Complexity

Technologies-Based Advanced Machine Learning Models: Applications in Civil Engineering 2021

Lead Guest Editor: Haitham Abdulmohsin Afan
Guest Editors: Mostafa Al-Emran and M. Z. Naser

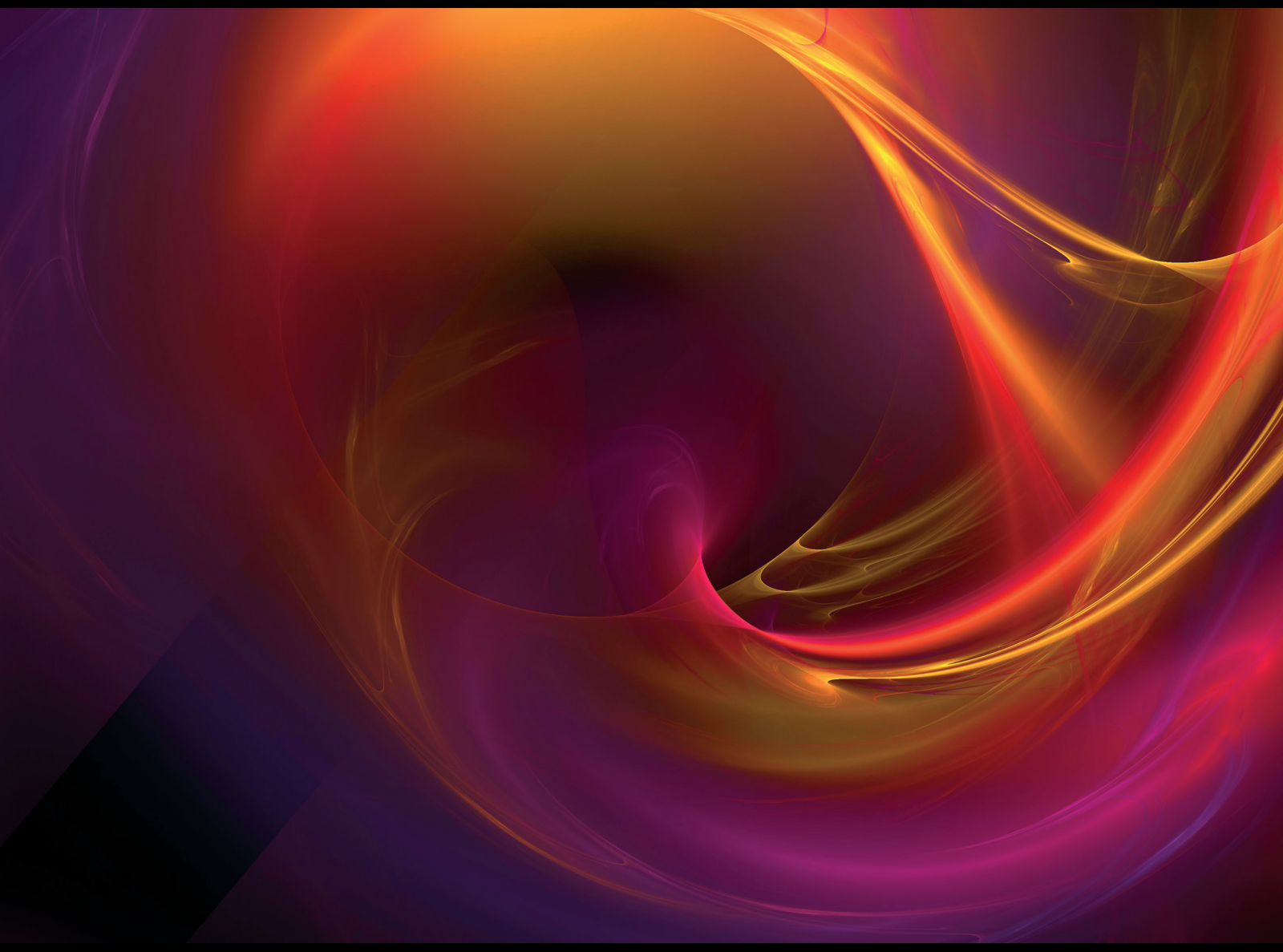

Technologies-Based Advanced Machine Learning Models: Applications in Civil Engineering 2021

Complexity

Technologies-Based Advanced Machine Learning Models: Applications in Civil Engineering 2021

Lead Guest Editor: Haitham Abdulmohsin Afan
Guest Editors: Mostafa Al-Emran and M. Z. Naser

Contents

A New Bayesian Network-Based Generalized Weighting Scheme for the Amalgamation of Multiple Drought Indices
Muhammad Ahmad Raza, Mohammed M. A. Almazah, Nadhir Al-ansari, Ijaz Hussain, Fuad S. Al-Duais, and Mohammed A. Naser
Research Article (23 pages), Article ID 8260317, Volume 2023 (2023)

A Systematic Literature Review on Robust Swarm Intelligence Algorithms in Search-Based Software Engineering
Alam Zeb, Fakhrud Din, Muhammad Fayaz, Gulzar Mehmood, and Kamal Z. Zamli
Review Article (22 pages), Article ID 4577581, Volume 2023 (2023)

Fluid Flow Behavior Prediction in Naturally Fractured Reservoirs Using Machine Learning Models
Mustafa Mudhafar Shawkat, Abdul Rahim Bin Risal, Noor J. Mahdi, Ziauddin Safari, Maryam H. Naser, and Ahmed W. Al Zand
Research Article (19 pages), Article ID 7953967, Volume 2023 (2023)

Developing an Integrative Data Intelligence Model for Construction Cost Estimation
Zainab Hasan Ali, Abbas M. Burhan, Murizah Kassim, and Zainab Al-Khafaji
Research Article (18 pages), Article ID 4285328, Volume 2022 (2022)

Application of Extreme Learning Machine Algorithm for Drought Forecasting
Muhammad Ahmad Raza, Mohammed M. A. Almazah, Zulfiqar Ali, Ijaz Hussain, and Fuad S. Al-Duais
Research Article (28 pages), Article ID 4998200, Volume 2022 (2022)

Design of System-of-System Acquisition Analysis Using Machine Learning
Fahad H. Alshammari
Research Article (15 pages), Article ID 4981539, Volume 2022 (2022)

Wind Effects on Rectangular and Triaxial Symmetrical Tall Building Having Equal Area and Height
Astha Verma, Rahul Kumar Meena, Hrishikesh Dubey, Ritu Raj, and S. Anbukumar
Research Article (20 pages), Article ID 4815623, Volume 2022 (2022)

Optimising the Selection of Input Variables to Increase the Predicting Accuracy of Shear Strength for Deep Beams
Mohammed Majeed Hameed, Faidhalrahman Khaleel, Mohamed Khalid AlOmar, Siti Fatin Mohd Razali, and Mohammed Abdulhakim AlSaadi
Research Article (23 pages), Article ID 6532763, Volume 2022 (2022)

Characterization of Meteorological Drought Using Monte Carlo Feature Selection and Steady-State Probabilities
Rizwan Niaz, Fahad Tanveer, Mohammed M. A. Almazah, Ijaz Hussain, Soliman Alkhatib, and A.Y. Al-Razami
Research Article (19 pages), Article ID 1172805, Volume 2022 (2022)

Compressive Strength Prediction Using Coupled Deep Learning Model with Extreme Gradient Boosting Algorithm: Environmentally Friendly Concrete Incorporating Recycled Aggregate

Mayadah W. Falah, Sadaam Hadee Hussein, Mohammed Ayad Saad, Zainab Hasan Ali, Tan Huy Tran, Rania M. Ghoniem, and Ahmed A. Ewees

Research Article (22 pages), Article ID 5433474, Volume 2022 (2022)

Hindawi
Complexity
Volume 2023, Article ID 8260317, 23 pages
https://doi.org/10.1155/2023/8260317

Research Article

A New Bayesian Network-Based Generalized Weighting Scheme for the Amalgamation of Multiple Drought Indices

Muhammad Ahmad Raza,[1,2] **Mohammed M. A. Almazah**,[3] **Nadhir Al-ansari**,[4] **Ijaz Hussain**,[1] **Fuad S. Al-Duais**,[5,6] **and Mohammed A. Naser**[3]

[1]*Department of Statistics, Quaid-i-Azam University, Islamabad, Pakistan*
[2]*Federal Urdu University, Arts, Sciences and Technology, Islamabad, Pakistan*
[3]*Department of Mathematics, College of Sciences and Arts (Muhyil), King Khalid University, Muhyil 61421, Saudi Arabia*
[4]*Department of Civil, Environmental and Natural Resources Engineering, Lulea University of Technology, 971 87 Lulea, Sweden*
[5]*Mathematics Department, College of Humanities and Science, Prince Sattam Bin Abdulaziz University, Al Aflaj, Saudi Arabia*
[6]*Administration Department, Administrative Science College, Thamar University, Thamar, Yemen*

Correspondence should be addressed to Nadhir Al-ansari; nadhir.alansari@ltu.se and Ijaz Hussain; ijaz@qau.edu.pk

Received 2 March 2022; Revised 10 December 2022; Accepted 4 April 2023; Published 21 April 2023

Academic Editor: Ning Cai

Drought is one of the most multifaceted hydrologic phenomena, affecting several factors such as soil moisture, surface runoff, and significant water shortages. Therefore, monitoring and assessing drought occurrences based on a single drought index are inadequate. The current study develops a multiscalar weighted amalgamated drought index (MWADI) to amalgamate multiple drought indices. The MWADI is mainly based on the normalized average dependence posterior probabilities (ADPPs). These ADPPs are obtained from Bayesian networks (BNs)-based Markov Chain Monte Carlo (MCMC) simulations. Results have shown that the MWADI correlates more with the standardized precipitation index (SPI) and the standardized precipitation temperature index (SPTI). As proposed, the MWADI synthesizes drought characteristics of different multiscalar drought indices to reduce the uncertainty of individual drought indices and provide a comprehensive drought assessment.

1. Introduction

Drought has complex nature and slow onset characteristics that have severe impacts on several sectors worldwide [1]. The vulnerabilities of drought differ from other natural hazards in numerous ways [2]. The abrupt and enigmatic features of drought make it the costliest and least understood hazard [3]. The American Meteorological Association classified drought into four categories including meteorological, hydrological, agricultural, and socioeconomic [4, 5]. Each drought category has different causes and consequences [6, 7]. For instance, meteorological drought occurs due to a lack of precipitation. It significantly impacts various sectors such as ecology, agricultural productions, and industrial productions [8]. It causes serious environmental and socioeconomic issues at regional and global scales [9, 10]. Meteorological drought can trigger linked climatic hazards such as pollution and heatwave [11]. Precise drought monitoring of drought requires reliable information, assessment, and evidence-based decisions [12]. Moreover, drought indices play a vibrant role in risk assessment for accurately identifying drought occurrence, severity, and spatial extent [13].

Drought indices are essential for quantifying drought duration, severity, and spatial extent [14, 15]. Various drought indices based on single and multiple climatic parameters have been developed to monitor and assess the drought characteristics [16]. The widely used drought indices are the Palmer drought severity index (PDSI) [17], the surface water supply index (SWSI) [8, 18], the standardized

precipitation index (SPI) [19], the effective drought index (EDI) [20], the standardized precipitation and evapotranspiration index (SPEI) [21], and the standardized precipitation temperature index (SPTI) [22]. Moreover, the SPI is the most well-known drought index proposed by the World Meteorological Organization (WMO). However, the selection and calculation of drought indices depend on the availability of data-related input climatic indicators [23]. Furthermore, due to the complex nature of hydroclimatic parameters, traditional meteorological drought indices cannot obtain full information for accurate drought characterization [24].

Individual drought indices have certain deficiencies in assessing drought severities [25]. The substantial complexity of the hydrological process depends upon multiple climatic factors such as precipitation, temperature, and evapotranspiration [26]. Single drought indices are incapable of considering certain drought-induced causes, leading to inaccurate drought assessment [27]. However, a very few composite and hybrid drought indices have been observed in recent decades [28]. The vegetation drought response index (VegDRI) is one of the best examples of a comprehensive drought index based on the SPI, the PDSI, and the NDVI [29]. Numerous drought indices are constructed using linear combinations, principal component analysis, and entropy weight method by considering a linear relationship among standardized drought indices [30]. However, regardless of the type of drought, the interactions among the numerous influencing factors in the environment should be considered for drought monitoring. Generally, drought conditions are associated with multiple meteorological and climatic variables [31]. Therefore, a comprehensive drought index based on a strong probabilistic structure can provide more accurate information about drought monitoring and assessing drought conditions.

Bayesian networks (BNs) are powerful probabilistic graphical models that explicitly capture the known dependence structure among stochastic variables such as drought indices (DIs) with probabilities through directed acyclic graphs (DAGs) [32]. The BNs have wide applications in various fields, viz., computer science [33], business analytics [34], agriculture [35], genetics [36], and environmental sciences [37, 38]. BNs are appropriate methods to estimate climate change impact and drought risk assessment [39]. The researchers have used the BN algorithm to develop new frameworks in different fields. For instance, it is used for flood prediction [40] and forecasting the dependence structure among health outcomes and hazardous pollutants [41]. Shin et al. (2020) used BNs to propagate the relationships of hydrological drought in different time intervals. Ávila and Ballari [42] used BNs to develop new homogeneous climate zone indices. Appraisal of the latest literature indicated that BNs are emerging in meteorological and climatic studies. The potential of probabilistic graphical models based on BNs for drought assessment and developing new comprehensive drought indices could be helpful. Since droughts are a slowly evolving phenomenon, a robust spatial and temporal relationship exists among drought indices [43]. Therefore, they can be amalgamated using BNs to combine the strengths of several drought indices.

The current study aims to develop a comprehensive drought index to improve the monitoring and assessment of drought. For this purpose, the current research uses the BN theory to synthesize drought monitoring characteristics of three standardized drought indices, including the SPI, the SPEI, and the SPTI. The proposed framework based on the Bayesian network theory also integrates the seasonal component of several seasonally segregated drought indices. It provides a scientific basis for an effective drought mitigation plan [44]. Moreover, the Gilgit-Baltistan province is selected to validate the current research.

2. Materials and Methods

2.1. Data Description and Study Area. The six synoptic gauged meteorological stations have been selected, including Astore, Bunji, Chilas, Gilgit, Gupis, and Skardu. The monthly time series data of precipitation and temperature (maximum and minimum) have been used to develop the MWADI. The input data for 47 years ranging from 1970 to 2016 have been acquired from the Karachi Data Processing Center (KDPC) through the Pakistan Meteorological Department (PMD). The spatial distribution map and location information of selected meteorological stations of Gilgit-Baltistan province is shown in Figure 1. The study area lies between 34.5125°N–37.0826°N latitude and 72.508°E–77.01°E longitude. The terrain feature of the study area is high-elevation mountainous. The GB province comprises the upper catchment areas of the Indus River and its major tributaries. The source of precipitation in GB is the typical continental monsoon in summer and the western depression in winter. The average annual rainfall in GB province is 231.5 inches. However, the region's temporal and spatial distributions of precipitation are not homogenous. The mean average annual precipitation at these selected meteorological stations significantly varies, as shown in Table 1. According to the above characteristics of topography, hydrology, and geomorphology, the region's climate is classified into different categories. The climate classification of selected meteorological stations is given in the last column of Table 1. These climate classifications are known as Köppen climate classifications [45]. Köppen [46] classified the climate of any region into five categories, which were further divided into subcategories. According to Köppen classification, the climate of Astore is considered humid-continental, and Gilgit and Bunji are considered cold desert, while Chilas, Gupis, and Skardu are classified as cold semiarid. The descriptive statistics of spatial variables (longitude, latitude, and elevation) and meteorological variables (precipitation and minimum and maximum temperature) are given in Table 1. It includes the mean and standard deviation (SD) of the average annual precipitation of selected meteorological stations. It provides varying features of the minimum and maximum temperature.

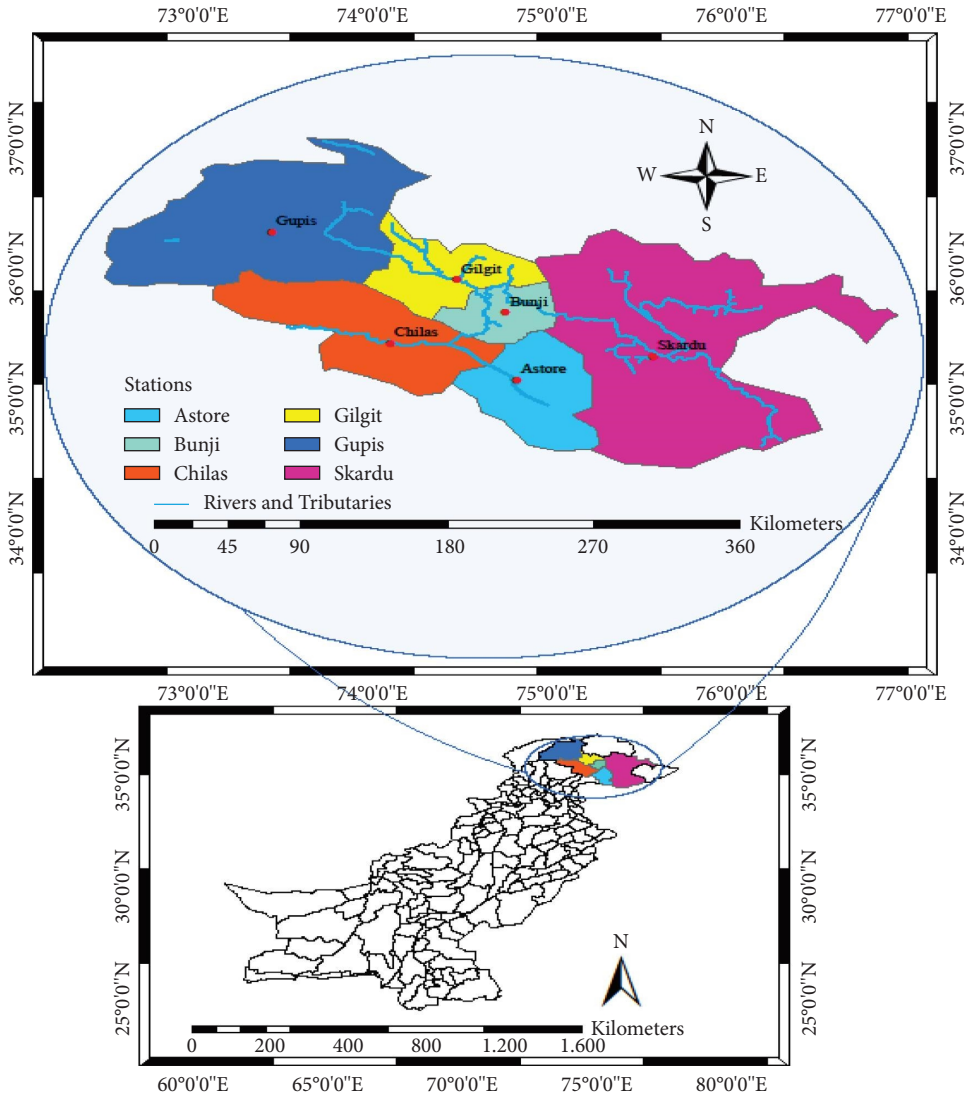

Figure 1: The map of the study region and distribution of meteorological stations.

Table 1: Descriptive statistics of average annual meteorological variables (precipitation and minimum and maximum temperature), regional spatial characteristics, and climate (Köppen classification).

Station	Precipitation		Temp. min		Temp. max		Latitude	Longitude	Elevation (m)	Climate
	Mean	SD	Min	Max	Min	Max				
Astore	471.8	129.3	2.36	5.23	13.90	17.47	35.3570°E	74.8624°N	2546	Humid continental
Bunji	163.4	61.5	9.57	13.6	22.33	25.48	35.6431°E	74.6342°N	1453	Cold desert
Chilas	190.6	93.9	12.32	15.53	24.57	27.97	35.4222°E	74.0946°N	1265	Cold semiarid
Gilgit	140.7	49.4	6.15	9.26	22.45	25.92	35.8819°E	74.4643°N	1500	Cold desert
Gupis	190.4	145.2	4.19	8.33	16.99	20.54	36.2274°E	73.4421°N	3030	Cold semiarid
Skardu	231.9	95.5	3.31	6.17	16.29	20.81	35.3247°E	75.551°N	2228	Cold semiarid

2.2. A Brief Description of Multiscalar Standardized Drought Indices. Standardized drought indices (SDIs) play a vibrant role in drought risk assessment and the sustainable development of water resources [9]. Therefore, defining drought features specific to drought intensity, duration, and patterns is very important [21]. Thus, the multiscaler drought indices, such as the SPI, the SPEI, and the SPTI, are selected as input hydroclimatic variables to develop the MWADI. The standardized precipitation index (SPI) is the most widely used drought index applied to regional and global studies. The World Meteorological Organization (WMO) ratified the SPI for meteorological drought [47]. It is a probabilistic and spatially invariant indicator for a different type of drought analysis [48]. The SPI utilizes only precipitation and has the inherited capability to be calculated at various time scales [49]. The standardized precipitation evapotranspiration

index (SPEI) is a climatic water balance variant of the SPI based on precipitation and potential evapotranspiration. It possesses the multiscalar capability of the SPI by considering its simple mathematical procedure and utilizing temperature variability. The computation procedure of the SPEI is followed by guidelines provided in [50]. The standardized precipitation temperature index (SPTI) is another multiscalar drought selected as the input climatic indicator of our proposed framework. The calculation procedure of the SPTI is quite like the SPI and the SPEI.

The above-stated drought indices are standardized, i.e., cumulative distribution function (CDF) values of a normal probability distribution. For any time scale, the zero value of SDIs (the SPI, the SPEI, and the SPTI) stated that there is no deviation from the average precipitation. A positive value indicates that the precipitation is higher than the average precipitation. In contrast, a negative value of drought shows that precipitation is smaller than the average precipitation.

2.3. Seasonality of Drought Indices. Drought predictions using seasonally integrated drought indices are helpful in freshwater resource management and ecological preservation [51]. Seasonal segregation of drought indices can compute hybrid and comprehensive drought indices for precise drought characterization [52, 53]. The seasonal climate forecast usually ranges from a few weeks to a year but is mainly selected at a monthly scale [54], as various hydrological and climatological studies are based on monthly defined seasonal indices [55, 56]. Similarly, current study indorses monthly defined seasonal drought indices as input variables.

2.4. Bayesian Networks (BNs). Bayesian networks (BNs) are probabilistic graphical models that can describe concise conditional dependence structures among a set of random variates through directed acyclic graphs (DAG) [57]. A DAG consists of nodes representing random variables and arcs or edges that quantify the conditional dependence of random variates (nodes) [39, 58]. The direction of edges or arcs represents the causal relationship among the random variables, and if nodes did not connect through some arc, they are considered conditionally independent. The conditional independence of nodes enables BNs to efficiently represent complex probability distributions [59]. The causal relationship between random variables (nodes) is defined as conditional probability based on prior information or statistically observed correlations [60]. Each node possesses signified states or levels [61]. BNs are constructed for the identification of the dependence structure among random variables. The learning of BNs from data for inference and decision-making is based on Markov Chain Monte Carlo (MCMC) algorithms [62, 63] using an improved Metropolis–Hastings sampler [64, 65].

In the Bayesian network theory, to learn the Bayesian networks from some observed dataset E, the posterior probability of network G can be computed using the Bayes rule.

$$P(G|E) = \frac{P(E|G)P(G)}{P(E)}, \tag{1}$$

where $P(E|G)$ is the marginal likelihood function of observed data given the DAG G', $P(G)$ is the prior density of DAG, and $P(E)$ is the normalizing factor. Then, the posterior probability of any hypothesis of interest can be computed by averaging all networks. For a detailed description of Bayesian learning, the Bayesian model average approach, and marginal posterior of features (edges), see [66].

2.5. Proposed Framework for the Bayesian Network-Based Generalized Weighting Scheme for Amalgamation of Multiple Drought Indices. The main objective of this study is to introduce a Bayesian network-based new weighting scheme for amalgamating multiple seasonal drought indices to develop a new comprehensive drought index. The central part of the study is based on three standardized drought indices (the SPI, the SPEI, and the SPTI) and the Bayesian network procedure. The details of these methodologies have already been discussed in Sections 2.2 and 2.3. A schematic diagram of the proposed framework is shown in Figure 2. Further implication and execution of the framework comprise different phases, which are as follows.

Phase 1. Selection and calculation of SDIs (the SPI, the SPEI, and the SPTI): The selection of drought indices can influence the obtained information about drought monitoring, its areal extent, and duration. Most of the SDIs are region-specific and have inherited complexities. Therefore, single and multiple meteorological variables based on drought indices (the SPI, the SPEI, and the SPTI) have been selected for the current study, and their calculation procedure is briefly described in Section 2.2.

Phase 2. Seasonal segregation of SDIs: In this phase, full-length time series datasets of already calculated SDIs are separated with respect to months by considering each month as a season for seasonal, temporal formation [56, 67]. These seasonal drought indices are then considered as input variables for structural BNs.

Phase 3. The implication of BNs to obtain potion quantities (weights): The key objective of the current study is to estimate the probabilistic dependence structure of seasonal standardized drought indices (the SPI, the SPEI, and the SPTI) at each selected meteorological station. The marginal posterior probabilities of feature edges (nodes/variables) are approximated through Markov Chain Monte Carlo (MCMC) simulations. Three independent MCMC simulations have run on each time series dataset to obtain convergence, and the marginal posterior probabilities are averaged. The marginal posterior probabilities describe the dependence structure among input variables (seasonal SDIs).

Let SDI_j be the list of candidate standardized drought indices and Y_{ijt} be the time series data of i^{th} season (month)

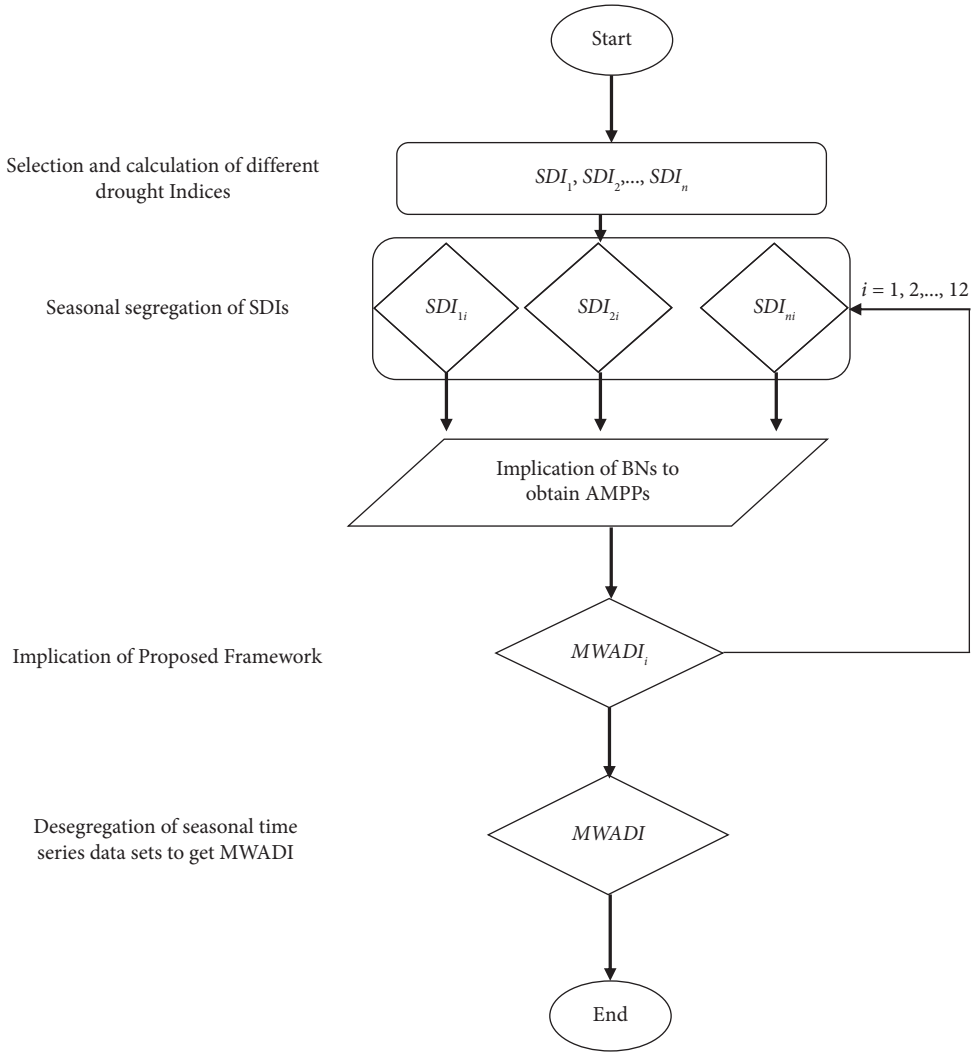

Figure 2: Graphical representation of the proposed framework.

related to j^{th} SDI at any individual meteorological station, where t shows the time index and $(i = 1, 2, \ldots, 12)$, $(j = 1, 2, 3)$. This step aims to calculate potion quantities being used as normalizing weights of the proposed framework to calculate the new seasonally synthesized amalgamated drought index. The realization of nodes (SDI_j) and edges are defined as follows:

$$f\left(y_{i1}, y_{i2}, y_{i3}\right) = P\left(Y_{i1} = y_{i1}, Y_{i2} = y_{i2}, Y_{i3} = y_{i3}\right). \quad (2)$$

Equation (2) describes the relative importance of each seasonal SDI through marginal posterior probabilities, which can also be defined as dependence probability. A single run of MCMC simulation gives the following result:

$$\begin{array}{c} \\ \mathrm{SPI} \\ \mathrm{SPEI} \\ \mathrm{SPTI} \end{array} \begin{array}{c} \begin{array}{ccc} \mathrm{SPI} & \mathrm{SPEI} & \mathrm{SPTI} \end{array} \\ \begin{bmatrix} \pi_{11} & \pi_{12} & \pi_{13} \\ \pi_{21} & \pi_{22} & \pi_{23} \\ \pi_{31} & \pi_{32} & \pi_{33} \end{bmatrix} \end{array}. \quad (3)$$

The average dependence probability (ADP) for a single MCMC simulation of j^{th} seasonal SDI is denoted by $\pi_{.j}$ which is defined as follows:

$$\pi_{.j} = \frac{\pi_{1j} + \pi_{2j} + \pi_{3j}}{3}. \quad (4)$$

The grand average dependence probability (GADP) of j^{th} SDI is denoted by ω_j, finally obtained through averaging for all three MCMC simulations, and is mathematically defined as follows:

$$\omega_j = \frac{\left(\pi_{.j_1} + \pi_{.j_2} + \pi_{.j_3}\right)}{3}. \quad (5)$$

These grand averaged dependence probabilities are the actual probabilistic relative importance of SDIs at each meteorological station. Furthermore, these are considered as potion quantities to calculate normalizing weights ω_j' defined as follows:

$$\omega_j' = \frac{\omega_j}{\sum_{j=1}^{3}\omega_j}, \tag{6}$$

where ω_j' are the estimated parameters of the proposed model defined in equation (6). These parameters are estimated through the probabilistic dependence structure of BNs analytically evaluated through MCMC simulations.

Phase 4. The execution of the proposed model to obtain the seasonal MWADI:

In this phase, a probabilistic model is defined to synthesize information from different SDIs. In numerous studies, stochastic models such as copulas were employed to combine drought characteristics of different drought indices [68–70]. But BNs are structural probabilistic and powerful graphical algorithms to produce dependence probabilities of stochastic variates utilizing every bit of information [40, 63, 71]. Therefore, this study proposes a probabilistic model defined in equation (7), which synthesizes information obtained from seasonal multiscalar standardized drought indices.

$$\mathrm{MWADI}_i = \omega_1'\mathrm{SPI}_i + \omega_2'\mathrm{SPEI}_i + \omega_3'\mathrm{SPTI}_i, \tag{7}$$

where MWADI_i is a linear combination of SPI_i, SPEI_i, and SPTI_i. The linear combination is a mathematical way to combine different drought indices to synthesize the meteorological information related to drought characterization. The most innovative feature of MWADI_i is that the weights (parameters) are calculated through a probabilistic structure of BNs using MCMC simulations. The weights calculated using BNs define the role of different drought indices. The proposed model defined in equation (7) results in seasonal MWADI_i (Jan–Dec) at each station using probabilistic weights or parameters associated with different drought indices. After obtaining the seasonal MWADI_i (Jan–Dec), all 12-time series datasets will be combined to obtain the final MWADI. The outcome of the algorithm is a comprehensive multiscalar weighted amalgamated drought index (MWADI).

3. Results and Discussion

The latest development of drought indices emphasized incorporating complete information readily available in standardized drought indices. Therefore, three multiscalar standardized drought indices (the SPI, the SPEI, and the SPTI) have been used as input indicators to construct the proposed MWADI. The main steps involved in the construction and development of the MWADI are explained and executed in sequence.

3.1. Selection and Estimation of Input Variables (SDIs). The SPI, the SPEI, and the SPTI are estimated using their input meteorological variables for full-length time series data of precipitation and temperature (minimum and maximum) at selected meteorological stations. These drought indices are calculated using a parametric approach by selecting appropriate probability distributions [50]. The Bayesian information criterion (BIC) has been used to determine appropriate distribution using the propagate *R* Package (Spies, 2014). Detailed calculation procedures of these SDIs at these selected meteorological stations can be seen in [66]. Afterward, the datasets of these SDIs are further seasonally (monthly defined) segregated to integrate seasonal components. In this study, six meteorological stations have been selected, and 36 seasonal datasets have formed at each station. Hence, 216 seasonal datasets have been used as input variables to execute MCMC simulations.

3.2. The Implication of BNs for the Estimation of Parameters (Normalizing Weights). The Bayesian network theory has been applied to monthly separated time series data of various drought indices (the SPI, the SPEI, and the SPTI) for calculating their relative importance through the dependence probability structure. BN-based MCMC simulations were performed using seasonal SDIs at each selected meteorological station. BNs sorted out causal relationships between nodes (variable) through DAGs. In this study, seasonal SDIs are considered as nodes, and the arc's direction shows the hydrologic causality (conditional dependence) between nodes (SDIs). Three independent MCMC simulation runs are carried out on monthly separated time series datasets of the SPI, the SPEI, and the SPTI with 200,000 iterations to obtain experimental results. The marginal posterior probabilities or dependence probabilities for each simulation run are obtained using equation (2) for all 12 seasons (Jan–Dec) at each station. The average dependence probabilities (ADPs) are calculated using equation (4). Moreover, ADPs obtained through these independent simulation runs have not shown much variation, which shows the consistency and convergence of MCMC simulation runs. For more precise results, equation (5) calculates grand averaged dependence probabilities (GADPs) by averaging ADPs for all three simulation runs. Tables 2 and 3comprise average marginal posterior probabilities already named ADPs of three simulation runs and GADPs for January and February seasons at all meteorological stations. These GADPs show the relative importance of seasonal SDIs (the SPI, the SPEI, and the SPTI) over each other. The GADPs of the SPI, the SPEI, and the SPTI for January are 0.9907, 0.6528, and 0.6620, respectively, showing the SPI's dominance at the Astore station. While at Bunji station, these results are 0.7245, 0.6429, and 0.9184, respectively. Here, the SPTI dominates other indices, showing that the relative importance of SDIs substantially varies from station to station.

Furthermore, we have checked across seasonal probabilistic relative importance of SDIs (the SPI, the SPEI, and the SPTI). The GADPs for the February season at Astore station are 0.9814, 0.6643, and 0.6829, respectively. The comparison of GADPs across seasons shows that at Astore station, the SPI's dominance persisted. While at Bunji station for the February season, these probabilities are 0.8510, 0.6119, and 0.7608, respectively, depicting that dominance changed from the SPTI to the SPI. The spatial and seasonal variations of conditional relevance of different SDIs are shown in Figure 3. It indicates that SDIs have significant

Table 2: Bayesian network-based grand average dependence probabilities (ω_j) of SDIs for season-1 (January) at all meteorological stations.

Simulation Runs	SDIs	Astore			Bunji			Chilas			Gilgit			Gupis			Skardu		
		SPI	SPEI	SPTI	SPI	SPEI	SPTI	SPI	SPEI	SPTI	SPI	SPEI	SPTI	SPI	SPEI	SPTI	SPI	SPEI	SPTI
	SPI	0.0001	0.9821	1	0.0001	0.4537	1	0.0001	0.4274	1	0.0001	0.4798	1	0.0001	0.4474	1	0.0001	0.8639	1
Run-1	SPEI	0.9821	0.0001	0.3235	0.4537	0.0001	0.8327	0.4274	0.0001	0.8325	0.4798	0.0001	0.7821	0.4474	0.0001	0.8046	0.8639	0.0001	0.3272
	SPTI	1	0.3235	0.0001	1	0.8327	0.0001	1	0.8325	0.0001	1	0.7821	0.0001	1	0.8046	0.0001	1	0.3272	0.0001
ADP_1		0.9910	0.6528	0.6618	0.7268	0.6432	0.9164	0.7137	0.6299	0.9163	0.7399	0.6310	0.8911	0.7237	0.6260	0.9023	0.9320	0.5956	0.6636
	SPI	0.0001	0.9802	1	0.0001	0.4402	1	0.0001	0.4306	1	0.0001	0.4770	1	0.0001	0.4590	1	0.0001	0.7978	1
Run-2	SPEI	0.9802	0.0001	0.3280	0.4402	0.0001	0.8401	0.4306	0.0001	0.8262	0.4770	0.0001	0.7844	0.4590	0.0001	0.7944	0.7978	0.0001	0.4539
	SPTI	1	0.3280	0.0001	1	0.8401	0.0001	1	0.8262	0.0001	1	0.7844	0.0001	1	0.7944	0.0001	1	0.4539	0.0001
ADP_2		0.9901	0.6541	0.6640	0.7201	0.6402	0.9200	0.7153	0.6284	0.9131	0.7385	0.6307	0.8922	0.7295	0.6267	0.8972	0.8989	0.6258	0.7269
	SPI	0.0001	0.9821	1	0.0001	0.4533	1	0.0001	0.4233	1	0.0001	0.4884	0.9998	0.0001	0.4433	1	0	0.8135	1
Run-3	SPEI	0.9821	0.0001	0.3207	0.4533	0.0001	0.8376	0.4233	0.0001	0.8299	0.4886	0.0001	0.7676	0.4433	0.0001	0.8095	0.8135	0.0001	0.4686
	SPTI	1	0.3207	0.0001	1	0.8376	0.0001	1	0.8299	0.0001	1	0.7677	0.0001	1	0.8095	0.0001	1	0.4686	0.0001
ADP_3		0.9910	0.6513	0.6603	0.7266	0.2266	0.9188	0.7117	0.2116	0.9149	0.7443	0.2442	0.8837	0.7216	0.2216	0.9047	0.9068	0.4068	0.7343
GADP		0.9907	0.6528	0.6620	0.7245	0.6429	0.9184	0.7136	0.6283	0.9148	0.7409	0.6299	0.8890	0.7250	0.6263	0.9014	0.9125	0.7083	0.7083

Table 3: Bayesian network-based grand average dependence probabilities (ω_j) of SDIs for February at all stations.

Simulation Runs	SDIs	Astore			Bunji			Chilas			Gilgit			Gupis			Skardu		
		SPI	SPEI	SPTI	SPI	SPEI	SPTI	SPI	SPEI	SPTI	SPI	SPEI	SPTI	SPI	SPEI	SPTI	SPI	SPEI	SPTI
	SPI	0.0001	0.9661	1	0.0001	0.6938	1	0.0001	0.4204	1	0.0001	0.4876	1	0.0001	0.4967	1	0.0001	0.3337	1
Run-1	SPEI	0.9661	0.0001	0.3676	0.6938	0.0001	0.5231	0.4204	0.0001	0.8527	0.4876	0.0001	0.7487	0.4967	0.0001	0.8615	0.3337	0.0001	0.9976
	SPTI	1	0.3676	0.0001	1	0.5231	0.0001	1	0.8527	0.0001	1	0.7487	0.0001	1	0.8615	0.0001	1	0.9976	0.0001
ADP_1		0.9831	0.6669	0.6838	0.8469	0.6084	0.7615	0.7102	0.6366	0.9264	0.7438	0.6181	0.8743	0.7484	0.6791	0.9307	0.6669	0.6656	0.9988
	SPI	0.0001	0.9602	1	0.0001	0.7042	1	0.0001	0.4098	1	0.0001	0.4978	1	0.0001	0.5020	1	0.0001	0.3647	1
Run-2	SPEI	0.9602	0.0001	0.3696	0.7042	0.0001	0.5247	0.4098	0.0001	0.8550	0.4978	0.0001	0.7399	0.5020	0.0001	0.8596	0.3647	0.0001	0.9969
	SPTI	1	0.3696	0.0000	1	0.5247	0.0001	1	0.8550	0.0001	1	0.7399	0.0001	1	0.8596	0.0001	1	0.9969	0.0001
ADP_2		0.9801	0.6649	0.6848	0.8521	0.6144	0.7623	0.7049	0.6324	0.9275	0.7489	0.6188	0.8700	0.7510	0.6808	0.9298	0.6824	0.6808	0.9985
	SPI	0.0001	0.9623	1	0.0001	0.7083	1	0.0001	0.4247	1	0.0001	0.4874	1	0.0001	0.5065	1	0.0001	0.3262	1
Run-3	SPEI	0.9623	0.0001	0.3601	0.7083	0.0001	0.5171	0.4247	0.0001	0.8407	0.4874	0.0001	0.7491	0.5065	0.0001	0.8574	0.3262	0.0001	0.9967
	SPTI	1	0.3601	0.0001	1	0.5171	0.0001	1	0.8407	0.0001	1	0.7491	0.0001	1	0.8574	0.0001	1	0.9967	0.0001
ADP_3		0.9811	0.4811	0.6800	0.8541	0.3541	0.7586	0.7124	0.2124	0.9203	0.7437	0.2437	0.8745	0.7533	0.2533	0.9287	0.6631	0.1631	0.9984
GADP		0.9814	0.6643	0.6829	0.8510	0.6119	0.7608	0.7092	0.6339	0.9247	0.7454	0.6284	0.8729	0.7509	0.6806	0.9298	0.6708	0.6693	0.9985

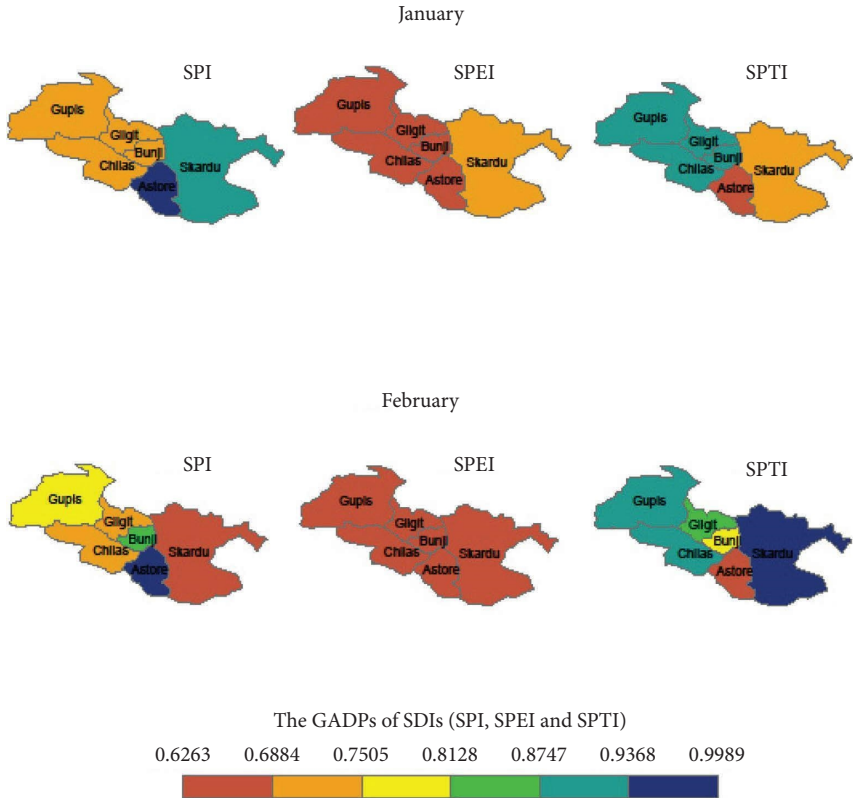

Figure 3: Spatial and seasonal dominance of different SDIs (the SPI, the SPEI, and the SPTI).

seasonal and spatial relevance at some meteorological stations. The GADPs (probabilistic relative importance) of SDIs are further normalized according to equation (6) to obtain the final potion quantities of the algorithm considered as estimates of the parameters of the proposed model. Results for all the 12 seasons (Jan–Dec) and all selected stations are given in Table 4. For ease of understanding, the presentation of experimental results is presented only for the specific season; however, the results for the other seasons can be presented accordingly.

3.3. Execution of the Proposed Model. The proposed model defined in equation (7), the MWADI, is a linear combination of three multiscalar standardized drought indices whose weights (parameters) are calculated using probabilistic structural BNs. The results of these estimated parameters of the proposed model for all the seasons (Jan–Dec) at selected stations are presented in Table 4. The outcome of the proposed model is also the seasonal MWADI for a specific season at each meteorological station. After calculating seasonal MWADIs (Jan–Dec), all 12-time series are then desegregated to obtain an outcome named MWADI. The process is repeated at each meteorological station to obtain the MWADI. The outcome of the proposed algorithm is a seasonally integrated multiscalar amalgamated drought index (MWADI) for any individual meteorological station. The MWADI and input SDIs can be calculated at various temporal scales to monitor drought conditions, but for convenience, results are given for a one-month time scale.

A validation experiment was carried out to assess the accuracy of the drought severity characterized by the MWADI by comparing the count plots, scatter plots, temporal plots, and correlation coefficients. Figures 4–6 show the scatter plots of seasonal MWADI with the SPI, the SPEI, and the SPTI for all seasons Jan–Dec at the Astore station. The MWADI is highly correlated with these drought indices, and the correlation test was applied, and it is observed that the MWADI is significantly correlated with all other SDI's at p value <0.001. Figure 7 shows that the MWADI is slightly less correlated with the SPEI while strongly correlated with the SPI and the SPTI. The overall correlation coefficient values between the MWADI and other SDIs (the SPI, the SPEI, and the SPTI) are 0.93, 0.84, and 0.98, respectively. Results related to the correlation coefficient between the MWADI and other SDIs for all seasons at selected stations are presented in Table 5. The strong relationship between the MWADI and other meteorological SDIs reflects that the MWADI can more precisely monitor and characterize meteorological drought.

The drought occurrence frequency is one of the important factors of drought characterization. Drought severity is classified into seven mutually exclusive categories. Several studies already endorse these classifications [19, 21, 72, 73]. The comparison of different drought categories characterized by the MWADI and other SDIs is presented by count plots, as shown in Figure 8. The frequency of different drought categories significantly varied from one SDI to another and seemed quite uncertain. Because different drought indices give contradictory outcomes

Table 4: Estimated parameters (ω_j') of the proposed model at all meteorological stations for all seasons (Jan–Dec).

Seasons	Astore			Bunji			Chilas			Gilgit			Gupis			Skardu		
	SPI	SPEI	SPTI	SPI	SPEI	SPTI	SPI	SPEI	SPTI	SPI	SPEI	SPTI	SPI	SPEI	SPTI	SPI	SPEI	SPTI
Jan	0.4297	0.2831	0.2872	0.3170	0.2813	0.4018	0.3162	0.2784	0.4054	0.3279	0.2787	0.3934	0.3218	0.2780	0.4001	0.4138	0.2931	0.2931
Feb	0.4215	0.2853	0.2933	0.3827	0.2752	0.3421	0.3127	0.2795	0.4078	0.3333	0.2765	0.3903	0.3180	0.2883	0.3938	0.2868	0.2862	0.4270
Mar	0.3592	0.3198	0.3210	0.3133	0.2803	0.4064	0.3322	0.2880	0.3798	0.3430	0.2769	0.3801	0.3279	0.2779	0.3942	0.2839	0.2834	0.4327
Apr	0.3767	0.3010	0.3223	0.3158	0.2809	0.4033	0.3381	0.2797	0.3822	0.3430	0.2768	0.3801	0.3918	0.2763	0.3318	0.2892	0.2891	0.4217
May	0.3072	0.2957	0.3971	0.2947	0.2867	0.4186	0.2976	0.2850	0.4174	0.2993	0.2862	0.4145	0.2979	0.2847	0.4173	0.2870	0.2870	0.4261
Jun	0.2899	0.2832	0.4268	0.3165	0.2871	0.3964	0.3141	0.2788	0.4072	0.3237	0.2845	0.3918	0.3139	0.2815	0.4046	0.3029	0.2838	0.4133
Jul	0.2853	0.2830	0.4316	0.3038	0.2912	0.4051	0.3117	0.2805	0.4079	0.3117	0.2881	0.4002	0.3144	0.2858	0.3997	0.2972	0.2849	0.4179
Aug	0.2901	0.2856	0.4244	0.2952	0.2882	0.4166	0.3057	0.2810	0.4133	0.2998	0.2830	0.4172	0.3119	0.2804	0.4077	0.2864	0.2847	0.4289
Sep	0.3717	0.2933	0.3350	0.3063	0.2802	0.4135	0.3294	0.2814	0.3891	0.3285	0.2774	0.3941	0.3329	0.2779	0.3892	0.2874	0.2872	0.4254
Oct	0.3556	0.2817	0.3627	0.3711	0.2757	0.3532	0.3367	0.2784	0.3849	0.3845	0.2751	0.3403	0.3727	0.2753	0.3520	0.2840	0.2840	0.4319
Nov	0.3494	0.2815	0.3691	0.3410	0.2744	0.3846	0.3174	0.2827	0.3999	0.3356	0.2759	0.3884	0.3414	0.2750	0.3836	0.2857	0.2840	0.4303
Dec	0.3451	0.2835	0.3714	0.3480	0.2747	0.3773	0.3179	0.2832	0.3988	0.3423	0.2746	0.3832	0.3403	0.2749	0.3848	0.3099	0.3098	0.3803

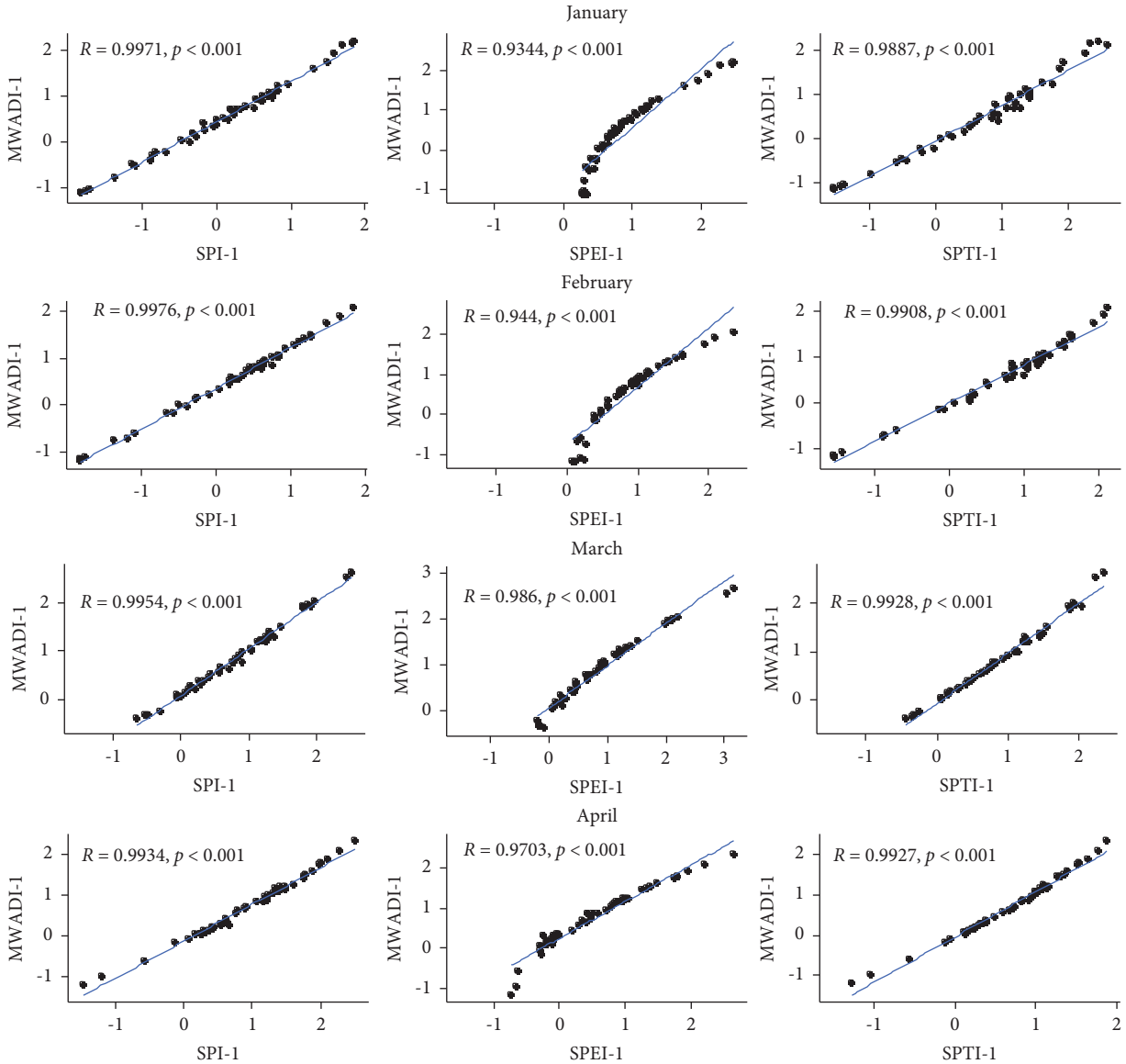

Figure 4: The scatter diagram and correlation coefficient R values between the seasonal MWADI and the SPI, the SPEI, and the SPTI (January–April) at Astore.

related to drought characterization. Furthermore, inaccurate drought characterization may mislead to drought mitigation policymakers. As the MWADI synthesized the climatic and meteorological characteristics of different SDIs (the SPI, the SPEI, and the SPTI), the drought characterization through the MWADI is considered more reliable. It reduces the uncertainty of drought characterization through different drought indices. The near normal (NN) drought class has a significantly higher proportion than other extreme classes. Extreme dry and extreme wet classes have comparatively lower count proportions but still can be catastrophic for linked ecosystems.

The temporal behavior of the MWADI and other SDIs (the SPI, the SPEI, and the SPTI) for the Astore station is shown in Figure 9. The SPI, the SPEI, and the SPTI were used to characterize short and long-term drought conditions. The graphical representation shows the evolution and termination of dry and wet conditions during 1970–2016. The red spikes and patches show the severity and duration of drought similarly; some blue spikes represent a few high precipitation events producing wet spells that cause flash flood events. The MWADI, the SPI, and the SPTI showed similar drought trends from 1970 to 2016, indicating the high correlation among these indices. This graphical evidence also clarifies the variation in defining drought classifications by the MWADI and other SDIs. The temporal behavior of the MWADI for a one-month time scale at all selected meteorological stations is presented in Figure 10. These statistical and graphical results indicate that the main advantage of the MWADI is its probabilistic graphical feature for characterizing and analyzing drought conditions. As the probabilistic structure of BNs is based on the cause-and-effect relationship between climatic and meteorological indicators therefore, a comprehensive drought index

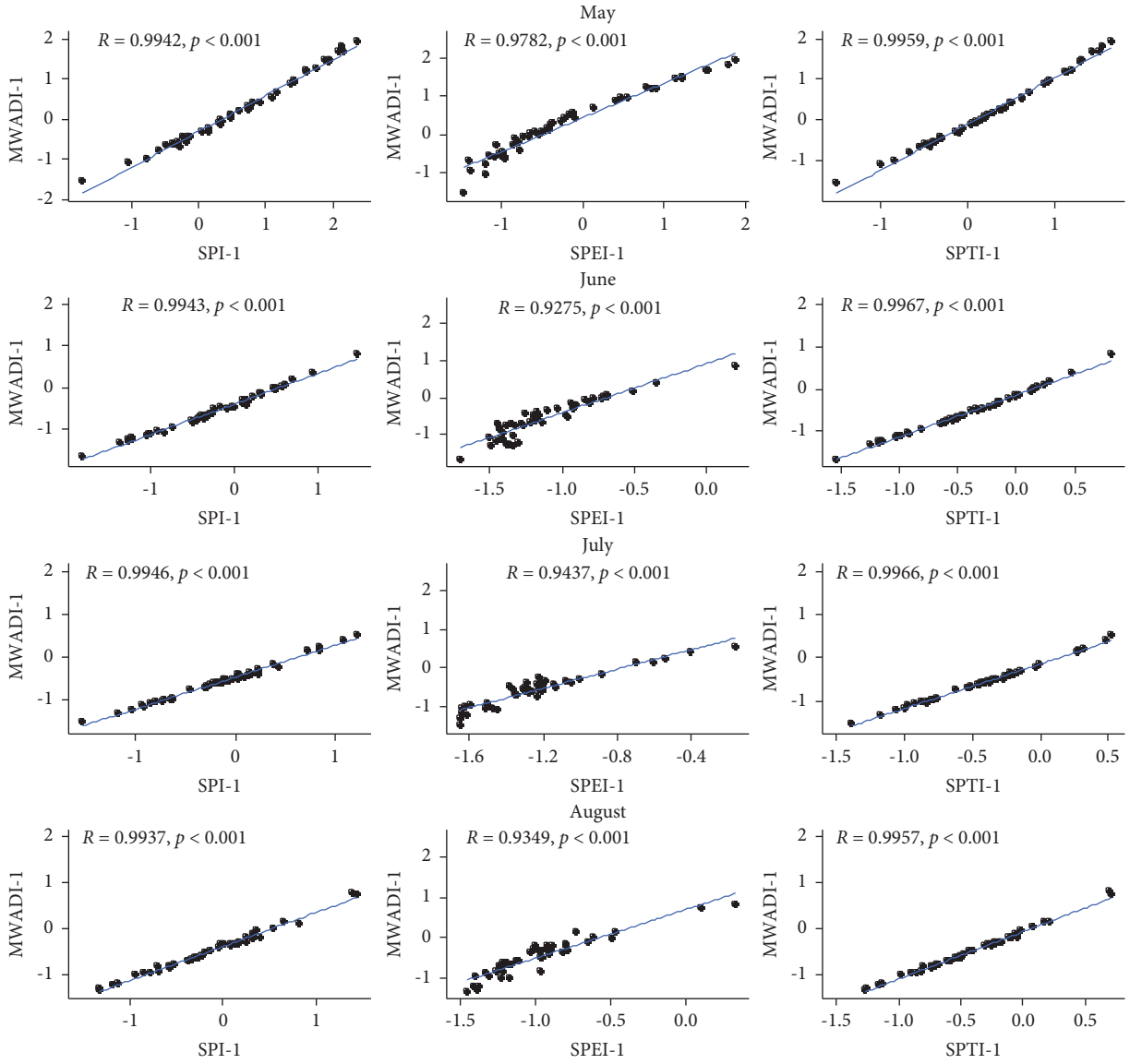

Figure 5: The scatter diagram and correlation coefficient R values between the seasonal MWADI and the SPI, the SPEI, and the SPTI (May–August) at Astore.

calculated through probabilistic structural and graphical algorithms reduces the uncertainties. The newly developed MWADI comprises various characteristics inherited by its multiple input multiscalar meteorological indicators. The MWADI can be easily implemented to display drought conditions across higher-order time scales. The temporal behavior of the MWADI at 6-month and 12-month time scales is presented in Figures 11 and 12 simultaneously. However, the proposed MWADI could be easily generalized by using more hydroclimatic and agricultural indicators as input variables for hydrological and agricultural drought assessment. Drought is a recurring threat to linked ecosystems, creating issues related to freshwater resources. The Bayesian network-based MWADI seems more promising for drought characterization to cope with such kinds of challenges.

The current study uses the SPI, the SPEI, and the SPTI as input indicators. These meteorological indicators are based on precipitation and mean monthly temperature, which defines the limits of the MWADI. The scope of the proposed index can be enhanced by using more input indicators based on soil moisture and remote sensing data. Similarly, different

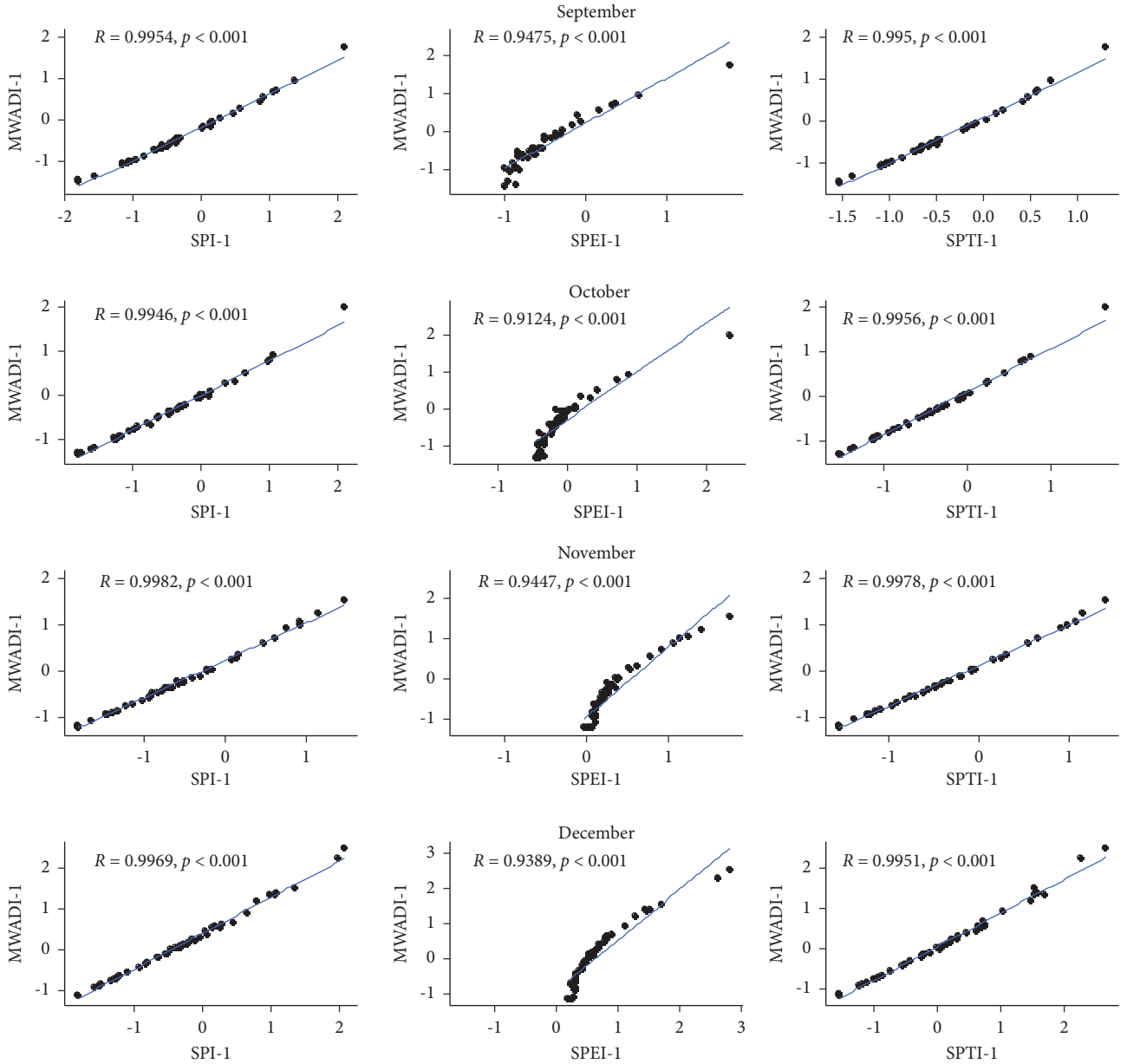

Figure 6: The scatter diagram and correlation coefficient R values between the seasonal MWADI and the SPI, the SPEI, and the SPTI (September–December) at Astore.

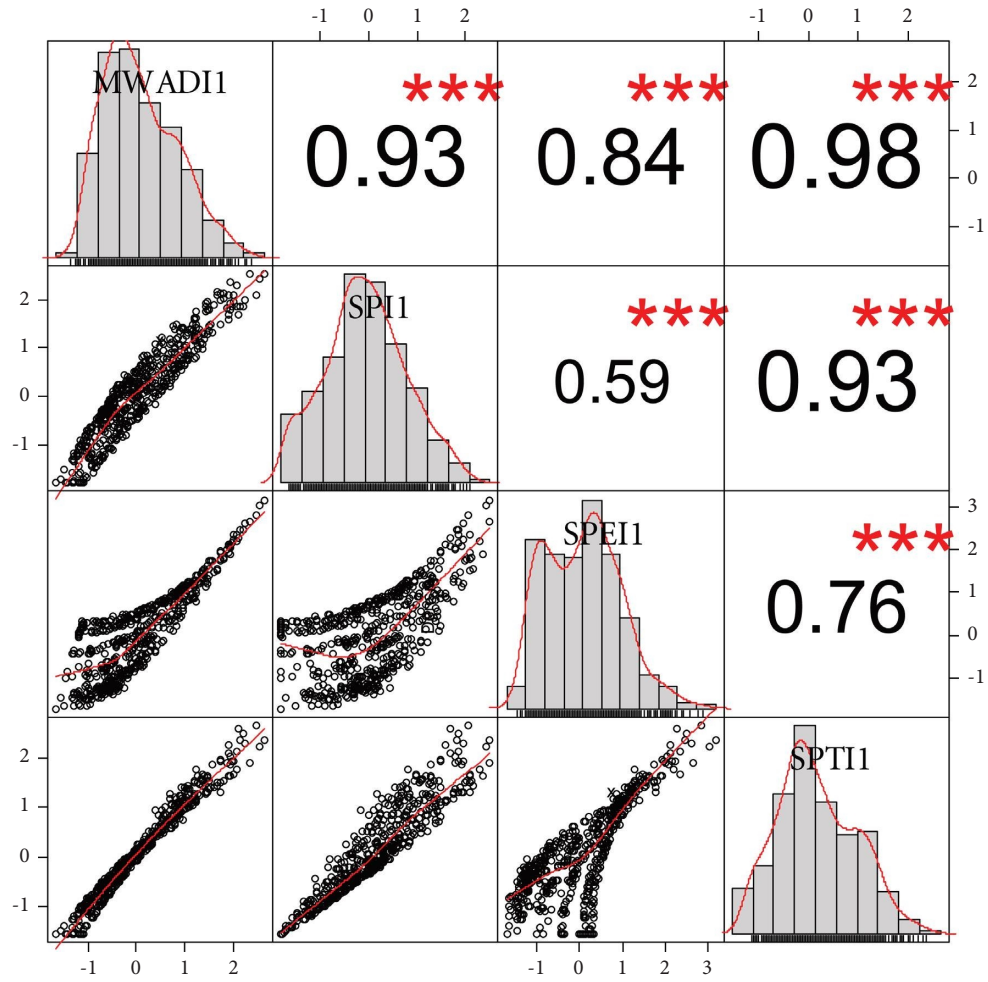

Figure 7: The correlation chart of the MWADI with other SDIs (the SPI, the SPEI, and the SPTI) at the Astore station.

Table 5: The correlation coefficient (r) for $MWADI_i$ with $SPI_i, SPEI_i$ and $SPTI_i$ at all meteorological stations for all seasons ($i = 1, 2, \cdots, 12$).

Seasons		Astore			Bunji			Chilas			Gilgit			Gupis			Skardu		
		SPI	SPEI	SPTI	SPI	SPEI	SPTI	SPI	SPEI	SPTI	SPI	SPEI	SPTI	SPI	SPEI	SPTI	SPI	SPEI	SPTI
Jan	MWADI	0.9971	0.9344	0.9887	0.9986	0.8824	0.9976	0.9986	0.8824	0.9976	0.9985	0.8329	0.9973	0.9984	0.9065	0.9976	0.9790	0.9236	0.9512
Feb		0.9976	0.9440	0.9908	0.9951	0.7957	0.9917	0.9951	0.7957	0.9916	0.9982	0.8384	0.9977	0.9940	0.7116	0.9967	0.9849	0.9383	0.9935
Mar		0.9954	0.9860	0.9928	0.9950	0.8875	0.9967	0.9950	0.8875	0.9967	0.9960	0.8571	0.9963	0.9958	0.8809	0.9968	0.9899	0.9590	0.9967
Apr		0.9934	0.9703	0.9927	0.9958	0.9276	0.9971	0.9958	0.9276	0.9971	0.9946	0.8806	0.9952	0.9951	0.8499	0.9937	0.9883	0.9565	0.9969
May		0.9942	0.9782	0.9959	0.9921	0.9202	0.9961	0.9921	0.9202	0.9961	0.9947	0.9107	0.9974	0.9911	0.9061	0.9947	0.9850	0.9596	0.9971
Jun		0.9943	0.9275	0.9967	0.9948	0.7784	0.9976	0.9948	0.7784	0.9976	0.9960	0.7629	0.9978	0.9937	0.8540	0.9954	0.9827	0.8107	0.9840
Jul		0.9946	0.9437	0.9966	0.9935	0.8725	0.9970	0.9935	0.8725	0.9970	0.9942	0.8262	0.9966	0.9927	0.7865	0.9951	0.9802	0.8382	0.9839
Aug		0.9937	0.9349	0.9957	0.9919	0.9055	0.9959	0.9919	0.9056	0.9959	0.9956	0.9070	0.9973	0.9939	0.8933	0.9950	0.9785	0.9027	0.9893
Sep		0.9954	0.9475	0.9950	0.9958	0.9022	0.9975	0.9958	0.9022	0.9975	0.9974	0.8699	0.9980	0.9935	0.8608	0.9945	0.9827	0.9391	0.9922
Oct		0.9946	0.9124	0.9956	0.9992	0.8855	0.9989	0.9992	0.8855	0.9989	0.9935	0.7857	0.9921	0.9944	0.8069	0.9939	0.9761	0.9112	0.9936
Nov		0.9982	0.9447	0.9978	0.9992	0.9005	0.9984	0.9992	0.9005	0.9984	0.9993	0.9029	0.9990	0.9987	0.8589	0.9986	0.9911	0.9607	0.9962
Dec		0.9969	0.9389	0.9951	0.9987	0.8538	0.9961	0.9987	0.8538	0.9961	0.9993	0.8889	0.9977	0.9986	0.8349	0.9964	0.9914	0.9456	0.9978

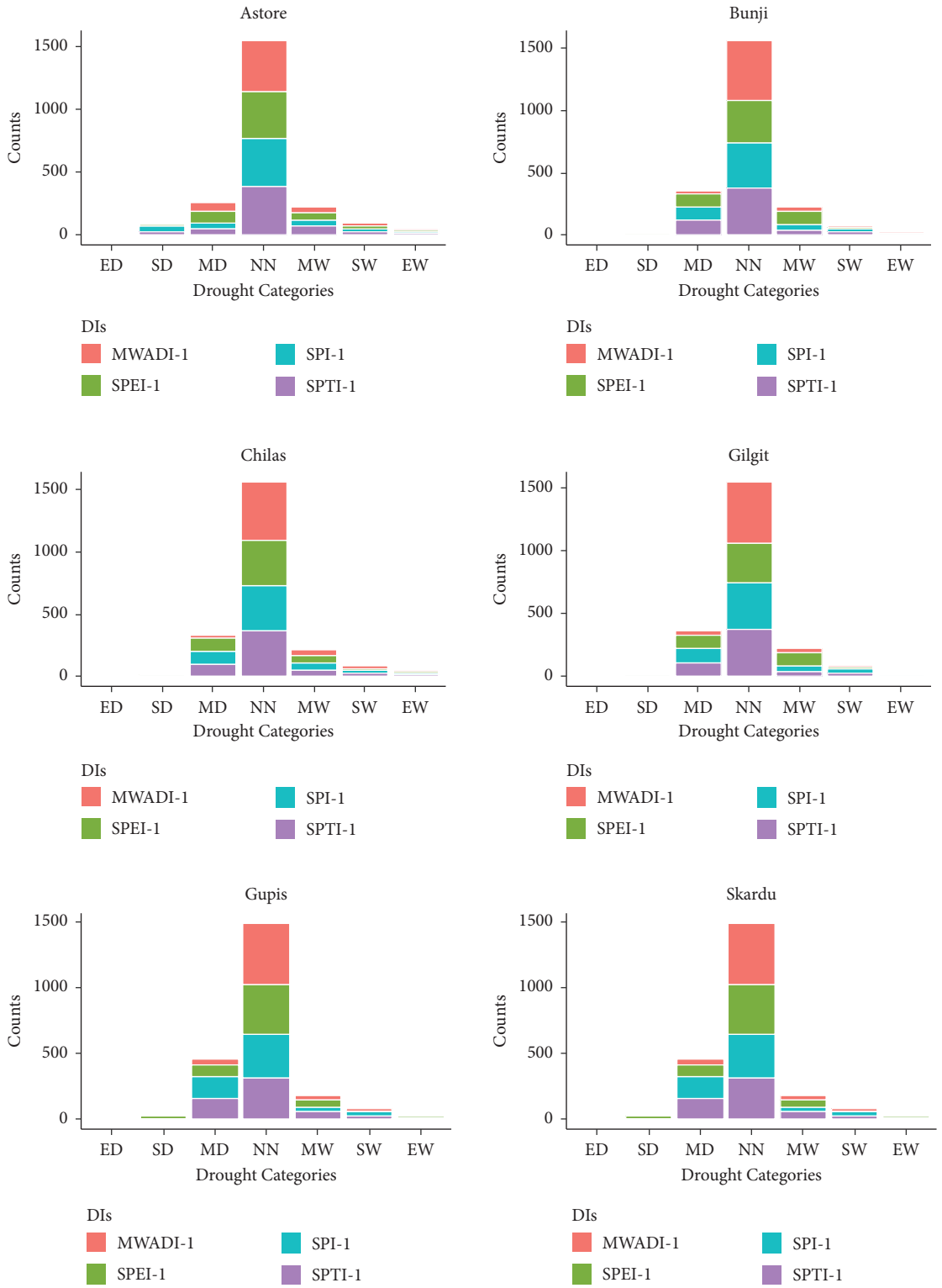

Figure 8: Count plots of MWADI-1, SPI-1, SPEI-1, and SPTI-1 at all stations.

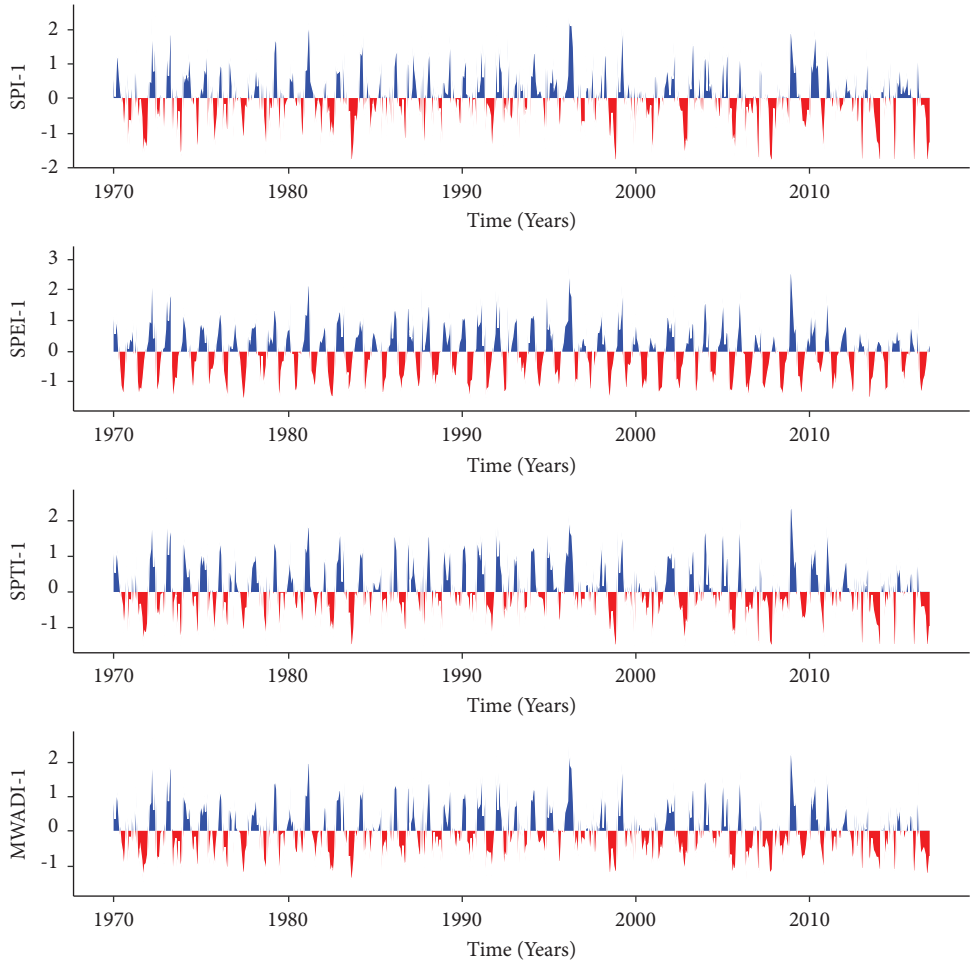

Figure 9: Temporal plots comparison of MWADI-1 with SPI-1, SPEI-1, and SPTI-1 at the Astore station.

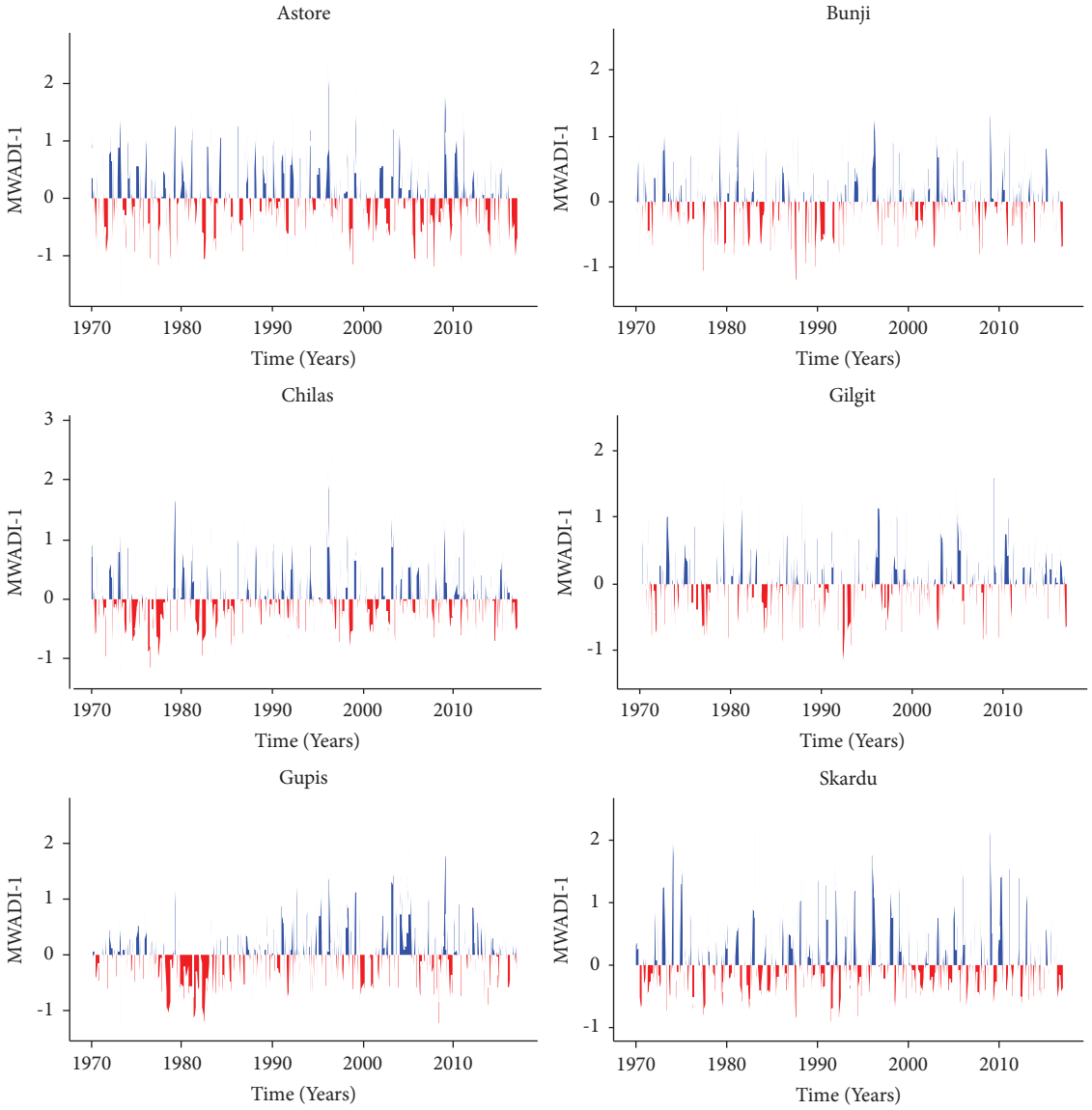

Figure 10: Temporal behavior of the MWADI at one-month time scale at all stations.

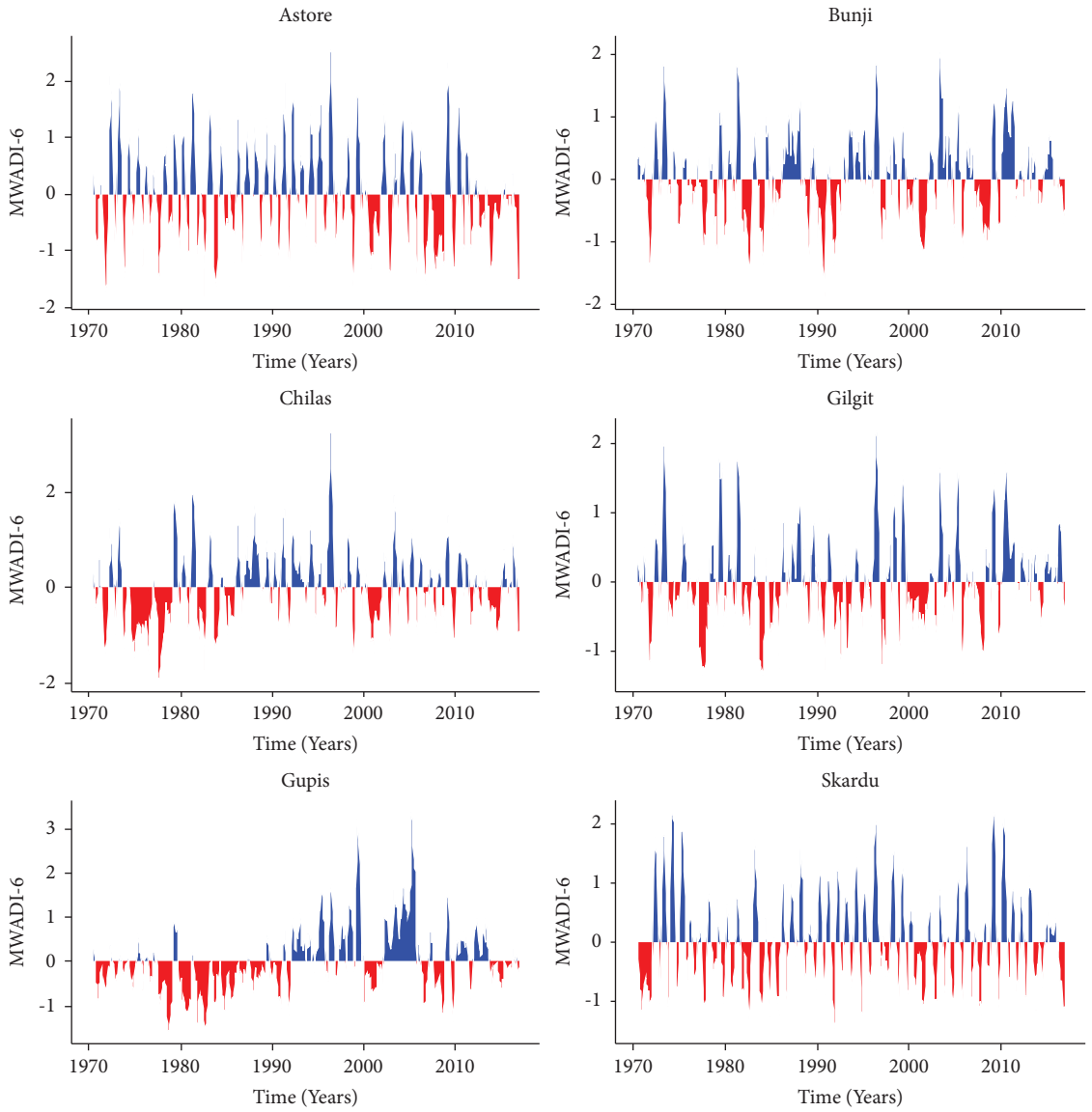

Figure 11: Temporal behavior of the MWADI at 6-month time scale at all stations.

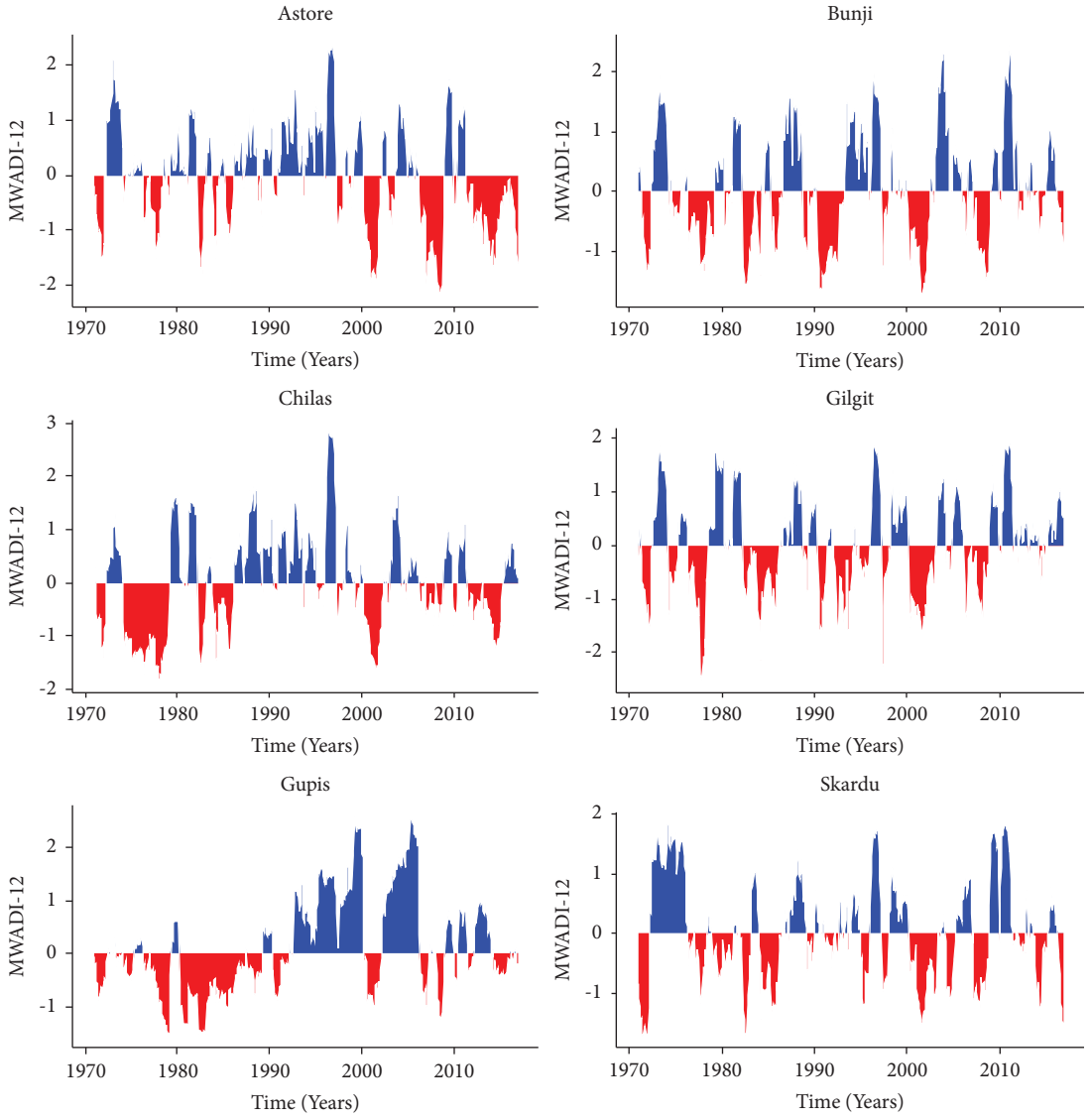

Figure 12: Temporal behavior of the MWADI at 12-month time scale at all stations.

drought indices could be combined using alternative stochastic and multivariate algorithms such as copulas and principal component analysis (PCA), which can be considered as future directions.

4. Conclusion

The use of a single drought index provides insufficient information related to the drought assessment. Due to the complex nature and widespread impacts of drought, applying a single index creates uncertainty for drought assessment and monitoring. Therefore, a new comprehensive procedure is required to minimize the uncertainty of drought evaluation. In this regard, the current study proposes a new framework, known as the multiscalar weighted amalgamated drought index (MWADI), that synthesizes information from multiple drought indices. The MWADI is mainly based on the ADPPs. Furthermore, these ADPPs are based on Bayesian networks (BNs)-based Monte Carlo Markov Chain (MCMC) simulations. The MWADI reconciles different drought indices and helps decision-makers to understand drought-related uncertainties. The drought severity and episodes estimated by the MWADI are compared and verified by temporal plots, count plots, and correlation charts. Moreover, the results of the MWADI are compared with the SPI, the SPEI, and the SPTI to estimate the drought events (impacts). The associated outcomes of the MWADI show a positive relationship with the SPI and the SPTI. Therefore, the MWADI can capture small changes in drought patterns and comprehensive drought risk assessment at the selected climatic zone.

Data Availability

The secondary data used to validate the proposed methods are available from the corresponding authors upon request.

Conflicts of Interest

The authors declare that they have no conflicts of interest.

Acknowledgments

Their authors extend their appreciation to the Deanship of Scientific Research at King Khalid University for funding this work through large groups Research project under grant number (RGP.2/23/44). And this study was supported via funding from Prince Sattam bin Abdulaziz University (project number (PSAU/2023/R/1444)).

References

[1] M. Agnoletti, A. Errico, A. Santoro, A. Dani, and F. Preti, "Terraced landscapes and hydrogeological risk. Effects of land abandonment in Cinque Terre (Italy) during severe rainfall events," *Sustainability*, vol. 11, no. 1, p. 235, 2019.

[2] A. AghaKouchak, A. Farahmand, F. S. Melton et al., "Remote sensing of drought: progress, challenges, and opportunities," *Reviews of Geophysics*, vol. 53, no. 2, pp. 452–480, 2015.

[3] D. A. Wilhite and M. H. Glantz, "Understanding: the drought phenomenon: the role of definitions," *Water International*, vol. 10, no. 3, pp. 111–120, 1985.

[4] R. R. Heim Jr, "A review of twentieth-century drought indices used in the United States," *Bulletin of the American Meteorological Society*, vol. 83, no. 8, pp. 1149–1166, 2002.

[5] A. Kaur and S. K. Sood, "Artificial intelligence-based model for drought prediction and forecasting," *The Computer Journal*, vol. 63, no. 11, pp. 1704–1712, 2020.

[6] N. Wanders and Y. Wada, "Human and climate impacts on the 21st century hydrological drought," *Journal of Hydrology*, vol. 526, pp. 208–220, 2015.

[7] S. H. Pour, A. K. A. Wahab, and S. Shahid, "Physical-empirical models for prediction of seasonal rainfall extremes of Peninsular Malaysia," *Atmospheric Research*, vol. 233, Article ID 104720, 2020.

[8] U. Büntgen, O. Urban, P. J. Krusic et al., "Recent European drought extremes beyond Common Era background variability," *Nature Geoscience*, vol. 14, no. 4, pp. 190–196, 2021.

[9] A. K. Mishra and V. P. Singh, "A review of drought concepts," *Journal of Hydrology*, vol. 391, no. 1-2, pp. 202–216, 2010.

[10] S. Mohamadi, S. S. Sammen, F. Panahi et al., "Zoning map for drought prediction using integrated machine learning models with a nomadic people optimization algorithm," *Natural Hazards*, vol. 104, no. 1, pp. 537–579, 2020.

[11] L. Gu, J. Chen, J. Yin et al., "Projected increases in magnitude and socioeconomic exposure of global droughts in 1.5 and 2 C warmer climates," *Hydrology and Earth System Sciences*, vol. 24, no. 1, pp. 451–472, 2020.

[12] P. Wang, W. Qiao, Y. Wang, S. Cao, and Y. Zhang, "Urban drought vulnerability assessment–A framework to integrate socioeconomic, physical, and policy index in a vulnerability contribution analysis," *Sustainable Cities and Society*, vol. 54, Article ID 102004, 2020.

[13] E. Gidey, O. Dikinya, R. Sebego, E. Segosebe, and A. Zenebe, "Analysis of the long-term agricultural drought onset, cessation, duration, frequency, severity and spatial extent using Vegetation Health Index (VHI) in Raya and its environs, Northern Ethiopia," *Environmental Systems Research*, vol. 7, no. 1, pp. 13–18, 2018.

[14] M. D. Svoboda and B. A. Fuchs, *Handbook of Drought Indicators and Indices*, World Meteorological Organization, Geneva, Switzerland, 2016.

[15] S. R. Chikabvumbwa, N. Salehnia, R. Manzanas, C. Abdelbaki, and A. Zerga, "Assessing the effect of spatial–temporal droughts on dominant crop yield changes in Central Malawi," *Environmental Monitoring and Assessment*, vol. 194, no. 2, pp. 63–16, 2022.

[16] A. Malik, Y. Tikhamarine, S. S. Sammen, S. I. Abba, and S. Shahid, "Prediction of meteorological drought by using hybrid support vector regression optimized with HHO versus PSO algorithms," *Environmental Science & Pollution Research*, vol. 28, no. 29, pp. 39139–39158, 2021.

[17] W. C. Palmer, *Meteorological Drought*, US Weather Bureau, Washington, DC, USA, 1965.

[18] B. A. Shafer and L. E. Dezman, "Development of surface water supply index (SWSI) to assess the severity of drought condition in snowpack runoff areas," in *Proceedings of the Western Snow Conference*, Reno, Nevada, January, 1982.

[19] T. B. McKee, N. J. Doesken, and J. Kleist, "The relationship of drought frequency and duration to time scales," in *Proceedings of the 8th Conference on Applied Climatology*, vol. 17, no. 22, pp. 179–183, American Meteorological Society, Boston, MA, USA, January, 1993.

[20] H. R. Byun and D. A. Wilhite, "Objective quantification of drought severity and duration," *Journal of Climate*, vol. 12, no. 9, pp. 2747–2756, 1999.

[21] S. M. Vicente-Serrano, S. Beguería, and J. I. López-Moreno, "A multiscalar drought index sensitive to global warming: the standardized precipitation evapotranspiration index," *Journal of Climate*, vol. 23, no. 7, pp. 1696–1718, 2010.

[22] Z. Ali, I. Hussain, M. Faisal et al., "A novel multiscalar drought index for monitoring drought: the standardized precipitation temperature index," *Water Resources Management*, vol. 31, no. 15, pp. 4957–4969, 2017.

[23] H. R. Byun and D. W. Kim, "Comparing the effective drought index and the standardized precipitation index," *Economics of drought and drought preparedness in a climate change context. López-Francos A.(comp.), López-Francos A.(collab.). Options Méditerranéennes. Sér. A. Séminaires Méditerranéens*, vol. 95, pp. 85–89, 2010.

[24] S. Kim, P. Parhi, H. Jun, and J. Lee, "Evaluation of drought severity with a Bayesian network analysis of multiple drought indices," *Journal of Water Resources Planning and Management*, vol. 144, no. 1, Article ID 05017016, 2018.

[25] M. Waseem, M. Ajmal, and T. W. Kim, "Development of a new composite drought index for multivariate drought assessment," *Journal of Hydrology*, vol. 527, pp. 30–37, 2015.

[26] L. Gu, J. Chen, J. Yin, C. Y. Xu, and H. Chen, "Drought hazard transferability from meteorological to hydrological propagation," *Journal of Hydrology*, vol. 585, Article ID 124761, 2020.

[27] T. Ji, G. Li, H. Yang, R. Liu, and T. He, "Comprehensive drought index as an indicator for use in drought monitoring integrating multi-source remote sensing data: a case study covering the Sichuan-Chongqing region," *International Journal of Remote Sensing*, vol. 39, no. 3, pp. 786–809, 2018.

[28] G. Qaiser, S. Tariq, S. Adnan, and M. Latif, "Evaluation of a composite drought index to identify seasonal drought and its associated atmospheric dynamics in Northern Punjab, Pakistan," *Journal of Arid Environments*, vol. 185, Article ID 104332, 2021.

[29] J. F. Brown, B. D. Wardlow, T. Tadesse, M. J. Hayes, and B. C. Reed, "The Vegetation Drought Response Index (VegDRI): a new integrated approach for monitoring drought stress in vegetation," *GIScience and Remote Sensing*, vol. 45, no. 1, pp. 16–46, 2008.

[30] K. C. Mo and D. P. Lettenmaier, "Objective drought classification using multiple land surface models," *Journal of Hydrometeorology*, vol. 15, no. 3, pp. 990–1010, 2014.

[31] H. Han, J. Bai, J. Yan, H. Yang, and G. Ma, "A combined drought monitoring index based on multi-sensor remote sensing data and machine learning," *Geocarto International*, vol. 36, no. 10, pp. 1161–1177, 2021.

[32] D. Heckerman, "Learning in graphical models, chapter A tutorial on learning with bayesian networks," *Adaptive Computation and Machine Learning*, pp. 301–354, MIT Press, Cambridge, MA, USA, 1999.

[33] P. Johnson, M. Ekstedt, and R. Lagerstrom, "Automatic probabilistic enterprise IT architecture modeling: a dynamic bayesian networks approach," in *Proceedings of the 2016 IEEE 20th International Enterprise Distributed Object Computing Workshop (EDOCW)*, pp. 1–8, IEEE, Vienna, Austria, September, 2016.

[34] L. Duan and Y. Xiong, "Big data analytics and business analytics," *Journal of Management Analytics*, vol. 2, no. 1, pp. 1–21, 2015.

[35] E. Pérez-Miñana, P. J. Krause, and J. Thornton, "Bayesian Networks for the management of greenhouse gas emissions in the British agricultural sector," *Environmental Modelling & Software*, vol. 35, pp. 132–148, 2012.

[36] M. Scutari, P. Howell, D. J. Balding, and I. Mackay, "Multiple quantitative trait analysis using Bayesian networks," *Genetics*, vol. 198, no. 1, pp. 129–137, 2014.

[37] L. Kaikkonen, T. Parviainen, M. Rahikainen, L. Uusitalo, and A. Lehikoinen, "Bayesian networks in environmental risk assessment: a review," *Integrated Environmental Assessment and Management*, vol. 17, no. 1, pp. 62–78, 2021.

[38] P. A. Aguilera, A. Fernández, R. Fernández, R. Rumí, and A. Salmerón, "Bayesian networks in environmental modelling," *Environmental Modelling & Software*, vol. 26, no. 12, pp. 1376–1388, 2011.

[39] A. Sperotto, J. L. Molina, S. Torresan, A. Critto, M. Pulido-Velazquez, and A. Marcomini, "A Bayesian Networks approach for the assessment of climate change impacts on nutrients loading," *Environmental Science & Policy*, vol. 100, pp. 21–36, 2019.

[40] Y. Wu, W. Xu, J. Feng, S. Palaiahnakote, and T. Lu, "Local and global Bayesian network based model for flood prediction," in *Proceedings of the 2018 24th International Conference on Pattern Recognition (ICPR)*, pp. 225–230, IEEE, Beijing, China, August, 2018.

[41] C. Vitolo, M. Scutari, M. Ghalaieny, A. Tucker, and A. Russell, "Modeling air pollution, climate, and health data using Bayesian Networks: a case study of the English regions," *Earth and Space Science*, vol. 5, no. 4, pp. 76–88, 2018.

[42] R. Ávila and D. Ballari, "A bayesian network approach to identity climate teleconnections within homogeneous precipitation regions in Ecuador," in *Proceedings of the Conference on Information Technologies and Communication of Ecuador*, pp. 21–35, Springer, Cham, Switzerland, November, 2019.

[43] S. C. Kao and R. S. Govindaraju, "A copula-based joint deficit index for droughts," *Journal of Hydrology*, vol. 380, no. 1-2, pp. 121–134, 2010.

[44] S. Chen, W. Zhong, S. Pan, Q. Xie, and T. W. Kim, "Comprehensive drought assessment using a modified composite drought index: a case study in Hubei Province, China," *Water*, vol. 12, no. 2, p. 462, 2020.

[45] D. Cui, W. Yuan, C. Chen, and R. Han, "Identification of colorectal cancer-associated macrophage biomarkers by integrated bioinformatic analysis," *International Journal of Clinical and Experimental Pathology*, vol. 14, pp. 1–8, 2021.

[46] W. Köppen, "Die Wärmezonen der Erde, nach der Dauer der heissen, gemässigten und kalten Zeit und nach der Wirkung der Wärme auf die organische Welt betrachtet," *Meteorologische Zeitschrift*, vol. 1, no. 21, pp. 5–226, 1884.

[47] J. Sheffield, E. F. Wood, N. Chaney et al., "A drought monitoring and forecasting system for sub-Sahara African water resources and food security," *Bulletin of the American Meteorological Society*, vol. 95, no. 6, pp. 861–882, 2014.

[48] N. B. Guttman, "Accepting the standardized precipitation index: a calculation algorithm 1," *JAWRA Journal of the American Water Resources Association*, vol. 35, no. 2, pp. 311–322, 1999.

[49] A. K. Mishra and V. R. Desai, "Drought forecasting using stochastic models," *Stochastic Environmental Research and Risk Assessment*, vol. 19, no. 5, pp. 326–339, 2005.

[50] J. H. Stagge, L. M. Tallaksen, L. Gudmundsson, A. F. Van Loon, and K. Stahl, "Candidate distributions for

climatological drought indices (SPI and SPEI)," *International Journal of Climatology*, vol. 35, no. 13, pp. 4027–4040, 2015.
[51] Z. Hao, V. P. Singh, and Y. Xia, "Seasonal drought prediction: advances, challenges, and future prospects," *Reviews of Geophysics*, vol. 56, no. 1, pp. 108–141, 2018.
[52] E. Dutra, L. Magnusson, F. Wetterhall et al., "The 2010–2011 drought in the Horn of Africa in ECMWF reanalysis and seasonal forecast products," *International Journal of Climatology*, vol. 33, no. 7, pp. 1720–1729, 2013.
[53] K. C. Mo and B. Lyon, "Global meteorological drought prediction using the North American multi-model ensemble," *Journal of Hydrometeorology*, vol. 16, no. 3, pp. 1409–1424, 2015.
[54] J. H. Yoon, K. Mo, and E. F. Wood, "Dynamic-model-based seasonal prediction of meteorological drought over the contiguous United States," *Journal of Hydrometeorology*, vol. 13, no. 2, pp. 463–482, 2012.
[55] B. O. Ayugi, W. Wen, and D. Chepkemoi, "Analysis of spatial and temporal patterns of rainfall variations over Kenya," *Studies*, vol. 6, no. 11, 2016.
[56] Y. G. Yang, J. F. Hu, H. L. Xiao, S. B. Zou, and Z. L. Yin, "Spatial and temporal variations of hydrological characteristic on the landscape zone scale in alpine cold region," *Huan jing ke xue= Huanjing kexue*, vol. 34, no. 10, pp. 3797–3803, 2013.
[57] J. Pearl, "Bayesian networks: a model cf self-activated memory for evidential reasoning," in *Proceedings of the 7th conference of the Cognitive Science Society*, pp. 15–17, University of California, Irvine, CA, USA, August, 1985.
[58] J. Pearl, *Probabilistic Reasoning in Intelligent Systems: Networks of Plausible Inference*, Elsevier, Amsterdam, Netherlands, 2014.
[59] N. Friedman and D. Koller, "Being Bayesian about network structure. A Bayesian approach to structure discovery in Bayesian networks," *Machine Learning*, vol. 50, no. 1, pp. 95–125, 2003.
[60] S. Dey and J. A. Stori, "A Bayesian network approach to root cause diagnosis of process variations," *International Journal of Machine Tools and Manufacture*, vol. 45, no. 1, pp. 75–91, 2005.
[61] I. Ben-Gal, *Encyclopedia of Statistics in Quality and Reliability*John Wiley & Sons, Hoboken, NJ, USA, 2007.
[62] D. Madigan, J. York, and D. Allard, "Bayesian graphical models for discrete data," *International Statistical Review/ Revue Internationale de Statistique*, vol. 63, no. 2, pp. 215–232, 1995.
[63] D. Madigan, A. E. Raftery, C. Volinsky, and J. Hoeting, "Bayesian model averaging," in *Proceedings of the AAAI Workshop on Integrating Multiple Learned Models*, pp. 77–83, Portland, OR, USA, August, 1996.
[64] P. Giudici and R. Castelo, "Improving Markov chain Monte Carlo model search for data mining," *Machine Learning*, vol. 50, no. 1/2, pp. 127–158, 2003.
[65] M. Grzegorczyk and D. Husmeier, "Improving the structure MCMC sampler for Bayesian networks by introducing a new edge reversal move," *Machine Learning*, vol. 71, no. 2-3, pp. 265–305, 2008.
[66] A. Raza, I. Hussain, Z. Ali et al., "A seasonally blended and regionally integrated drought index using Bayesian network theory," *Meteorological Applications*, vol. 28, no. 3, 2021.
[67] S. Madadgar and H. Moradkhani, "A Bayesian framework for probabilistic seasonal drought forecasting," *Journal of Hydrometeorology*, vol. 14, no. 6, pp. 1685–1705, 2013.
[68] M. Kavianpour, M. Seyedabadi, and S. Moazami, "Spatial and temporal analysis of drought based on a combined index using copula," *Environmental Earth Sciences*, vol. 77, no. 22, pp. 769–812, 2018.
[69] J. Won, J. Choi, O. Lee, and S. Kim, "Copula-based Joint Drought Index using SPI and EDDI and its application to climate change," *Science of the Total Environment*, vol. 744, Article ID 140701, 2020.
[70] Y. Li, Y. Gong, and C. Huang, "Construction of combined drought index based on bivariate joint distribution," *Alexandria Engineering Journal*, vol. 60, no. 3, pp. 2825–2833, 2021.
[71] J. Y. Shin, H. H. Kwon, J. H. Lee, and T. W. Kim, "Probabilistic long-term hydrological drought forecast using Bayesian networks and drought propagation," *Meteorological Applications*, vol. 27, no. 1, 2020.
[72] B. Zhang, X. Zhao, J. Jin, and P. Wu, "Development and evaluation of a physically based multiscalar drought index: the Standardized Moisture Anomaly Index," *Journal of Geophysical Research: Atmospheres*, vol. 120, no. 22, pp. 11,575–11,588, 2015.
[73] X. Li, B. He, X. Quan, Z. Liao, and X. Bai, "Use of the standardized precipitation evapotranspiration index (SPEI) to characterize the drying trend in southwest China from 1982–2012," *Remote Sensing*, vol. 7, no. 8, pp. 10917–10937, 2015.

Hindawi
Complexity
Volume 2023, Article ID 4577581, 22 pages
https://doi.org/10.1155/2023/4577581

Review Article

A Systematic Literature Review on Robust Swarm Intelligence Algorithms in Search-Based Software Engineering

Alam Zeb,[1] **Fakhrud Din**,[1] **Muhammad Fayaz**,[2] **Gulzar Mehmood**,[3] **and Kamal Z. Zamli**[4]

[1]*Faculty of Information Technology, Department of Computer Science & IT, University of Malakand, Lower Dir 18800, KPK, Pakistan*
[2]*Department of Computer Science, University of Central Asia, Naryn, Kyrgyzstan*
[3]*Department of Computer Science, IQRA National University, Swat Campus 19220, Peshawar, Pakistan*
[4]*Faculty of Science and Technology, Universitas Airlangga, C Campus JI. Dr. H. Soekamo, Mulyorejo, Surabaya 60115, Indonesia*

Correspondence should be addressed to Muhammad Fayaz; muhammad.fayaz@ucentralasia.org

Received 1 May 2022; Revised 4 September 2022; Accepted 7 October 2022; Published 23 February 2023

Academic Editor: Haitham Abdulmohsin Afan

Swarm intelligence algorithms are metaheuristics inspired by the collective behavior of species such as birds, fish, bees, and ants. They are used in many optimization problems due to their simplicity, flexibility, and scalability. These algorithms get the desired convergence during the search by balancing the exploration and exploitation processes. These metaheuristics have applications in various domains such as global optimization, bioinformatics, power engineering, networking, machine learning, image processing, and environmental applications. This paper presents a systematic literature review (SLR) on applications of four swarm intelligence algorithms i.e., grey wolf optimization (GWO), whale optimization algorithms (WOA), Harris hawks optimizer (HHO), and moth-flame optimizer (MFO) in the field of software engineering. It presents an in-depth study of these metaheuristics' adoption in the field of software engineering. This SLR is mainly comprised of three phases such as planning, conducting, and reporting. This study covers all related studies published from 2014 up to 2022. The study shows that applications of the selected metaheuristics have been utilized in various fields of software engineering especially software testing, software defect prediction, and software reliability. The study also points out some of the areas where applications of these swarm intelligence algorithms can be utilized. This study may act as a guideline for researchers in improving the current state-of-the-art on generally adopting these metaheuristics in software engineering.

1. Introduction

The goal of optimization is to find a solution that either minimizes or maximizes a criterion known as the objective function, fitness function, or cost function. A solution known as a feasible solution or admissible solution is required to solve the objective function under given constraints [1]. An optimization algorithm works iteratively until a specified number of iterations or when a specific amount of time is reached to enhance a given criterion [2].

Many real-life optimization problems in engineering, science, and business are complicated and, thus, no exact solutions can be provided in a fair amount of time. To tackle such problems, approximate algorithms are used. Approximate algorithms are further divided into specific heuristics and metaheuristics. Specific heuristics being problem-dependent solve specific problems, whereas metaheuristics are general-purpose strategies used to solve a huge number of optimization problems [3].

Generally, metaheuristics solve instances of hard problems through exploration of the search space where the solution is supposed to be found. There are mainly three objectives of metaheuristics: (1) providing a fast solution to a given problem; (2) tackling large problems; and (3) obtaining robust algorithms. Furthermore, metaheuristics are flexible and simple to design as well as implement [3].

In Search-Based Software Engineering (SBSE), metaheuristic search techniques are applied to optimization problems in software engineering. The main objective of SBSE is to move problems related to software engineering to machine-based search instead of human-based search. This is accomplished by using various techniques of metaheuristics as well as operations research [4]. Near-optimal solutions are acceptable in various engineering disciplines, and software engineering is no exception. It is due to this fact that metaheuristic techniques are applicable to solving software engineering problems. Thus, difficult problems can be solved using such search-based techniques with acceptable solutions where perfect solutions are infeasible or impossible [5].

Various swarm intelligence algorithms such as GWO, WOA, HHO, and MFO algorithms have been applied in numerous domains such as machine learning, networks, engineering optimization, environmental modeling, image processing, power dispatch problems, and medical and bioinformatics [6–9]. Some of the recent nature-inspired metaheuristic algorithms include monarch butterfly optimization (MBO) proposed by Wang et al. [10], slime mould algorithm (SMA) proposed by Li et al. [11], moth search (MS) algorithm proposed by Wang [12], marine predators algorithm (MPA) presented by Faramarzi et al. [13], hunger games search (HGS) presented by Yang et al. [14], and colony predation algorithm (CPA) developed by Tu et al. [15].

This paper presents a systematic literature review on applications of four swarm intelligence algorithms, namely, GWO, WOA, HHO, and MFO, in the domain of software engineering. Our motivation comes from the fact that, as per our knowledge, there is no such systematic review available. Also, a review study paper helps researchers with aggregated knowledge on a given topic in one place. Table 1 shows various fields in software engineering that utilize these swarm intelligence algorithms. It also points out various areas in software engineering where these algorithms could be utilized. The main contributions of this SLR are as follows:

(i) The SLR presents applications of four swarm-based metaheuristics i.e., GWO, WOA, HHO, and MFO in the field of software engineering.

(ii) The SLR analyzes 46 relevant studies from 2014 to 2022 according to several research questions.

(iii) This study points out new areas in software engineering where the selected metaheuristics could be utilized thus it identifies further research opportunities in the field.

Many swarm intelligence algorithms are available and are gaining prominence as they offer reasonable solutions to complex problems. These algorithms are mainly inspired by biological systems such as animal-based and insect-based. We have chosen four swarm intelligence algorithms, one from each group, i. e., GWO from animal-based, MFO from insect-based, HHO from bird-based, and WOA from fish-based groups. Also, the selected algorithms are relatively new, therefore, working on these will provide the current state-of-the-art. Moreover, these algorithms are popular among swarm intelligence algorithms, which is obvious from the number of their applications in various fields, including software engineering. Based on the above scenario, we have chosen these four algorithms for our SLR.

The Grey Wolf Optimizer is a metaheuristic algorithm that is inspired by grey wolves. It works by mimicking grey wolves in nature, such as their leadership hierarchy and hunting mechanism. Similarly, WOA is a nature-inspired metaheuristic optimization algorithm that mimics the social behavior of humpback whales. The bubble-net hunting strategy is the main inspiration for WOA. The third metaheuristic algorithm included in our study is HHO, which is a nature-inspired and population-based swarm intelligence algorithm. It is inspired by the chasing style and cooperative behavior of Harris' hawks in nature, known as surprise pounce. The fourth and last swarm intelligence algorithm included in our study is also a nature-inspired optimization algorithm called the MFO algorithm. Transverse orientation, the navigation method of moths in nature, is the main inspiration for this algorithm.

Recent applications of the GWO include Al-Momani et al. [16] used GWO to optimize the fixed parameters of the supercritical power plant (SCPP). Results were compared with GA which confirmed the superiority of GWO over GA for parameter identification of the SCPP model. Hao and Sobhani [17] utilized chaotic GWO to identify important functional parameters of solid oxide fuel cells. The adaptive GWO was applied to a 5 kW dynamic tubular stack. The result showed significant performance compared with existing well-known methods for optimization. Bardhan et al. [18] proposed a hybrid approach based on GWO and an artificial neural network (ANN) to find the load-carrying capability of concrete-filled steel tube (CFST) columns. The author also employed an enhanced version of GWO (EGWO) and created two hybrid models, ANN-AGWO and ANN-EGWO, to estimate CFST columns' load-carrying capacity. According to the results, the ANN-AGWO outperformed other methods. Dhar et al. [19] proposed a modified GWO for parameter tuning of the model of a direct deposition process of austenitic steel that utilizes the technique of extreme gradient boost. Results showed GWO's performance in tuning the parameters of the eth model was satisfactory. Yin and Sun [20] introduced distributed multiobjective GWO (DMOGWO) to solve the large-scale multiarea interconnected power systems (LMIPSs) problems. Results confirmed the better performance of the proposed method in solving LMIPS problems.

It is worth noting that these optimization methods do not guarantee the best solution, and since these are mostly used in NP-hard problems, they offer near-optimal solutions. Moreover, these metaheuristics come with their shortcomings, such as trapping in local optima. To avoid being trapped in local optima, various solutions have been proposed by offering variants of these metaheuristics, such as Hu et al. [21] tried to overcome GWO's shortcomings by developing a variant of GWO. The proposed GWOCMA-LOL uses CMAES, levy flight, and orthogonal learning strategies. According to the results, the proposed algorithm

Table 1: Swarm intelligence algorithms' areas of applications in software engineering.

Algorithms	Fields covered by the algorithm	Gaps to be covered by these algorithms
GWO	(i) Software testing (ii) Software bug/defect prediction (iii) System reliability (iv) Software requirements analysis (v) Agile software development (vi) Software effort estimation (vii) Software project scheduling problem (viii) Software usability (ix) Next release problem (x) Project cost estimation (xi) Software release planning (xii) Software risk management	(i) Software vulnerability prediction (ii) Software organization (iii) Software re-modularization (iv) Maintenance/evolution system integration (v) Software module clustering (vi) Finding good designs (vii) Reverse and re-engineering through transformation and re-factoring (viii) User-based fitness evaluation for aesthetic aspects of software engineering (ix) Avionics software (x) Automotive software (xi) Software configuration (xii) Software component allocation (xiii) Structural testing (xiv) Mutation testing (xv) Worst-and-best case execution time testing (xvi) Issue of boundary value analysis (xvii) Partition testing
WOA	(i) Software testing (ii) Software bug/defect prediction (iii) System reliability (iv) Software requirements analysis (v) Software effort estimation (vi) Software project scheduling problem (vii) Next release problem	
HHO	(i) Software testing (ii) Software bug/defect prediction	
MFO	(i) Software testing (ii) Software bug/defect prediction (iii) Software usability	

outperformed the original algorithm by resolving its shortcomings.

This paper is organized as follows: An overview of GWO is presented in the *Overview* section. The adopted research methodology is discussed in the *Methodology* section. Results obtained from the review study are presented in the *Results* section. Section *Discussion* summarizes the SLR and provides insights obtained from the study. Section *Threats to Validity* outlines the potential threats to validity. Finally, the *Conclusion* section concludes the literature review work.

2. Overview

This section presents an overview of the swarm intelligence algorithms included in our study. It explores sources of inspiration as well as mathematical models of these algorithms.

2.1. Grey Wolf Optimizer (GWO). The Grey Wolf Optimizer is an instance of a swarm intelligence technique that is inspired by the social hierarchy as well as the hunting behavior of the grey wolf (*Canis lupus*) of the Canidae family. They stay at the top of the food chain, being apex predators. They usually live in packs with an average size of 5 to 12 wolves. The group dictates a strict social dominant hierarchy [6, 22]. A multi-objective variant of the same algorithm, the Muli-Objective Grey Wolf Optimizer (MOGWO), is proposed by Mirjalili [23] for optimization of problems having more than one objective.

At the top of the hierarchy is the alpha, which leads the group. Beta, the subordinate wolves are next to alpha in the social hierarchy. They help the alphas with making decisions as well as other activities. In case the alpha becomes too old or passes away, the beta becomes the alpha. At the bottom of the hierarchy are the omega wolves, which are dominated by other dominant wolves. The fourth type in the hierarchy is delta, which has dominance over the omega but submits to alpha and beta. Delta wolves include caretakers, hunters, sentinels, scouts, and elders [22].

Like their social hierarchy, grey wolves also exhibit interesting social behavior during group hunting. They follow a set of efficient steps during group hunting, such as chasing, encircling, harassing, and attacking the prey. This behavior enables them to control big prey [6, 22]. Figure 1 shows the flowchart of GWO.

2.2. Mathematical Model of GWO. This section presents the mathematical models of the social behavior of grey wolves such as encircling and hunting the prey [22].

2.2.1. Encircling the Prey. The encircling behavior of grey wolves is depicted mathematically by the following equations:

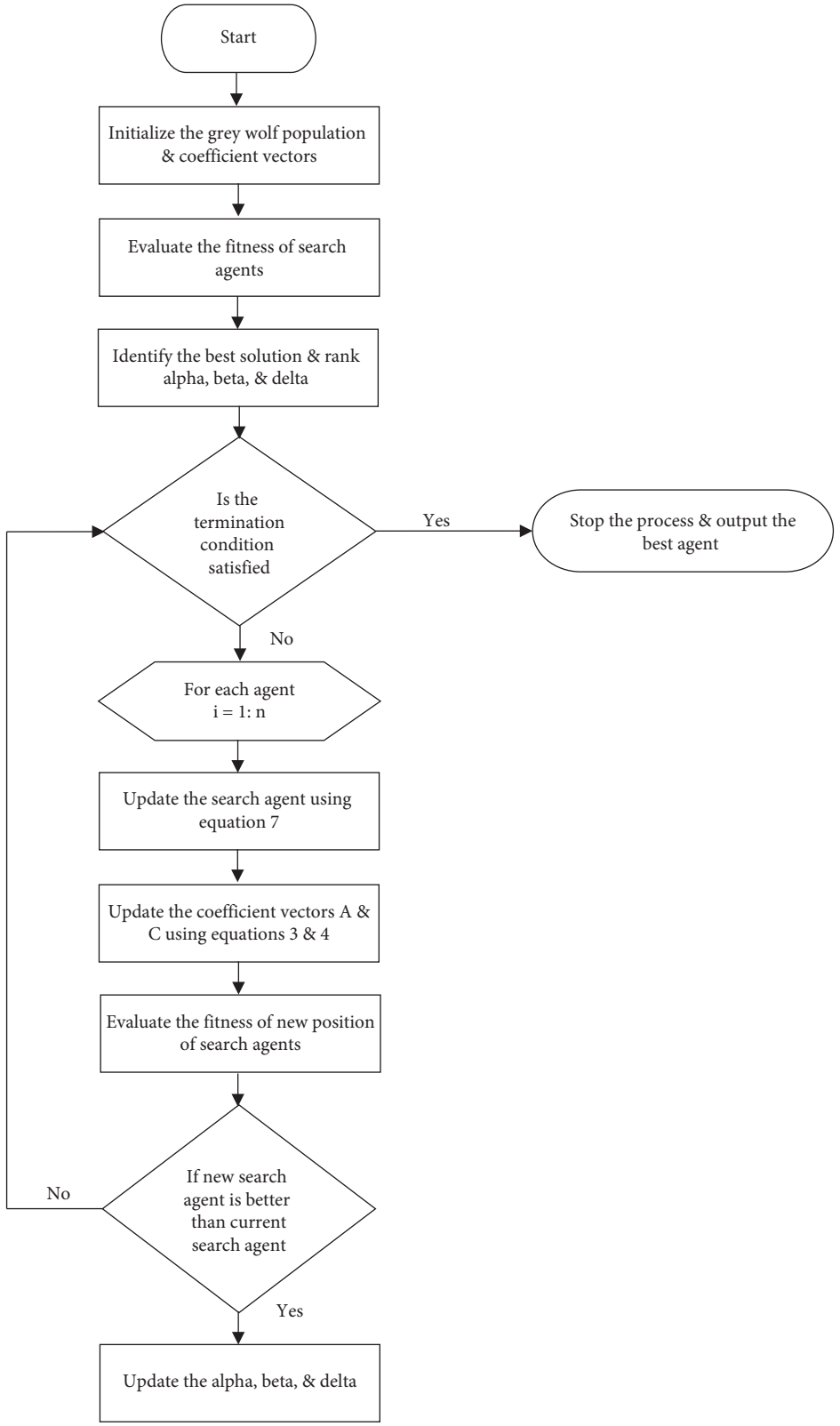

Figure 1: Flowchart of Grey Wolf Optimization (GWO) algorithm.

$$\vec{D} = \left|\vec{C}.\vec{X_p}(t) - \vec{X}(t)\right|, \quad (1)$$

$$\vec{X}(t+1) = \vec{X_p} - \vec{A}.\vec{D}, \quad (2)$$

where the current iteration is shown by t, grey wolf's position vector is indicated by $\vec{X}$ and position vector of prey is indicated by $\vec{X_p}$. $\vec{A}$ and $\vec{C}$ represent the coefficient vectors calculated as follows:

$$\vec{A} = 2\vec{a}.\vec{r_1} - \vec{a}, \quad (3)$$

$$\vec{C} = 2.\vec{r_2}, \quad (4)$$

where r_1 and r_2 are random vectors in the range [0, 1] while components of $\vec{a}$ are decreased from 2 to 0 linearly as iterations proceed.

2.2.2. Hunting. In a given abstract search space, the best candidate solution is supposed to be alpha whereas beta, and delta are supposed to know the prey's potential location i. e., the best solution. The top three solutions obtained are saved. Other search agents such as omegas update their positions according to the position of the best search agents. This concept is depicted mathematically by the following equations:

$$\begin{aligned}&\vec{D_\alpha} = \left|\vec{C_1}.\vec{X_\alpha} - \vec{X}\right|, \vec{D_\beta} = \left|\vec{C_2}.\vec{X_\beta} - \vec{X}\right|, \vec{D_\delta} = \left|\vec{C_3}.\vec{X_\delta} - \vec{X}\right|,\\ &\vec{X_1} = \vec{X_\alpha} - \vec{A_1}.\left(\vec{D_\alpha}\right), \vec{X_2} = \vec{X_\beta} - \vec{A_2}.\left(\vec{D_\beta}\right), \vec{X_3} = \vec{X_\delta} - \vec{A_3}.\left(\vec{D_\delta}\right),\end{aligned} \quad (5)$$

where $\vec{D_\alpha}, \vec{D_\beta}$ and $\vec{D_\delta}$ are vectors showing distance between prey's location $\vec{X}$ and alpha, beta, and delta, respectively.

$\vec{X_\alpha}, \vec{X_\beta}$ and $\vec{X_\delta}$represent the position vectors of alpha, beta and delta respectively. $\vec{X_1}, \vec{X_2}$ and $\vec{X_3}$ represent the next location of alpha, beta, and delta, respectively. Whereas, $\vec{C_1}, \vec{C_2}, \vec{C_3}, \vec{A_1}, \vec{A_2}$ and $\vec{A_3}$ are coefficient vectors defined by equations (3) and (4)

$$\vec{X}(t+1) = \frac{\vec{X_1} + \vec{X_2} + \vec{X_3}}{3}, \quad (6)$$

where $\vec{X}(t+1)$ represent the next location of the prey i.e., the average of the best three solutions so far to be obliged by other search agents such as omega for updating their position.

2.3. Whale Optimization Algorithm (WOA). WOA is a nature-inspired metaheuristic optimization algorithm proposed by Mirjalili and Lewis [24] in 2016 which mimics the social behavior of humpback whales. The bubble-net hunting strategy is the main inspiration for WOA. The Whale optimization algorithm is a nature-inspired metaheuristic optimization algorithm proposed by Mirjalili and Lewis [24] in 2016 which mimics the social behavior of humpback whales. Whales feel emotions and are considered intelligent animals. Humpback whales (Megaptera novaeangliae) are among the biggest baleen whales. An adult humpback whale almost grows to the size of a school bus.

The humpback whales follow an interesting special hunting method known as the bubble-net feeding method. Small fish and schools of krill are the preferred prey of humpback whales. They forage by creating distinctive bubbles along a "9"-shaped or circle. Their two maneuvers related to bubbles are named "upward-spirals" and "double-loops". In "upward-spirals" the humpback whales take dives and create bubbles in a spiral shape around the prey, whereas "double-loops" consists of three stages: coral loop, lobtail, and capture loop [24].

2.4. Mathematical Model of WOA. This section presents the mathematical model of the unique foraging behavior of humpback whales such as searching for prey, encircling prey, and spiral bubble-net feeding maneuver [24].

2.4.1. Encircling the Prey. The following equations mathematically depict the encircling behavior of humpback whales:

$$\begin{aligned}\vec{D} &= \left|\vec{C}.\vec{X^*}(t) - \vec{X}(t)\right|\\ \vec{X}(t+1) &= \vec{X^*}(t) - \vec{A}.\vec{D},\end{aligned} \quad (7)$$

where the current iteration is shown by t, $\vec{X}$ represents the position vector, and X^* represents the the position vector of the optimal solution.

The following equations calculate vectors $\vec{A}$ and $\vec{C}$ as

$$\vec{A} = 2\vec{a}.\vec{r} - \vec{a}, \quad (8)$$

$$\vec{C} = 2.\vec{r}, \quad (9)$$

where $\vec{r}$ is a random vectors in the range [0, 1] while $\vec{a}$ decreases from 2 to 0 linearly as iterations proceed.

2.4.2. Bubble-Net Attacking Method. The bubble-net behavior represents the exploitation phase. It is modeled mathematically by using two approaches as follows:

(1) *Shrinking Encircling Mechanism.* To achieve this behavior, the value of $\vec{a}$ in equation (8) is decreased which further decreases the fluctuation range of $\vec{A}$.

(2) *Spiral Updating Position.* In this approach, the distance between the whale and prey is calculated first. Positions of

whale and prey are represented by (X, Y) and $,(X^*, Y^*)$, respectively. Then the helix-shaped movement of humpback whales is mimicked using the spiral equation as follows:

$$\overrightarrow{X}(t+1) = \overrightarrow{D'}.e^{bl}.\cos(2\pi l) + \overrightarrow{X^*}(t), \tag{10}$$

where $\overrightarrow{D'} = |\overrightarrow{X^*}(t) - \overrightarrow{X}(t)|$ shows the i^{th} whale's distance to the prey i.e., the optimal solution so far, b defines the logarithmic spiral's shape, l indicates a random number in the range $[-1, 1]$, whereas "." indicates element-wise multiplication.

The following equation models the foraging behavior of humpback whales by assuming a 50% probability each for the shrinking encircling mechanism and the spiral model to update the whales' position during the optimization process:

$$\overrightarrow{X}(t+1) = \begin{cases} \overrightarrow{X^*}(t) - \overrightarrow{A}.\overrightarrow{D}, & \text{if } p < 0.5, \\ \overrightarrow{D'}.e^{bl}.\cos(2\pi l) + \overrightarrow{X^*}(t), & \text{if } p \geq 0.5, \end{cases} \tag{11}$$

where p indicates a random number in the range [0, 1].

2.4.3. Search for Prey. The humpback whales also search randomly for prey. This random search represents the exploration phase. Unlike the exploitation phase, the position of a search agent in the exploration phase is updated randomly as opposed to the optimal search agent found so far. This mechanism as well as $|\overrightarrow{A}| > 1$ enables the WOA algorithm for a global search. The following equation presents the mathematical model:

$$\begin{aligned} \overrightarrow{D} &= \left|\overrightarrow{C}.\overrightarrow{X_{\text{rand}}} - \overrightarrow{X}\right|, \\ \overrightarrow{X}(t+1) &= \left|\overrightarrow{X_{\text{rand}}} - \overrightarrow{A}.\overrightarrow{D}\right|, \end{aligned} \tag{12}$$

where $\overrightarrow{X_{\text{rand}}}$ represents a random position vector i.e., a random whale out of the current population.

2.5. Harris Hawks Optimizer (HHO). The next metaheuristic algorithm included in our study is HHO, which is a nature-inspired and population-based swarm intelligence algorithm proposed by Heidari et al. [25] in 2019. It is inspired by the chasing style and cooperative behavior of Harris' hawks (Parabuteo unicinctus) in nature, known as surprise pounce. The Harris' hawks are considered intelligent birds and are found in the southern half of Arizona, USA.

To capture prey, Harris' hawks use "surprise pounce" as the main strategy. This tactic is also called the "seven kills" strategy. Using this strategy, the detected rabbit is attacked from different directions, and the hawks concurrently converge on the escaping rabbit. The "seven kills" approach may take seconds or several minutes to capture prey depending on its escaping capabilities. Harris' hawks demonstrate various chasing styles based on the escaping patterns of prey as well as the circumstances [25].

2.6. Mathematical Model of HHO. This section mathematically models the exploratory as well as exploitative phases of the HHO algorithm inspired by various hunting strategies of Harris' hawks [25].

2.6.1. Exploration Phase. The following equation models the exploration mechanism of HHO. The perch behavior in HHO is based on two strategies (1) perch based on the positions of other members, which is modeled in equation (13) [ref] for the condition of $q < 0.5$, or (2) random perch on tall trees, which is modeled in Equation (13) for the condition of $q \geq 0.5$.

$$X(t+1) = \begin{cases} X_{\text{rand}}(t) - r_1\left|X_{\text{rand}}(t) - 2r_2X(t)\right|, & \text{if } q \geq 0.5, \\ \left(X_{\text{rabbit}}(t) - X_m(t)\right) - r_3\left(LB + r_4(UB - LB)\right), & \text{if } q < 0.5, \end{cases} \tag{13}$$

where $X(t+1)$ represents hawks' position vector in the next iteration t, $X_{\text{rabbit}}(t)$ represents rabbit's position, $X(t)$ represents hawks' current position vector, r_1, r_2, r_3, r_4, and q represent random numbers inside in the range (0,1), LB and UB represent variables' upper and lower bounds, $X_{\text{rand}}(t)$ shows a hawk randomly selected out of the current population, and average position of hawks' current population is represented by X_m which is defined by equation 14:

$$X_m(t) = \frac{1}{N}\sum_{i=1}^{N} X_i(t), \tag{14}$$

where $X_i(t)$ represents each hawks' location in iteration t and the total number of hawks is represented by N.

During the escape, the prey's energy decreases considerably which can be modeled mathematically as

$$E = 2E_0\left(1 - \frac{t}{T}\right), \tag{15}$$

where E shows the prey's escaping energy, T represents the maximum number of allowed iterations, and E_0 represents the initial energy.

2.6.2. Exploitation Phase. Harris' hawks attack by performing a surprise pounce on the prey. However, prey often succeeds in escaping, which gives rise to various chasing

styles. Based on the chasing strategies as well as escaping behaviors, HHO has four strategies to model the attacking stage. Suppose r represents the prey's escape chance, $(r < 0.5)$ means successful escape while $(r \geq 0.5)$ shows unsuccessful escape before surprise pounce. A hard or soft besiege is performed by the hawks to catch the prey. Here, the parameter E is utilized to decide between soft and hard besiege processes. The soft besiege is performed when $|E| \geq 0.5$ and when $|E| \leq 0.5$, the hard besiege takes place.

(1) *Soft Besiege*. The behavior is performed when $r \geq 0.5$ and $|E| \geq 0.5$ as modeled by the following rules:

$$\begin{aligned} X(t+1) &= \Delta X(t) - E|JX_{\text{rabbit}}(t) - X(t)|, \\ \Delta X(t) &= X_{\text{rabbit}}(t) - X(t), \end{aligned} \tag{16}$$

where $\Delta X(t)$*represents* the difference between the rabbit's position vector and the current location in iteration t, r_5 represents a random number in the range (0,1), and $J = 2(1 - r_5)$ randomly presents the rabbit's jumping strength during the escaping procedure.

(2) *Hard Besiege*. When $r \geq 0.5$ and $|E| < 0.5$, the prey has low escaping energy. In this scenario, the following equation updates the current positions:

$$X(t+1) = X_{\text{rabbit}}(t) - E|\Delta X(t)|. \tag{17}$$

(3) *Soft Besiege with Progressive Rapid Dives*. When $|E| \geq 0.5$ and $r < 0.5$, the rabbit's energy level is still high enough for a successful escape. Thus, prior to surprise pounce, a soft besiege is constructed. The following equation updates the hawks' position in the soft besiege phase:

$$X(t+1) = \begin{cases} Y, & \text{if} F(Y) < F(X(t)), \\ Z, & \text{if} F(Z) < F(X(t)), \end{cases} \tag{18}$$

where Y and Z are obtained using equations (19) and (20) respectively as follows:

$$Y = X_{\text{rabbit}}(t) - E\left|JX_{\text{rabbit}}(t) - X(t)\right|, \tag{19}$$

$$Z = Y + S \times LF(D), \tag{20}$$

where D represents the dimension of the problem and S represents a random vector by size $1 \times D$ and LF represents the levy flight function defined by equation (21).

$$LF(x) = 0.01 \times \frac{u \times \sigma}{|v|^{1/\beta}}, \sigma = \left(\frac{\Gamma(1+\beta) \times \sin(\pi\beta/2)}{\Gamma(1+\beta/2) \times \beta \times 2^{\beta-1/2}}\right)^{1/\beta}, \tag{21}$$

where u, v represents random values in the range (0,1) and β represents a default constant with the value 1.5.

(4) *Hard Besiege with Progressive Rapid Dives*. When $|E| < 0.5$ and $r < 0.5$, a hard besiege is constructed before the surprise pounce as the rabbit lacks the energy to escape. The following equation models the hard besiege condition:

$$X(t+1) = \begin{cases} Y, & \text{if} F(Y) < F(X(t)), \\ Z, & \text{if} F(Z) < F(X(t)), \end{cases} \tag{22}$$

where Y and Z are defined by equations (23) and (24), respectively,

$$Y = X_{\text{rabbit}}(t) - E\left|JX_{\text{rabbit}}(t) - X_m(t)\right|, \tag{23}$$

$$Z = Y + S \times LF(D), \tag{24}$$

where $X_m(t)$ is defined by equation (14).

2.7. Moth-Flame Optimizer (MFO). Another swarm intelligence algorithm included in our study is also a nature-inspired optimization proposed by Mirjalili [26] in 2015 called the MFO algorithm. Transverse orientation, the navigation method of moths in nature, is the main inspiration for this algorithm. Moths are butterfly-like insects with over 160,000 different species.

Moths have an interesting navigation method at night. They utilize moonlight when flying at night using a mechanism known as transverse orientation. Using this method, a moth flies in a straight path by maintaining a fixed angle with respect to the moon. This is an effective method that guarantees flying in a straight line [26].

However, moths are observed flying spirally around the lights. This is because the transverse orientation only works when the light is far away, like the moon. Using artificial lights, they want to keep a similar angle with the light to fly in a straight line. However, this behavior only creates a useless and deadly spiral fly path for moths. In the end, they converge toward the light. The Mothflame optimization algorithm is inspired by this behavior [26].

2.8. Mathematical Model of MFO. MFO is consisted of moths and flames. Moths as search agents are represented in a matrix as follows:

$$M = \begin{bmatrix} m_{1,1} & m_{1,2} & \cdots & \cdots & m_{1,d} \\ m_{2,1} & m_{2,2} & \cdots & \cdots & m_{2,d} \\ \vdots & \vdots & \vdots & \vdots & \vdots \\ m_{n,1} & m_{n,2} & \cdots & \cdots & m_{n,d} \end{bmatrix}, \tag{25}$$

where n represents the number of moths and d represents the dimension.

Also, an array is used to store the fitness of the corresponding moth as follows:

$$OM = \begin{bmatrix} OM_1 \\ OM_2 \\ \vdots \\ OM_n \end{bmatrix}, \tag{26}$$

where n represents the number of moths.

Furthermore, the best positions discovered by moths are represented as flames which are stored matrix F and their fitness value is stored in an array OF.

The spiral moment of moths around flames is modeled as follows:

$$S\left(M_i, F_j\right) = D_i.e^{bt}.\ \cos(2\pi t) + F_j, \tag{27}$$

where D_i shows the distance of the i^{th} moth for the j^{th} flame, b is a constant which define the logarithmic spiral's shape, and t indicates a random number in the range $[-1, 1]$.

D is defined by the following equation:

$$D_i = \left|F_j - M_i\right|, \tag{28}$$

where M_i represents the i^{th} moth and F_j represents the jth flame.

For exploitation as well as convergence, the flames decrease in number as depicted in the following equation:

$$\text{flameno} = \text{round}\left(N - l * \frac{N-1}{T}\right), \tag{29}$$

where the current number of iteration is represented by l, maximum number of flames are shown by N, and the maximum number of iterations is shown by T.

3. Research Methodology

This Systematic Literature Review (SLR) follows the proposed methodology of Kitchenham and Charters [27]. Various discrete activities comprise our work. These activities can be divided into three phases, such as planning, conducting, and reporting the SLR. The first phase, namely, planning of the study is comprised of the research questions addressed by the SLR, identifying the data sources, forming the search strategy, data extraction process, and synthesis.

3.1. Research Questions. This systematic literature review explores the applications of GWO, WOA, HHO, and MFO in software engineering. Specification of research questions (RQs) is an essential part of any SLR. For the accomplishment of the SLR, the following RQs are included:

RQ1: What is the evaluation of studies published on the GWO, WOA, HHO, and MFO algorithms in software engineering?

RQ2: What are the applications of GWO, WOA, HHO, and MFO in software engineering?

RQ3: Which individuals, organizations, and countries are actively involved in searched-based software engineering using GWO, WOA, HHO, and MFO?

RQ4: What are the potential applications of GWO, WOA, HHO, and MFO in software engineering?

3.2. Data Sources and Search Strategy. Based on [28], our search string incorporates two essential search terms, namely, "Creature Name" and "Domain". The first term mentions algorithms such as GWO, WOA, HHO, and MFO inspired by the social behavior of grey wolves, humpback whales, Harris' hawks, and moths, respectively. The second term describes the fields where the social behavior of grey wolves has been mimicked, such as software engineering. This term is accompanied by appropriate synonyms.

The Boolean AND has been used to combine the major search terms of our search string, whereas the Boolean OR has been used to incorporate the synonyms as well as related terms. The following is the search string used in our SLR.

("grey wolf optimizer," OR, GWO, OR "whale optimization algorithm," OR, WOA, OR "Harris hawks optimization," OR, HHO, OR "moth-flame optimization" OR MFO) AND ("software engineering" OR "software development" OR "software testing" OR "requirements engineering" OR "usability engineering" OR software OR testing).

For the accumulation of related publications, academic data sources such as IEEExplore, ACM Digital Library, SpringerLink, and ScienceDirect have been searched. Most of our publications of interest came from using Google Scholar. Publications and contributions came from journals, books, and conferences.

This SLR includes full-text studies citing GWO, WOA, HHO, and MFO in software engineering and was published from 2014 until 2022. Major search terms must be part of each study. Furthermore, the written language of these publications must be English. The titles and abstracts of these papers are investigated to ensure they fit the SLR. Personal blogs, web pages, and studies that do not cite the mentioned swarm intelligence algorithms are excluded from the SLR. The exclusion and inclusion criteria for the selection of studies are summarized in Figure 2.

3.3. Data Extraction and Synthesis. To address the research questions, this section explores the strategy of extracting and analyzing data from selected studies. A list comprised of various data items is obtained from the selected studies. Table 2 presents the recorded information which will be used for providing answers to the research questions (RQs). Also, the individual data items associated with the relevant research questions are shown in Table 2.

We applied the search string to various digital libraries such as IEEExplore, ACM Digital Library, SpringerLink, and ScienceDirect and obtained 68, 24, 275, and 2270 studies, respectively. We also used Google Scholar and using a search string, 2446 studies were obtained. Our search provided a total of 5083 studies, as shown in Table 3. Primary studies were obtained from the search results by using the PRISMA flow diagram as shown in Figure 3.

The PRISMA flow diagram consists of various steps such as identification, screening, eligibility, and inclusion, as depicted in Figure 3. All studies are identified through electronic databases by using the search string in the first step, i. e., identification. A total of 5083 studies have been identified. In the second step, namely, screening, irrelevant and grey studies are removed and outcomes in 103 studies are based on the inclusion and exclusion criterion 1. Duplicate studies were removed based on exclusion criterion 2, which resulted in 68 studies. More studies are excluded based on exclusion criteria 3 and 4 and we are left with 54 studies. In the eligibility step, 48 studies are found to be eligible. After reading these 48 studies, they are found to be relevant and are considered primary studies for this SLR. However, Section *Quality assessment criteria* further assesses the selected papers based on quality assessment criteria.

3.4. Quality assessment Criteria. After the implementation of inclusion and exclusion criteria, a quality assessment for each study is performed to determine its credibility as well as relevance. Being a supplementary criterion, it helps in excluding studies having low quality based on some given

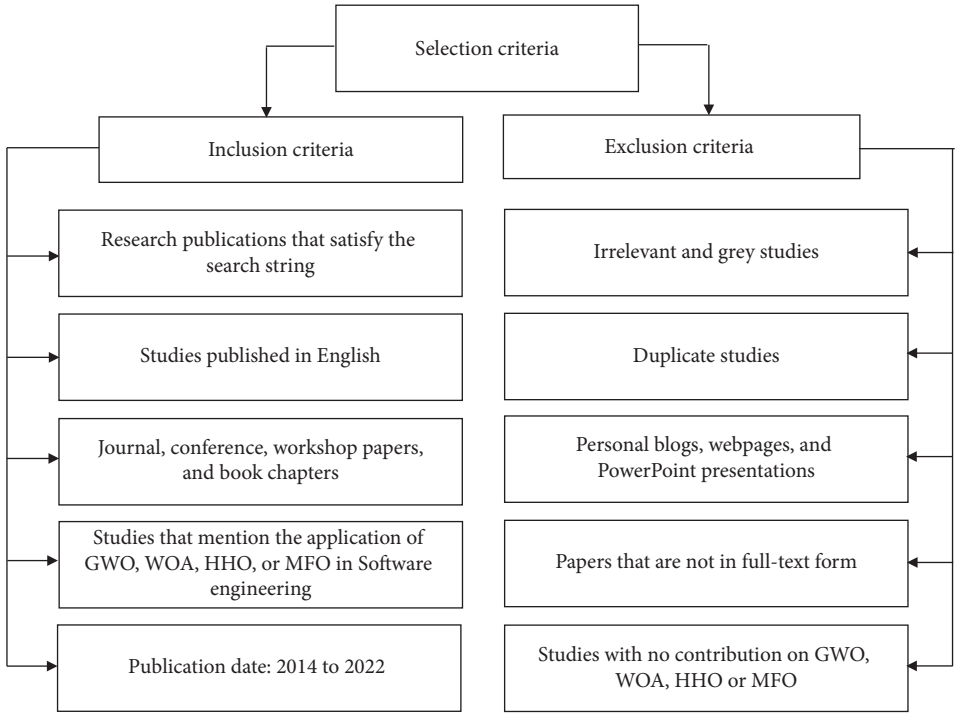

Figure 2: Summary of selection criteria.

Table 2: Data items from selected studies for recording information.

ID	Data item	Description	Relevant RQ
D1	Year of publication	What is publication year of the article?	RQ1
D2	Name of author	Who are the authors of the article?	RQ1
D3	Title of paper	What is the article's title?	RQ1
D4	Subject area	The published article explores which knowledge area?	RQ1
D5	Document type	The article belongs to which document type?	RQ1
D6	Source	What is the article's source such as journal, conference, or book?	RQ1
D7	Swarm based intelligence	What swarm-based intelligence algorithms are involved in search-based software engineering?	RQ2
D8	Case study	Which case study is explored in the paper?	RQ2
D9	Affiliation	The study is published in which affiliated institutes/organizations?	RQ3
D10	Country	Which country has the research institute that has published the study?	RQ3
D11	Application	What are the potential applications of GWO, WOA, HHO, and MFO in software engineering?	RQ4

Table 3: Databases with number of published studies.

ID	Database	Obtained studies	Electronic database's web link
DB1	IEEExplore	68	https://ieeexplore.ieee.org
DB2	ACM digital library	24	https://dl.acm.org
DB3	SpringerLink	275	https://link.springer.com
DB4	ScienceDirect	2270	https://www.sciencedirect.com
DB5	Google scholar	2446	https://scholar.google.com

weights and certain thresholds. The following questions are used to determine the quality assessment criteria:

Q1. Does the research state its aims clearly?

Q2. Does the research compare its proposed estimation method with existing methods?

Q3. Does the study analyze its limitations explicitly?

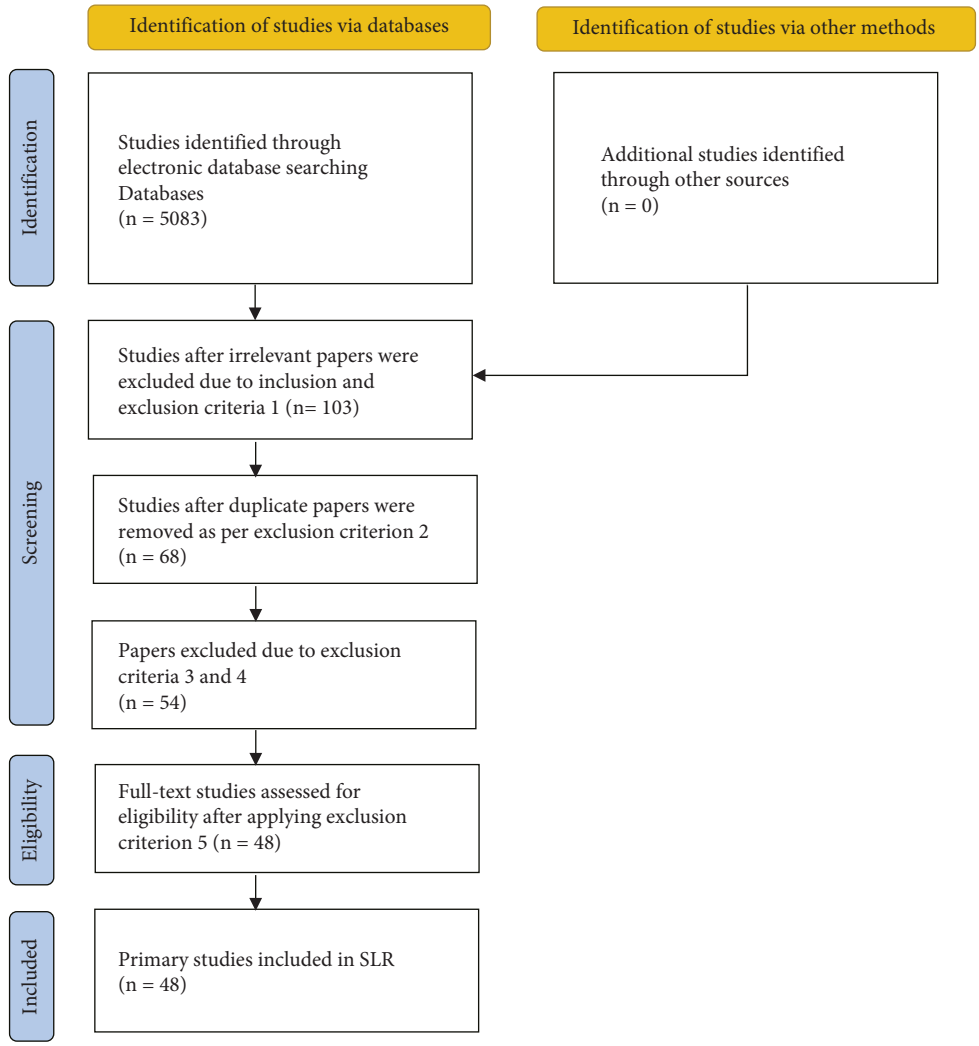

Figure 3: PRISMA flow diagram for selection of primary studies.

Q4. Does the study have citations?

Each question is assigned a weight of 0.25. Since there are a total of four questions, therefore, the combined weight is 1. Thus the total score for a single study can be given as:

0.00 (No)

0.25 (Rarely)

0.50 (Partly)

0.75 (Mostly)

1.00 (Yes)

Based on the abovementioned criterion, a study is included if it scores 0.5 or above, which means out of the four given assessment criteria, it must fulfill at least two.

As a result of the application of this quality assessment, 02 more studies are discarded with a 0.25 (rarely) score each. In other words, all the studies with an assigned score of "partly, mostly, and yes" are included in the SLR. Finally, 46 studies were selected for this SLR. Scores based on quality assessment criteria for the selected studies are given in Table 4. The authors shared the same opinion throughout the selection process.

4. Results

This section provides answers to the RQs by analyzing the selected studies. Detailed outcomes of the literature analysis are presented in this section.

Frequency of published studies based on GWO, WOA, HHO, and MFO in software engineering (RQ1).

The identified studies are analyzed to find out the frequency as well as the advancement of publications based on the selected metaheuristics in software engineering. Figure 4 shows year-wise publication of the selected studies with an average of 05 studies per year. The figure also shows the increased number of publications in recent years. Many research studies indicate that variants of the selected metaheuristics have been used in software engineering, as depicted in Table5. Figure 5 illustrates the type of selected publications. According to the figure, 76% are articles, 22% are inproceeding, and 2% are incollection of the identified studies. Figure 6 illustrates various fields in software engineering in the identified publications. Table 6 shows various journals and conferences associated with the identified research work. It is evident from Table 6 that 4 papers have

Table 4: Selected papers with quality assessment scores.

Study	Score
S1	Mostly
S2	Mostly
S3	Partly
S4	Yes
S5	Partly
S6	Mostly
S7	Mostly
S8	Mostly
S9	Mostly
S10	Mostly
S11	Mostly
S12	Partly
S13	Mostly
S14	Mostly
S15	Yes
S16	Mostly
S17	Mostly
S18	Partly
S19	Mostly
S20	Partly
S21	Partly
S22	Mostly
S23	Partly
S24	Partly
S25	Mostly
S26	Partly
S27	Mostly
S28	Mostly
S29	Yes
S30	Mostly
S31	Mostly
S32	Mostly
S33	Yes
S34	Partly
S35	Mostly
S36	Mostly
S37	Mostly
S38	Mostly
S39	Mostly
S40	Mostly
S41	Mostly
S42	Mostly
S43	Mostly
S44	Mostly
S45	Mostly
S46	Mostly

been published in "IEEE Access", 2 papers each have been published in Springer and "International Journal of Intelligent Engineering and Systems," while one paper each has been published in the rest of the journals and conferences.

4.1. Applications of GWO, WOA, HHO, and MFO in Software Engineering (RQ2). The identified studies discuss various applications of the selected metaheuristics, i.e., GWO, WOA, HHO, and MFO, in software engineering. Figure 7 shows the selected algorithms used by our study. It is clear from the figure that GWO tops the list with 51%, WOA comes second with 30%, while MFO and HHO are at third and fourth positions with 13% and 6% respectively. Table 7 summarizes these applications. The following paragraphs discuss these applications in detail.

Altaie et al. [47] generated a test suite to increase the coverage of paths based on GWO and PSO. According to the results, the PSO algorithm performed better than the GWO algorithm. Jyoti and Sharma [44] proposed an enhanced version of WOA (Ambha_WOA) using 12 test case suites obtained from SIR and GitHub repositories. The new algorithm was compared with WOA using various performance metrics such as fault detection ratio metric, precision and recall, and classification accuracy. NP-statistical tests were conducted for result validation. Wang and Zhao [56] used WOA with chaos initialization for the automatic test case generation method. By using the improved WOA, the method aimed at one path at a time for optimizing the population as well as finding the optimal value. Kaur [51] utilized HHO for extracting the optimal test cases. Sharma and Saha [39] combined MFO and the Firefly Algorithm (FA) for test path generation. The authors used five object-oriented benchmark applications for verification. The full coverage of the path was confirmed by the results. Agrawal et al. [43] used a hybrid WOA for the regression test case selection approach. The proposed approach improved the fault detection ability as per the obtained results. Hassan et al. [55] utilized WOA for t-way test suite generation with constraint support. Results confirmed competitive outcomes for WOA as compared with existing metaheuristics. Harikarthik et al. [54] used the regression test case prioritization mechanism for generating test cases. Then, they used the kernel fuzzy c-means (KFCM) clustering technique for clustering the test cases. They utilized WOA for the weight optimization process. Rastogi [30] used the GWO and FA (GWFF) methods to optimize the Test Case (TC) and generate path coverage in less execution time. The GWFF showed better performance in terms of fitness values when compared with Particle Swarm Optimization (PSO), Bee Colony Algorithm (BCA), and Cuckoo Search (CS). Sunitha [49] proposed a technique that makes use of optimal test prioritization in the Cloud using KFCM to overcome the shortcomings of various algorithms and to find an accurate optimization of existing software applications. The technique has two steps. Firstly, the KFCM technique was applied based on a similarity feature in organizing the test cases in software applications. Secondly, GWO was applied to achieve an optimal solution. Sharma and Saha [53] used MFO for model-based software testing based on object orientation. According to the results, for large software applications, MFO outperformed other metaheuristics, i.e., FA and ACO in creating optimized test cases. Metwally [52] used MFO to create a technique for automatic test data generation which in a single run could generate the whole test suite. According to the results, the new technique outperformed the random generator. Badanahatti and Murthy [48] used cloud-based regression testing. The proposed technique has three stages, namely, test case generation, clustering, and test case prioritization. As per the results, the proposed method preceded the minimum implementation time of the available technique. Gupta and

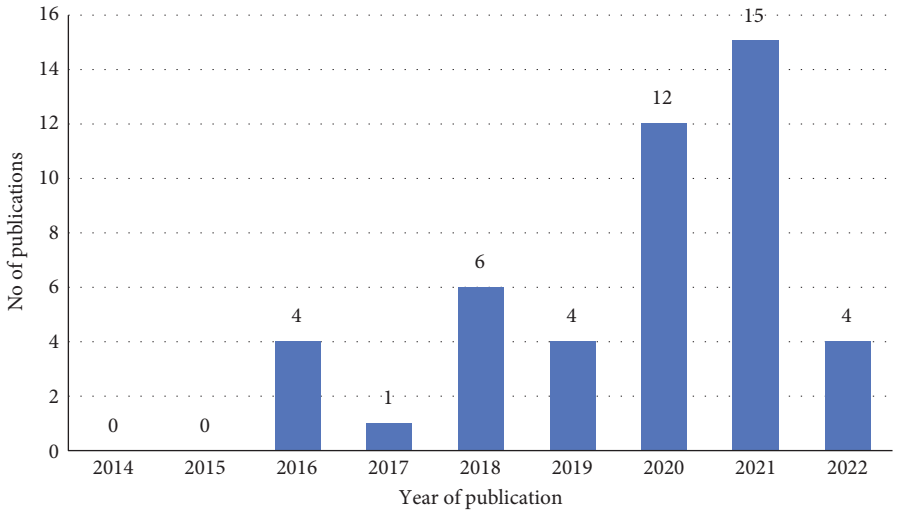

Figure 4: Frequency of published study by year.

Table 5: Summary of the selected metaheuristics' variants used in software engineering.

Variant	Short name	Effectiveness compared with	Efficiency/performance evaluated/validated by	Case study	Publication year	Authors [ref.]
Chaotic grey wolf optimization algorithm	CGWO	GWO, PSO, GA, and WO	Pham-Zhang (PZ) model and testing effort functions (TEFs)	Parameter optimization of software reliability growth model	2021	Dhavakumar and gopalan [29]
Grey Wolf-FireFly method	GWFF	BCA, PSO, and CS	Mean time between failures (MTBF)	Software test case mechanism	2019	Rastogi [30]
Agile risk prioritization–grey wolf optimization	ARP-GWO	Existing agile	Usability goals achievement metric (UGAM) and index of integration (IoI)	Risk prioritization in agile software development	2021	Prakash and viswanathan [31]
Modified grey wolf optimization	MGWO	GWO, MBBAT, MWOA, and MMFO	Software development life cycle (SDLC) models	Software usability	2021	Jain [32]
Multi-objective grey wolf optimizer	MOGWO	NSGA2, MOTLBO, and SPEA2	8 quality indicators, i.e., fairness indicators, uncertainty indicators, and multi-objective optimizations indicators (MOO)	Multi objective next realease problem (MONRP)	2021	Ghasemi [33]
Improved grey wolf optimizer	IGWO	GWO	Real world failure datasets, statistical comparison metrics	Parameter estimation of software reliability growth models (SRGMs)	2021	Musa [34]
Hybrid grey wolf optimizer	HGWO	PSO, ABC, DABC, CGA, and MGA	Two groups of datasets	Parameter estimation of software reliability growth models (SRGMs)	2019	Alneamyand dabdoob [35]
Whale and grey wolf optimization algorithm	WGW	Replacement access, library and ID card project (RALIC) dataset	RALIC dataset	Prioritization of software requirements	2018	Masadeh et al. [36]
Enhanced binary harris hawk optimization algorithm	EBHHO	BGOA, ESBHHO, BALO, BWOA, BBA, BGSA, and GA	Datasets in the field of software fault prediction (SFP)	Software fault prediction	2020	Thaher and arman [37]

Table 5: Continued.

Variant	Short name	Effectiveness compared with	Efficiency/performance evaluated/validated by	Case study	Publication year	Authors [ref.]
Island binary moth flame optimization	IsBMFO	BMFO	21 public software datasets	Software defect prediction	2021	Khurma et al. [38]
Moth firefly algorithm	MFA	MFO and FA	5 object-oriented benchmark applications	Path testing	2020	Sharma and saha [39]
Enhanced binary moth flame optimization	EBMFO	BGOA, BGSA, WOA, BBA, and BALO	15 different software fault projects obtained from PROMISE public software engineering repository	Software fault prediction	2020	Tumar et al. [40]
Modified mothflame optimization	MMFO	MFO, BBAT, and MBBAT	The dataset with 23 features	Usability feature selection	2020	Gupta et al. [41]
Modified whale optimization algorithm	MWOA	WOA, GWO, PSO, and DABC	34 benchmark function	Parameter estimation of SRGMs	2021	Lu and ma [42]
Hybrid whale optimization algorithm	HWOA	BAT and ACO	Subject programs retrieved from the software artifact infrastructure repository	Regression test case selection	2020	Agrawal et al. [43]
Ambha_Whale optimization algorithm	Ambha_WOA	WOA	12 test case suites taken from GitHub and SIR repositories	Test case suite selection	2022	Jyoti and sharma [44]
Tournament selection method with binary WOA	TBWOA	BGWO, BGSA, BPSO, BALO, BBA, and BSSA	17 SFP datasets from the PROMISE repository	Software fault prediction	2021	Hassouneh et al. [45]
Multi-objective whale optimization algorithm	MOWOA	NSGA2, MOTLBO, and SPEA2	8 quality indicators i.e., fairness indicators, uncertainty indicators, and multi-objective optimizations indicators (MOO)	Multi objective next release problem (MONRP)	2021	Ghasemi [33]
Modified whale optimization algorithm	MWOA	WOA	3 real measured test/debug data sets	Parameter estimation of SRGMs	2018	Lu and ma [46]

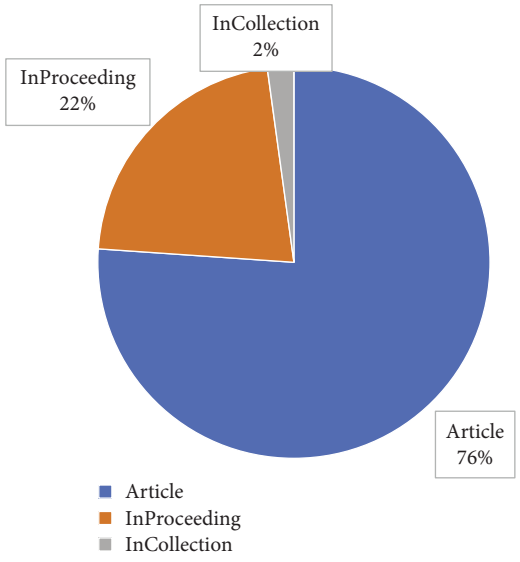

Figure 5: Document type of identified studies.

Gupta [50] utilized Biographical Based Optimization (BBO) and GWO in test suite prioritization as well as minimization. The performance was then evaluated with other meta-heuristic algorithms.

Rhmann [57] utilized GWO and random forest (RF) for predicting software vulnerability. According to the results, the proposed technique, i.e., GW-RF, outperformed machine learning techniques for software vulnerability prediction. Mohammad et al. [59] proposed a multi-objective HHO for binary classification problems using the Adaptive Synthetic Sampling (ADASYN) Technique. The authors used a healthcare dataset. Results confirmed the significant performance of the proposed model. Almayyan [58] evaluated different feature selection algorithms such as GWO, CS, Bat, and PSO for the prediction of software defects. The NASA dataset benchmarks were analyzed using three clustering algorithms such as X-Means, Farthest First, and Self Organizing Map (SOM). The proposed clustering model was used to build an efficient predictive model with an acceptable number of features as well as a good detection

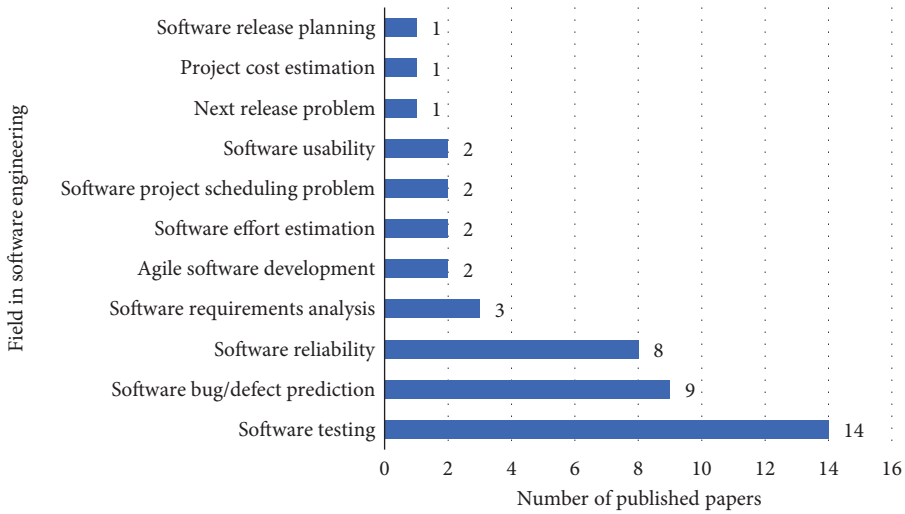

Figure 6: Ratio of identified studies by various fields in software engineering.

rate. Khurma et al. [38] proposed a binary variant of MFO (BMFO) by using the island BMFO (IsBMFO) model for the software defect prediction (SDP) problem. Results showed that IsBMFO, followed by support vector machine (SVM) classification, outperformed other models for the SDP problem, with an average G-mean of 78%. Alsghaier and Akour [60] developed an approach for software fault prediction by combining the genetics algorithm (GA) with the SVM classifier and WOA. It was then applied to 24 datasets, and the results confirmed the improved performance of the software fault prediction process. Hassouneh et al. [45] utilized WOA to present an efficient wrapper Feature Selection (FS) approach. The WOA was enhanced with nature selection operators to improve its efficacy in dealing with FS tasks. Zhu et al. [61] developed an enhanced metaheuristic search-based feature selection algorithm named EMWS by utilizing WOA and simulated annealing (SA). The results confirmed the superiority of EMWS. Thaher and Arman [37] proposed an enhanced binary version of HHO (EBHHO) for the FS problem. The authors used the Adaptive Synthetic (ADASYN) oversampling technique to reduce the dimensionality of the dataset using the FS technique. Results showed the superiority of EBHHO over the basic HHO. Tumar et al. [40] proposed an enhanced binary MFO (EBMFO) as a wrapper feature selection with ADASYN for software fault prediction. According to the results, the EBMFO improved the overall performance of classifiers.

Dhavakumar and Gopalan [29] used the Chaotic GWO algorithm (CGWO) in the Software Reliability Growth Model (SRGM). SRGM utilizes optimization algorithms to advance the parameters by dividing them into stages. However, by using CGWO, the technique is upgraded by using all the parameters simultaneously. Lu and Ma [42] proposed a modified WOA (MWOA) for predicting software reliability. Using software fault historical data, MWOA is used to predict the faults during software testing. Also, for the accurate estimation of software faults, the authors developed a modified sigmoid model (MSM). Musa [34] adopted the Improved GWO (IGWO) to estimate the optimum parameters for SRGMs. The proposed method utilizes seven real-world failure datasets. As per the results, the proposed method of IGWO performs better than the existing GWO. Gupta et al. [64] applied Random Walk GWO (RW-GWO) to determine the optimal redundancies to optimize the system reliability and the optimum cost of two distinct complex systems with constraints imposed on system reliability. The comparison proved the efficiency of the RW-GWO. Alneamy and Dabdoob [63] proposed the binding of the GA and the GWO algorithms for the estimation of the parameters of SRGMs. According to the results, the proposed binding GWO-RGA performed better than the previous binding HGWO in terms of accuracy of parameter estimation as well as performance using the same datasets. Lu and Ma [46] proposed a modified WOA (MWOA) and a three-stage SRGM. The parameters of three-stage SRGMs are estimated using MWOA. Results showed that using MWOA with the three-stage model is more helpful in estimating the software faults. Salahaldeen et al. [35] estimated the parameters of SRGMs depending on failure data. A hybrid GWO (HGWO) was used by combining the GWO with the Real Coded Genetic Algorithm (RGA). According to the results, all other algorithms, such as PSO, ABC, Classic GA (CGA), the Dichotomous Artificial Bee Colony (DABC), and the Modified GA (MGA), were outperformed by the GWO. Sheta and Abdel-Raouf [62] explored the GWO algorithm to estimate the SRGM's parameters to minimize the difference between the actual and estimated number of failures of the software. Three different SRGM models, namely, the Power Model (POWM), the Exponential Model (EXPM), and the Delayed S-Shaped Model (DSSM), were evaluated. The study was conducted using three different datasets.

Alzaqebah et al. [66] utilized the WOA to prioritize the software requirements. The proposed technique was compared with the analytical hierarchy process (AHP). According to the results, the proposed technique outperformed the AHP technique with an approximate margin of 40%. Masadeh et al. [36] proposed a hybrid approach

Table 6: Number of papers published in various journals or conferences.

Name of journal or conference	No of published studies
IEEE Access	4
International Journal of Intelligent Engineering & Systems	2
Springer	2
2016 IEEE 27th International Symposium on Software Reliability Engineering (ISSRE)	1
2018 17th International Symposium on Distributed Computing and Applications for Business Engineering and Science (DCABES)	1
2018 9th International Conference on Information and Communication Systems (ICICS)	1
2020 10th International Conference on Cloud Computing, Data Science & Engineering	1
2020 11th International Conference on Information and Communication Systems (ICICS)	1
2020 6th International Engineering Conference "Sustainable Technology and Development"(IEC)	1
2021 11th International Conference on Cloud Computing, Data Science & Engineering (Confluence)	1
2021 16th International Conference on Emerging Technologies (ICET)	1
2021 5th International Conference on Intelligent Systems, Metaheuristics & Swarm Intelligence	1
Advances in Systems Science and Applications	1
Applied Intelligence	1
Cluster Computing	1
Computing	1
International Journal for Research in Applied Science and Engineering Technology	1
International Journal of Advanced Computer Science and Applications	1
International Journal of Applied Metaheuristic Computing (IJAMC)	1
International Journal of Artificial Intelligence and Applications (IJAIA)	1
International Journal of Computer Applications	1
International Journal of Computer Applications in Technology	1
International Journal of Distributed Systems and Technologies (IJDST)	1
International Journal of Recent Research and Review	1
International Journal of Recent Technology and Engineering (IJRTE)	1
IOP Conference Series: Materials Science and Engineering	1
Journal of Algorithms & Computational Technology	1
Journal of Ambient Intelligence and Humanized Computing	1
Journal of Information and Optimization Sciences	1
Journal of Intelligent & Fuzzy Systems	1
Journal of Systems and Software	1
Mathematics	1
Modern Applied Science	1
Soft Computing	1
Soft computing for problem solving	1
Soft Computing Methods for System Dependability	1
Software: practice and experience	1
Specialusis Ugdymas	1
TELKOMNIKA (Telecommunication Computing Electronics and Control)	1
Webology	1
Wireless Communications and Mobile Computing	1

using WOA and GWO algorithms (WGW) for the prioritization of software requirements. The RALIC dataset was used to evaluate the proposed method. Compared with the RALIC dataset, the proposed method showed 91% accuracy in requirements prioritization. In [65], Masadeh et al. applied GWO to prioritize the requirements of a software project in an ordered list. Results were compared and evaluated with the AHP technique based on average running time and dataset size. According to the results, the RP-GWO performed better than the AHP mechanism by approximately 30%.

Prakash and Viswanathan [31] proposed a technique based on Agile Risk Prioritization and GWO (ARP–GWO) for risk prioritization. By using the technique, risk factors were prioritized during the development of agile software. The effectiveness of ARP-GWO was analyzed using performance metrics such as Usability Goals Achievement Metric and Index of Integration. The results showed enhancements in comparison with the available agile process. Also, the author [67] performed a comparative study of five effective metaheuristic algorithms, namely, Ant Colony Optimization (ACO), PSO, GA, GWO, and AHP, to prioritize the risks in agile environments. As per results, GWO performed better in the prioritization of risks in an agile environment based on accuracy, reliability, running time, and error rate.

Khan et al. [68] presented a Deep Neural Network (DNN) model based on GWO and StrawBerry Algorithm (SBA) for software effort estimation. Nine benchmark functions were applied to validate the performance of the

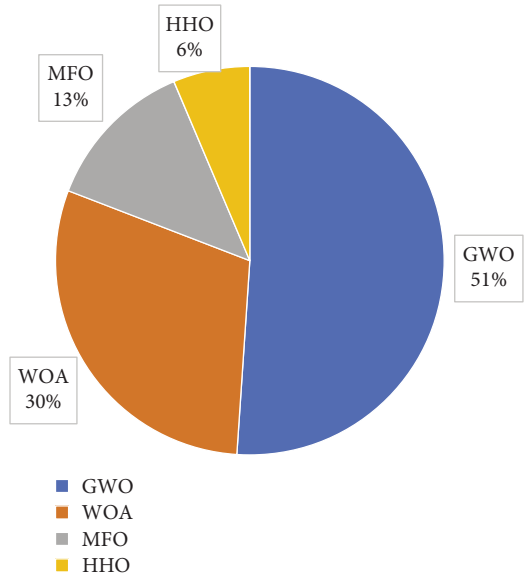

Figure 7: Swarm intelligence algorithm used by the identified studies.

Table 7: Summary of selected metaheuristics' applications.

Application area	No. of publications	[Ref.]
Software testing	14	[30, 39, 43, 44, 47–56]
Software bug/defect prediction	9	[37, 38, 40, 45, 57–61]
System reliability	8	[29, 34, 35, 42, 46, 62–64]
Software requirements analysis	3	[36, 65, 66]
Agile software development	2	[31, 67]
Software effort estimation	2	[68, 69]
Software project scheduling problem	2	[70, 71]
Software usability	2	[32, 41]
Next release problem	1	[33]
Software release planning	1	[72]
Project cost estimation	1	[73]
Software release planning	1	[72]
Software risk management	1	[74]

two algorithms. The proposed DNN model (GWDNNSB) produced better results for learning rate selection and initial weights as compared with the available work. Fadhil and Alsarraj [69] applied the WOA with the Constructive Cost Model II (COCOMO II) to solve the problem of ideal transactions. The NASA 93 dataset was used by the algorithm. The proposed approach based on the Mean Magnitude of Relative Error (MMRE) metric showed the best results.

Alabajee et al. [70] explored GWO for solving the software project scheduling problem (SPSP) by seeking an optimum solution. The authors compared results with the intelligent water drop algorithm (IWD), max-min ant system hyper cube framework (MMAS-HC), ACO, FA, intelligent water drop autonomous search (IWDAS), and intelligent water drop algorithm standard version (IWDSTD). According to the results, GWO showed better optimizing performance than the rest of the algorithms. Also, Alreffaee and Alabajee [71] proposed WOA to resolve SPSP by utilizing three datasets. The algorithm gave good results.

Jain [32] proposed a modified GWO (MGWO) algorithm for the selection of crucial features in a hierarchical software model. As per the results, MGWO outperformed other relevant optimizers in terms of accuracy. Gupta et al. [41] introduced a modified MFO (MMFO) for usability feature selection. Results confirmed the better performance of the proposed algorithm.

Ghasemi [33] proposed a multi-objective version of GWO and WOA by solving the bi-objective next release problem (NRP). The two algorithms with three other evolutionary algorithms were used to solve instances of the NRP problem from four different datasets. To satisfy the constraints of the NRP problem, a roulette wheel, and a cost-to-score ratio were used. According to the results, MOWOA outperformed others whereas, with reduced budget constraints, MOGWO performed better.

Hassan and Khan [73] implemented GWO, the Harmony Search Algorithm (HSA), and the SBA for software cost estimation. The NASA dataset was used, and to find a better algorithm, MMRE was utilized. GWO outperformed other algorithms regarding MMRE reduction.

Verma et al. [72] presented GWO's application in software release planning, considering warranty based on the proposed mathematical model used to measure software systems' reliability growth. The software cost model is based on fault reduction factor, fault removal efficiency, and error generation. The fault dataset of ERP systems was used to validate the model.

Prakash and Viswanathan [74] used the GWO algorithm to prioritize the risks involved in software development. The proposed method of software risk prioritization (SRP-GWO) was compared with other techniques such as PSO, AHP, average ranking, categorizing scale, and Delphi. Five attributes, namely, adaptability, simplicity, accuracy, consistency, and running time, were used for evaluation. According to the results, the proposed method outperformed other techniques.

4.2. Countries, Organization and Active Individuals Involved in Searched-Based Software Engineering Using GWO, WOA, HHO, and MFO (RQ3). This study finds active researchers, affiliated organizations and countries involved in research regarding the selected metaheuristics in software engineering. According to the top researchers' ranking, Abdullah Alzaqebah, Amjad Hudaib, Prakash Balasubramanian, Raja Masadeh, and Viswanathan Vadivel are the topmost researchers with 3 publications each.

Anju Saha, Ankur Choudhary, Arun Prakash Agrawal, Deepak K Gupta, Jamal Salahaldeen Alneamy, Kezhong Lu, Marrwa Abd-AlKareem Alabajee, Marwah M. A. Dabdoob, Rashmi Sharma, Taghreed Riyadh Alreffaee and Zongmin Ma have 2 publications each, as shown in Figure 8. Top organizations affiliated by authors are also ranked which shows that.

"Vellore Institute of Technology, Chennai, India," "The University of Jordan, Amman, Jordan" and "The World Islamic Sciences and Education University, Amman, Jordan" are at the top with 3 publications each.

"University of Mosul, Iraq", "Maharaja Agrasen Institute of Technology, Delhi, India", "Nanjing University of Aeronautics and Astronautics, Jiangsu, China" and "Chizhou University, Anhui, China" have 2 publications each as illustrated in Figure 9.

Lastly, active countries having the highest number of published articles on selected metaheuristics in software engineering are ranked as per details given in Figure 10. According to the ranking, India is the most active country with 20 publications; Iraq is in the 2nd position with 6 publications; Jordan has 5 publications; China and Saudi Arabia have 4 publications each; Pakistan, Egypt, and Palestine have 3 publications each; Iran, Malaysia, and Vietnam have 2 papers each, whereas Brazil, Kuwait, Libya, Nepal, Poland, Portugal, Russia, and the USA have 1 publication each.

4.3. Potential Applications of GWO, WOA, HHO, and MFO in Software Engineering (RQ4). Various metaheuristic algorithms are used in different fields of software engineering. Ranichandra [75] utilizes ACO for enhancing estimation accuracy in analogy-based software cost estimation by proposing the non-orthogonal space distance (NoSD) technique. Prajapati and Kumar [76] address the issues related to multiple objective optimization of software remodularization using a customized version of PSO known as PSO-based multi-objective software remodularization (PSO-MoSR). In [77], Al-Azzoni and Iqbal use GA and ACO to demonstrate a software framework for solving instances of software component allocation problems. In [78], Wang propose a novel hybrid metaheuristic algorithm, CVTMaker, which may help publishers identify ideal crowdsourced virtual teams (CVTs). Sun et al. [79] utilize PSO with a reverse edge known as REPSO for multi-objective software module clustering problem (MOSMCP), which divides the complex software system into subsystems to obtain a perfect structure. Prajapati and Chhabra [80] use PSO-based module clustering (PSOMC) for Software Module Clustering problem. Tang et al. [81] propose two metaheuristic search algorithms, i. e., coordinate descent and genetic algorithms, for exploring the configuration space of Hadoop for high-performing configurations which perform significantly better than the default configuration settings. In [82], Haraty et al. use simulated annealing (SA) for state-based software testing, especially web applications. Mann et al. in [83] propose a path-specific approach for automatic test case generation (ATCG) using GA, PSO, and ABC. In the same paper, another approach, i. e., a test case prioritization (TCP), is also proposed using PSO.

Likewise, the selected metaheuristics i. e., GWO, WHOA, HHO, and MFO are used in most areas of software engineering due to their usefulness in terms of simplicity, flexibility, and scalability. They lead to the desired convergence by keeping a good balance between exploration and exploitation, which are the basic search behaviors of metaheuristic algorithms.

Applications of GWO, WOA, HHO, and MFO, in software engineering discusses applications of these swarm intelligence algorithms in various fields of software engineering, such as software testing, software reliability, next release problem, agile software development, and software requirements analysis, as given in Table 7. Metaheuristics algorithms are useful in optimization; therefore, problems that come under the realm of optimization problems could be solved using metaheuristics such as GWO. The following are some of the areas of software engineering where the applications of the selected swarm intelligence algorithms can potentially be used:

(i) Software vulnerability prediction

(ii) Software organization

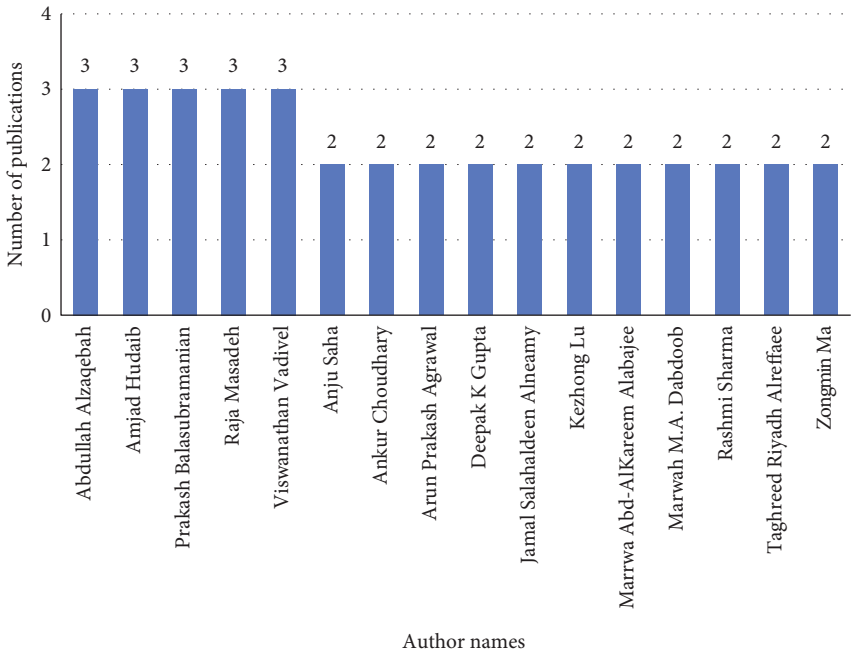

Figure 8: The top researchers using GWO in software engineering.

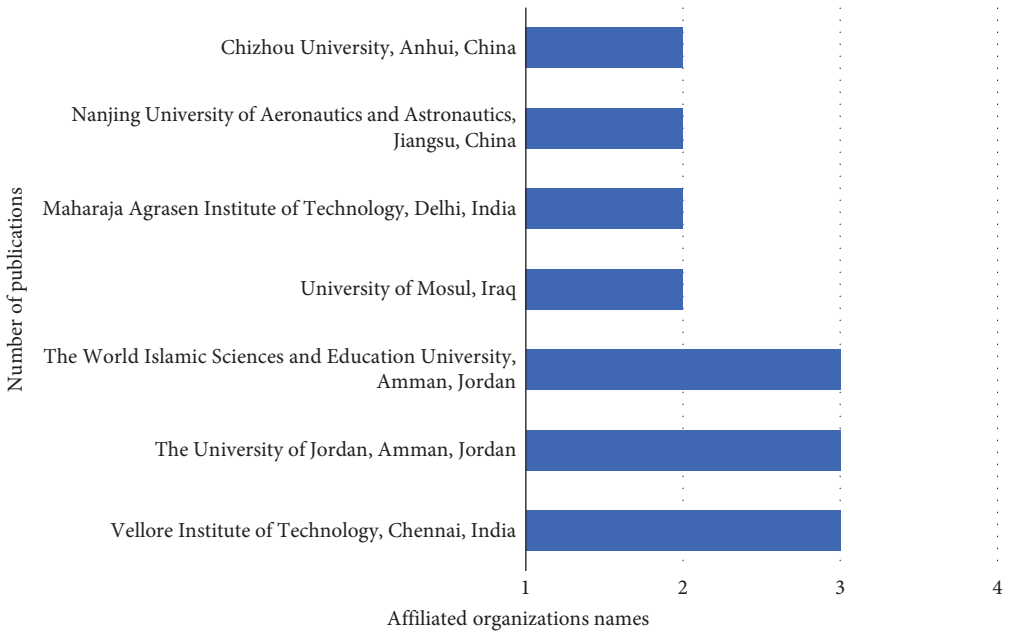

Figure 9: The top affiliated organizations using GWO in software engineering.

(iii) Software re-modularization
(iv) Maintenance/evolution system integration
(v) Software module clustering
(vi) Finding good designs
(vii) Reverse and re-engineering through transformation and re-factoring
(viii) User-based fitness evaluation for aesthetic aspects of software engineering
(ix) Avionics software
(x) Automotive software
(xi) Software configuration
(xii) Software component allocation
(xiii) Software testing
    (1) Structural testing
    (2) Mutation testing
    (3) Worst-and-best case execution time testing
    (4) Issue of boundary value analysis
    (5) Partition testing

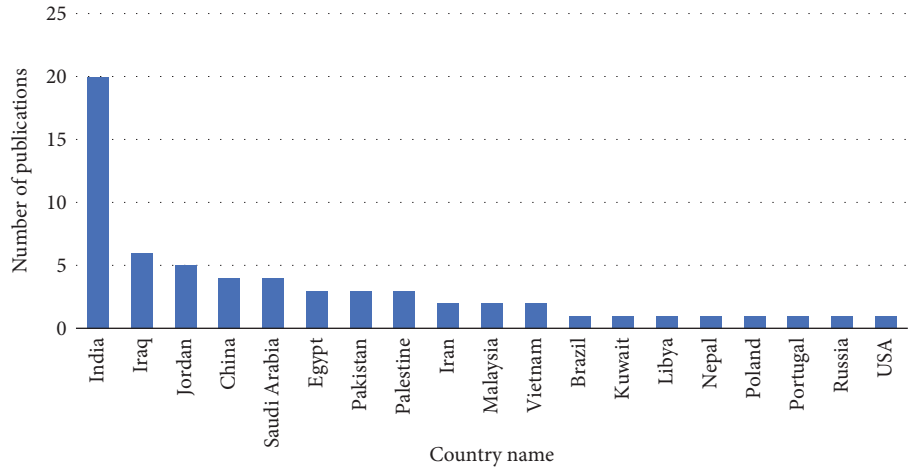

Figure 10: Active countries using GWO in software engineering.

5. Discussion

In this paper, we selected four swarm intelligence algorithms, i.e., GWO, WOA, HHO, and MFO, to study their applications in the field of software engineering. Our study presented an in-depth analysis of the applications of these metaheuristics in software engineering from 2014 up to 2022.

Our SLR is comprised of three phases, such as planning, conducting, and reporting. In the planning phase, we composed research questions that laid the foundation of our SLR. Data sources were then identified, such as IEEEXplore, ACM Digital Library, Springer Link, and ScienceDirect. We then formed a search strategy for extracting relevant literature. The PRISMA was utilized to obtain the primary studies for the SLR. The PRISMA flow diagram consists of various steps such as identification, screening, eligibility, and inclusion, as shown in Figure 3. Using PRISMA, 48 studies were found to be eligible. The identified studies were further subjected to quality assessment criteria and as a result, 2 more papers were dropped. Thus, a total of 46 papers were finally selected for our SLR.

According to the identified studies, GWO is the most used metaheuristic algorithm with 51% usage, WOA has 30% usage, MFO has 13% usage, and HHO has 6% usage, as shown in Figure 7. Also, our analysis showed that the selected metaheuristics have mostly been used in software testing, software defect prediction, and software reliability as shown in 6. Our study also revealed an increase in recent years in the usage of metaheuristic algorithms in software engineering, as evident in Figure 4. Furthermore, the top journals where the identified studies have been published are "IEEE Access," "Springer," and "International Journal of Intelligent Engineering and Systems."

As per the No Free Lunch theorem, no metaheuristic could solve all problems but a specific range of problems. Moreover, metaheuristics are easy to use and implement but they do not always guarantee the solution. To overcome some of the drawbacks of metaheuristics such as being trapped in local optima, researchers have developed variants of the existing metaheuristics as shown in detail in Table 5. Despite their shortcomings, metaheuristics are still popular as they provide near-optimal solutions to some of the hard problems such as NP-hard.

5.1. Threats to Validity. Various challenges can affect the validity of literature mapping or review studies. The following recommendations and guidelines can be used as compensation for the threats of this study:

(i) Coverage of relevant literature: This study includes publications that cite the selected metaheuristics, i.e., GWO, WOA, HHO, and MFO in software engineering from the time of GWO's invention to the present time, as GWO is the oldest among the selected swarm intelligence algorithms. New studies using the selected metaheuristics in software engineering published after our submission are beyond the scope of this study.

(ii) Coverage of research questions: The research questions may not cover all the aspects of state-of-the-art research on the selected metaheuristics in software engineering. Brainstorming is used to address this threat by optimally identifying the collection of research questions to cover the current research in this study.

6. Conclusion

This paper presented an in-depth literature study based on various applications of the selected metaheuristics, i.e., GWO, WOA, HHO, and MFO in the field of software engineering. The review study analyzed 46 papers published from 2014 to 2022 mentioning applications of the selected metaheuristics in the field of software engineering. Variants of the selected metaheuristics were also included in this study. This paper analyzed the selected papers according to the research questions of our SLR. This paper has mentioned countries, organizations, and authors actively involved in applying these metaheuristics in the field of software

engineering. The paper has also presented a detailed discussion on various applications of the selected metaheuristics in software engineering which revealed that these algorithms have mostly been used in software testing, software defect prediction, and software reliability. The study also pointed out areas of software engineering where these algorithms could be utilized. Hopefully, the current study may be helpful for new researchers using these swarm intelligence algorithms in software engineering for further enhancements.

Data Availability

This is a review article and all the data are discussed in the paper.

Conflicts of Interest

The authors declare that they have no conflicts of interest.

References

[1] B. Chopard and M. Tomassini, *An Introduction to Metaheuristics for Optimization*, Springer, Berlin/Heidelberg, Germany, 2018.

[2] J. K. Mykel and A. W. Tim, *Algorithms for Optimization*, Mit Press, Cambridge, Massachusetts, 2019.

[3] T. El-Ghazali, *Metaheuristics: from design to implementation*, Vol. 74, John Wiley & Sons, , Hoboken, New Jersey, U.S, 2009.

[4] M. Harman, S. Afshin Mansouri, and Y. Zhang, "Search-based software engineering: trends, techniques and applications," in *ACM Computing Surveys (CSUR)*vol. 45, no. 1, , pp. 1–61, ACM, 2012.

[5] M. Harman and B. F. Jones, "Search-based software engineering," in *Information and Software Technology*vol. 43, no. 14, , pp. 833–839, Elsevier, 2001.

[6] H. Faris, "Grey wolf optimizer: a review of recent variants and applications," in *Neural Computing & Applications*vol. 30, no. 2, , pp. 413–435, Springer, 2018.

[7] F. S. Gharehchopogh and H. Gholizadeh, "A comprehensive survey: whale Optimization Algorithm and its applications," *Swarm and Evolutionary Computation*, vol. 48, pp. 1–24, 2019.

[8] H. M. Alabool, D. Alarabiat, L. Abualigah, and A. A. Heidari, "Harris hawks optimization: a comprehensive review of recent variants and applications," *Neural Computing & Applications*, vol. 33, pp. 8939–8980, 2021.

[9] M. Shehab, L. Abualigah, H. Al Hamad, H. Alabool, M. Alshinwan, and A. M. Khasawneh, "Moth–flame optimization algorithm: variants and applications," *Neural Computing & Applications*, vol. 32, pp. 9859–9884, 2020.

[10] G.-G. Wang, S. Deb, and Z. Cui, "Monarch butterfly optimization," *Neural Computing & Applications*, vol. 31, pp. 1995–2014, 2019.

[11] S. Li, H. Chen, M. Wang, A. A. Heidari, and S. Mirjalili, "Slime mould algorithm: a new method for stochastic optimization," *Future Generation Computer Systems*, vol. 111, pp. 300–323, 2020.

[12] G. G. Wang, "Moth search algorithm: a bio-inspired metaheuristic algorithm for global optimization problems," *Memetic Computing*, vol. 10, pp. 151–164, 2018.

[13] A. Faramarzi, M. Heidarinejad, S. Mirjalili, and A. H. Gandomi, "Marine predators algorithm: a nature-inspired metaheuristic," *Expert Systems with Applications*, vol. 152, Article ID 113377, 2020.

[14] Y. Yang, H. Chen, A. A. Heidari, and A. H. Gandomi, "Hunger games search: visions, conception, implementation, deep analysis, perspectives, and towards performance shifts," *Expert Systems with Applications*, vol. 177, Article ID 114864, 2021.

[15] J. Tu, H. Chen, M. Wang, and A. H. Gandomi, "The colony predation algorithm," *Journal of Bionics Engineering*, vol. 18, pp. 674–710, 2021.

[16] A. Al-Momani, O. Mohamed, and W. Abu Elhaija, "Multiple processes modeling and identification for a cleaner supercritical power plant via Grey Wolf Optimizer," *Energy*, vol. 252, Article ID 124090, 2022.

[17] P. Hao and B. Sobhani, "Application of the improved chaotic grey wolf optimization algorithm as a novel and efficient method for parameter estimation of solid oxide fuel cells model," *International Journal of Hydrogen Energy*, vol. 46, no. 73, Article ID 36454, 2021.

[18] A. Bardhan, R. Biswas, N. Kardani et al., "A novel integrated approach of augmented grey wolf optimizer and ann for estimating axial load carrying-capacity of concrete-filled steel tube columns," *Construction and Building Materials*, vol. 337, no. 2022, Article ID 127454, 2022.

[19] A. R. Dhar, D. Gupta, S. S. Roy, A. K. Lohar, and N. Mandal, "Covariance matrix adapted grey wolf optimizer tuned eXtreme gradient boost for bi-directional modelling of direct metal deposition process," *Expert Systems with Applications*, vol. 199, Article ID 116971, 2022.

[20] L. Yin and Z. Sun, "Distributed multi-objective grey wolf optimizer for distributed multi-objective economic dispatch of multi-area interconnected power systems," *Applied Soft Computing*, vol. 117, Article ID 108345, 2022.

[21] J. Hu, H. Chen, A. A. Heidari et al., "Orthogonal learning covariance matrix for defects of grey wolf optimizer: insights, balance, diversity, and feature selection," *Knowledge-Based Systems*, vol. 213, Article ID 106684, 2021.

[22] S. Mirjalili, S. M. Mirjalili, and A. Lewis, "Grey wolf optimizer," in *Advances in Engineering Software*vol. 69, , pp. 46–61, Elsevier, 2014.

[23] S. Mirjalili, "Multi-objective grey wolf optimizer: a novel algorithm for multi-criterion optimization," in *Expert Systems with Applications*vol. 47, , pp. 106–119, Elsevier, 2016.

[24] S. Mirjalili and A. Lewis, "The whale optimization algorithm," *Advances in Engineering Software*, vol. 95, pp. 51–67, 2016.

[25] A. A. Heidari, S. Mirjalili, H. Faris, I. Aljarah, M. Mafarja, and H. Chen, "Harris hawks optimization: algorithm and applications," *Future Generation Computer Systems*, vol. 97, pp. 849–872, 2019.

[26] S. Mirjalili, "Moth-flame optimization algorithm: a novel nature-inspired heuristic paradigm," *Knowledge-Based Systems*, vol. 89, pp. 228–249, 2015.

[27] B. Kitchenham and S. Charters, *Guidelines for Performing Systematic Literature Reviews in Software Engineering*Elsevier, Amsterdam, Netherlands, 2007.

[28] M. Kader, "A systematic review on emperor penguin optimizer," in *Neural Computing and Applications*, pp. 1–21, Springer, Berlin/Heidelberg, Germany, 2021.

[29] P. Dhavakumar and N. P. Gopalan, "An efficient parameter optimization of software reliability growth model by using chaotic grey wolf optimization algorithm," *Journal of Ambient Intelligence and Humanized Computing*, vol. 12, pp. 3177–3188, 2021.

[30] P. Rastogi, "An optimal software test case mechanism using grey wolf-FireFly method," *International Journal of Intelligent Engineering and Systems*, vol. 12, no. 2, pp. 22–32, 2019.

[31] B. Prakash and V. Viswanathan, "ARP–GWO: an efficient approach for prioritization of risks in agile software development," *Soft Computing*, vol. 25, no. 7, pp. 5587–5605, 2021.

[32] R. Jain, *Feature Selection Algorithm for Usability Engineering: A Nature Inspired Approach"*Springer, Berlin/Heidelberg, Germany, 2021.

[33] M. Ghasemi, "Multi-objective whale optimization algorithm and multi-objective grey wolf optimizer for solving next release problem with developing fairness and uncertainty quality indicators," *Applied Intelligence*, vol. 51, pp. 1–30, 2021.

[34] A. A. Musa, "Parameter estimation of software reliability growth models: a comparison between grey wolf optimizer and improved grey wolf optimizer," in *Proceedings of the 2021 11th International Conference on Cloud Computing, Data Science & Engineering (Confluence)*, pp. 611–617, IEEE, Amity University, India, January, 2021.

[35] J. Salahaldeen and M. Marwan, "The use of original and hybrid grey wolf optimizer in estimating the parameters of software reliability growth models," *International Journal of Computer Application*, vol. 167, pp. 12–21, 2017.

[36] R. Masadeh, A. Hudaib, and A. Alzaqebah, "Wgw: A hybrid approach based on whale and grey wolf optimization algorithms for requirements prioritization," *Advances in Systems Science and Applications*, vol. 18, pp. 63–83, 2018.

[37] T. Thaher and N. Arman, "Efficient multi-swarm binary Harris hawks optimization as a feature selection approach for software fault prediction," in *Proceedings of the 2020 11th International Conference on Information and Communication Systems (ICICS)*, pp. 249–254, IEEE, Irbid, Jordan, April, 2020.

[38] R. A. Khurma, H. Alsawalqah, I. Aljarah, M. A. Elaziz, and R. Damasevicius, "An enhanced evolutionary software defect prediction method using island moth flame optimization," *Mathematics*, vol. 9, p. 1722, 2021.

[39] R. Sharma and A. Saha, "An integrated approach of class testing using firefly and moth flame optimization algorithm," *Journal of Information and Optimization Sciences*, vol. 41, pp. 599–612, 2020.

[40] I. Tumar, Y. Hassouneh, H. Turabieh, and T. Thaher, "Enhanced binary moth flame optimization as a feature selection algorithm to predict software fault prediction," *IEEE Access*, vol. 8, pp. 8041–8055, 2020.

[41] D. Gupta, A. K. Ahlawat, A. Sharma, and J. J. P. C. Rodrigues, "Feature selection and evaluation for software usability model using modified moth-flame optimization," *Computing*, vol. 102, pp. 1503–1520, 2020.

[42] K. Lu and Z. Ma, "A modified whale optimization algorithm for parameter estimation of software reliability growth models," *Journal of Algorithms & Computational Technology*, vol. 15, Article ID 174830262110344, 2021.

[43] A. P. Agrawal, A. Choudhary, and A. Kaur, "An effective regression test case selection using hybrid whale optimization algorithm," *International Journal of Distributed Systems and Technologies*, vol. 11, pp. 53–67, 2020.

[44] B. Jyoti and A. K. Sharma, "An enhanced Whale Optimisation Algorithm for test case suite selection: ambha_WOA," *Specialusis Ugdymas*, vol. 1, pp. 4356–4372, 2022.

[45] Y. Hassouneh, H. Turabieh, T. Thaher, I. Tumar, H. Chantar, and J. Too, "Boosted whale optimization algorithm with natural selection operators for software fault prediction," *IEEE Access*, vol. 9, Article ID 14239, 2021.

[46] K. Lu and Z. Ma, "Parameter estimation of software reliability growth models by a modified whale optimization algorithm," in *Proceedings of the 2018 17th International Symposium on Distributed Computing and Applications for Business Engineering and Science (DCABES)*, pp. 268–271, IEEE, Wuxi, China, October, 2018.

[47] A. M. Altaie, T. M. Tawfeeq, and M. G. Saeed, "Automated test suite generation tool based on GWO algorithm," *Webology*, vol. 19, pp. 3835–3849, 2022.

[48] S. Badanahatti and Y. S. S. R. Murthy, "Optimal test case prioritization in cloud based regression testing with aid of KFCM," *International Journal of Intelligent Engineering and Systems*, vol. 10, no. 3, pp. 96–105, 2017.

[49] B. Sunitha, "Prioritization of software applications in cloud using GWO algorithm," *International Journal for Research in Applied Science and Engineering Technology*, vol. 6, no. 5, pp. 2070–2075, 2018.

[50] D. Gupta and V. Gupta, *Test Suite Prioritization Using Nature Inspired Meta-Heuristic Algorithms*Springer, Berlin/Heidelberg, Germany, 2016.

[51] A. Kaur, "An approach to extract optimal test cases using AI," in *Proceedings of the 2020 10th International Conference on Cloud Computing, Data Science & Engineering (Confluence)*, pp. 649–654, Noida, India, January, 2020.

[52] A. S. Metwally, "WAP: a novel automatic test generation technique based on moth flame optimization," in *Proceedings of the 2016 IEEE 27th International Symposium on Software Reliability Engineering (ISSRE)*, pp. 59–64, IEEE, Ottawa, ON, Canada, October, 2016.

[53] R. Sharma and A. Saha, "Optimal test sequence generation in state based testing using moth flame optimization algorithm," *Journal of Intelligent and Fuzzy Systems*, vol. 35, pp. 5203–5215, 2018.

[54] S. K. Harikarthik, V. Palanisamy, and P. Ramanathan, "Optimal test suite selection in regression testing with testcase prioritization using modified Ann and Whale optimization algorithm," *Cluster Computing*, vol. 22, no. S5, Article ID 11425, 2019.

[55] A. A. Hassan, S. Abdullah, K. Z. Zamli, and R. Razali, "Combinatorial test suites generation strategy utilizing the whale optimization algorithm," *IEEE Access*, vol. 8, Article ID 192288, 2020.

[56] J. Wang and W. Zhao, "Automatic test case generation method based on improved whale optimization algorithm," in *Proceedings of the 2021 5th International Conference on Intelligent Systems, Metaheuristics & Swarm Intelligence*, pp. 7–16, Victoria Seychelles, April, 2021.

[57] W. Rhmann, "Software vulnerability prediction using grey wolf-optimized random forest on the unbalanced data sets," *International Journal of Applied Metaheuristic Computing*, vol. 13, pp. 1–15, 2022.

[58] W. Almayyan, "Towards predicting software defects with clustering techniques," *International Journal of Artificial Intelligence and Applications (IJAIA)*, vol. 12, p. 1, 2021.

[59] U. G. Mohammad, S. Imtiaz, M. Shakya, A. Almadhor, and F. Anwar, "An optimized feature selection method using ensemble classifiers in software defect prediction for healthcare systems," *Wireless Communications and Mobile Computing*, vol. 202214 pages, 2022.

[60] H. Alsghaier and M. Akour, "Software fault prediction using whale algorithm with genetics algorithm," *Software: Practice and Experience*, vol. 51, pp. 1121–1146, 2021.

[61] K. Zhu, S. Ying, N. Zhang, and D. Zhu, "Software defect prediction based on enhanced metaheuristic feature selection optimization and a hybrid deep neural network," *Journal of Systems and Software*, vol. 180, Article ID 111026, 2021.

[62] A. F. Sheta and A. Abdel-Raouf, "Estimating the parameters of software reliability growth models using the grey wolf optimization algorithm," *International Journal of Advanced Computer Science and Applications*, vol. 7, p. 4, 2016.

[63] J. S. Alneamy and M. M. A. Dabdoob, "Proposed binding between genetic algorithm and grey wolf optimizer to estimate the parameters of software reliability growth models," *International Journal of Recent Research and Review*, 2019.

[64] S. Gupta, K. Deep, and A. Assad, "Reliability–redundancy allocation using random walk gray wolf optimizer," in *Soft Computing for Problem Solving*, pp. 941–959, Springer, Berlin/Heidelberg, Germany, 2020.

[65] R. Masadeh, A. Alzaqebah, and A. Hudaib, "Grey Wolf algorithm for requirements prioritization," *Modern Applied Science*, vol. 12, p. 54, 2018.

[66] A. Alzaqebah, R. Masadeh, and A. Hudaib, "Whale optimization algorithm for requirements prioritization," in *Proceedings of the 2018 9th International Conference on Information and Communication Systems (ICICS)*, pp. 84–89, IEEE, Irbid, Jordan, April, 2018.

[67] B. Prakash and V. Viswanathan, "A comparative study of meta-heuristic optimisation techniques for prioritisation of risks in agile software development," *International Journal of Computer Applications in Technology*, vol. 62, pp. 175–188, 2020.

[68] M. S. Khan, F. Jabeen, S. Ghouzali, Z. Rehman, S. Naz, and W. Abdul, "Metaheuristic algorithms in optimizing deep neural network model for software effort estimation," *IEEE Access*, vol. 9, Article ID 60309, 2021.

[69] A. A. Fadhil and R. G. Alsarraj, "Exploring the whale optimization algorithm to enhance software project effort estimation," in *Proceedings of the 2020 6th international engineering conference âĂIJSustainable Technology and development(IEC)*, pp. 146–151, Victoria Seychelles, March, 2020.

[70] M. A. A. Alabajee, D. R. Ahmed, and T. R. Alreffaee, "Solving software project scheduling problem using grey wolf optimization," *TELKOMNIKA (Telecommunication Computing Electronics and Control)*, vol. 19, pp. 1820–1829, 2021.

[71] T. R. Alreffaee and M. A. A. Alabajee, "Solving software project scheduling problem using whale optimization algorithm," in *IOP Conference Series: Materials Science and Engineering*vol. 928, IOP Publishing, Article ID 032084, 2020.

[72] V. Verma, N. Neha, and A. G. Aggarwal, "Software release planning using grey wolf optimizer," in *Soft Computing Methods for System Dependability*IGI Global, Hershey, Pennsylvania, 2020.

[73] C. A. Hassan and M. S. Khan, "An effective nature inspired approach for the estimation of software development cost," in *Proceedings of the 2021 16th International Conference on Emerging Technologies (ICET)*, pp. 1–6, IEEE, Islamabad, Pakistan, December, 2021.

[74] B. Prakash and V. Viswanathan, "Risk prioritization for software development using grey wolf optimization," *International Journal of Recent Technology and Engineering (IJRTE)*, vol. 7, 2019.

[75] S. Ranichandra, "Optimizing non-orthogonal space distance using ACO in software cost estimation," *Mukt Shabd J*, vol. 9, pp. 1592–1604, 2020.

[76] A. Prajapati and S. Kumar, "PSO-MoSR: a PSO-based multi-objective software remodularisation," *International Journal of Bio-Inspired Computation*, vol. 15, pp. 254–263, 2020.

[77] I. Al-Azzoni and S. Iqbal, "Meta-heuristics for solving the software component allocation problem," *IEEE Access*, vol. 8, Article ID 153067, 2020.

[78] H. Wang, "Solving team making problem for crowdsourcing with hybrid metaheuristic algorithm," in *Proceedings of the Genetic and Evolutionary Computation Conference Companion*, pp. 318-319, Boston, MA, USA, August, 2018.

[79] J. Sun, Y. Xu, and S. Wang, "PSO with reverse edge for multi-objective software module clustering," *International Journal of Performability Engineering*, vol. 14, p. 2423, 2018.

[80] A. Prajapati and J. K. Chhabra, "A particle swarm optimization-based heuristic for software module clustering problem," *Arabian Journal for Science and Engineering*, vol. 43, pp. 7083–7094, 2018.

[81] C. Tang, K. Sullivan, and B. Ray, "Searching for high-performing software configurations with metaheuristic algorithms," in *Proceedings of the 40th International Conference on Software Engineering: Companion Proceeedings*, pp. 354-355, Gothenburg, Sweden, December, 2018.

[82] R. A. Haraty, N. Mansour, and H. Zeitunlian, "Metaheuristic algorithm for state-based software testing," *Applied Artificial Intelligence*, vol. 32, pp. 197–213, 2018.

[83] M. Mann, P. Tomar, and O. P. Sangwan, "Bio-inspired metaheuristics: evolving and prioritizing software test data," *Applied Intelligence*, vol. 48, pp. 687–702, 2018.

Hindawi
Complexity
Volume 2023, Article ID 7953967, 19 pages
https://doi.org/10.1155/2023/7953967

Research Article

Fluid Flow Behavior Prediction in Naturally Fractured Reservoirs Using Machine Learning Models

Mustafa Mudhafar Shawkat,[1] **Abdul Rahim Bin Risal**,[1] **Noor J. Mahdi**,[2] **Ziauddin Safari**,[3] **Maryam H. Naser**,[4] **and Ahmed W. Al Zand**[5]

[1]*Department of Petroleum Engineering, School of Chemical and Energy Engineering, Faculty of Engineering, Universiti Teknologi Malaysia, Johor Bahru 81310, Malaysia*
[2]*Department of Civil Engineering, Al-Maarif University College, Ramadi, Iraq*
[3]*Department of Civil Engineering, Faculty of Engineering, Takhar University, Taleqan, Afghanistan*
[4]*Building and Construction Techniques Engineering Department, Al-Mustaqbal University College, Hillah 51001, Iraq*
[5]*Department of Civil Engineering, Faculty of Engineering and Built Environment, Universiti Kebangsaan Malaysia (UKM), Bangi 43600, Selangor, Malaysia*

Correspondence should be addressed to Ziauddin Safari; zia.safari2011@gmail.com

Received 3 June 2022; Revised 15 October 2022; Accepted 29 November 2022; Published 20 February 2023

Academic Editor: Mostafa Al-Emran

The naturally fractured reservoirs are one of the most challenging due to the tectonic movements that are caused to increase the permeability and conductivity of the fractures. The instability of the permeability and conductivity effects on the fluid flow path causes problems during the transfer of the fluids from the matrix to the fractures and fluid losses during production. In addition, these complications made it difficult for engineers to estimate fluid flow during production. The fracture properties' study is important to model the fluid flow paths such as the fracture porosity, permeability, and the shape factor, which are considered essential in the stability of fluid flow. To examine this, this research introduced new models including decision tree (DT), random forest (RF), K-nearest regression (KNR), ridge regression (RR), and LASSO regression model,. The research studied the fracture properties in naturally fractured reservoirs like the fracture porosity (FP) and the shape factor (SF). The datasets used in this study were collected from previous studies "i.e., Texas oil and gas fields" to build an intelligence-based predictive model for fluid flow characteristics. The prediction process was conducted based on interporosity flow coefficient, storativity ratio, wellbore radius, matrix permeability, and fracture permeability as input data. This study revealed a positive finding for the adopted machine learning (ML) models and was superior in using statistical accuracy metrics. Overall, the research emphasized the implementation of computer-aided models for naturally fractured reservoir analysis, giving more details on the extensive execution techniques, such as injection or the creation of artificial cracks, to minimize hydrocarbon losses or leakage.

1. Introduction

1.1. Background. Naturally fractured reservoirs are the result of natural processes that present the diastrophism and volume shrinkage that lead to fractures that have dispersed as a consistently linked network across the reservoir [1]. The tectonic processes have evolved in reservoirs, fractured reservoirs are frequently found in weak reservoir rocks with poor porosity [2]. Due to that, the fracture is extended and large, where it is often referred to as the large fracture [3]. If the granular porosity is high but the rocks are fragile, the fracture is relatively small and limited in quantity, often referred to as microfractures [1]. The naturally fractured reservoirs are different from the conventional reservoirs [4, 5]. In addition, the tectonic movements affected by the behavior of the fracture during transfer and production of the fluids flow due to the high conductivity and permeability of the natural fractures [6]. The conductivity and

permeability of the fractures factor minimize the fracture porosity of the fluids that cause low storage capacity [6]. In contrast, the conductivity of the matrix increases storage capacity with low permeability, which causes an increase in the matrix porosity [7]. According to previous studies, matrix porosity is higher than fracture porosity in the naturally fractured reservoirs, which the fluids store in the matrix [8].

Multiphase flow modeling in naturally fractured reservoirs has been considered an issue for petroleum reservoir engineers [9, 10]. Warren and Root have shown a dual-porosity model which presents multiphase behavior in fractured reservoirs [11]. In the dual-porosity model, there are two characteristic regions: matrix and fracture [12]. The naturally fractured reservoirs present one of the most difficult reservoirs in the petroleum industry due to the fracture properties like permeability and porosity, where the natural fracture permeability is higher than the matrix permeability in a dual-porosity system [12]. The hydrocarbons flow from the matrix to the fractures and from these to the wellbore where the fractures cannot store these fluids, which cause fluid flow losses. An obstacle of the fluid flow can be seen in Figure 1 [13].

The motivation is always focused on developing a reliable mathematical model for modeling naturally fractured reservoir properties such as fracture porosity (FP) and the shape factor (SF). In the literature, ML models are one of the technologies that contribute to the systematization of fluid flow by forming speculative models based on hypotheses and equations modeling the properties of petroleum fluids [14]. Hence, the focus of the current investigation is to test different versions of ML models for the prediction of FP and SF. The models are built based on the characteristics of oil and gas, such as matrix porosity, permeability, pressure, and temperature.

1.2. Literature Review. Modeling of the naturally fractured reservoirs is one of the challenges due to the generation of the complex fractures and the conductivity factor of fractures that affect fluids paths [15]. Although fractures covered 20% of world reserves, naturally fractured reservoirs represented the risk reservoirs in drilling, production, and modeling processes due to fracture pressure that sometimes-caused loss in hydrocarbons production [16]. Two studies were conducted to investigate the naturally fractured reservoirs functionally [11, 17]. Both studies relied on the modeling of the naturally fractured, double-connected system, which was divided into two areas, the matrix and the fracture. The authors concluded that the fracture is central to the permeability of hydrocarbons and that the fluid flows from the matrix to the fracture depending on the geometric parameters of the fracture such as permeability and porosity [18]. Li et al. [19] extended the study of fluid leakage in areas of tectonic stress. To examine this, the tectonic movements affected the fracture behavior, which causes losses in the fluids of low-permeability formations. This examined some of the factors affecting the leakage of fluids by making a model for analyzing the leakage of fluids in naturally fractured gas fields. Turn to Warren and Root [11], the authors have provided a suitable solution to this problem and were able to arrive at these parameters, the actual shape, dimensions, and fluid flow properties of the reservoir, where the same scenario had been adopted later in [20, 21].

Two quadruple porosity models (QPM) that include a triple-fracture network with a single matrix system were presented by Dreier et al. [22] for naturally fractured reservoirs (NFR). The pressure-transient features of QPM are analysed and evaluated using these models: Warren and Root theory with various forms of matrix-to-fracture flow regimes, wellbore storage, and skin are commonly employed in well-test analysis, and the parameters storativity ratio and interporosity flow coefficient are significant in describing such reservoirs. Perez Garcia [23] improved the earlier simulation-based investigations, relying mainly on the Warren and Root equations as well as the Gilman model. The author came to the conclusion that the well-test data was reliable but more investigations and development assumptions were required for fracture reservoirs.

In order to boost the productivity of naturally fractured reservoirs, acid fracturing procedures are used. The effectiveness of the therapy is influenced by a number of factors, including treatment circumstances and reservoir characteristics. It is possible to measure the effectiveness of acid fracturing stimulations using a variety of methods [24]. Only a few models, however, took into account the natural fractures (NFs) present in the hydrocarbon reservoirs [25], using an ML model. Hence, the goal of this work is to develop an effective model to calculate the efficacy of acid fracturing therapy in naturally fractured reservoirs. This study estimates the increase in hydrocarbon production brought on by the use of acid fracturing treatments and takes into account the interactions between naturally occurring and artificially generated cracks. The reservoir features and treatment parameters of more than 3000 scenarios were utilized to create and validate the artificial neural network (ANN) model [26]. The created model takes into account the formation permeability, injection rate, natural fracture spacing, and treatment volume as reservoir and treatment characteristics [27]. To evaluate the effectiveness of the model's prediction, the percentage error and correlation coefficient were also calculated. The performance of acid fracturing treatments can be predicted quite accurately using the proposed model. The testing datasets yielded a correlation coefficient of 0.94 and a percentage error of 6.3%.

A novel ML model based on an improved learning process was established to offer a precise and timely forecast for increased productivity [28]. In order to assess the validity of the new equation, validation data were employed. A 6.8% average absolute error and a 0.93 correlation coefficient were obtained, demonstrating the excellent dependability of the suggested correlation. The originality of this work is in creating a solid and trustworthy model to forecast productivity gains from acid fracturing in naturally fractured reservoirs. By offering quick and accurate calculations, the novel correlation can be used to enhance the treatment design for naturally fractured reservoirs [29]. In order to

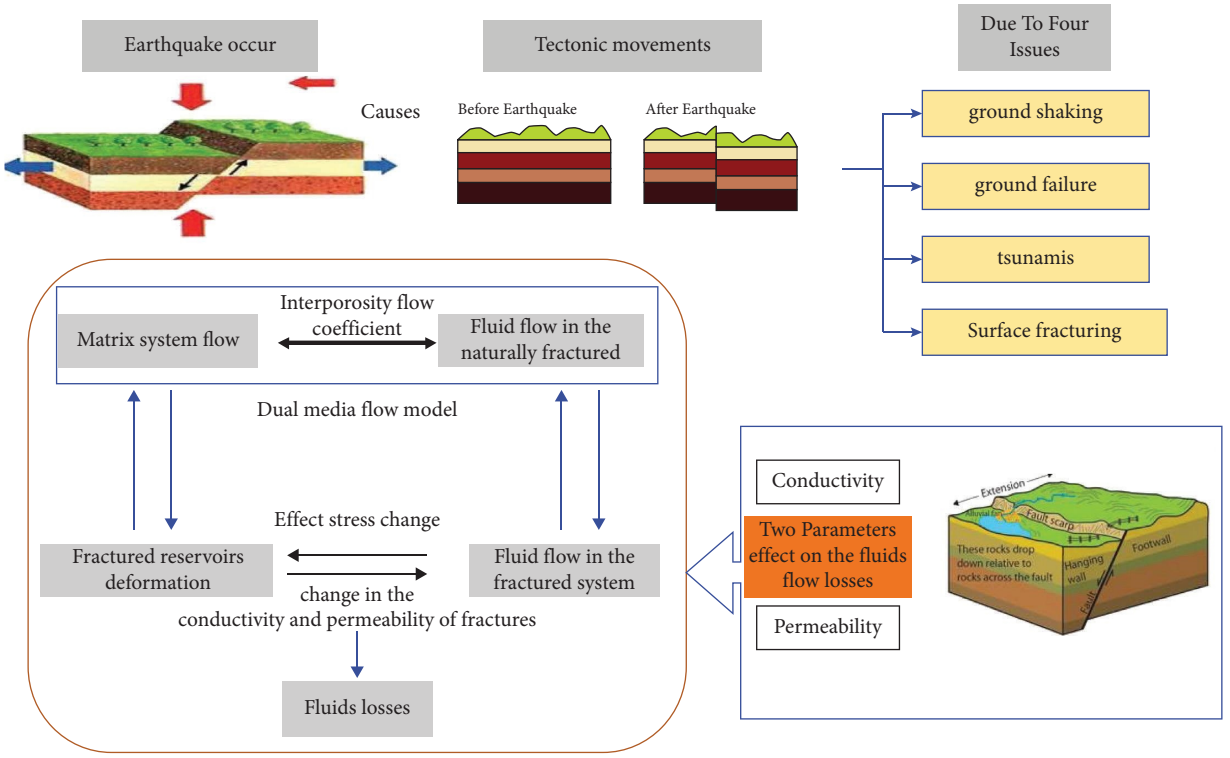

Figure 1: Fluid flow losses in the naturally fractured reservoirs.

estimate fracture permeability under complex physics, an integrated workflow based on the ML model was proposed (e.g., inertial effect) [30]. The methodology is being used for the first time to scale up rocks [31]. The suggested model provides a practical and accurate replacement for conventional upscaling techniques that can be quickly integrated into workflows for reservoir characterization and modeling.

Analysis of pressure-transient well tests is a crucial technique for figuring out reservoir properties [32]. Due to the analysts' inexperience, the validity of the data from the well-test analysis could be questioned [33]. A one-dimensional convolutional neural network (1D CNN) was tested to create an autonomous model for well-tested data interpretation [34]. Both the associated parameters and the type of curve can be automatically identified by the model [35]. Without adjusting the model architecture or using hyperparameters, a combined automatic interpretation model with four conventional well-test models were conducted. According to the findings, the 1D CNN model outperformed the ANN model. Three field cases are used to further validate the automatic interpretation model. Based on the reported literature review, the current research was inspired to develop a new methodology based on a soft computing model that is associated with theoretical study in the conditions of simulation data as well as being specialized based on the assumptions [36]. Our paper focuses to solve the fluids losses problem by modeling the fluids flow in the fractured reservoirs through using machine learning technique. This paper depends on the two parameters which are interporosity flow coefficient and storativity ratio to determine the fluid flow behavior.

1.3. The Objective of This Study. The previous studies used empirical methodologies and modern models such as ML models for diverse oil and gas datasets. This leads to the continuous issue in fluid flow paths due to the changes of the fracture's characteristic such as high conductivity and permeability of fractures. In conjunction with modern technology, the aim of this research is to make use of the applicability of ML models for predicting the shape factor and the fracture porosity. The models evaluated the fluid flow in the naturally fractured reservoirs. Predictive models were established using five different related input parameters. The assumption of the characteristics of the oil and gas datasets allows the ML models to build more than one model for the same datasets and compare them to get the best two models. The expected research outcome is to develop a reliable alternative technology for the petroleum industry where it can participate in sustainability and management.

2. Data Descriptions

This study specializes in analyzing the fluid flow behavior in naturally fractured reservoirs during production. The actual data consist of oil and gas data were obtained from Texas field. The actual data take account of the matrix permeability, fracture permeability, wellbore radius, interporosity flow coefficient, and the storativity ratio as inputs while the fracture porosity as outputs. To accomplish that, the study changed the input and output of Texas field data such that storativity ratio, interporosity flow coefficient, matrix permeability, fracture permeability, and wellbore radius are input data, while the shape factor and fracture porosity are output data. The conditions of input and output data were

put as temperature 150 Fahrenheit, pressure 3,626 psi, and matrix porosity 22% for oil and 15% for gas, radius 1,000 ft, where these conditions are the same as Texas field's conditions with some changes in the assumptions [23]. These data are implemented on the basis that the flow is radial, taking into account that there is no Darcy's law and no skin factor [37].

3. Machine Learning Methods

This section presented the utilized ML models adopted for fluid flow data simulation. ML models are built to describe the effect of the shape factor and the fracture on the treatment of the hydrocarbon's leakage. Five different types of ML models were developed, including decision tree regression, random forest regression, LASSO regression, K-N neighbors' regression, and ridge regression models. Figure 2 presented the flowchart of the conducted methodological mechanism for this study.

3.1. Decision Trees Model. Decision tree regression (DT) was developed by [38] as a powerful ML model for both classification and regression tasks [39, 40]. In the DT algorithm, features (extracted from a specific dataset) are arranged in a symbolic tree-shaped manner, with terminal and internal nodes representing leaves and splits, respectively [41]. A tree is shaped by following a set of fundamental principles. Multiple trees are combined to form a set of rules that can be used in the prediction step. The technique first builds a tree from the training dataset, after which it splits the original data into two branches using a binary split procedure. The new growth branches are subjected to the separation process, and this is continued when a new branch becomes inseparable, and the accompanying node achieves the minimum size and evolves into a terminal node [42]. DTR's principles are easy to understand and follow a logical pattern that can be described as a tree; this is a significant advantage of the DT over other models. However, despite being quicker than other AI models, DTR frequently is not the right choice for time-series problems [43] because it frequently does not generate accurate results when there are issues of nonlinearity or noisy datasets.

3.2. Random Forest Model. Random forest model was first developed by [44], and since its introduction, it has been used widely in many fields of science and engineering for prediction purposes [45–47]. The RF model is strongly advised for scenarios with numerous input variables. Regarding a random vector, RF is an individual uniform distribution to each tree in the forest. Although RF is preferred when the trees, *eta*, and *mtry* are of an appropriate size, the maximal depth can be adjusted according to the complexity of the data [48]. The RF model in this study was built using *library (random forest)*. The significant hyperparameters, such as *ntree*, *eta*, *max depth*, and *mtry*, were set to 140, 4, 6, and 2 accordingly in order to reduce overfitting issues. When regression trees are built using distinct bootstraps for each tree, the potential features in those trees can be modeled using such algorithms [49]. For the purposes of predicting the targeted parameters, every tree in the forest was treated equally. The first set was utilized for the growth of the trees and then for the assessment of each tree's classification error [50]. The RF prediction's output is represented thus,

$$y = \frac{1}{n_{\text{tree}}} \sum_{i=1}^{n_{\text{tree}}} y_i(x), \tag{1}$$

where y = the average prediction output from the overall number of trees and $y_i(x)$ = the trees' discrete prediction for output vector x. Model overfitting was avoided by using the ten-fold cross-validation procedure thrice. The tree was initially built for each predictor and was then followed-up with its growth to ensure optimal weight and minimal computed error. The significance of the predictors, as well as the self-adjusted growth of the selected trees, must be ranked using the RF approach. The RF model performed well across all the response predictors based on the employed performance indicators.

3.3. K-Nearest Neighbor Regression Model. The KNR classification was developed as a relatively new technique for the parametric estimation of unknown probabilities [51]. The KNR was mainly built for classification patterns with an understanding of the K-nearest neighbor rule [52]. The KNR concept relies on the distance between the distributions to categorize each piece of data that contains the majority of nearest neighbors [53]. The prediction process of KNR depends on the use of classifiers and regression, wherein the regression aspect uses previously processed data to predict future data. Statistical methods, such as linear regression, are typically used to process the regression; however, the use of the linear regression method is limited only to some databases. This study implemented regression for the prediction of the fracture porosity and the shape factor based on gas and oil filled data observations. The problem with regression is predicting the result of a preprocessed parameter using a certain collection of independent variables. The result can be expressed as $G = G_n$ if the KNR is performed using n nearest neighbors. Then, the average of the results is used to determine the outcome. The solution will then be given as

$$G = \frac{G_n}{2}. \tag{2}$$

At that point, KNR prediction initiates the outcome of the neighbor, and prediction can be done by determining the Euclidean distance (ED) between the case point and the query based on the existing dataset.

$$D(z, q) = \sqrt{(z - q)^2}, \tag{3}$$

where z represents the query point and q represents the case point from the existing dataset.

3.4. Ridge Regression Model. In conditions whilst linearly impartial variables are closely correlated, RR model is a way of calculating the coefficients of a couple of regression fashions [54]. It has been applied in different engineering

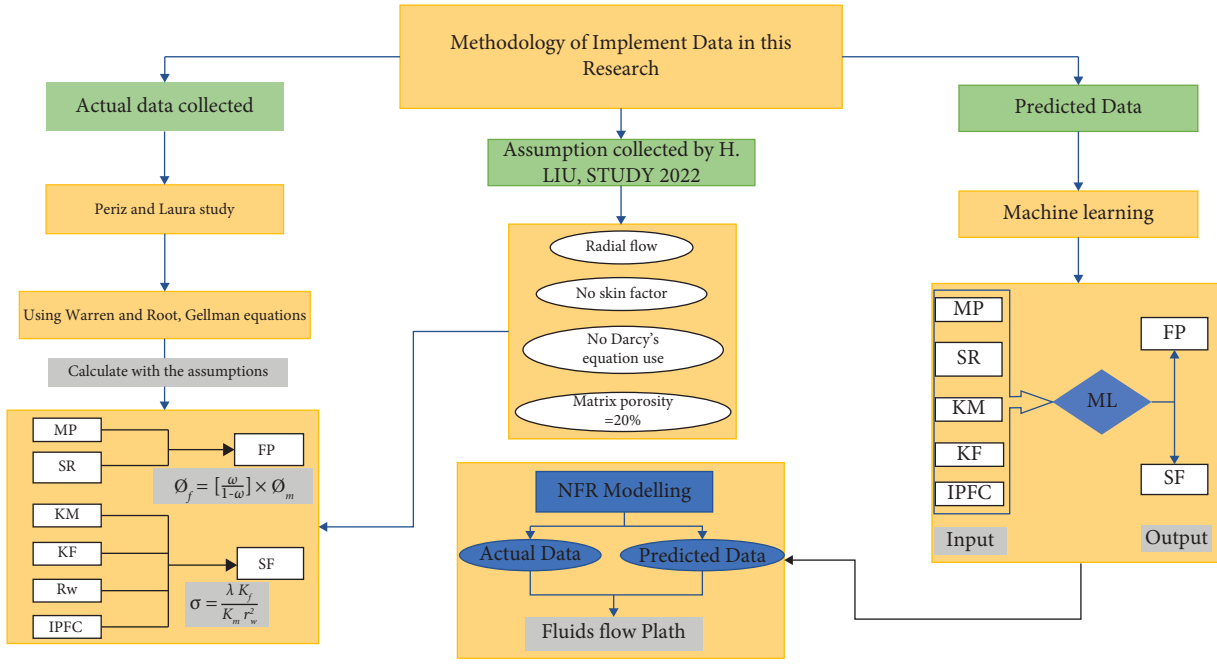

Figure 2: Methodology of databases modeling application.

and science domains and approved for its capacity. Amongst different areas and patterns of the RR model, equations are presented as follows [55]:

$$\widehat{B} = (X^T X)^{-1} X^T y, \tag{4}$$

where X^T is the transpose of X. By contrast, the ridge regression estimator to evaluate $(\widehat{B})$ the fracture porosity.

$$M_{\text{ridge}} = \left(X^T \widehat{X} + KIp\right)^{-1} X^T y, \tag{5}$$

where Ip is the $p \times p$ identity matrix, and $K > 0$ indicates a large number. The form along the diagonal of I is known as a ridge.

3.5. Lasso Model. Lasso is a commonly used sparse regression technique that relies on the sparse assumption for parameter regularization [56]. It is an innovative method for variable selection during regression tasks that operates by minimizing the residual sum of squares under the condition that the sum of absolute values of the coefficients is less than a constant [57]. It was first discussed in relation to least squares. The following is a summary of the basic Lasso framework. Assume a sample of N cases with p variables and a single outcome for each of the N instances. Consider that y_i is the response variable while $x_i = (x_1, x_2, x_3, \ldots, x_{np})$. T represents the covariate vector for the i^{th} case, $\beta = (\beta_1, \beta_2, \ldots, \beta_p)^T$. Hence, Lasso is aimed to solve the regression problem using nonlinearity functional properties.

4. Results and Discussion

In this section, the results of the adopted ML models were presented based on the radial flow in the fluid modeling of fracture reservoirs. Radial flow was concerned with the analysis of the flow of fluids along a radius. The volume for the wellbore radius is not large enough to cover the modeling of an entire well by ML models. The present results provide a slight improvement over the previous results of the data provided by Perez [23].

One of the most popular graphical presentation on the predictability evaluation is the scatter plot between the actual observations and the predictive models results, which was adopted here for assessment. All models were developed based on the predictability and interoperability of fluid flow losses. The modeling results for the DT model for the gas flow were reported in Figure 3 (Figure 3(a): fracture porosity, and Figure 3(b): shape factor). The DT model attained a determination coefficient ($R^2 \approx 0.80$) for fracture porosity and $R^2 \approx 0.94$ for the shape factor. This was formed in harmony with the established previous research of [23]. The modeling of Perez's data is assumed to be actual if our results build on the predicted data. On the other hand, the results for the oil flow characteristic are given in (Figure 4(a): fracture porosity ($R^2 \approx 0.93$) and Figure 4(b): shape factor ($R^2 = 0.94$)).

In the same manner, the scatter plots for the other ML models are (i.e., RF "Figure 5: gas flow and Figure 6: oil flow," KNR "Figure 7: gas flow and Figure 8: oil flow," RR "Figure 9: gas flow and Figure 10: oil flow" and Lasso "Figure 11: gas flow and Figure 12: oil flow"). The superior prediction accuracies were observed for the gas flow fracture porosity using the Lasso model over the testing phase with ($R^2 \approx 0.97$). However, gas flow shape factor prediction achieved using KNR ($R^2 \approx 0.96$). It is true that all models relative accomplished their results over ($R^2 = 0.85$) as an indicator for acceptable results. However, the motivation here is to target the more accurate model which is relatively near to the factual field observations with $R^2 \approx 1$. For the oil flow, the fracture porosity and shape factor were predicted accurately using the Lasso model.

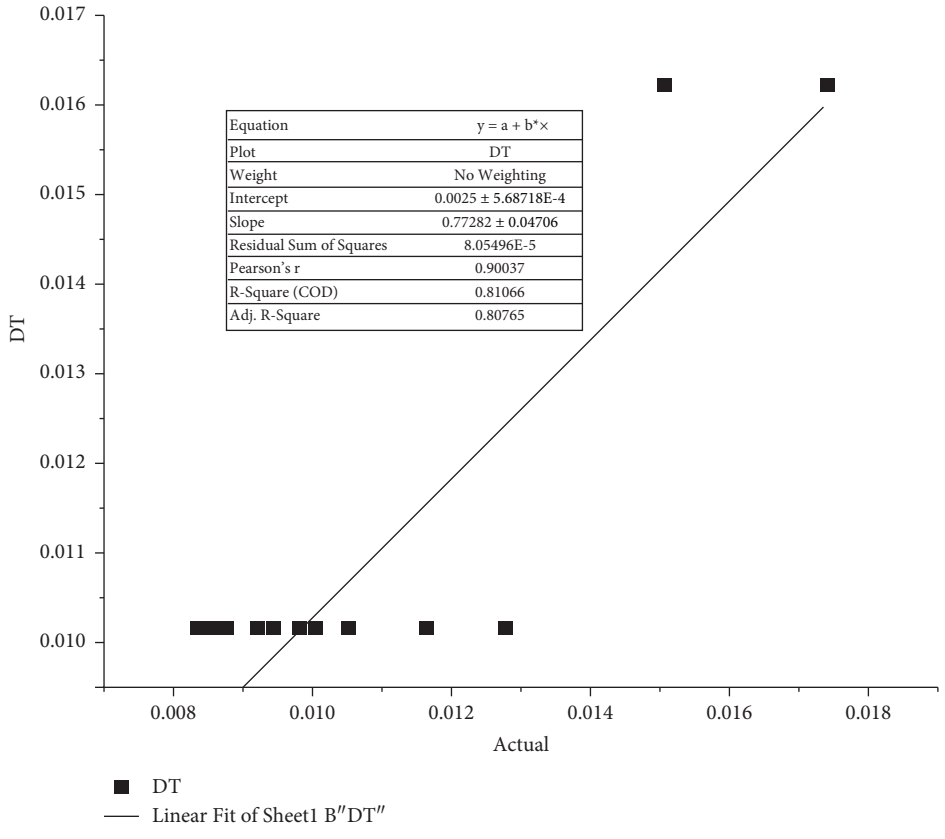

(a)

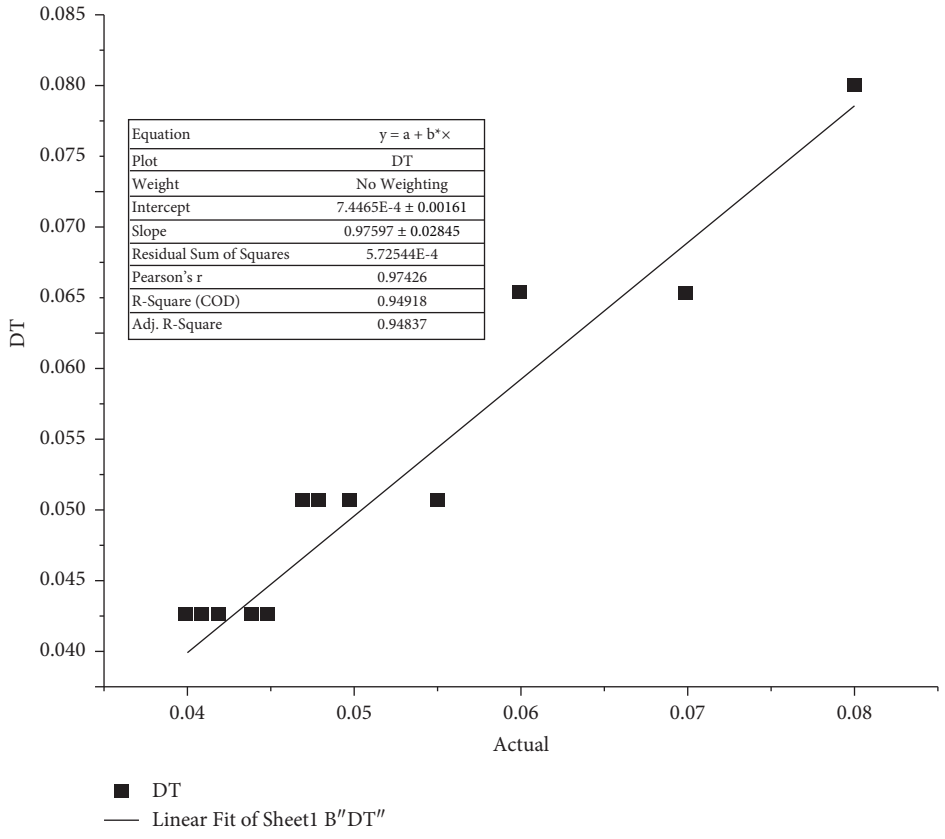

(b)

Figure 3: The decision tree model scatter plots for the testing phase of the gas flow: (a) fracture porosity and (b) shape factor.

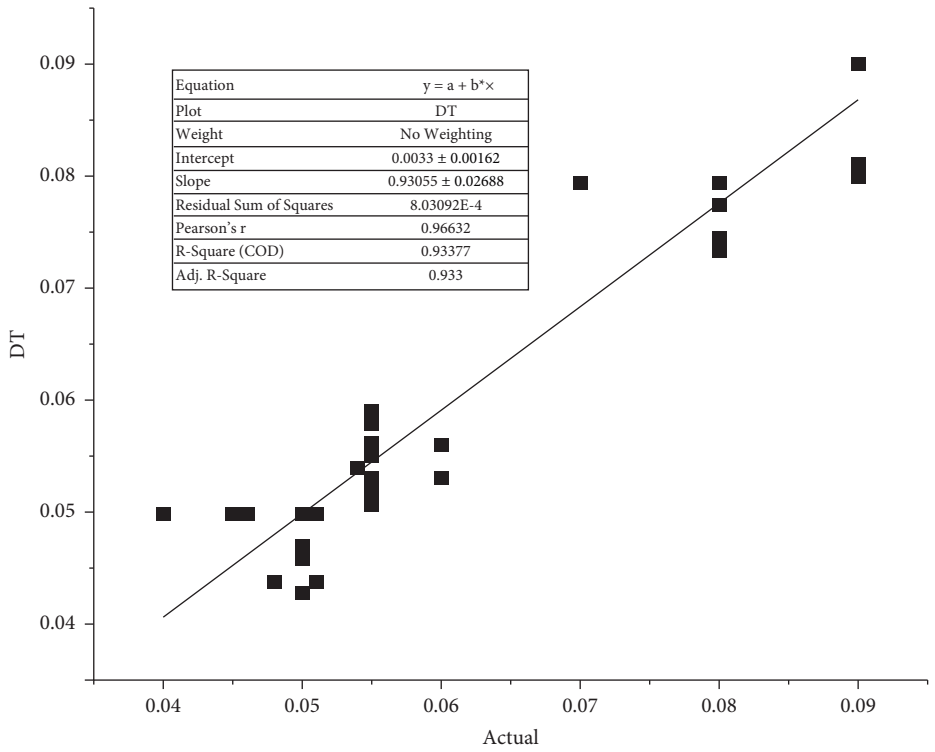

(a)

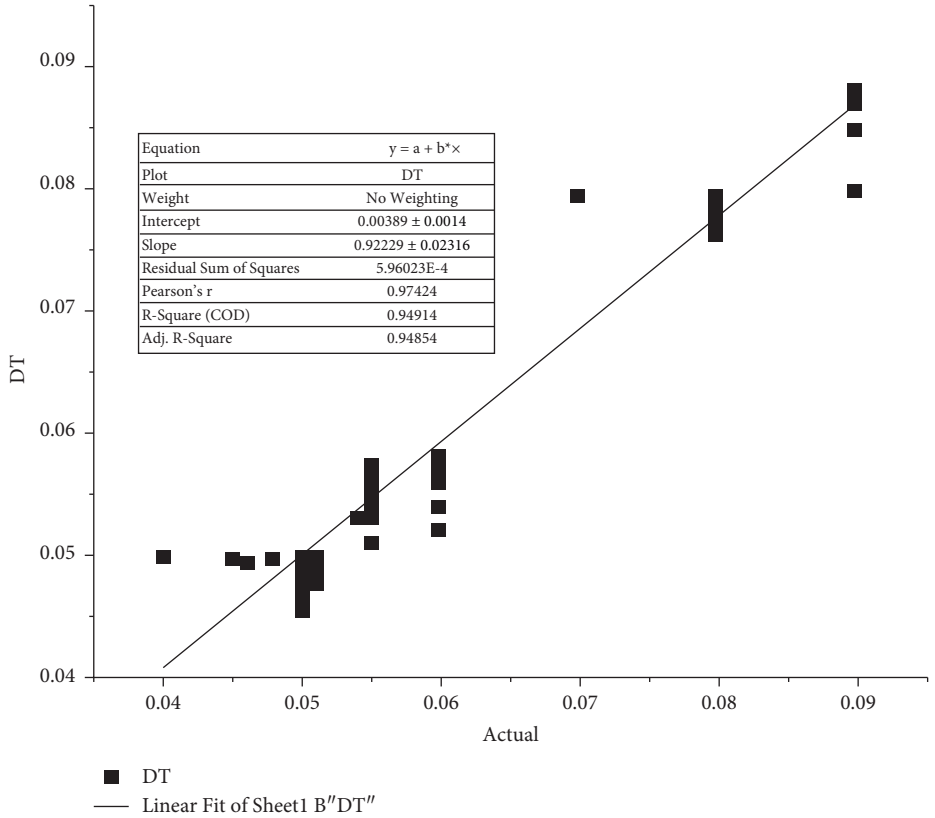

(b)

Figure 4: The decision tree model scatter plots for the testing phase of the oil flow: (a) fracture porosity in oil system and (b) shape factor.

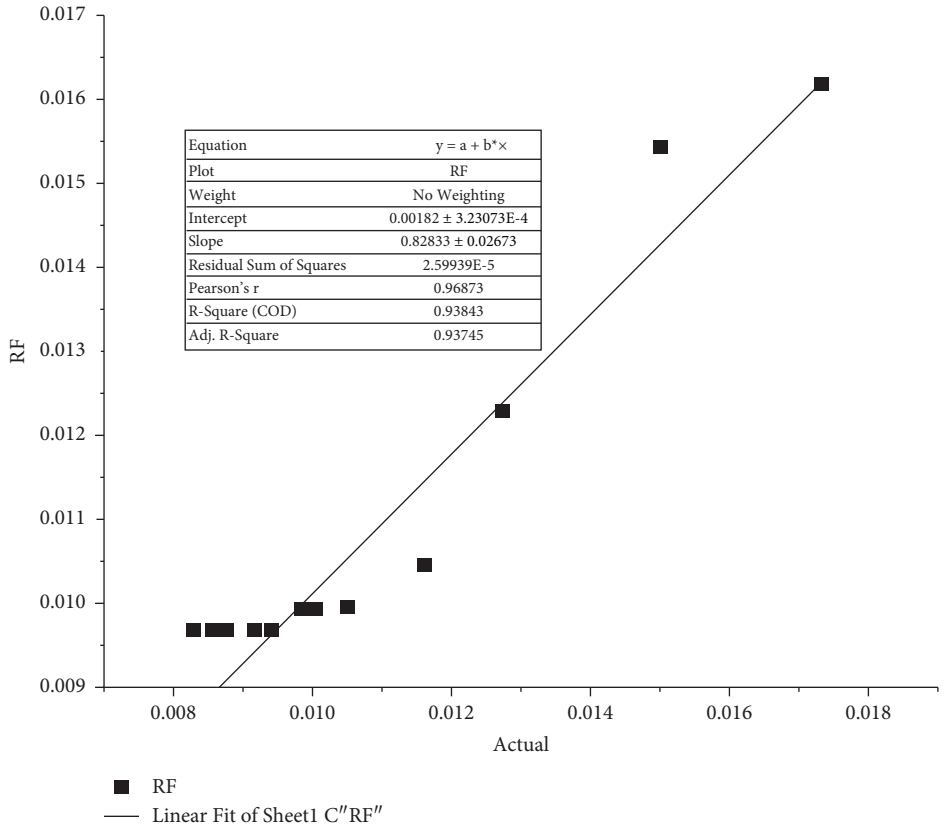

(a)

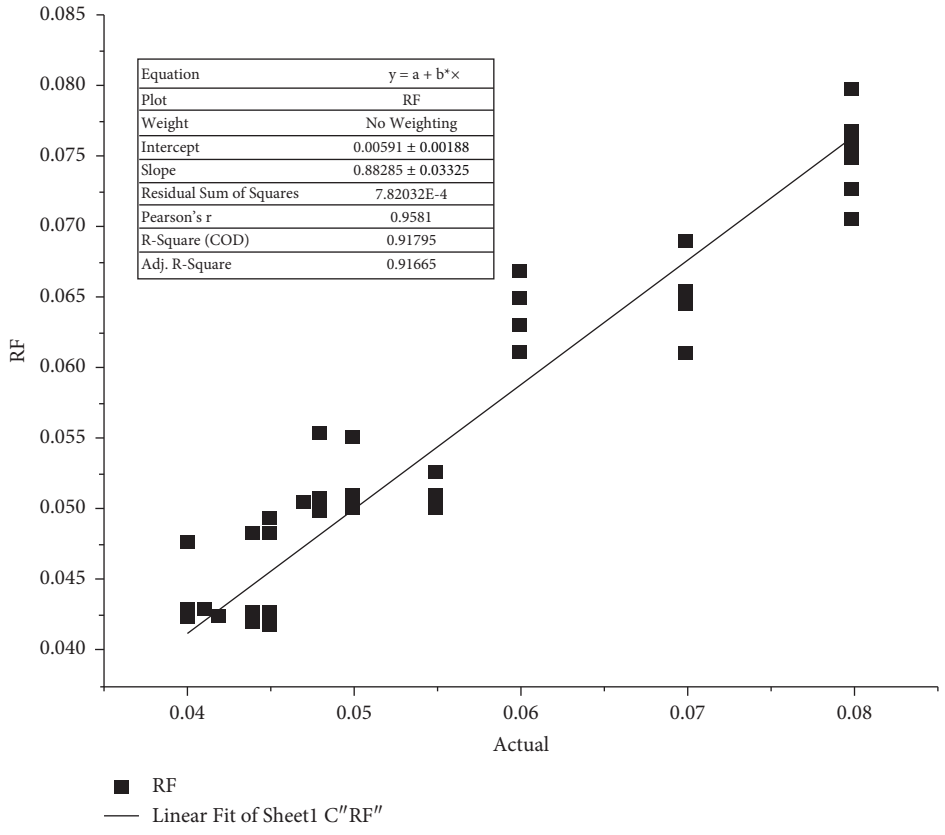

(b)

Figure 5: The random forest model scatter plots for the testing phase of the gas flow: (a) fracture porosity in oil system and (b) fracture porosity.

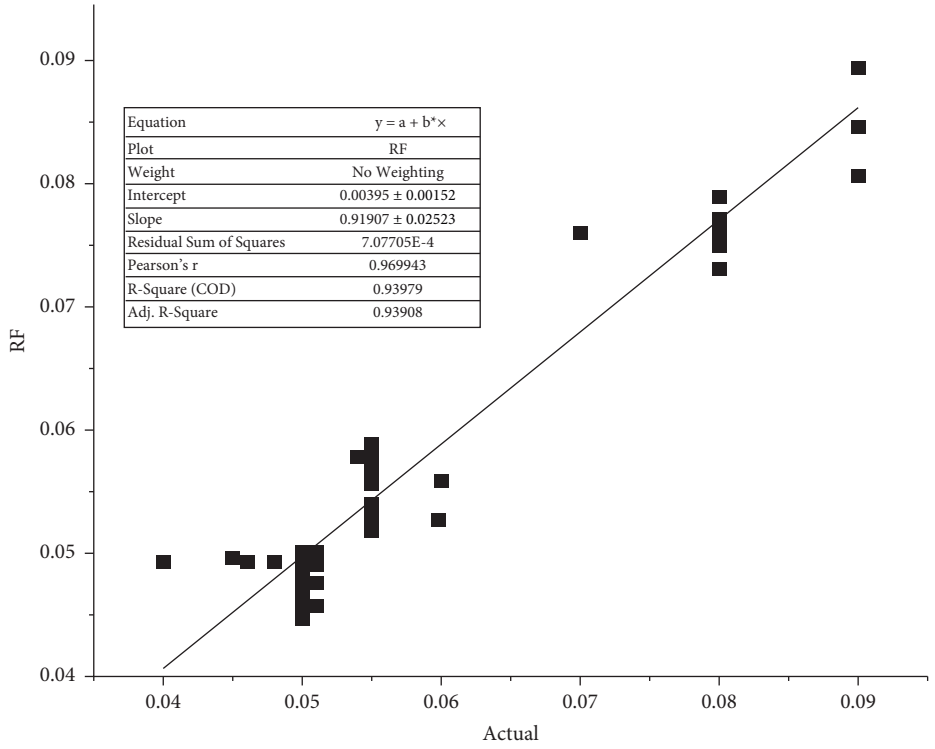

(a)

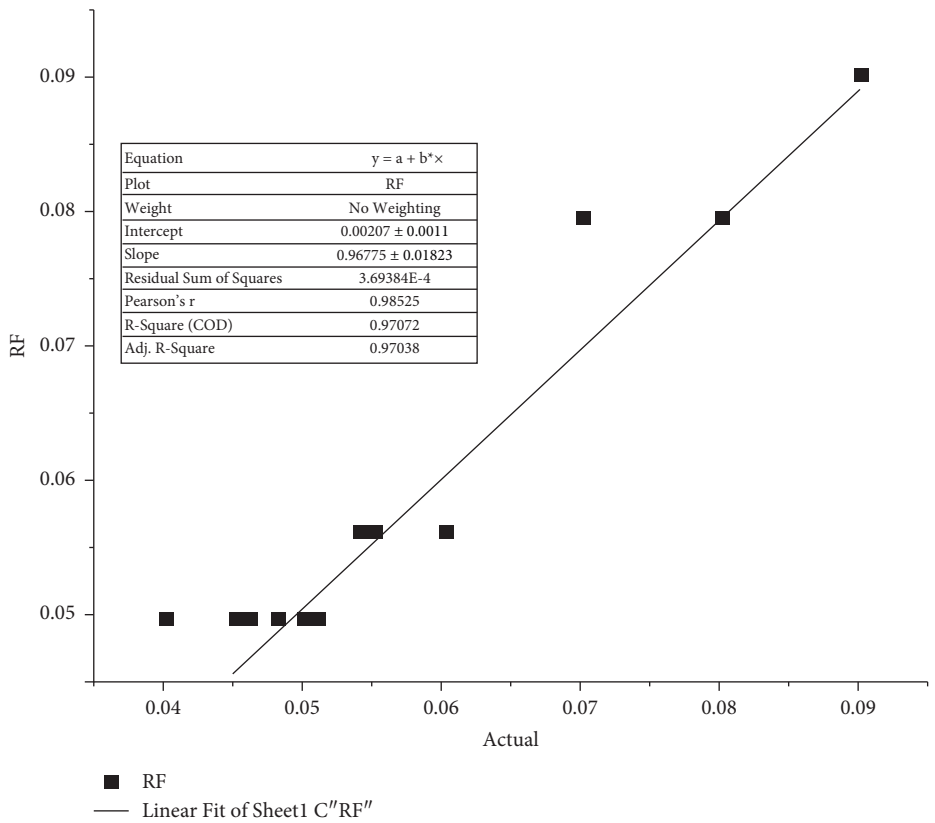

(b)

Figure 6: The random forest model scatter plots for the testing phase of the oil flow: (a) fracture porosity in oil system and (b) shape factor.

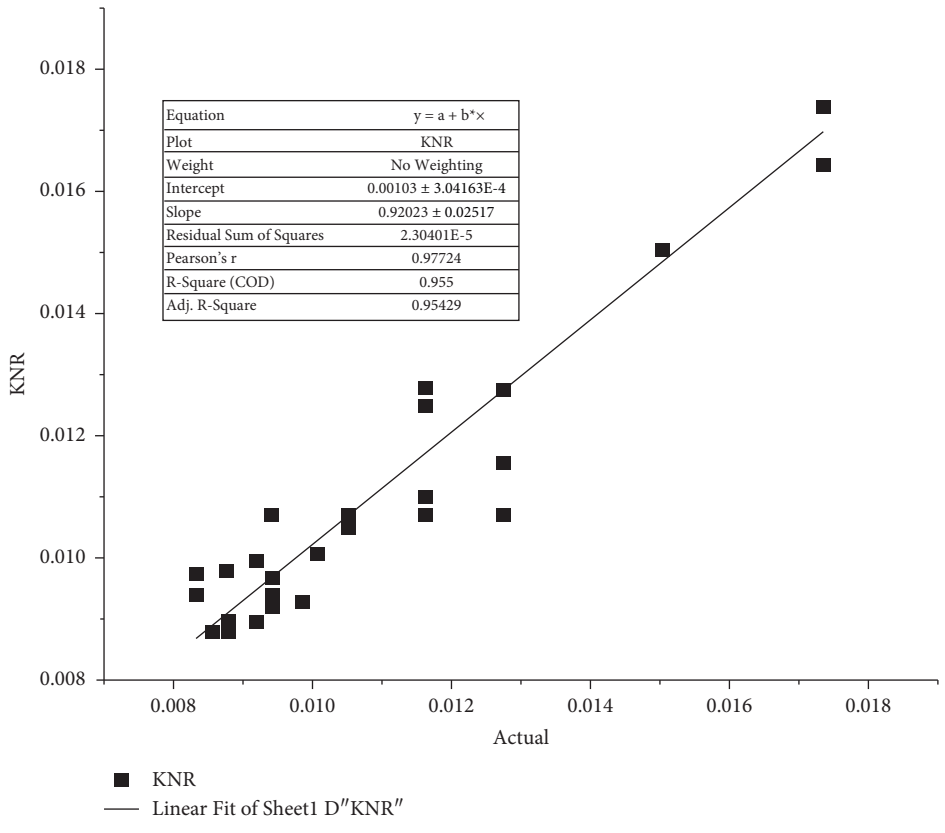

(a)

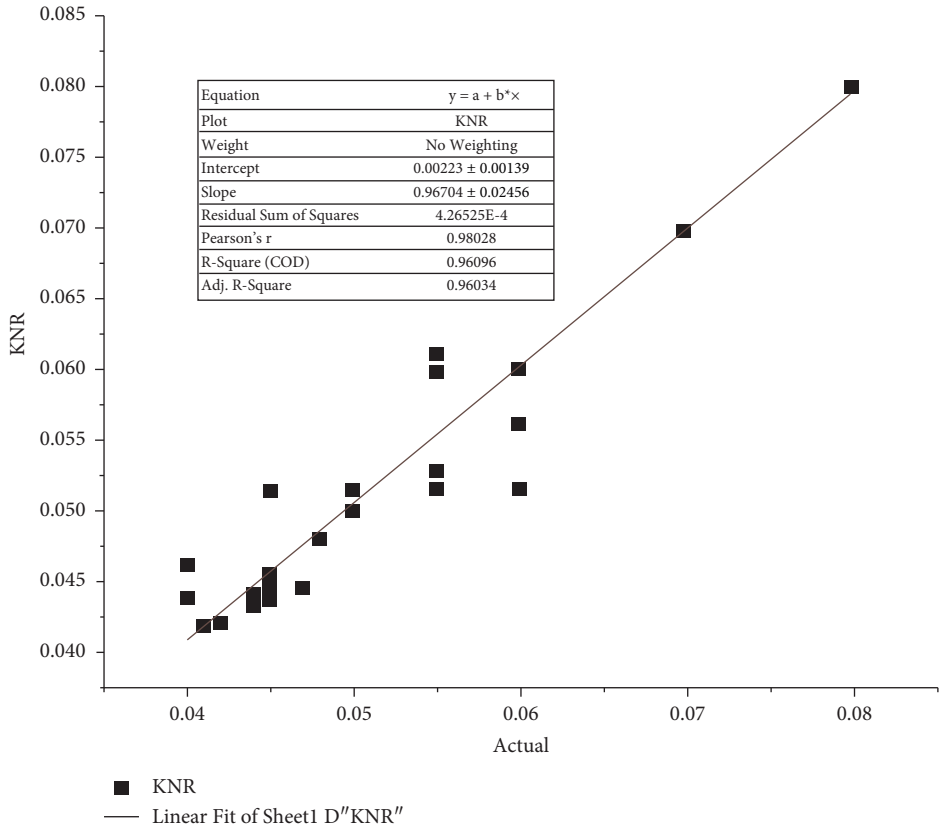

(b)

Figure 7: The K-nearest regression model scatter plots for the testing phase of the gas flow: (a) fracture porosity in oil system and (b) fracture porosity.

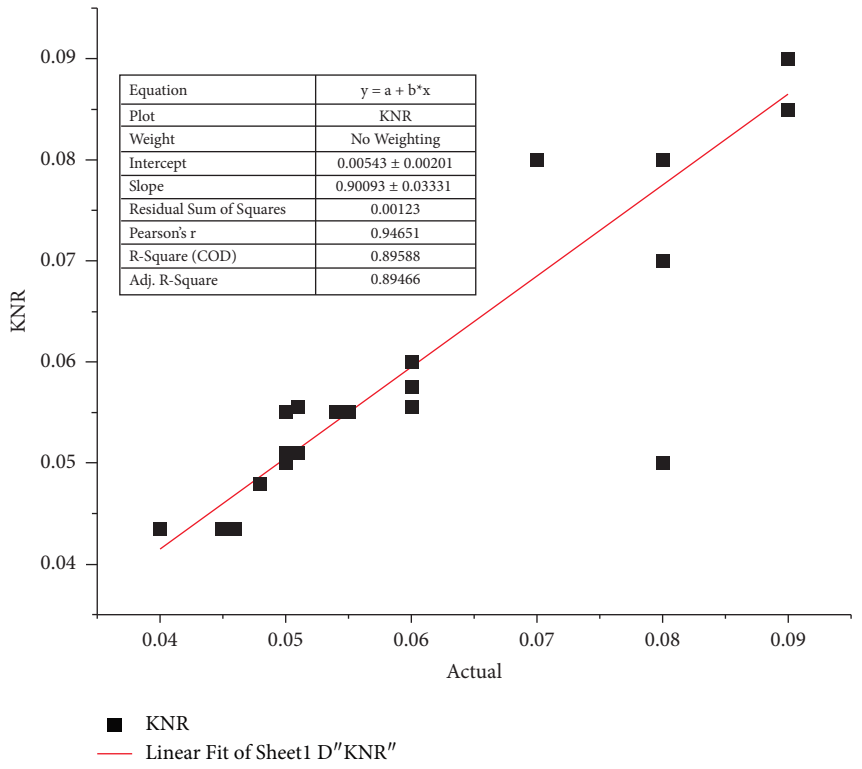

(a)

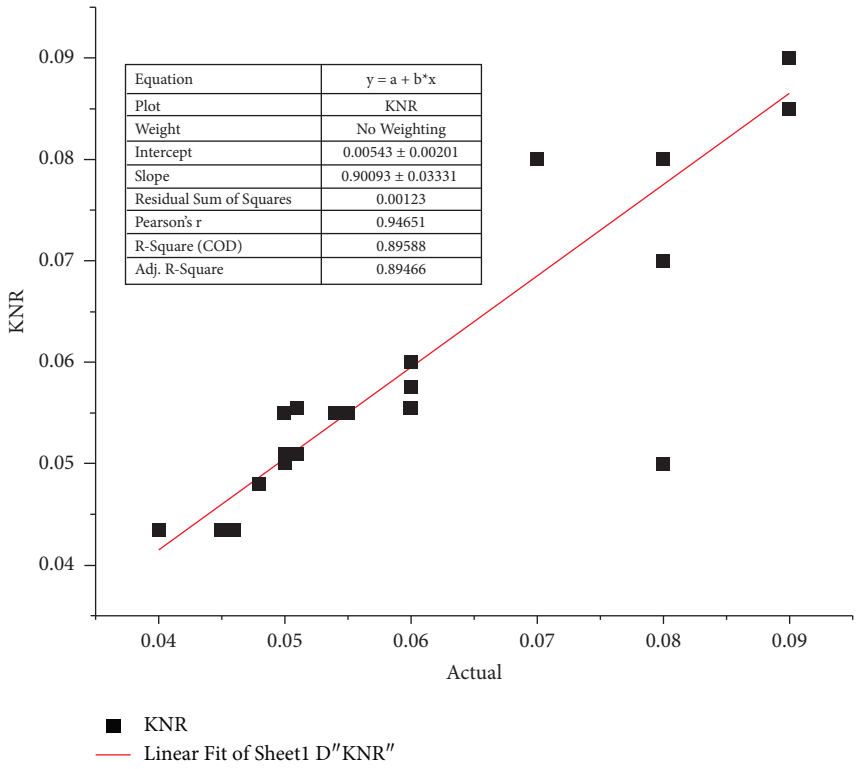

(b)

Figure 8: The K-Neighbor regression model scatter plots for the testing phase of the oil flow: (a) fracture porosity and (b) shape factor.

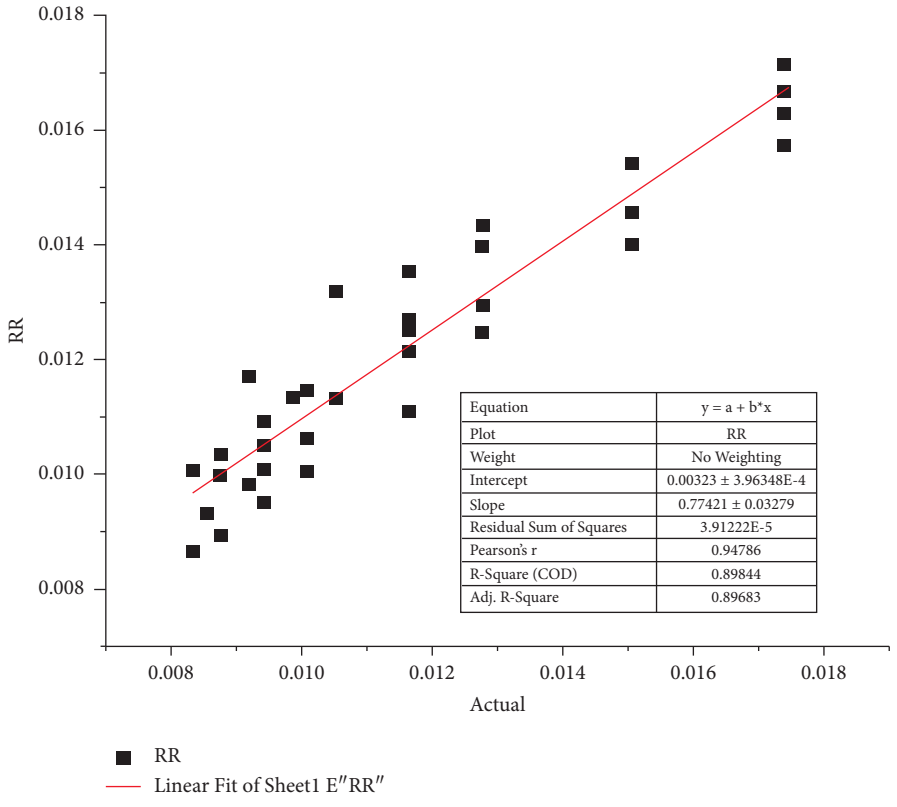

(a)

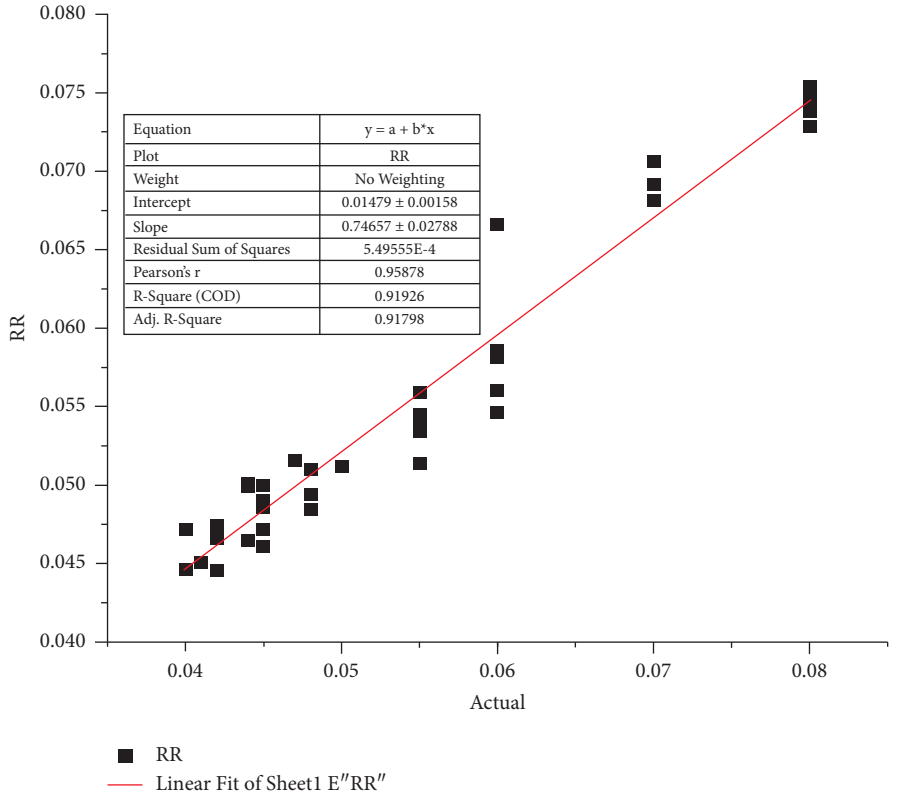

(b)

Figure 9: The Ridge regression model scatter plots for the testing phase of the gas flow: (a) fracture porosity in oil system and (b) fracture porosity.

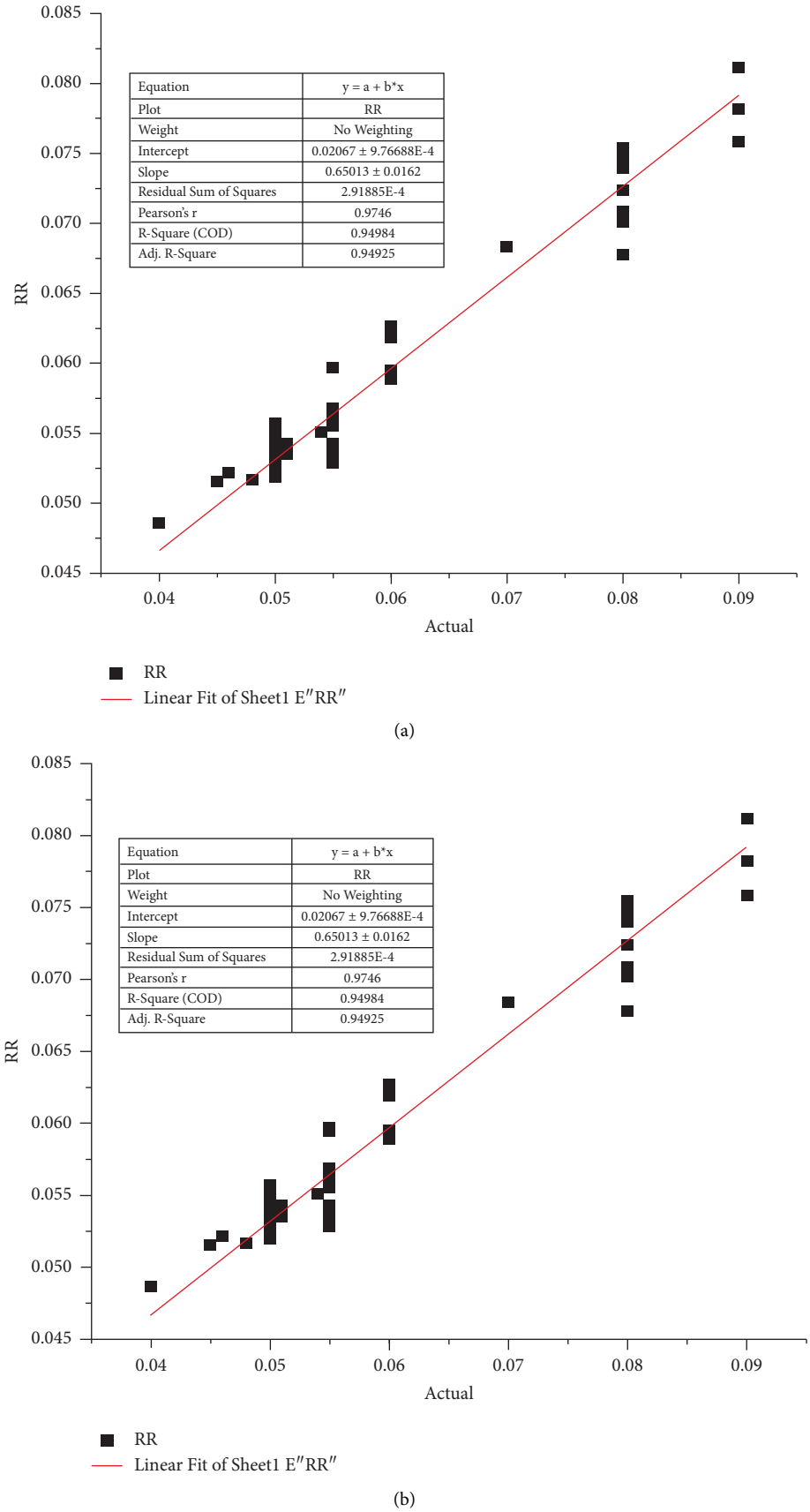

Figure 10: The Ridge regression model scatter plots for the testing phase of the oil flow: (a) fracture porosity and (b) shape factor.

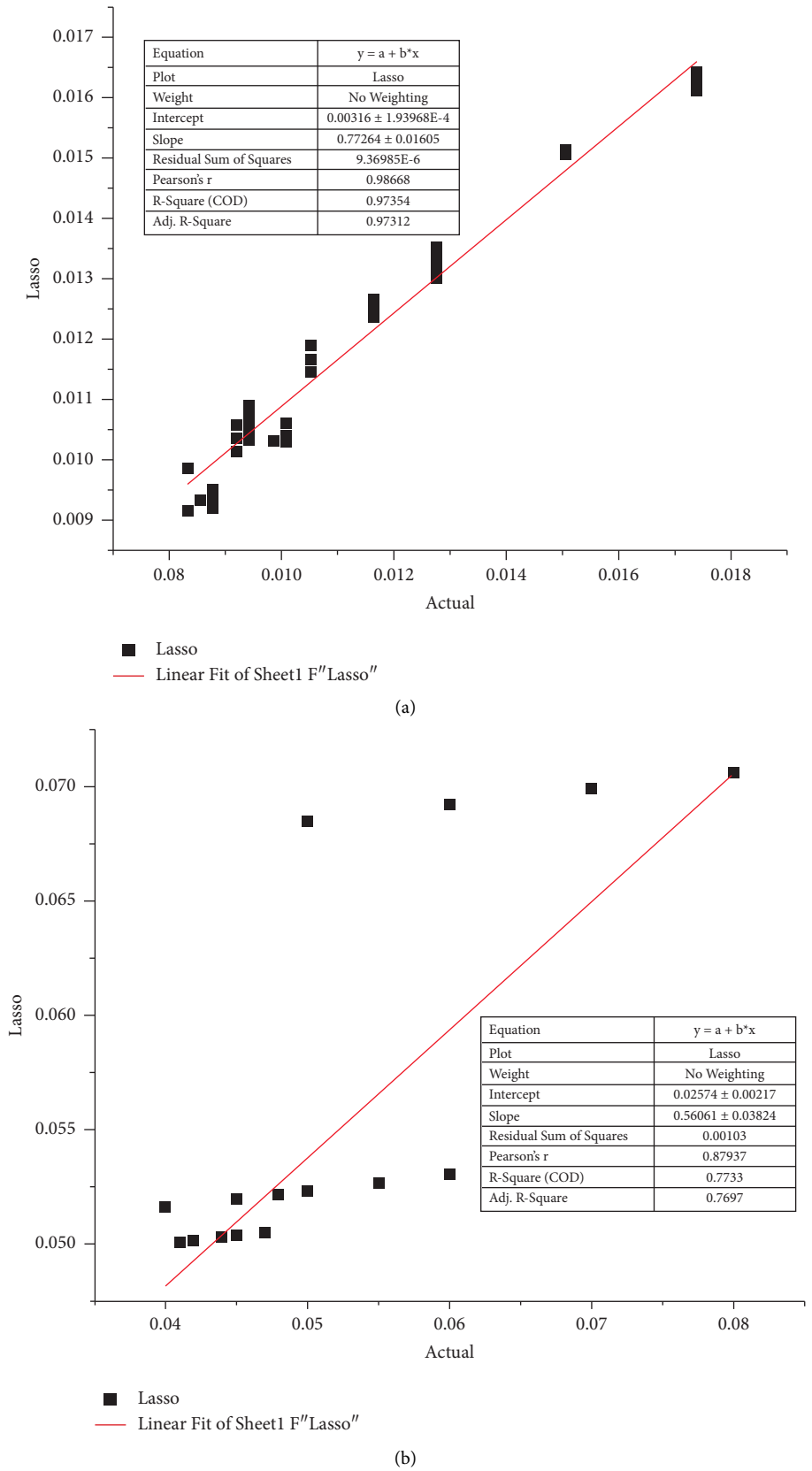

Figure 11: The Lasso model scatter plots for the testing phase of the gas flow: (a) fracture porosity in oil system and (b) fracture porosity.

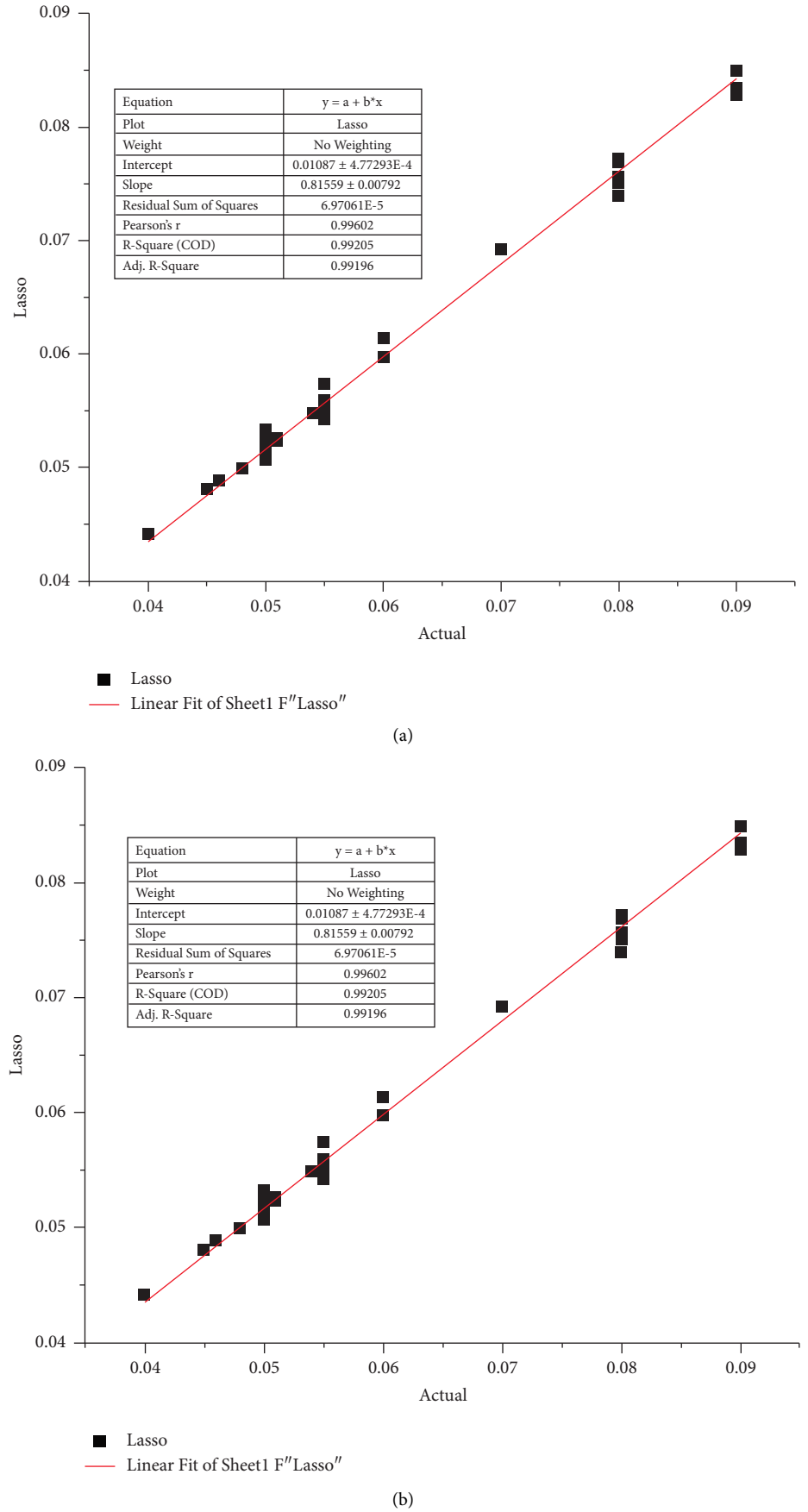

Figure 12: The Lasso model scatter plots for the testing phase of the oil flow: (a) fracture porosity and (b) shape factor.

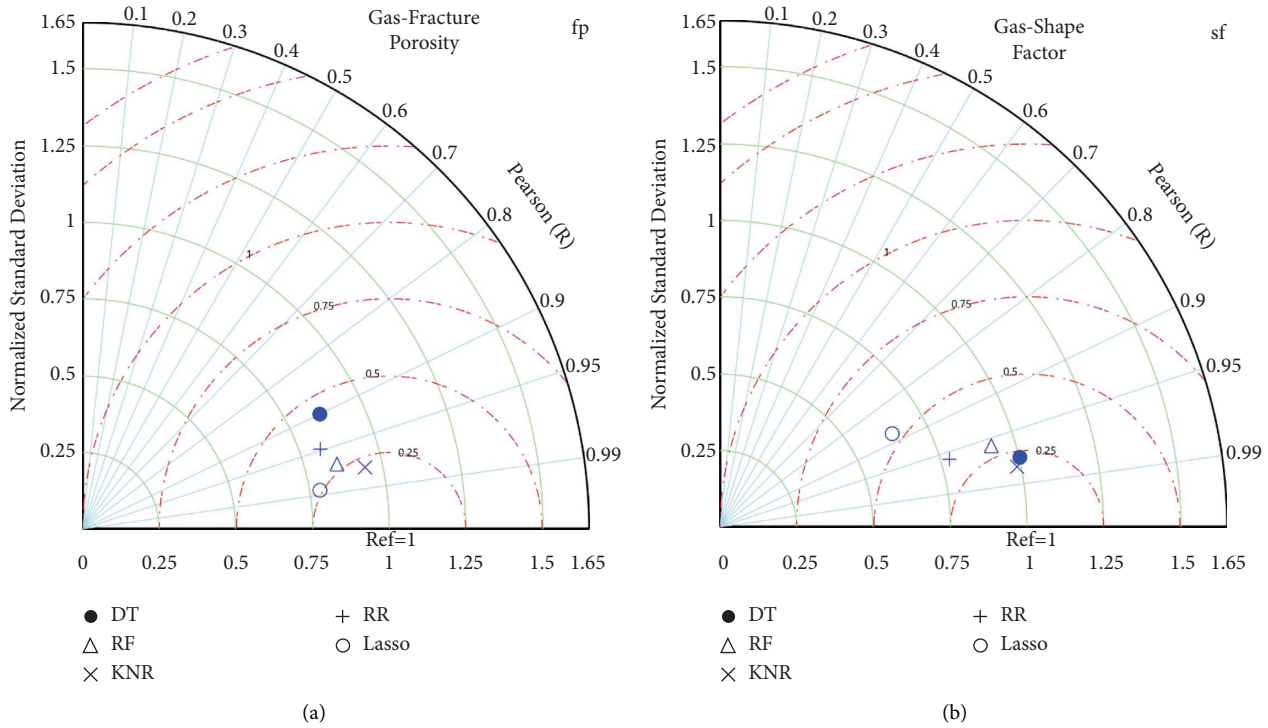

Figure 13: Taylor diagram presentation for the gas flow fracture porosity and shape factor prediction using different machine learning models.

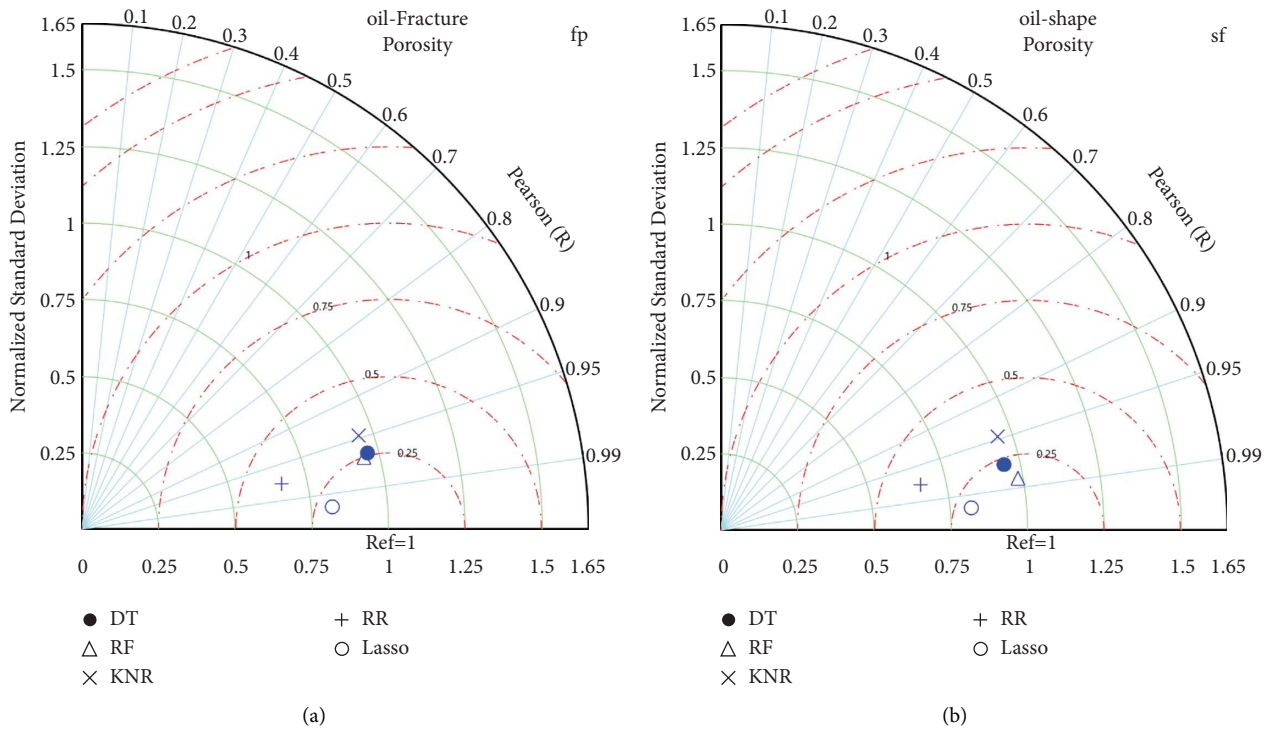

Figure 14: Taylor diagram presentation for the oil flow fracture porosity and shape factor prediction using different machine learning models.

Table 1: The calculated performance metrics for the gas flow fracture porosity over the testing phase.

Model	R^2	KGE	RMSE	MAPE (%)
DT	0.811	0.826	0.001	10.1
RF	0.938	0.851	0.001	6.4
KNR	0.955	0.937	0.001	4.1
RR	0.898	0.803	0.001	8.9
Lasso	0.974	0.779	0.001	7.7

Table 2: The calculated performance metrics for the gas shape factor over the testing phase.

Model	R^2	KGE	RMSE	MAPE (%)
DT	0.949	0.972	0.003	4.7
RF	0.918	0.91	0.004	5.8
KNR	0.961	0.975	0.003	2.8
RR	0.919	0.774	0.004	6.7
Lasso	0.773	0.617	0.007	11.7

Table 3: The calculated performance metrics for the oil fracture porosity over the testing phase.

Model	R^2	KGE	RMSE	MAPE (%)
DT	0.934	0.948	0.003	3.7
RF	0.94	0.938	0.003	4.1
KNR	0.896	0.927	0.004	1.9
RR	0.95	0.666	0.005	5.8
Lasso	0.992	0.819	0.002	3

Table 4: The calculated performance metrics for the oil shape factor over the testing phase.

Model	R^2	KGE	RMSE	MAPE (%)
DT	0.949	0.94	0.003	3.5
RF	0.971	0.977	0.002	2.3
KNR	0.896	0.928	0.004	1.9
RR	0.95	0.666	0.005	5.8
Lasso	0.992	0.819	0.002	3

It is even better to explore more logical and scientifically acknowledged graphical presentation of the developed ML models [58]. A graphical based on root mean square error (RMSE), correlation, and standard deviation was generated in Figures 13(a) and 13(b) "gas flow presented in the form of fracture porosity and shape factor" and Figures 14(a) and 14(b) "oil flow presented in the form of fracture porosity and shape factor." Based on Figure 13(a), the KNR model presented the closest coordinate to the actual observation of gas flow fracture porosity. However, the prediction of gas flow shape factor was visualized using DT and KNR "relatively close coordinates" (Figure 13(b)). In Figure 14(a), Lasso models indicated nearer location for the fracture porosity; on the other hand, both models Lasso and RF showed relatively closer prediction performance for the shape factor of the oil flow (Figure 14(b)).

The modeling results further assessed using some statistical metrics based on the perfect fit of goodness (i.e., determination coefficient (R^2) and Kling–Gupta efficiency (KGE)) and absolute error indicators (i.e., root mean square error (RMSE) and mean absolute percentage error (MAPE)) [59]. Tables 1 and 2 reported the modeling results for the gas flow fracture porosity and shape factor, respectively. By examining all the performance metrics of the Table 1, it clearly appears that performing more than two or more statistical indicators can give more informative results of the adopted ML models. Although the Lasso model revealed the superior correlation value, the KNR model gave the minimal value for the MAPE metric in which by validating with KGE metric, it is clearly a valid model for prediction superiority for the fracture porosity of gas flow. On the other hand, Tables 3 and 4 presented the modeling results of the oil flow fracture porosity and shape factor, respectively. Over the testing phase, the KNR model reported the best modeling results for the fracture porosity and shape factor prediction based on the multiple metrics evaluation.

Based on the performance metrics in Tables 1–4, modeling superiority for the attained prediction results distributed between RF, KNR and Lasso models. Indeed, this is a factual thing for the ML models behavior through the learning process in which depending on the how much capacity can be attained during the learning mechanisms of the models. This can be elaborated also due to the distribution of the fracture points in one line which prove that the fracture conductivity factor has a big impact oil than gas [60]. Generally, the radial flow is distributed as parabolic that points of fluids spread systemically due to the shape factor in gas flow [61].

5. Conclusions

Reliably predicting distributed fluids flow in the naturally fractured reservoirs is achievable using ML models applied to a group of oil and gas datasets of Texas field calibrated with the fracture porosity and shape factor data. The fracture porosity and shape factor respond to the distinct characteristics of fractures such as conductivity and permeability factor in different ways. The results of this study lead to the following conclusions:

(i) When the fracture characteristics variables were used collectively in the trained models, it was definitively determining the suitable type of flow for oil and gas (pseudosteady state flow or radial flow).

(ii) Based on the five available input variables, the following two output variables are shown to be most effective when used in combination to predict the movement of the fluids in the naturally fractured reservoirs. These input variables are matrix permeability, fracture permeability, wellbore radius, interporosity flow coefficient, and storativity ratio, while the output variables are the fracture porosity and shape factor.

(iii) ML models confirmed their potential in predicting the ail/gas flow fracture porosity and shape factor.

(iv) Some limitations were observed that sometimes ML models cannot work well in the development of the behavior of the naturally fractured reservoir characteristics due to their instability in one pattern as same as conventional reservoirs and this causes it difficult to predict.

Data Availability

The data used to support the findings of this study are available from the corresponding author upon request.

Conflicts of Interest

The authors declare that they do not have any conflicts of interest.

References

[1] W. Narr, D. S. Schechter, and L. B. Thompson, "Naturally fractured reservoir characterization," *Society of Petroleum Engineers Richardson*, vol. 112, 2006.

[2] G. Penuela, E. A. Idrobo, A. Ordonez, C. E. Medina, and N. S. Meza, "A new material-balance equation for naturally fractured reservoirs using a dual-system approach," in *Proceedings of the SPE Western Regional Meeting 2001*, Richardson, TX, USA, March 2001.

[3] A. Ordonez, G. Peñuela, E.-A. Idrobo, and C. E. Medina, "Recent advances in naturally fractured reservoir modeling," *CT&F - Ciencia, Tecnología y Futuro*, vol. 2, no. 2, pp. 51–64, 2001.

[4] J.-C. Guo, R.-S. Nie, and Y.-L. Jia, "Dual permeability flow behavior for modeling horizontal well production in fractured-vuggy carbonate reservoirs," *Journal of Hydrology*, vol. 464, pp. 281–293, 2012.

[5] X. Du, Z. Lu, D. Li, Y. Xu, P. Li, and D. Lu, "A novel analytical well test model for fractured vuggy carbonate reservoirs considering the coupling between oil flow and wave propagation," *Journal of Petroleum Science and Engineering*, vol. 173, pp. 447–461, 2019.

[6] D. Li, W. Jiao, F. Yue, X. Xiang, and L. Pan, "Natural fractures and their effects on reservoir reconstruction in lower cambrian shale, southeast chongqing, China," *Energy Exploration and Exploitation*, vol. 33, no. 6, pp. 769–783, 2015.

[7] B. L. Beckner, *Improved Modeling of Imbibition Matrix/fracture Fluid Transfer in Double Porosity Simulators*, Stanford University, Stanford, CA, USA, 1990.

[8] M. Frey, C. Bossennec, L. Seib, K. Bär, E. Schill, and I. Sass, "Interdisciplinary fracture network characterization in the crystalline basement: a case study from the Southern Odenwald, SW Germany," *Solid Earth*, vol. 13, no. 6, pp. 935–955, 2022.

[9] H. K. Hawez, R. Sanaee, and N. H. Faisal, "A critical review on coupled geomechanics and fluid flow in naturally fractured reservoirs," *Journal of Natural Gas Science and Engineering*, vol. 95, Article ID 104150, 2021.

[10] H. Hawez, R. Sanaee, and N. H. Faisal, "Multiphase flow modelling in fractured reservoirs using A novel computational fluid dynamics approach," in *Proceedings of the 55th US Rock Mechanics/Geomechanics Symposium*, Houston, TX, USA, June 2021.

[11] J. E. Warren and P. J. Root, "The behavior of naturally fractured reservoirs," *Society of Petroleum Engineers Journal*, vol. 3, no. 3, pp. 245–255, 1963.

[12] J. R. Gilman, J. L. Bowzer, and B. W. Rothkopf, "Application of short-radius horizontal boreholes in the naturally fractured yates field," *SPE Reservoir Engineering*, vol. 10, no. 1, pp. 10–15, 1995.

[13] E. R. Rangel-German and A. R. Kovscek, "Matrix-fracture shape factors and multiphase-flow properties of fractured porous media," in *Proceedings of the SPE Latin American and Caribbean Petroleum Engineering Conference 2005*, Rio de Janeiro, Brazil, June 2005.

[14] P. C. Eze and L. Y. Hu, "Natural fracture presence prediction in unconventional reservoirs using machine learning and geostatistical methods - workflow and HFTS1 case," in *Proceedings of the 10th Unconventional Resources Technology Conference*, American Association of Petroleum Geologists, Denver, CO, USA, July 2022.

[15] A. Aghabarari and M. Ghaedi, "Evaluation of the effects of homogenizing matrix block sizes on the simulation of naturally fractured reservoirs," *Journal of Petroleum Science and Engineering*, vol. 213, Article ID 110373, 2022.

[16] B. E. M. Lima and L. F. De Ros, "Deposition, diagenetic and hydrothermal processes in the Aptian Pre-Salt lacustrine carbonate reservoirs of the northern Campos Basin, offshore Brazil," *Sedimentary Geology*, vol. 383, pp. 55–81, 2019.

[17] G. I. Barenblatt, I. Zheltov, and I. N. Kochina, "Basic concepts in the theory of seepage of homogeneous liquids in fissured rocks [strata]," *Journal of Applied Mathematics and Mechanics*, vol. 24, no. 5, pp. 1286–1303, 1960.

[18] H. Kazemi, L. S. Merrill, K. L. Porterfield, and P. R. Zeman, "Numerical simulation of water-oil flow in naturally fractured reservoirs," *Society of Petroleum Engineers Journal*, vol. 16, no. 6, pp. 317–326, 1976.

[19] Y. Li, J. Guo, J. Zhao, and Y. Yue, "A new model of fluid leak-off in naturally fractured gas fields and its effects on fracture geometry," *Journal of Canadian Petroleum Technology*, vol. 46, no. 12, 2007.

[20] H. Pulido, F. Samaniego, J. Rivera, R. Camacho, and C. Suárez, "Decline curve analysis for naturally fractured reservoirs with transient interporosity flow," in *Proceedings of the 27th Workshop on Geothermal Reservoir Engineering Stanford University*, Stanford, CA, USA, January 2002.

[21] S. Gerami, M. Pooladi-Darvish, and L. Mattar, "Decline curve analysis for naturally fractured gas reservoirs: a study on the applicability of pseudo-time and material balance pseudo-time," in *Proceedings of the International Petroleum Technology Conference*, Dubai, UAE, December 2007.

[22] J. Dreier, E. Ozkan, and H. Kazemi, "New analytical pressure-transient models to detect and characterize reservoirs with multiple fracture systems," in *Proceedings of the SPE International Petroleum Conference in Mexico*, Bakersfield, CA, USA, March 2004.

[23] L. E. Perez Garcia, *Integration of Well Test Analysis into Naturally Fractured Reservoir Simulation*, Texas A&M University, College Station, TX, USA, 2006.

[24] M. Akbari, M. Javad Ameri, S. Kharazmi, Y. Motamedi, and M. Pournik, "New correlations to predict fracture conductivity based on the rock strength," *Journal of Petroleum Science and Engineering*, vol. 152, pp. 416–426, 2017.

[25] M. S. Aljawad, M. P. Schwalbert, M. Mahmoud, and A. Sultan, "Impacts of natural fractures on acid fracture design: a modeling study," *Energy Reports*, vol. 6, pp. 1073–1082, 2020.

[26] M. S. Aljawad, M. P. Schwalbert, D. Zhu, and A. D. Hill, "Improving acid fracture design in dolomite formations utilizing a fully integrated acid fracture model," *Journal of Petroleum Science and Engineering*, vol. 184, Article ID 106481, 2020.

[27] M. S. Aljawad, H. Aljulaih, M. Mahmoud, and M. Desouky, "Integration of field, laboratory, and modeling aspects of acid fracturing: a comprehensive review," *Journal of Petroleum Science and Engineering*, vol. 181, Article ID 106158, 2019.

[28] Y. Chen, H. Wang, Y. Wang, and G. Ma, "Numerical evaluation of a fracture acidizing treatment in a three-dimensional fractured carbonate reservoir," *Journal of Natural Gas Science and Engineering*, vol. 81, Article ID 103440, 2020.

[29] A. M. Hassan, M. S. Aljawad, and M. A. Mahmoud, "Predicting the productivity enhancement after applying acid fracturing treatments in naturally fractured reservoirs utilizing artificial neural network," in *Proceedings of the Abu Dhabi International Petroleum Exhibition & Conference*, SPE, Abu Dhabi, UAE, November 2021.

[30] G. M. Lomize, "Water flow through jointed rock," *Gosenergoizdat, Moscow*, vol. 127, 1951 (in Russian).

[31] S. Marelli and B. Sudret, "UQLab: A framework for uncertainty quantification in matlab," *Vulnerability, Uncertainty, and Risk*, American Society of Civil Engineers, Reston, Virginia, USA, 2014.

[32] M. Alajmi and T. Ertekin, "The development of an artificial neural network as a pressure transient analysis tool for applications in double-porosity reservoirs," in *Proceedings of the Asia Pacific Oil and Gas Conference and Exhibition*, SPE, Jakarta, Indonesia, October 2007.

[33] O. F. Allain and R. N. Horne, "Use of artificial intelligence in well-test interpretation," *Journal of Petroleum Technology*, vol. 42, no. 3, pp. 342–349, 1990.

[34] A. M. AlMaraghi and A. H. El-Banbi, "Automatic reservoir model identification using artificial neural networks in pressure transient analysis," in *Proceedings of the SPE North Africa Technical Conference and Exhibition*, SPE, Cairo, Egypt, September 2015.

[35] A. A. Awotunde, "Estimation of well test parameters using global optimization techniques," *Journal of Petroleum Science and Engineering*, vol. 125, pp. 269–277, 2015.

[36] X. dong Wang, Y. fang Zhou, and W. jing Luo, "A study on transient fluid flow of horizontal wells in dual-permeability media," *Journal of Hydrodynamics*, vol. 22, no. 1, 2010.

[37] L. Mei, H. Zhang, L. Wang, Q. Zhang, and J. Cai, "Fractal analysis of shape factor for matrix-fracture transfer function in fractured reservoirs," *Oil & Gas Science and Technology*, vol. 75, p. 47, 2020.

[38] K.-M. Osei-Bryson, "Evaluation of decision trees: a multi-criteria approach," *Computers & Operations Research*, vol. 31, no. 11, pp. 1933–1945, 2004.

[39] A. Sharafati, S. B. Haji Seyed Asadollah, D. Motta, and Z. M. Yaseen, "Application of newly developed ensemble machine learning models for daily suspended sediment load prediction and related uncertainty analysis," *Hydrological Sciences Journal*, vol. 65, no. 12, 2020.

[40] A. Priyam, G. R. Abhijeeta, A. Rathee, and S. Srivastava, "Comparative analysis of decision tree classification algorithms," *International Journal of Current Engineering and Technology*, vol. 3, no. 2, pp. 334–337, 2013.

[41] S. Y. Kim and A. Upneja, "Majority voting ensemble with a decision trees for business failure prediction during economic downturns," *Journal of Innovation & Knowledge*, vol. 6, no. 2, pp. 112–123, 2021.

[42] M. Xu, P. Watanachaturaporn, P. K. Varshney, and M. K. Arora, "Decision tree regression for soft classification of remote sensing data," *Remote Sensing of Environment*, vol. 97, no. 3, pp. 322–336, 2005.

[43] G. K. F. Tso and K. K. W. Yau, "Predicting electricity energy consumption: a comparison of regression analysis, decision tree and neural networks," *Energy*, vol. 32, no. 9, pp. 1761–1768, 2007.

[44] L. Breiman, *Machine Learning*, vol. 45, no. 1, pp. 5–32, 2001.

[45] T. Tiyasha, T. M. Tung, S. K. Bhagat et al., "Functionalization of remote sensing and on-site data for simulating surface water dissolved oxygen: development of hybrid tree-based artificial intelligence models," *Marine Pollution Bulletin*, vol. 170, Article ID 112639, 2021.

[46] Z. M. Yaseen, Z. H. Ali, S. Q. Salih, and N. Al-Ansari, "Prediction of risk delay in construction projects using a hybrid artificial intelligence model," *Sustainability*, vol. 12, no. 4, p. 1514, 2020.

[47] M. Belgiu and L. Drăguţ, "Random forest in remote sensing: a review of applications and future directions," *ISPRS Journal of Photogrammetry and Remote Sensing*, vol. 114, pp. 24–31, 2016.

[48] S. Nickel, W. Schroder, W. Wosniok et al., "Modelling and mapping heavy metal and nitrogen concentrations in moss in 2010 throughout Europe by applying Random Forests models," *Atmospheric Environment*, vol. 156, pp. 146–159, 2017.

[49] A. O. Al-Sulttani, M. Al-Mukhtar, A. B. Roomi, A. Farooque, K. M. Khedher, and Z. M. Yaseen, "Proposition of new ensemble data-intelligence models for surface water quality prediction," *IEEE Access*, vol. 9, 2021.

[50] P. Zhang, R. P. Chen, and H. N. Wu, "Real-time analysis and regulation of epb shield steering using random forest," *Automation in Construction*, vol. 106, 2019.

[51] J. C. Bezdek, S. K. Chuah, and D. Leep, "Generalized k-nearest neighbor rules," *Fuzzy Sets and Systems*, vol. 18, no. 3, pp. 237–256, 1986.

[52] H. Samet, "K-nearest neighbor finding using MaxNearestDist," *IEEE Transactions on Pattern Analysis and Machine Intelligence*, vol. 30, no. 2, pp. 243–252, 2008.

[53] G. Batista and D. F. Silva, "How k-nearest neighbor parameters affect its performance," in *Argentine Symposium on Artificial Intelligence*, pp. 1–12, Citeseer, Princeton, NJ, USA, 2009.

[54] H. Tao, S. Q. Salih, M. K. Saggi et al., "A newly developed integrative bio-inspired artificial intelligence model for wind speed prediction," *IEEE Access*, vol. 8, pp. 83347–83358, 2020.

[55] M. H. J. Gruber, *Improving Efficiency by Shrinkage: The James-Stein and ridge Regression Estimators*, Routledge, Oxfordshire, UK, 2017.

[56] J. Ranstam and J. A. Cook, "LASSO regression," *British Journal of Surgery*, vol. 105, no. 10, p. 1348, 2018.

[57] R. Tibshirani, "Regression shrinkage and selection via the lasso," *Journal of the Royal Statistical Society: Series B*, vol. 58, no. 1, pp. 267–288, 1996.

[58] K. E. Taylor, "Summarizing multiple aspects of model performance in a single diagram," *Journal of Geophysical Research: Atmospheres*, vol. 106, no. 7, pp. 7183–7192, 2001.

[59] A. Botchkarev, "Performance metrics (error measures) in machine learning regression, forecasting and prognostics: properties and typology," 2018, https://arxiv.org/abs/1809.03006.

[60] S. Afzali, N. Rezaei, S. Zendehboudi, and I. Chatzis, "Computational fluid dynamic simulation of multi-phase flow in fractured porous media during water-alternating-gas injection process," *Journal of Hydrology*, vol. 610, Article ID 127852, 2022.

[61] A. Rossi, F. Alberini, and E. Brunazzi, "Identification of suspension state using passive acoustic emission and machine learning in a solid–liquid mixing system," *Chemical Engineering Research and Design*, vol. 177, pp. 273–282, 2022.

Hindawi
Complexity
Volume 2022, Article ID 4285328, 18 pages
https://doi.org/10.1155/2022/4285328

Research Article

Developing an Integrative Data Intelligence Model for Construction Cost Estimation

Zainab Hasan Ali,[1] **Abbas M. Burhan**,[1] **Murizah Kassim**,[2,3] **and Zainab Al-Khafaji**[4]

[1]*Civil Engineering Department, College of Engineering, University of Baghdad, Baghdad, Iraq*
[2]*Institute for Big Data Analytics and Artificial Intelligence (IBDAAI), Universiti Teknologi MARA, Shah Alam 40450, Selangor, Malaysia*
[3]*School of Electrical Engineering, College of Engineering, Universiti Teknologi MARA, Shah Alam 40450, Selangor, Malaysia*
[4]*Building and Construction Techniques Engineering Department, Al-Mustaqbal University College, Babylon 51001, Iraq*

Correspondence should be addressed to Zainab Al-Khafaji; zainab.sattar@mustaqbal-college.edu.iq

Received 15 July 2022; Accepted 1 September 2022; Published 29 September 2022

Academic Editor: Haitham Abdulmohsin Afan

Construction cost estimation is one of the essential processes in construction management. Project cost is a complex engineering problem due to various factors affecting the construction industry. Accurate cost estimation is important in construction management and significantly impacts project performance. Artificial intelligence (AI) models have been effectively implemented in construction management studies in recent years owing to their capability to deal with complex problems. In this research, extreme gradient boosting is developed as an advanced input selector algorithm and coupled with three AI models, including random forest (RF), artificial neural network (ANN), and support vector machine (SVM) for cost estimation. Datasets were gathered based on a survey conducted on 90 building projects in Iraq. Statistical indicators and graphical methods were used to evaluate the developed models. Several input predictors were used, and XGBoost highlighted inflation as the most crucial parameter. The results indicated that the best prediction was attained by XGBoost-RF using six input parameters, with r-squared and the mean absolute percentage error equal to 0.87 and 0.25, respectively. The comparison results revealed that all AI models showed good prediction performance when applied to datasets affected by more than two parameters. The outcomes of this research revealed an optimistic strategy that can help decision makers select the influencing parameters in the early phases of project management. Also, developing a prediction model with high precision results can assist the project's estimators in decreasing the errors in the cost estimation process.

1. Introduction

The construction industry is complex and comprises parties such as owners, contractors, and consultants [1, 2]. The construction sector affects the global economy of countries, so many studies have explored methods to improve the performance of construction projects [3–5]. Due to its global impact, several scholars measure the project performance's success to understand it better. The construction project's success can be measured by achieving the project within the estimated cost, duration, and specifications [6, 7]. Implementing a project with successful performance is challenging with growing awareness of the environment and customer requirements changing [8]. The construction industry is dynamic and complex since it needs the implementation of successful project management strategies [9, 10]. Unsuccessful strategies cause cost and schedule overruns, leading to undesirable results and reducing customer satisfaction [11–13].

Consequently, there is a need to develop effective strategies and methods to mitigate risks and uncertainties in a construction project [14, 15]. The construction project management sector mainly includes the initial design phase, detailed design phase, construction cost estimation, project bidding phase, construction phase, and final delivery after completion [16–18]. Cost is an essential criterion of project

performance due to its impact on feasibility studies and choosing design alternatives [19]. Cost studies describe and evaluate the costs of buildings and other construction projects [20]. These studies seek to maximize the project's revenue by using the available resources. Cost estimation is essential in construction and significantly impacts project management [21]. Accuracy of cost estimation is considered a necessary factor of project success during various phases of project construction [22, 23]. Accurate cost estimation affects the project's profitability, owner's satisfaction, and financial decision [24]. Inaccurate cost estimation leads to problems like cost overruns and project parties' disputes [25, 26]. Several studies on cost management indicated that accurate cost estimation affects the profitability of construction projects at the tender phase and is a vital part of project survival [27, 28]. They also showed that establishing accurate cost estimation ensures the contract's profit at the tendering phase.

Cost estimation is performed by a coordination role of tender managers and technical experts called estimators. The existing cost estimation methods require complete information about construction projects and are costly and time consuming [29, 30]. During the tendering phase, estimators have little information; therefore, they depend on their knowledge and expertise to attain the estimated cost [31]. The level of knowledge is different among estimators, which can affect the accuracy of the cost estimation process [13]. Many studies have used statistical and artificial intelligence techniques to prevent these problems and accurately estimate construction costs [13, 32, 33]. Several studies performed the regression method as a traditional technique for cost estimation [34–37]. This method is easy and has achieved simple results. However, this technique cannot handle a complex system's nonlinear relationship among parameters. Recently, computer-aided algorithms have been successfully conducted in construction management studies. AI models can handle the complexity and nonlinearity of construction projects and help the project's parties understand the uncertainties and incomplete information at the early stage of the construction process [38–41].

The capacity of artificial neural network (ANN) and support vector machine (SVM) models in estimating the cost and duration of road projects was analysed [42]. The comparison analysis showed that SVM has higher accuracy and fewer errors than the ANN model. Two researchers presented the ordinary least square regression (OLSR) for construction cost forecasting of the Pune region in India [43, 44]. The model was applied over a 12-year prediction period and attained 91%–97% accuracy. The SVM model's capability in estimating the residential building's conceptual cost was studied by the authors in [45]. The results showed that the model achieved low mean absolute percentage errors, with values ranging between 7% and 8.19%. Another study used SVM to estimate the cost of bridge construction [46]. The study showed that the SVM model could estimate the cost during the initial process of project construction. The model obtained the highest performance results with a correlation coefficient equal to 0.974. An ANN model was trained with a backpropagation algorithm for early performance estimation of buildings in India [47]. The study revealed the ability of the ANN model in cost prediction and its importance to the financial investors in the construction project. The precision of construction cost prediction was improved by integrating a genetic algorithm (GA) with the ANN model [48]. The study reported that the developed model attained a high predictive performance equal to 0.9471 and assisted project managers at the beginning of the project. Principal component analysis (PCA) and particle swarm optimization (PSO) were combined with the SVM model to predict cost of substation projects [49]. The developed model was compared with PCA-SVM and PSO-SVM, and the study demonstrated that the integration of three algorithms achieved better prediction outputs than other models, which can help decision makers in substation projects. Twenty AI techniques for construction cost estimation of field canal improvement projects were compared by the author in [50]. The author concluded that the extreme gradient boosting (XGBoost) algorithm gained the best prediction results with r-squared equal to 0.929. Three AI methods, namely, multilayer perceptron (MLP), radial basis function neural network (RBFNN), and general regression neural network (GRNN), were developed for cost prediction of road projects [51]. The study showed that GRNN gained better prediction results than other models, with R^2 equal to 0.9595. The study also indicated that ANN obtained fewer prediction errors and could handle limited information during the early phases of the construction process. The study by the authors in [52] used three machine learning algorithms: MLP, GRNN, and RBFNN, with a process-based method for cost prediction at the early stage of project management. The study confirmed that the GRNN algorithm provided better outcomes than other models, which can help project managers predict construction costs in the contracting phase, where several input parameters are unknown at this stage. The labor cost of the BIM project was explored by integrating a simple linear regression (SLR) with the random forest (RF) model [53]. The study demonstrated the effectiveness of the hybrid model in the cost estimation process. An optimization algorithm called PSO was integrated with the ANN model to improve the performance of the cost prediction of high-rise residential buildings [54]. The study concluded that the PSO-ANN model has higher prediction precision and generalization than the single ANN algorithm.

The ability of RF, SVM, and multilinear regression (MLR) to predict the cost overrun of high-rise buildings' engineering services was examined [55]. The authors showed that the RF model achieved better prediction results than the other two AI models. Based on the reported studies, AI algorithms can be applied successfully for cost estimation. These studies indicated that the performance of these algorithms is affected by the algorithm's structure and the abstraction of input variables. The correlation statistics, factor analysis, and relative importance index are the popular methods used by past studies [56–59].

In these studies, data were collected based on personal opinions and expert surveys, leading to bias in the existing approaches. Moreover, the current method explores the

Table 1: Descriptive measures of the cost data for the training phase.

	Minimum	Maximum	Mean	Median	Std. deviation	Skewness	Kurtosis
Ground floor area (m^2)	200	5320	1622	1370	1196.252	1.127	0.466
Total floor area (m^2)	355	9088	3135	2525	2214.788	1.079	0.466
Floor number	1	6	2.762	2	1.711	0.651	−1.052
Elevator number	0	4	0.794	0	1.002	1.073	0.349
Footing type (raft = 1; separated = 2)	—	—	—	—	—	—	—
Inflation (%)	0.1	7.5	2.484	1.8	2.161	0.775	−0.656
Duration (days)	122	731	357.6	348	137.171	0.715	0.652
Cost ($)	26756	6451519	1975260	1321630	1623076	0.903	−0.312

linear relationship between input and output predictors. Based on that, exploring an advanced method that can investigate the complex system of cost estimation parameters is very important to achieve accurate results [38]. Furthermore, integrating a new feature selection method with AI algorithms is significant for construction management engineering to get accurate prediction performance [60]. Recently, the XGBoost algorithm has been explored as an advanced version of the feature selection approach in engineering problems. XGBoost is a recent version of gradient boosting and has been applied effectively as an input selection method by civil engineering scholars [61, 62]. The research scope of applying AI algorithms in construction management is still limited, so exploring a new cost estimation method is the motivation of this research.

Developing effective predictive models that can achieve accurate performance is a vital issue in the early phases of engineering management. The construction industry in Iraq has a special issue due to the risky conditions and exceptional political circumstances that had happened in this region [2]. The instability of political and economic conditions has a massive impact on the performance of construction projects. Due to economic and political circumstances, most constructed projects have failed to be completed within the specified budget [63]. Thus, developing an integrative model using AI algorithms in cost management can improve cost performance by evaluating, controlling, and monitoring the project cost under uncertain conditions.

The current study is achieved by integrating the XGBoost algorithm with three AI algorithms, namely, RF, SVM, and ANN. XGBoost was used to select the influencing parameters of the prediction process, and then, the AI model used these parameters. The attained results are analysed and discussed by using statistical and visualization methods. The output of this study can assist a project manager in selecting the influencing parameters at the early stage of a construction project. Also, introducing an integrated model with high precision results helps project estimators reduce errors in the cost estimation phase.

2. Construction Cost Data Explanation

This study used public building projects in Iraq as a case study for the modelling process and used their dataset. These projects are managed by the Iraqi government, so developing an accurate precision model can help decision makers by producing precious results. The information in the dataset was collected from the survey conducted on 90 construction projects between 2016 and 2021. The information was gathered from historical records of construction projects, including project drawings, bills of quantities, and project schedules. The dataset includes information on ground floor area (GFA), total floor area (TFA), floor number (FN), elevator number (EN), footing type (FT), inflation (F), duration (D), and construction cost (C). The inflation data were collected from the Iraqi central bank (https://cbiraq.org/). Tables 1 and 2 show the descriptive measures of the cost data for the training-testing phase. The statistical descriptions include minimum, maximum, mean, median, standard deviation, skewness, and kurtosis. For the training process, the mean value of construction cost is 1623076 $, while for the testing phase, the mean value is 2571431 $. The maximum and minimum values of project duration are 731 days and 122 days for the training phase, while for the testing phase, they are 150 days and 787 days. It can be seen that the datasets for the training and testing phases are well distributed. It is near the normal distribution because the mean and median values of the datasets are close to each other.

3. Method Overview

3.1. Extreme Gradient Boosting (XGBoost). XGBoost is an advanced version of tree-based boosting modelling introduced by Chen and Guestrin [62], which is applied effectively in input selection problems [64, 65]. The boosting algorithm's concept uses an iteration process for learning the functional relationship between the target and predictor values [66]. Through this iterative process, the individual trees are trained sequentially on the residual output of the previous trees to reduce the training errors [67]. The algorithm uses a cache-aware structure and a regularized method for boosting learning. The mathematical expression of prediction can be shown as follows:

$$\widehat{Y} = \phi(X) = \frac{1}{n}\sum_{k=1}^{n} f_k(X), \tag{1}$$

where $\widehat{Y}$ is the predicted value of the target, X represents the input variable, K is the value ranging between 1 and n, f_k is the function between input and output variables, and n is the number of trained functions by boosting trees. The loss

Table 2: Descriptive measures of the cost data for the testing phase.

	Minimum	Maximum	Mean	Median	Std. deviation	Skewness	Kurtosis
Ground floor area (m^2)	239	3940	1490	1394	882.414	0.991	0.713
Total floor area (m^2)	344	9800	4086	3840	2692.433	0.384	−1.068
Floor number	1	6	3.222	3	1.625	0.483	−1.089
Elevator number	0	4	1.37	1	1.182	0.501	−0.936
Footing type (raft = 1; separated = 2)	—	—	—	—	—	—	—
Inflation (%)	0.1	7.5	3.319	2.1	2.674	0.297	−1.474
Duration (days)	150	787	404.7	364	177.036	0.468	−0.770
Cost ($)	160147	6104878	2571431	2215402	1940152	0.409	−1.345

function in XGBoost must be minimized to train several functions f_k, as shown in the following expression:

$$\mathscr{L}(\phi) = \sum_i l(\hat{y}_i, y_i) + \sum_k \Omega(f_k),$$
$$\Omega(f_k) = \gamma T + \frac{1}{2}\lambda \|w\|^2, \tag{2}$$

where $\mathscr{L}(\phi)$ is the regularized function, i represents the loss function measurement between $\hat{y}_i$ (prediction value) and y_i (actual value), Ω is a regularization term that prevents the building of additional trees in the model from decreasing overfitting and error. γ is the leaf's complexity, T is the leaves' number in the tree model, λ is the penalty parameter, and w is the score vector on the leaves.

In the input selection process, the main aim of XGBoost is to produce the feature importance of input variables [68]. According to Hastie et al. [69], the algorithm uses gain, frequency, and cover to calculate feature importance. The gain method calculates the role of each feature in the model's development. Frequency is the weight representing the occurrence number for each feature in the boosted trees. The cover method shows the number of samples related to each feature. XGBoost uses the following expression to calculate the importance of the feature:

$$N_v = \sum_{L=1}^{L} \sum_{l=1}^{X=1} I\left(V_L^l, v\right),$$
$$\left(V_L^l, v\right) = f(x) = \begin{cases} 1\, if\, V_L^l = v, \\ 0, \text{otherwise}, \end{cases} \tag{3}$$

where L is the tree' number, N is the number of a node for each leaf, (V_L^l) represents the feature of node l, and I is the indicator function.

3.2. Random Forest (RF). Random forest (RF) is an ensemble algorithm introduced by Breiman [70] and based on combining multiple decision trees to produce a robust prediction model. It has been used effectively for classification and regression problems in several areas of construction management [71–73]. The RF model can deal with many input variables and work efficiently with outliers and unbalanced datasets. The algorithm reduces overfitting results and performs accurately with simple computation processes [74]. The RF model uses bootstrap and random space techniques to improve the predictive model's performance [75, 76]. In the RF model, the algorithm uses a bootstrap method to choose new training sets from the original data randomly, and these new data will be utilized to develop a regression tree (n_{tree}). The number of split m_{try} for each node in the regression tree is computed using a stochastic random space technique.

The modelling steps to develop the RF model are as follows: First, we generate a new training dataset using a bootstrap algorithm where two-thirds of the original data (in bag data) are used to train the developed model. After that, several regression trees were built based on bootstrap samples, and these regression trees were used to develop the RF model. The RF model is created by training a sequence of regression trees. The variance between the trees can be measured by randomly choosing the optimal number of attributes based on maximum depth values. These computations increase the ability of the RF model to reduce the errors in prediction results. The RF model is built by training a sequence of regression trees. Finally, the algorithm collects the output value for each tree and calculates the final prediction using the average method [77]. The mathematical calculation of the RF technique is expressed as follows:

$$y' = \frac{1}{n_{\text{tree}}} \sum_{i=1}^{n_{\text{tree}}} f_i(x), \tag{4}$$

where y' represents the prediction value of the RF model, n_{tree} is the number of regression trees, and $f_i(x)$ is the regression tree model based on input value (x). The schematic diagram of the RF algorithm is described in Figure 1.

3.3. Artificial Neural Network (ANN). Artificial algorithms such as ANN and other machine learning algorithms have been introduced recently. These models have been characterized by their capabilities in handling complex datasets and producing accurate results [78]. The artificial neural network is a mathematical expression, building its components by emulating the biological structure of the human brain [79]. The main element of the ANN model is the series of connected layers called neurons. Several types of ANN exist; scholars commonly apply a feedforward ANN with a backpropagation algorithm [80]. The popularity of the backpropagation algorithm in ANN applications is gained by its capacity to learn ANN networks based on a supervised learning algorithm [81]. In this method, the error in prediction results is computed by comparing the predicted values with actual variables. The weights in the ANN model are updated by backpropagation to reduce the expected error

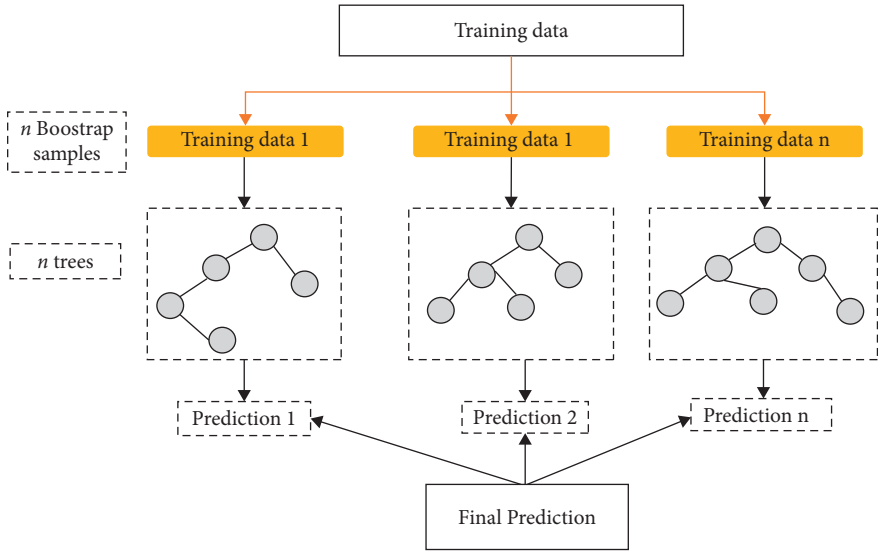

Figure 1: Schematic diagram of the RF algorithm.

to the allowable value. Feedforward ANN consists of input, hidden, and output layer components. In this type of ANN, moving information is performed directly from the input to the output neurons without returning in the reversed direction. The number of neurons in the input and output layer is based on the number of input and output variables in the ANN model. In the hidden layer, neurons nonlinearly transform input variables into the output layer [82]. Hidden layers in the ANN algorithm can be expressed mathematically as follows:

$$v_i = \left(1 + \exp\left(-1 \times \sum_{i=1}^{1} x_i w_{ij}\right)\right)^{-1}, \tag{5}$$

where v_i represents the hidden layer, x_i is the input parameters, and w_{ij} refers to the weight between input and hidden layers. The value of the output layer can be computed as follows:

$$y = \left(1 + \exp\left(-1 \times \sum_{j=1}^{1} v_j w_{ij}\right)\right)^{-1}. \tag{6}$$

The design of an ANN network requires identifying the number of neurons and hidden layers. According to previous studies, the best prediction results can be achieved using one or two layers [83, 84]. The optimum input variables can attain the best performance during the training process. The relationship between input and output variables is designed to improve prediction performance by training ANN. For each repeated process, the biases and weights are modified by the algorithm to reduce the error measures between the original and predicted values. The errors of the expected value can be presented as follows:

$$\text{Error} = 0.5(d - y)^2, \tag{7}$$

where d represents the actual value and y is the predicted value achieved by the ANN model. The presentation of the ANN model is shown in Figure 2.

3.4. Support Vector Machine (SVM). Support vector machine is a supervised machine learning algorithm developed as a method that uses a hyperplane to divide the data and measure the nearest position between the external point and the hyperplane [85]. SVM is a popular algorithm commonly used by scholars to improve the estimated process of engineering problems [86, 87]. The algorithm simulates the errors between actual and predicted parameters by measuring the distance from the SVM margin. The SVM model can be expressed mathematically as follows:

$$M = \{x_1, y_1), x_2, y_2), \ldots, x_n y_n). \tag{8}$$

M represents the training dataset and x and y are the input and output parameters. SVM uses the following function to learn the dataset during the training phase:

$$f(x) = w \cdot \varphi(x) + b, \tag{9}$$

where w represents the weight indicator, $\varphi(x)$ is the nonlinear function of input parameter x, and b is a scalable term. The standard error of the prediction process is minimized using the following equation:

$$\begin{aligned} &\min\varphi(w, \xi) = 0.5w^2 + C\left(\sum_{i=1}^{n} \xi_i\right)\varphi(x_i) + b, \\ &\text{subjected to } M_i\left(w^M x_i + b\right) \geq \varepsilon + \xi_i, \xi \geq 0, \end{aligned} \tag{10}$$

where ξ refers to the slag variable, C is a penalty variable controlling the error between regularization and empirical prediction, and ε is the function corresponding to the accuracy of the training process. The SVM model can be optimized by using Lagrange multipliers and optimum generic functions as shown in the following expression:

$$f(x, a_i, a_i^*) = \sum_{i=1}^{n} (a_i - a_i^*) K(x, x_i) + b, \tag{11}$$

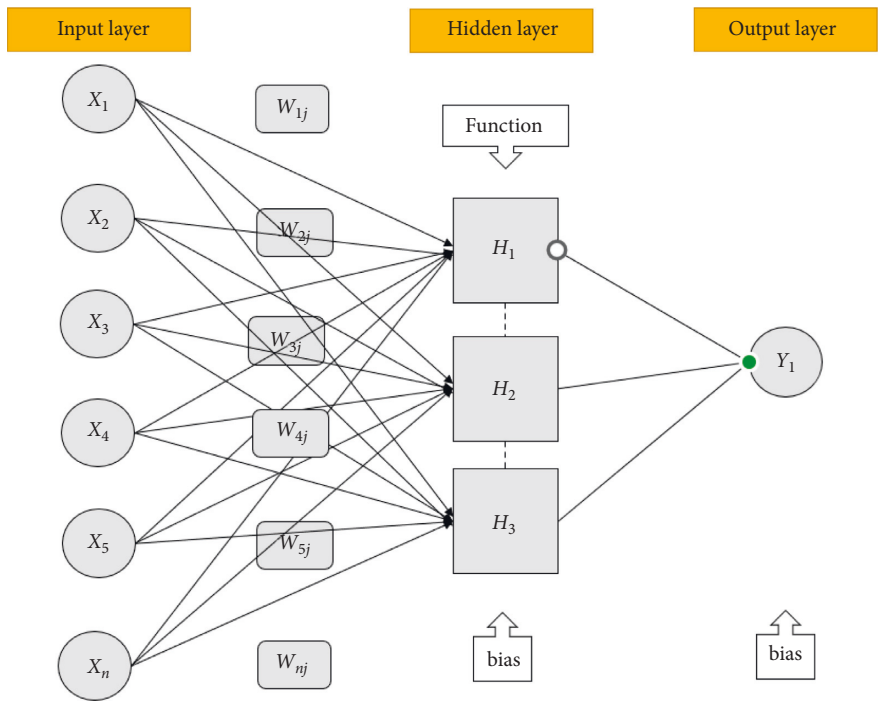

Figure 2: Structure diagram of the ANN model.

where $K(x \text{ and } x_i)$ represents the kernel function. The main feature of the SVM algorithm in regression problems is that it correlates input and output parameters using a nonlinear relationship. The SVM model's kernel function helps the algorithm generate nonlinear mappings in high-dimensional space. The SVM model has four kernel functions: linear, sigmoid, polynomial, and radial basis function (RBF) [87]. The RBF kernel function is simple, effective, and reliable and has been used in several complex studies [88]. The RBF nonlinear equation was used in this study, and the kernel function was defined depending on three parameters: C, ε, and γ where the optimal values of this equation can be reached using the trial and error method. The illustrative diagram of the SVM algorithm is depicted in Figure 3.

4. Model Development and Performance Assessment

In the present study, the construction cost estimation of the building projects in Iraq was explored. First, input selection was made to abstract the appropriate features for the prediction process. Due to the complex nature of cost estimation, the XGBoost algorithm was developed to choose the most important parameters. XGBoost was integrated with popular AI algorithms, namely, RF, ANN, and SVM. The hybrid model was developed using the R programming language (version 4.1.1). Three libraries called XGBoost, Matrix, and ggplot2 were applied to construct the XGBoost algorithm. The best results of feature selection were attained using the xgb importance function. For the SVM model, library (dplyr), library (caret), library (ggplot2), and library (kernlab) were used. Function train control was applied to control the following parameters: method (cv), number (), and set as 5-fold cross-validation. The radial basis function was applied in this study using the svmRadial function. The RF algorithm was designed using the library (ranger) and ranger function. The designed parameters are as follows: num.trees set as 200, mtry equal to 3, and min.node size used as 3. In the case of the ANN model, library neuralnet with one hidden layer and resilient backpropagation were applied to enhance model prediction. The performance of the developed model was assessed by using several statistical evaluators, including coefficient of determination (R^2), error measures (i.e., mean absolute error (MAE), root mean square error (RMSE), and mean absolute percentage error (MAPE)), Nash–Sutcliffe efficiency (Nash) and Willmott's index (WI) [89, 90]. The process of the presented AI models is shown in Figure 4.

5. Result and Discussion

5.1. Results Analysis. In this research, the ability of three AI algorithms, namely, RF, ANN, and SVM, was examined to estimate the cost of construction projects. The authors introduced the XGBoost model to determine the best combination of input parameters. The developed models were built based on different combinations extracted from the XGBoost model. Input combinations were constructed using the important parameters selected by the XGBoost algorithm, as shown in Figure 5. Figure 5 shows the relative importance values of input features using the XGBoost algorithm. The XGBoost results show that the inflation parameter (F) is the most important cost estimation, followed by the total and ground floor area. The results also indicated that the elevator number and the footing type gained the least significant scores by XGBoost. To determine the impact

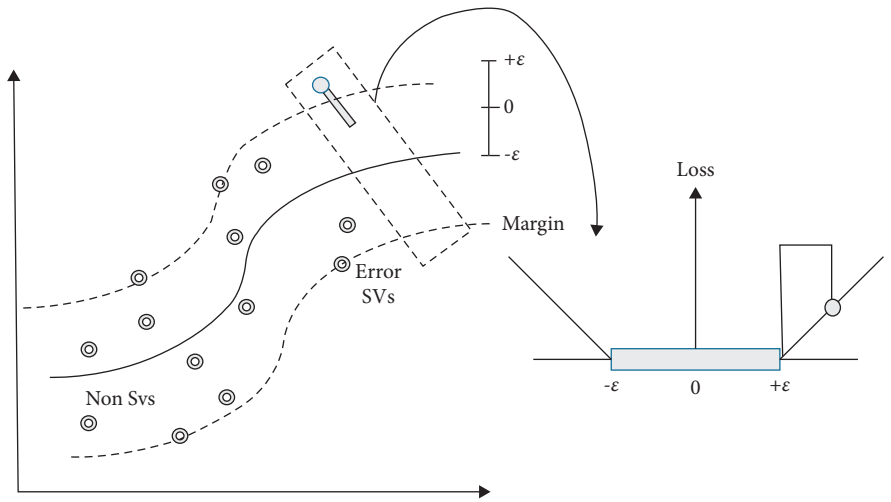

Figure 3: Illustrative diagram of the SVM algorithm.

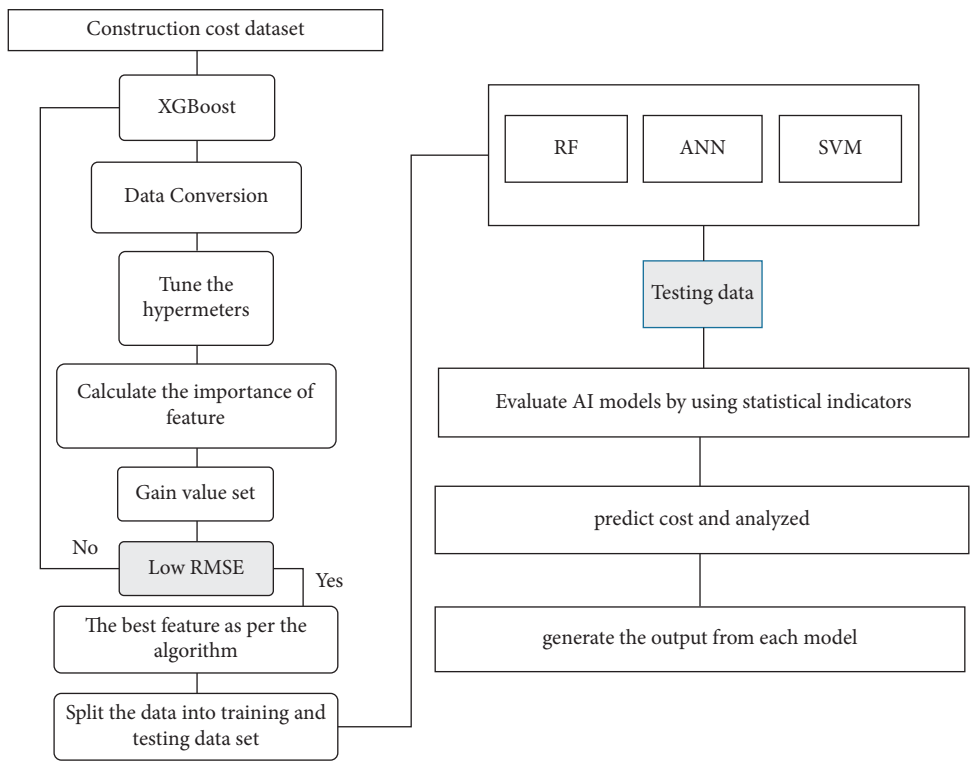

Figure 4: The proposed AI model for construction cost estimation.

of input variables on the performance of predictive models, several combinations were constructed and tested by each model. Seven models were developed for each algorithm (Model I, Model II, Model III, ..., Model VII), including variables from one to seven input parameters.

Tables 3 and 4 show the statistical measurements of the presented computer-aided algorithms for the training and testing phase. The tabulated measurements revealed that both the XGBoost-RF and XGBoost-ANN models have excellent performance for the training phase when using more than two input variables. The XGBoost-SVM model achieved less predictive performance than the other AI models for all input combinations, and the best accuracy was attained by using three input parameters. The best results for the training phase are demonstrated by XGBoost-ANN–Model V with $R^2 = 0.97551$, RMSE = 253464.6776, MAE = 151999.7328, MAPE = 0.40876, Nash = 0.97522, and WI = 0.99376. For the testing phase, the results revealed that increasing the number of input variables leads to increased predictive accuracy for all AI models. RF outperformed SVM and ANN models, and the

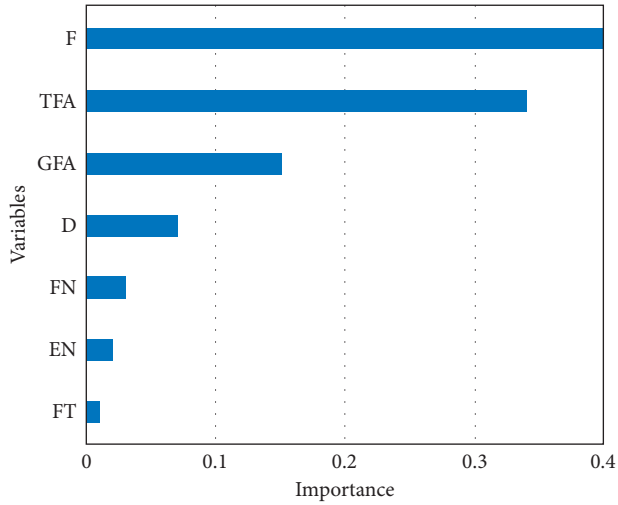

Figure 5: Feature selection of the XGBoost algorithm.

Table 3: Performance measures of AI models for training data.

	R^2	RMSE	MAE	MAPE	Nash	WI
XGBoost-RF model						
Model I	0.76081	788890.3191	604981.6715	0.99102	0.75994	0.93074
Model II	0.70272	879643.0411	589663.4386	0.63845	0.70154	0.90834
Model III	0.91381	472714.8598	339706.5592	0.43244	0.91381	0.97704
Model IV	0.92352	446670.1333	328896.3663	0.44469	0.92304	0.97921
Model V	0.96647	323123.8558	208083.017	0.36537	0.95973	0.98879
Model VI	0.93993	394961.8018	274148.5711	0.41215	0.95603	0.98446
Model VII	0.90717	495125.5653	337773.447	0.43415	0.90544	0.97555
XGBoost-ANN model						
Model I	0.69691	860530.7166	839959.9524	0.77566	0.61666	0.83414
Model II	0.88621	582676.712	290912.5011	0.26372	0.86904	0.96865
Model III	0.95504	341388.8802	224162.0108	0.37779	0.95505	0.98838
Model IV	0.95569	338911.6945	214402.0251	0.40876	0.95569	0.98856
Model V	0.97551	253464.6776	151999.7328	0.40876	0.97522	0.99376
Model VI	0.95603	337627.8199	226863.17	0.41546	0.71921	0.91102
Model VII	0.70773	1108463.447	872191.1237	0.95867	0.52607	0.75929
XGBoost-SVM model						
Model I	0.71722	838810.8081	666081.6149	0.63946	0.71436	0.91413
Model II	0.89679	527105.4427	333897.5918	0.40414	0.89283	0.97276
Model III	0.80479	717164.8809	466107.817	0.64501	0.80161	0.93934
Model IV	0.80151	735499.0773	491505.0568	0.65881	0.79134	0.93388
Model V	0.8031	715627.4657	451267.6691	0.53051	0.80246	0.94242
Model VI	0.72157	853201.115	542534.255	0.60776	0.79545	0.93821
Model VII	0.80124	727702.5318	450836.0521	0.54879	0.79574	0.93678

best performance was achieved by XGBoost-RF-Model VI with $R^2 = 0.87211$, RMSE = 693311.4488, MAE = 424619.6505, MAPE = 0.25539, Nash = 0.86739, and WI = 0.962557.

The developed AI models are also evaluated by graphical presentations like scatter plots, box plots, and Taylor diagrams. Figures 6–8 illustrate scatter plots for the testing phase for the three hybrid models (XGBoost-RF, XGBoost-ANN, and XGBoost-SVM). The XGBoost-RF model exhibits a good prediction with R^2 greater than 0.81 for all combinations except for Model I, where R^2 decreases to 0.6215. In the ANN algorithm, the developed model performs well with R^2 maxed out at 0.83 when increasing the number of input combinations for models V, VI, and VII, as shown in Figure 6. The SVM model shows an enhancement in the prediction accuracy when the number of combinations increases, except for Models VI and VII, where R^2 reduces to 0.7579.

Figure 9 shows a box plot presentation to illustrate the residual error between the observed and estimated values of cost estimation. The results showed that XGBoost-RF-Model III and XGBoost-RF-Model V gained the minimum residual plot with an error value of less than 50%. For the ANN model, the minimum positive error was attained by Models V and VII, while Models V and VI gained the minimum

Table 4: Performance measures of AI models for testing data.

	R^2	RMSE	MAE	MAPE	Nash	WI
XGBoost-RF model						
Model I	0.62154	1227246.543	874941.6745	0.55214	0.58448	0.88937
Model II	0.66971	831959.7023	619292.1689	0.35191	0.80904	0.94221
Model III	0.87382	804900.462	582701.9977	0.30825	0.82126	0.9404
Model IV	0.8553	859581.3363	591577.1935	0.2804	0.79615	0.92993
Model V	0.85961	823500.3632	554104.6337	0.25399	0.81291	0.93815
Model VI	0.87211	693311.4488	424619.6505	0.25539	0.86739	0.962557
Model VII	0.86511	706201.1783	461238.6876	0.26279	0.86241	0.961966
XGBoost-ANN model						
Model I	0.59486	1297368.569	919557.1617	0.56905	0.53564	0.88069
Model II	0.75537	1150901.062	763471.3537	0.33141	0.63458	0.9049
Model III	0.73428	1004876.227	578230.6713	0.28253	0.72142	0.9241
Model IV	0.7481	979906.0497	523097.5798	0.28778	0.7351	0.92872
Model V	0.85042	750698.034	459356.0909	0.26579	0.84453	0.95641
Model VI	0.84828	864172.2326	570128.7514	0.23589	0.79398	0.93062
Model VII	0.83202	836314.9646	545942.9388	0.23004	0.80704	0.93977
XGBoost-SVM model						
Model I	0.64182	1158278.86	803076.3523	0.80044	0.62987	0.89511
Model II	0.77873	946666.831	713338.1417	0.38731	0.75276	0.92379
Model III	0.81801	879551.0025	631843.2588	0.33659	0.78658	0.93023
Model IV	0.8256	856049.4301	586251.8811	0.26047	0.79783	0.93494
Model V	0.83321	826462.8309	542359.3988	0.23651	0.81156	0.94219
Model VI	0.78213	907434.4113	623458.3053	0.24091	0.77283	0.93306
Model VII	0.75791	958666.6949	633398.3941	0.24339	0.74646	0.92462

negative error. In the XGBoost-SVM model, combinations with 2 to 7 input parameters show a reduction in the error value, and the minimum error was achieved by Models III, IV, and V with a residual error of less than 50%. The maximum residual error was demonstrated by Model I for all the developed models with a negative error value of less than 85%.

Another graphical method (i.e., the Taylor diagram) was constructed to evaluate the developed models based on correlation and standard deviation [91]. Figure 10 illustrates the Taylor diagram for the three AI algorithms with different input combinations for tested data. Based on the constructed Taylor diagram, the XGBoost-RF model attained the nearest position to the actual cost using three and six input parameters (i.e., Model III and Model VI). The rest of the combinations of the RF model demonstrate good prediction performance, except for Model I, which attained less correlation value than the other combinations.

XGBoost-ANN and XGBoost-SVM models achieved the best performance using five input variables (i.e., Model V). XGBoost-ANN attained the nearest distance to the actual cost using three models (i.e., Model V, Model VI, and Model VII), whereas the remaining models achieved the farthest distance with a correlation value of less than 0.9. For XGBoost-SVM, only three models gained the best performance using three, four, and five input parameters, whereas the poorest performance was achieved using one input variable.

5.2. Validation against Previous Studies. To confirm the ability of the introduced AI models in cost estimation, it is necessary to validate these models against the developed AI models in past studies. An ANN algorithm was developed to estimate the construction cost of highway projects in India [92]. The study showed that the ANN model could estimate construction cost with an R of 0.94. In another study, the developed approach gained a correlation coefficient of 0.97 for the cost prediction of bridge construction by using an SVM model with 27 input variables [46]. The investigation of three AI algorithms called multivariate adaptive regression spline (MARS), extreme learning machine (ELM), and partial least square regression (PLS) was performed to estimate the construction cost of field canal projects [93]. According to the reported results, the MARS model attained the best results with an $R^2 = 0.94$ and five input parameters. Previous studies also reported hybrid models as effective models for cost estimation, such as ANN-GA and RF-SLR [48, 53]. The previous studies gained an acceptable performance in cost estimation. However, they only focused on single models and gave little attention to hybrid models. Also, they developed AI models based on all input parameters. This study combined the XGBoost algorithm with AI models to enhance the cost estimation accuracy. It can be noticed that XGBoost-RF achieved good estimation performance with r-squared ranging from 0.87 to 0.91 for both testing and training phases using only three input variables.

5.3. Discussion. Using an AI approach in complex construction projects is highly recommended to get accurate estimation process results and simulate the nonlinear relationships between input and output parameters. Using XGBoost as an advanced input selector revealed that inflation, total floor area, and ground floor area are the most important variables in cost estimation. The comparison

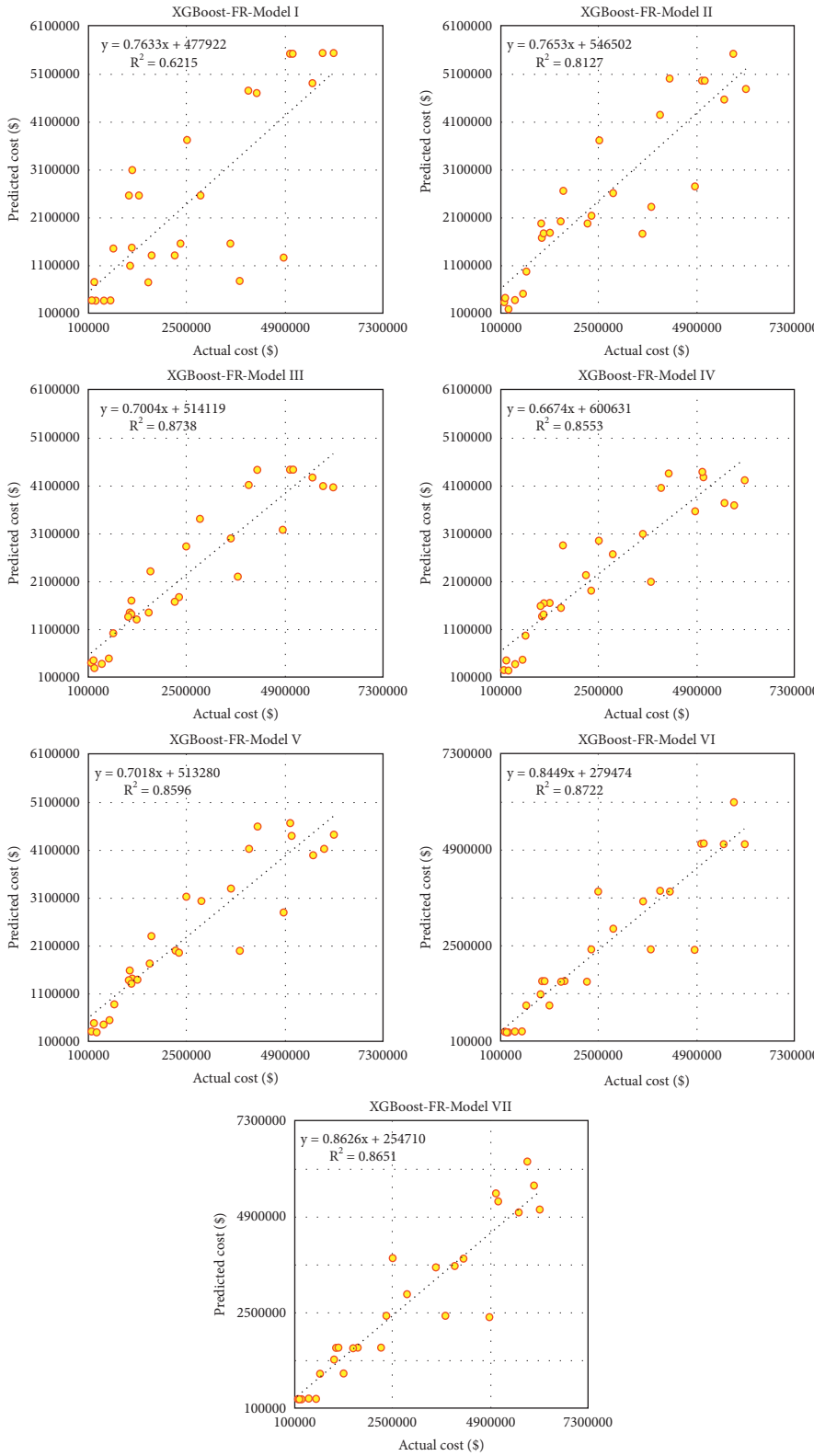

Figure 6: Scatter plot presentation of the XGBoost-RF model for tested data.

results between AI models showed the ability of the developed algorithms to predict construction costs because all models attained good predictive performance except for models that used one input variable. The XGBoost-RF model showed a significant enhancement in the prediction process using only three input parameters where $R^2 = 0.87$ and MAPE = 0.308 and minimum negative error, as shown in Table 4 and Figure 9. Applying an RF model with six input

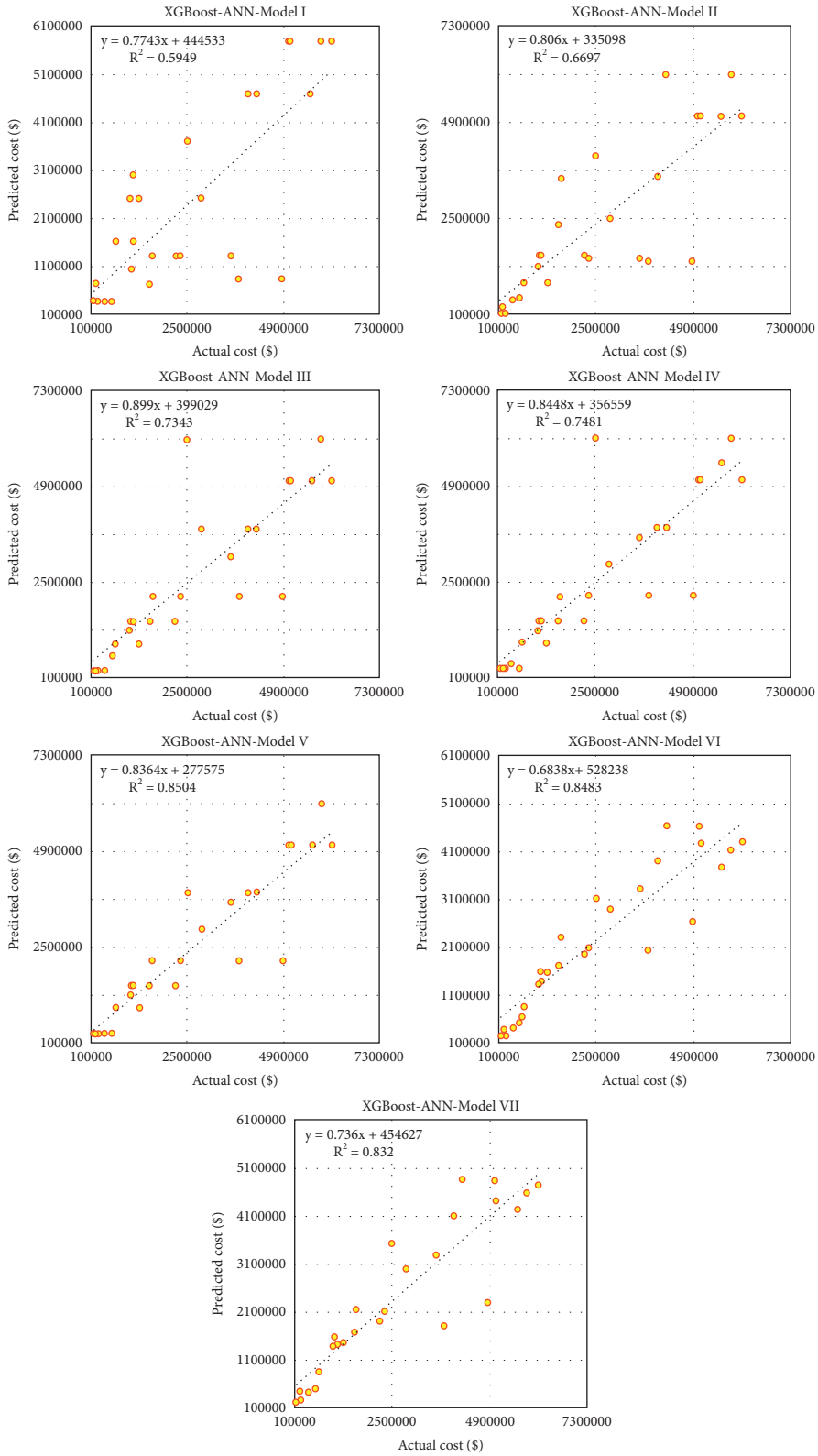

Figure 7: Scatter plot presentation of the XGBoost-ANN model for tested data.

parameters (i.e., XGBoost-RF-Model VI) led to reducing MAPE to 0.25 and producing a residual plot with no outlier points.

The poor performance was achieved by the RF algorithm in Model I and Model II, where the gained R^2 was less than 0.7 and the residual error was high, as illustrated in Figures 8

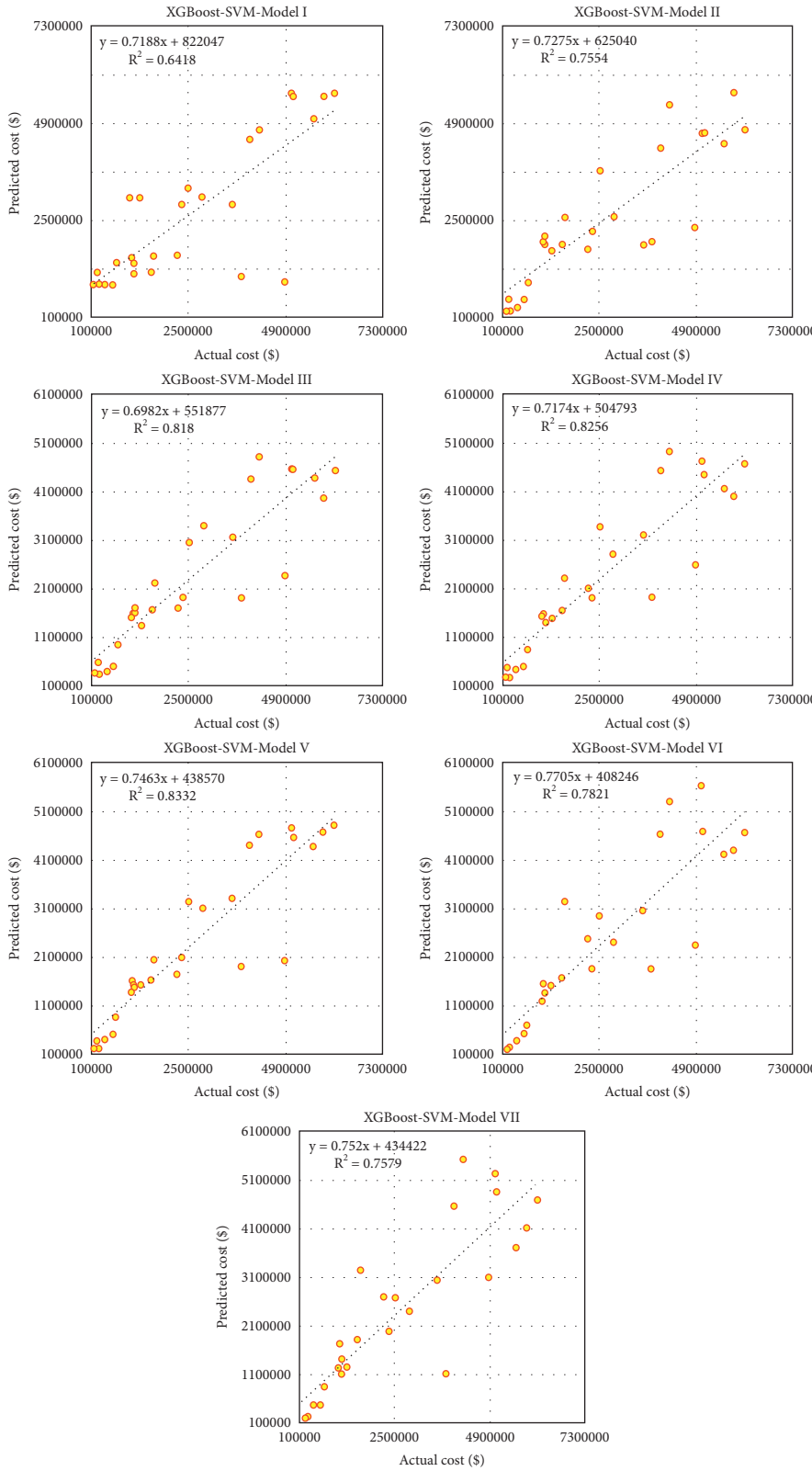

Figure 8: Scatter plot presentation of the XGBoost-SVM model for tested data.

and 9. For the ANN algorithm, the model increased its prediction performance by increasing the number of input parameters, and the best R^2 was achieved by XGBoost-ANN-Model V with RMSE equal to 750698.034, as reported in Table 4. The XGBoost-ANN-Model revealed the poorest results of Model I with high residual errors and the farthest distance to actual cost (see Figures 9 and 10). In the case of the SVM model, three models (i.e., Model III, Model IV, and

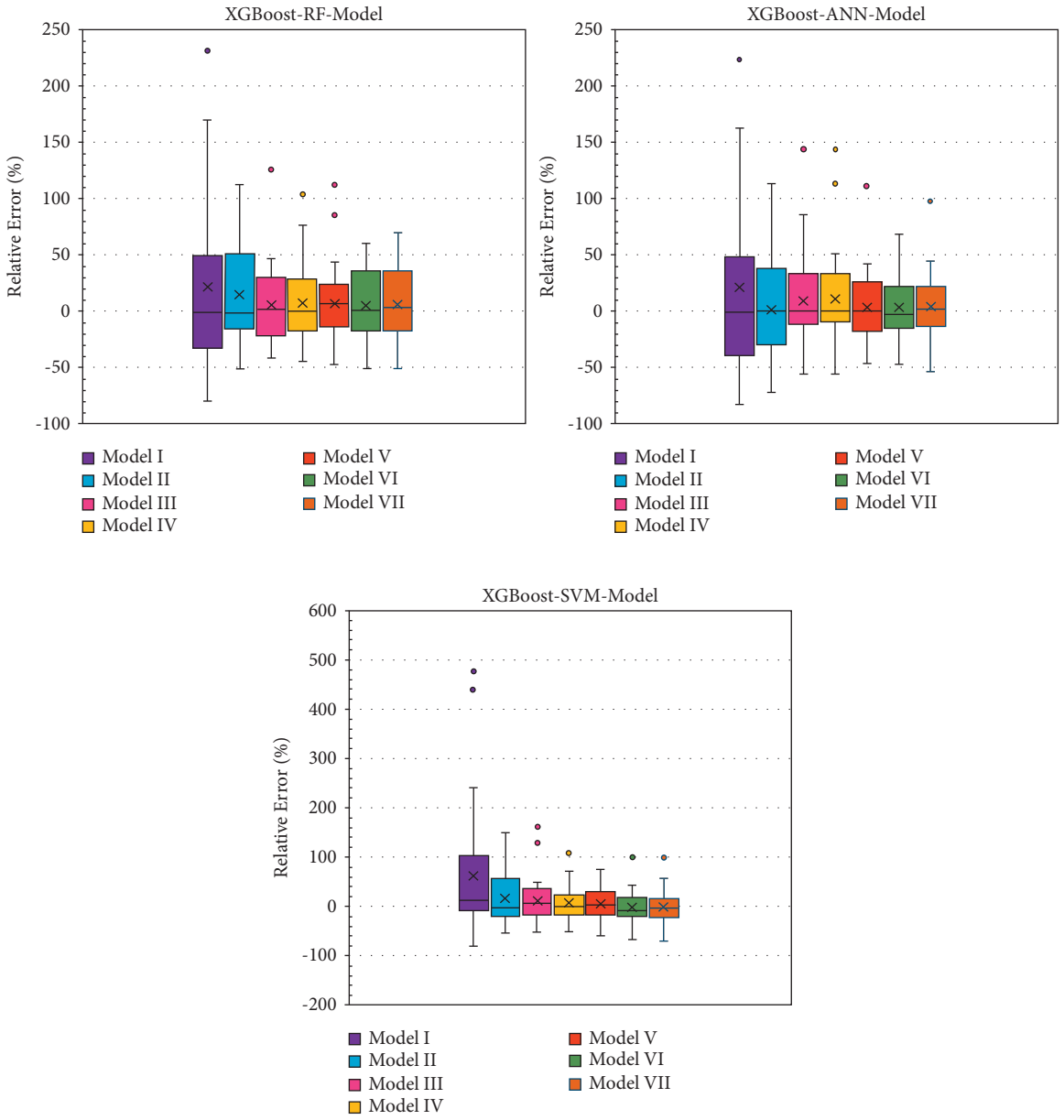

Figure 9: Box plot presentation of the developed AI models for the testing phase.

Model V) illustrated good performance with r-squared maxed out at 0.8, as depicted in Figure 7. The other combinations of the XGBoost-SVM model achieved good predictive accuracy with R^2 greater than 0.7, except for Model I that showed the lowest correlation coefficient and farthest position to the observed value, as shown in Figures 8 and 10. Based on the evaluation results, all AI models exhibited good performance when the number of input variables was increased in the estimation process. RF and SVM models performed better than ANN when using a few input variables, especially when applied to one input parameter. The comparison results revealed that integrating XGBoost with AI models enhanced the prediction accuracy by selecting the appropriate parameters for the modelling process. The integrated XGBoost algorithm with AI models revealed that using three input parameters, i.e. inflation, the total floor area, and the ground floor area, is necessary to get the accurate performance of cost estimation. The results revealed that increasing input variables from three to six reduced the error percentage and increased modelling efficiency. The results also showed that tree-based models outperformed classical models in their ability to handle complex models based on a few input variables. The reported results indicated that the RF model was able to understand the complex nature of construction cost estimation. The integrated XGBoost algorithm with AI models revealed the robustness of using predictive models when limited input variables are known by the project's stockholders. These results indicate the ability of the developed model to be used under uncertain circumstances. For future studies, other advanced selection algorithms like GA can be tested to simulate the complex behaviour among modelling parameters. Also,

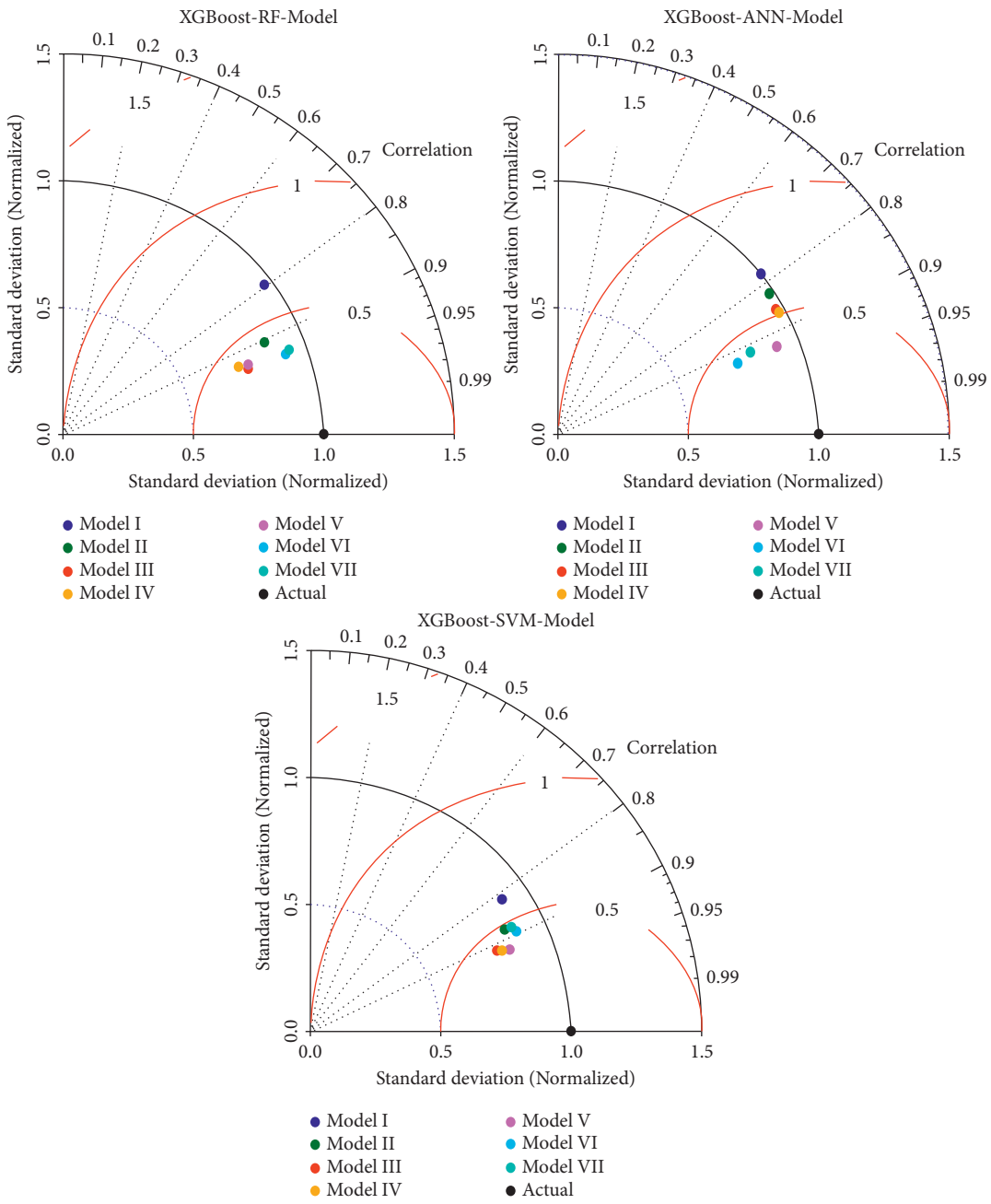

Figure 10: Taylor diagram of the developed AI models for the testing phase.

recent algorithms such as deep neural networks can be integrated with input selector algorithms to get low errors and more accurate results [94, 95].

6. Conclusions

Developing a reliable predictive model is an essential issue in construction cost estimation. In this research, the XGBoost algorithm was used to select the correlated parameters of the modelling process and hybridized with three AI models, namely, RF, ANN, and SVM, to estimate the construction cost. Datasets were collected based on the survey of 90 building projects constructed between 2016 and 2021. The results showed that the most correlated variables selected by XGBoost are inflation, the total floor area, and the ground floor area. For prediction performance, all AI models showed good reliability in the prediction process when applied to input variables of more than 2. The XGBoost-RF model revealed a high correlation coefficient in all combinations except for Model I, where R is below the acceptable performance level. The graphical evaluation showed that XGBoost-RF-Model VI gained the best performance with an r-squared of more than 0.8 and low residual error. The results also indicated that tree models could deal with complex systems and get accurate results based on the limited number of input variables. More input parameters should be investigated for future direction, and the GA

algorithm can be explored to generate significant feature selection. Also, a new deep learning algorithm can be presented to enhance the capability of predictive models.

Data Availability

The used data in the current research study can be obtained from the corresponding author upon request.

Conflicts of Interest

The authors declare no conflicts of interest.

Acknowledgments

The authors would like to thank the Institute for Big Data Analytics and Artificial Intelligence (IBDAAI), Kompleks Al-Khawarizmi, Universiti Teknologi MARA (UiTM), 40450 Shah Alam, Selangor, Malaysia, for the support in publishing this paper. In addition, the authors would like to thank Al-Mustaqbal University College (MUC-E-0122) for providing technical support for this research. This research was funded by Universiti Teknologi MARA. The authors would also like to thank the support received by the University of Baghdad.

References

[1] P. V. Ingle and G. Mahesh, "Construction project performance areas for Indian construction projects," *International Journal of Construction Management*, vol. 22, no. 8, pp. 1443–1454, 2020.

[2] W. Jing, H. I. Naji, R. N. Zehawi, Z. H. Ali, N. Al-Ansari, and Z. M. Yaseen, "System dynamics modeling strategy for civil construction projects: the concept of successive legislation periods," *Symmetry*, vol. 11, no. 5, p. 677, 2019.

[3] D. Myers, *Construction Economics: A New Approach*, Routledge, London, 2016.

[4] D.-G. Owusu-Manu, D. J. Edwards, A. Mohammed, W. D. Thwala, and T. Birch, "Short run causal relationship between foreign direct investment (FDI) and infrastructure development," *Journal of Engineering, Design and Technology*, vol. 17, no. 6, pp. 1202–1221, 2019.

[5] D. Bryde, "Perceptions of the impact of project sponsorship practices on project success," *International Journal of Project Management*, vol. 26, no. 8, pp. 800–809, 2008.

[6] J. Pollack, J. Helm, and D. Adler, "What is the Iron Triangle, and how has it changed?" *International Journal of Managing Projects in Business*, vol. 11, no. 2, pp. 527–547, 2018.

[7] A. M. Araba, Z. A. Memon, M. Alhawat, M. Ali, and A. Milad, "Estimation at completion in civil engineering projects: review of regression and soft computing models," *Knowledge-Based Engineering and Sciences*, vol. 2, no. 2, pp. 1–12, 2021.

[8] M. R. Haas, "Knowledge gathering, team capabilities, and project performance in challenging work environments," *Management Science*, vol. 52, no. 8, pp. 1170–1184, 2006.

[9] S. Hwang, "Dynamic regression models for prediction of construction costs," *Journal of Construction Engineering and Management*, vol. 135, no. 5, pp. 360–367, 2009.

[10] K. H. Mohammad, N. S. Ali, and B. M. Najm, "Assessment of the cost and time impact of variation orders on construction projects in Sulaimani governorate," *Journal of Engineering*, vol. 27, no. 2, pp. 106–125, 2021.

[11] A. Akintoye, "Analysis of factors influencing project cost estimating practice," *Construction Management & Economics*, vol. 18, no. 1, pp. 77–89, 2000.

[12] T. Huo, H. Ren, and W. Cai, G. Q. Shen, Measurement and dependence analysis of cost overruns in megatransport infrastructure projects: case study in Hong Kong," *Journal of Construction Engineering and Management*, vol. 144, no. 3, Article ID 5018001, 2018.

[13] E. Matel, F. Vahdatikhaki, S. Hosseinyalamdary, T. Evers, and H. Voordijk, "An artificial neural network approach for cost estimation of engineering services," *International Journal of Construction Management*, vol. 22, no. 7, pp. 1274–1287, 2019.

[14] D. D. Ahiaga-Dagbui and S. D. Smith, "Neural networks for modelling the final target cost of water projects," *Proceedings of the 28th Annu. ARCOM Conf*, pp. 307–316, Edinburgh, UK, September 2012.

[15] A. Jaafari, "Management of risks, uncertainties and opportunities on projects: time for a fundamental shift," *International Journal of Project Management*, vol. 19, no. 2, pp. 89–101, 2001.

[16] S. Demirkesen and B. Ozorhon, "Impact of integration management on construction project management performance," *International Journal of Project Management*, vol. 35, no. 8, pp. 1639–1654, 2017.

[17] S. Banihashemi, M. R. Hosseini, H. Golizadeh, and S. Sankaran, "Critical success factors (CSFs) for integration of sustainability into construction project management practices in developing countries," *International Journal of Project Management*, vol. 35, no. 6, pp. 1103–1119, 2017.

[18] S. Kim, S. Chang, and D. Castro-Lacouture, "Dynamic modeling for analyzing impacts of skilled labor shortage on construction project management," *Journal of Management in Engineering*, vol. 36, no. 1, Article ID 4019035, 2020.

[19] Z. Shehu, I. R. Endut, A. Akintoye, and G. D. Holt, "Cost overrun in the Malaysian construction industry projects: a deeper insight," *International Journal of Project Management*, vol. 32, no. 8, pp. 1471–1480, 2014.

[20] D. R. Al-Tawal, M. Arafah, and G. J. Sweis, "A model utilizing the artificial neural network in cost estimation of construction projects in Jordan," *Engineering Construction and Architectural Management*, vol. 28, no. 9, pp. 2466–2488, 2020.

[21] M. O. Sanni-Anibire, R. Mohamad Zin, and S. O. Olatunji, "Developing a preliminary cost estimation model for tall buildings based on machine learning," *International Journal of Management Science and Engineering Management*, vol. 16, no. 2, pp. 134–142, 2021.

[22] A. Enshassi, S. Mohamed, and I. Madi, "Factors affecting accuracy of cost estimation of building contracts in the Gaza Strip," *Journal of Financial Management of Property and Construction*, vol. 10, no. 2, 2005.

[23] I. Attarzadeh and S. H. Ow, "Proposing a new software cost estimation model based on artificial neural networks," *2nd International Conference on Computer Engineering and Technology*, vol. 3, pp. V3–V487, 2010.

[24] J. Ahn, S. H. Ji, S. J. Ahn et al., "Performance evaluation of normalization-based CBR models for improving construction cost estimation," *Automation in Construction*, vol. 119, Article ID 103329, 2020.

[25] M. Alzara, J. Kashiwagi, D. Kashiwagi, and A. Al-Tassan, "Using PIPS to minimize causes of delay in Saudi Arabian construction projects: university case study," *Procedia Engineering*, vol. 145, pp. 932–939, 2016.

[26] A. Enshassi, S. Mohamed, and M. Abdel-Hadi, "Factors affecting the accuracy of pre-tender cost estimates in the Gaza

Strip," *Journal of Construction in Developing Countries*, vol. 18, no. 1, 2013.

[27] A. Akintoye and E. Fitzgerald, "A survey of current cost estimating practices in the UK," *Construction Management & Economics*, vol. 18, no. 2, pp. 161–172, 2000.

[28] I. ElSawy, H. Hosny, and M. A. Razek, "A neural network model for construction projects site overhead cost estimating in Egypt," arXiv Prepr, 2011, https://arXiv1106.1570.

[29] L. Sabol, *Challenges in Cost Estimating with Building Information Modeling*, pp. 1–16, IFMA world Work, Washington, DC, 2008.

[30] M. Barakchi, O. Torp, and A. M. Belay, "Cost estimation methods for transport infrastructure: a systematic literature review," *Procedia Engineering*, vol. 196, pp. 270–277, 2017.

[31] M.-Y. Cheng, H.-C. Tsai, and E. Sudjono, "Conceptual cost estimates using evolutionary fuzzy hybrid neural network for projects in construction industry," *Expert Systems with Applications*, vol. 37, no. 6, pp. 4224–4231, 2010.

[32] O. Alshboul, A. Shehadeh, G. Almasabha, and A. S. Almuflih, "Extreme gradient boosting-based machine learning approach for green building cost prediction," *Sustainability*, vol. 14, no. 11, p. 6651, 2022.

[33] K. Upreti, U. K. Singh, R. Jain, K. Kaur, and A. K. Sharma, "Fuzzy logic based support vector regression (SVR) model for software cost estimation using machine learning," in *ICT Systems and Sustainability*, pp. 917–927, Springer, Berlin, Germany, 2022.

[34] A. H. Al-Momani, "Construction cost prediction for public school buildings in Jordan," *Construction Management & Economics*, vol. 14, no. 4, pp. 311–317, 1996.

[35] D. J. Lowe, M. W. Emsley, and A. Harding, "Predicting construction cost using multiple regression techniques," *Journal of Construction Engineering and Management*, vol. 132, no. 7, pp. 750–758, 2006.

[36] F. Shutian, Z. Tianyi, and Z. Ying, "Prediction of construction projects' costs based on fusion method," *Engineering Computations*, vol. 34, no. 7, pp. 2396–2408, 2017.

[37] H. Son, C. Kim, and C. Kim, "Hybrid principal component analysis and support vector machine model for predicting the cost performance of commercial building projects using pre-project planning variables," *Automation in Construction*, vol. 27, pp. 60–66, 2012.

[38] R. Wang, V. Asghari, C. M. Cheung, S.-C. Hsu, and C.-J. Lee, "Assessing effects of economic factors on construction cost estimation using deep neural networks," *Automation in Construction*, vol. 134, Article ID 104080, 2022.

[39] Z. M. Yaseen, Z. H. Ali, S. Q. Salih, and N. Al-Ansari, "Prediction of risk delay in construction projects using a hybrid artificial intelligence model," *Sustainability*, vol. 12, no. 4, p. 1514, 2020.

[40] H. T. Almusawi and A. M. Burhan, "Developing a model to estimate the productivity of ready mixed concrete batch plant," *Journal of Engineering*, vol. 26, no. 10, pp. 80–93, 2020.

[41] H. Sanikhani, R. C. Deo, P. Samui et al., "Survey of different data-intelligent modeling strategies for forecasting air temperature using geographic information as model predictors," *Computers and Electronics in Agriculture*, vol. 152, pp. 242–260, 2018.

[42] I. Peško, V. Mucenski, M. Seslija et al., "Estimation of costs and durations of construction of urban roads using ANN and SVM," *Complexity*, vol. 2017, p. 13, 2017.

[43] S. S. Arage and N. V Dharwadkar, "Cost estimation of civil construction projects using machine learning paradigm," in *Proceedings of the 2017 International Conference on I-SMAC (IoT in Social, Mobile, Analytics and Cloud)(I-SMAC)*, pp. 594–599, Palladam India, February 2017.

[44] S. S. Arage and N. V. Dharwadkar, "Prediction and estimation of civil construction cost using linear regression and neural network," *International Journal of Intelligent Systems Design and Computing*, vol. 2, no. 1, pp. 28–44, 2018.

[45] M. Juszczyk, "Residential buildings conceptual cost estimates with the use of support vector regression," *MATEC Web of Conferences*, vol. 196, p. 04090, 2018.

[46] M. Juszczyk, "On the search of models for early cost estimates of bridges: an SVM-based approach," *Buildings*, vol. 10, no. 1, p. 2, 2019.

[47] V. Chandanshive and A. R. Kambekar, "Estimation of building construction cost using artificial neural networks," *J. Soft Comput. Civ. Eng.*vol. 3, no. 1, pp. 91–107, 2019.

[48] S. T. Hashemi, O. M. Ebadati E, and H. Kaur, "A hybrid conceptual cost estimating model using ANN and GA for power plant projects," *Neural Computing & Applications*, vol. 31, no. 7, pp. 2143–2154, 2019.

[49] T. Lin, T. Yi, C. Zhang, and J. Liu, "Intelligent prediction of the construction cost of substation projects using support vector machine optimized by particle swarm optimization," *Mathematical Problems in Engineering*, vol. 2019, Article ID 7631362, 10 pages, 2019.

[50] H. H. Elmousalami, "Artificial intelligence and parametric construction cost estimate modeling: state-of-the-art review," *Journal of Construction Engineering and Management*, vol. 146, no. 1, 2020.

[51] K. Tijanić, D. Car-Pušić, and M. Šperac, "Cost estimation in road construction using artificial neural network," *Neural Computing & Applications*, vol. 32, no. 13, pp. 9343–9355, 2020.

[52] D. Car-Pusic, S. Petruseva, V. Zileska Pancovska, and Z. Zafirovski, "Neural network-based model for predicting preliminary construction cost as part of cost predicting system," *Advances in Civil Engineering*, vol. 2020, Article ID 8886170, 13 pages, 2020.

[53] C.-H. Huang and S.-H. Hsieh, "Predicting BIM labor cost with random forest and simple linear regression," *Automation in Construction*, vol. 118, Article ID 103280, 2020.

[54] D. Ye, "An algorithm for construction project cost forecast based on particle swarm optimization-guided BP neural network," *Scientific Programming*, vol. 2021, p. 8, 2021.

[55] S. Shoar, N. Chileshe, and J. D. Edwards, "Machine learning-aided engineering services' cost overruns prediction in high-rise residential building projects: application of random forest regression," *Journal of Building Engineering*, vol. 50, Article ID 104102, 2022.

[56] Y.-M. Cheng, "An exploration into cost-influencing factors on construction projects," *International Journal of Project Management*, vol. 32, no. 5, pp. 850–860, 2014.

[57] M. Gunduz and O. L. Maki, "Assessing the risk perception of cost overrun through importance rating," *Technological and Economic Development of Economy*, vol. 24, no. 5, pp. 1829–1844, 2018.

[58] K. C. Iyer and K. N. Jha, "Factors affecting cost performance: evidence from Indian construction projects," *International Journal of Project Management*, vol. 23, no. 4, pp. 283–295, 2005.

[59] L. Zhao, J. Mbachu, and Z. Liu, "Identifying significant cost-influencing factors for sustainable development in construction industry using structural equation modelling," *Mathematical Problems in Engineering*, vol. 2020, p. 16, 2020.

[60] H. A. Afan, M. F. Allawi, A. El-Shafie et al., "Input attributes optimization using the feasibility of genetic nature inspired

algorithm: application of river flow forecasting," *Scientific Reports*, vol. 10, no. 1, pp. 4684–4715, 2020.

[61] D. Chakraborty, H. Elhegazy, H. Elzarka, and L. Gutierrez, "A novel construction cost prediction model using hybrid natural and light gradient boosting," *Advanced Engineering Informatics*, vol. 46, Article ID 101201, 2020.

[62] T. Chen and C. Guestrin, "Xgboost: a scalable tree boosting system," *Proceedings of the 22nd Acm Sigkdd International Conference on Knowledge Discovery and Data Mining*, pp. 785–794, San Francisco, California, USA, August 2016.

[63] H. Al-Ageeli and A. S. Alzobaee, "The most influential factor on the stumble and failure of the governmental projects," *Journal of Engineering*, vol. 22, no. 3, pp. 93–110, 2016.

[64] H. Tao, M. Habib, I. Aljarah, H. Faris, H. A. Afan, and Z. M. Yaseen, "An Intelligent Evolutionary Extreme Gradient Boosting Algorithm Development for Modeling Scour Depths under Submerged Weir," *Inf. Sci. (Ny)*, vol. 570, 2021.

[65] H. Tao, S. M. Awadh, S. Q. Salih, S. S. Shafik, and Z. M. Yaseen, "Integration of extreme gradient boosting feature selection approach with machine learning models: application of weather relative humidity prediction," *Neural Computing & Applications*, vol. 34, no. 1, pp. 515–533, 2021.

[66] H. Tao, S. Salih, A. Y. Oudah et al., "Development of new computational machine learning models for longitudinal dispersion coefficient determination: case study of natural streams, United States," *Environmental Science and Pollution Research*, vol. 29, no. 24, pp. 35841–35861, 2022.

[67] S. Alves Basilio and L. Goliatt, "Gradient boosting hybridized with exponential natural evolution strategies for estimating the strength of geopolymer self-compacting concrete," *Knowledge-Based Engineering and Sciences*, vol. 3, no. 1, pp. 1–16, 2022.

[68] Y. Wang and X. S. Ni, "A XGBoost Risk Model via Feature Selection and Bayesian Hyper-Parameter Optimization," arXiv Prepr, 2019, https://arXiv1901.08433.

[69] K. Nordhausen, "The elements of statistical learning: data mining, inference, and prediction, second edition by trevor Hastie, robert tibshirani, jerome friedman," *International Statistical Review*, vol. 77, no. 3, p. 482, 2009.

[70] L. Breiman, "Using iterated bagging to debias regressions," *Machine Learning*, vol. 45, no. 3, pp. 261–277, 2001.

[71] J. Zhou, X. Shi, K. Du, X. Qiu, X. Li, and H. S. Mitri, "Feasibility of random-forest approach for prediction of ground settlements induced by the construction of a shield-driven tunnel," *International Journal of Geomechanics*, vol. 17, no. 6, Article ID 4016129, 2017.

[72] Y. Zhang, A. Javanmardi, Y. Liu et al., "How does experience with delay shape managers' making-do decision: random forest approach," *Journal of Management in Engineering*, vol. 36, no. 4, Article ID 4020030, 2020.

[73] X. Liu, Y. Song, W. Yi, X. Wang, and J. Zhu, "Comparing the random forest with the generalized additive model to evaluate the impacts of outdoor ambient environmental factors on scaffolding construction productivity," *Journal of Construction Engineering and Management*, vol. 144, no. 6, Article ID 4018037, 2018.

[74] S. K. Bhagat, T. Tiyasha, A. Kumar et al., "Integrative artificial intelligence models for Australian coastal sediment lead prediction: an investigation of in-situ measurements and meteorological parameters effects," *Journal of Environmental Management*, vol. 309, Article ID 114711, 2022.

[75] B. Leo, "Bagging Predictors," *Mach. Learn*, vol. 24, 1996.

[76] T. K. Ho, "The random subspace method for constructing decision forests," *IEEE Transactions on Pattern Analysis and Machine Intelligence*, vol. 20, no. 8, pp. 832–844, 1998.

[77] M. A. Khan, S. A. Memon, F. Farooq, M. F. Javed, F. Aslam, and R. Alyousef, "Compressive strength of fly-ash-based geopolymer concrete by gene expression programming and random forest," *Advances in Civil Engineering*, vol. 2021, p. 17, 2021.

[78] B. Salman and M. M. Kadhum, "Predicting of load carrying capacity of reactive powder concrete and normal strength concrete column specimens using artificial neural network," *Knowledge-Based Eng. Sci.*vol. 3, no. 1, pp. 45–53, 2022.

[79] A. De Fenza, A. Sorrentino, and P. Vitiello, "Application of artificial neural networks and probability ellipse methods for damage detection using lamb waves," *Composite Structures*, vol. 133, pp. 390–403, 2015.

[80] C. Yan, Z. Yousef, S. A. Alireza et al., "A Review Study of Application of Artificial Intelligence in Construction Management and Composite Beams," vol. 39, no. 6, 2021.

[81] J. J. Hopfield, "Neural networks and physical systems with emergent collective computational abilities," *Proceedings of the National Academy of Sciences*, vol. 79, no. 8, pp. 2554–2558, 1982.

[82] H. Adeli, "Neural networks in civil engineering: 1989–2000," *Computer-Aided Civil and Infrastructure Engineering*, vol. 16, no. 2, pp. 126–142, 2001.

[83] R. Lippmann, "An introduction to computing with neural nets," *IEEE ASSP Magazine*, vol. 4, no. 2, pp. 4–22, 1987.

[84] D. E. Rumelhart, G. E. Hinton, and R. J. Williams, *Learning Internal Representations by Error Propagation*, California Univ San Diego La Jolla Inst for Cognitive Science, 1985.

[85] V. N. Vapnik, *The Nature of Statistical Learning Theory*, vol. 8, no. 6, 2000.

[86] G. Zhang, Z. H. Ali, M. S. Aldlemy et al., "Reinforced concrete deep beam shear strength capacity modelling using an integrative bio-inspired algorithm with an artificial intelligence model," *Engineering with Computers*, vol. 38, 2020.

[87] S. Raghavendra N and P. C. Deka, "Support vector machine applications in the field of hydrology: a review," *Applied Soft Computing*, vol. 19, pp. 372–386, 2014.

[88] K. P. Wu and S. D. Wang, "Choosing the kernel parameters for support vector machines by the inter-cluster distance in the feature space," *Pattern Recognition*, vol. 42, no. 5, pp. 710–717, 2009.

[89] R. E. Walpole, R. H. Myers, S. L. Myers, and K. Ye, *Probability and statistics for engineers and scientists*, Vol. 5, Macmillan, New York, 1993.

[90] H. V. Gupta, H. Kling, K. K. Yilmaz, and G. F. Martinez, "Decomposition of the mean squared error and NSE performance criteria: implications for improving hydrological modelling," *Journal of Hydrology*, vol. 377, no. 1–2, pp. 80–91, 2009.

[91] K. E. Taylor, "Summarizing multiple aspects of model performance in a single diagram," *Journal of Geophysical Research: Atmospheres*, vol. 106, no. D7, pp. 7183–7192, 2001.

[92] G. Mahalakshmi and C. Rajasekaran, "Early cost estimation of highway projects in India using artificial neural network," *Lecture Notes in Civil Engineering*, vol. 25, pp. 659–672, 2019.

[93] S. Shartooh Sharqi and A. Bhattarai, "Evaluation of several machine learning models for field canal improvement project cost prediction," *Complexity*, vol. 2021, p. 12, 2021.
[94] J. A. Khalaf, A. A. Majeed, M. S. Aldlemy et al., "Hybridized deep learning model for perfobond rib shear strength connector prediction," *Complexity*, vol. 2021, p. 21, 2021.
[95] M. W. Falah, S. H. Hussein, M. A. Saad et al., "Compressive strength prediction using coupled deep learning model with extreme gradient boosting algorithm: environmentally friendly concrete incorporating recycled aggregate," *Complexity*, vol. 2022, p. 22, 2022.

Hindawi
Complexity
Volume 2022, Article ID 4998200, 28 pages
https://doi.org/10.1155/2022/4998200

Research Article

Application of Extreme Learning Machine Algorithm for Drought Forecasting

Muhammad Ahmad Raza[1,2] **Mohammed M. A. Almazah**[3,4] **Zulfiqar Ali**[5] **Ijaz Hussain**[1] **and Fuad S. Al-Duais**[6,7]

[1]*Department of Statistics, Quaid-i-Azam University, Islamabad, Pakistan*
[2]*Department of Statistics, Federal Urdu University of Arts, Science and Technology Islamabad, Islamabad, Pakistan*
[3]*Department of Mathematics, College of Sciences and Arts (Muhyil), King Khalid University, Muhyil 61421, Saudi Arabia*
[4]*Department of Mathematics and Computer, College of Sciences, Ibb University, Ibb 70270, Yemen*
[5]*College of Statistical and Actuarial Sciences, University of the Punjab, Lahore, Pakistan*
[6]*Mathematics Department, College of Humanities and Science, Prince Sattam Bin Abdulaziz University, Al Aflaj, Saudi Arabia*
[7]*Administration Department, Administrative Science College, Thamar University, Thamar, Yemen*

Correspondence should be addressed to Muhammad Ahmad Raza; maraza@stat.qau.edu.pk and Ijaz Hussain; ijaz@qau.edu.pk

Received 6 March 2022; Revised 5 August 2022; Accepted 16 August 2022; Published 20 September 2022

Academic Editor: M. Z. Naser

Drought is a complex and frequently occurring natural hazard in many parts of the world. Therefore, accurate drought forecasting is essential to mitigate its adverse impacts. This research has inferred the implication and the appropriateness of the extreme learning machine (ELM) algorithm for drought forecasting. For numerical evaluation, time series data of the Standardized Precipitating Temperature Index (SPTI) are used for nine meteorological stations located in various climatological zones of Pakistan. To assess the performance of ELM, this research includes parallel inferences of multilayer perceptron (MLP) and autoregressive integrated moving average (ARIMA) models. The performance of each model is assessed using root mean square error (RMSE), mean absolute error (MAE), mean absolute percent error (MAPE), Kling-Gupta efficiency (KGE), Willmott index (WI), and Karl Pearson's correlation coefficient. Generally, graphical results illustrated an excellent performance of the ELM algorithm over MLP and ARIMA models. For training data of SPTI-1, ELM's best performance has observed at Chitral station (RMSE = 0.374, KGE = 0.838, WI = 0.960, MAE = 0.272, MAPE = 259.59, $R = 0.93$). For SPTI-1 at Astore station, the numerical results are (RMSE = 0.688, KGE = 0.988, WI = 0.997, MAE = 0.798, MAPE = 247.35). The overall results indicate that the ELM outperformed by producing the smallest RMSE, MAE, and MAPE values and maximum values for KGE, WI, and correlation coefficient values at almost all the selected meteorological stations for (1, 3, 6, 9, and 12) month time scales. In summary, this research endorses the use of ELM for accurate drought forecasting.

1. Introduction

Drought is a recurrent natural climatic phenomenon that occurs virtually in most parts of the world. A drought is a recurrent event due to a lack of precipitation for an extended period of time in a particular region [1, 2]. Like other natural hazards, drought is steady and sometimes considered a creeping phenomenon as it is a gradually evolving natural hazard due to climatic fluctuations [3, 4]. Generally, the impacts of drought have effect on agriculture, livestock, ecological system, socio-economic, and energy sectors [5, 6]. Moreover, drought can be categorized as meteorological, hydrological, agricultural, and socio-economic drought. Therefore, it requires the investigator to consider individual opinions to define a specific type of drought [1, 2, 7, 8].

Due to the complex nature of drought, it is difficult to monitor and assess its impact [1, 2, 6]. An accurate prediction of drought is considered difficult, especially its onset

or end [9, 10]. Prolonged droughts adversely impact the economic agriculture and social sectors. These massive drought impacts are due to sudden and widespread climate changes [11]. Drought can lead to devastating economic effects, with worldwide losses of around $9 billion per annum; the US livestock industry faced a $400 million loss during a severe drought in 2002 [12]. A comprehensive early warning system for drought is necessary to reduce its devastating impact. However, a few studies are conducted to mitigate this stochastic natural hazard [13–15]. Recently, numerous drought indices have been developed to identify and monitor droughts and introduce mitigation policies [16–19]. Reference [20] proposed a new drought indicator, i.e., Normalized Ecosystem Drought Index (NEDI), to observe dryness conditions in the pattern of a transitional ecosystem. It is expected that dryness conditions can be quantified better by using NEDI.

Numerically expressed drought indices are more understandable than natural rainfall data [1, 2, 21]. Drought indices can be a valuable tool to detect the initiation and termination of drought levels necessary for recovery planning, mitigation, and decision-making [22, 23]. Drought indices aim to quantify how drought conditions evolve and classify the severity of drought events. These indices made easy droughts modeling using stochastic time series, neural network algorithms, and water balance models. The most commonly used drought indices are Palmer Drought Severity Index (PDSI) [24], Surface Water Supply Index (SWSI) [25], Standardized Precipitation Index (SPI) [26], Effective Drought Index (EDI), and Standardized Precipitation and Evapotranspiration Index (SPEI) [27]. Ali et al. [28] proposed a multiscalar drought index named as Standardized Precipitation Temperature Index (SPTI). These drought indices were calculated using different meteorological variables [29]. Different drought indices were used to characterize, estimate, and forecast drought conditions.

The current long-range drought forecasts have minimal reliability [30]. Existing conventional stochastic models are inadequate for accurate drought predictions [31]. The recently developed machine learning (ML) models have extensive application in climatology including Naïve Bayes classifier, Bayesian networks [32], support vector machine (SVM), wavelet gene expression programming [33], maximum entropy, and artificial neural networks (ANNs). Results of several studies affirmed that the ML models perform comparatively better than conventional stochastic and dynamic models for drought estimation [34, 35]. ANN models act like a human brain and can be classified according to their neuron structure, number of hidden layers, and activation functions. Many researchers have successfully applied MLP neural networks for drought estimation and forecasting [36, 37]. The MLP is capable of accurately forecasting soil temperature in semi-humid and arid regions [38]. Aghelpour et al. [39] improved agriculture drought modeling by coupling the dragonfly optimization algorithm with SVM. Furthermore, [40] efficiently modeled RDI using hybrid support vector regression (SVR) coupled with firefly algorithm (FA), whale optimization algorithm (WOA), and wavelet analysis (WA). The results proved that hybrid and coupled SVR techniques improved drought forecasting. Although ML models have an outstanding reputation in estimation, prediction, and forecasting, many have slow computing times [41]. Among the class of ANN algorithms, ELM is being widely used in various fields and has gained fame in climatology and engineering [42–47]. Mouatadid and Adamowski [48] efficiently forecasted urban water demand for Montreal (Canada) using ELM.

This research aims to infer the implication and the appropriateness of the extreme learning machine (ELM) algorithm for drought forecasting. In previous research, ELM has been implemented in different disciplines, including classification [49], regression [50, 51], clustering [52, 53], feature selection [54], pattern recognition [55], image processing [56] estimating sediment transport [57], and drought forecasting [30, 58, 59].The ELM has significantly faster learning, improved generalization performance, minimum human intervention, and accurate forecasting performance [60].

2. Materials and Methods

2.1. Data and Study Area. The application of this research is based on nine meteorological stations scattered around Pakistan. The topographic map of the study region and distribution of selected meteorological stations is shown in Figure 1. The study area is situated in the southeastern part of Asia and lies between 23.8° to 37°N latitude and 60.9° to 75.37°E longitude. The region is classified into clusters comprising different meteorological stations with diverse spatial characteristics [61]. Hence, selecting these meteorological stations aims to cover the maximum climatic variability. In addition, the study area encompasses five major river basins, Ravi, Chenab, Sutlej, Jhelum, and the Indus River. These rivers are the backbone of the country's agriculture industry and hydropower projects.

For this research, time series data of the monthly precipitation and minimum and maximum air temperatures were collected from the Karachi Data Processing Center (KDPC) through the Pakistan Meteorological Department (PMD). The length of the data ranges from January 1951 to December 2016. The full-length data were split into two parts. January 1951 to December 2013 is considered the training data set, and the remaining three years, January 2014 to December 2016, is considered the test data set. The climatological forecast needs more accuracy for future hazard mitigation because long-range climatological forecasts compromise accuracy. Here, the errors and irregularities were detected and removed by the KDPC itself. Additionally, missing data were adjusted by generating values using cumulative distributions over lead periods.

2.2. Standardized Precipitation Temperature Index (SPTI). The Standardized Drought Indices (SDIs) have extensive applications for drought monitoring. SDIs are standardized and spatially invariant tools for monitoring and assessing drought characteristics. In the literature, various authors have offered numerous methods for SDIs. Example includes

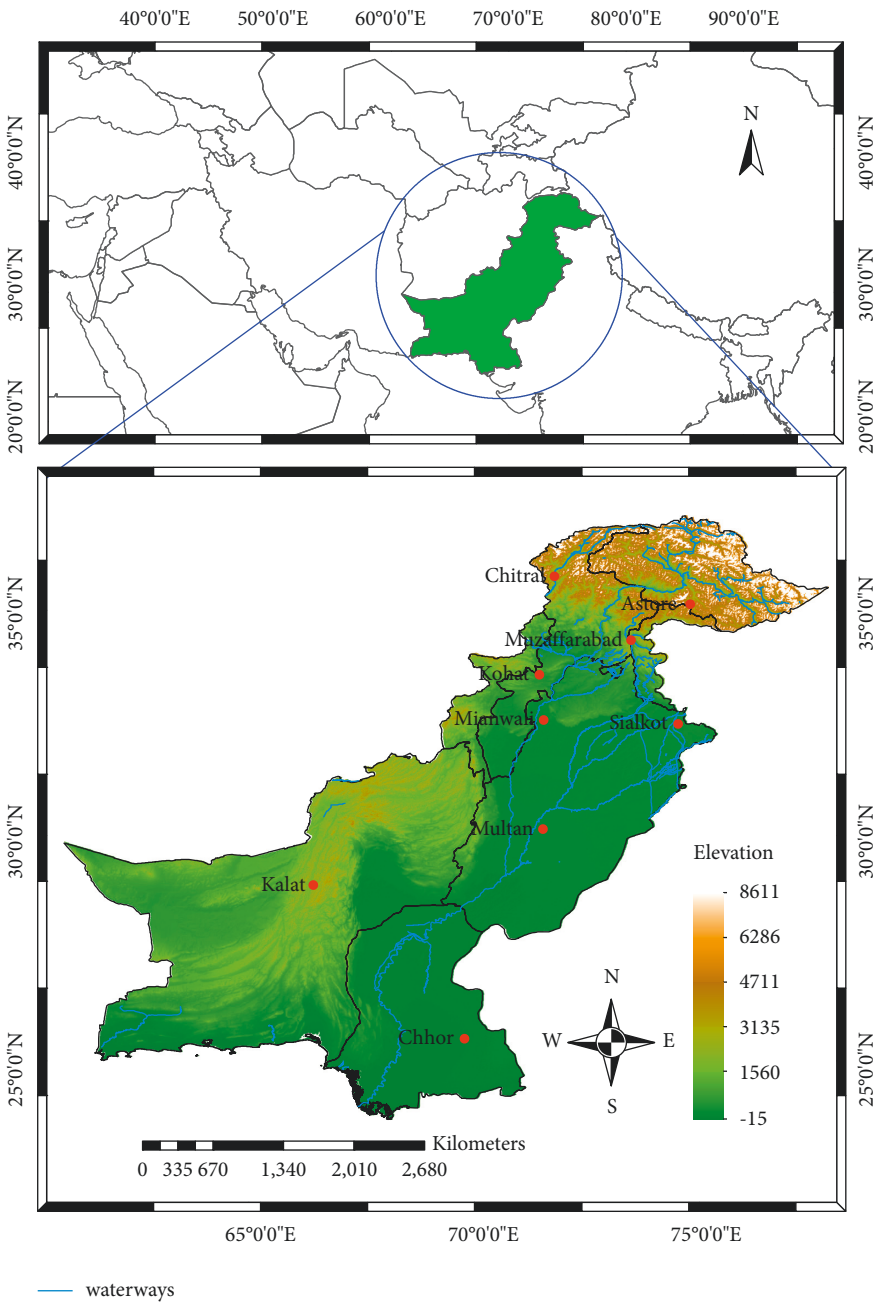

Figure 1: Topographic map of the study area and geographical distribution of meteorological stations.

the Standardized Precipitation Index (SPI) [26], Standardized Precipitation Evapotranspiration Index (SPEI) [27], and Standardized Precipitation Temperature Index (SPTI) [28]. Precipitation and temperature are two essential climatology indicators, revealing the vital dynamics of climate and hydrology. Therefore, a standardized drought index based on these two meteorological variables is more beneficial for drought monitoring and forecasting. Therefore, the SPTI has been chosen as SDI for monitoring and forecasting drought. The mathematical calculation of SPTI is quite similar to SPI; more detailed discussion can be accessed in [41]. SPTI is a multiscalar drought index and can be calculated for different time scales (1–48). Positive and negative values of the index

Table 1: Drought classification of the SPTI index.

SPTI values	Classes	Cumulative probabilities
≤−2	Extreme drought (ED)	0.000–0.023
−1.9 to −1.5	Severe drought (SD)	0.023–0.067
−1.49 to −1	Moderate drought (MD)	0.067–0.159
−0.99 to 0.99	Near normal (NN)	0.159–0.841
1 to 1.49	Moderate wet (MW)	0.841–0.933
1.5 to 1.9	Severe wet (SW)	0.933–0.977
≥2	Extreme wet (EW)	0.977–1

indicate drought and wet conditions. These drought conditions are classified in Table 1 [62, 63].

SPTI is a modified form of the De-Martonne Aridity Index (DAI) (de Martonne, 1926). The mathematical properties of SPTI are utterly similar to SPI, an extensively used index for drought prediction in many parts of the world. For SPTI, we need to calculate DAI based on the monthly total precipitation and average monthly temperature. The next step is to fit an appropriate distribution to calculate a cumulative probability for standardization. However, many researchers used Gamma distribution for standardization. The index values are subjected to fitted distribution, and none of the single distribution can be appropriate for all the stations and for various time scales. Therefore, the 32 candidate distributions have been fitted on DAI at different lead time scales. The Bayesian Information Criterion (BIC) has been used as a threshold to assess the appropriateness of a distribution.

2.3. Candidate Algorithms. An artificial neural network (ANN) is a computational paradigm. It is a data-driven technique in which information goes through a biological structure of neurons with multiple layers introduced in the 1950s. It did not impose any constraints on input variables to train the model like other stochastic models. These algorithms are brilliant and learn from existing relationships among the observations of input and auxiliary variables. ANN can manage high-dimensional and high-frequency complex datasets [58]. ANN algorithms have broad applications in mathematics, engineering, medicine, economics, neurology, and hydrology [64–67]. Kuligowski and Barros [68] claimed that weather prediction could be improved using ANN algorithms. This class of algorithms can be helpful in the field of climatology to forecast natural hazards like drought. Multilayer perceptron (MLP) is considered one of the useful and fully connected feedforward artificial neural networks. It usually consists of three layers of multiple nodes, including an input layer, multiple hidden layers (usually two hidden layers with multiple hidden nodes) with a nonlinear activation function, and an output layer. The neuron structure and estimation accuracy of MLP make it prominent among the other ANN algorithms. Error back-propagation is one of the supervised learning techniques used to train MLP. Another stochastic algorithm used for drought prediction is the ARIMA process [69].

2.3.1. Seasonal Autoregressive and Integrated Moving Average Model (SARIMA). Yule [70] pioneered to introduce autoregressive (AR) models that the time series being analyzed is a linear function of its previous lag values. Slutzky [71] modeled time series as a function of past residual terms named as moving average model (MA). Wold [72] merged both AR and MA specifications and introduced a new generalized form of ARMA specifications used to model all stationary time series by choosing the appropriate order of "AR" and "MA" terms into the model. Time series data generally have trends (non-stationary). Non-stationary time series can be modeled by appropriate differencing the series into stationary. The series that is transformed from non-stationary to stationary by differencing is known as integrated series. The ARIMA has a systematic way of identification, estimation, and diagnostic checking approach to reach an appropriate model. Many hydrologic and meteorological time series data have inherited seasonal components [73]. These kinds of data can be efficiently modeled with the seasonal ARIMA model, which requires only a few parameters to be estimated [74]. The seasonal ARIMA model is described as ARIMA(p, d, q) $(P, D, Q)_s$, where (p, d, q) is the non-seasonal component of the ARIMA specifications, while $(P,D,Q)_s$ is the seasonal component of the ARIMA model. The general seasonal ARIMA specifications are as follows:

$$\phi_p(B)\Phi_P(B^s)\nabla^d\nabla_s^{D'}D_t = \theta_q(B)\Theta_Q(B^s)\alpha_t. \quad (1)$$

Here, "p" is the order of non-seasonal autoregressive terms, "q" is the no of non-seasonal MA terms to be included in the model. Similarly, "P" is the seasonal autoregressive terms, and "Q" is the number of seasonal MA terms, ∇^d is the difference operator of non-seasonal series with "d" levels to make the series stationary, $\nabla^{D'}$ is the difference operator of seasonal series with D' no of differencing to get integrated stationary series, where "s" is the length of the season. The mathematical details of ARIMA specifications can be observed in [75]. The development of ARIMA specifications included identification, estimation, and diagnostic checking. By following these steps, a parsimonious ARIMA specification can be selected for estimation and forecasting a time series.

2.3.2. Extreme Learning Machine (ELM). The extreme learning machine (ELM) is a modern single hidden layer feedforward neural network (SLFN) algorithm proposed by [76]. The proposed novel machine learning algorithm (ELM) operates identically to feedforward back-propagation ANN (FFBP-ANN) and least-squares support vector regression LSSVR models. It has shown its candidacy among the ANN algorithms to solve complex linear and nonlinear regression problems. It contains a single hidden layer of multiple hidden nods. However, most of the ANN-based methods have specific limitations such as slow computation, learning epochs, larger biases, and tuning parameters (weights). To overcome such weaknesses and the frailty of ANN methods, a state-of-the-art algorithm known as extreme learning machine (ELM) gained fame in the class of ANN algorithms [77].

Studies have revealed that even with randomly generated weights of hidden nodes, ELM can attain the universal approximation feature of SLFNs [46, 47, 78]. In the proposed method, the input weights are assigned randomly, and the output weights can be solved uniquely by the least-squares method of generalized inverse function [76]. If hidden node input weights and biases are chosen randomly, SLNFs can be considered a linear system. The output weights are determined analytically through the generalized inverse operation of the hidden layer output matrices because these weights connect the hidden layer to the output layer of the linear

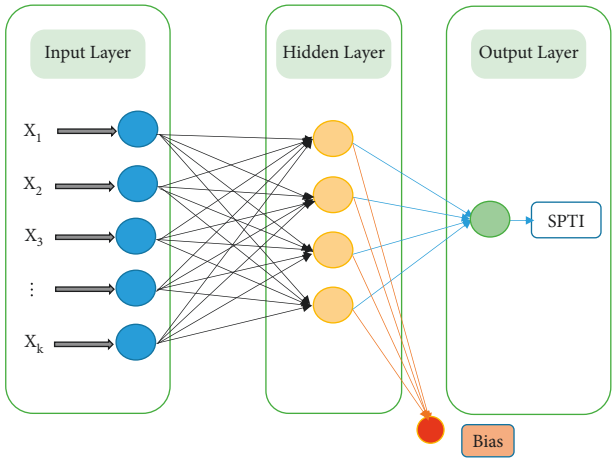

Figure 2: The topological structure of the extreme learning machine network. The input layer is the lag values of SPTI, the hidden layer contains randomly assigned hidden nodes, and the output layer generates predicted values of SPTI.

system. The ELM can solve regression problems with shorter simulation times than FFBP-ANN and LSSVR algorithms and makes ELM a thousand times faster [59, 79–81]. It contains common properties of high generalization performance. The topological structure of the ELM algorithm is given in Figure 2, where three layers of neurons are used to develop the architecture.

Input layer where the input variables are introduced, the single hidden layer contain variable number of neurons where data are processed and analyzed and the output layer produce desired results through their activation function. The activation function used in the ELM algorithm is a sigmoid function $g(x) = 1/(1 + e^{-x})$, and while training ELM, most of the time is utilized while calculating the Moore-Penrose generalized inverse $H^{\dagger}$ of the hidden layer.

Huang et al. [76] claimed that the maximal margin property of SVM and the minimal norm of weight theory of ELM is consistent. ELM and SVM perform equally well for standard optimization. For M random distinct samples (y_i, t_i), where $y_i = [y_{i1}, y_{i2}, \ldots, y_{im}]^T \in R^m$ and $t_i = [t_{i1}, t_{i2}, \ldots t_{il}]^T \in R^l$, standard ELM with N hidden nodes and with activation function $g(y)$ are mathematically modeled as

$$\sum_{i=1}^{\widehat{N}} \gamma_i g_i\left(y_j\right) = \sum_{i=1}^{\widehat{N}} \gamma_i g\left(\omega_i . y_j + b_i\right) = o_j j = 1, 2, 3, \ldots, M, \tag{2}$$

where $\omega_i = [\omega_{i1}, \omega_{i2}, \ldots, \omega_{im}]^T$ is the weight vector connecting the i^{th} hidden node and input nodes. $\gamma_i = [\gamma_{i1}, \gamma_{i2}, \ldots, \gamma_{il}]^T$ is the weight vector connecting the i^{th} hidden node and output nodes, and bi is the threshold of i^{th} hidden node. $\omega_i . y_j$ denote the inner product of ω_i and y_j.

$$H\gamma = T, \tag{3}$$

$$H\left(\omega_1, \omega_2, \ldots \omega_{\widehat{M}}, b_1, b_2, \ldots, b_{\widehat{M}}, y_1, y_2, \ldots, y_M\right) = \begin{bmatrix} g(\omega_1 . y_1 + b_1) & \cdots & g\left(\omega_{\widehat{M}} . y_1 + b_{\widehat{M}}\right) \\ \vdots & \cdots & \vdots \\ g(\omega_1 . y_M + b_1) & \cdots & g\left(\omega_{\widehat{M}} . y_M + b_{\widehat{M}}\right) \end{bmatrix}_{\widehat{M} \times M}, \tag{4}$$

$$\gamma = \begin{bmatrix} \gamma_1^T \\ \gamma_2^T \\ \vdots \\ \gamma_{\widehat{M}}^T \end{bmatrix}_{\widehat{M} \times l}, \text{ and } T = \begin{bmatrix} t_1^T \\ t_2^T \\ \vdots \\ t_M^T \end{bmatrix}_{M \times l}. \tag{5}$$

ELM attains optimal generalization performance as long as the chosen number of hidden nodes is sufficiently high. In our simulation through ELM with sigmoid activation function, the number of hidden nodes is selected automatically to attain optimal prediction and forecast performance.

2.4. Model Evaluation Metrics. A model performance assessment needs calibration of an existed link between observed and predicted hydrological patterns. The fundamental performance assessment method is through a visual inspection of empirical and predicted or forecasted time series. For the quantitative evaluation of algorithms, around 20 performance metrics select a hydrological model [82]. It has been observed that the choice of an appropriate model significantly changed if precision-based metrics were used instead of error-based metrics [83]. Numerous accuracy measurement criteria were developed, but each tool has inherited pros and cons, and none of the metrics is universally accepted and can be used as a threshold [84]. In this study, some error-based performance metrics have been used for cross-validation, including root mean square error (RMSE), mean absolute error (MAE), and mean absolute percentage error (MAPE). The Kling-Gupta efficiency (KGE) and Willmott Index of agreement (WI) are also better ways to assess the performance of stochastic, machine

Table 2: Summary statistics of rainfall (in mm) and spatial characteristics of selected stations.

Station	Min	Q1	Median	Mean	Q3	Max	Latitude	Longitude	Time range
Astore	0	10.97	26.35	40.64	54.52	248.7	35.3570°E	74.8624°N	1954–2016
Chhor	0	0	0	18.89	11.47	381	25.5114°E	69.7823°N	1951–2016
Chitral	0	3.72	20.2	38.51	58.48	281.4	35.7699°E	71.7741°N	1965–2016
Kalat	0	0	1.35	15.35	16.23	546.0	29.0523°E	66.5879°N	1951–2016
Kohat	0	12.51	33	47.98	65.7	419.6	33.5889°E	71.4429°N	1954–2016
Mianwali	0	3.95	22.1	43.6	60.12	530	32.5839°E	71.5370°N	1960–2016
Multan	0	0.01	4.1	16.85	19.2	231.2	30.1575°E	71.5247°N	1951–2016
Muzaffarabad	0	46.33	97.85	125.65	178.07	721	34.3551°E	73.4769°N	1955–2016
Sialkot	0	8.28	33.05	80.692	96.3	917.6	32.4945°E	74.5229°N	1951–2016

learning, and hydrologic models [85, 86]. Another way to assess an algorithm's prediction performance is to calculate the simple correlation coefficient between observed and predicted values of the input variable (SPTI) as a closeness measure. Similar performance metrics are used to assess the forecast ability of candidate algorithms.

The RMSE is the deviation of estimated or predicted values "$\widehat{D}$" from actual or observed values "D" of drought indices, computed for "T" different predictions given in

$$\text{RMSE} = \sqrt{\frac{1}{h}\sum_{t=T}^{T+h}\left(D_{t+1} - \widehat{D}_{t+1|T}\right)^2}. \tag{6}$$

Since RMSE is positively affected by outliers, therefore we need some robust measures toward extreme values. Mean absolute error (MAE) is less influenced by extreme values than RMSE [87]. Equation (7) describes the mathematical structure of the MAE.

$$MAE = \frac{1}{h}\sum_{t=T}^{T+h}\left(\left|D_{t+1} - \widehat{D}_{t+1|T}\right|\right). \tag{7}$$

Another accuracy measure is the mean absolute percentage error (MAPE), a unit-free tool to assess an algorithm's prediction and forecast ability. Unlike other performance metrics, MAPE is a scaled independent metric. These performance metrics or accuracy measures are extensively being used in the field of climatology. The mathematical form of MAPE is given in

$$\text{MAPE} = \frac{100}{h}\sum_{t=T}^{T+h}\left(\left|\frac{D_{t+1} - \widehat{D}_{t+1|T}}{D_{t+1}}\right|\right). \tag{8}$$

Kling-Gupta efficiency index was developed to assess the performance model by comparing estimated and observed time series data [88].

$$\text{KGE} = 1 - \sqrt{(r-1)^2 + (\alpha-1)^2 + (\beta-1)^2}. \tag{9}$$

Here, "r," α, and β in the KGE index illustrate the correlation coefficient, standard deviation ratio, and average ratio of observed and predicted values of SPTI, respectively.

Willmott [89] proposes an index named Willmott Index of agreement (WI) as a standardized measure of the degree of model prediction error.

$$WI = 1 - \left[\frac{\sum_{t=T}^{T+h}\left(D_{t+1} - \widehat{D}_{t+1|T}\right)^2}{\sum_{t=T}^{T+h}\left(\left|D_{t+1} - \overline{D}_{t+1}\right| + \left|\widehat{D}_{t+1} - \overline{D}_{t+1}\right|\right)^2}\right], 0 \le WI \le 1. \tag{10}$$

A model with minimum values of RMSE, MAE, MAPE, the maximum value of KGE index, and the value of WI close to "1" will be selected and proposed as an adequate algorithm for the estimation of existing drought phenomena and forecasting future drought episodes.

3. Results

The descriptive statistics of meteorological and climatic variables are briefly detailed by using five-number summary statistics. The numerical results related to Minimum (Min.), first quartile (Q_1), Median, Mean, and third quartile (Q_3) are expressed in Table 2. These results indicated that the annual and seasonal meteorological characteristics of the selected meteorological stations are quite diverse.

Muzaffarabad has the highest mean monthly precipitation (125.65 mm), and the lowest mean monthly precipitation recorded was (15.35 mm) at Kalat. Sialkot has the highest maximum rainfall in a month (917.6 mm), and Chhor has observed the lowest maximum rainfall in a month (11.47 mm), while minimum rainfall at all selected locations was zero (0 mm). The precipitation source at these stations varies, such as heavy rainfall occurring at some stations in the monsoon season (June-Sep). However, precipitation exponentially declined after September and lasted till December until the western depression started in winter. At the same time, western depression causes rainfall in the winter season (Dec-Mar). The above statistics exhibit the dry and wet season cycles at a few stations. Temperature is another climatic variable used to calculate SPTI, so similar descriptive statistics for minimum and maximum temperature are expressed in Table 3. Results show that the total monthly minimum and maximum temperatures are highly apparent and distinguishable for all the stations.

3.1. Estimation of SPTI. At the very early stage of the computational analysis, we first prepared time series data of the SPTI index for all the stations by following the guidelines [90]. As described in Section 2.2, CDFs of the appropriate probability functions are standardized for all the stations and

Table 3: Summary statistics of minimum and maximum temperatures (Celsius) at selected meteorological stations.

Station	Minimum temperature						Maximum temperature						Elevation (m)
	Min	Q1	Median	Mean	Q3	Max	Min	Q1	Median	Mean	Q3	Max	
Astore	−12.1	−2.5	4.2	3.982	10.7	17.5	−0.5	7.285	16.65	15.63	23.9	29.9	2546
Chhor	1.9	10.38	19.7	18.01	25.32	28.4	23.4	31.5	35.6	34.88	38.2	44.2	4
Chitral	−4.5	1.6	7.8	8.565	14.6	22	5.3	14.2	24.05	23.4	32.83	38.2	1493
Kalat	−11.9	−1.1	6.2	5.808	12.425	23.2	5	15.18	22.35	22.17	29.8	37.1	2007
Kohat	2.7	10.28	17.9	17.07	24.73	29.3	14.3	22.3	30.9	29.54	36.3	43.9	489
Mianwali	0.7	8.6	17.2	16.89	25.73	30.7	14.5	24.48	33.65	31.59	38	44	210
Multan	1	9.6	19.25	18.23	27.02	30.8	17.2	26.5	34.75	32.55	38.5	45.2	122
Muzaffarabad	0.9	6.65	13.75	13.57	20.73	24.7	12.2	20.48	29.1	27.51	33.83	39.9	737
Sialkot	2.1	9.2	18	16.69	24.3	28.8	13.5	23.7	32	29.77	34.6	43.4	256

Table 4: The candidacy of appropriate distributions according to their respective BIC values for SPTI-1.

Distribution	Mianwali	Sialkot	Muzaffarabad	Astore	Chitral	Multan	Kalat	Chhor	Kohat
2P beta	−260.71	−387.86	−278.31	−280.10	−216.46	−63.88	−418.16	−244.53	−228.65
3P Weibull	−472.53	−718.58	−555.22	−480.83	−400.89	−317.25	−638.60	−444.44	−622.28
4P beta	−463.53	−722.18	−584.52	−469.79	−393.88	−311.66	−664.62	−434.07	−616.67
Arcsine	−211.50	−322.48	−364.18	−272.85	−194.87	−38.61	−353.11	−178.98	−216.75
Burr	−49.90	−291.37	−351.96	−347.29	−87.23	259.98	−111.45	197.60	−315.30
Cauchy	−218.97	−414.95	−460.90	−367.96	−227.51	−87.98	−498.98	−289.68	−322.84
Chi	−292.62	−424.20	−186.90	−247.93	−245.62	113.16	−220.02	130.71	−315.76
Chi-square	−321.57	−546.12	−456.49	−441.42	−271.12	125.40	−179.55	136.71	−588.65
Cosine	−5.68	−181.37	−403.03	−192.31	−48.26	267.44	−64.93	206.84	−159.22
Curv. trapezoidal	−163.25	−349.64	−555.47	−375.44	−169.25	−117.58	−60.78	−236.04	−415.05
Exponential	−128.46	−375.68	−561.96	−401.81	−163.06	106.66	−407.55	−244.95	−496.17
F-dist	−295.38	−613.36	−361.98	−457.56	−248.41	158.37	−180.79	152.12	−490.64
Gamma	−316.77	−648.41	−557.36	−477.56	−268.29	−70.08	−441.22	−246.11	−584.11
Gen. ext. value	−320.78	−565.13	−526.85	−456.48	−316.84	−242.60	−620.84	−441.41	−431.50
Gen. normal	−366.43	−633.43	−533.60	−476.01	−358.69	−303.25	−627.76	−443.34	−466.85
Gumbel	−179.72	−379.06	−527.12	−389.62	−195.10	−35.02	−431.30	−244.43	−376.46
Inv. chi-square	−148.95	−274.23	−379.11	−273.05	−162.67	15.23	−356.13	−200.45	−239.52
Inv. Gamma	−298.53	−536.09	−421.80	−396.36	−296.90	−174.70	−535.77	−276.36	−325.84
Inv. Gaussian	−178.04	−440.80	−429.50	−356.23	−229.22	−55.60	−485.95	−253.33	−252.24
Johnson SB	−364.48	−633.93	−547.57	−478.62	−357.49	−298.02	−623.36	−445.58	−463.74
Johnson SU	−361.60	−628.62	−528.86	−471.37	−354.24	−298.52	−623.36	−445.58	−461.94
Laplace	−184.73	−413.96	−480.10	−382.24	−201.82	−41.51	−439.14	−245.85	−339.58
Logistic	−176.53	−360.75	−496.70	−365.07	−190.99	−30.47	−425.80	−243.25	−333.03
Log-normal	−319.29	−610.18	−470.78	−478.07	−301.39	−139.80	−486.30	−259.66	−453.97
Normal	−169.86	−345.46	−498.92	−357.27	−184.07	−21.42	−418.91	−240.70	−327.01
Rayleigh	−171.77	−356.66	−524.70	−373.83	−186.34	−23.85	−420.65	−241.01	−358.02
Scaled t-dist	−241.83	−423.80	−494.18	−369.08	−242.48	−122.45	−535.64	−356.41	−330.06
Skewed-normal	−167.53	−360.64	−558.46	−384.42	−182.86	−19.95	−417.15	−236.57	−400.74
Trapezoidal	−134.44	−326.85	−548.58	−361.71	−171.10	−8.78	−409.37	−231.50	−389.97
Triangular	−91.67	−331.66	−553.32	−366.35	−175.48	24.70	−413.76	−236.04	−394.58
Uniform	−94.00	−244.30	−269.41	−274.09	−124.13	170.57	−80.62	144.85	−261.94
von Mises	−169.96	−348.32	−392.92	−364.93	−184.39	−21.44	−419.38	−240.71	−331.99

time scales. The minimum BIC value criterion decides the appropriateness of the probability function. Besides, we have assessed the quantile plot of theoretical and empirical densities. Thirty-two highly parameterized and extreme value distributions are included in our candidate list. The parameter estimation of these distributions and the computation of BIC values are based on *Propagate* [91] package of R language. Table 4 shows the BIC values calculated by fitting all the candidate distributions on SPTI-1 at selected meteorological stations, and with the lowest value of BIC, a distribution is chosen as the appropriate fitted distribution.

Furthermore, in Sialkot, Muzaffarabad, and Kalat stations, the BIC values of the "four-parameter Beta" distribution are the lowest among other distributions (Sialkot, −722.18; Muzaffarabad, −584.52; Kalat, −664.62). Only in Chhor station, "Johnson S_U-distribution" has given better fitness results (Chhor, −445.58). We have observed that the "Three Parameter Weibull" distribution with the lowest BIC

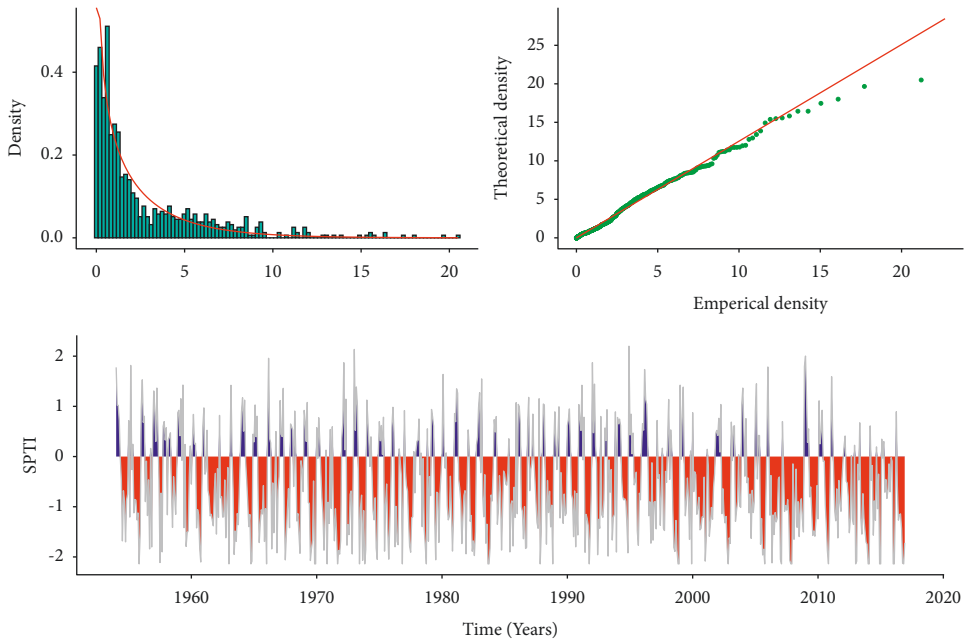

Figure 3: Histogram, QQ-plot, and temporal plot of SPTI-1 at Astore station.

Table 5: Appropriate distributions with their respective BIC values for different time scales at nine meteorological stations.

Stations	SPTI-1		SPTI-3		SPTI-6		SPTI-9		SPTI-12	
	Distribution	BIC	Distribution	BIC	Distribution	BIC	Distribution	BIC	Distribution	BIC
Mianwali	3P Weibull	−472.53	3P Weibull	−455.20	Gamma	−535.73	Laplace	−351.26	Chi-square	−326.56
Sialkot	4P beta	−722.18	Generalized normal	−600.22	Gamma	−581.78	Gumbel	−636.77	Gumbel	−548.40
Muzaffarabad	4P beta	−584.52	Rayleigh	−670.62	Chi-square	−739.36	Log-normal	−964.72	Chi-square	−866.88
Astore	3P Weibull	−480.83	Gen. extreme value	−558.42	Skewed-normal	−745.38	Rayleigh	−756.25	Triangular	−717.03
Chitral	3P Weibull	−400.89	Generalized normal	−565.65	Triangular	−467.11	Normal	−478.68	Laplace	−430.01
Multan	3P Weibull	−317.25	4P beta	−390.52	Gumbel	−417.03	Trapezoidal	−496.07	Skewed-normal	−355.40
Kalat	4P beta	−664.62	4P beta	−798.51	4P beta	−963.70	4P beta	−475.47	Trapezoidal	−500.91
Chhor	Johnson SU	−444.44	3P Weibull	−353.93	4P beta	−337.40	Exponential	−282.64	Laplace	−287.91
Kohat	3P Weibull	−622.28	Gumbel	−466.94	Inverse Gaussian	−590.98	Triangular	−391.63	Trapezoidal	−381.36

values is the most dominant (see bold values in Table 4). For the Astore station, the histogram of the appropriate probability function, the associated quantile plot, and the temporal behavior of the standardized time series data of SPTI-1 are presented in Figure 3.

For ease of convenience, other station plots are skipped. The red spikes indicated the drought severity and conditional dependence structure among drought episodes. The selected probability distributions with respective BIC values for all the time scales (1, 3, 6, 9, and 12) are presented in Table 5. Finally, standardized time series data of SPTI for selected time scales at all the selected meteorological stations have been prepared using appropriate probability distributions.

3.2. ELM and Its Comparative Assessment. In this research, we have assessed the performance of ELM with MLP and ARIMA in two phases. For all the individual stations selected for the current study, full-length data were divided into two independent parts, the training set and the validation set (test data). For most stations, precipitation and temperature records were available from 1951 to 2016. In the training phase, 64 years of monthly precipitation and minimum and maximum air temperature data from January 1951 to December 2013 are used to train candidate algorithms. In the testing phase, the rest of the 36 months of data (2014–2016) are considered test data to validate forecasting results. Simulations for ELM and MLP are carried out using R package *nnfor* [92], and *forecast* package for R language [93]

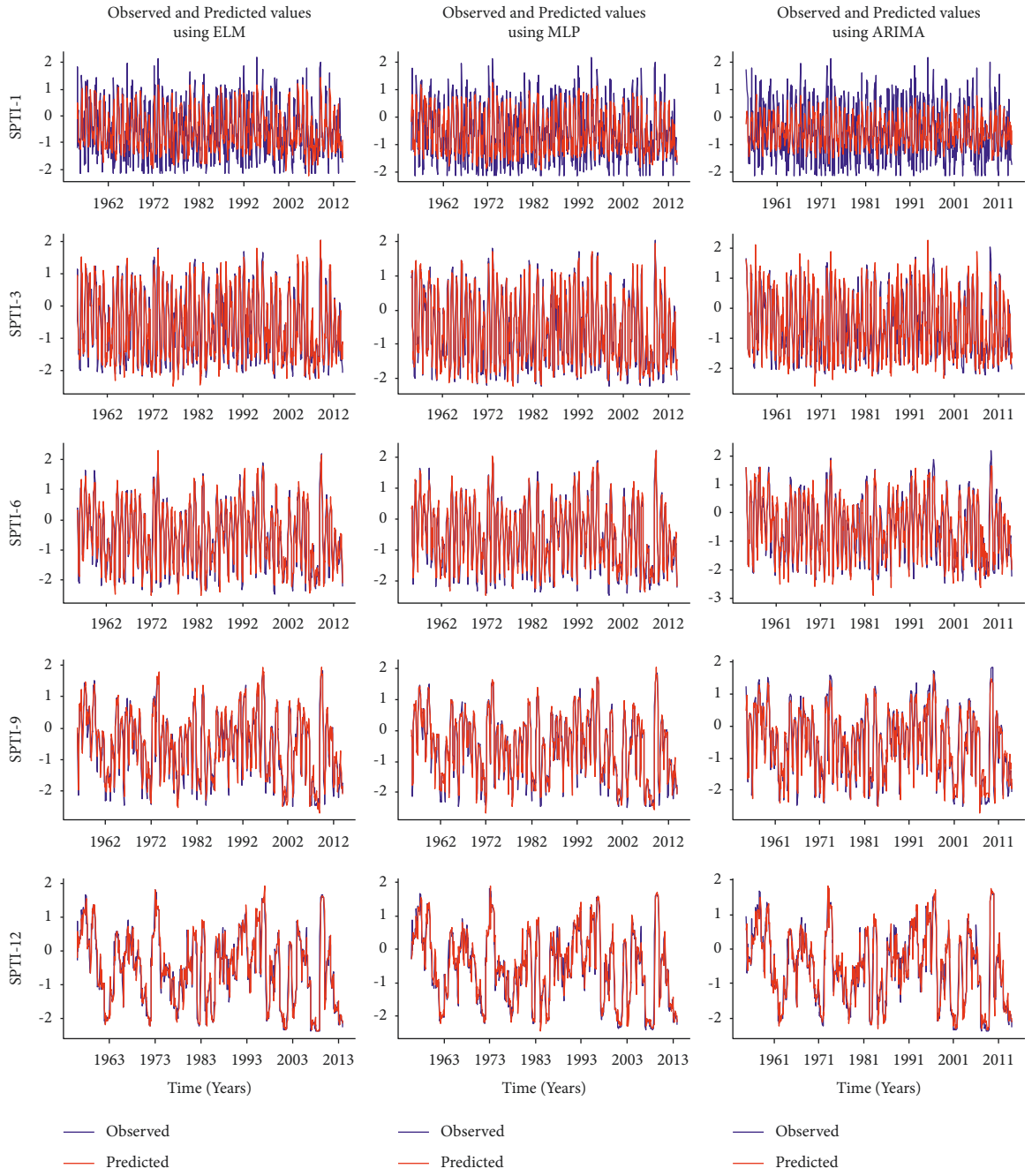

Figure 4: Performance assessment of ELM, MLP, and ARIMA models through co-movement of observed and predicted values of SPTI at Astore station for the training phase.

was used to select the appropriate order of seasonal and non-seasonal specifications of the ARIMA model.

Furthermore, all the ELM, MLP, and ARIMA simulations are carried out in the R 3.5.3 environment running on core i7 with a clock speed of 2.3 GHz CPU. The optimum order of ARIMA specifications with the estimated parameters is detailed in Table 6. These optimum specifications were attained by running all possible ARIMA models, including all possible seasonal and non-seasonal lag values of the input time series. The ELM algorithm was trained using 23 input layer nodes and a single hidden layer with 100 hidden nodes. The algorithm is repeated 20 times, and the estimated outcomes are combined using the median operator. ELM assigns random weights to each hidden node. Furthermore, it assigns start weights to input layer nodes and generalized weights to hidden layer nodes. These weights are estimated using least absolute shrinkage and selection operator (LASSO) to keep the model parsimonious. The parametric network structure still forms a large dimension matrix, which is not feasible to illustrate

Table 6: The estimated parameters of optimum selected ARIMA models at all selected meteorological stations with (1, 3, 6, 9, and 12) month time scales.

Stations		Optimum model	Drift	ϕ_1	ϕ_2	ϕ_3	ϕ_4	ϕ_5	θ_1	θ_2	θ_3	θ_4	Φ_1	Φ_2	Θ_1	Θ_2
Astore	SPTI-1	ARIMA $(5, 0, 1)\ (2, 0, 0)_{12}$	—	0.808	−0.047	−0.123	0.040	−0.157	−0.579	—	—	—	0.171	0.164	—	—
	SPTI-3	ARIMA $(2, 0, 2)\ (2, 1, 0)_{12}$	—	−0.005	0.114	—	—	—	0.815	0.546	—	—	−0.611	−0.315	—	—
	SPTI-6	ARIMA $(1, 0, 0)\ (2, 1, 0)_{12}$	−0.002	0.837	—	—	—	—	—	—	—	—	−0.648	−0.350	—	—
	SPTI-9	ARIMA $(2, 0, 1)\ (2, 0, 0)_{12}$	—	1.632	−0.710	—	—	—	−0.576	—	—		0.212	0.168	—	—
	SPTI-12	ARIMA $(2, 0, 0)\ (0, 0, 1)_{12}$	—	1.05	−0.067	—	—	—	—	—	—	—	—	—	−0.777	—
Chhor	SPTI-1	ARIMA $(1, 0, 0)\ (2, 0, 0)_{12}$	—	0.179	—	—	—	—	—	—	—	—	0.317	0.219	—	—
	SPTI-3	ARIMA $(4, 0, 0)\ (2, 1, 0)_{12}$	—	0.696	0.035	−0.249	0.101	—	—	—	—	—	−0.681	−0.370	—	—
	SPTI-6	ARIMA $(1, 0, 0)\ (2, 1, 0)_{12}$	0.001	0.813	—	—	—	—	—	—	—	—	−0.649	−0.348	—	—
	SPTI-9	ARIMA $(2, 0, 0)\ (2, 0, 0)_{12}$	—	1.000	−0.191	—	—	—	—	—	—	—	0.274	0.162	—	—
	SPTI-12	ARIMA $(1, 0, 1)\ (0, 0, 1)_{12}$	—	0.957	—	—	—	—	0.080	—	—	—	—	—	−0.711	—
Chitral	SPTI-1	ARIMA $(1, 0, 0)\ (1, 1, 0)_{12}$	—	0.123	—	—	—	—	—	—	—	—	−0.539	—	—	—
	SPTI-3	ARIMA $(2, 0, 2)\ (1, 1, 0)_{12}$	−0.001	0.005	0.077	—	—	—	0.782	0.520	—	—	−0.527	—	—	—
	SPTI-6	ARIMA $(1, 0, 0)\ (1, 1, 0)_{12}$	−0.002	0.823	—	—	—	—	—	—	—	—	−0.524	—	—	—
	SPTI-9	ARIMA $(2, 0, 2)\ (1, 1, 0)_{12}$	−0.003	0.008	0.788	—	—	—	0.922	0.043	—	—	−0.540	—	—	—
	SPTI-12	ARIMA $(1, 0, 0)\ (0, 0, 1)_{12}$	—	0.978	—	—	—	—	—	—	—	—	—	—	−0.643	—
Kalat	SPTI-1	ARIMA $(4, 1, 1)\ (0, 0, 21)_{12}$	—	0.319	0.038	0.028	−0.067	—	−0.987	—	—	—	—	—	0.216	0.191
	SPTI-3	ARIMA $(2, 0, 2)\ (2, 1, 0)_{12}$	0.001	0.046	0.249	—	—	—	0.779	0.449	—	—	−0.669	−0.344	—	—
	SPTI-6	ARIMA $(1, 0, 0)\ (2, 1, 0)_{12}$	—	0.880	—	—	—	—	—	—	—	—	−0.710	−0.360	—	—
	SPTI-9	ARIMA $(0, 0, 1)\ (2, 0, 0)_{12}$	—	—	—	—	—	—	0.085	—	—	—	0.215	0.307	—	—
	SPTI-12	ARIMA $(3, 1, 0)\ (0, 0, 2)_{12}$	—	0.120	0.077	0.037	—	—	—	—	—	—	—	—	−0.782	−0.052
Kohat	SPTI-1	ARIMA $(1, 0, 0)\ (2, 0, 0)_{12}$	—	0.157	—	—	—	—	—	—	—	—	0.165	0.261	—	—
	SPTI-3	ARIMA $(5, 0, 0)\ (2, 0, 0)_{12}$	—	0.912	−0.104	−0.511	0.473	−0.121	—	—	—	—	0.141	0.224	—	—
	SPTI-6	ARIMA $(4, 0, 1)\ (2, 0, 0)_{12}$	—	0.074	0.838	−0.096	−0.209	—	0.959	—	—	—	0.102	0.176	—	—
	SPTI-9	ARIMA $(5, 0, 4)\ (2, 0, 0)_{12}$	—	−0.340	0.288	−0.283	0.203	0.441	1.449	1.168	1.374	0.900	0.130	0.264	—	—
	SPTI-12	ARIMA $(1, 0, 2)\ (2, 0, 2)_{12}$	—	0.978	—	—	—	—	0.091	0.067	—	—	−0.335	−0.134	−0.462	−0.119
Mianwali	SPTI-1	ARIMA $(5, 1, 0)\ (2, 0, 0)_{12}$	—	−0.813	−0.640	−0.537	−0.395	−0.176	—	—	—	—	0.257	0.304	—	—
	SPTI-3	ARIMA $(2, 0, 3)\ (2, 1, 0)_{12}$	0.001	0.504	0.139	—	—	—	0.254	0.156	−0.410	—	−0.634	−0.350	—	—
	SPTI-6	ARIMA $(0, 1, 0)\ (2, 0, 0)_{12}$	—	—	—	—	—	—	—	—	—	—	0.254	0.141	—	—
	SPTI-9	ARIMA $(0, 1, 0)\ (2, 0, 0)_{12}$	—	—	—	—	—	—	—	—	—	—	0.328	0.284	—	—
	SPTI-12	ARIMA $(0, 1, 0)\ (0, 0, 1)_{12}$	—	—	—	—	—	—	—	—	—	—	—	—	−0.656	—
Multan	SPTI-1	ARIMA $(1, 0, 2)\ (2, 0, 0)_{12}$	—	0.941	—	—	—	—	−0.861	−0.116	—	—	0.213	0.149	—	—
	SPTI-3	ARIMA $(4, 0, 4)\ (2, 0, 0)_{12}$	—	−0.161	—1.031	−0.002	−0.091	—	0.941	1.761	0.852	0.676	0.187	—	—	—
	SPTI-6	ARIMA $(2, 0, 4)\ (2, 0, 0)_{12}$	—	0.023	−0.120	—	—	—	0.922	0.956	0.897	0.861	0.106	0.151	—	—
	SPTI-9	ARIMA $(0, 1, 0)\ (2, 0, 0)_{12}$	—	—	—	—	—	—	—	—	—	—	0.184	0.202	—	—
	SPTI-12	ARIMA $(2, 1, 1)\ (1, 0, 1)_{12}$	—	0.251	−0.05	—	—	—	−0.296	—	—	—	−0.130	—	−0.495	—
Muzaffarabad	SPTI-1	ARIMA $(1, 0, 0)\ (2, 0, 0)_{12}$	—	0.094	—	—	—	—	—	—	—	—	0.251	—	—	—
	SPTI-3	ARIMA $(5, 0, 1)\ (2, 0, 0)_{12}$	—	1.629	−0.749	−0.450	0.807	−0.365	−0.760	—	—	—	0.248	0.241	—	—
	SPTI-6	ARIMA $(3, 0, 1)\ (2, 0, 0)_{12}$	—	1.509	−0.561	−0.067	—	—	−0.553	—	—	—	0.206	0.150	—	—
	SPTI-9	ARIMA $(4, 0, 4)\ (2, 0, 0)_{12}$	—	0.561	−0.076	−0.551	0.656	—	0.427	0.489	0.823	0.039	0.188	0.324	—	—
	SPTI-12	ARIMA $(1, 0, 2)\ (1, 0, 1)_{12}$	—	0.972	—	—	—	—	0.036	0.066	—	—	−0.030	—	−0.690	—

Table 6: Continued.

Stations		Optimum model	Drift	ϕ_1	ϕ_2	ϕ_3	ϕ_4	ϕ_5	θ_1	θ_2	θ_3	θ_4	Φ_1	Φ_2	Θ_1	Θ_2
Sialkot	SPTI-1	ARIMA (2, 0, 2) $(2, 0, 0)_{12}$	—	0.895	−0.854	—	—	—	−0.769	0.714	—	—	0.231	0.251	—	—
	SPTI-3	ARIMA (3, 0, 2) $(2, 1, 0)_{12}$	0.001	−0.024	0.026	−0.042	—	—	0.697	0.457	—	—	−0.619	−0.320	—	—
	SPTI-6	ARIMA (2, 0, 2) $(2, 0, 0)_{12}$	—	1.605	−0.686	—	—	—	−0.768	0.078	—	—	−0.680	−0310	—	—
	SPTI-9	ARIMA (2, 0, 2) $(1, 1, 0)_{12}$	0.001	1.857	−0.891	—	—	—	—1.059	0.180	—	—	−0.472	—	—	—
	SPTI-12	ARIMA (1, 0, 0) $(0, 0, 2)_{12}$	—	0.968	—	—	—	—	—	—	—	—	—	—	−0.665	0.077

Table 7: Prediction performance of ELM, MLP, and ARIMA algorithms using training data for SPTI with 1–12 month time scales at selected meteorological stations.

	Station	RMSE			KGE			WI			MAE			MAPE (%age)		
		ELM	MLP	ARIMA	ELM	MLP	ARIMA	ELM	MLP	ARIMA	ELM	MLP	ARIMA	ELM	MLP	ARIMA
SPTI-1	Astore	0.523	0.836	0.841	0.712	0.517	0.349	0.909	0.748	0.664	0.395	0.660	0.671	470.151	9318.622	633.715
	Chhor	0.387	0.598	0.632	0.719	0.533	0.333	0.910	0.771	0.663	0.281	0.449	0.500	445.292	335.141	749.993
	Chitral	0.374	0.680	0.762	0.838	0.680	0.671	0.960	0.847	0.825	0.272	0.533	0.582	259.592	161.335	324.699
	Kalat	0.402	0.624	0.681	0.721	0.556	0.308	0.907	0.778	0.643	0.302	0.492	0.558	517.220	1870.592	903.828
	Kohat	0.583	0.948	0.967	0.642	0.383	0.130	0.880	0.666	0.490	0.461	0.766	0.776	608.050	856.133	331.864
	Mianwali	0.416	0.734	0.823	0.735	0.503	0.308	0.918	0.748	0.625	0.323	0.588	0.679	675.666	978.739	576.477
	Multan	0.489	0.782	0.795	0.613	0.292	0.319	0.872	0.616	0.425	0.382	0.637	0.674	592.744	365.638	1005.901
	Muzaffarabad	0.537	0.796	0.837	0.571	0.425	0.110	0.891	0.722	0.600	0.412	0.636	0.655	660.512	348.687	834.538
	Sialkot	0.523	0.774	0.822	0.755	0.592	0.404	0.923	0.799	0.708	0.412	0.627	0.662	436.879	238.422	380.266
SPTI-3	Astore	0.305	0.506	0.558	0.922	0.872	0.847	0.978	0.939	0.925	0.218	0.377	0.425	270.129	115.508	396.597
	Chhor	0.275	0.431	0.474	0.905	0.834	0.781	0.970	0.923	0.905	0.190	0.305	0.356	266.512	126.178	351.577
	Chitral	0.252	0.403	0.461	0.950	0.917	0.902	0.985	0.961	0.951	0.177	0.296	0.345	89.236	46.108	128.119
	Kalat	0.342	0.504	0.543	0.902	0.850	0.824	0.967	0.927	0.914	0.235	0.362	0.403	202.446	93.793	164.865
	Kohat	0.395	0.580	0.625	0.874	0.811	0.709	0.959	0.710	0.880	0.291	0.431	0.473	206.435	125.313	242.491
	Mianwali	0.330	0.539	0.632	0.908	0.833	0.772	0.972	0.921	0.889	0.238	0.394	0.472	180.319	76.808	163.529
	Multan	0.416	0.660	0.684	0.863	0.746	0639	0.952	0.877	0.843	0.295	0.485	0.522	196.750	92.480	175.258
	Muzaffarabad	0.348	0.522	0.557	0.825	0.820	0.522	0.964	0.917	0.894	0.263	0.388	0.428	249.060	189.263	490.751
	Sialkot	0.317	0.476	0.531	0.763	0756	0.801	0.970	0.927	0.907	0.229	0.355	0.408	230.092	557.723	263.315
SPTI-6	Astore	0.287	0.351	0.455	0.945	0.912	0.894	0.991	0.981	0.949	0.198	0.248	0.347	75.918	86.424	129.332
	Chhor	0.255	0.353	0.430	0.939	0.916	0.859	0.979	0.960	0.936	0.155	0.229	0.307	98.630	131.632	181.744
	Chitral	0.247	0.299	0.402	0.964	0.955	0.925	0.986	0.978	0.962	0.167	0.211	0.306	81.651	52.158	131.476
	Kalat	0.316	0.380	0.439	0.956	0.942	0.897	0.993	0.976	0.952	0.193	0.240	0.301	79.513	300.351	238.315
	Kohat	0.883	0.455	0.507	0.922	0.957	0.823	0.968	0.983	0.930	0.695	0.313	0.370	173.514	253.266	703.016
	Mianwali	0.319	0.409	0.488	0.912	0.898	0.866	0.972	0.953	0.933	0.218	0.272	0.332	209.504	98.576	422.293
	Multan	0.382	0.478	0.481	0.922	0.872	0.841	0.993	0.963	0.937	0.264	0.318	0.337	179.676	99.793	136.787
	Muzaffarabad	0.390	0.471	0.527	0.885	0.753	0.343	0.959	0.944	0.914	0.278	0.337	0.395	158.979	114.439	364.869
	Sialkot	0.298	0.375	0.432	0.889	0.882	0.691	0.975	0.959	0.944	0.199	0.249	0.314	117.078	97.213	149.507
SPTI-9	Astore	0.288	0.346	0.434	0.949	0.936	0.874	0.980	0.971	0.951	0.197	0.248	0.309	76.933	62.029	194.755
	Chhor	0.283	0.355	0.433	0.943	0.910	0.764	0.977	0.951	0.907	0.158	0.221	0.289	150.828	92.464	129.091
	Chitral	0.263	0.308	0.443	0.958	0.955	0.914	0.984	0.979	0.957	0.185	0.222	0.319	116.527	58.645	86.048
	Kalat	0.284	0.344	0.409	0.951	0.945	0.927	0.982	0.974	0.963	0.169	0.210	0.241	115.838	171.454	201.090
	Kohat	0.318	0.371	0.415	0.942	0.765	0.846	0.975	0.875	0.939	0.220	0.259	0.302	89.845	123.001	117.730
	Mianwali	0.264	0.307	0.388	0.948	0.948	0.916	0.982	0.975	0.961	0.184	0.219	0.277	466.118	96.627	164.084
	Multan	0.366	0.436	0.547	0.928	0.905	0.862	0.968	0.953	0.928	0.247	0.294	0.352	143.634	90.969	124.937
	Muzaffarabad	0.323	0.385	0.471	0.938	0.921	0.849	0.975	0.964	0.941	0.240	0.289	0.357	180.985	107.083	712.336
	Sialkot	0.298	0.334	0.423	0.947	0.938	0.895	0.976	0.970	0.951	0.202	0.234	0.310	121.539	1223.05	552.815
SPTI-12	Astore	0.311	0.336	0.300	0.951	0.945	0.938	0.973	0.977	0.978	0.203	0.216	0.204	115.137	158.271	131.494
	Chhor	0.302	0.340	0.302	0.946	0.933	0.864	0.974	0.967	0.973	0.151	0.154	0.158	97.432	241.040	60.678
	Chitral	0.348	0.372	0.340	0.940	0.936	0.923	0.971	0.968	0.973	0.214	0.218	0.213	94.942	83.428	144.242
	Kalat	0.240	0.284	0.257	0.973	0.968	0.966	0.989	0.985	0.987	0.122	0.131	0.124	51.690	59.213	457.499
	Kohat	0.301	0.342	0.302	0.952	0.944	0.939	0.978	0.972	0.978	0.203	0.224	0.204	146.081	78.430	131.950
	Mianwali	0.254	0.277	0.254	0.968	0.959	0.328	0.985	0.982	0.984	0.169	0.180	0.167	97.518	94.950	70.970
	Multan	0.342	0.383	0.362	0.935	0.814	0.899	0.957	0.813	0.962	0.216	0.229	0.225	412.644	80.412	142.043
	Muzaffarabad	0.344	0.370	0.335	0.941	0.935	0.927	0.972	0.968	0.972	0.246	0.260	0.242	111.260	90.649	165.662
	Sialkot	0.329	0.364	0.329	0.938	0.932	0.911	0.972	0.966	0.971	0.209	0.224	0.213	108.491	114.554	92.435

Table 8: Pearson's correlation coefficient between the observed and predicted values of SPTI 1–12 month time scales using ELM, MLP, and ARIMA algorithms at selected meteorological stations.

Scale	Astore			Chhor			Chitral			Kalat			Kohat			Mianwali			Multan			Muzaffarabad			Sialkot		
	ELM	MLP	ARIMA	ELM	MLP	ARIMA	ELM	MLP	ARIMA	ELM	MLP	ARIMA	ELM	MLP	ARIMA	ELM	MLP	ARIMA	ELM	MLP	ARIMA	ELM	MLP	ARIMA	ELM	MLP	ARIMA
SPTI-1	0.87	0.59	0.56	**0.86**	0.62	0.54	**0.93**	0.74	0.69	**0.86**	0.63	0.52	**0.84**	0.48	0.39	**0.88**	0.59	0.43	**0.84**	0.41	0.32	**0.84**	0.56	0.48	**0.88**	0.66	0.60
SPTI-3	0.96	0.88	0.86	**0.95**	0.86	0.83	**0.97**	0.93	0.90	**0.94**	0.86	0.84	**0.92**	0.83	0.80	**0.95**	0.85	0.80	**0.91**	0.78	0.75	**0.93**	0.85	0.82	**0.94**	0.86	0.83
SPTI-6	0.96	0.94	0.90	**0.96**	0.92	0.88	**0.97**	0.96	0.93	**0.95**	0.93	0.91	**0.94**	0.90	0.87	**0.94**	0.91	0.87	**0.93**	0.89	0.89	**0.93**	0.89	0.86	**0.95**	0.92	0.89
SPTI-9	0.96	0.94	0.91	**0.96**	0.28	0.84	**0.97**	0.96	0.92	**0.97**	0.95	0.93	**0.95**	0.77	0.89	**0.96**	0.95	0.92	**0.94**	0.91	0.86	**0.95**	0.93	0.89	**0.95**	0.94	0.91
SPTI-12	0.96	0.95	0.96	**0.95**	0.93	**0.95**	0.94	0.94	**0.95**	**0.98**	0.97	**0.98**	**0.96**	0.95	**0.96**	**0.97**	0.96	**0.97**	0.77	0.92	**0.93**	**0.95**	0.94	**0.95**	**0.95**	0.93	0.94

Table 9: Forecast performance of ELM, MLP, and ARIMA algorithms for SPTI with 1–12 month time scales at nine meteorological stations.

	Station	RMSE			KGE			WI			MAE			MAPE (%age)		
		ELM	MLP	ARIMA	ELM	MLP	ARIMA	ELM	MLP	ARIMA	ELM	MLP	ARIMA	ELM	MLP	ARIMA
SPTI-1	Astore	0.688	1.034	0.893	0.988	0.771	0.671	0.997	0.897	0.884	0.798	0.855	0.865	247.353	251.284	364.431
	Chhor	0.579	0.600	0.559	0.871	0.712	0.541	0.999	0.730	0.663	0.531	0.447	0.468	559.287	269.288	396.060
	Chitral	0.643	0.647	0.690	0.909	0.685	0.678	0.979	0.836	0.823	0.495	0.510	0.520	142.102	193.952	414.532
	Kalat	0.776	0.832	0.727	0.952	0.779	0.767	0.998	0.966	0.976	0.676	0.731	0.684	500.369	824.503	616.762
	Kohat	0.956	0.970	1.031	0.979	0.930	0.900	0.999	0.992	0.954	0.791	0.815	0.869	528.066	1136.164	268.277
	Mianwali	0.773	0.984	0.801	0.961	0.753	0.690	0.998	0.954	0.923	0.652	0.818	0.655	309.146	369.444	860.231
	Multan	0.714	0.666	0.824	0.986	0.428	0.687	0.997	0.740	0.885	0.612	0.577	0.706	545.568	1291.204	3958.975
	Muzaffarabad	0.764	0.743	0.724	0.937	0.877	0.673	0.997	0.966	0.994	0.605	0.597	0.553	321.810	3469.574	455.340
	Sialkot	0.720	0.745	0.822	0.931	0.902	0.914	0.995	0.989	0.982	0.554	0.593	0.663	91.037	151.493	269.868
SPTI-3	Astore	0.764	0.896	0.607	0.970	0.744	0.511	0.991	0.865	0.760	0.589	0.735	0.488	797.800	63.992	84.646
	Chhor	0.563	0.503	0.539	0.866	0962	0.678	0.821	0.873	0.871	0.438	0.366	0.385	193.072	159.359	141.894
	Chitral	0.468	0.522	0.514	0.921	0.709	0.820	0.965	0.908	0.918	0.408	0.396	0.405	2354.06	79.394	150.935
	Kalat	0.987	1.247	1.152	0.996	0.858	0.678	0.999	0.956	0.758	0.850	1.067	0.899	329.382	314.217	199.070
	Kohat	0.771	0.775	0.873	0.974	0.965	0.73	0.994	0.993	0.891	0.729	0.668	0.726	116.387	330.497	134.998
	Mianwali	1.104	1.221	1.041	0.997	0.961	0.943	0.997	0.987	0.956	0.914	1.014	0.806	1082.42	561.266	173.703
	Multan	0.801	0.790	0.982	0.894	0.927	0.938	0.999	0.997	0.978	0.660	0.654	0.826	210.083	193.947	210.070
	Muzaffarabad	0.791	0.785	0.777	0.967	0.856	0.873	0.999	0.990	0.996	0.602	0.686	0.601	230.935	809.403	334.650
	Sialkot	0.681	0.725	0.768	0.938	0.924	0.628	0.996	0.977	0.811	0.520	0.532	0.601	265.276	259.027	201.413
SPTI-6	Astore	0.402	0.670	0.482	0.962	0.607	0.541	0.985	0.782	0.733	0.492	0.582	0.408	46.301	343.207	37.464
	Chhor	0.819	0.889	0.669	0.910	0.687	0.456	0.998	0.967	0.876	0.702	0.771	0.475	697.320	269.541	73.976
	Chitral	0.374	0.405	0.399	0.961	0.862	0.846	0.984	0.935	0.943	0.308	0.325	0.308	172.828	140.348	140.661
	Kalat	0.972	0.792	1.231	0.965	0.921	0.933	0.993	0.884	0.976	0.807	0.666	1.022	1364.65	335.608	184.772
	Kohat	0.957	0.930	0.869	0.924	0.876	0.759	0.990	0.948	0.918	0.764	0.841	0.719	89.183	301.444	109.716
	Mianwali	1.411	2.148	1.457	0.974	0.788	0.885	0.999	0.975	0.987	1.319	1.868	1.145	347.413	215.620	298.005
	Multan	0.783	1.209	1.076	0.931	0.781	0.926	0.999	0.999	0.991	0.673	0.982	0.886	222.776	194.657	173.698
	Muzaffarabad	0.771	1.176	0.872	0.989	0.935	0.893	0.999	0.995	0.981	0.648	0.822	0.695	2458.04	214.159	4533.34
	Sialkot	0.880	0.733	0.656	0.953	0.944	0.928	0.998	0.991	0.994	0.756	0.670	0.557	776.441	532.295	178.914
SPTI-9	Astore	0.634	0.647	0.874	0.968	0.728	0.783	0.990	0.857	0.869	0.496	0.542	0.776	41.230	49.977	101.519
	Chhor	1.134	1.328	0.961	0.949	0.936	0.945	0.994	0.996	0.829	0.944	1.151	0.760	358.134	243.020	584.953
	Chitral	0.372	0.504	0.383	0.953	0.863	0.820	0.984	0.921	0.910	0.322	0.406	0.297	53.696	3157.85	34.444
	Kalat	0.428	1.133	0.782	0.991	0.724	0.845	0.999	0.892	0.935	0.876	0.982	0.713	187.052	360.125	50.731
	Kohat	1.032	1.042	0.836	0.941	0.932	0.774	0.992	0.987	0.962	0.840	0.791	0.617	98.190	87.813	72.893
	Mianwali	1.350	2.062	1.457	0.970	0.924	0.616	0.998	0.982	0.964	1.429	1.895	1.145	253.908	162.066	298.005
	Multan	0.746	0.690	1.148	0.973	0.873	0.898	0.999	0.998	0.999	0.609	0.595	0.946	1139.22	1061.42	134.464
	Muzaffarabad	0.763	0.800	0.761	0.985	0.948	0.938	0.999	0.979	0.990	0.634	0.660	0.592	78.798	144.126	88.432
	Sialkot	0.765	0.681	0.839	0.925	0.904	0.851	0.997	0.996	0.985	0.589	0.485	0.655	94.806	227.032	221.098
SPTI-12	Astore	0.258	0.754	1.229	0.962	0.721	0.770	0.992	0.906	0.869	0.215	0.658	1.202	10.936	68.122	187.249
	Chhor	0.670	0.707	0.728	0.987	0.975	0.879	0.996	0.935	0.921	0.566	0.600	0.648	197.918	1307.50	2828.820
	Chitral	0.521	0.524	0.772	0.996	0.747	0.678	0.999	0.922	0.854	0.406	0.413	0.653	38.710	35.631	117.257
	Kalat	1.346	1.216	1.168	0.975	0.994	0.612	0.998	0.998	0.804	1.179	1.026	0.984	1739.84	558.414	343.401
	Kohat	0.615	1.066	0.963	0.981	0.959	0.900	0.997	0.995	0.981	0.860	0.790	0.819	84.522	66.743	144.398
	Mianwali	1.402	1.513	1.484	0.994	0.882	0.775	0.999	0.989	0.837	1.629	1.298	1.273	147.015	180.588	169.143
	Multan	0.561	1.072	0.664	0.995	0.916	0.870	0.998	0.974	0.970	0.434	0.997	0.553	60.976	1233.10	223.381
	Muzaffarabad	0.720	1.117	0.754	0.985	0.756	0.890	0.997	0.899	0.962	0.564	0.780	0.586	49.482	257.156	94.969
	Sialkot	0.793	0.727	0.766	0.945	0.926	0.922	0.993	0.992	0.973	0.630	0.593	0.593	61.040	181.003	1734.785

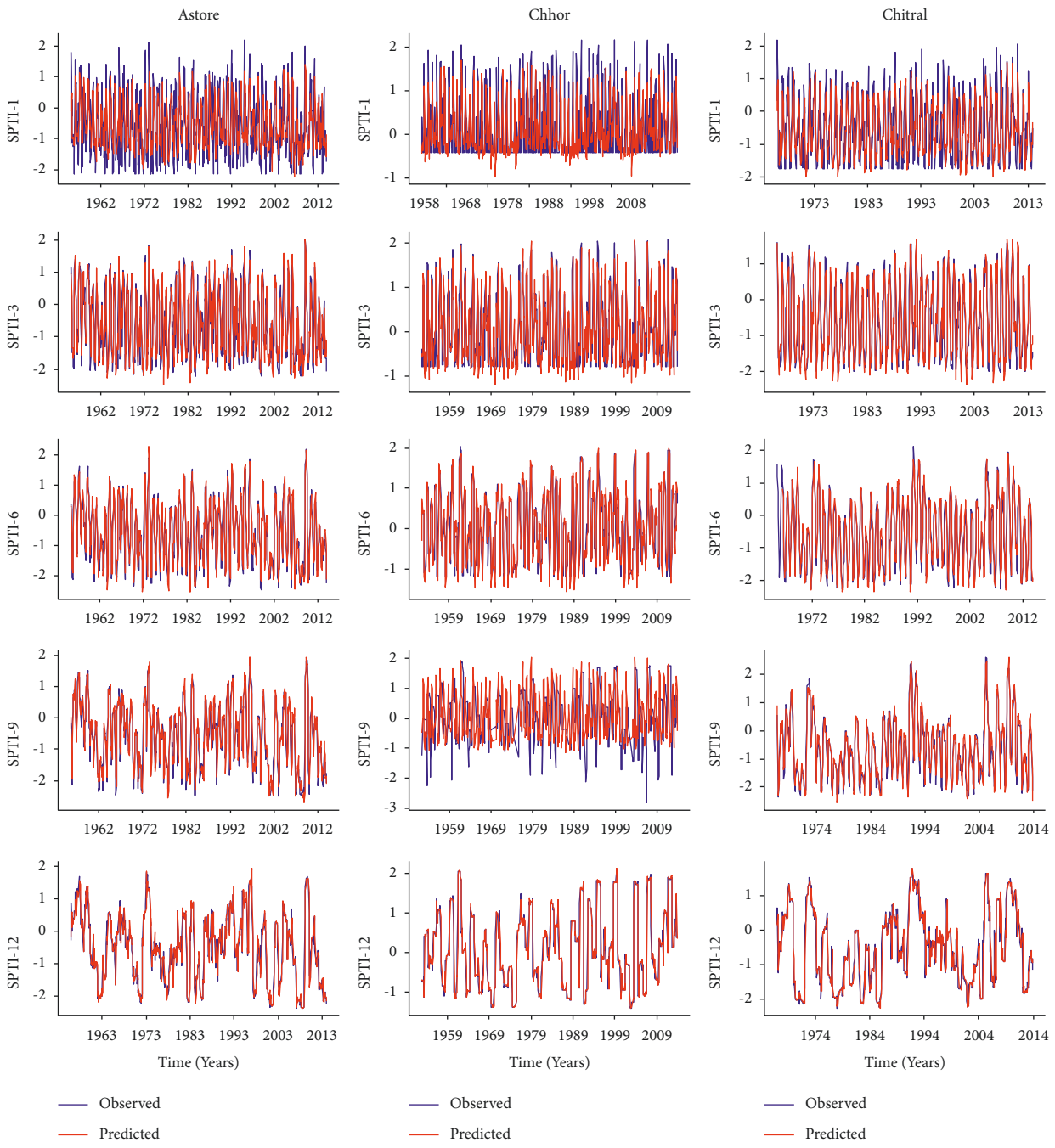

Figure 5: Co-movement of the observed and predicted values of SPTI using ELM at Astore, Chhor, and Chitral stations for the training phase.

numerically in a tabulated form. Furthermore, MLP is trained using two hidden layers containing 10 and 5 hidden nodes, respectively, to get optimum results.

The MLP algorithm drastically increases as we increase the number of hidden layers or by increasing the number of nodes of hidden layers. Hence, the structure of MLP is finalized with 23 nodes of the input layer, two hidden layers with 10 and 5 nodes, respectively, and a single output layer. This parsimonious structure still forms a larger matrix of user-defined parameters. Due to complexity and numeric hazard, the estimated results for user-defined parameters are skipped. The performance of ELM, MLP, and ARIMA algorithms was assessed using performance assessment metrics, including RMSE, MAE, MAPE, KGE, and Willmott index of agreement.

Table 7 provides numerical results of these performance assessment metrics using training data sets for ELM, MLP, and ARIMA models at selected meteorological stations with (1, 3, 6, 9, and 12) month lead time scales. Results indicate that ELM performs better than MLP and ARIMA models. For the assessment of candidate models, the numerical results of all statistical metrics for SPTI-1 are illustrated with

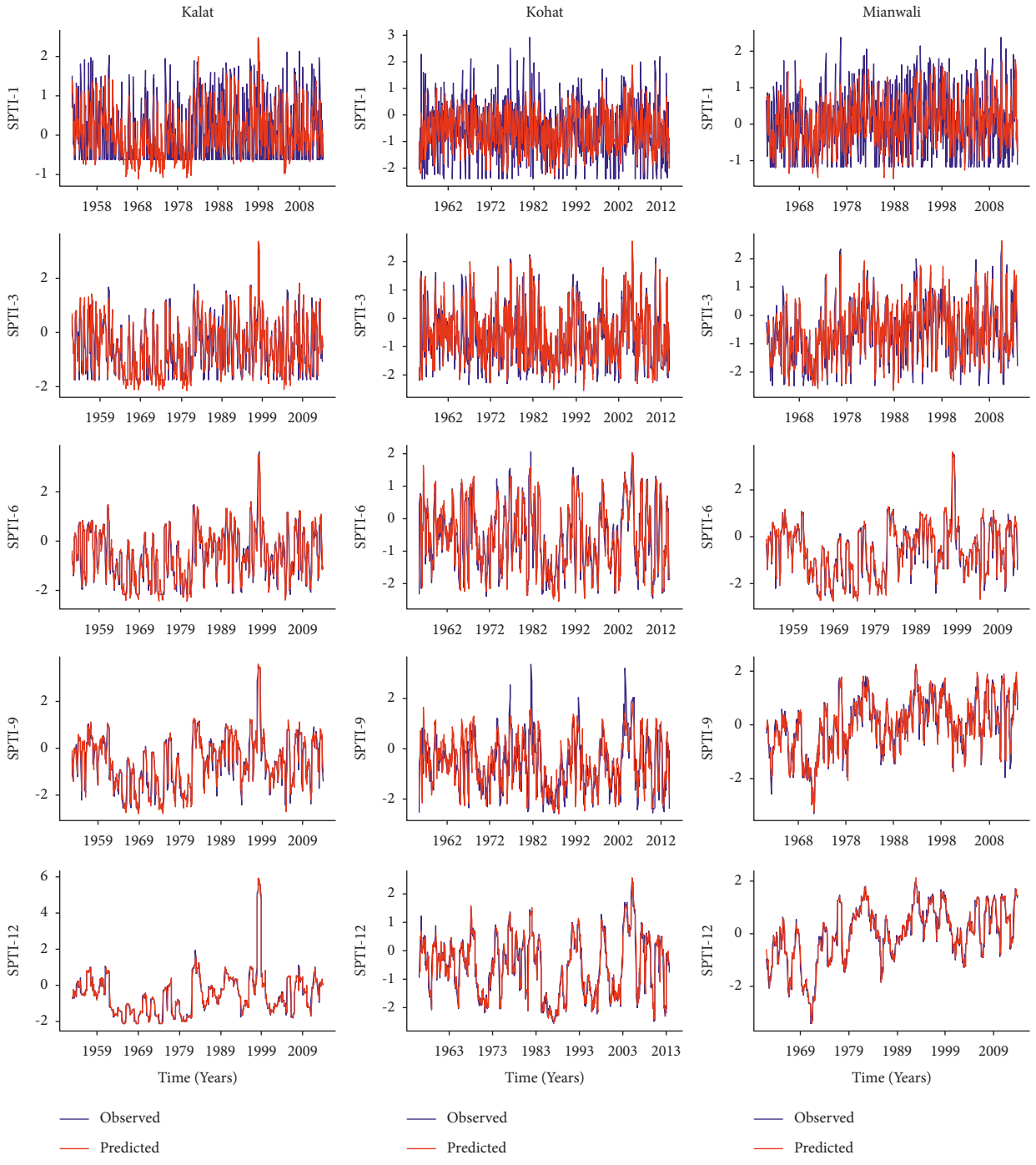

Figure 6: Co-movement of the observed and predicted values of SPTI using ELM at Kalat, Kohat, and Mianwali stations for the training phase.

details. The best performance of ELM has been observed at Chitral, with a minimum value of RMSE (0.374). However, MLP best performed at Chhor station with a minimum value of RMSE as 0.598, and the ARIMA model overall best performed at the Chhor station with RMSE (0.632). While using MAE, the minimum values for ELM, MLP, and ARIMA are 0.272, 0.449, and 0.5, respectively. As for MAPE, these quantities are 259.59, 161.33, and 324.7, respectively. The values KGE for ELM, MLP, and ARIMA models at Astore station are 0.712, 0.517, and 0.314, respectively.

Similarly, the numeric quantities of WI at the Astore station are 0.999, 0.748, and 0.664, respectively. The KGE index indorses ELM's superior performance at all the stations by providing maximum values as compared to MLP and ARIMA. Similarly, Willmott's agreement "WI" index consistently provides the highest values for the ELM algorithm. KGE and WI are considered the most appropriate metrics for the performance assessment of meteorological and hydrological models. The KGE is calculated using the correlation coefficient, the ratio of variations, and the ratio of

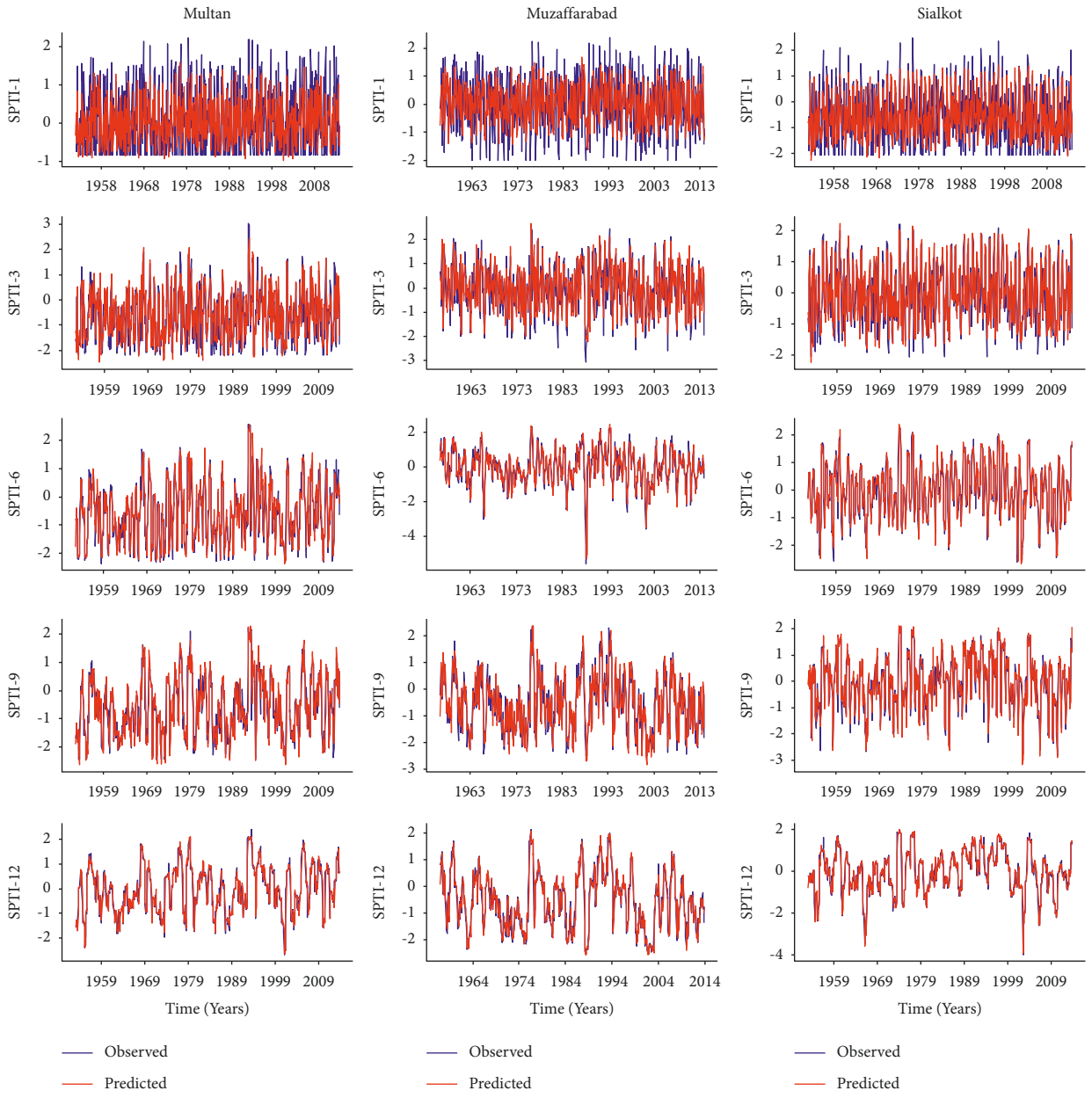

Figure 7: Co-movement of the observed and predicted values of SPTI using ELM at Muzaffarabad, Multan, and Sialkot stations for the training phase.

averages of predicted and observed series using equation (9). The values of "WI" for the ELM model for all the selected stations are close to 1, which endorses the ELM as the best performing model. The similar superior performance of ELM continued for other time scales at selected stations. Overall results for the training phase show that the ELM model has shown good agreement at all selected stations.

As the time scale of the drought index increases, the performance of the proposed algorithm improves. As a result, the ELM algorithm showed superior performance to its competitive algorithms (MLP and ARIMA). A comparison of all the performance assessment metrics concluded that ELM algorithm is selected as the adequate model for the estimation and forecasting of drought indices (see Table 7).

The consistency and co-movement of the observed and estimated values of SPTI are further assessed while employing Karl Pearson's product-moment correlation coefficient. Table 8 shows the numerical results of the correlation coefficient between the observed and predicted values of SPTI using ELM, MLP, and ARIMA models for training data. The quantitative results of the Astore station for ELM, MLP, and ARIMA are 0.87, 0.59, and 0.56, respectively, indicating a better agreement of ELM to predict SPTI-1 contrary to other candidate algorithms. At Chitral station, values of correlation are (0.93, 0.74, and 0.69). For SPTI-3 at Astore station, these results are 0.96, 0.88, and 0.86, respectively, and at Chitral station, the correlation values for ELM, MLP, and ARIMA are 0.97, 0.93, and 0.90.

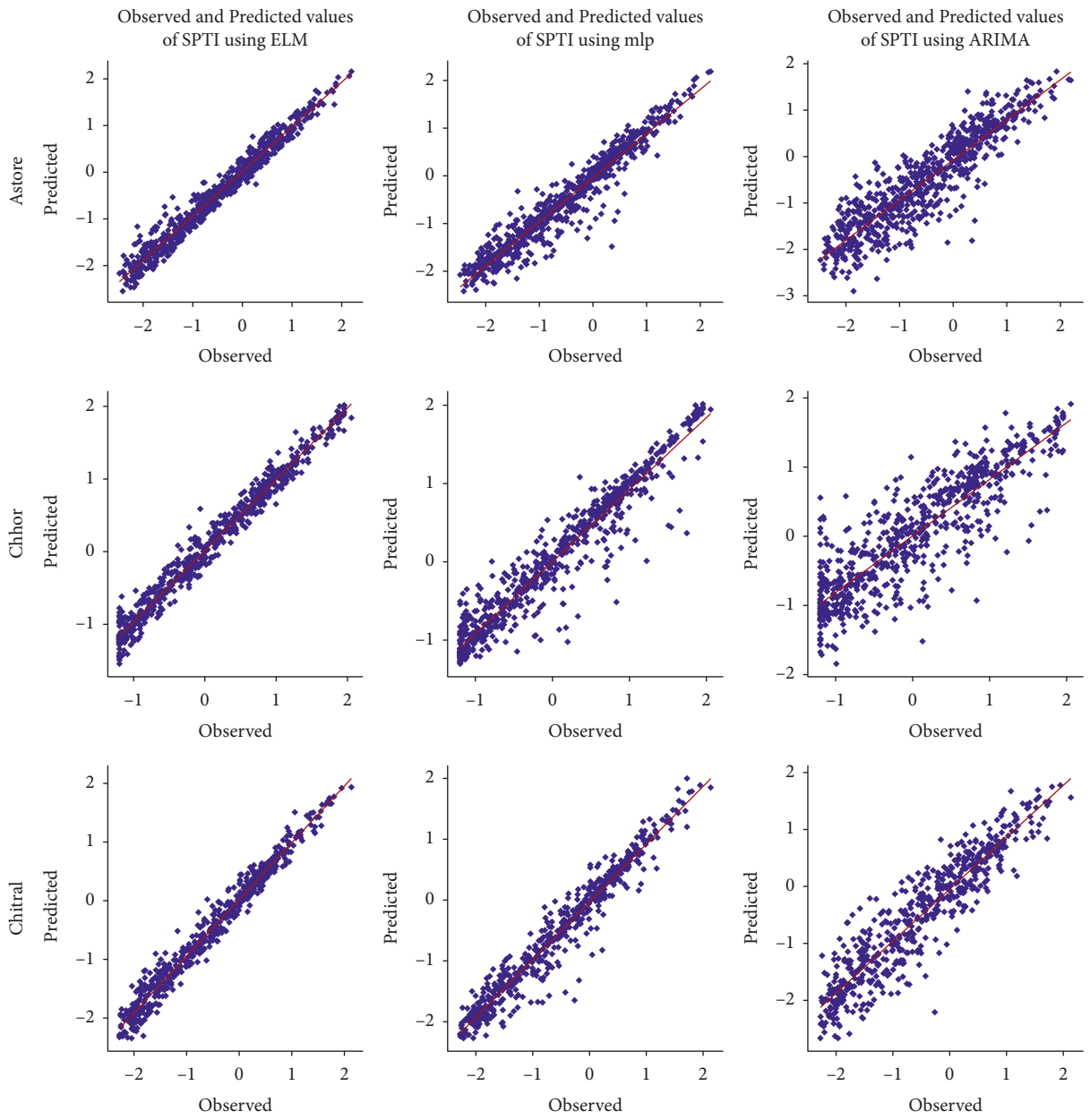

Figure 8: Scatter plots of the observed and predicted values of SPTI-6 using ELM, MLP, and ARIMA at Astore, Chhor, and Chitral stations for the training phase.

These numerical results clearly illustrated that the performance of the ELM model significantly improved as the time scale increased. A similar pattern of the superior prediction performance of ELM continued for other time scales at all the selected stations. Although all the models have shown reasonable prediction performance, quantitative results evidently confirmed that the estimated values of SPTI using the ELM model strongly correlate with the observed values of SPTI for any time scale.

Usually, climatic and meteorological studies comprise high-frequency datasets that require fast algorithms. So, speed is a notable characteristic for determining the reliability of the algorithm. The algorithm selection for climatic studies is subjective in terms of speed and relative efficiency. ELM has the novelty of being the fastest algorithm among the ANN class to solve complex datasets. ELM algorithm training and testing time were almost 32 times faster than ANN, indicating ELM's supremacy over other ANN algorithms [58].

The functional relationship between the actual (observed) and predicted values of SPTI using ELM and other algorithms for the "Astore" station is shown in Figure 4 using a line graph, which depicts significantly less variation among the observed values of SPTI and the predicted values using ELM.

MLP and ARIMA were unable to capture all the shocks in historical values of SPTI, and departure from observed values was significant. Here, the ELM algorithm reflects

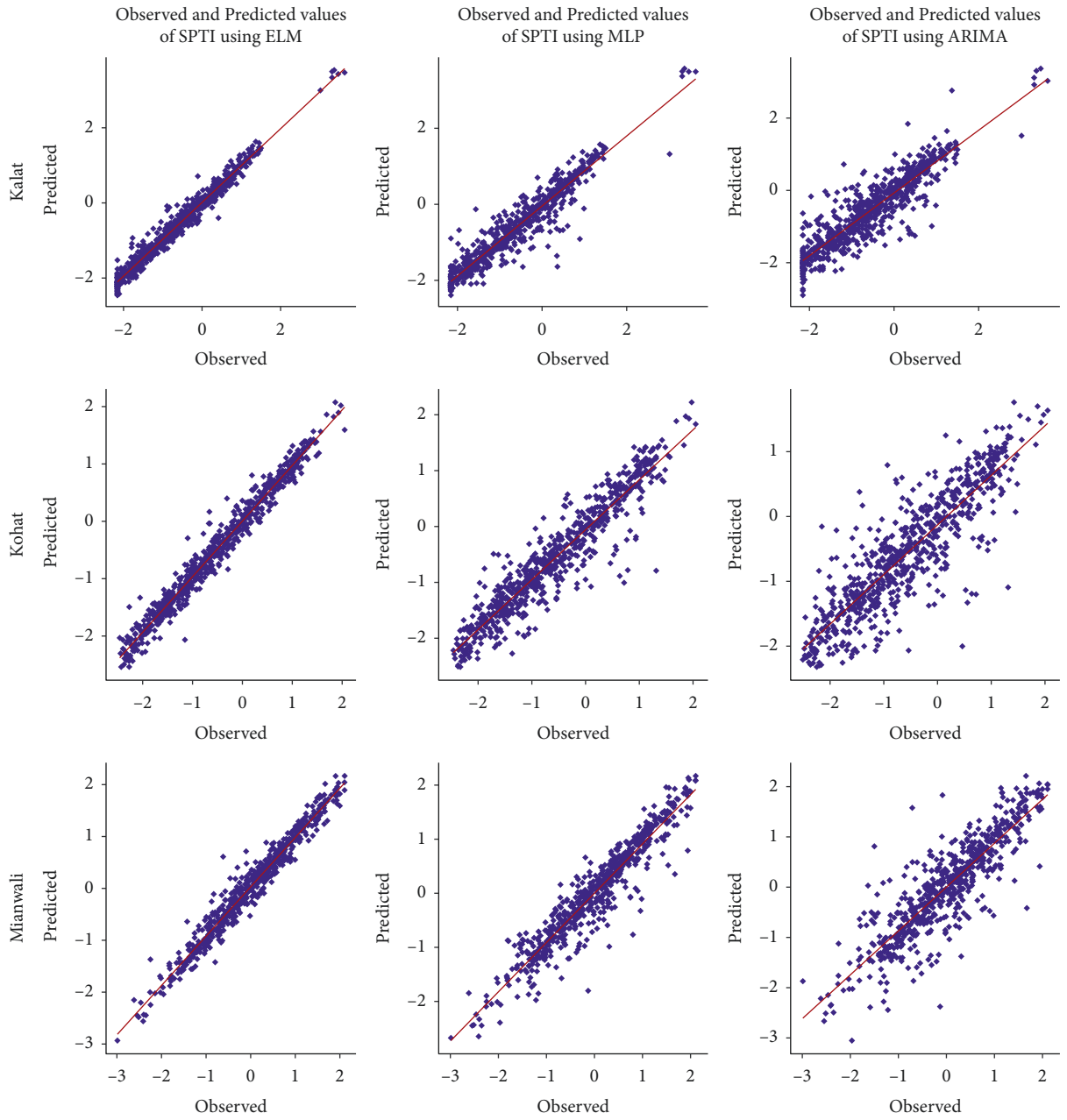

Figure 9: Scatter plots of the observed and predicted values of SPTI using ELM, MLP, and ARIMA at Kalat, Kohat, and Mianwali stations for the training phase.

more precise and accurate predictions. Figures 5– detail the ELM's prediction performance for all the time scales at the selected stations, which depicts the ELM algorithm's better prediction performance.

It was observed that as the time scale increases, the prediction performance of algorithms substantially improves. For SPTI-12, significantly fewer deviations have been observed among drought index's paired (observed and predicted) values. These multi-line plots indicate that the ELM model incurred smaller errors than the two counterparts. The predicted values using ELM model follow the observed values of SPTI more precisely. These graphical presentations show that the ELM model has shown more accuracy than MLP and ARIMA models for estimating SPTI for various lead time scales at selected meteorological stations.

Scatter plots of the observed and predicted time series data sets are another way to assess the prediction performance of probabilistic, machine learning, and ANN algorithms. Figures 8–10 show the scatter plots of the historical observed and predicted values of SPTI-6 using ELM, MLP, and ARIMA models at all the selected meteorological stations. Predicted values through the ELM model have shown a strong correlation with the observed values of SPTI

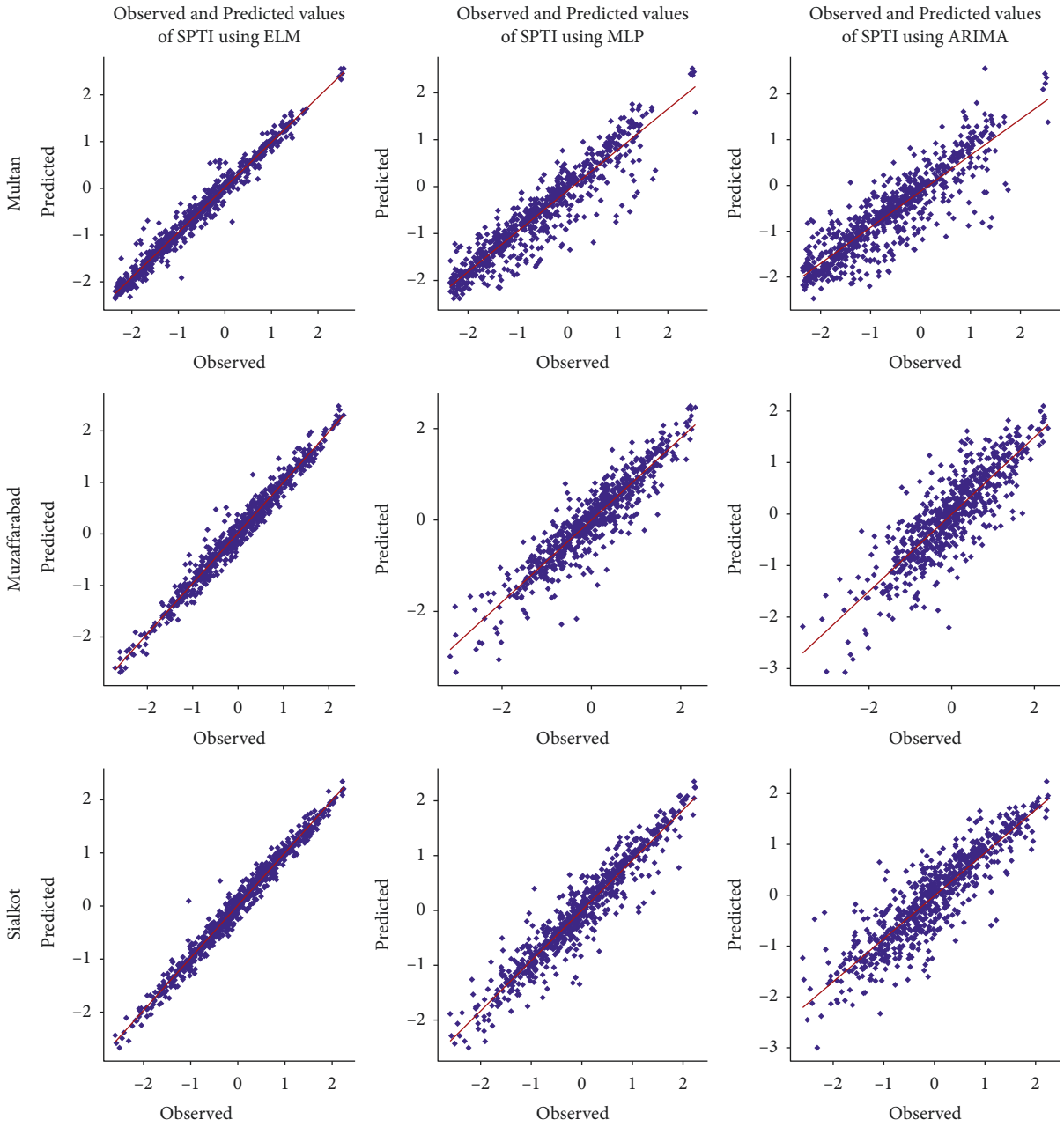

Figure 10: Scatter plots of the observed and predicted values of SPTI using ELM, MLP, and ARIMA at Muzaffarabad, Multan, and Sialkot stations for the training phase.

through scatter plots. Another graphical presentation endorses the superior performance of ELM. We can observe that the ELM algorithm showed more accuracy and can potentially predict drought conditions in any climatic zone.

Figure 11 represents the Taylor diagrams for the Astore station with (1, 3, 6, 9, and 12) month time scales for the training phase. Taylor diagrams are the more comprehensive and precise way to represent the estimation and forecast ability of a model. The similarity between the predicted and actual values of SPTI is evaluated in terms of correlation (as a measure of closeness), and the variation is assessed by the standard deviation (SD) and the RMSE. For SPTI-1, the correlation of modeled data using the ELM algorithm with actual observations was about 0.9, followed by MLP and ARIMA with 0.6 each. As time scale increases, the prediction performance of algorithms significantly improves. For SPTI-3, the ELM algorithm is significantly closer to the actual values as its correlation is about (0.97) as compared to MLP (0.9) and ARIMA (0.85). The Taylor diagram exhibits the superior performance of ELM algorithm for estimating SPTI with (1, 3, 6, 9, and 12) month lead time scales (see Figure 11). Figure 12 illustrates the violin plots related to the training phase of ELM and other candidate models. The red dot represents the mean value, a thick white bar represents the interquartile, and a thin blue line represents the whole data set distribution. These are the components of the

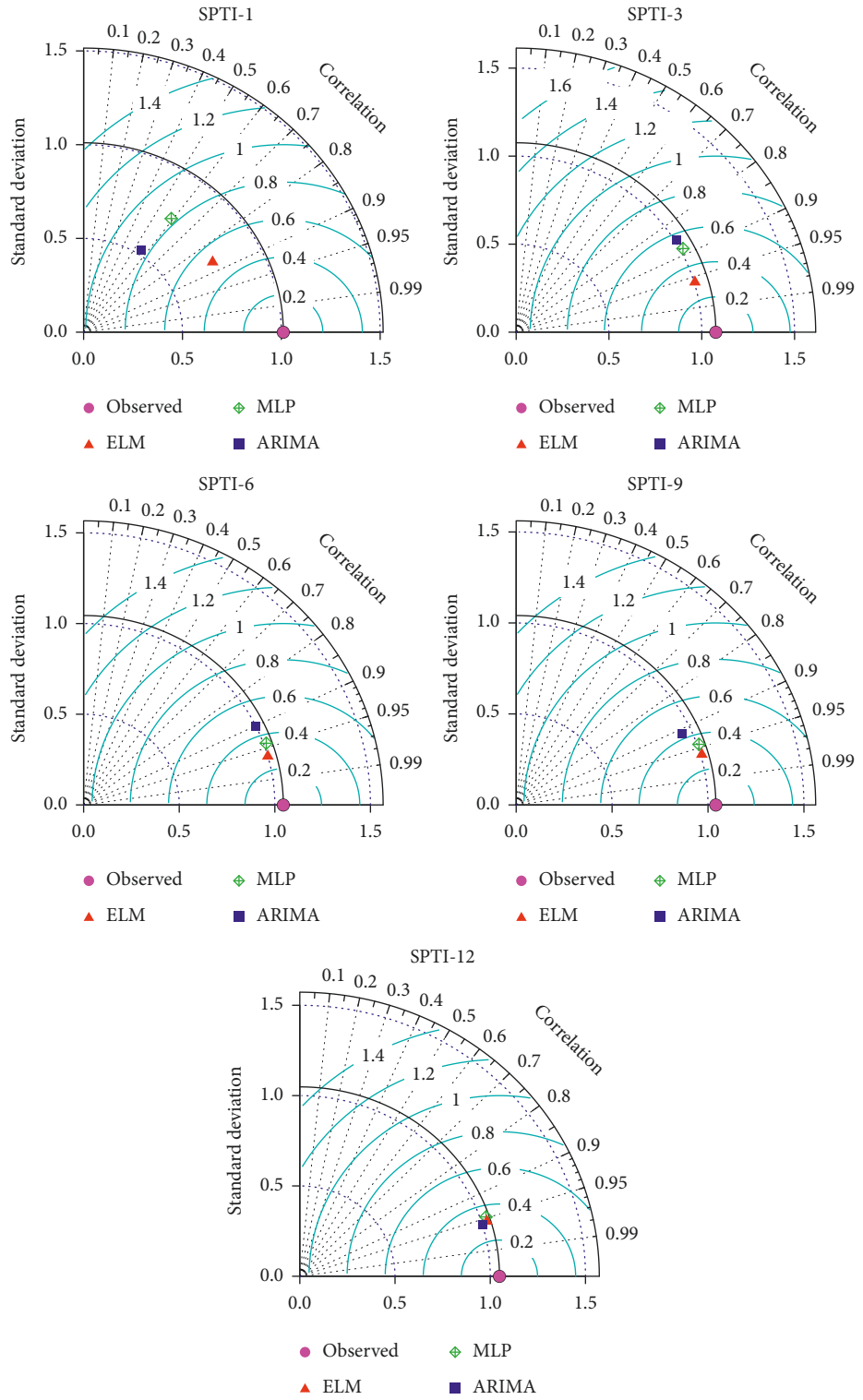

Figure 11: Taylor diagrams for the evaluation of the prediction performance of ELM, MLP, and ARIMA algorithms at Astore station with different time scales in the training phase.

boxplot, but the colored area on both sides of the blue line is the estimated kernel density of the shape of the distribution of data. Higher probabilities are associated with wider parts of the diagram, and thinner sections show lower probabilities. This is another systematic way to compare the prediction performance of models. It is noticeable that the mean of the predicted and observed values of SPTI-6 for the ELM model was almost similar for all the stations, whereas other models have slight variations. All the models have shown reasonable agreement but Violin diagrams of ELM

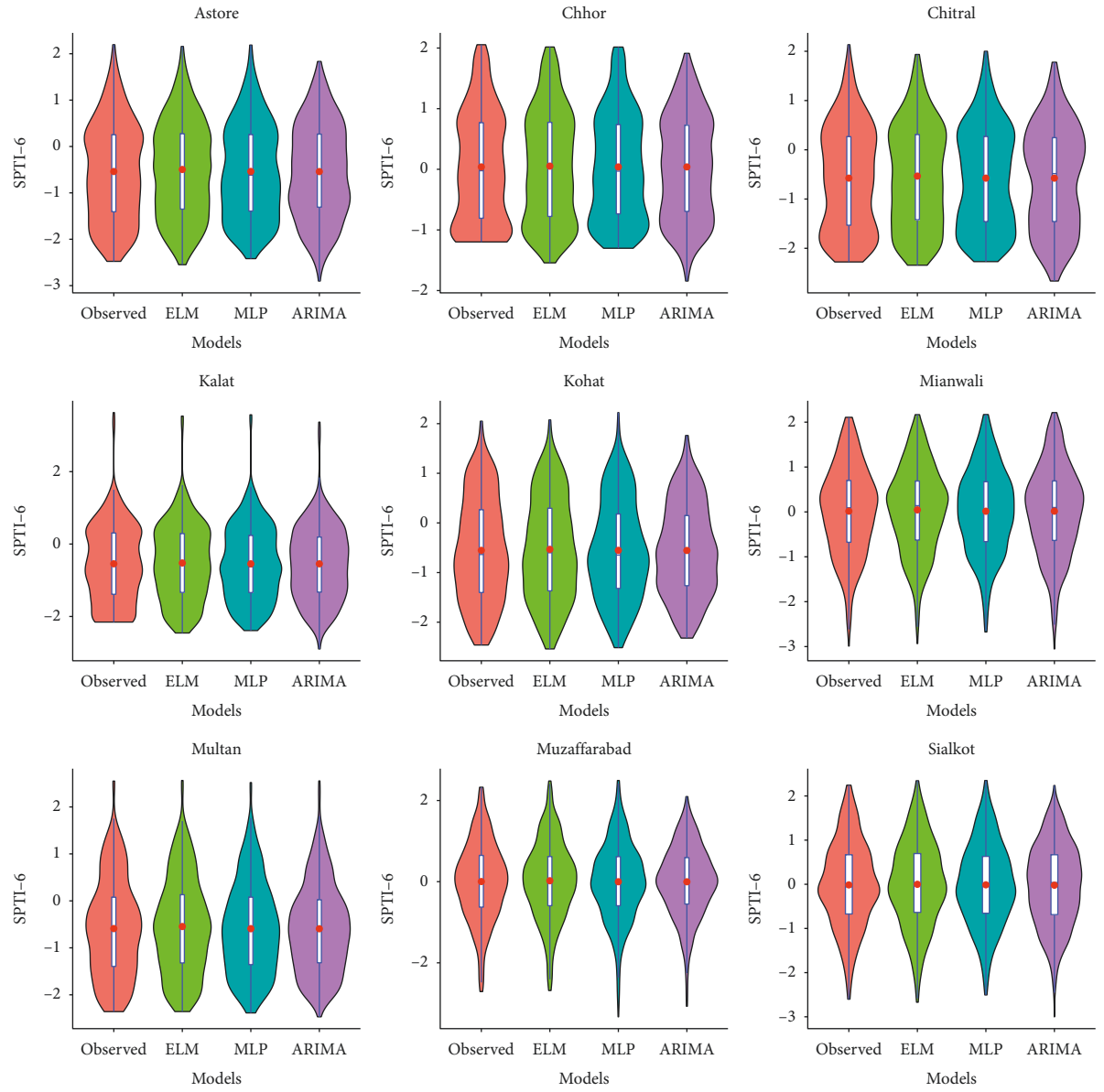

Figure 12: Violin plots of the observed SPTI-6 and the modeled data using ELM, MLP, and ARIMA models at all the selected meteorological stations in the training phase.

and observed data are nearly identical. These graphical illustrations affirmed that the proposed ELM model is better in estimating the actual values of SPTI at all selected meteorological stations.

After calibrating and validating algorithms for training datasets, the proposed algorithm's generalization capability has been assessed in the next step. Finally, out of the sample forecast of SPTI for all the lead time scales, (1–12) is carried out for 36 months from 2014 to 2016. These forecasts are considered sufficient for drought preparedness and mitigation policies. Similar performance metrics have been used to analyze the difference between the observed and forecasted values of SPTI for different time scales at all selected meteorological stations. Numerical results related to these performance metrics are given in Table 9. If the comparison of KGE was made at Astore station, the values of KGE for ELM, MLP, and ARIMA models are 0.988, 0.771, and 0.671, respectively. The KGE for the ELM model is significantly higher than its counterparts for all the time scales at all the selected meteorological stations, which clearly endorses the better forecast capability of the ELM model. Similarly, WI and MAE quantitative results also ratified that the ELM model outperformed the ANN and ARIMA models. RMSE and MAPE endorsed ELM as a better forecasting model for most stations.

The functional relationship between the observed and forecasted values of SPTI using ELM, MLP, and ARIMA models for all the time scales at Astore stations is illustrated in Figure 13 for the test phase starting from January 2014 to December 2016 for 36 months. A significantly smaller degree of deviation in SPTI for the ELM model and observed values of SPTI were exhibited. Although MLP has shown a

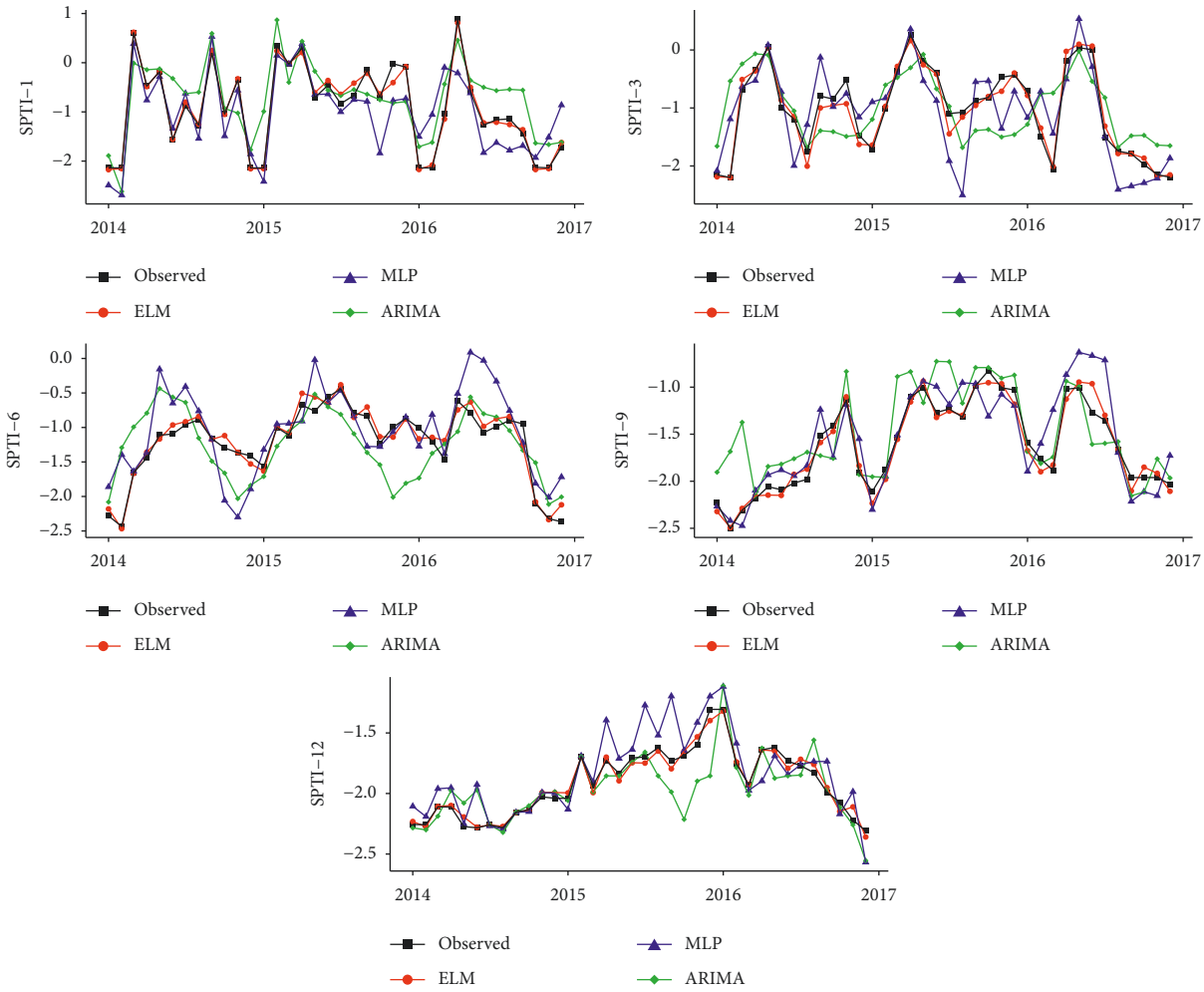

Figure 13: Observed and forecasted SPTI by ELM, MLP, and ARIMA models at Astore station for 1, 3, 6, 9, and 12 month lead time scales.

reasonably good forecast performance compared to the stochastic seasonal ARIMA model, the ELM model evidently shows superior forecast performance.

In order to check the appropriateness of the ELM model, scatter plots were prepared using time series data of the observed and forecasted SPTI at Astore station for all lead time scales (Figure 14). These scatter plots have shown a significant difference in the forecast performance of ELM and other models. The scatter plots depict the correlation, goodness-of-fit, and the extent of agreement between the observed and forecasted SPTI. The ELM model also clearly outperformed MLP and ARIMA models for the testing phase for all the selected time scales.

3.3. Discussion. Drought is a multifaceted and commonly occurring hazard in several parts of the world. Its impacts are prevalent in the agriculture, socio-economic, and energy sectors. However, precise drought monitoring and estimation techniques can assist in decreasing the vulnerability of society to drought. The primary objective of the current study was to test the appropriateness and usefulness of the ELM model relative to other ANN (MLP) models and stochastic (ARIMA) models for drought forecasting. The prediction and forecast performance of ELM is compared with other ANN algorithms (MLP) and statistical stochastic (ARIMA) models. The prediction and forecast performance of models is assessed using numerous performance metrics, including RMSE, MAE, MAPE, KGE, WI, and Karl Pearson's correlation coefficient. The quantitative assessment revealed that both the ANN models (ELM and MLP) performed better than the stochastic model (ARIMA), and among the ANN models, ELM has shown supremacy by producing the smallest RMSE, MAE, and MAPE values and the maximum values for KGE, WI, and correlation coefficient for almost all the meteorological stations.

Furthermore, ELM shows better agreement for both the training and test phases to predict the SPTI at all climatic stations than its counterparts. The efficiency of ELM, contrary to other models, is evident based on the performance metrics. A similar forecast performance has continued for higher-order time scales, consistent with earlier studies [30, 58]. Computational time consumed by drought modeling algorithms also needs to be optimized. Usually, large datasets are used as input variables for real-time drought modeling, which affects the computational performance of different models in terms of time. The ELM model is

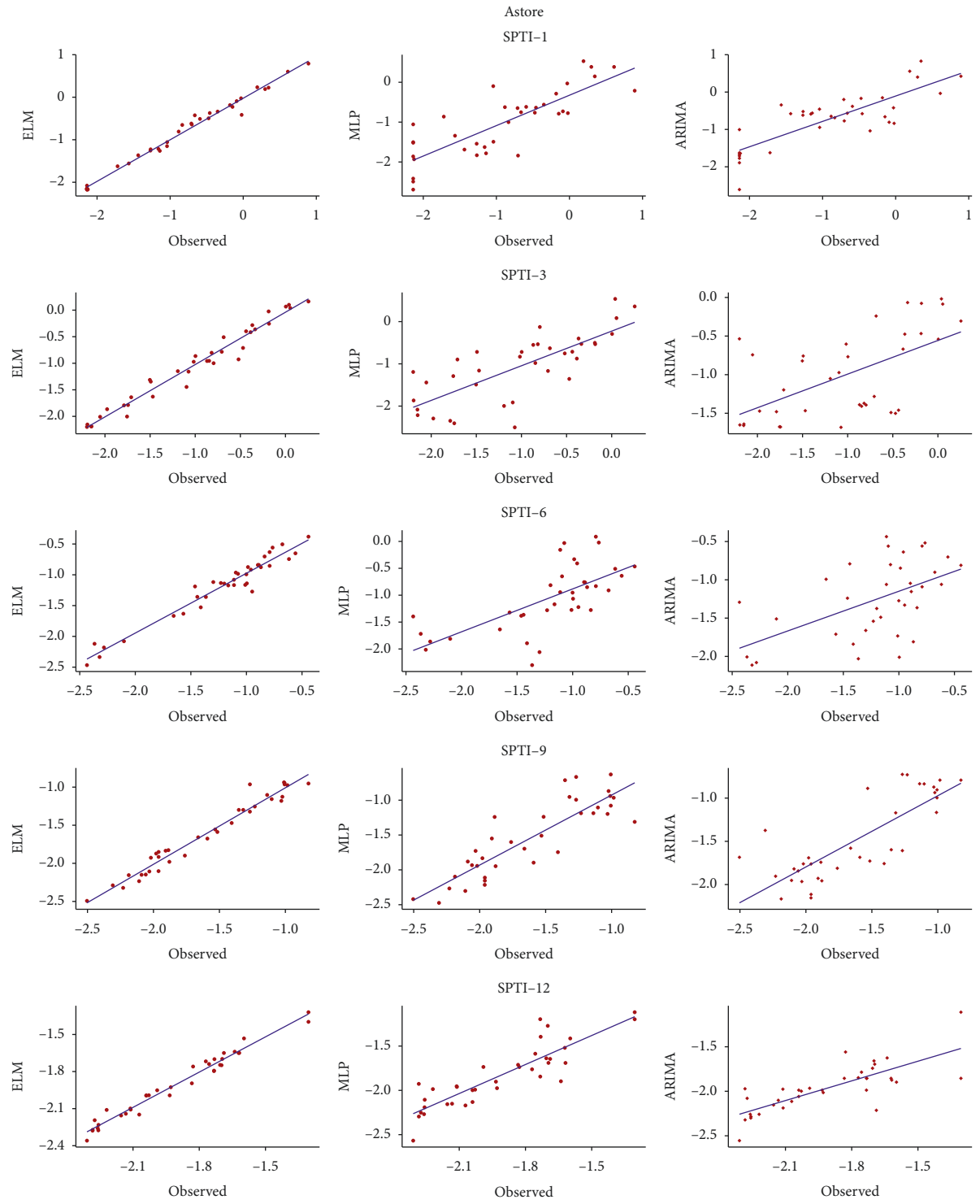

Figure 14: Scatter plots of the observed and forecasted values of SPTI using ELM, MLP, and ARIMA models at Astore station with all lead time scales for the test phase. The least-squares regression line is also included.

significantly faster than its counterparts. By evaluating all the numerical results of performance metrics and different graphical illustrations, it can be easily concluded that the ELM model attains the most accurate drought forecasting performance during training and test phases. The study revealed that ELM is the most appropriate, reliable, and efficient algorithm for drought prediction and forecasting. This study suggests that ELM can be used as an early warning drought forecasting tool for developing drought mitigation policies.

4. Conclusions

The reliable, efficient, and faster drought forecasting algorithms are useful for freshwater resource managers and drought mitigation policymakers. The current study examines the forecast performance of new machine learning (ELM) model using the Standardized Precipitating Temperature Index (SPTI). For application, meteorological time series datasets of monthly precipitation and minimum and maximum temperatures were collected from nine meteorological stations located in various climatological zones of Pakistan. Further, the prediction and forecast performance of the ELM model was compared with MLP and ARIMA models using different statistical performance metrics and graphical illustrations. The primary objective of the study was to investigate the appropriateness of the ELM model for predicting the nonlinear and complex temporal behavior of SPTI. The ELM model outperformed MLP and ARIMA models by producing the smallest root mean square error, mean absolute error, mean absolute percent error values, and maximum values for KGE, WI, and Karl Pearson's correlation coefficient for all the selected meteorological stations for different selected time scales. KGE and WI unanimously endorsed ELM as the best forecasting model at all the stations. Moreover, by comparing forecasting results for a one-month time scale, RMSE clearly affirmed ELM as superior forecasting model for five stations including Astore (RMSE = 0.688), Chitral (RMSE = 0.643), Kohat (RMSE = 0.956), Mianwali (RMSE = 0.773), and Sialkot (RMSE = 0.720). Furthermore, MLP better performed at Multan (RMSE = 0.666) and ARIMA at three of the meteorological stations containing Chhor (RMSE = 0.559), Kalat (RMSE = 0.727), and Muzaffarabad (RMSE = 0.724). While using MAE as a performance measure, the ELM algorithm performs better for six [94] stations (Astore 0.798, Chitral 0.495, Kalat 0.676, Kohat 0.791, Mianwali 0.652, and Sialkot 0.554), MLP for two [95] stations (Chhor 0.447 and Multan 0.577), and ARIMA for one of the stations (Astore 0.765). MAPE recognizes [96] ELM as an appropriate algorithm [97] for seven stations (Astore 247.3, Chitral 142.1, Kalat 500.3, Mianwali 309.1, Multan 545.5, Muzaffarabad 321.8, and Sialkot 91.0) and MLP (Chhor 269.2) and ARIMA (Kohat 268.2) for one station. Contrary [98] to MLP and ARIMA models, the ELM model has [99] the super-fast computation capability of [100] drought modeling. These performance [101] comparisons clearly ratified the novelty and [102] appropriateness of the proposed ELM algorithm.

In summary, this study suggests that ELM can be used as an early warning drought forecasting tool for developing drought mitigation policies using time series data of the Standardized Precipitating Temperature Index. The scope of the study can be enhanced by using wavelet data mining transformation to get the optimized forecast performance of the ELM model. ML algorithms have certain limitations, like requiring fast computing hardware. ANN models (ELM and MLP) have complex network structures among the machine learning algorithms. Another limitation of ANN algorithms is that there is no specific rule to determine the final network structure. Instead, the appropriate network structure is finalized through trial-and-error-based.

Data Availability

Data and codes can be provided on request.

Conflicts of Interest

The authors declare that they have no conflicts of interest.

Authors' Contributions

All authors have an equal contribution.

Acknowledgments

The authors appreciate the Deanship Scientific Research at King Khalid University for funding this work through large groups (project under grant number RGP.2/34/43).

References

[1] C. Liu, C. Yang, Q. Yang, and J. Wang, "Spatiotemporal drought analysis by the standardized precipitation index (SPI) and standardized precipitation evapotranspiration index (SPEI) in Sichuan Province, China," *Scientific Reports*, vol. 11, no. 1, pp. 1280–1314, 2021.

[2] D. G. Miralles, D. L. Schumacher, J. Keune, and P. A. Dirmeyer, "Drought spatiotemporal propagation via land feedbacks," in *Proceedings of the EGU General Assembly Conference Abstracts*, pp. EGU21–1505, 2021, April.

[3] B. Sobhani and V. S. Zengir, "Correction to: modeling, monitoring and forecasting of drought in south and southwestern Iran, Iran," *Modeling Earth Systems and Environment*, vol. 7, no. 1, p. 641, 2021.

[4] I. Semenova, "Some meteor-ological aspects of severe agricul-tural drought in the Northern Black Sea region in 2019-2020," *Environmental Sciences Proceedings*, vol. 8, no. 1, p. 18, 2021.

[5] C. King-Okumu, D. Tsegai, R. P. Pandey, and G. Rees, "Less to lose? Drought impact and vulnerability assessment in disadvantaged regions," *Water*, vol. 12, no. 4, p. 1136, 2020.

[6] W. R. L. Anderegg, A. T. Trugman, G. Badgley, A. G. Konings, and J. Shaw, "Divergent forest sensitivity to repeated extreme droughts," *Nature Climate Change*, vol. 10, no. 12, pp. 1091–1095, 2020.

[7] E. Eris, Y. Cavus, H. Aksoy, H. I. Burgan, H. Aksu, and H. Boyacioglu, "Spatiotemporal analysis of meteorological drought over Kucuk Menderes river basin in the Aegean region of Turkey," *Theoretical and Applied Climatology*, vol. 142, no. 3-4, pp. 1515–1530, 2020.

[8] M. N. Sattar, M. Jehanzaib, J. E. Kim, H. H. Kwon, and T. W. Kim, "Application of the hidden Markov Bayesian classifier and propagation Concept for probabilistic assessment of meteorological and hydrological droughts in South Korea," *Atmosphere*, vol. 11, no. 9, p. 1000, 2020.

[9] V. Diaz, G. A. Corzo Perez, H. A. Van Lanen, D. Solomatine, and E. A. Varouchakis, "An approach to characterise spatio-temporal drought dynamics," *Advances in Water Resources*, vol. 137, Article ID 103512, 2020.

[10] S. S. Askarimarnani, A. S. Kiem, and C. R. Twomey, "Comparing the performance of drought indicators in Australia from 1900 to 2018," *International Journal of Climatology*, vol. 41, no. S1, pp. E912–E934, 2021.

[11] D. J. Frame, S. M. Rosier, I. Noy et al., "Climate change attribution and the economic costs of extreme weather

events: a study on damages from extreme rainfall and drought," *Climatic Change*, vol. 162, no. 2, pp. 781–797, 2020.

[12] D. Wagner, "Arizona drought: Trees, animals stressed," *USA Today*, vol. 8, 2007.

[13] V. T. Jadhav, N. S. Kute, V. A. Chavan, and S. N. Bhalerao, "Effect of drought mitigation strategies on growth, yield and economics of pigeonpea (Cajanus cajan L. Millsp)," *Journal of Food Legumes*, vol. 33, no. 1, pp. 58–60, 2020.

[14] N. Bandyopadhyay, C. Bhuiyan, and A. K. Saha, "Drought mitigation: critical analysis and proposal for a new drought policy with special reference to Gujarat (India)," *Progress in Disaster Science*, vol. 5, Article ID 100049, 2020.

[15] D. E. Wendt, A. F. Van Loon, B. R. Scanlon, and D. M. Hannah, "Managed aquifer recharge as a drought mitigation strategy in heavily-stressed aquifers," *Environmental Research Letters*, vol. 16, no. 1, Article ID 014046, 2021.

[16] L. C. Botterill and M. J. Hayes, "Drought triggers and declarations: science and policy considerations for drought risk management," *Natural Hazards*, vol. 64, no. 1, pp. 139–151, 2012.

[17] R. Niaz, I. Hussain, Z. Ali, and M. Faisal, "A novel framework for regional pattern recognition of drought intensities," *Arabian Journal of Geosciences*, vol. 14, no. 16, pp. 1644–1716, 2021a.

[18] R. Niaz, X. Zhang, Z. Ali et al., "A new propagation-based framework to enhance competency in regional drought monitoring," *Tellus A: Dynamic Meteorology and Oceanography*, vol. 73, no. 1, pp. 1975404–1975413, 2021b.

[19] M. A. Faiz, Y. Zhang, N. Ma, F. Baig, F. Naz, and Y. Niaz, "Drought indices: aggregation is necessary or it is only the researcher's choice," *Water Supply*, vol. 21, no. 8, pp. 3987–4002, 2021.

[20] M. A. Faiz, D. Liu, Q. Fu et al., "Assessment of dryness conditions according to transitional ecosystem patterns in an extremely cold region of China," *Journal of Cleaner Production*, vol. 255, Article ID 120348, 2020.

[21] H. Wang, Y. Pan, and Y. Chen, "Comparison of three drought indices and their evolutionary characteristics in the arid region of northwestern China," *Atmospheric Science Letters*, vol. 18, no. 3, pp. 132–139, 2017.

[22] L. Li, D. She, H. Zheng, P. Lin, and Z. L. Yang, "Elucidating diverse drought characteristics from two meteorological drought indices (SPI and SPEI) in China," *Journal of Hydrometeorology*, vol. 21, no. 7, pp. 1513–1530, 2020.

[23] Q. Liu, S. Zhang, H. Zhang, Y. Bai, and J. Zhang, "Monitoring drought using composite drought indices based on remote sensing," *Science of The Total Environment*, vol. 711, Article ID 134585, 2020.

[24] W. C. Palmer, "Meteorological drought," Research paper no. 45, p. 58, US Weather Bureau, Washington, DC, US Weather Bureau, 1965.

[25] B. A. Shafer and L. E. Dezman, "Development of surface water supply index (swsi) to assess the severity of drought condition in snowpack runoff areas," in *Proceedings of the western snow conference, Colorado State University*, pp. 164–174, Western Snow Conference, Fort Collins, CO, April 1982.

[26] T. B. McKee, N. J. Doesken, and J. Kleist, "The relationship of drought frequency and duration to time scales," in *Proceedings of the 8th Conference on Applied Climatology*, pp. 179–183, Amer. Meteor. Soc, Anaheim California, January 1993.

[27] S. M. Vicente-Serrano, S. Beguería, and J. I. López-Moreno, "A multiscalar drought index sensitive to global warming: the standardized precipitation evapotranspiration index," *Journal of Climate*, vol. 23, no. 7, pp. 1696–1718, 2010.

[28] Z. Ali, I. Hussain, M. Faisal et al., "A novel multiscalar drought index for monitoring drought: the standardized precipitation temperature index," *Water Resources Management*, vol. 31, no. 15, pp. 4957–4969, 2017a.

[29] R. Niaz, I. Hussain, X. Zhang et al., "Prediction of drought severity using model-based clustering," *Mathematical Problems in Engineering*, vol. 2021, pp. 2021–2110, 2021c.

[30] R. C. Deo, M. K. Tiwari, J. F. Adamowski, and J. M. Quilty, "Forecasting effective drought index using a wavelet extreme learning machine (W-ELM) model," *Stochastic Environmental Research and Risk Assessment*, vol. 31, no. 5, pp. 1211–1240, 2017.

[31] O. Aiyelokun, G. Ogunsanwo, A. Ojelabi, and O. Agbede, "Gaussian Naïve Bayes classification algorithm for drought and Flood risk Reduction," in *Intelligent Data Analytics for Decision-Support Systems in Hazard Mitigation*, pp. 49–62, Springer, Singapore, 2021.

[32] A. Raza, I. Hussain, Z. Ali et al., "A seasonally blended and regionally integrated drought index using Bayesian network theory," *Meteorological Applications*, vol. 28, no. 3, Article ID e1992, 2021.

[33] S. Mehdizadeh, F. Ahmadi, and A. Kozekalani Sales, "Modelling daily soil temperature at different depths via the classical and hybrid models," *Meteorological Applications*, vol. 27, no. 4, Article ID e1941, 2020a.

[34] S. Mohamadi, S. S. Sammen, F. Panahi et al., "Zoning map for drought prediction using integrated machine learning models with a nomadic people optimization algorithm," *Natural Hazards*, vol. 104, no. 1, pp. 537–579, 2020.

[35] A. Mokhtar, M. Jalali, H. He et al., "Estimation of SPEI meteorological drought using machine learning algorithms," *IEEE Access*, vol. 9, pp. 65503–65523, 2021.

[36] H. Bonakdari, H. Moeeni, I. Ebtehaj, M. Zeynoddin, A. Mahoammadian, and B. Gharabaghi, "New insights into soil temperature time series modeling: linear or nonlinear?" *Theoretical and Applied Climatology*, vol. 135, no. 3-4, pp. 1157–1177, 2019.

[37] I. Ebtehaj and H. Bonakdari, "Comparison of genetic algorithm and imperialist competitive algorithms in predicting bed load transport in clean pipe," *Water Science and Technology*, vol. 70, no. 10, pp. 1695–1701, 2014.

[38] M. Zeynoddin, H. Bonakdari, I. Ebtehaj, F. Esmaeilbeiki, B. Gharabaghi, and D. Zare Haghi, "A reliable linear stochastic daily soil temperature forecast model," *Soil and Tillage Research*, vol. 189, pp. 73–87, 2019.

[39] P. Aghelpour, B. Mohammadi, S. Mehdizadeh, H. Bahrami-Pichaghchi, and Z. Duan, "A novel hybrid dragonfly optimization algorithm for agricultural drought prediction," *Stochastic Environmental Research and Risk Assessment*, vol. 35, no. 12, pp. 2459–2477, 2021.

[40] F. Ahmadi, S. Mehdizadeh, and B. Mohammadi, "Development of bio-inspired-and wavelet-based hybrid models for reconnaissance drought index modeling," *Water Resources Management*, vol. 35, no. 12, pp. 4127–4147, 2021.

[41] Z. Ali, I. Hussain, M. Faisal et al., "Forecasting drought using multilayer perceptron artificial neural network model," *Advances in Meteorology*, vol. 2017, pp. 1–9, 2017b.

[42] N. Acharya, N. A. Shrivastava, B. K. Panigrahi, and U. C. Mohanty, "Development of an artificial neural network-based multi-model ensemble to estimate the northeast

monsoon rainfall over south peninsular India: an application of extreme learning machine," *Climate Dynamics*, vol. 43, no. 5-6, pp. 1303–1310, 2014.

[43] A. Belayneh and J. Adamowski, "Standard precipitation index drought forecasting using neural networks, wavelet neural networks, and support vector regression," *Applied computational intelligence and soft computing*, vol. 2012, pp. 1–13, 2012.

[44] M. Şahin, Y. Kaya, M. Uyar, and S. Yıldırım, "Application of extreme learning machine for estimating solar radiation from satellite data," *International Journal of Energy Research*, vol. 38, no. 2, pp. 205–212, 2014.

[45] K. J. Waciko and B. Ismail, "SARIMA-ELM hybrid model versus SARIMA-MLP hybrid model," *International Journal of Statistics and Applied Mathematics*, vol. 5, no. 2, pp. 01–08, 2020.

[46] C. Deina, M. H. do Amaral Prates, C. H. R. Alves et al., "A methodology for coffee price forecasting based on extreme learning machines," *Information Processing in Agriculture*, 2021.

[47] S. C. Nayak, B. Satyanarayana, B. P. Kar, and J. Karthik, "An extreme learning machine-based model for Cryptocurrencies prediction," in *Smart Computing Techniques and Applications*, pp. 127–136, Springer, Singapore, 2021.

[48] S. Mouatadid and J. Adamowski, "Using extreme learning machines for short-term urban water demand forecasting," *Urban Water Journal*, vol. 14, no. 6, pp. 630–638, 2017.

[49] A. Toprak, "Extreme learning machine (elm)-based classification of benign and malignant cells in breast cancer," *Medical Science Monitor*, vol. 24, pp. 6537–6543, 2018.

[50] G. B. Huang, H. Zhou, X. Ding, and R. Zhang, "Extreme learning machine for regression and multiclass classification," *IEEE Transactions on Systems, Man, and Cybernetics, Part B (Cybernetics)*, vol. 42, no. 2, pp. 513–529, 2012.

[51] S. J. Hadi, S. I. Abba, S. S. Sammen, S. Q. Salih, N. Al-Ansari, and Z. M. Yaseen, "Non-linear input variable selection approach integrated with non-Tuned data Intelligence model for streamflow pattern simulation," *IEEE Access*, vol. 7, pp. 141533–141548, 2019.

[52] Q. He, X. Jin, C. Du, F. Zhuang, and Z. Shi, "Clustering in extreme learning machine feature space," *Neurocomputing*, vol. 128, pp. 88–95, 2014.

[53] J. Chen, Y. Zeng, Y. Li, and G. B. Huang, "Unsupervised feature selection based extreme learning machine for clustering," *Neurocomputing*, vol. 386, pp. 198–207, 2020.

[54] M. Y. Zhai, R. H. Yu, S. F. Zhang, and J.-H. Zhai, "Feature selection based on extreme learning machine," in *Proceedings of the 2012 2012 International Conference on Machine Learning and Cybernetics*, pp. 157–162, IEEE, Xi'an, China, July 2012.

[55] Y. Wan, S. Song, G. Huang, and S. Li, "Twin extreme learning machines for pattern classification," *Neurocomputing*, vol. 260, pp. 235–244, 2017.

[56] G. Di Leo, G. Fabbrocini, and C. Liguori, "ELM image processing for melanocytic skin lesion diagnosis based on 7-point checklist: a preliminary discussion," in *Proc. Int. Symp. Meas. For Res. and Ind. Appl*, E. Kayafas and V. Loumos, Eds., pp. 474–479, IMEKO, Budapest, Hungary, 2004.

[57] I. Ebtehaj, H. Bonakdari, and S. Shamshirband, "Extreme learning machine assessment for estimating sediment transport in open channels," *Engineering with Computers*, vol. 32, no. 4, pp. 691–704, 2016.

[58] R. C. Deo and M. Şahin, "Application of the extreme learning machine algorithm for the prediction of monthly Effective Drought Index in eastern Australia," *Atmospheric Research*, vol. 153, pp. 512–525, 2015.

[59] G. Huang, G. B. Huang, S. Song, and K. You, "Trends in extreme learning machines: a review," *Neural Networks*, vol. 61, pp. 32–48, 2015.

[60] S. Ding, X. Xu, and R. Nie, "Extreme learning machine and its applications," *Neural Computing & Applications*, vol. 25, no. 3-4, pp. 549–556, 2014.

[61] Z. Ali, I. Hussain, M. Faisal, A. M. Shoukry, S. Gani, and I. Ahmad, "A framework to identify homogeneous drought characterization regions," *Theoretical and Applied Climatology*, vol. 137, no. 3-4, pp. 3161–3172, 2019.

[62] X. Li, B. He, X. Quan, Z. Liao, and X. Bai, "Use of the standardized precipitation evapotranspiration index (SPEI) to characterize the drying trend in southwest China from 1982–2012," *Remote Sensing*, vol. 7, no. 8, pp. 10917–10937, 2015.

[63] R. Niaz, I. Hussain, Z. Ali et al., "A novel spatially weighted accumulative procedure for regional drought monitoring," *Tellus A: Dynamic Meteorology and Oceanography*, vol. 72, no. 1, pp. 1838194–1838213, 2020.

[64] E. D. Martonne, "L'indice d'aridité," *Bulletin de 'Association de géographes français*, vol. 3, no. 9, pp. 3–5, 1926.

[65] M. Kumar, N. S. Raghuwanshi, and R. Singh, "Artificial neural networks approach in evapotranspiration modeling: a review," *Irrigation Science*, vol. 29, no. 1, pp. 11–25, 2011.

[66] S. S. Sammen, T. A. Mohamed, A. H. Ghazali, A. H. El-Shafie, and L. M. Sidek, "Generalized regression neural network for prediction of Peak Outflow from Dam Breach," *Water Resources Management*, vol. 31, no. 1, pp. 549–562, 2017.

[67] S. S. Sammen, M. A. Ghorbani, A. Malik et al., "Enhanced artificial neural network with Harris Hawks optimization for predicting Scour Depth Downstream of Ski-Jump Spillway," *Applied Sciences*, vol. 10, no. 15, p. 5160, 2020.

[68] R. J. Kuligowski and A. P. Barros, "Localized precipitation forecasts from a numerical weather prediction model using artificial neural networks," *Weather and Forecasting*, vol. 13, pp. 1194–1204, 1998.

[69] P. Han, P. X. Wang, S. Y. Zhang, and D. H. Zhu, "Drought forecasting based on the remote sensing data using ARIMA models," *Mathematical and Computer Modelling*, vol. 51, no. 11-12, pp. 1398–1403, 2010.

[70] G. U. Yule, "Why do we sometimes get nonsense-correlations between Time-Series?--a study in sampling and the nature of time-series," *Journal of the Royal Statistical Society*, vol. 89, pp. 1–63, 1926.

[71] E. Slutzky, "The summation of random causes as the source of cyclic processes," *Econometrica*, vol. 5, no. 2, pp. 105–146, 1937.

[72] H. Wold, "A study in the analysis of stationary time series," Doctoral dissertation, p. 214, Almqvist & Wiksell, Uppsala, Almqvist & Wiksell, 1938.

[73] M. H. Alsharif, M. K. Younes, and J. Kim, "Time series ARIMA model for prediction of daily and monthly average global solar radiation: the case study of Seoul, South Korea," *Symmetry*, vol. 11, no. 2, p. 240, 2019.

[74] A. K. Mishra and V. R. Desai, "Drought forecasting using stochastic models," *Stochastic Environmental Research and Risk Assessment*, vol. 19, no. 5, pp. 326–339, 2005.

[75] D. Xu, Q. Zhang, Y. Ding, and H. Huang, "Application of a hybrid ARIMA–SVR model based on the SPI for the forecast of drought—a case study in Henan Province, China," *Journal*

of Applied Meteorology and Climatology, vol. 59, no. 7, pp. 1239–1259, 2020.

[76] G. B. Huang, Q. Y. Zhu, and C. K. Siew, "Extreme learning machine: theory and applications," *Neurocomputing*, vol. 70, no. 1-3, pp. 489–501, 2006.

[77] I. Ebtehaj and H. Bonakdari, "Bed load sediment transport estimation in a clean pipe using multilayer perceptron with different training algorithms," *KSCE Journal of Civil Engineering*, vol. 20, no. 2, pp. 581–589, 2016.

[78] G. B. Huang, M. B. Li, L. Chen, and C. K. Siew, "Incremental extreme learning machine with fully complex hidden nodes," *Neurocomputing*, vol. 71, no. 4-6, pp. 576–583, 2008.

[79] B. L. S. da Silva, F. K. Inaba, E. O. T. Salles, and P. M. Ciarelli, "Fast deep stacked networks based on extreme learning machine applied to regression problems," *Neural Networks*, vol. 131, pp. 14–28, 2020.

[80] S. R. Mugunthan and T. Vijayakumar, "Design of improved Version of sigmoidal function with biases for classification Task in ELM Domain," *Journal of Soft Computing Paradigm*, vol. 3, no. 2, pp. 70–82, 2021.

[81] Q. Fan, L. Niu, and Q. Kang, "Regression and multiclass classification using sparse extreme learning machine via smoothing group L 1/2 regularizer," *IEEE Access*, vol. 8, pp. 191482–191494, 2020.

[82] C. W. Dawson, R. J. Abrahart, and L. See, "HydroTest: a web-based toolbox of evaluation metrics for the standardized assessment of hydrological forecasts," *Environmental Modelling & Software*, vol. 22, no. 7, pp. 1034–1052, 2007.

[83] N. Mehdiyev, D. Enke, P. Fettke, and P. Loos, "Evaluating forecasting methods by considering different accuracy measures," *Procedia Computer Science*, vol. 95, pp. 264–271, 2016.

[84] P. J. Gleckler, K. E. Taylor, and C. Doutriaux, "Performance metrics for climate models," *Journal of Geophysical Research*, vol. 113, no. D6, p. D06104, 2008.

[85] F. Ahmadi, S. Mehdizadeh, and V. Nourani, "Improving the performance of random forest for estimating monthly reservoir inflow via complete ensemble empirical mode decomposition and wavelet analysis," *Stochastic Environmental Research and Risk Assessment*, pp. 1–16, 2022.

[86] S. Mehdizadeh, F. Ahmadi, A. Danandeh Mehr, and M. J. S. Safari, "Drought modeling using classic time series and hybrid wavelet-gene expression programming models," *Journal of Hydrology*, vol. 587, Article ID 125017, 2020b.

[87] D. G. Fox, "Judging air quality model performance: a summary of the AMS workshop on dispersion model performance, woods hole, Mass., 8–11 September 1980," *Bulletin America Meteorology Social*, vol. 62, pp. 599–609, 1981.

[88] H. V. Gupta, H. Kling, K. K. Yilmaz, and G. F. Martinez, "Decomposition of the mean squared error and NSE performance criteria: Implications for improving hydrological modelling," *Journal of hydrology*, vol. 377, no. 1-2, pp. 80–91, 2009.

[89] C. J. Willmott, "On the validation of models," *Physical Geography*, vol. 2, no. 2, pp. 184–194, 1981.

[90] J. H. Stagge, L. M. Tallaksen, L. Gudmundsson, A. F. Van Loon, and K. Stahl, "Candidate distributions for climatological drought indices (SPI and SPEI)," *International Journal of Climatology*, vol. 35, no. 13, pp. 4027–4040, 2015.

[91] A. N. Spiess, "Propagate: propagation of Uncertainty," R package version 1.0-4, 2014.

[92] N. Kourentzes, "Nnfor: time series forecasting with neural networks," 2019, https://CRAN.R-project.org/package=nnfor.

[93] R. J. Hyndman and Y. Khandakar, "Automatic time series forecasting: the forecast package for R," *Journal of Statistical Software*, vol. 27, no. 3, pp. 1–22, 2008.

[94] G. E. Box and G. M. Jenkins, *Time Series Analysis: Forecasting and Control San Francisco*, Holden Day, Calif, 1976.

[95] J. J. Harou, M.-A. Josue, T. Zhu et al., "Economic consequences of optimized water management for a prolonged, severe drought in California," *Water Resources Research*, vol. 46, no. 5, 2010.

[96] K. L. Hsu, H. V. Gupta, and S. Sorooshian, "Artificial neural network modeling of the rainfall-runoff process," *Water Resour. Res.*vol. 31, no. 10, pp. 2517–2530, 1995.

[97] S. S. Lin, S. L. Shen, A. Zhou, and H. M. Lyu, "Assessment and management of lake eutrophication: a case study in Lake Erhai, China," *Science of the Total Environment*, vol. 751, Article ID 141618, 2021.

[98] F. Mekanik, M. A. Imteaz, S. Gato-Trinidad, and A. Elmahdi, "Multiple regression and Artificial Neural Network for long-term rainfall forecasting using large scale climate modes," *Journal of Hydrology*, vol. 503, pp. 11–21, 2013.

[99] A. Mellit, A. Massi Pavan, E. Ogliari, S. Leva, and V. Lughi, "Advanced methods for photovoltaic output power forecasting: a review," *Applied Sciences*, vol. 10, no. 2, p. 487, 2020.

[100] J. Rhee and J. Im, "Meteorological drought forecasting for ungauged areas based on machine learning: using long-range climate forecast and remote sensing data," *Agricultural and Forest Meteorology*, vol. 237-238, pp. 105–122, 2017.

[101] A. Sugathan and S. Gregory, "Analysis of AEP prediction against production data of commercial wind turbines in Sweden," Thesis, p. 51, 2021.

[102] C. M. Zealand, D. H. Burn, and S. P. Simonovic, "Short term streamflow forecasting using artificial neural networks," *Journal of Hydrology*, vol. 214, no. 1-4, pp. 32–48, 1999.

Hindawi
Complexity
Volume 2022, Article ID 4981539, 15 pages
https://doi.org/10.1155/2022/4981539

WILEY | Hindawi

Research Article

Design of System-of-System Acquisition Analysis Using Machine Learning

Fahad H. Alshammari

College of Computing and Information Technology, Shaqra University, Shaqra, Saudi Arabia

Correspondence should be addressed to Fahad H. Alshammari; fahad.h@su.edu.sa

Received 13 May 2022; Revised 20 June 2022; Accepted 23 June 2022; Published 21 July 2022

Academic Editor: Haitham Abdulmohsin Afan

A system of system's ability to function is derived from the integration of systems from different sources. An SOS's systems serve two purposes: first, to accomplish their own specific aims, and second, to provide resources to the SOS as a whole. In the last few decades, machine learning and data analytics have been widely used in system design and acquisitions. Every organisation that acquires a sophisticated system employs some type of data analytics to evaluate the system's independent objectives, which is universally accepted. Data analytics and decision-making regarding the independent system is rarely shared across SOS stakeholders, even though the systems contribute to and benefit from the larger SOS. The goal of this research is to determine how the exchange of data sets and the corresponding analytics by SOS stakeholders can improve SOS capacity. Predicting SOS capabilities by exchanging relevant data sets and prescribing information connections between systems, we propose to use machine learning techniques. This article serves as an intermediate analysis of the above research work and aims to estimate the benefit of information sharing among the SOS stakeholders. In this research, we have applied different machine learning models to the IBM HR analytics data set to determine the corresponding analytics by SOS stakeholders that can improve SOS capacity. We propose using machine learning techniques to forecast SOS capabilities through the sharing of relevant data sets, and we prescribe the information linkages across systems to make this possible. This paper provides an update on the progress being made toward the aforementioned research project, and its primary focus is on developing a method to put a dollar amount on the benefits of information sharing among the many parties involved in the SOS.

1. Introduction

A system of systems (SOS) is a collection of many heterogeneous distributed systems that have been acquired independently and continue to operate and be managed independently [1]. The system-of-systems capability relies on the systems' ability to work together effectively, notwithstanding their independence [2]. For acquisition decisions, it is crucial to take into account more than just one system; rather, it is necessary to take into account all of the systems within the SOS [3].

Through the use of collected and previously used data, predictive data analytics may foresee and forecast future consequences [4]. In Babylonian times, data was stored on tablets to anticipate harvest, but a dramatic leap in the ability to reason over enormous volumes of data arose in the 1940s with the advent of computer development [5, 6], storage, and machine learning techniques [7]. In the 1940s and 1950s, data analytics models were utilised to anticipate the consequences of nuclear chain reactions in the Manhattan Project and weather forecasts using the ENIAC computer [8]. Data analytics that is used to produce or prescribe the optimum courses of action in light of available information is known as prescriptive data analytics [9].

1.1. Problem Statement. In the decades following World War II, the requirement to optimise the course of action encouraged the development of the operations research discipline, which eventually led to "Analytics 1.0" for the introduction of data-based decision-making in corporations [10]. Enormous companies such as Google and Amazon

have adopted Analytics 2.0 as the new paradigm for processing large amounts of structured and unstructured data (also known as big data) [11–13]. "Analytics 3.0" is a term used to describe the ability of organisations to incorporate this "big data" into their decision-making process, which is shaped by the volume, variety, velocity, and validity of data [4]. To say that most successful firms use Analytics 3.0 for business and product development is not a generalisation.

Analytics 3.0 deployment presents a unique challenge for the acquisition and development of SOS capabilities, as each of the contributing organisations employs a different set of predictive and prescriptive analytics tools for their respective systems (the Literature Review of Machine Learning Techniques and Applications in the DOD provides details on predictive machine learning techniques as applied primarily in the DOD application space) [7]. All SOS stakeholders rarely have access to these analyses and the underlying data sets [14–16].

1.2. Motivation. SOS is a diverse enterprise, and in this article, we pursue research toward an information-centric framework that aids early-stage decisions at the corporate level. Digital engineering (DE) and its related components in other engineering tasks [17], such as model-based systems engineering (MBSE) for the systems engineering domain, provide an important backdrop for our work. Digital models are employed by DE and MBSE throughout the acquisition process. Many people are focused on how to implement DE/MBSE and the desire to have models work together rather than how well the extended enterprise (or "acquisition ecosystem") is aware of and trusts the various data sets that underpin models and development processes that use them, which is a more demanding issue. Data management and analytic deployment techniques that establish synergies between multiple enterprise entities and link stakeholders, resources, policy, and economics between various systems are among our objectives in this area. Data aspects such as survey categories, types of variables, ownership/privacy of data, and the interconnection of data sets are examined in the framework. These data sets exist at the local system level but may not be shared with SOS/enterprise or vice versa for SOS acquisition. Predictive and prescriptive analytics can be used because of data access, and this allows us to explain how sharing and connecting data sets can lead to better results at the SOS level. An example is used to demonstrate how valuable techniques from the field of data science/machine learning can be used. As this is a relatively new field of study, we are focusing on determining which of the most persistent research problems deserve further investigation.

1.3. Contributions. The contributions of this study are as follows:

(a) We have determined how the exchange of data sets and the corresponding analytics by SOS stakeholders can improve SOS capacity

(b) We have predicted SOS capabilities by exchanging relevant data sets, and prescribing information connections between systems, we propose to use machine learning techniques

(c) This article serves as an intermediate analysis of the above research work and aims to estimate the benefit of information sharing among the SOS stakeholders

(d) We have applied different machine learning models to the IBM HR analytics data set to determine the corresponding analytics by SOS stakeholders that can improve SOS capacity

(e) We propose using machine learning techniques to forecast SOS capabilities through the sharing of relevant data sets, and we prescribe the information linkages across systems to make this possible

(f) This paper provides an update on the progress being made toward the aforementioned research project, and its primary focus is on developing a method to put a dollar amount on the benefits of information sharing among the many parties involved in the SOS

2. Literature Review

SOS's ability to function is derived from the integration of systems from different sources. An SOS's systems serve two purposes: first, to accomplish their own specific aims, and second, to provide resources to the SOS as a whole. In the last few decades, machine learning and data analytics have been widely used in system design and acquisitions. Every organisation that acquires a sophisticated system employs some type of data analytics to evaluate the system's independent objectives, which is universally accepted. Data analytics and decision-making regarding the independent system are rarely shared across SOS stakeholders, even though the systems contribute to and benefit from the larger SOS. Certain areas of knowledge acquisition can be greatly aided by the use of machine learning algorithms. We have initiated a systematic examination into how to transfer the functions of knowledge-based systems onto those machine learning systems that supply the requisite information, given the potential of machine learning for knowledge acquisition.

In Dahmann et al. [4] research, there are various parallels and differences between NCE system and SOS, which highlights the implications for system engineering and acquisition. The first half of this study provides an overview of our current understanding of SOS and the implications of this understanding for SE. It then studies the attributes of NCE systems and compares them to those of SOS systems in order to conclude. The study concludes with an examination of the implications of these findings for systems engineering and procurement practices.

There are significant development hurdles in all three dimensions of military capabilities, including technological, operational, and programmatic aspects of the system of systems development. A scarcity of tools exists for determining how to create and evolve SOS in a way that takes into account both performance and risk considerations. In the study by Colombi et al. [18], the application of methodologies from financial engineering and operations research is beneficial in the optimisation of portfolios. The authors

make it easier for SOS architectures to evolve by offering a framework that allows for architectural selection at a certain evolutionary decision epoch. Generic nodes on a network are used to model hierarchies of interconnected systems. These generic nodes, subject to connectivity and compatibility constraints, collaborate to achieve broad capability objectives. Portfolio algorithms are capable of dealing with a wide range of problems, including uncertain data, poor performance between nodes, and development risk. This naval warfare scenario demonstrates how to identify "portfolios" of available systems from a list of candidate systems by using a search algorithm. For example, by allowing the optimisation problem to handle the more mathematically intensive elements of the decision-making process (e.g., the feasibility of solutions and optimality), the number of connection rules, the feasibility of solutions, and optimality are all decreased. As a result, while making final decisions, human decision-makers can concentrate their efforts on picking the appropriate risk aversion weights.

In the past, programme managers have utilised technical performance measures (TPMs) to establish whether or not a programme is on pace to reach its performance objectives. It is possible to build a deterministic method of estimating the operational performance of a project by utilising TPMs throughout the project's lifecycle. When it comes to a set of systems that are universally accepted, TPMs, on the other hand, can be difficult to compute (SOS). For a deterministic state similar to TPM usage, an SOS performance measure (SPM) has been developed and proven. It serves the same function as TPMs and may be used in the same way. The reality reveals that several of the SOS components are subject to significant uncertainty during the development process of the system. As a result, in order to more precisely account for an SOS's ability to achieve its desired performance, it is necessary to take this unpredictability into account. In order to account for this uncertainty, [18] develops an extension of the SPM concept known as a stochastic SPM. To demonstrate how this expansion of the SPM technique improves its effectiveness, an antisubmarine warfare (ASW) operation is used in this example.

How typical systems engineering activities have evolved to enable SOS-level systems engineering is discussed in detail in the Department of Defence's Systems Engineering Guide for Systems of Systems, which was just released this month. According to the study conducted for this handbook, modelling and simulation are helpful in the development of SOS systems. While some modelling and simulation are currently being used, more support would be advantageous if models could be generated rapidly and used to assist in decision-making when it is needed. In order to achieve these objectives, the Systems Modelling Language (SysML) is employed in [18] research.

System-of-systems procurements might include the purchase of many systems, or they can be purchased as stand-alone items. A considerably more common occurrence in the United States Department of Defence (DOD) is the acquisition of one or more new systems that are intended to interoperate with existing systems as part of a system of systems (SOS) with additional capabilities. The success of any SOS acquisition is dependent on the effectiveness of the contract structures and acquisition processes used. The difficulties associated with the acquisition of SOS are recognised in this work, and the findings are explored. According to the findings, the SOS acquisition should be accompanied by a significant systems engineering effort, as well as modifications to the existing contractual processes, frameworks, and organisational structures, before being finalised. As a result of [18], modifications to current and future Department of Defence SOS procurement are recommended.

SOS (system-of-systems) management faces a major issue in dealing with the possibility for member systems to evolve in an uncontrolled manner. Organisations become more inefficient, more expensive, and less able to respond rapidly to changing circumstances when they lack control over evolution. In order to achieve common aims, systems of systems (SOS) connect together a variety of systems that were designed independently and to various standards. The objectives and aims of the member systems are preserved, as is a great deal of their autonomy. As a result, there is an increased possibility that decisions on evolution will be made unilaterally within member systems, which could have negative consequences for the SOS's stability, efficiency, and trustworthiness. A modified version of HAZOPS (hazard and operability study) is used in [18] to examine the hazards associated with SOS evolution and presents a technique to assist nonspecialist end users in identifying, organising, and discussing this information. The report uses a case study of a recent RAF (royal aviation force) Nimrod air crash to examine the methodology, and the official inquiry revealed serious flaws in the Nimrod SOS's operation. Conclusions and future prospects for research are discussed in the paper, which concludes that the technique proposed would be a valuable support for SOS evolution processes.

The authors need to look more closely at how the BMDS interacts with other systems, especially those built by other agencies. Interstitials are used in the context of systems interoperability, interoperability, and integration. The authors believe the SOS literature has not given enough attention to this problem. The BMDS is an excellent case study for the SOS because many of its components are existing programmes of record. The pieces work as intended, but their performance metrics may not match the SOS's higher-level requirements. Interoperability is a BMDS challenge to achieving predictable national capacity. Some of the new capabilities requested by national leaders may include changes to kill chains, C2 structures, coordination, and performance. To attain these new capabilities, record programmes must be changed and system components integrated. SOS engineers must objectively evaluate competing solutions and trade-offs. Reference [18] provides a variety of technological methods for integrating a complex adaptive SOS. New mathematical tools such as graph-theoretic modelling and simulation techniques such as agent-based modelling will be introduced. Finally, new design maturity measures will be introduced. This study will use the theatrical BMDS design and interstitials to depict the integration domain. They may assist the BMDS to reach its full

potential by focusing on the interstitial area of the overall BMDS SOS build and applying suitable technical rigour and engineering due diligence.

Data management strategies for business analytic capability growth should be informed by continuing research into developing an information-centric framework. Data collecting aspects (e.g., survey categories, types of variables, ownership/privacy of data, and connection of data sets) are examined in the framework to determine the type and effectiveness of predictive and prescriptive analytics that can be used. Using a system-of-systems engineering approach, the authors of [19] take into account all key stakeholders' interests, resources, and operations; policies and economics of data gathering and curation; and the various predictive/prescriptive analytic deployments that can be achieved. Data architectures and analytic components across an organisation are envisioned to be orchestrated in an integrated manner to maximise informational synergy and to extend the analytic capabilities of prescriptive and predictive elements that are deployed in an organisation. When it comes to predictive and prescriptive analytic applications, minor, straightforward modifications in how data is acquired have a significant impact. Using the concept problem, the framework's ideas are seen in action.

The best practices of OSSD projects are merged with new capabilities for virtual system acquisition in [20], which analyses and develops concepts that will lead to that combination of capabilities. With the use of virtual systems, it is possible to drastically cut acquisition prices and cycle times for software-intensive systems while simultaneously improving them. Implementing electronic government applications makes use of modern information technology and processes (IT). Using open-source software development in the creation, deployment, and ongoing expansion of complex software system applications is a relatively recent strategy in the field of software system development. The development of large-scale, user-friendly, and highly reliable software systems necessitates the development of new resources, products, techniques, and production environments, all of which are being rethought as part of the open-source movement. The open acquisition is a brand-new concept that brings together the best of open-source software development with cutting-edge electronic government processes to create a revolutionary new way of doing business. This study describes the development of an open acquisition framework for virtual system acquisition, as well as its demonstration. Furthermore, this study highlights the next steps to be taken in order to deploy open acquisition approaches inside this framework.

Instead of the traditional document-centric approach, the model-centered approach (MBSE) is used instead. The development of SOSs lends itself well to a model-centric approach, particularly when the model can describe the independence of the systems that make up the SOSs in question. Using an agent-based paradigm, the system of systems (SOS) and each individual system can be regarded as distinct entities, each with its own dynamics and interactions. Each system must establish its own agenda and priorities in order to contribute to the growth of the system of systems (SOSs). System-to-system interactions may be required in order to achieve the overall aims and capabilities of the SOS. The research of [3] investigates an acknowledged system of systems (SOSs) and the various systems that are associated with it, which are represented in an agent-based model (ABM). Individual system agents' decisions are recorded in the ABM's decision models for system dynamics, system-to-system, and system-of-system discussions. ABM, which integrates the key elements that drive SOS dynamics, can be used to test and analyse the dynamics of individual systems and the dynamics of the system as a whole.

Teams of designers are necessary to possess a diverse variety of design and decision-making abilities when working on large-scale engineering systems. Using formal and computational approaches that have been well-defined for system integration and design optimisation, it is possible to obtain optimal performance for complex systems. Engineers may be ill-suited to handle this type of project, according to design best practices. During their graduate studies, students from four distinct graduate programmes collaborated to build a distributed, sophisticated system. The design histories of the teams reveal three ineffective approaches: global searches rather than local searches, optimising each design parameter independently, and sequential rather than concurrent optimisation processes, according to the results of the analysis. Optimisation of systems was overlooked in favour of optimising the performance of individual subsystems, with no attention given to the impact of changes in individual subsystems on the performance of the system as a whole. Engineers should be taught how to integrate systems as a whole, according to [21].

Cook [2] defines "systems of systems" (SOS) as a subset of large monolithic systems that differ in terms of system characteristics and acquisition methodologies. A distinguishing element of this research is that systems of systems (SOS) are formed from component systems that are acquired through a variety of asynchronous activities. Considering our position as a defence contractor, the authors believe that the current acquisition paradigm does not appropriately address the purchase of component parts for military systems and systems components. The study identifies more particular challenges that must be addressed, as well as alternative mitigating methods that can be implemented. Capacity development and acquisition in broad force areas should be prioritised over project-centric capacity development and acquisition, and top-down, force-structure planning should be given more prominence. The importance of system features such as adaptability, flexibility, and open interfaces should also increase as a result of these developments.

Reference [22] discusses a system engineering process that can be used in the building of advanced military systems and systems of systems. In order to accommodate this, the process has been split down into its constituent elements, with each stage being described in great depth. It is discussed how to utilise legacy equipment while also ensuring that new parts are seamlessly and synergistically integrated. As part of the integration and testing of these systems of systems, it will

be necessary to develop new dimensions and measurement systems in order to assess performance. Whenever these systems are used by the military, it becomes necessary to examine whether or not a new doctrine, standards, and procedures are required.

When it comes to "systems of systems," the implementation and control of these systems vary significantly from the implementation and control of individual systems. Because of this, the systems engineering processes required to ensure the proper implementation of systems of systems differ dramatically from those commonly applied to individual systems. Successful implementation of systems of systems necessitates the use of a multi-tiered systems engineering technique that goes beyond the conventional single-system approach, according to the finding of [23].

Although information systems (IS) were supposed to have a significant impact on socioeconomic and human development in developing countries, the benefits have been less than expected. Many elements influence an information system's long-term survival (IS). Africa's technology transfer efforts have relied too largely on foreign finance and technology. Informed by local needs and structures, relevant information systems must be designed locally. Reference [24] recommends that information systems be acquired, developed, and implemented in Zambia (Africa) based on local demands and structures. Five public interest user companies in Zambia were researched in detail, as were literature evaluations on IT acquisition, development, and deployment in South Africa, Kenya, India, and the developing world. Obstacles to sector growth in Zambia include people, technology, and poor execution. Before citizens enjoy locally created and manufactured goods and services, their mindsets must be altered. The sector's growth will be accelerated if authors recognise the value of tiny steps and developing talent while acquiring information systems. A paradigm (the acquisition, development, and implementation framework; ADIF) has been designed to ensure that information system investments are maximised.

Our understanding of the system of systems (SOSs) engineering and management has expanded and evolved along with it. SOS engineering (SoSE) is still looking for a way to provide meaning to this kind of uncertainty, whereas systems engineering has developed frameworks and architectures to do so. SOS literature is reviewed to show that in a dynamic, complex environment, an SoSE management framework is required to meet the needs of constant technological improvement. According to the findings of [1], there are two ways to describe SOS: (1) using distinguishing traits and (2) viewing SOS as a network to which "best practices" for network management can be applied to SoSE. In order to construct an efficient SoSE management framework, the authors rely on these two theories. Use the modified FCAPS network principles for this purpose in order to achieve this goal (SoSE management conceptual areas). There are various SoSE management frameworks that employ these qualities as a starting point. As the last example, the authors use a well-documented and well-known SOS (i.e., integrated deepwater system) to demonstrate how the SoSE domain can be better understood, engineered, and managed.

Increasing evidence suggests that airborne particulate matter is a factor in numerous diseases. The authors of [25] need to know how particulate matter impacts air filters if they are going to design effective filtration devices. We are building an air filter testing setup and automating the data collection process. An air filter's performance can be monitored over time using a data-gathering system. Deterioration can be seen, even if the quality of air filters does not reach dangerous levels. In order to train and test a machine learning model that can evaluate air filter quality, the obtained data is used for this purpose with 99% accuracy; this machine learning is a significant tool in the evaluation of air filters. Finally, a data-gathering system and user interface have been developed that greatly decreases the amount of time needed to test filters. Data collection systems can also alert operators when filters need to be changed or other problems arise with the equipment. An effort to develop a system for automatically determining when the test equipment needs to be repaired and recalibrated failed.

E-procurement software refers to the use of data and communication advancements via the Internet to complete all phases of procurement. With this new arrangement of electronic acquisition software, the majority of firms are succeeding while some fall short. During this investigation, steel companies in Pakistan were surveyed by [26] for their use of electronic acquisition software. Achievement variables for electronic acquisition are influenced by the examination's goal. For this inquiry, a semiorganised discussion from the acquisition administrators of selected associations was held to discuss the differentiating proof of accomplishment components in their organisations. From eight firms, a sample size of 150 respondents participated in a study survey to get quantitative data on the influence of electronic acquisition software's success. The data are broken down using SPSS v22, and a variety of analyses are carried out. Electronic acquisition software has been adopted by every single company, but some practices such as e-sourcing and e-proposal accommodation have not been implemented because of a lack of education in the market, as well as a fear of using new technology at the provider/merchant end, according to the study.

There are a lot of ways to model the acquisition process in [27]. Starting with Winston Royce's waterfall model, authors then go on to more complex and detailed waterfall models, such as the "V" and spiral models. As a result, we will also take a look at other acquisition methods. These many models are all a part of the acquisition process's progression, according to our perspective. Simplification of the procedure is getting more and more feasible and economical as technology progresses. For example, authors have seen an upsurge in concurrent engineering and concurrent design. We will look at models for this cycle and how they connect to the acquisition, research, development, test, and evaluation cycles in the planning and marketing life cycle.

In [8], systems engineering (SE) considerations for integrating independently useful systems into a bigger system that has unique capabilities (a system of systems (SOS)) inside the Department of Defence (DOD) are addressed. The

handbook is designed to be a resource for systems engineers who assist SOS work, notably as part of a SE team for an SOS, and it draws on the experiences of existing SOS SE practitioners. SE for SOS may now be better understood and guided because of this first draught of the guide. In some circumstances, the book raises awareness of issues that may need to be addressed by systems engineers undertaking SOS work, but it does not provide practical recommendations. In the future, the guide will develop in scope and content as more people get familiar with SOS.

A number of sources have asserted that the technological and management maturity of the acquirer is a significant element in SISA's success and that best practices should be followed. Because of a lack of understanding of how and why SISA techniques affect software-intensive system development, the Department of Defence (DOD) has been cautious to use SISA practices in its development processes. A hybrid software process simulation modelling approach is employed in [28] to investigate the implications of SISA strategies on both the acquirer and the developer. It is possible to represent the dynamic and discrete properties of SISA programmes using our technique (e.g., the interactions between acquisition and development organisations and the effects of numerous SISA practices). The outcomes of this study will shed light on the various ways in which the activities of the acquirer have an impact on the developer's development cycle.

To build on and extend guidance published by the United States Department of Defence on systems engineering (SE) of systems of systems (SOS), [7] develops and presents an approach to SOS SE that transforms the core elements of SOS SE, their interrelationships, and the artefacts and data used in SOS decision-making from a trapeze model to a more familiar and intuitive time-sequenced wave model representation. A more user-friendly version of the information has been provided, and it is consistent with the progressive development methodologies that are common in the advancement of SOS capabilities. A wave model is developed; its important characteristics are discussed; and examples of SOS efforts reflecting this perspective of SOS SE are provided in the paper. Finally, the study explains how the information necessary for a successful SOS SE is generated, where it belongs in the wave model, how it changes over time, and where it is generally stored.

Machine learning techniques have the potential to significantly improve the efficiency of some knowledge acquisition processes. As a result of the potential that machine learning has for knowledge acquisition, we have begun a systematic investigation into how to convert the functionality of knowledge-based systems to machine learning systems that can offer the necessary information. Reference [29] attempts to give a comprehensive definition of machine learning systems and their associated application domains, which authors believe they will be able to do in the near future.

Reference [30] introduces the concept of system-of-systems difficulties, as well as the key qualities that distinguish them from other types of issues. Following that, the significant ramifications for the aeronautical design community are highlighted. Due to the fact that they concentrate on a network of systems and dynamic behaviour rather than a single system and static behaviour, there are two important characteristics that stand out. The community's existing ability to handle the methodological criteria for examining these characteristics is also restricted. Future transportation concepts are conceptualised as a system of systems in order to better grasp their repercussions. The "proto-method" for dealing with this class of difficulties is introduced and investigated in the transportation sector, as well as prospective approaches to constructing successful models and simulations for transportation. Because the vast bulk of the existing literature on systems of systems is devoted to the study of defence systems, it is vital that civil transportation be included in this research. Currently, civil transportation is not included in this research.

A "system of systems" (SOS) is created by integrating many independent but interdependent systems, each of which can function independently, to produce a larger system with greater capabilities. In the aerospace and defence industries, clients increasingly want broad capabilities and solutions rather than individual equipment. Choosing the correct mix of present and future systems is critical to the SOS design process. Including elements of a future system complicates resource allocation by mandating a dynamic resource. Reference [10] calculates the cost of flying on an unbuilt new plane. Based on this statement, it is an NLP difficulty. MINLP methodologies are employed to address the problem, albeit at a high computational expense. Using a response surface technology improves airline design while reducing computer costs. In a similar way to multi-disciplinary optimisation, the problem can be decomposed into allocation and aircraft design domains, yielding solutions at a cheaper computing cost. The MDO-motivated decomposition strategy appears promising for several SOS design difficulties.

A system of unmanned aerial vehicles (UAVs), including vehicles, networks, and operating plans, must be created at the same time as a part of an integrated system. The challenge in designing areas of unified design space that are not merely a collection of poorly optimised discrete entities is that even at the conceptual level, the resulting complexity can quickly become unmanageable. In order to abstract the integrated system, an object-oriented modelling technique must be employed for the modelling of the integrated system. When [31] strategy is used, it increases the efficiency with which the combined system-of-systems design space may be searched more successfully. The economic viability of an imagined service provider in UAV-based package delivery architecture is analysed in terms of trade-offs between vehicle performance and network topology. When compared to previous approaches, the object-oriented solution offers greater modelling flexibility than those approaches.

An acquisition strategy's identification and handling of possible threats to the company's long-term existence is one of the most critical components of the process. It is necessary to integrate a large number of systems in order to support

business processes that span numerous firms or organisations. New risks, such as a large and diverse user base, as well as increasing unpredictability, are incorporated into this operational framework by [32], making the development and implementation of an acquisition plan more difficult to accomplish. The incorporation of these concepts into an acquisition plan can help alleviate some of the problems mentioned above.

Reference [33] describes an IBM-compatible laptop-based data collection and analysis system (PC). Conventional bus slots connect the computer to a D/A converter. The programme supports eight analogue signals, four of which can be plotted on the computer's screen as data is acquired. Data can be stored in ASCII or small binary files to speed up input and output. After a data collection cycle, data can be easily scaled and plotted for review. The extra data reduction features allow for smoothing data and cross plots between any two variables. This technology replaces traditional tape recorders and strip chart recorders by saving data in a format that computers can access in the future. The device is portable and runs on a 12-volt automobile battery. This approach records and displays vehicle motion and driver/rider response characteristics. In between runs, data can be processed and examined fast to impact future test conditions. The strategy works with several typical laptop computers that have easily accessible PC buses. Two current systems that could be used are Datavue Snap 1 + 1 and GRID Case Exp.

Many people use the term "systems of systems," but there is no agreement on what they are, how to differentiate them from "conventional systems," or how their development differs from other systems. To aid in their creation, [34] offers a definition, a limited taxonomy, and a foundational set of architectural principles. Apparently, the taxonomic term "system of systems" is a misnomer. "Collaborative systems" is a better term for grouping. Misclassification is also addressed in this work, and the paper's authors outline how to avoid it in system design. As a result of the classification, the primary structuring heuristics for systems of systems have been identified. Another is the realisation that the architecture of a system of systems is communications. Nonphysical architecture is the set of standards that enable meaningful communication among the components.

The purpose of this literature study is twofold: first, to catalogue the numerous ML approaches that can be used to solve SOS acquisition challenges and to map their input, output, and data needs, and second, to evaluate how these approaches are used to solve a variety of Department of Defence issues. A common theme that has emerged from the assessment of relevant literature is that these techniques are often applied in silos, with results and data sets being kept secret from higher-level decision-makers and the Society of Organizational Learning (SoL). Our research is distinct because we want to examine how various systems perform independent local predictive analytics and how to optimally communicate diverse data sets throughout the SOS hierarchy in order to prescribe the SOS capabilities.

3. Materials and Methods

Due to a lack of communication or judgement in a multi-objective SOS acquisition situation [35], it is usual to see different interpretations of the aims from several officers, developers, and managers. Disparities in requirements defined by different contributors to the SOS have an impact on the ultimate performance and cost, which is the subject of this study. System capabilities and the indices by which they contribute to SOS capability have been defined. They are all desirable. When calculating each SOS capacity, a normalised sum of the capabilities of the separate systems used is used in the relevant area.

3.1. Problem Formulation. Consider, for example, the capabilities of a system of systems, as shown in Figure 1. The system of systems is defined in the definition phase, whereas the abstraction phase defines the links between the various components. According to this arrangement, system β_1 is made up of systems α_1 and α_2, whereas system β_2 includes systems α_3 and α_4. Identifying the correct information pathways and integrating data sets for predictive and prescriptive analytics becomes important when suppliers 1, supplier 2, and system 1 management are all integrated into the same system. Data sets may need to be connected between systems 1 and 2 and between suppliers 1, 2, and 3 in order for the SOS level to function properly, according to this rationale. However, achieving complete connectivity between all SOS components and constituents may not be a practical goal. This raises the challenge of how to determine which data sets should be linked by assessing the influence of their connectedness on the SOS and the figures of merit. Figure 1 shows the conceptual model of the study.

An analytical solution is impossible due to the problem's complexity and magnitude in real-world implementations. By first constructing an SOS capability measure by collecting different systems from inside the DOD application domain, we demonstrate how SOS capability evolves due to sharing preferences between sub-hierarchical systems while keeping the autonomous system goals. To that end, we will study the use of machine learning techniques to forecast and prescribe the connection of data sets across various hierarchical levels. SOS acquisition issue formulation is the primary emphasis of this paper's interim update; however, a future update will explore methods for selecting machine learning techniques.

3.2. Framework. A synthetic problem was created to run simulations using Python and interface with other existing system-of-systems (SOS) analytical tools. The synthetic problem is an IBM HR-based analytics for employee attrition, which was chosen since it is a multi-domain problem involving education, employee satisfaction, job satisfaction, job performance, performance rating, relationship, and work-life balance. The systems in IBM interact to provide logistical support and system-level capabilities to achieve

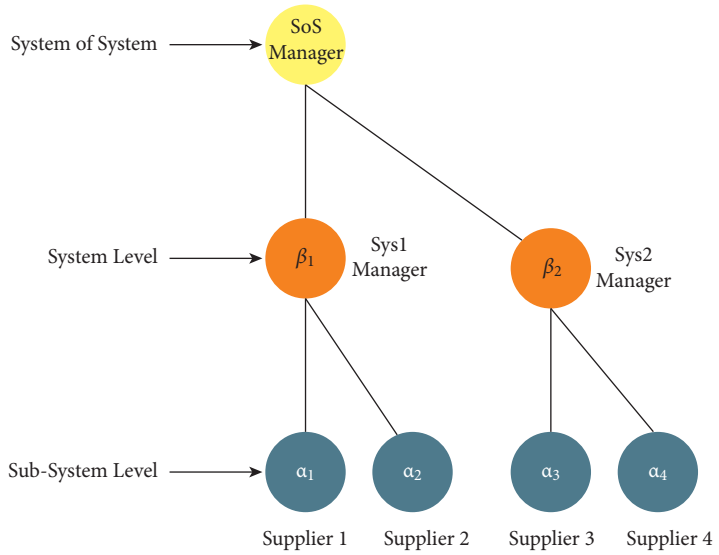

Figure 1: Conceptual model.

certain SOS-level capabilities. Figure 2 shows the framework of the current study:

System capabilities and the indices by which they contribute to SOS capability have been specified. They are all desired. Each SOS capacity is derived from the total of the individual system capabilities in the relevant domain. Portfolios including information about various architectures and their associated SOS performance index and cost are generated for each case. Some systems provide the required capabilities, while others give the necessary support, making up a portfolio.

3.3. Data Set Description. Employee attrition is caused by a variety of circumstances, such as a lack of job satisfaction, a lack of work-life balance, or a lack of opportunities for advancement (https://www.kaggle.com/datasets/pavansubhasht/ibm-hr-analytics-attrition-dataset). To keep things interesting, IBM data scientists generated this fictitious data set. Table 1 shows the data set description and features distribution.

Figure 3 shows the attrition level in data set and frequency distribution of label 0 or 1.

Figure 4 shows the attrition distribution on the basis of travel readiness.

Figure 5 shows the distribution of attrition on the basis of the department of employees.

Figure 6 shows the attrition on the basis of education level and the distribution of frequencies on the basis of qualification level.

3.4. Data Preprocessing. Processing raw data into a comprehensible format is known as preprocessing. Because we cannot do anything with raw data, it is a critical phase in the data mining process. Before using machine learning or data mining methods, make sure the data is of high quality. It is just a set of procedures that convert or alter data. It is a prealgorithm process of data transformation. In the context of data processing, the term refers to the use of a computer to

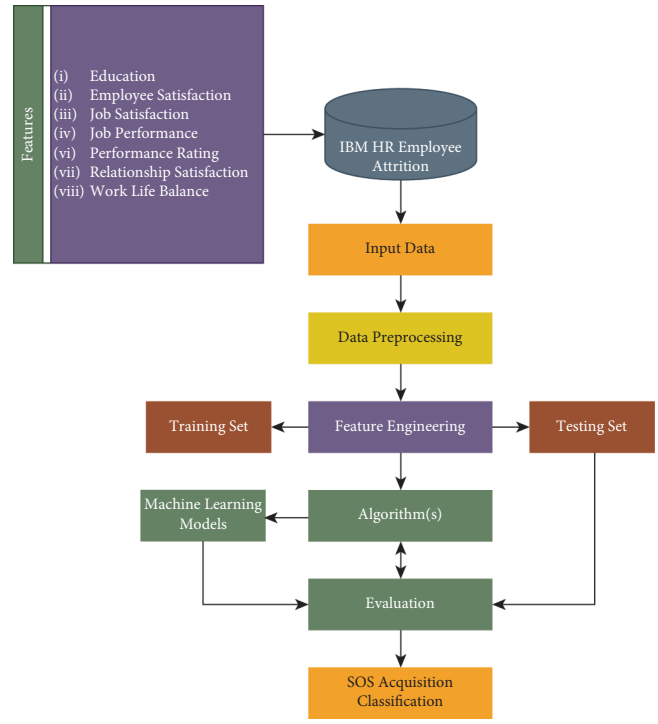

Figure 2: Framework.

extract, convert, or otherwise alter data. Before data can be used, it must be preprocessed. Processing raw data into a clean data set is known as preprocessing. Before running the algorithm, the data set is preprocessed to look for anomalies such as missing values, noisy data, and other irregularities. Figure 7 shows feature correlation matrix.

3.5. Feature Engineering. In machine learning and statistical modelling, feature engineering refers to the process of selecting and transforming the most relevant variables from

Table 1: Features' description.

Feature	Description	Features labels and values	Type of variable
Education	Education level of applicants and candidates	(1) "Below college" (2) "College" (3) "Bachelor" (4) "Master" (5) "Doctor"	Input
Employee satisfaction	Level of satisfaction from an employee as described by the company	(1) "Low" (2) "Medium" (3) "High" (4) "Very high"	Input
Job satisfaction	Job satisfaction level of an employee while searching and joining a job	(1) "Low" (2) "Medium" (3) "High" (4) "Very high"	Input
Job performance	Performance of employee during job in a company	(1) "Low" (2) "Medium" (3) "High" (4) "Very high"	Input
Performance rating	Performance rating shown by company as per the performance of employee	(1) "Low" (2) "Good" (3) "Excellent" (4) "Outstanding"	Input
Relationship satisfaction	Behaviour and relationship of satisfaction level with other employees	(1) "Low" (2) "Medium" (3) "High" (4) "Very high"	Input
Work-life balance	Balance between job and life	(1) "Bad" (2) "Good" (3) "Better" (4) "Best"	Input
Attrition	Strength and acquisition	0 or 1 No or yes	Output

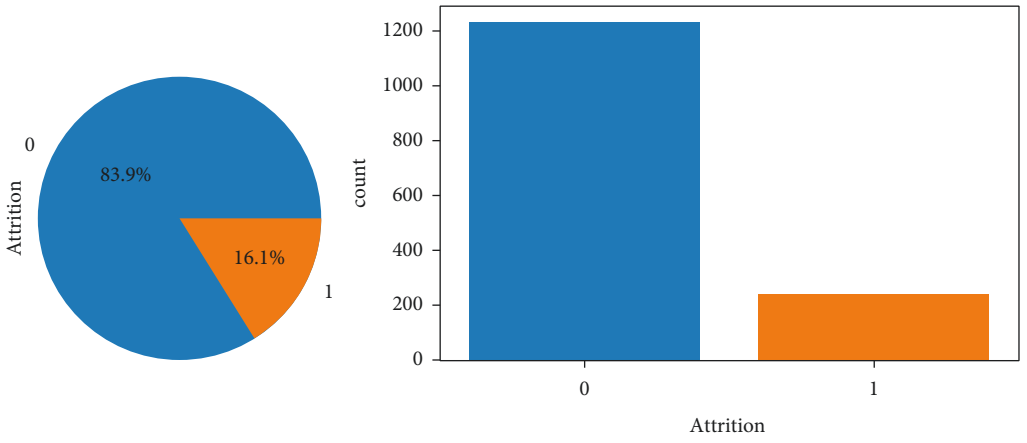

Figure 3: Attrition level.

raw data in order to build a predictive model. Engineers use domain expertise to extract features from raw data via feature engineering or feature extraction. The goal is to enhance the quality of machine learning outcomes by providing these additional attributes in addition to the raw data that would otherwise be provided. Figure 7 shows the feature correlation matrix showing the correlation of most related features.

3.6. Classification Models. This study's objective is to determine how SOS stakeholders may improve SOS capacity

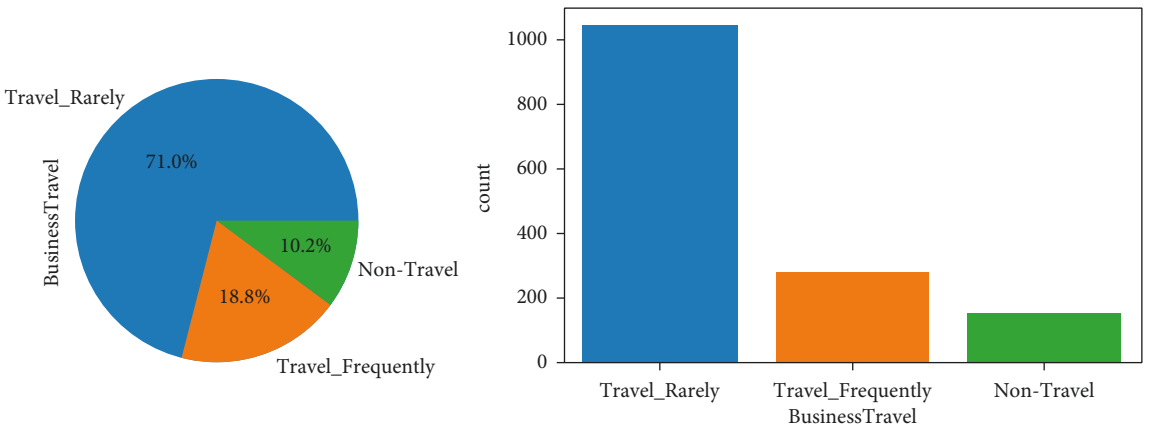

Figure 4: Distribution on the basis of travel readiness.

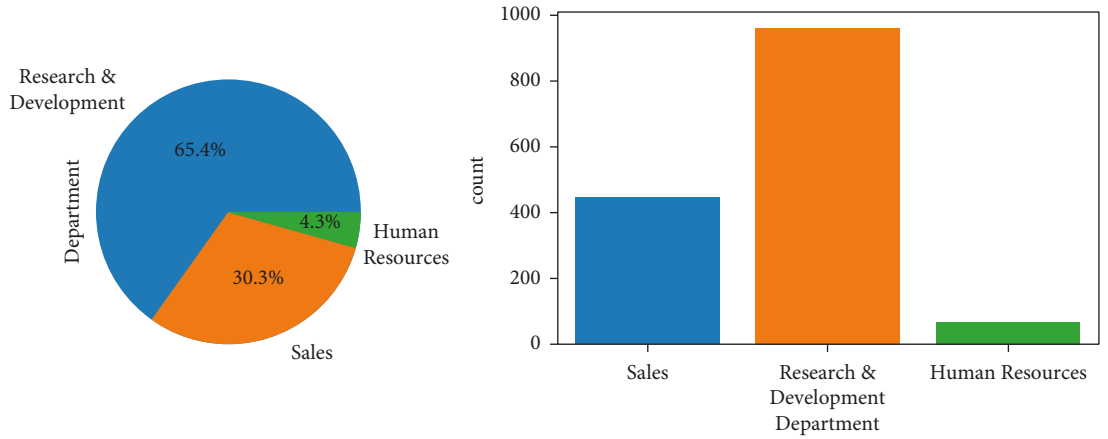

Figure 5: Attrition on the basis of the department of employees.

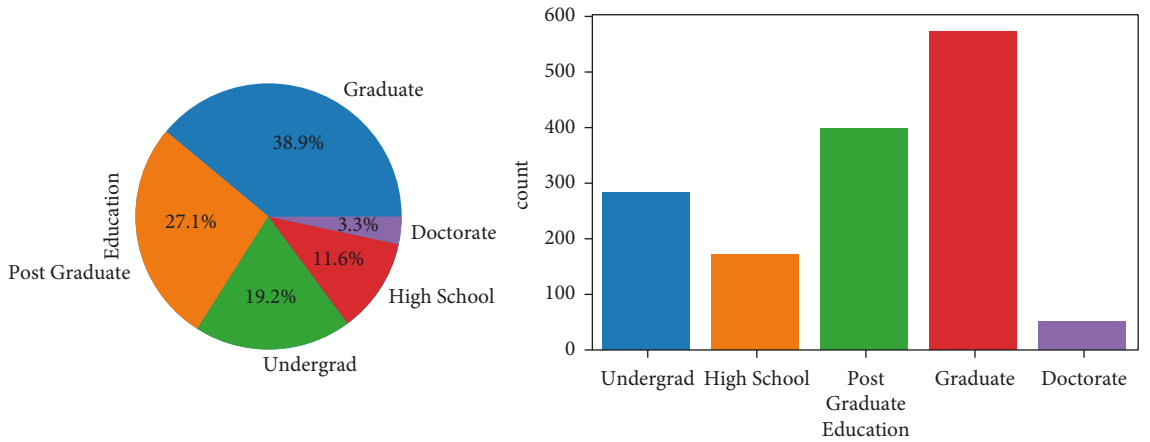

Figure 6: Attrition on the basis of education level.

by exchanging statistics and the corresponding analytics. We suggest using machine learning approaches to predict SOS capabilities through the exchange of relevant data sets and the prescription of information linkages between systems. Using data from previous research, this article estimates the value of exchanging information among SOS stakeholders. Using a variety of machine learning algorithms, we were able to identify the SOS stakeholders who are most likely to benefit from using the corresponding insights. For this purpose, we are using the following models:

(a) Support vector machine

(b) Logistic regression

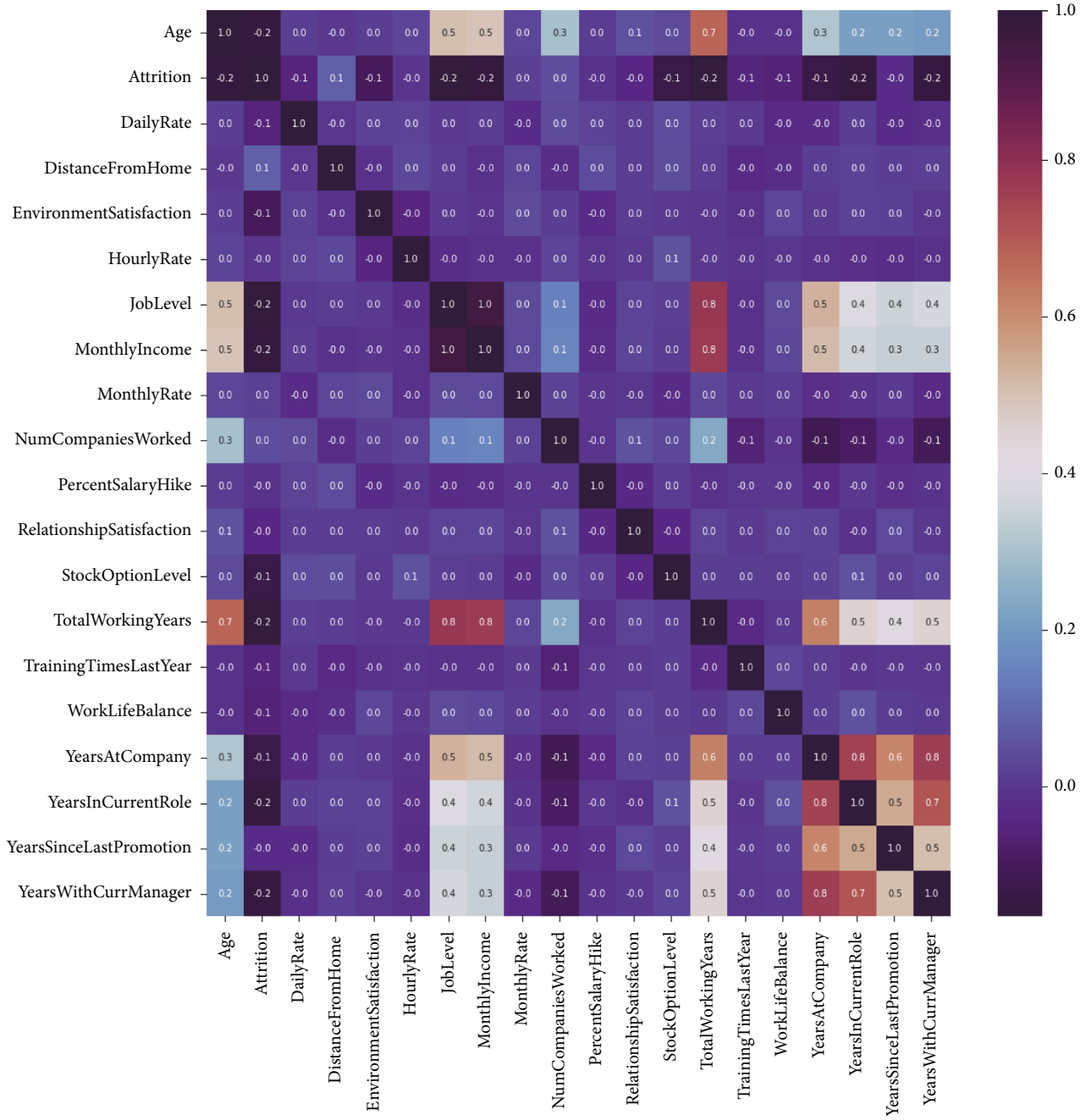

Figure 7: Feature correlation matrix.

(c) Decision trees

4. Results and Discussion

Predicting SOS capabilities through the interchange of relevant data sets and the prescription of information linkages between systems is something we propose doing using machine learning methodologies. The value of information exchange among SOS stakeholders is estimated in this article based on past research. We were able to identify the SOS stakeholders most in need of the corresponding insights by utilising a range of machine learning algorithms.

4.1. Support Vector Machine. For the attrition of employees, SVM has shown promising results. We have used different kernels of SVM for the prediction of attrition in employees through IBM data sets. The confusion matrix in Figure 8 shows that SVM has shown good performance with 2,400 true positive and 12 true negative values.

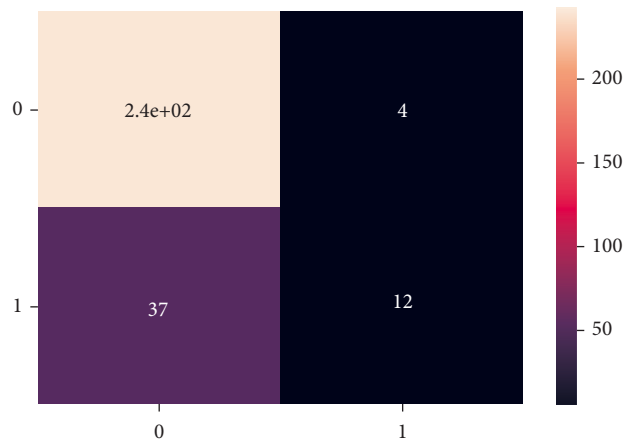

Figure 8: Confusion matrix of collective SVM kernel response.

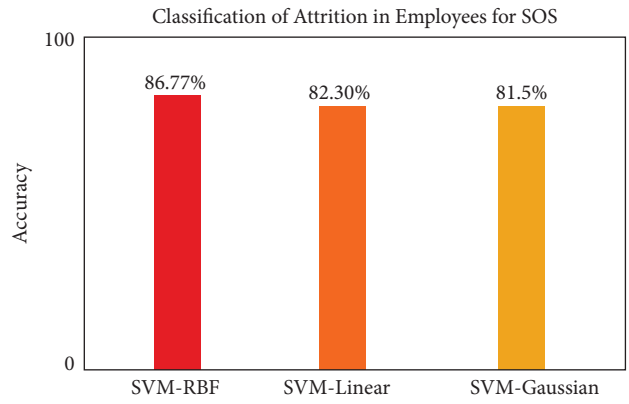

Figure 9: Performance of SVM.

Figure 9 shows the performance of SVM models for the prediction of attrition in employees for SOS acquisition. SVM-RBF kernel has shown the highest accuracy of 86.77%.

4.2. Logistic Regression. For the attrition of employees, LR has shown promising results. We have used LR for the prediction of attrition in employees through IBM data sets. The confusion matrix in Figure 10 shows that LR has shown good performance with 2,400 true positive and 9 true negative values.

Figure 11 shows the performance of LR models for the prediction of attrition in employees for SOS acquisition. LR has shown the highest accuracy of 84.6%.

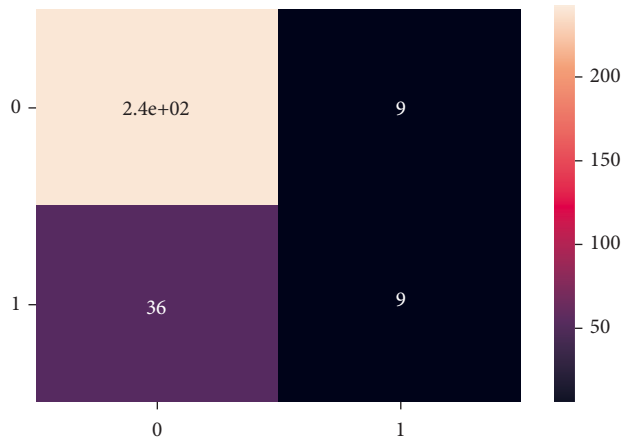

Figure 10: Confusion matrix of LR response.

4.3. Decision Trees. For the attrition of employees, decision trees has shown promising results. We have used decision trees for the prediction of attrition in employees through IBM data sets. The confusion matrix in Figure 12 shows that decision trees has shown good performance with 2,400 true positive and 9 true negative values.

Figure 13 shows the performance of decision trees models for the prediction of attrition in employees for SOS acquisition. Decision trees have shown the highest accuracy of 83.5%.

Further models have been compared with these three models but do not perform well. We have compared SVM, LR, and DT with naïve Bayes, KNN, and random forests. Table 2 shows the comparative analysis of ML models.

Comparatively, ML models have shown good accuracy for the classification of attrition in employees in IBM data

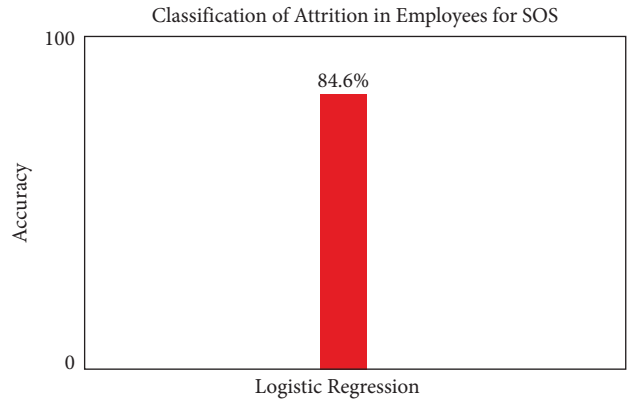

Figure 11: Performance of LR.

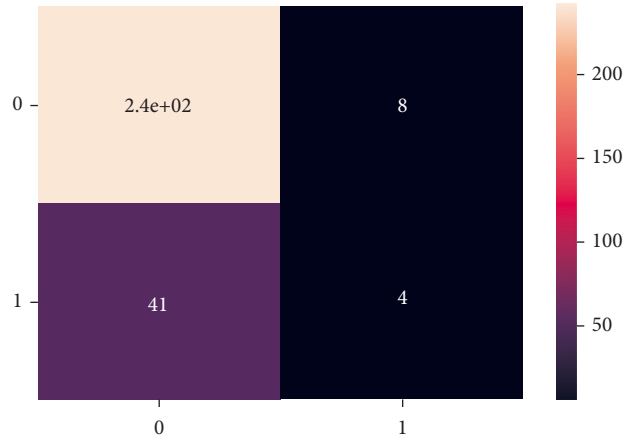

Figure 12: Confusion matrix of decision trees response.

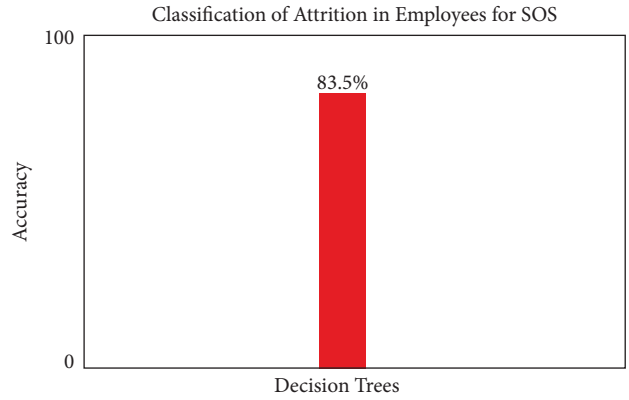

Figure 13: Performance of LR.

Table 2: Comparative analysis of ML models.

Model	Training testing ratio	Accuracy (%)
SVM	70:30	86.5
LR	70:30	85
DT	70:30	83
RF	70:30	72
NB	70:30	71.5
KNN	70:30	60.7

sets. Table 3 shows the comparative analysis of the current study with the previous state-of-the-art methods:

We recommend applying methodologies from machine learning in order to create predictions about the capabilities of SOS by exchanging critical data sets and prescribing information linkages between various systems. This can be done by trading off-key data sets. The purpose of this essay is to act as a sort of intermediary analysis of the research

Table 3: Comparative analysis.

Reference	Techniques	Data sets	Outcome	Accuracy (%)
Crossley et al. [10]	Multi-disciplinary analysis	Pertinent data sets	SOS acquisition	78.00
Gorod et al. [1]	NN	Pertinent data sets	SOS acquisition	75.55
Cook [2]	SVM	Pertinent data sets	SOS acquisition	83.00
Dahmann et al. [4]	NN	Pertinent data sets	SOS acquisition	80.00
Our proposed method	SVM, LR, DT	Pertinent data sets	SOS acquisition	86.50, 85.00, 83.00

endeavour that was discussed earlier. In addition to this, the purpose of the paper is to conduct an analysis of the benefits of information sharing among the stakeholders in SOS. Within the scope of this investigation, we used a number of distinct machine learning models in the IBM HR analytics data set in order to determine which types of analytics, when carried out by SOS stakeholders, had the potential to result in an expansion of SOS capacity. With a rate of 86.77%, SVM RBF has demonstrated the highest level of accuracy in the classification of acquisition as attrition of personnel.

5. Conclusions

The ability of a system to work is obtained from the integration of systems coming from a variety of diverse sources. The systems that make up an SOS have two main functions: first, to achieve the goals that are unique to them, and second, to supply the SOS as a whole with the resources that it needs. In the most recent few decades, one of the most common applications of machine learning and data analytics has been in the process of designing systems and acquiring new ones. It is a commonly understood practice that each company that invests in a complex system will use some form of data analytics in order to evaluate the system's individual goals. Even if the systems contribute to and benefit from the wider SOS, data analytics and decision-making on the separate system are rarely shared among SOS stakeholders. The purpose of this study is to investigate the ways in which the stakeholders in SOS can increase their capacity by exchanging data sets and the analytics that correlate to those data sets. We suggest using machine learning approaches in order to make predictions about the capabilities of SOS by trading off-key data sets and prescribing information links between different systems. This article is intended to serve as an intermediate analysis of the study effort described above. Additionally, the article's goal is to evaluate the benefit of information sharing across the SOS stakeholders. In this study, we deployed several different machine learning models to the IBM HR analytics data set in order to evaluate which analytics, when performed by SOS stakeholders, can lead to an increase in SOS capacity. SVM RBF has shown the best accuracy in the classification of acquisition as attrition of employees with 86.77%. Since a fully connected data enterprise is probably not feasible in practice, one of the main challenges we hope to overcome as this project progresses is determining which data sets need to be connected throughout the SOS. Current efforts are directed toward elucidating the role that machine learning can play in predicting the SOS capability, giving access to system-level decision-making loops, and prescribing the next steps for establishing information flows between systems in the SOS. A fully connected data enterprise is probably not realistic in practice; hence, one of the primary issues in future we want to overcome as this project continues is selecting which data sets need to be connected throughout the SOS. Current work focuses on clarifying the role machine learning can play in predicting SOS capabilities given system-level decision-making loops and prescribing future actions for building information flows between SOS systems.

Data Availability

The data used to support the findings of this study are available from the author upon request.

Ethical Approval

The paper does not deal with any ethical problems.

Conflicts of Interest

The author declares that there are no conflicts of interest in this work.

Acknowledgments

This study could not be started, nor achieved without Shaqra University encouragement, and its continued support.

References

[1] A. Gorod, B. Sauser, and J. Boardman, "System-of-systems engineering management: a review of modern history and a path forward," *IEEE Systems Journal*, vol. 2, no. 4, pp. 484–499, 2008.

[2] S. C. Cook, "2.3.1 on the acquisition of systems of systems," *INCOSE International Symposium*, vol. 11, no. 1, pp. 383–390, 2001.

[3] P. Acheson, C. Dagli, and N. K. Ergin, "Model based systems engineering for system of systems using agent-based modeling," *Procedia Computer Science*, vol. 16, pp. 11–19, 2013.

[4] J. Dahmann, K. J. Baldwin, and G. Rebovich, *Systems of Systems and Net-Centric Enterprise Systems*, MITRE CORP MCLEAN VADEPARTMENT OF DEFENSE WASHINGTON DCMITRE CORP BEDFORD MA, Washington, „ 2009.

[5] J. M. Vicente-Samper, E. Avila-Navarro, and J. M. Sabater-Navarro, "Data acquisition devices towards a system for monitoring sensory processing disorders," *IEEE Access*, vol. 8, pp. 183596–183605, 2020.

[6] Q. A. Ng, X. Wang, C. P. Tan, M. B. M. Nor, N. S. Damanhuri, and J. G. Chase, "Network data acquisition and monitoring/ system for intensive care mechanical ventilation treatment," *IEEE Access*, vol. 9, pp. 91859–91873, 2021.

[7] J. Dahmann, G. Rebovich, J. Lane, R. Lowry, and K. Baldwin, "An implementers' view of systems engineering for systems of systems," in *es of the 2011 IEEE International Systems Conference*, pp. 212–217, Montreal, QC,, April 2011.

[8] A. Odusd and T. Sse, *Systems engineering guide for systems of systems*, Vol. 36, Department of defence, , Washington, , USA, 2008.

[9] G. u Rehman, A. Ghani, M. Zubair, M. I Saeed, and D. Singh, "SOS Socially Omitting Selfishness in IoT for Smart and Connected Communities," *International Journal of Communication Systems*, pp. 1–25, 2020.

[10] W. A. Crossley, M. Mane, and A. Nusawardhana, "Variable resource allocation using multidisciplinary optimization: initial investigations for system of systems," in *Proceedings of the 10th AIAA/ISSMO Multidisciplinary Analysis and Optimization Conference*, vol. 5, pp. 3372–3388, Albany, NY, USA, September 2004.

[11] Q. Wenqi, Z. Qingxi, G. Chang, and L. Chade, "Fine Doppler shift acquisition algorithm for BeiDou software receiver by a look-up table," *Journal of Systems Engineering and Electronics*, vol. 31, no. 3, pp. 612–625, 2020.

[12] H. Attia, Gaya, A. Alamoudi et al., "Wireless geophone sensing system for real-time seismic data acquisition," *IEEE Access*, vol. 8, pp. 81116–81128, 2020.

[13] L. Yang, H. Gao, D. Yu, S. Pan, Y. Zhou, and Y. Gai, "Design of a novel fully automatic ocean spectra acquisition and control system based on the real-time solar angle Analyzing and tracking," *IEEE Access*, vol. 9, pp. 4752–4768, 2021.

[14] Y. Zhao, P. Ye, J. Meng, K. Yang et al., Compensation module design for overlapping band in band-interleaved data acquisition systems based on hybrid particle swarm optimization algorithm," *IEEE Access*, vol. 8, pp. 178835–178848, 2020.

[15] A. A. Abud, G. L. Miotto, and R. Sipos, "Experience and performance of persistent memory for the DUNE data acquisition system," *IEEE Transactions on Nuclear Science*, vol. 68, no. 8, pp. 2159–2164, 2021.

[16] V. Frolov, S. Huber, I. Konorov et al., "Data acquisition system for the COMPASS++/AMBER experiment," *IEEE Transactions on Nuclear Science*, vol. 68, no. 8, pp. 1891–1898, 2021.

[17] S. K. Weber, G. L. Miotto, J. Almeida, P. H Blanc, A. Dias, and G. Malaguti, H. Manninen, J. Pfeifer, S. Ravat et al., Data acquisition system of the CLOUD experiment at CERN," *IEEE Transactions on Instrumentation and Measurement*, vol. 70, pp. 1–13, 2021.

[18] J. Colombi, M. John, M. E. Miller et al., "Model based systems engineering with department of Defense architectural framework," *Systems Engineering*, vol. 14, no. 3, pp. 305–326, 2012.

[19] N. Davendralingam, A. Maheshwari, and A. Raz, "Predictive and Prescriptive Analytics via System of Systems Engineering: Informational Determinants for Enterprise-Level Effectiveness," in *Proceedings of the Council of Engineering Systems Universities Global Conference 2018*, Tokyo, Japan, June 2018.

[20] W. Scacchi, "Open Acquisition: Combining Open Source Software Development with System Acquisition," pp. 1–26, 2002, https://www.ics.uci.edu/~wscacchi/Papers/DAU/OpenAcquisition.pdf.

[21] J. Austin-Breneman, T. Honda, and M. C. Yang, "A study of student design team behaviors in complex system design," *Journal of Mechanical Design*, vol. 134, no. 12, 12 pages, 2012.

[22] C. L. Roe, "A systems engineering process for systems of systems," *INCOSE International Symposium*, vol. 9, no. 1, pp. 1214–1220, 1999.

[23] P. G. Carlock, J. A. Scardina, S. C. Decker, R. E. Fenton, and C. W. Pate, "1 agency-level systems engineering for "systems of systems"," *INCOSE International Symposium*, vol. 9, no. 1, pp. 1–7, 1999.

[24] A. M Maka and J. Phiri, *Information Systems Acquisition, Development and Implementation Framework*, The University of Zambia, Lusaka, Zambia, 2019.

[25] Ö. A Karlsson, "Data Acquisition System with Filter Design and Implementation of a Data Acquisition System with Filter Quality Evaluation," Master's Thesis, KTH Royal Institute of Technology, Stockholm, Sweden, 2019.

[26] R. Khalique, M. Asim, and S. Manzoor, "Electronic-acquisition Software's key factors and subsequent impact: points of view from user's," *European Journal of Business and Management Research*, vol. 5, no. 1, 2020.

[27] D. A. Delaurentis, B. Sketch, and P. Balasubramani, "A system-of-systems approach to enterprise analytics design," *Acquistion Research Program Sponsored Report Series*, Purdue University, West Lafayette, IN, USA, 2021.

[28] L. Yilmaz and J. Phillips, "Software process change," in *Proceedings of the Lecture Notes in Computer Science*, vol. 3966, pp. 234–241, Shanghai, China, May 2006.

[29] V. L. Shalin, E. J. Wisniewski, K. R. Levi, and P. D. Scott, "A formal analysis of machine learning systems for knowledge acquisition," *International Journal of Man-Machine Studies*, vol. 29, no. 4, pp. 429–446, 1988.

[30] D. A. DeLaurentis, "Understanding transportation as a system-of-systems design problem," in *Proceedings of the 43rd AIAA Aerospace Sciences Meeting and Exhibit*, pp. 15083–15096, Reno, Nevada, January 2005.

[31] H. Pfaender, D. DeLaurentis, and D. N. Mavris, "An object oriented approach for conceptual design exploration of UAV-based system-of-systems," in *Proceedings of the 2nd AIAA "Unmanned Unlimited" Conf. and Workshop & Exhibit*, San Diego, CA, USA, September 2003.

[32] R. Creel and B. Ellison, *System-of-systems Influences on Acquisition Strategy Development*, pp. 1–12, Softw Eng Inst, Pittsburgh,PA, USA, 2013.

[33] R. W. Allen, J. R. Hogue, T. J. Rosenthal, and Z. Parseghian, "Data acquisition and analysis system based on a lap-top computer," *Transportation Research Record*, vol. 1213, pp. 82–89, 1989.

[34] M. W. Maier, "Architecting principles for systems-of-systems," *Systems Engineering: The Journal of the International Council on Systems Engineering*, vol. 1, pp. 267–284, 1999.

[35] D. A. Delaurentis, C. Guariniello, and P. Balasubramani, "ACQUISITION RESEARCH PROGRAM SPONSORED REPORT SERIES," *A System-Of-Systems Approach to Enterprise Analytics Design*, Naval Postgraduate School, Monterey, USA, 2016.

Hindawi
Complexity
Volume 2022, Article ID 4815623, 20 pages
https://doi.org/10.1155/2022/4815623

Research Article

Wind Effects on Rectangular and Triaxial Symmetrical Tall Building Having Equal Area and Height

Astha Verma,[1] Rahul Kumar Meena,[2] Hrishikesh Dubey,[2] Ritu Raj,[2] and S. Anbukumar[2]

[1]*Department of Civil Engineering, Govind Ballabh Pant University of Agriculture and Technology, Pantnagar, India*
[2]*Department of Civil Engineering, Delhi Technological University, New Delhi, India*

Correspondence should be addressed to Ritu Raj; rituraj@dtu.ac.in

Received 25 February 2022; Revised 11 May 2022; Accepted 23 May 2022; Published 20 July 2022

Academic Editor: Mostafa Al-Emran

The study aims to investigate wind effects on the equal area and the same height building model having the plan cross-sectional shape in the form of regular and irregular shape bulidings. The ratio of modification in the cross-sectional shape is kept same for regular and irregular shaped models because limited studies are available for such type of comparison. The responses of the structure to resist the wind load is increased by applying these modifications in the corner configuration such as corner cut, chamfer, and fillet in the plan shape of the structure. The numerical study is performed using ANSYS CFX and wind incidence angle varies in the range of 0° to 180° at the interval of 15°. The results of velocity and pressure distribution are presented in the form of pressure contours and wind force coefficients for all four-building models which are presented in the form of a graph. The comparison of numerical simulation results on two models are compared with the different international standards and with the experimental results. The regular shape with a corner cut and a "Y"-shaped structure with a fillet corner model performed the best among all models for resisting overall wind force. The results of pressure distribution of all four models are presented in the form of pressure contours for 0° and 90° wind angles.

1. Introduction

The tall structure is the most appropriate solution for the current situation since land availability in the conventional shape is approaching at saturation. The population is also booming and there is a scarcity of space available for individual residences consequently, accommodating such a large population within the available land is feasible with tall buildings. Various international standards [1–10] are already discussed different parameters to design tall buildings. There is significant constraint on the design of tall buildings as the majority of international standards are silent on the modification of the shape of plan cross-sectional area buildings. Tavakoli et al. [11] discussed the important aspects of high rise buildings. Dadkhah et al. [12] investigated the performance of the steel structure during an earthquake. Kamgar and Rahgozar [13] analyzed different lateral resisting systems to resist lateral loads which are produced during an earthquake. Kamgar et al. [14] investigated the soil-structure interaction for a different storey outrigger braced building resting on two different types of soil. Dadkhah et al. [15] performed nonliner seismic analyses using incremental dynamic analysis, which is most accurate and time-consuming, and also need a high computational cost. Dadkhah et al. [16] presented the optimization of a tuned mass damper to improve the seismic performance of a six storey steel structure based on the ductility damage index. Kamgar and Samani [17] conducted the numerical study for evaluating the effect of length to the height ratio on the behavior of a concrete frame retrofitted with steel infill plates and observed that the value of absorbed energy by two diagonal viscous dampers is higher than that of the chevron viscous damper. Numerous studies have been conducted in the subject of wind engineering, the majority of which focus on modifying the shape or height of the structure but the current study focuses on equal area structures of regular and

irregular shapes. When the regular shape of the rectangular building model is contrasted to the irregular shape of the "Y"-shaped building model, the designer can choose the shape of the building when constructing such shapes.

Investigation of wind effects is possible through two techniques like wind tunnel and CFD, the various amount of research is already conducted through the wind tunnel, such as Kwok [18] studied the effect of wind on the shape of a building by applying different measures to control the wind effect and found that the building with the chamfer corner is best among all to resist the along and across wind response. Jozwiak et al. [19] presented the aerodynamic interference effect on pressure distribution on the building model and observed that there is a significant difference in pressure distribution with and without modeling of the boundary layer. Pal et al. [20] presented the experimental investigation performed in an open circuit boundary layer wind tunnel on the "fish plan shape" and observed that pressure on the windward face in the case of a fish shape is less than the square shape when the wind incidence angle is 0°. Nagar et al. [21] performed an experiment in BLWT on the "H" shaped model and found that pressure increases until the wind incidence angle reach up to 60° wind, and it was found that the interference factor for the square and the "H" shaped building is less than one. Pal et al. [22] carried out a comparative study of wind-induced mutual interference effects on the twin square and the fish plan shaped model, which is having equal volume, and the experiment is performed in the boundary layer wind tunnel at the length scale of 1 : 300. This is observed from the experimental study that the drag and lift force for the fish shaped model is lesser than that of the square shaped model in the case of 0° and 180° wind. Nagar et al. [23] investigated the wind-induced interference effect between two plus shaped high rise buildings on mean and RMS pressure coefficients and concluded that these interference effects on local wind pressure are significantly higher on the windward side face near the recessed corner. Pal et al. [24] performed an experimental investigation on a square and a remodeled triangle shaped building at the length scale of 1 : 300. This is found that the front-to-front interference case of the remodeled triangle shaped model performed best in resisting along and across the wind. The maximum suction of the testing model at the FBI condition is decreased by nearly 40% to that of the isolated case of the SPS model at the same condition. Amin and Ahuja [25] presented a review on an aerodynamic modification such as corner cut, chamfering, rounding, horizontal slots, vertical slots, dropping of corners, and many more to the shape of the tall building. The major outcome from this review is that the opening along the cross-wind direction at the top significantly reduces the wind excitation of the building, and the tapering of tall buildings has significant effects on wind force in across wind direction than that of the along wind response. Blackmore [26] estimated the wind effects on and around the building model, wind forces are dynamic and fluctuate continuously in both magnitude and position. Most of the international standards considered static loads and having limitations. Bhattacharyya and Dalui [27] presented the study on the "*E*" plan shaped building, which has symmetry about both the axis and wind response is measured from 0° to 330° at the interval of 30°. The result obtained from the experimental study and numerical study were compared. Various amounts of research work is performed using the wind tunnel test, however, this study is performed by using the k-ε turbulence model and most of the studies in the present times are performed using the k-ε turbulence model to obtained the solution using the numerical simulation.

Numerical simulation is the better option for the estimation of wind loads because the wind tunnel test is time taking and costly, and it also needs heavy machinery and resources to investigate the wind effects. Various studies are also available and presented on the various aspect of CFD simulation, such as Tominaga and Stathopoulos [28] investigated the turbulent scalar flux by assuming the gradient diffusion hypothesis using Reynold averaged Navier stock equation in CFD. Blocken [29] discussed the important aspect of CFD for defining urban physics and gave ten important tips and tricks towards the accurate and reliable simulations. Behera et al. [30] performed an experiment in the boundary layer wind tunnel to investigate the wind interference effect on tall buildings with varying plan ratios, and observed that the interference zone extends over a larger area as the building plan ratio increases. Tamura et al. [31] performed a series of wind tunnel tests to determine the aerodynamic performance and pedestrian level wind characteristics of different super tall buildings having square, rectangular, and elliptic plan with corner cuts. Mittal et al. [32] performed the numerical simulation on tall buildings and discussed the effect of the shorter building placed in front of a taller building. Blocken et al. [33] conducted the CFD simulation of the atmospheric boundary layer and discussed the effect of using wall function. The accuracy of CFD simulation can be seriously compromised when wall function roughness modification based on the experimental data for sand grain roughened pipes and channels are applied at the bottom of the computational domain. Numerical studies are already conducted on the different types of the plan shape structure, such as Tian et al. [34] on a rectangular shape, Gaur and Raj [35] on corner modification on a square and a plus shaped building, Raj et al. [36], Keerthana and Harikrishna [37]on the "*H*" plan, Kumar and Raj [38] on an octagonal plan shape, Raj et al. [39] obtained response of a square and a plus shaped building by varying wind loads, Gaur et al. [40] studied the interference effect using CFD, Mukherjee et al. [41], Sanyal and Dalui [42–45], Goyal et al. [46] on the "Y" shape, Meena et al. [47], Kumar and Raj [48] on the "L" shape, Raj and Ahuja [49], on the "+" shape, Sanyal and Dalui [50] on the rectangular shape having some modification, Meena et al. [51] investigated the wind effects on the regular shaped structure having a rectangular plan with various corner modifications, Mallick et al. [52] on the "*C*" shape, Amin and Ahuja [53] on the side ratio of a rectangular building, Amin and Ahuja [54] obtained response of a tall building against the wind load. The considerable outcomes after modifying the shapes of the structure are as the Strouhal number is not sensitive to the aspect ratio, flow reattachment of the separated shear layer in the corner cut model present suction into corners, which is further

caused in the reduction of drag, interference position of the building is highly effecting principal building pressure distribution, the length/width (side ratio) makes changes into the upwash, downwash, and the stagnation zone on upstream of flow, shielding effects were the main factors which is controlling the spacing between the buildings, highest wind velocity is obtained at the edges of the windward side and minimum at the leeward side, maximum suction is observed at the corner of the building, it is important to give due consideration for suction on the corner region, by increasing the L/W ratio horizontal force coefficient and overturning moment coefficient increases by the significant amount, the model with the rounded corner is best to reduce wind loads and overturning moments, in comparison of the chamfer corner, rounded corner are efficient in reducing the wind load, deflection is observed due to the presence of vortices in the wake region of buildings, the accuracy of the k-ε turbulence model is more than the SST model.

The current study will examine the wind pressure on tall structures of both regular and irregular shapes. The majority of earlier research has concentrated on the wind effects of either regular or irregular shaped buildings, however, the current study examines the results of these two types of buildings by altering the corners. This study is particularly noteworthy because the cross-sectional area and height of the building model are kept constant to minimize wind loads. Numerous corner modifications, such as chamfer, fillet, and corner cut, are also employed and the ratio of cuts is maintained, allowing the designer to select the most efficient structure for the situation. Additionally, two models are validated and the numerical simulation results are compared to experimental results and a number of relevant standards. Furthermore, the result of velocity streamlines is illustrated graphically in the form of contours, pressure distribution, and wind force coefficient for wind incidence angles ranging from 0° to 180° at 15°-degree intervals.

2. Methodology

The present study concentrates on the investigation of wind effects and compares the results of the regular and irregular shaped models. The numerical simulation results are validated before the starting of the work and the results of numerical simulation are found identical with experimental results.

2.1. Method of Study. The present study is performed using the numerical simulation tool ANSYS CFX and investigated the wind effects on tall buildings having an equal plan area and same height. Most of the available studies are either for regular shape or for irregular shape, but these studies present the comparison among such shapes having both regular and irregular shape. The geometry is selected and applied in the CFX-Pre setup. After the geometry, the meshing is performed and flow physics are defined in the solution and simulation is performed and the results are presented in different graphical forms.

2.2. Numerical Simulation. Numerical simulation is performed using ANSYS CFX and boundary conditions used into this simulation are kept as the boundary condition used by Raj [55] in the experiment performed in the boundary layer wind tunnel at IIT Roorkee, India. The numerical simulation performed into this study is performed using the k-ε turbulence model [56].

(i) k-ε turbulence model

This method is generally used to solve a complex fluid problem and it is a two-equation model. The solution is generated after solving two different equations during the entire numerical simulation. This model performs nearly equivalent to the experimental problem and the k-ε model also uses the scalable wall-function to increase the efficiency of the solver and this model performs more robustness in the case of the fine mesh.

It is very less expensive and mostly used to simulate turbulent flow characteristics. The solution is solved by two transport equations, i.e., turbulent kinetic energy (k) and the turbulent dissipation rate (ε). It has the positive advantage of not including any geometry-related parameters in the modeling. Turbulent kinetic energy and the turbulence dissipation rate are two variables introduced into the system of equations for the model. The values for turbulence are calculated according to turbulence eddy dissipation using

(ii) Basic equations

The basic equation used to study fluid flow problems using Navier-Stokes and continuity equation.

(iii) Navier stokes equation is written as

$$\frac{\partial(\rho u_i)}{\partial t} = -\frac{\partial(\rho u_i u_j)}{\partial x_j} - \frac{\partial P}{\partial x_j} + \frac{\partial}{\partial_{x_j}}\left[\mu\left(\frac{\partial_{u_i}}{\partial_{x_j}} + \frac{\partial_{u_j}}{\partial_{x_i}}\right)\right] + F. \tag{1}$$

(iv) Continuity equation is written as

$$\frac{\partial_\rho}{\partial_t} + \frac{\partial_{\rho_i}}{\partial_{x_i}} = 0. \tag{2}$$

The standard k-ε model uses the following transport equations for the turbulence kinetic energy and turbulence dissipation.

$$\rho\frac{\partial k}{\partial t} + \rho\overline{u_i}\frac{\partial k}{\partial x_j} = \tau_{ij}\frac{\partial \overline{u_i}}{\partial x_j} - \rho\varepsilon + \frac{\partial}{\partial_{x_j}}\left[\left(\mu + \frac{\mu_t}{\sigma_\varepsilon}\right)\frac{\partial \varepsilon}{\partial x_j}\right]. \tag{3}$$

Momentum equation is written as

$$\frac{\partial(\rho U_i)}{\partial t} = -\frac{\partial(\rho U_i U_j)}{\partial x_j} - \frac{\partial P}{\partial x_i} + \frac{\partial}{\partial_{x_j}}\left[\mu_{eff}\left(\frac{\partial_{U_i}}{\partial_{x_j}} + \frac{\partial_{U_j}}{\partial_{x_i}}\right)\right] + S_M. \tag{4}$$

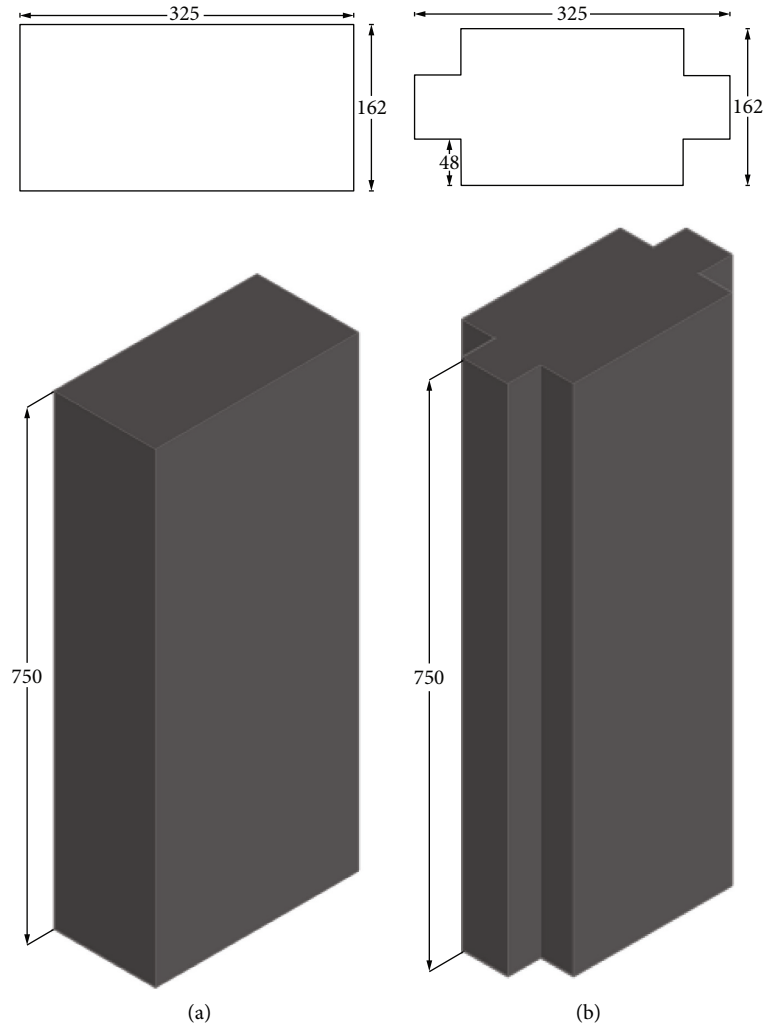

Figure 1: Regular shaped building model (a) rectangle and (b) rectangle with corner cuts.

2.2.1. Advantages

(1) It performs best for the boundary layer separation fluid problem.

(2) It is the most use turbulence model for validation purposes.

(3) Generally, it is used by the industrialist to solve the complex fluid problem.

(4) It provided the solution based on boundary conditions.

2.2.2. Disadvantage

(1) It does not perform well in the case where flow is changing instantaneously.

(2) It is unable to generate the accurate solution for the rotating fluid problem.

(3) It is notable to generate the accurate solution for a low Reynold number.

2.3. Geometrical Configuration of Model. The regular shape of a rectangular building Figure 1 represents the building having no corner modification, corner cut model and irregular shaped model of Y-shape is represented in Figure 2 are considered in this study. The plan cross-sectional area and height are kept the same for the study so that the results can be compared on an equal volume building model. Both sorts of building models have the same modification ratio.

2.4. Meshing and Domain. Meshing contains important flow features, which are dependent upon the flow parameters, such as grid refinement inside the wall boundary layer. The meshing applied after the geometry and the name selection for each part of geometry are required before meshing to understand the CFX-Pre about the geometry. The name selection is required to define flow physics. It is better to provide name selection before the meshing so that the surface mesh exactly matches with nodes on the two sides of the boundary, which allows a more accurate fluid solution

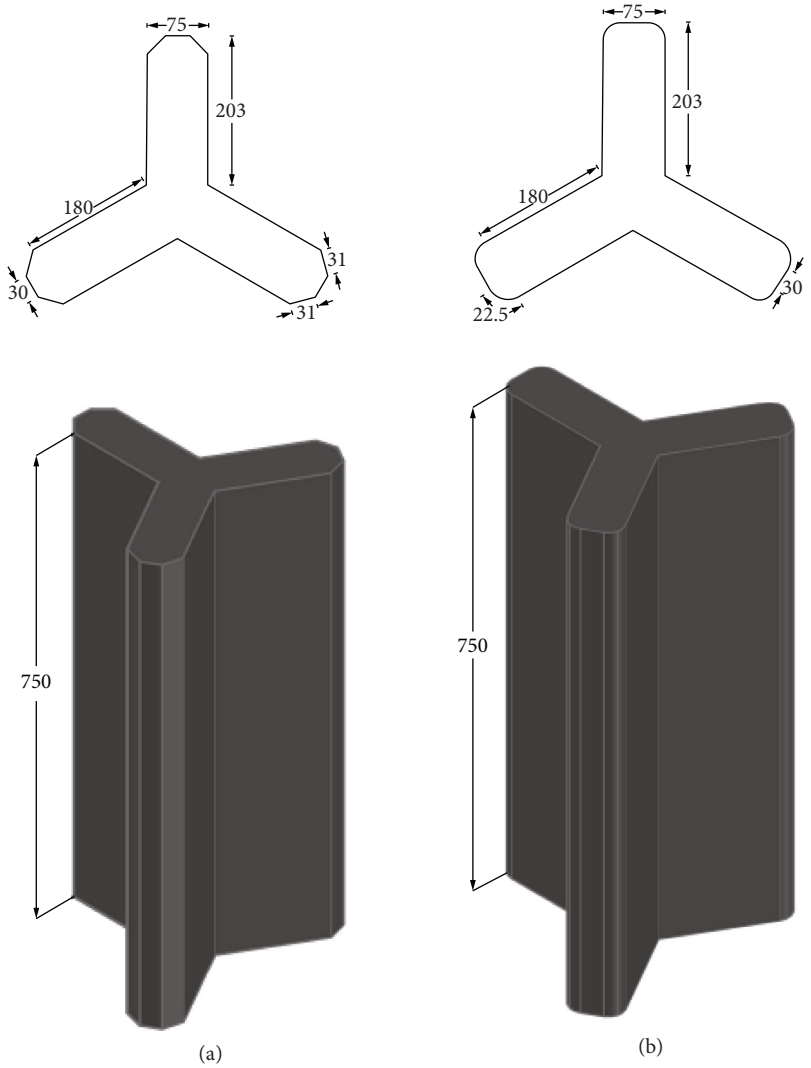

Figure 2: Y-shape building model (a) Y-shape with chamfer and (b) Y-shape with fillet.

[57]. Name selection also helps the program to control the inflation, i.e., automatically select for the wall and inflation automatically provided during the auto mesh generation. The meshing is represented in Figure 3 for domain, building, and inflation.

The mesh generation steps are automatically worked into the program; however, this can be controlled by varying the element size, type of mesh to generate, and where and how the mesh should be refined. Tetra dominant meshing, which is patch independent, is suitable for the CAD model having many surface patches and if the geometry has small edges then this is suitable [58]. Hex meshing is used both in general sweep and thin sweep; it is also recommended for the model which has the clean cad geometry. Mapped and free meshing is adopted where the fluid problem needs a different type of meshing like structured (mapped) and unstructured (free); however, this is suitable for the problem where the sweeping method does not work without extensive geometry decomposition.

Inflation is provided to capture the flow properly at the interface and the same can be provided by various methods

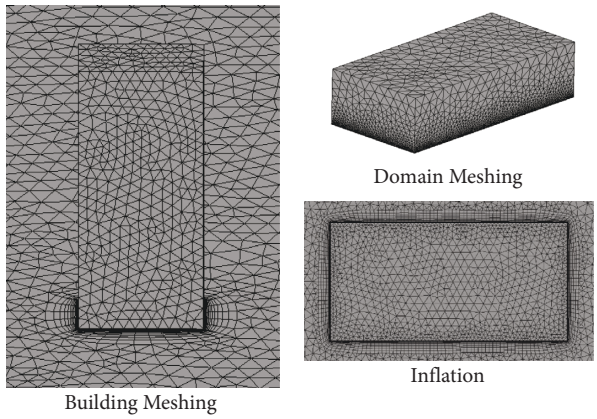

Figure 3: CFD model representing meshing.

available in the CFD model. Smooth transition is the default option and it uses the local tetrahedron elements size to compute each local height and total height so that the rate of volume change is smooth. Each triangle that is being inflated

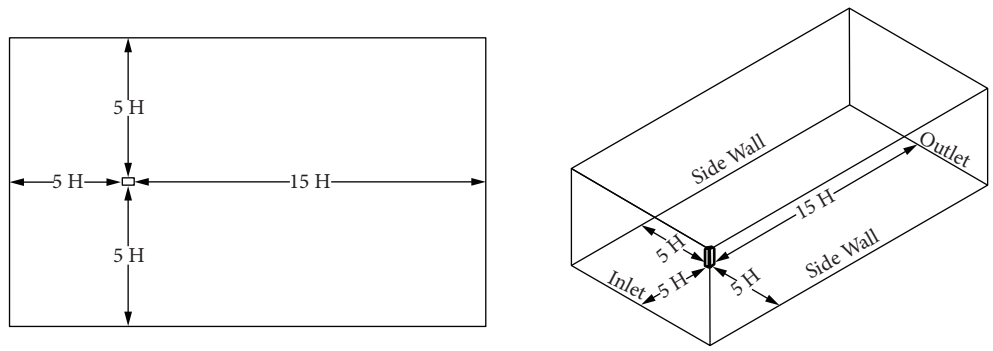

Figure 4: CFD domain.

will have an initial height that is computed with respect to its area averaged at the nodes. This means that for the uniform mesh, the initial height will be roughly same, while for a varying mesh, the initial height will vary. An increment in the value of the growth rate that controls the reduction in the total height of inflation layers.

The numerical simulation predicts the result based on boundary conditions, as the finite element method work well with boundary conditions. Inlet wind speed is provided as the power law where the reference height in the simulation is considered as 1 m, while the reference velocity is defined as 10 m/s. The wall of the domain is considered as a free slip wall, while the ground of the domain is a rough wall [43].

The faces of the model are considered as no slip. Wall function defines that if a coarse mesh near the wall than it assumes that the logarithmic low applies as wall function. At the same time, the fine mesh near the wall and various turbulence models account for a low Reynold number. Wall functions are useable to low Reynold number problems. In general, if the fine mesh is defined near the wall then the gradient changes are considered automatically by the solver. The domain is represented in Figure 4 in both the top and isometric view. A domain feature is considered after the various recondition provided by the past studied [59–62] numerical model. No-slip walls is the wall where fluid immediately next to the wall assumes the velocity of the wall as zero; free slip wall is the wall where the shear stress at the wall is zero and the velocity of the fluid near the wall is not retarded by the wall friction effects.

2.5. Grid Sensitivity. In this study a grid sensitivity study is performed on model-A and tabulated in Table 1, which is having no corner modification into the rectangular shape model. A grid sensitivity study is essential to CFD programming as it helps to achieve the proper meshing size, which predicts the most accurate result for the numerical simulation. For the present study GS-3 is adopted for all the wind incidence angle.

2.6. Mean Wind Speed and Turbulence Intensity Profile

2.6.1. Mean Wind Speed. Wind flow over the tall building involves complex flow patterns, although wind flow is generally separated from the surface, where the flow is mostly recirculating. Flow patterns are unsteady around the buildings model, therefore creating turbulence. The development of turbulences near the ground level is observed due to the presence of other obstacles. Such effects are also considered while calculating the turbulence intensity and wind flow up to the gradient height and after that it becomes constant.

Mean wind speed defined in the CFX-Pre is represented in Figure 5, the variation in the form of a power law between height and mean wind speed is as follows:

$$\frac{U(Z)}{U\left(Z_{ref}\right)} = \left(\frac{Z}{Z_{ref}}\right)^{n}, \tag{5}$$

where $U(Z)$ = mean velocity at height Z; $U(Z_{\text{ref}})$ = mean velocity at reference height Z_{ref}; and n = power law exponent, a measure of ground roughness, varies between 0.13 and 0.15 in open terrain.

The variation in the mean wind speed with height is generally expressed in an alternate form in a logarithmic form.

$$\frac{U(Z)}{U_{*}} = \left(\frac{1}{k}\right) ln\left(\frac{Z}{Z_{o}}\right). \tag{6}$$

Also, a simplification of this logarithmic equation is as follows:

$$\frac{U(Z)}{U_{(Z_{\text{ref}})}} = \frac{\ln\left(Z/Z_{o}\right)}{\ln\left(Z_{\text{ref}}/Z_{o}\right)}, \tag{7}$$

where U_{*} = shear velocity; k = Von Karman constant, 0.4; ln = natural log function; and Z_{o} = effective roughness length, another measure of ground roughness, varies from 0.01 to 0.05 meters in open terrain.

2.6.2. Turbulent Intensity. Turbulence intensity is a non-dimensional quantity derived from the variance and for the mean wind speed.

$$I_{z} = \frac{\sigma_{z}}{U(z)}, \tag{8}$$

where I_{z} = turbulence intensity at height z; σ_{z} = standard deviation of the wind speed at height z; and $U(z)$ = mean wind speed at a reference height.

Table 1: Mesh independent test result for model-A.

Name	Type of meshing	No of elements	Mean external pressure Face				% error				Reynold No
			A	*B*	*C*	*D*	*A* (%)	*B* (%)	*C* (%)	*D* (%)	
GS-1	Coarse	957324	0.59	−0.49	−0.24	−0.49	36	32	26	32	
GS-2	Medium-1	1284687	0.73	−0.56	−0.27	−0.56	10	16	12	16	
GS-3	Medium-2	**1439589**	**0.78**	**−0.64**	**−0.30**	**−0.64**	**3**	**2**	**0**	**2**	3.56×10^6 to 3.90×10^6
GS-4	Medium-3	1561140	0.81	−0.69	−0.32	−0.69	1	5	6	5	
GS-5	Fine	2497236	1.02	−0.98	−0.43	−0.98	33	33	30	33	

Bold values are indicating that if the GS-3 case is adopted for the numerical simulation, then the percentage error will be less in comparison to other meshing cases investigated in this study.

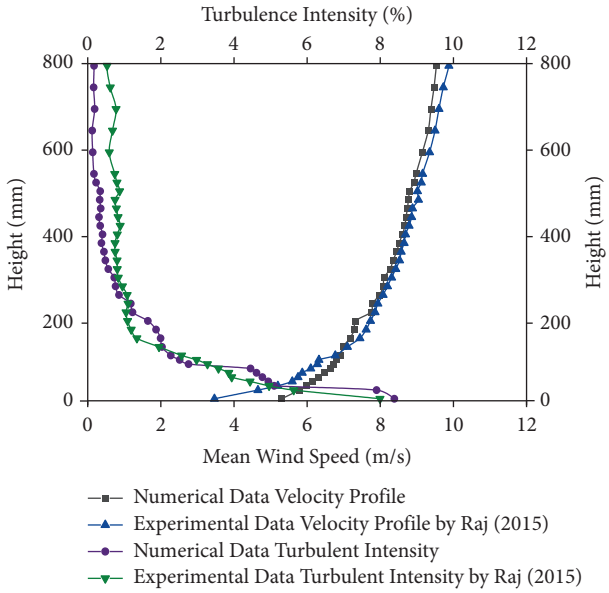

Figure 5: Variation of mean wind speed and turbulent intensity with height.

2.7. Validation. Validation is a prerequisite part of numerical simulation and two different models are considered in this study to validate with available international standards and an experimental study. Such buildings model are selected and external C_p compared with the available experimental results. This is also clearly depicted in Figure 6 that the result obtained in this numerical simulation show nearly an identical result for the pressure coefficient.

The results plotted for the normal and corner cut rectangular building model are representing a very close match with the experimental results. Therefore, the result obtained in this study are very much accurate for designing the model, which are considered in this entire study. The rectangular shape model is also simulated for the wind load at 0° and 90° wind and a pressure coefficient is compared with available international standards mentioned at Table 2.

The external pressure coefficient "C_p" is calculated using (9).

$$C_p = \frac{p - p_o}{(1/2)\rho U_H^2}, \tag{9}$$

where p = pressure derived from the external lines plotted on the model; p_o = static pressure at reference height; ρ = air density (1.225 kg/m^3); U_H = mean wind velocity at the building reference height.

3. Result and Discussion

CFD postprocessed results enables the visualization and analysis of wind effects in variety of graphical representations. The pressure distribution along the face is a function of the shape and size and the same is illustrated using contours. The wind response is also represented graphically in the form of the wind force coefficient.

3.1. Velocity Contours. Velocity contours are represented for model-A in Figures 7 and 8. The main cause of the pressure difference is the velocity field around and along with the building model. The velocity at downstream is mentioned at Figure 7, and the size of the wake is increasing with respect to the frontal exposed area, which changes according to wind incidence angle.

Velocity along the height of model-A is depicted in Figure 8 and the wind velocity distribution pattern is illustrating the variation of the wind at the downstream. The suction observed in the case of 15° and 75° are of the same type. The suction on the roof of the building is also observed and demonstrated in Figure 8.

3.2. Wind Forces. The wind-generated effect in the form of wind force is evaluated after the numerical simulation performed on the building model. The value of F_x and F_y are obtained using CFD postprocessed result while the frontal exposed area is calculated at each wind incidence angle. Drag force is calculated as per equations (16) and (17). Along wind force, i.e., the drag for model-A, is obtained a maximum of −4.72 is between 60° and 120°, while the minimum 0.0 is noted when the wind is striking to the model at 0° and 90°. The corner cut model of rectangular shape, i.e., model-B, has the highest magnitude of drag is −4.39 in the case of 30° and 150° wind and the smallest drag is 0.04 in the case of 0° and 180° wind. The maximum amount of drag is reduced for model-B with respect to model-A.

$$F_x = \left(0.5\rho_{U_h^2}.A_p\right)C_{f_x},$$
$$F_y = \left(0.5\rho_{U_h^2}.A_p\right)C_{f_y}. \tag{10}$$

An irregular "Y" shaped model having corner modifications such as model-C and D are having chamfer and fillet, respectively, the drag is measured using numerical

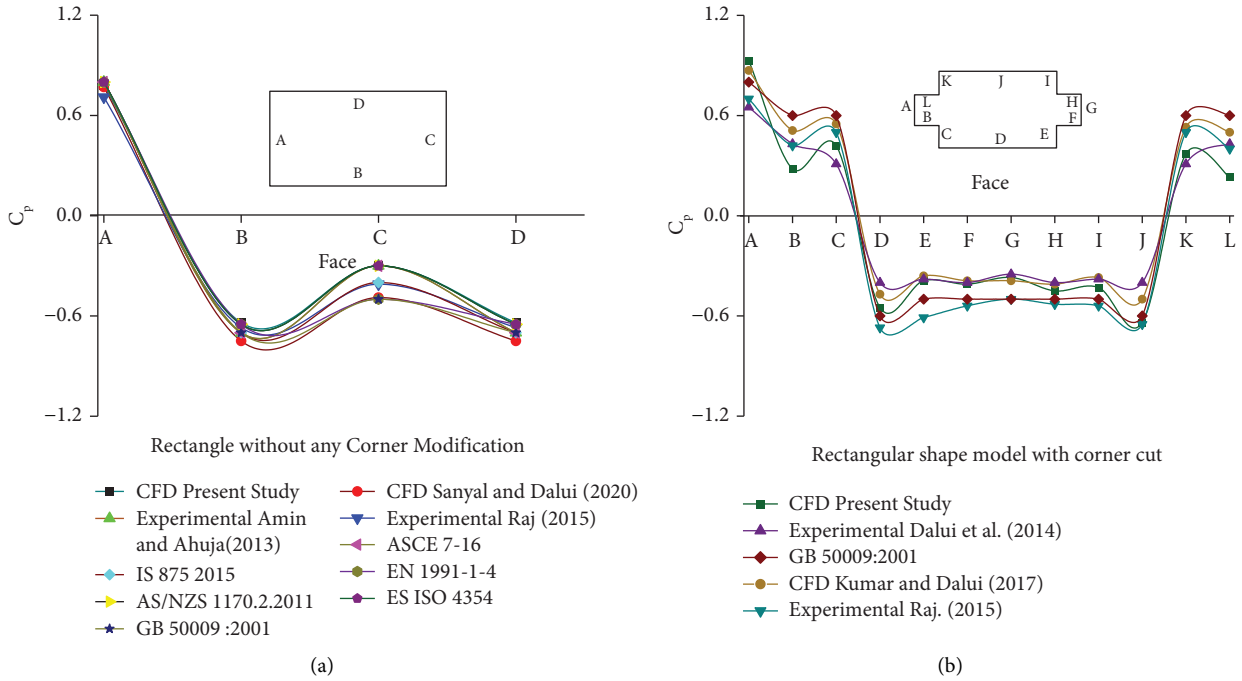

Figure 6: Validation result: (a) rectangular shape and (b) corner cut model.

Table 2: Comparison of average face pressure coefficient (*Cp*) on the rectangular shape tall building.

International code	Wind angle (°)	Windward side	Side wall	Leeward side
CFD results	0	0.78	−0.64	−0.30
	90	0.70	−0.61	−0.45
IS 875 (part 3)	0	0.7	−0.7	−0.4
	90	0.8	−0.5	−0.1
ASCE/SEI 7-16	0	0.8	−0.7	−0.5
	90	0.8	−0.7	−0.5
AS/NZS 1170.2.2011	0	0.8	−0.65	−0.5
	90	0.8	−0.65	−0.5
EN 1991-1-4	0	0.8	−0.5	−0.7
	90	0.8	−0.5	−0.7
BS 6399-2	0	0.8	−0.5	−0.7
	90	0.8	−0.5	−0.7
GB 50009-2001	0	0.8	−0.5	−0.7
	90	0.8	−0.5	−0.7
NSCP 2015	0	0.8	−0.5	−0.7
	90	0.8	−0.5	−0.7
ES/ISO 4354: 2012	0	0.8	−0.65	−0.7
	90	0.8	−0.65	−0.7

simulation and graphically plotted in Figure 9. The drag is also measured for model-C (chamfer-Y shape) and the maximum magnitude is −9.44 in the case of 150° wind. Model-D (fillet–Y shape) is investigated for along wind forces and the maximum drag of −7.92 is noticed in the case of 150° wind, while the lowest drag is −0.04 in the case of 180° wind is noticed for model-D.

The across wind, i.e., lift force in the *y*-direction, is calculated and graphically plotted in Figure 10 for model-A, B, C, and D. The regular shaped model of the rectangular shape (model-A & B) is having some different type of corner modification so that lift force can be reduced on the tall building by making some modification in the corners. The maximum lift of −13.73 is noted in the case of 90° wind for model-A, while the smallest of −5.23 is spotted in the case of 0° and 180° wind. Model-B (corner cut rectangle) is having the highest lift of −11.28 in the case of 90° wind, while the lowest lift of −4.73 is detected in the case of 15° and 165° wind.

The irregular "Y" shaped model-C and *D* are numerically investigated for the across wind response and lift force for model-D (fillet-Y) is having the maximum lift force of

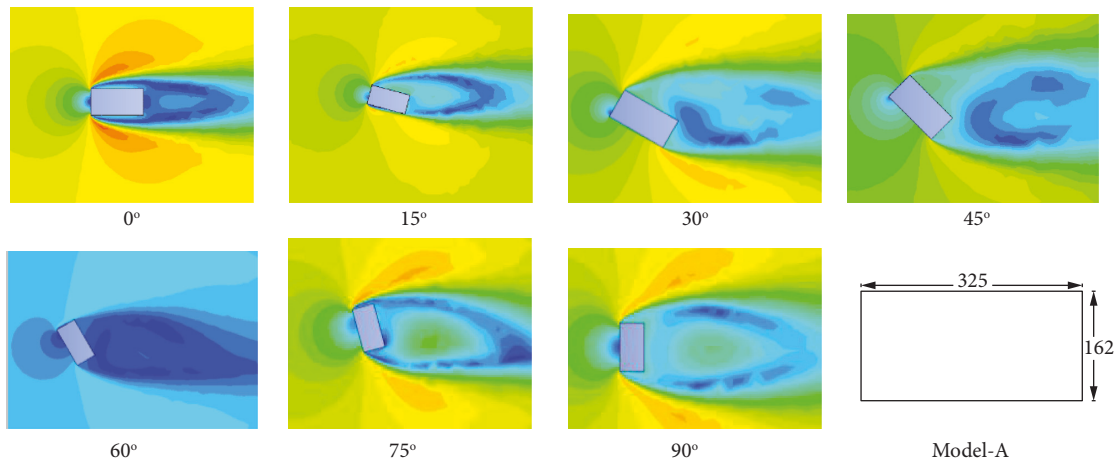

Figure 7: Velocity contours building model-A in plan.

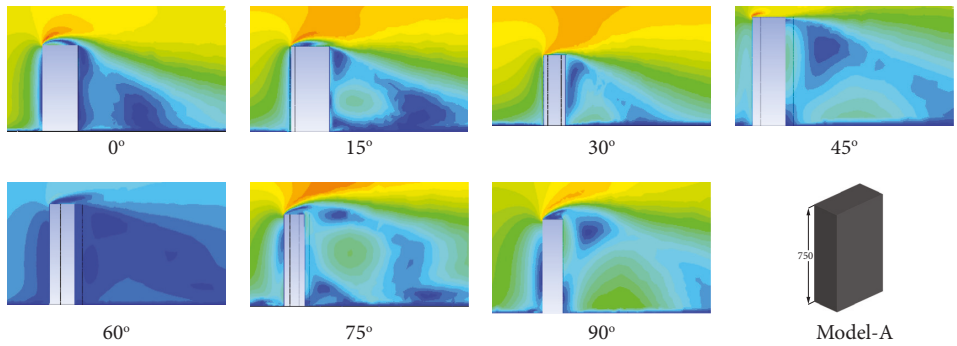

Figure 8: Velocity contours for model-A in elevation.

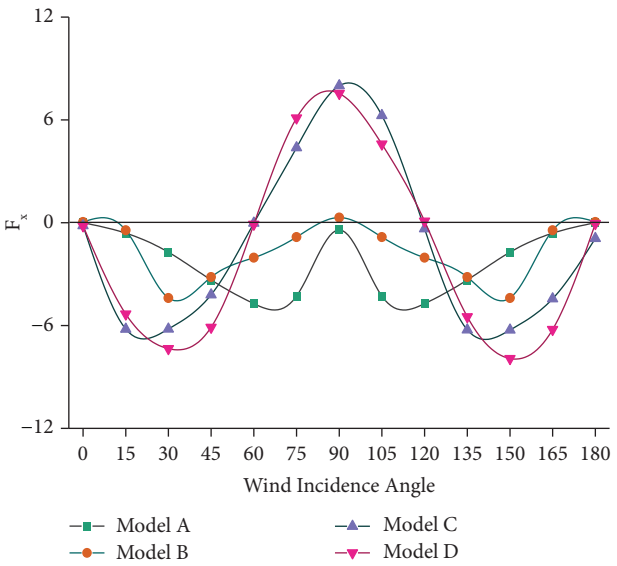

Figure 9: Wind force coefficient in x-direction F_x.

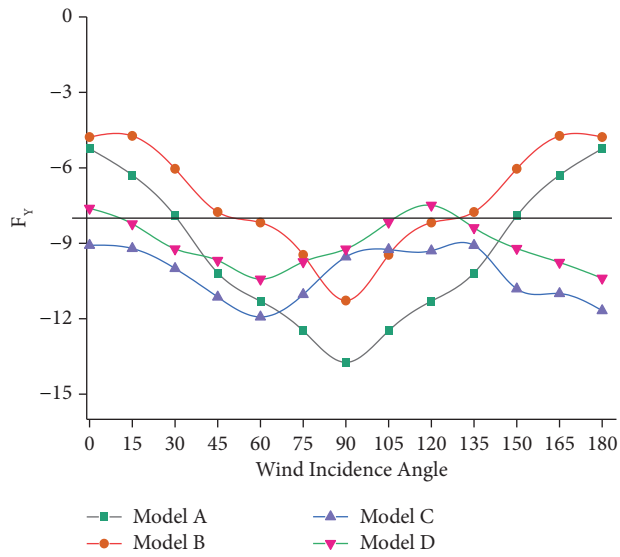

Figure 10: Wind force coefficient in y-direction F_y.

−11.92 in 60° wind, while the minimum of −9.08 for 0° wind 135° wind. The along wind, lift force is found greatest of −10.42 in the case of model-D (fillet-Y) for 60° wind, while the smallest of −7.6 is noticed in the case of 0° wind. Among the Y-shaped model, the lowest lift force is observed for the model having a fillet corner into each limb of the "Y" shape [63].

3.3. Pressure Contours. Pressure distribution is represented in the form of contours for each surface of the building model. Pressure distribution for rectangular building model-A is represented in Figure 11 for 0° wind, while for 90° wind, the pressure distribution pattern along the height of the

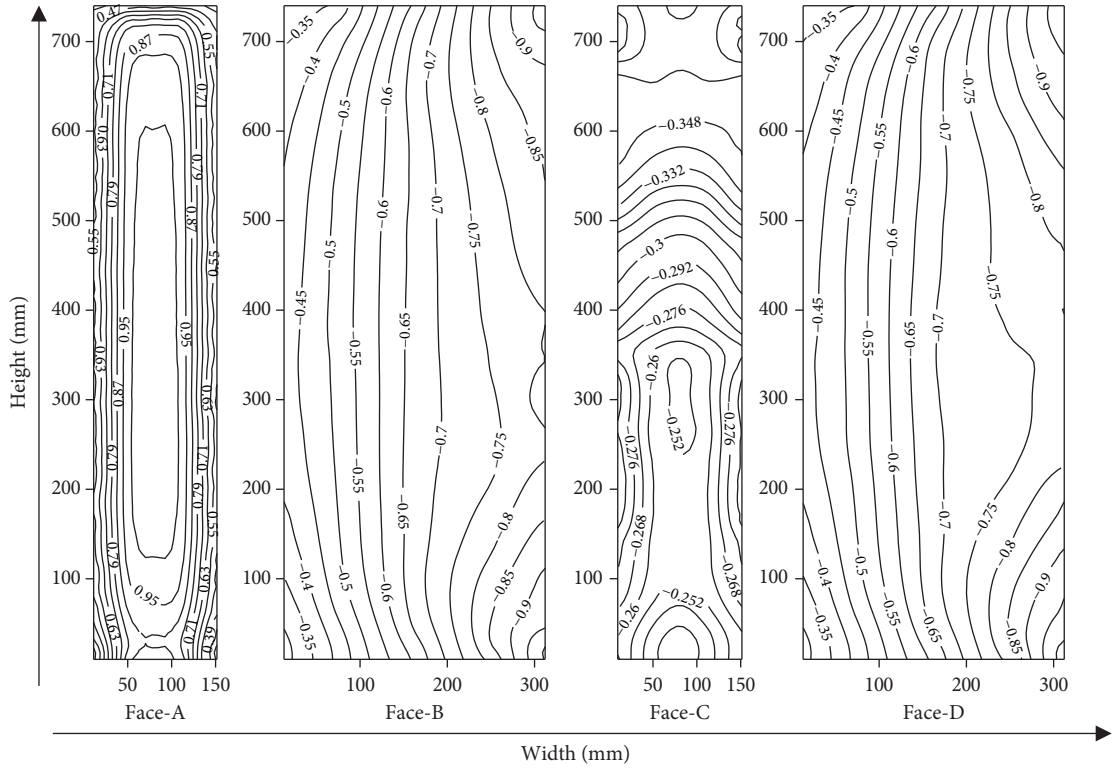

Figure 11: Pressure contours at 0° wind for model-A.

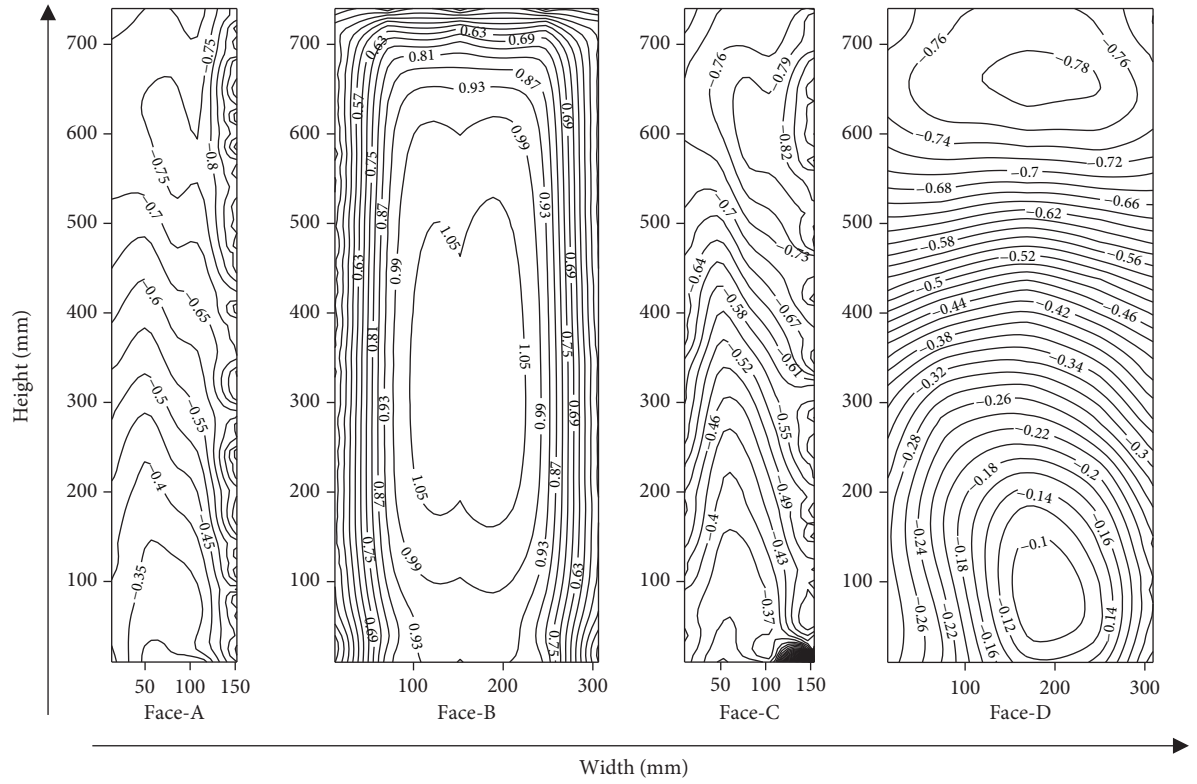

Figure 12: Pressure contours at 90° wind for model-A.

model is represented in Figure 12. The pressure on the wind ward face in both the case is having nearly the same pressure distribution pattern. The maximum pressure is observed in the case of 0° wind of 0.95 in the central part of face-A, while face-B in 90° wind is having the maximum of around 1.05, which is more than face-A for 0° wind because of the face

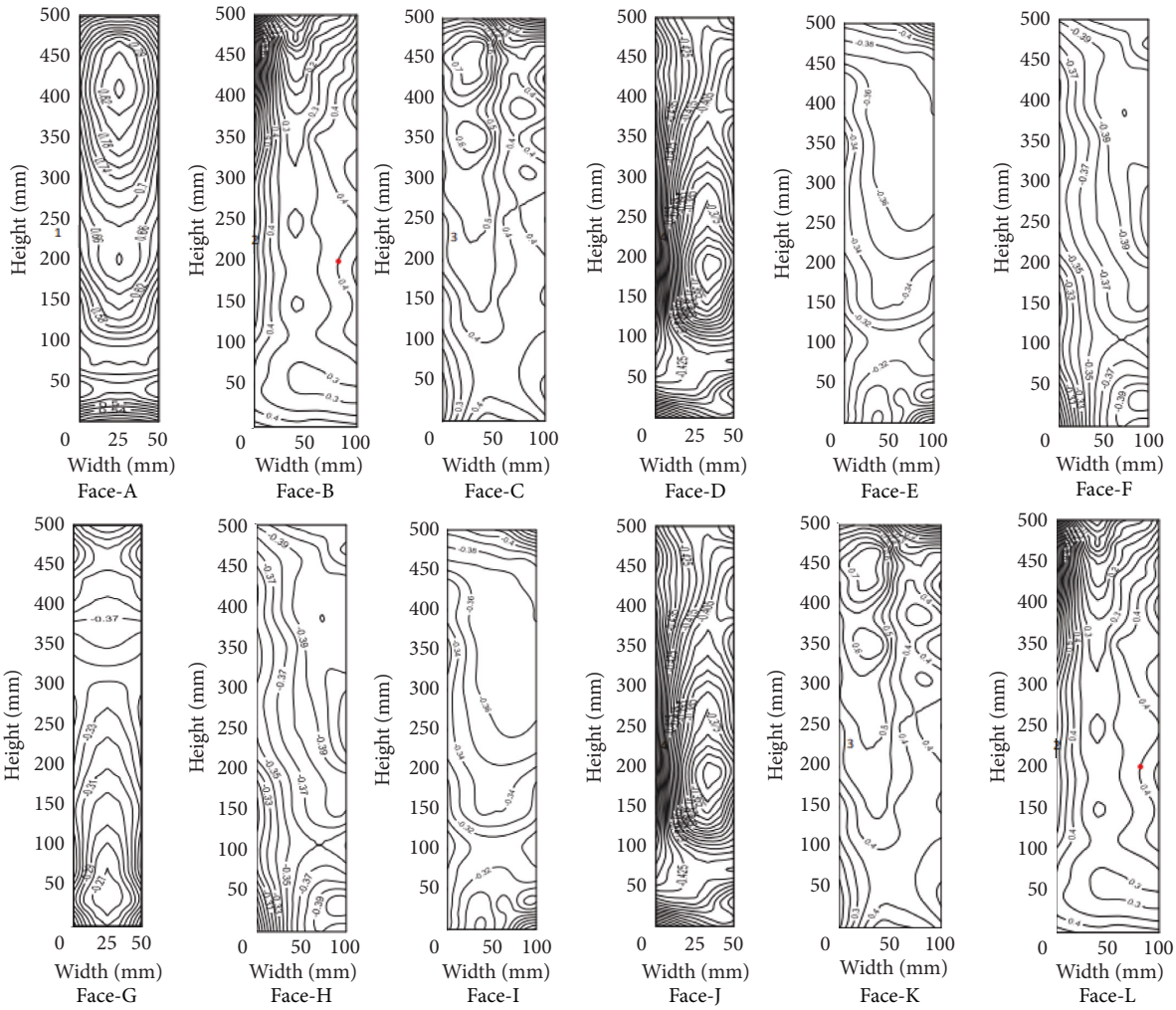

Figure 13: Pressure contours for 0° wind "+" shape [63].

width is increased and that is why the pressure exposure area is increased. For 0° wind, pressure along face-B starts to increase from upstream to downstream of wind, this is because of reattachment of flow. Face-B and face-D is having almost the same pressure distribution pattern, this is because of the symmetric faces of a building model. Leeward face, i.e., face-C, is having suction (negative pressure) and the maximum is on the bottom part of the building, while suction is increased at face-C from base to top of the model.

Figure 12 represents the pressure distribution variation of model-A. Pressure is presented in the form of contours, which is varying as per the shape and size of the particular face. In the case of 90° wind angle, face-A and face-C are having almost the identical pressure distribution pattern. This is increased from the ground of the model to the top of the building model. Also, pressure in the negative is increased as the wind moves from upstream to downstream. Pressure along face-D (Leeward) is having highest negative pressure in the top one-third part of the building model.

Figure 13 is pictorially representing [63] the pressure distribution in the form of contours for the "+" shaped building model, while present studies numerically investigate the wind effects on model-B. Model-B (rectangular model having corner cuts) pressure contours for 0° wind is represented in Figure 14, while for 90° wind the pressure contours for model-B are represented in Figure 15. The nature of pressure distribution on windward face-A is identical and the maximum pressure of 1.04 is spotted on face-A, while the face-A of the "+" shaped building is having maximum of 1.06. This is clearly depicted that each face of model-B is having a pressure distribution pattern and is the same as that with the experimental study performed on the "+" shaped model [63]. The pressure distribution variation is not much dependent on the size of the face, while the height more or less controls the pressure patterns.

Model-C (Y-Chamfer) is investigated numerically for wind effects and the pressure distribution pattern for 0° wind is in Figure 16, and for 90° wind, pressure contours are represented in Figure 17. The maximum positive pressure of 0.55 is on face-D, while the maximum negative of −1.3 is on face-E. The pressure variation along the shape and size is

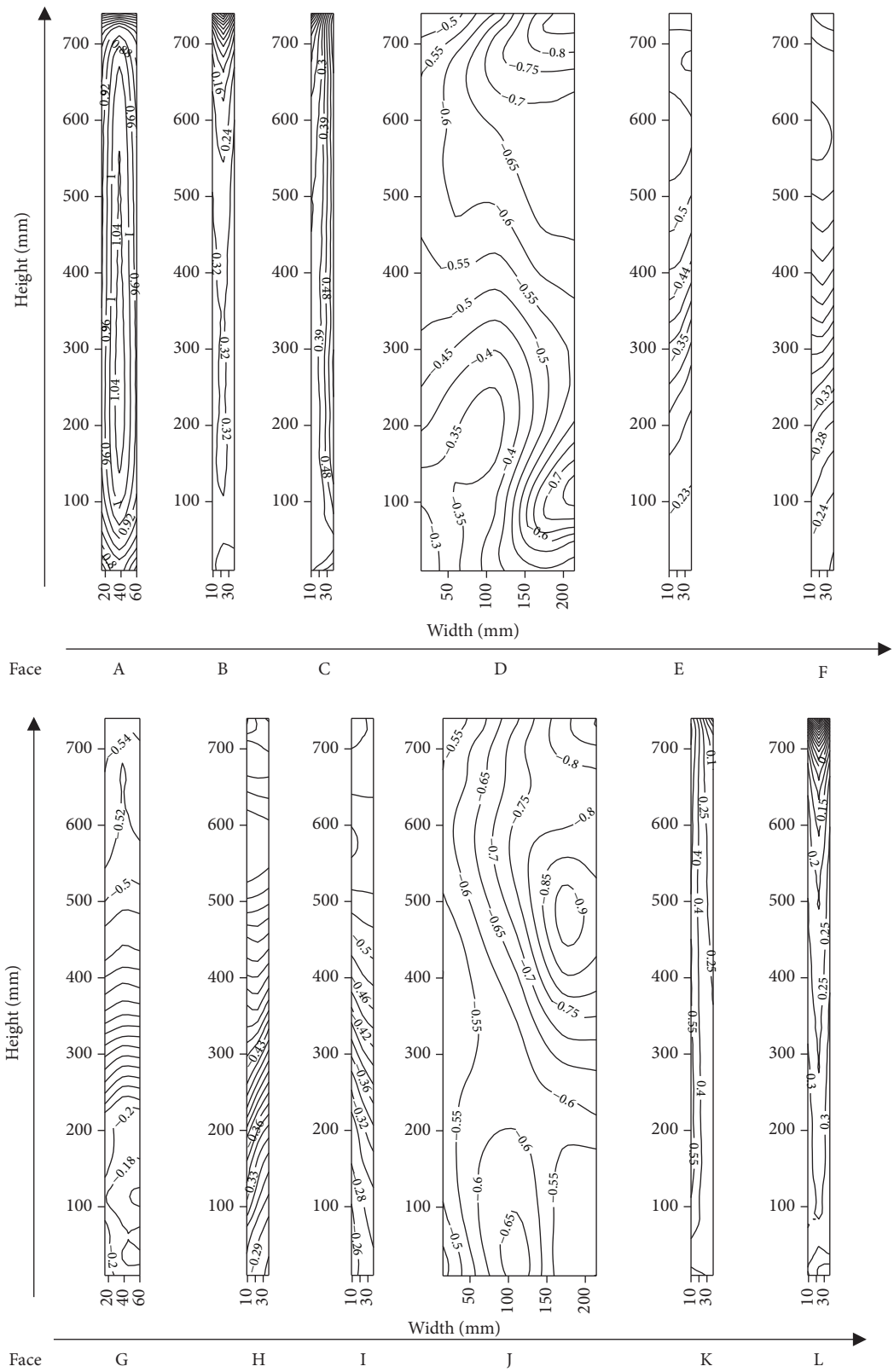

Figure 14: Pressure contour at 0° wind for model-B.

clearly demonstrating the magnitude of pressure as contours are showing with the label, and such labels are showing the increment or decrement in pressure. The actual phenomenon along model-C is valuable for the designer to investigate the wind effects on such types of corner configurations.

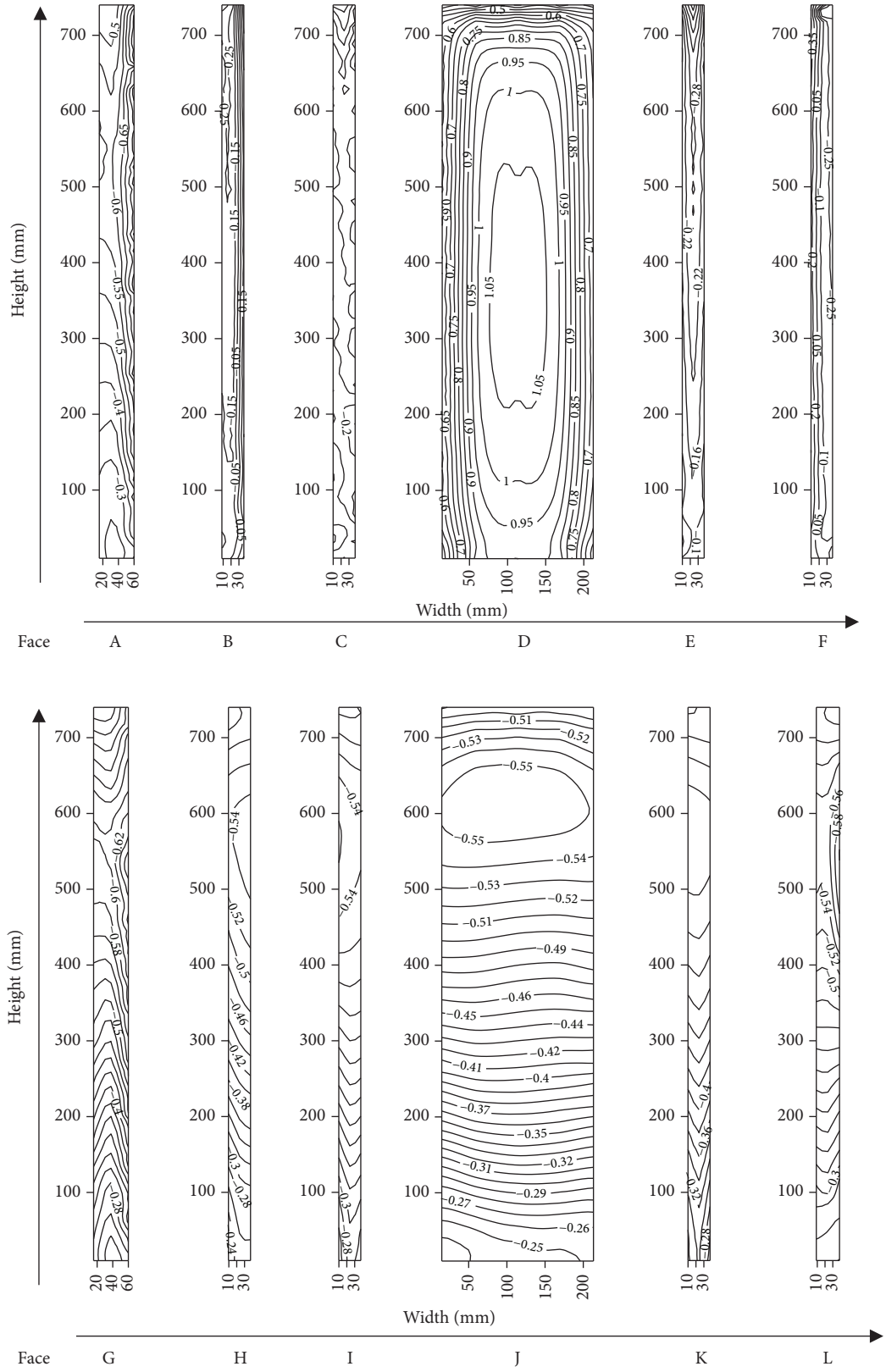

Figure 15: Pressure contour at 90° wind for model-B.

Pressure distribution on model-D is represented graphically in Figure 18 for 0° wind, while pressure contours in Figure 19 is for 90° wind. The positive pressure is observed on face-A, B, C, D, M, and N, while the negative pressure is noticed on face-E, F, G, H, I, J, K, L, and O in the case of 0° wind. The maximum positive pressure of 0.64 is observed on

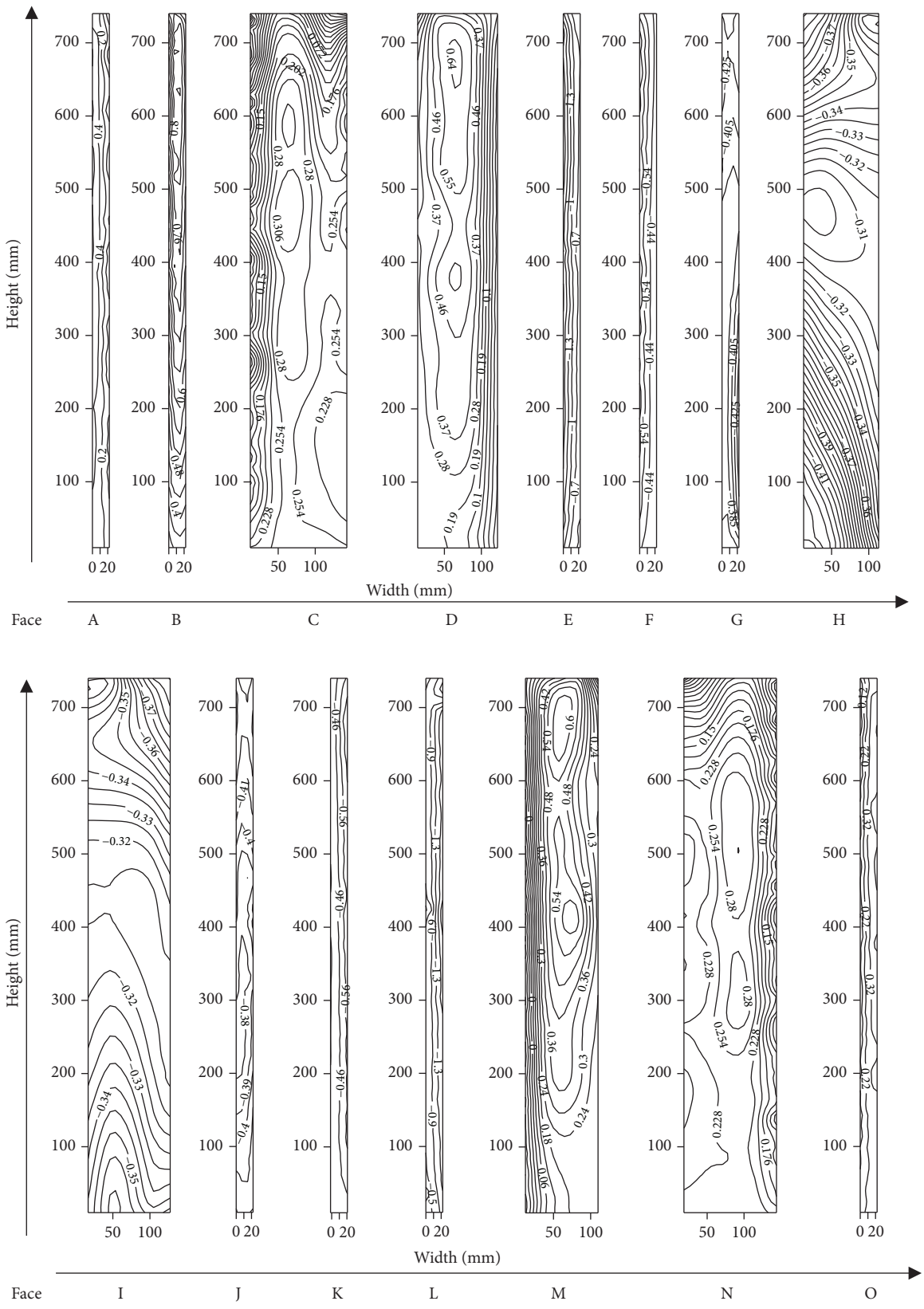

Figure 16: Pressure contours at 0° wind for model-C.

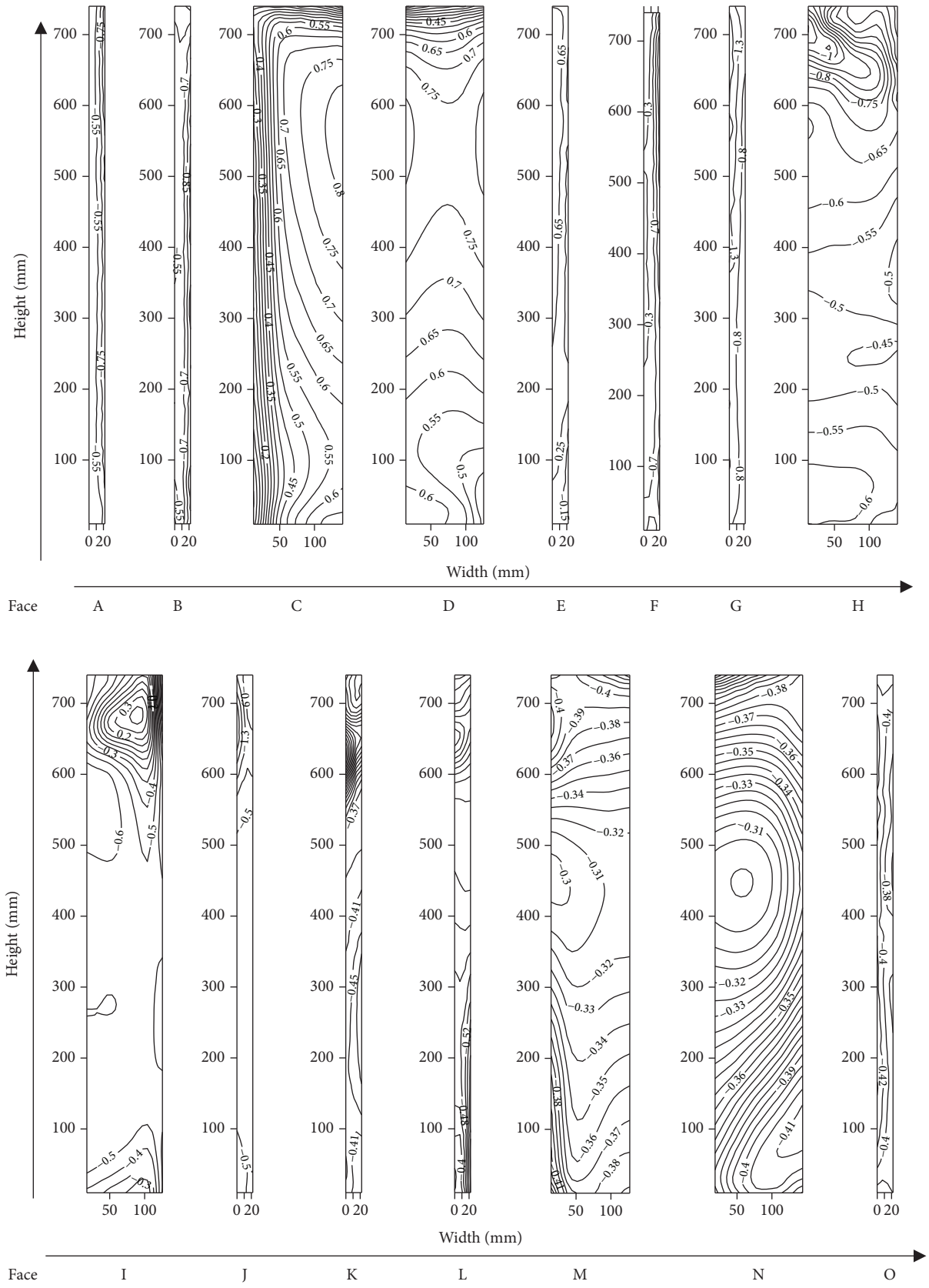

Figure 17: Pressure contours at 90° wind for model-C.

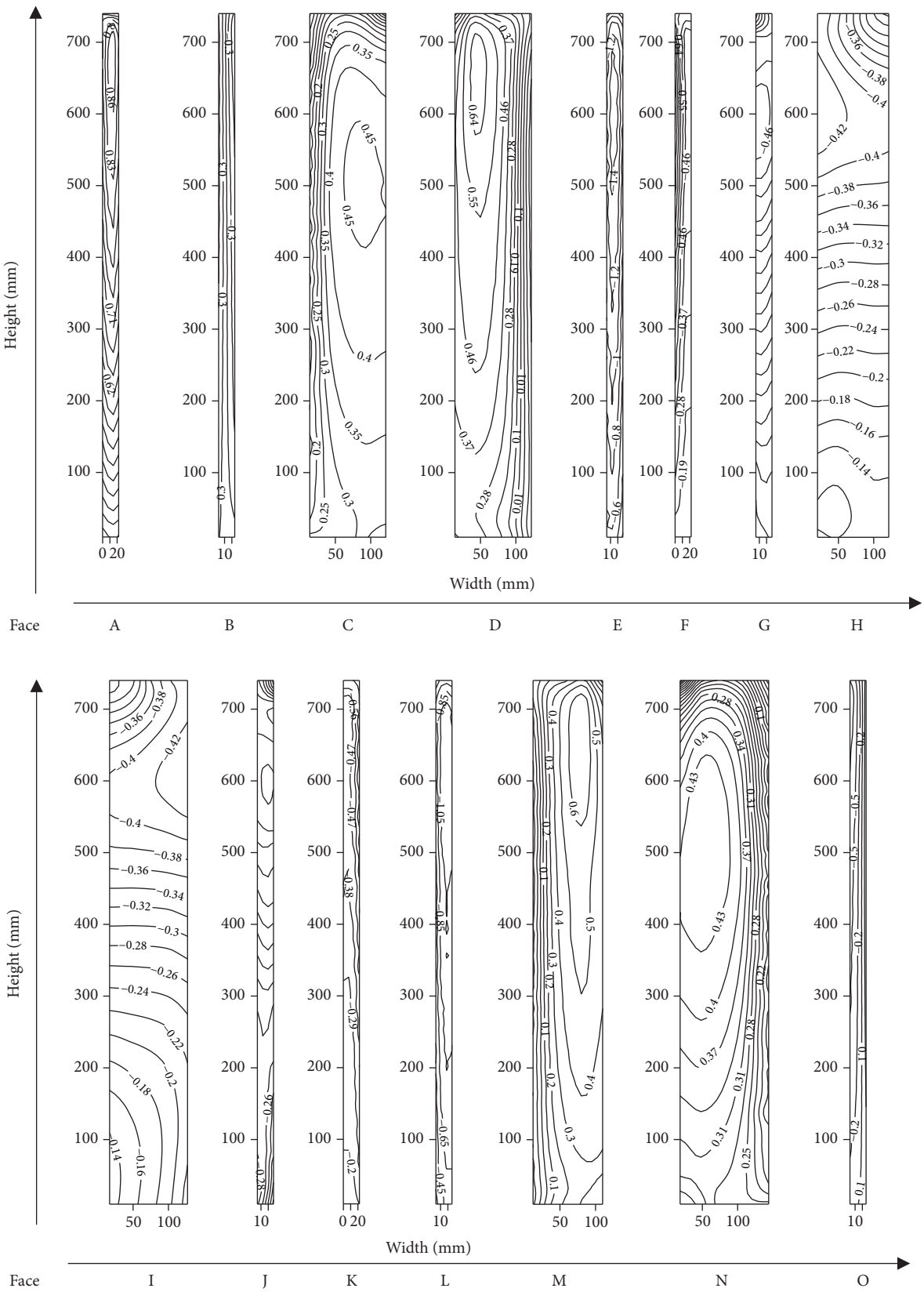

Figure 18: Pressure contours at 0° wind for model-D.

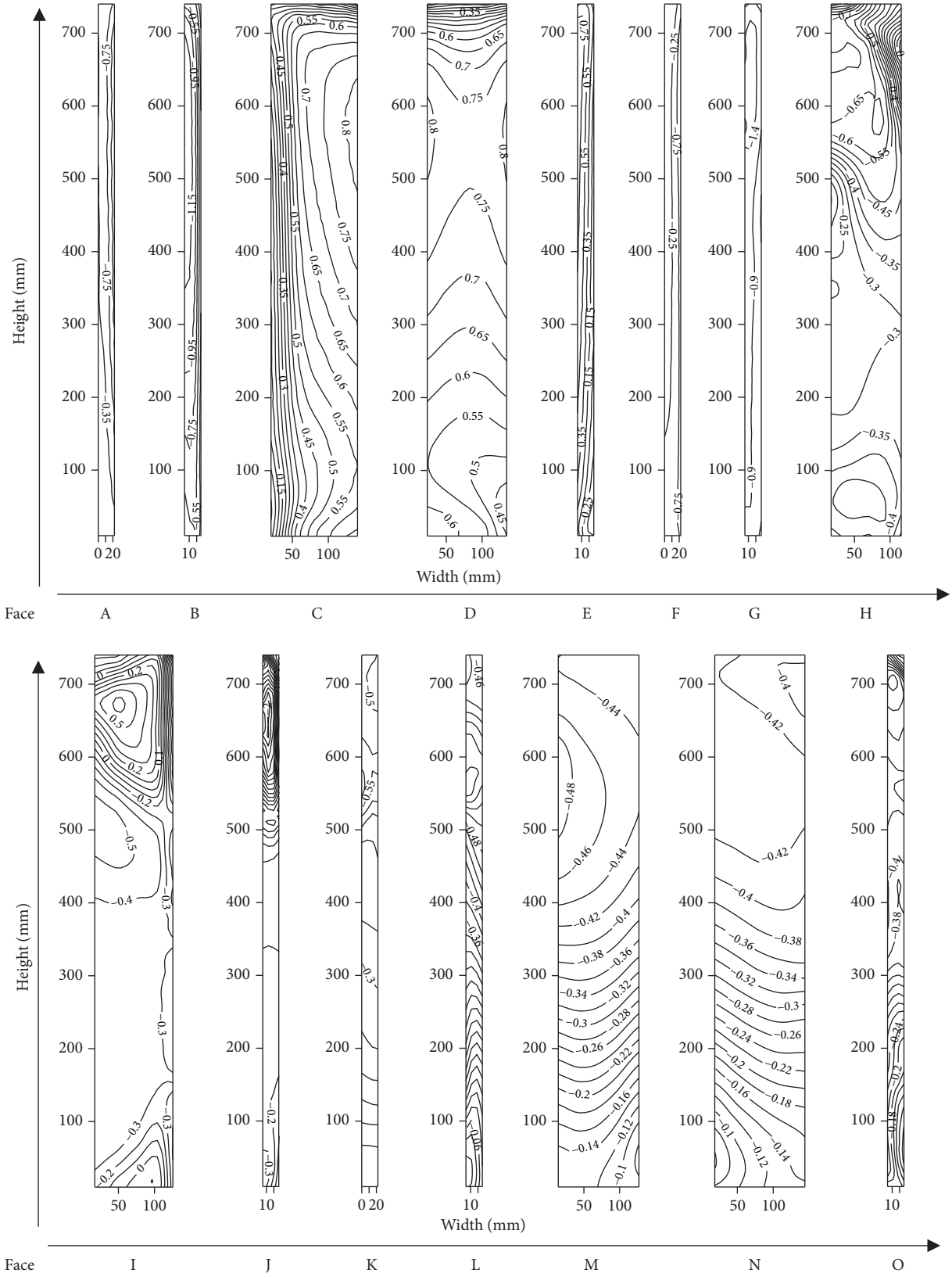

Figure 19: Pressure contours at 90° wind for model-D.

face-*D*, while the maximum suction of −1.4 is spotted on face-E in the case of 0° wind. Pressure contours for 90° wind for model-D (Y-fillet) is represented graphically Figure 19. The positive pressure is spotted on face-C, D, and E only in the case of 90° wind, while other faces are under the effect of negative pressure. The maximum positive pressure of 0.75 is observed on face-C and D, while the negative pressure of −1.4 is noticed on face-G for model-D (Y-fillet). This is also noticed from pressure contours that symmetrical faces are having same pressure distribution patterns.

4. Conclusion

The present numerical study is performed to investigate the wind effects on the corner effects of the tall building having various corners (corner cut, chamfer, and fillet) in the corner of the cross-sectional plan area of the building. The present study is performed using ANSYS CFX by utilizing the k-ε turbulence model. The wind incidence angle varies in the range of 0° to 180° at the interval of 15° each. All four building models have the same corner modification ratio, as well as the same area and height. Validation studies show the closer agreement of the numerical simulation result with the experimental studies and different international standards. Various results of the pressure distribution wind force coefficient are calculated and presented. The notable outcomes from the present are as follows:

(i) Validation investigations indicate a strong degree of congruence between numerical results and experimental results and a number of international standards. Validation is carried out on two distinct models of rectangles, one with a regular shape and one with a corner cut.

(ii) The shape of the building is having the significant effect in determining the wind load on the tall building, wind forces are varying with the wind incidence angle. A regular plan shape model with no corner modification and a model with corner modification exhibit identical along the wind response, but the overall lift is less for the model having corner modification.

(iii) The maximum wind forces at 30°, 90°, and 150° wind angles were observed for an irregular "Y" shaped building with modified corners. These types of structures are well-suited to withstand such high-intensity forces, if appropriate openings are provided in the cladding unit.

(iv) Among the regular shape models, a model with corner cuts is optimal; however, an irregular "Y" shaped model with fillet corners into each limb is optimal for resisting overall wind force. To avoid excessive wind loads, the base shear of all four buildings is also investigated.

(v) The majority of available international standards are silent on providing data for irregular shape models; however, this study investigates wind load information for such buildings.

(vi) The designer can choose the best model from one of these four models, since this study compares the wind effects on equal area building models with the same ratio of modifications and the results are presented in the form of pressure contours for the regular and irregular models.

4.1. Future Scope. The present study analyses and compares the result of the simple type of corner and corner cut on a regular shaped building model, while for irregular shaped modifications of chamfer and fillet shape is provided. Different types of modification can be applied and checked for stability against the wind load.

Nomenclature

ρ:	Density of air
F:	Body force per unit volume
u_i:	The filtered scale velocity field
μ:	Dynamic viscosity of air
t:	Time step
μ_t:	Eddy or turbulent viscosity
x, y, z:	System of rectangular cartesian coordinates
$\in$:	Dissipation rate of k
P:	Pressure
k:	von Karman's constant
u, v, w:	Fluctuating wind
τ_{ij}:	Turbulent stress tensor
z_o:	Reference height
z:	Height above the ground
n:	Power law index
v_z:	Mean wind speed at any height
v_o:	Mean wind speed at reference height
P:	Pressure at the point
P_0:	Static pressure at reference height
U_H:	Mean wind speed at reference height
C_F:	Force coefficient
C_M:	Base moment coefficient
A_p:	Area projected
H:	Height of the building model
β, β^*, σ^*, σ:	Closure coefficients
k:	Turbulent kinetic energy
$\overline{u_i u_j}$:	Reynold stress
i:	General values of u, v, w component at point
BLWT:	Boundary Layer Wind Tunnel
TTU:	Texas Tech University
SST:	Sher Stress Transport
GC:	Grid Convergence
ABL:	Atmospheric boundary layer flow
CFD:	Computational fluid dynamics
WT:	Wind Tunnel
atm:	Atmospheric.

Data Availability

All data, models, and code generated or used during the study appear in the submitted article. Data are available from

the corresponding author upon request in the form of contour plots and graphs.

Conflicts of Interest

The authors declare that they have no conflicts of interest.

Acknowledgments

The authors would like to express their sincere gratitude to the Delhi Technological University, Delhi, India, for providing funding to conduct the research work and for the institutional fellowship for the second author under Institutational fellowship for the Ph.D.

References

[1] I S, "Indian Standard Design Loads (Other than Earthquake) for Buildings and Structures-Code of Practice,part 3(wind loads)," Indian Standard, Mirzapur, I. S 875, 2015.

[2] As/Nzs, "Structural Design Actions - Part 2," As/Nzs:1170, p. 2, Wind actions. Standards Australia/Standards New Zealand, Sydney, Wind actions. Standards Australia/Standards New Zealand, 2011.

[3] Asce, "Minimum Design Loads and Associated Criteria for Buildings and Other Structures," *Structural Engineering Institute of the American Society of Civil Engineering, Reston*, 2017.

[4] Gb 50009-2001, *National Standard Of The People's Republic Of China*, General Administration of Quality Supervision, Inspection and Quarantine of The People's Republic of China, China, 2002.

[5] BE, *Code of Practice on Wind Effects in Hong Kong 2004*, pp. 68–70, Buildings Department, Hong Kong, 2004.

[6] NSCP C101-15, *National Structural Code of the Philippines 2015*, Association of Structural Engineers of the Philippines, Quezon, Philippines, 2015.

[7] Mnbc, *Myanmar National Building Code 2020*, International relation and legal Section Department of Building Minis, 2020.

[8] Ministry of Housing and Urban Development, "National building code," pp. 1–476, Federal. Repub. Nigera, Nigera West Africa, 2006.

[9] Mvcs, *National Building Regulations*, Bureau of indian standards, New Delhi, India, 2018.

[10] Bnbc, *Bangladesh National Building Code (BNBC) 2020*, House Build. Res. Inst, 2020.

[11] R. Tavakoli, R. Kamgar, and R. Rahgozar, "Optimal location of energy dissipation outrigger in high-rise building considering nonlinear soil-structure interaction effects," *Periodica Polytechnica: Civil Engineering*, vol. 64, pp. 887–903, 2020.

[12] M. Dadkhah, R. Kamgar, H. Heidarzadeh, A. Jakubczyk-Galczyńska, and R. Jankowski, "Improvement of performance level of steel moment-resisting frames using tuned mass damper system," *Applied Sciences*, vol. 10, pp. 34–38, 2020.

[13] R. Kamgar and P. Rahgozar, "Optimum location for the belt truss system for minimum roof displacement of steel buildings subjected to critical excitation," *Steel and Composite Structures*, vol. 37, pp. 463–479, 2020.

[14] R. Kamgar, R. Tavakoli, P. Rahgozar, and R. Jankowski, "Application of discrete wavelet transform in seismic nonlinear analysis of soil–structure interaction problems," *Earthquake Spectra*, vol. 37, 2021.

[15] M. Dadkhah, R. Kamgar, and H. Heidarzadeh, "Reducing the cost of calculations for incremental dynamic analysis of building structures using the discrete wavelet transform," *Journal of Earthquake Engineering*, vol. 26, 2020.

[16] M. Dadkhah, R. Kamgar, and H. Heidarzadeh, "Improving the nonlinear seismic performance of steel moment-resisting frames with minimizing the ductility damage index," *SN Applied Sciences*, vol. 3, 2021.

[17] R. Kamgar and M. R. B. Samani, "Numerical study for evaluating the effect of length-to-height ratio on the behavior of concrete frame retrofitted with steel infill plates," *Practice Periodical on Structural Design and Construction*, vol. 27, pp. 1–10, 2022.

[18] K. C. S. Kwok, "Effect of building shape on wind-induced response of tall building," *Advances in Wind Engineering*, vol. 28, pp. 381–390, 1988.

[19] R. Jozwiak, J. Kacprzyk, and J. A. Zuranski, "Wind Tunnel Investigation of Interference Effects on Pressure Distribution on a Building," *Journal of Wind Engineering and Industrial Aerodynamics*, vol. 57, 1995.

[20] S. Pal, R. K. Meena, R. Raj, and S. Anbukumar, "Wind tunnel study of a fish - plan shape model under different isolated wind incidences," vol. 5, pp. 353–366, 2021.

[21] S. K. Nagar, R. Raj, and N. Dev, "Experimental study of wind - induced pressures on tall buildings of different shapes," *Wind Struct. An Int. J*, vol. 5, pp. 441–453, 2020.

[22] S. Pal, R. Raj, and S. Anbukumar, "Comparative study of wind induced mutual interference effects on square and fish-plan shape tall buildings," *Sādhanā*, vol. 46, no. 2, p. 86, 2021.

[23] S. K. Nagar, R. Raj, and N. Dev, "Proximity effects between two plus-plan shaped high-rise buildings on mean and RMS pressure coefficients," *Scientia Iranica*, vol. 29, 2021.

[24] S. Pal, R. Raj, and S. Anbukumar, "Bilateral interference of wind loads induced on duplicate building models of various shapes," *Latin American Journal of Solids and Structures*, vol. 18, 2021.

[25] J. A. Amin and A. K. Ahuja, "Aerodynamic modifications to the shape of the buildings: a review of the state-of-the-art," *Asian J. Civ. Eng*, vol. 11, pp. 433–450, 2010.

[26] P. A. Blackmore, "The role of wind tunnel testing in the design of building structures," *Proceedings of the Institution of Civil Engineers - Structures and Buildings*, vol. 122, no. 3, pp. 253–265, 1997.

[27] B. Bhattacharyya and S. K. Dalui, "Experimental and numerical study of wind-pressure distribution on irregular-plan-shaped building," *Journal of Structural Engineering*, vol. 146, Article ID 04020137, 2020.

[28] Y. Tominaga and T. Stathopoulos, "Turbulent Schmidt numbers for CFD analysis with various types of flowfield," *Atmospheric Environment*, vol. 41, no. 37, pp. 8091–8099, 2007.

[29] B. Blocken, "Computational Fluid Dynamics for urban physics: importance, scales, possibilities, limitations and ten tips and tricks towards accurate and reliable simulations," *Building and Environment*, vol. 91, pp. 219–245, 2015.

[30] S. Behera, D. Ghosh, A. K. Mittal, Y. Tamura, and W. Kim, "The effect of plan ratios on wind interference of two tall buildings," *The Structural Design of Tall and Special Buildings*, vol. 29, 2020.

[31] Y. Tamura, X. Xu, H. Tanaka, Y. C. Kim, A. Yoshida, and Q. Yang, "Aerodynamic and pedestrian-level wind characteristics of super-tall buildings with various configurations," *Procedia Engineering*, vol. 199, pp. 28–37, 2017.

[32] A. K. Mittal, D. Ghosh, S. Behera, I. A. Siddiqui, and D. S. Dharmshaktu, "Wind flow simulation in the vicinity of tall buildings through CFD," in *Proceedings of the 8th Asia-Pacific Conf. Wind Eng. APCWE*, pp. 682–690, Chennai, India, December 2013.

[33] B. Blocken, T. Stathopoulos, and J. Carmeliet, "CFD simulation of the atmospheric boundary layer: wall function problems," *Atmospheric Environment*, vol. 41, no. 2, pp. 238–252, 2007.

[34] X. Tian, M. C. Ong, J. Yang, and D. Myrhaug, "Unsteady RANS simulations of flow around rectangular cylinders with different aspect ratios," *Ocean Engineering*, vol. 58, pp. 208–216, 2013.

[35] N. Gaur and R. Raj, "Aerodynamic mitigation by corner modification on square model under wind loads employing CFD and wind tunnel," *Ain Shams Engineering Journal*, vol. 13, 2021.

[36] R. Raj, T. Rana, T. Anchalia, and U. Khola, "Numerical study of wind excited action on H Plan-shaped tall building," *International Journal on Emerging Technologies*, vol. 11, pp. 591–605, 2020.

[37] M. Keerthana and P. Harikrishna, "Application of CFD for assessment of galloping stability of rectangular and H-sections," *Journal of Scientific & Industrial Research*, vol. 72, pp. 419–427, 2013.

[38] A. Kumar and R. Raj, "Study of pressure distribution on an irregular octagonal plan oval-shape building using CFD," *Civil Engineering Journal*, vol. 7, no. 10, pp. 1787–1805, 2021.

[39] R. Raj, A. Sharma, and S. Chauhan, *Response of Square and Plus Shaped Buildings on Varying Wind Loads*, in *Proceedings of the ASCE India Conference 2017*, pp. 206–215, New Delhi , India, December 2018.

[40] N. Gaur, R. Raj, and P. K. Goyal, "Interference effect on corner - configured structures with variable geometry and blockage configurations under wind loads using CFD," *Asian J. Civ. Eng*, vol. 22, 2021.

[41] S. Mukherjee, S. Chakraborty, S. K. Dalui, and A. K. Ahuja, "Wind induced pressure on 'Y' plan shape tall building," *Wind and Structures*, vol. 19, no. 5, pp. 523–540, 2014.

[42] P. Sanyal and S. K. Dalui, "Effect of corner modifications on Y' plan shaped tall building under wind load," *Wind Struct. An Int. J*, vol. 30, pp. 245–260, 2020.

[43] P. Sanyal and S. K. Dalui, "Effects of Side Ratio for 'Y' Plan Shaped Tall Building under Wind Load," *Building Simulation*, vol. 14, 2020.

[44] P. Sanyal and S. K. Dalui, "Effects of internal angle between limbs of "Y" plan shaped tall building under wind load," *Journal of Building Engineering*, vol. 33, Article ID 101843, 2021.

[45] P. Sanyal and S. K. Dalui, "Comparison of aerodynamic coefficients of various types of Y-plan-shaped tall buildings," *Asian Journal of Civil Engineering*, vol. 21, no. 7, pp. 1109–1127, 2020.

[46] P. K. Goyal, S. Kumari, S. Singh, R. K. Saroj, R. K. Meena, and R. Raj, "Numerical study of wind loads on Y plan-shaped tall building using CFD," *Civil Engineering Journal*, vol. 8, no. 2, pp. 263–277, 2022.

[47] R. K. Meena, R. Raj, and S. Anbukumar, *Numerical Investigation of Wind Load on Side Ratio of High-Rise Buildings Numerical Investigation of Wind Load on Side Ratio of High-Rise Buildings*, Springer, Singapore, 2021.

[48] A. Kumar and R. Raj, "CFD study of flow characteristics and pressure distribution on Re-entrant wing faces of L-shape buildings," *Civil Engineering and Architecture*, vol. 10, no. 1, pp. 289–304, 2022.

[49] R. Raj and A. K. Ahuja, "Wind loads on cross shape tall buildings," *J. Acad. Ind. Res*, vol. 2, pp. 111–113, 2013.

[50] P. Sanyal and S. K. Dalui, "Effects of courtyard and opening on a rectangular plan shaped tall building under wind load," *International Journal of Advanced Structural Engineering*, vol. 10, no. 2, pp. 169–188, 2018.

[51] R. K. Meena, R. Raj, and S. Anbukumar, "Wind excited action around tall building having different corner configurations," *Advances in Civil Engineering*, vol. 2022, Article ID 1529416, 2022.

[52] M. Mallick, A. Mohanta, A. Kumar, and V. Raj, "Modelling of wind pressure coefficients on C-shaped building models," *Modelling and Simulation in Engineering*, vol. 2018, Article ID 6524945, 2018.

[53] J. A. Amin and A. K. Ahuja, "Effects of side ratio on wind-induced pressure distribution on rectangular buildings," *Journal of Structures*, vol. 2013, pp. 1–12, 2013.

[54] J. A. Amin and A. K. Ahuja, "Characteristics of wind forces and responses of rectangular tall buildings," *International Journal of Advanced Structural Engineering*, vol. 6, no. 3, pp. 1–14, 2014.

[55] R. Raj, "Effects Of Cross-Sectional Shapes On Response Of Tall Buildings Under Wind Loads," iit Roorkee, 2015, http://hdl.handle.net/123456789/14664.

[56] P. J. Richards and R. P. Hoxey, "Appropriate boundary conditions for computational wind engineering models using the k-ϵ turbulence model," in *Proceedings of the 1st International Symposium on Computational Wind Engineering (CWE 92)*, pp. 145–153, Tokyo, Japan, August 1993.

[57] Ansys, *ANSYS Meshing User's Guide*, Taylor and francis group an informa business, UK, 2010.

[58] E. M. Alawadhi, "Meshing guide," *Finite Elem. Simulations Using ANSYS*, vol. 15317, pp. 407–424, 2020.

[59] Ansys, "ANSYS CFX-Solver Modeling Guide," ANSYS INC, 2020, http://www.ansys.com.

[60] J. Revuz, D. M. Hargreaves, and J. S. Owen, "On the domain size for the steady-state CFD modelling of a tall building," *Wind and Structures*, vol. 15, no. 4, pp. 313–329, 2012.

[61] J. Franke, A. Hellsten, H. Schlünzen, and B. Carissimo, *Best Practice Guideline for the Cfd Simulation of Flows in the Urban Environment. Cost 732: Quality Assurance and Improvement of Microscale Meteorological Models*, New Delhi, India, 2007.

[62] J. H. Ferziger and M. Peric, "Computational Methods for Fluid Dynamics," 2002, http://marefateadyan.nashriyat.ir/node/150.

[63] S. Chakraborty, S. K. Dalui, and A. K. Ahuja, "Experimental investigation of surface pressure on "+" plan shape tall building," *Jordan J. Civ. Eng*, vol. 8, pp. 251–262, 2014.

Hindawi
Complexity
Volume 2022, Article ID 6532763, 23 pages
https://doi.org/10.1155/2022/6532763

Research Article

Optimising the Selection of Input Variables to Increase the Predicting Accuracy of Shear Strength for Deep Beams

Mohammed Majeed Hameed,[1] **Faidhalrahman Khaleel**,[1] **Mohamed Khalid AlOmar**,[1] **Siti Fatin Mohd Razali**,[2] **and Mohammed Abdulhakim AlSaadi**[3]

[1]*Department of Civil Engineering, Al-Maarif University College, Ramadi, Iraq*
[2]*Department of Civil Engineering, Faculty of Engineering and Built Environment, Universiti Kebangsaan Malaysia (UKM), 43600 Bangi, Selangor, Malaysia*
[3]*Natural and Medical Sciences Research Center (NMSRC), University of Nizwa Sultanate of Oman, Nizwa, Oman*

Correspondence should be addressed to Mohammed Majeed Hameed; mohmmag1@gmail.com, Mohamed Khalid AlOmar; mohd.alomar@yahoo.com, and Mohammed Abdulhakim AlSaadi; m.hakim@unizwa.edu.om

Received 11 March 2022; Revised 19 May 2022; Accepted 28 May 2022; Published 4 July 2022

Academic Editor: M. Z. Naser

The deep beam in load transfer is very important as well as difficult to design due to its shear stress problems. Accurate estimation of shear stress would help engineers to get a safer design. One of the major obstacles in building an accurate prediction model is optimising the input variables. Therefore, developing an efficient algorithm to select the optimal input parameters that have the highest information content to represent the target and minimise redundant data is very important. The feature-section algorithm based on the combination of genetic algorithm and information theory (GAITH) was used to select the most important input combinations and introduce them into the prediction models. Four models were used in this study: locally weighted linear regression (LWLR) based on the radial basis kernel function, multiple linear regression (MLR), extreme learning machine (ELM), and random forest (RF). The study found that all applied models were significantly improved by the presence of the GAITH algorithm, except for the MLR model. The LWLR-GAITH model showed 29.15% to 47.88% higher performance accuracy in terms of root mean square error (RMSE) than the other hybrid models during the test phase. Moreover, the results of the standard models (without using the GAITH algorithm) proved the superiority of the LWLR model in reducing the RMSE by 34.51%, 55.17%, and 35.35% compared to RF, MLR, and ELM, respectively. Thus, the inclusion of the LWLR model with GAITH has demonstrated a reliable and applicable computer aid for modelling shear strength in deep beams.

1. Introduction

Since the 1950s, scientists have extensively studied the shear behaviour of beams made of deep reinforced concrete (RC) [1]. In general, it has long been known that deep beams can withstand far greater shear loads than slender beams due to their enormous ratio of shear span to depth ($(a/d) \leq 2.5$). Therefore, deep beams are often used as transfer beams in structures, in bridge arches as cap beams, in foundations as pile caps, and in other highly loaded structural members. The main difference between slender and deep beams is that shear deformation in slender beams is minimal and can be neglected, while it must be taken into account in the design and analysis of deep beams, as failure in the latter is mainly due to shear stresses [2]. Moreover, from a modelling point of view, deep beams contradict the concept of the standard plane and require different models than slender beams [3].

In deep beams, the internal arch action generates the shear strength by transferring the load directly to the column through concrete struts. Several factors influence the structural system of deep beams, such as the ratio of shear span to depth, the compressive strength of the concrete, the

yield strength of the horizontal and vertical reinforcement, and the ratio of the main reinforcement [4]. The RC behaviour of deep beams and specifically the shear strength has been quantitatively studied over several decades using various models and empirical approaches such as the strut and sill model, which is considered the most commonly used approach and has been adopted by various codes such as ACI 318-14 [5], CSA A23.3-14 [6], and EC2 [7], or mechanism analysis based on the upper bound theory of plasticity and the finite element approach. However, the design methods of these approaches are linear and therefore unable to capture the complex relationship between the vectors affecting the shear strength and the shear strength itself, in which, in turn, the obtained predicted value of the shear strength differs significantly from the actual value [8].

Different researchers have proposed different design methods to calculate the ultimate shear strength of RC deep beams [9–11]. These design codes are able to capture the nonlinear relationship between the numerous parameters and the ultimate shear strength of deep beams. However, when the results of these methods are compared with the results of experimental tests, they are conservative at best and poor at worst [12]. Furthermore, developing a model that correctly approximates the mathematical shear strength is a major challenge due to this relationship. Due to the inherent limitations of classical models, the prediction of shear strength remains limited to experimental tests [13]. Therefore, the ability of designers to predict shear strength is limited because it is impossible to create an accurate model that can correctly estimate the shear strength capacity using a mathematical formula [14].

In the last two decades, data-driven models based on artificial intelligence (AI) have become increasingly crucial for structural analysis and designing in civil engineering [15, 16]. The most critical applications of AI are the analysis of data sets obtained from experimentally or numerically generated data sets to produce closed-form formulae or numerical tools that predict parameters related to structural response and mechanical behaviour. Due to the low information content of the datasets and the high costs associated with their enrichment, it is essential to comprehensively analyse the available data and build the best possible prediction models, which can be done using AI modelling [17]. Moreover, AI models can capture relationships that are difficult to handle with conventional methods [18].

Table 1 provides some examples of the application of different AI and empirical models to predict shear strength. According to the work reviewed, researchers have focused too much on using various artificial and empirical models to estimate shear strength capacity. Since several predictors can affect the shear strength, the reviewed works used classical assumptions to determine the input combination. The most commonly used methods can be presented as follows:

(i) Trial and error approach (trying different combinations)

(ii) Linear correlation approach (selecting only the predictors with higher correlation with the shear strength capacity)

(iii) Using all available inputs

The use of the above methods has several drawbacks: (1) the applied model needs more time to complete the training and calibration phase, (2) the selection of input combinations may not represent all potential cases (primarily if the trial-and-error procedure is used), (3) the complexity of the modelling leads to difficulties in interpreting the model performance and the obtained results, and (4) the model is trained with lack or excessive and redundant information of the selected predictors, which may significantly affect the model performance and stability. Furthermore, the use of linear correlation may be misleading in some cases due to the complexity of the relationship between the shear strength of reinforcement beams and geometric, concrete, and steel parameters.

According to the previous papers published in the literature, many researchers used ANN models to estimate the shear strength in the deep beam. Therefore, in this work, ELM was used as a comparable model. Notably, this model is considered the new variant of ANN and has the advantage of good performance, speed, and ability to generalize. However, while reviewing prior research, we discovered a group of highly motivated scientists to adopt sophisticated models based on regression tree-based models. Thus, we select RF as a robust assembling model. The reason for selecting MLR is to see the efficiency of the other models compared to simple models and, in other words, to investigate if there is a significant difference between the nonlinear-based models and simple models like MLR.

Furthermore, the structures of the three models (RF, MLR, and ELM) are somewhat lacking in flexibility. In other words, these parametric approaches derive a general or global model. Therefore, after finishing the training phase, there will be one complex function to present the targeting problem, and all the data samples are subjected to that function. However, the LWLR is not necessary to specify a function to fit a model to all data in a sample. Thus, LWLR is more flexible and can model complex processes for which no theoretical model exists.

The main objective of this study is to determine the ability of the locally weighted linear regression (LWLR) model based on the Gaussian kernel function to predict the ultimate shear strength of reinforced concrete beams with and without web reinforcement. Moreover, the LWLR model proposed in this study is evaluated by comparing its performance with comparable models such as extreme learning machine (ELM), random forest (RF), and classical multiple linear regression (MLR). Furthermore, the second objective of this study is to use an efficient feature selection tool to select the best input parameters. Selecting the inputs with the highest information with the target and the most diminutive relationship with each other is considered a vital step to achieve the desired prediction accuracy. In this context, information theory is combined with the genetic algorithm as a feature selection tool to remove the variable (s) that contain redundant information that negatively affects the model's prediction ability. It is also the first time that the LWLR model has been used as a prediction tool in the concrete and structural fields.

Table 1: Examples of different SC models and empirical equations in modelling the shear strength.

Reference	Used method	Statistical parameter	Data division	Findings
[19]	ANN with training algorithms ANN-LM ANN-QN ANN-GG ANN-GD	R, RMSE, MAE, MAPE	70% for training and 30% for testing. 106 data.	ANN-GG has the best prediction accuracy.
[20]	NN	R	70% for training and 30% for testing. 233 data.	The results of the proposed model show great similarity with the test results
[3]	OSVM-AEW LS-SVM with SOS	R, R^2, MAE, MAPE, RMSE	67% for training and 33% for testing using a triple cross-validation approach.	OSVM-AEW has the best prediction accuracy
[21]	SVR-GA SVR ANN GBDTs	R^2, RMSE, MAE, NSE, WI	70% for training and 30% for testing. 217 test records.	SVR-GA gives better predictions than the other models.
[22]	GEP ANN	R, RMSE, MAE	70% for training, 10% for validation, and 20% for testing. 214 test records.	GEP has better prediction accuracy than ACI and CSA and shows very good agreement with the ANN model.
[4]	LS-SVR and SFA	R, RMSE, MAE, MAPE	70% for training and 30% for testing. 214 data set	LS-SVR with SFA has better prediction accuracy compared to the standard SVR.
[23]	ANN	Mean, STD, COV	—	ANN performed better than the ACI code, EURO code, zsutty method, and russo method.
[24]	Strut-and-tie model	AVG, COV	16 test specimens.	The results of the proposed model show great similarity with the test results.
[25]	CSTM	Mean, COV	355 test specimens.	The performance of CSTM is better than other STM models.
[26]	New analytical expression using strut-and-tie model (STM)	Mean, COV	111 test specimens.	The proposed model has better prediction accuracy compared to ACI 318-14 code.
[27]	GA	AVG, STD	50% for training and 50% for testing. 371 data records.	GA has better prediction accuracy compared to ACI 318-14 code.
[28]	Feedforward NN	Mean, STD	50% for training, 25% for validation, and 25% for testing. 433 data records.	The results of the proposed model are in agreement with the experimental and analytical data.
[29]	EMARS BPNN RBFNN SVM	R^2, RMSE, MAPE	10-fold cross-validation. 106 data set	The performance of EMARS is better than BPNN, RBFNN, and SVM.
[15]	RF AdaBoost GBRT XGBoost	R^2, RMSE, MAE, MAPE	10-fold cross-validation. 271 test records	The performance of the proposed models is better than the traditional machines single learning methods (DT, SVM, ANN)
[30]	SVR with RBF and polynomial kernel	R, RMSE	10-fold cross-validation	SVR with RBF and polynomial kernel gives better prediction accuracy compared to backpropagation neural network and empirical relations.

2. Methodology

2.1. Shear Strength of RC Deep Beams and Data Collection. Reinforced concrete (RC) deep beams are frequently used as load-bearing elements in bridge and building construction, so their mechanical behaviour should be carefully analysed and investigated. Since the span-to-depth ratio of RC deep beams is usually less than two, the load-bearing capacity of these structures is strongly influenced by the shear behaviour. It is well known that it is difficult to accurately model the shear behaviour of deep beams because the assumption of a plane cross section no longer holds. To overcome this difficulty, some researchers have applied well-known mechanics-driven models, including the soft truss model

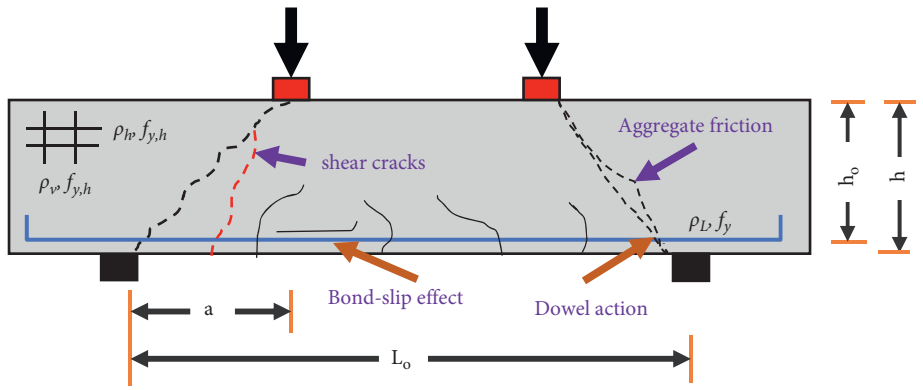

Figure 1: Failure types on reinforced deep beams.

[31, 32], the modified compression field method [33, 34], and the strut-and-tie model [25, 35]. Nevertheless, the associated shear strength mechanism is quite complex, as shown in Figure 1. Shear strength involves many complex behaviours, such as aggregate friction effect, flexure-shear interaction, shear transfer effect of web reinforcement, longitudinal reinforcement, dowel effect of longitudinal reinforcement, bond-slip effect, and size effect. There is no practical way to account for all these behaviours in a unified model, which leads to significant differences in the performance of existing models. Therefore, the main objective of this study is to use a robust prediction model to solve a classical problem in civil engineering.

A total of 271 test data on RC deep beams were collected from the open-source literature to train the models used in this work. These include 52 specimens from Lu [36], 37 specimens from Ludwig and Nunes [37], 25 specimens from Hameed et al. [38], 53 specimens from Hameed et al. [39], 12 specimens from Naser and Alavi [40], 12 specimens from Ludwig et al. [41], 6 specimens by Nguyen et al. [42], 12 specimens by Yaseen et al. [43], 19 specimens by Zhang et al. [44], 39 specimens by Gong, and 4 specimens by Gandomi et al. [45]. It is worth noting that the database contains a wide range of RC deep beams to improve the generativity of the model. Moreover, the dataset contains four types of RC deep beams: beams with horizontal web reinforcement, beams without web reinforcement, beams with horizontal and vertical reinforcement, and beams with vertical web reinforcement.

2.2. Multiple Linear Regression. Multiple linear regression (MLR) specifies the independent variable (Y) according to a linear equation in terms of more than two independent variables (X_i). The mathematical expression of MLR is as follows [46]:

$$Y = \beta_o + \sum_{i=1}^{n} \beta_i X_i + E. \tag{1}$$

Here, the MLR parameters (i.e., β_o and β_i) are calculated using the least-squares method (LS), and E is the unsystematic error. The fitness function should be defined to calculate the best fit line for the measured data set (Y). The following fitness function should be minimised.

$$Fitness = \frac{1}{2N} \sum_{j=1}^{N} \left(Yobs_j - Ypred_j\right)^2, \tag{2}$$

where N is the length of the data set used, and $Yobs_j - Ypred_j$ represent the actual or predicted values for the j^{th} sample. To simplify equation (2), a matrix can be derived from this equation as $(X\beta - Y)^T (X\beta - Y)$.

The derivative of the matrix with respect to β then gives $X^T (X\beta - Y)$. By the LS method, the term $X^T (X\beta - Y)$ should be zero and solved for β. Finally, the parameter β can be given by the following equation:

$$\beta = \left(X^T X\right)^{-1} X^T Y, \tag{3}$$

where X and Y are the training and target values.

2.3. Locally Weighted Linear Regression. The locally weighted linear regression (LWLR) model is an improved version of the MLR method. This method was invented by Chen et al. [47] to improve the efficiency of the classical MLR model. In the proposed technique, a weighting function is used to define the relationship between the input and output of the data sets. Moreover, the fitness function of LWLR can be defined as follows:

$$Fitness = \frac{1}{2N} \sum_{j=1}^{N} W_j \left(Yobs_j - Ypred_j\right)^2, \tag{4}$$

where the W in the above equation is the weight. Similar to MLR, the equation can be expressed as $((X\beta - Y)^T W (X\beta - Y)$. When the fitness function of the LWLR technique is derived in terms of β, the matrix $X^T W (X\beta - Y)$ is obtained. To calculate β, the matrix of $X^T W (X\beta - Y)$ should be zero. Consequently, β is expressed by

$$\beta = \left(X^T W X\right)^{-1} X^T W Y. \tag{5}$$

In the LWLR method, a kernel function is used as a weighted matrix. In this study, the radial basis function (RBF) is used to calculate the proposed matrix, which is expressed as follows [48]:

$$W_{ik} = \exp\left(-\Upsilon\left(X_i - X_j\right)^2\right), \tag{6}$$

where $(-\Upsilon(X_i - X_j)$ is the difference between variables X in samples i and j, while Y is a positive user-defined number.

2.4. Extreme Learning Machine. Extreme learning machine (ELM) is a novel machine learning approach introduced by Wakjira et al. [49] as a robust new learning algorithm for single hidden layer feedforward networks (SLFNs). ELM is thousands of times faster than conventional learning algorithms for feedforward networks and achieves higher generalisation performance [50]. Since ELM is encoded as SLFNs, many of the complications of gradient-based algorithms, such as learning rate, learning epochs, and local minima, are eliminated when using ELM. Moreover, even with randomly generated hidden nodes, ELM retains its ability to universally approximate SLFNs [51]. ELM networks consist of three layers: the input layer where the data are presented to the ELM network, the hidden layer where the basic computations are performed, and the output layer where the information from the hidden layer is transmitted to. In addition, the results of ELM are organised in the output layer. ELM randomly selects the input weights and biases for the hidden nodes and uses the least-squares solution to calculate the output weights analytically.

The ELM model can be mathematically expressed as

$$V_t = \sum_{m=1}^{i} B_m g_m(\alpha_m \cdot x_m + \beta_m), m = 1, 2, \ldots, n, \tag{7}$$

where V_t is the ELM target; i refers to the number of hidden nodes; B_m is the weight value connecting the m^{th} hidden node with the output node; $g_m(\alpha_m \cdot x_m + \beta_m)$ is the output function associated with i hidden nodes; and (α_m, β_m) are the hidden node parameters that are randomly initialised.

The above equation can be written compactly as follows:

$$MR = T, \tag{8}$$

where $\boldsymbol{M}$ is known as the output matrix of the hidden layer of the neural network.

$$\mathbf{M}(\alpha_1, \ldots, \alpha_i, \beta_1, \ldots, \beta_i, x_1, \ldots, x_i) = \begin{bmatrix} g_m(\alpha_1 \cdot x_1 + \beta_1) & \cdots & g_i(\alpha_i \cdot x_1 + \beta_i) \\ \vdots & & \vdots \\ g_m(\alpha_i \cdot x_i + \beta_1) & \cdots & g_i(\alpha_i \cdot x_1 + \beta_i) \end{bmatrix}_{N \times i}, \tag{9}$$

$$R = \begin{bmatrix} R_1^T \\ \vdots \\ R_i^T \end{bmatrix}, \tag{10}$$

$$T = \begin{bmatrix} t_1^T \\ \vdots \\ t_i^T \end{bmatrix}, \tag{11}$$

where $(\cdot)^T$ stands for the transposition operator and the sigmoid transfer function used in this study. Figure 2 illustrates the structure of ELM with a single hidden layer.

2.5. Random Forest (RF). RF is a machine learning approach often used to solve problems related to classification and regression. Basically, it is an extension of the method CART (classification and regression trees). Decision tree models generally have many advantages, such as simplicity, ease of use, and interpretability, but also many disadvantages, such as poor performance and unsatisfactory robustness. Therefore, RF can overcome the shortcomings of conventional decision trees by combining the performance of many randomised decorrelated decision trees to perform prediction or classification tasks efficiently. In addition, RF uses a modified version of the bootstrap aggregation approach, called bagging, in which a considerable collection of decorrelated, noisy, approximately unbiased trees is constructed and averaged to minimise model variance and instability problems [52]. The RF strategy involves aggregating multiple trees to improve overall prediction accuracy while achieving low variance and bias. Figure 3 shows RF as a forest of n trees.

RF is not only able to model high-dimensional, nonlinear relationships but is also resistant to overfitting, has relative robustness, estimates variable importance, and has few user-defined parameters [53]. The hyperparameters of the RF model strongly influence the performance of the models, so their values need to be determined precisely. The most critical hyperparameters are the number of regression trees, the proportion of the training dataset used to build the model, and the leaf nodes.

2.6. Feature Selection. Feature selection (FS) is a dimensionality technique used to eliminate the redundant and irreversible variables from the data set. This technique helps to use the minimum number of features that correctly describe a given problem in a given domain, resulting in more straightforward and accurate schemes. In machine learning, the tool FS is a fundamental concept that significantly impacts the performance of a prediction model. Machine learning models are highly influenced by the data features on

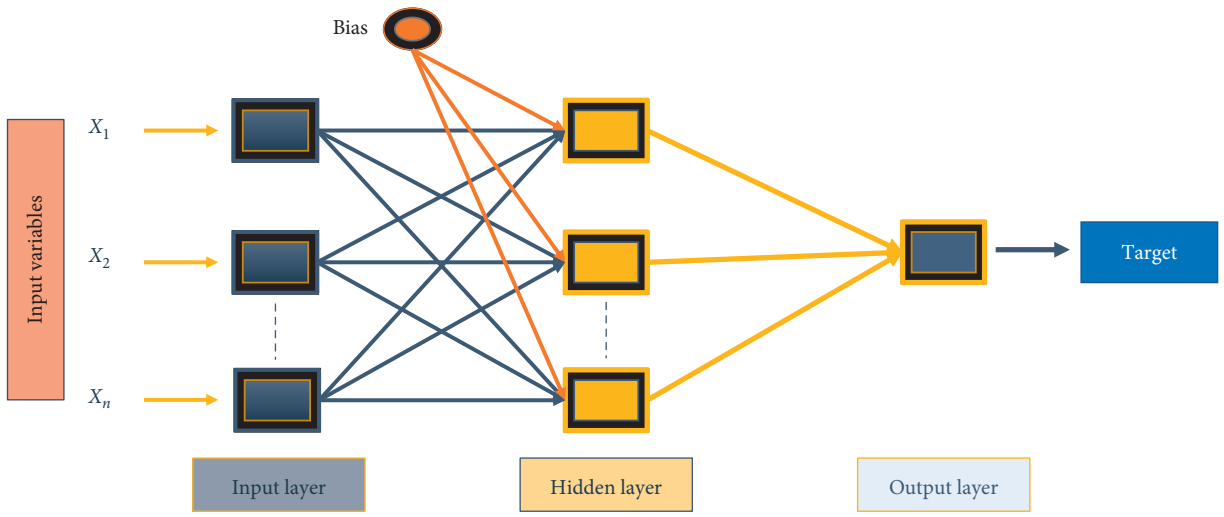

Figure 2: The basic ELM topology.

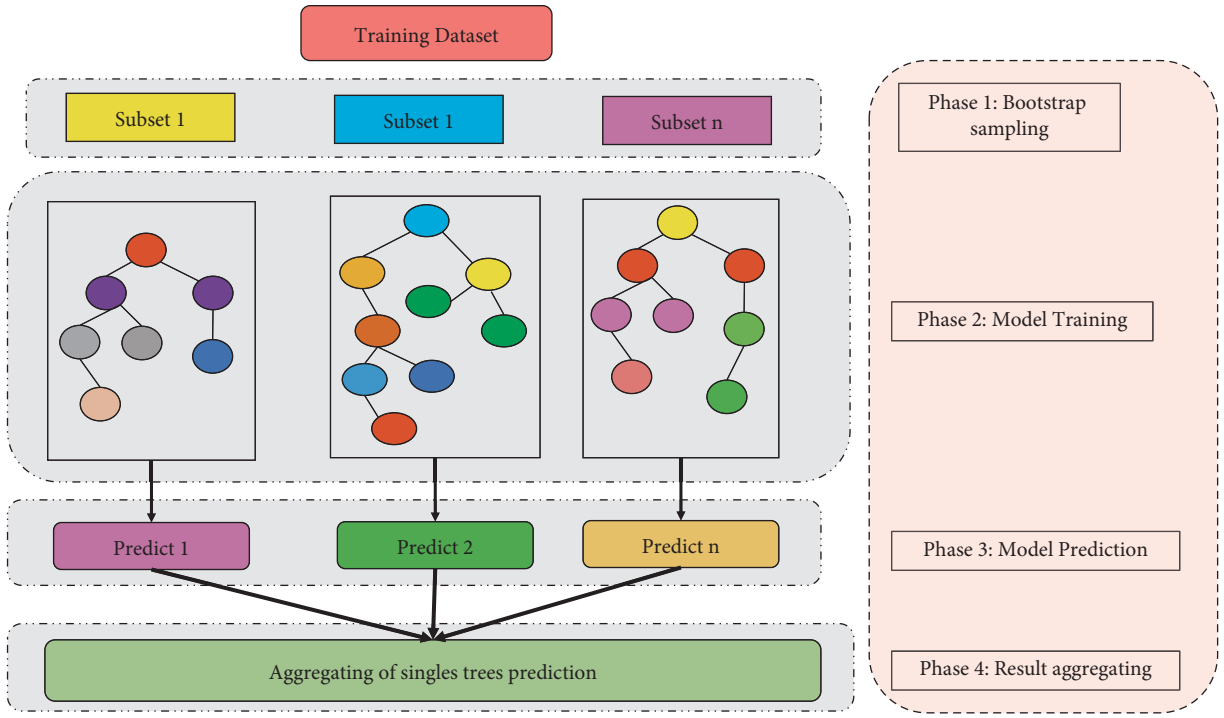

Figure 3: The basic structure of random forest (RF).

which they are trained. More specifically, the performance of a model can be affected by features that are not relevant or only partially relevant. The other advantages of using FS before training a prediction model can be summarised as follows:

(i) Overfitting is reduced by removing redundant data. When there is less redundant data, it is more challenging to make decisions based on noise data

(ii) Improves model accuracy: less misleading data means better modelling accuracy

(iii) Reduces training time: a smaller number of features reduces the algorithm's complexity and speeds up training

2.6.1. Information Theory. Information theory was introduced by Claude E. Shannon to study the quantitative aspects of information, including how coding affects information transmission [54]. Information theory originated as a mathematical study of whether it is possible to transmit information reliably and cheaply for a given source, channel, and fidelity criteria. Shannon's information theory defines information as anything that reduces or eliminates uncertainty. The model can achieve higher accuracy in classification tasks if it receives more information because the predicted classes of new instances are likely to match their actual classes [55]. Mutual information (MI) is defined in algorithmic information theory and has an "algorithmic" relationship. MI is a dimensionless quantity, usually

Algorithm : Selecting the best predictors by GA and mutual information.

Input: $I(Xh_n{}^{var}; Xh_m{}^{var})$ and $I(Xh_n{}^{var}; y_{target})$,

n = (1,…m): statistical data determined by the pervious algorithm;

N_{no} : desired number of predictors.

A = selective pressure.

G_{max}: maximum number of generations

N_P: population size.

Output: { j }: set the indexes of the selected predictors.

i. Generate a set with N_P chromosome $\{CR\}$ for the initial population. Each chromosome is a vector $CR = [j_1, j_2, \ldots j_{N_{no}}]$ including N_{no} neuron indexes j randomly generated without repeated elements.

ii. for generation =1 : G_{max} do

iii. Evaluating the population.

iv. for idx = 1 : N_P do

v. Calculating the V *and* P for for the individual CR using formula below , by the means of the calculated mutual information values for all elements of the chromosomes CR_{idx}

$$V = \frac{1}{N_{no}} \sum_{i=1}^{N_{no}} I(Xh_i; y)$$

$$P = \frac{1}{N_{no}{}^2} \sum_{i=1}^{N_{no}} \sum_{k=1}^{N_{no}} I(Xh_i; y_K)$$

Figure 4: The information theory algorithm

expressed in bits, and can be viewed as a means of reducing uncertainty about one random variable given knowledge of another. The MI between two random variables indicates how much uncertainty has been reduced. The lower the mutual information, the greater the reduction, and zero means that the variables are strictly independent [56]. Figure 4 shows the structure of information theory.

2.6.2. Genetic Algorithm. The genetic algorithm (GA) is one of the most widely used metaheuristic algorithms, a stochastic optimisation technique inspired by natural evolution [57]. Crossing and mutating chromosomes are an essential part of the GA process. Each chromosome acts as an individual solution to the target problem, which is ultimately expressed in a binary string. The chromosome population is essential in the GA process, and its initial values are randomly selected. Then, a chromosome (the best one) that solves the given problem very well is selected for reproduction [58]. The optimisation process of GA consists of six steps: initialisation, fitness calculation (objective function), conditional termination, selection, crossover, and mutation. The detailed process of GA is shown in Figure 5. In addition, only chromosomes that function perfectly are retained for further reproduction during the fitness evaluation step. The process of selection and reproduction is repeated several times to obtain better chromosomes. After selecting the best chromosomes, these chromosomes can produce offspring during the crossover process by exchanging string parts and gene combinations, resulting in a new solution. A

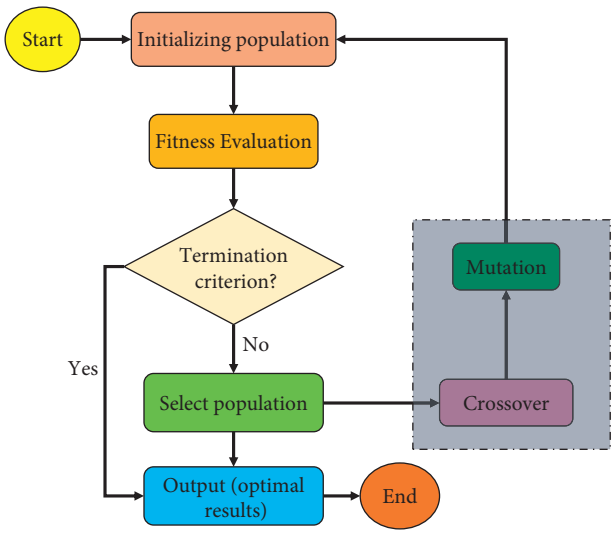

Figure 5: The basic structure of GA.

chromosome is nominated to change a randomly selected bit through a random exchange during the mutation process. The following step is to estimate the generated fitness and compare it with the termination criteria. The GA process is terminated when the termination criteria are met.

2.6.3. Genetic Algorithm-Based Information Theory. Information theory is generally used for input variable selection. Variable selection attempts to maximise the mutual

Input: $I\ (Xh_n{}^{\text{var}}; Xh_m{}^{\text{var}})$ and $I\ (Xh_n{}^{\text{var}}; y_{t\text{arget}})$
$n = (1, \ldots, m)$: statistical data determined by the previous algorithm (Figure 4);
N_{no}: the desired number of predictors;
A: selection pressure;
G_{max}: maximum number of generations;
N_P: size of the population; and
Output: $\{j\}$ set the indexes of the selected predictors.

(i) Generate a set of N_P chromosome {CR} for the initial population. Each chromosome is a vector $\text{CR} = [j_1, j_2, \ldots j_{N_{\text{no}}}]$ containing the indices of N_{no} neuron j generated randomly without repeating elements.
(ii) **For** generation = 1: G_{max}, **do**
(iii) Evaluate the population.
(iv) **For** $idx = 1$: N_P, **do**
(v) Calculate V and P for each CR using the following formula by the calculated values of mutual information for all elements of chromosomes $\text{CR}_{i\ dx}$.
$V = (1/N_{\text{no}}) \sum_{i=1}^{N_{\text{no}}} I(Xh_i; y)$
$P = (1/N_{\text{no}}{}^2) \sum_{i=1}^{N_{\text{no}}} \sum_{k=1}^{N_{\text{no}}} I(Xh_i; y_K)$
(vi) $\phi_{i\ dx} \leftarrow (V - P)$: storing the fitness of each idx;
(vii) **end for** (loop).
(viii) Rank the individuals according to their fitness $\phi_{i\ dx}$.
(ix) Store the genes of the best individual into $\{j\}$.
(x) Perform the crossover
(xi) $k \leftarrow 0$.
(xii) **For** $idx = 1$: N_{no}, **do**
(xiii) $k \leftarrow k + 1$.
(xiv) Choose the indices of the parents randomly using the asymmetric distribution [60].
(xv) $\omega_{j,i} = (1, 2) \leftarrow$ random number $\in\in [0, 1]$ with uniform distribution
(xvi) $\text{parent}_j, i = (1, 2) \leftarrow \text{round}\,(N_P\,(e^{a\omega_j} - 1)/(e^a - 1))$ [60];
(xvii) Storing the indices missing in both parents in $\{j_{\text{abse}}\}$.
(xviii) **Assembling the chromosome** CR_k^{son}.
(xix) **For** $n = 1$: N_{no}, **do**
(xx) Randomly select a parent (i.e., between parent 1 and 2) to get the n^{th} gene for the k^{th} of the individual in the new generation.
(xxi) $\text{CR}_{k,n}^{\text{son}} \leftarrow \text{CR}_{(\text{parent 1 or 2},n)}$
(xxii) Considering the constraint [40],
(xxiii) **If** there is duplicity of indices in CR_k^{son}, **then**
(xxiv) Pick up a new index for $\text{CR}_{k,n}^{\text{son}}$ from $\{j_{\text{abse}}\}$.
(xxv) **end if**
(xxvi) **end for**
(xxvii) **end for**
(xxviii) **end for**.

Algorithm 1: Selection of the best predictors by GA and mutual information.

information of input and output data, either directly or indirectly. However, this procedure is computationally intensive, as the joint probability distributions must be estimated in order to calculate the joint entropy. These computational costs can be avoided by selecting variables according to the minimum redundancy/maximum relevance principle, which maximises the mutual information indirectly and at a low cost. However, the problem of combinatorial optimisation, where all combinations of variables are examined, still requires a high computational cost. Due to this computational cost, some previous works have proposed a simple incremental algorithm to obtain a near-optimal solution. Since existing methods are limited, Clark [59] proposed a code that uses genetic algorithms for combinatorial optimisation. The arguments are the desired number of features (feat_numb), the matrix X in which each column is an example of a feature vector, and the target data Y which is a row vector. The output is a vector of feature indices that make up the optimal feature, where there is no relationship between the order and the importance of the feature set. The full details of this algorithm are provided (see Algorithm 1).

2.7. Model Development and Performance Evaluation. In this study, two scenarios are created to develop more reliable models to predict the shear strength values of the deep beams. Both scenarios are created using a dataset containing geometric parameters, steel, and concrete properties. Table 2 shows the statistical description of each parameter. The data set is divided into two groups: the training phase comprises two-thirds of the data, while the rest is used to test the accuracy of the models. All the input and output variables are normalised (between 0 and 1) to remove the influence of dimensions and improve the capabilities of the predicting models [61]. This method prevents numerical difficulties

Table 2: The statistical description of the input parameters used in this study.

Category	Variable	Unit	Max.	Mean	Min.	STD	IQR
Geometrical parameters	b	mm	305.000	122.810	76.000	44.244	30.000
	h	mm	915.000	523.476	254.000	147.671	160.000
	a	mm	1290.000	467.734	125.000	238.306	356.000
	h_o	mm	844.000	469.014	216.000	145.175	140.000
	l_o	mm	4065.000	1484.450	500.000	642.367	1100.000
	a/h_o	Non	2.700	1.063	0.220	0.518	0.960
	$l_{o/}h$	Non	5.000	2.925	0.910	1.064	1.570
Vertical web reinforcement	S_v	mm	457.500	154.679	0.000	122.820	165.100
	fy_v	MPa	586.000	292.920	0.000	175.846	227.400
	ρ_v	%	2.450	0.351	0.000	0.407	0.360
Horizontal web reinforcement	S_h	mm	801.000	67.816	0.000	96.034	101.250
	fy_h	MPa	586.000	213.697	0.000	207.344	437.400
	ρ_h	%	2.450	0.299	0.000	0.419	0.450
Longitudinal reinforcement	fy_l	MPa	504.800	361.755	210.000	86.698	131.000
	ρ_l	%	4.080	1.620	0.120	0.713	0.700
Concrete property	f'_c	MPa	73.600	30.891	12.260	14.830	23.350
Shear strength capacity	V_u	kN	1357.000	287.197	67.620	180.332	182.590

Table 3: The determination of the best input combination using the ITH-GA tool.

Combinations	Absent variable (s)	Models
$M1$	f_y	GAITH – ELM_{M1} GAITH – RF_{M1} GAITH – MLR_{M1} GAITH – $LWLR_{M1}$
$M2$	h_o, f_y	GAITH – ELM_{M2} GAITH – RF_{M2} GAITH – MLR_{M2} GAITH – $LWLR_{M2}$
$M3$	h_o, $f_{y,v}$, f_y	GAITH – ELM_{M3} GAITH – RF_{M3} GAITH – MLR_{M3} GAITH – $LWLR_{M3}$
$M4$	h_o, l_o/h, $f_{y,v}$, f_y	GAITH – ELM_{M4} GAITH – RF_{M4} GAITH – MLR_{M4} GAITH – $LWLR_{M4}$
$M5$	b, h_o, l_o/h, $f_{y,v}$, f_y	GAITH – ELM_{M5} GAITH – RF_{M5} GAITH – MLR_{M5} GAITH – $LWLR_{M5}$

from forming numerical attributes with more extensive ranges from dominating smaller ones. In this study, several scenarios are developed to estimate the shear strength of deep beams. The first scenario is created using standard models such as LWLR, MLR, RF, and ELM. However, the second scenario of this study involves the use of feature selection to choose the most optimal input combination by removing the variables that contain redundant information. However, the results of both scenarios are evaluated using various statistical measures such as coefficient of determination (R^2), Nash-Sutcliffe (NSE), Willmott index (WI), mean absolute error (MAE), uncertainty interval (U_{95}), and root mean square error (RMSE). In addition, various visualisations such as Taylor diagrams, scatter plots, line plots, and bar charts are produced to provide more information about the best prediction model and to allow better comparison between the models used. The mathematical expressions of the statistical matrices are explained as follows [62, 63]:

$$RMSE = \sqrt{\frac{1}{N}\sum_{i=1}^{N}\left(Yobs_i - Ypred_i\right)^2}, \tag{12}$$

$$MAE = \frac{1}{N}\sum_{i=1}^{N}\left|\left(Yobs_i - Ypred_i\right)\right|, \tag{13}$$

$$R^2 = 1 - \frac{\sum_{i=1}^{N}\left(Yobs_i - Ypred_i\right)^2}{\sum_{i=1}^{N}\left(Ypred_i - \mu\right)}, \tag{14}$$

$$\mathrm{WI} = 1 - \frac{\sum_{\mathrm{i=1}}^{\mathrm{n}}\left(Yobs_i - Ypred_i\right)^2}{\sum_{\mathrm{r=1}}^{\mathrm{n}}\left(\left|Ypred_i - \mu\right| + \left|Yobs_i - \mu\right|\right)^2}, \tag{15}$$

$$\mathrm{NSE} = 1 - \frac{1/\mathrm{n}\sum_{\mathrm{i=1}}^{\mathrm{n}}\left|Yobs_i - Ypred_i\right|}{\sum_{i=1}^{n}\left(Ypred_i - \mu\right)^2}, \tag{16}$$

$$U_{95} = \frac{1.96}{n}\sqrt{\sum_{i=1}^{n}\left(Yobs_i - \alpha\right)^2 + \sum_{i=1}^{n}\left(Yobs_i - Ypred_i\right)^2}, \tag{17}$$

where $Yobs_i - Ypred_i$ is the measured and predicted shear strength value of the i^{th} sample, M is the number of samples, and μ, α is the mean predicted and observed shear strength values.

3. Result and Discussion

In this part of the study, the results of four prediction models for predicting the ultimate shear strength of deep beams are presented. In this work, two scenarios are created to achieve

Table 4: The statistical description of the proposed models: first scenario.

Model	Training phase				Testing phase			
	MAE (kN)	RMSE (kN)	NSE	WI	MAE	RMSE (kN)	NSE	WI
LWLR	13.249	22.563	0.974	0.993	33.933	57.776	0.941	0.984
RF	18.138	28.613	0.958	0.988	49.068	77.712	0.892	0.964
MLR	36.924	48.692	0.879	0.967	61.165	89.651	0.857	0.953
ELM	23.194	31.045	0.951	0.987	51.999	78.200	0.891	0.968

Table 5: A comparison between the efficiency of the proposed models.

Model	Distribution of data in terms of relative error for each model							
	Training phase				Testing phase			
	5%	10%	15%	20%	5%	10%	15%	20%
LWLR	62.78	87.78	95.56	98.89	31.96	60.04	75.00	85.87
RF	54.44	80.00	90.00	92.22	22.83	45.65	65.22	75.00
MLR	22.22	43.33	60.56	72.78	17.39	30.43	47.83	59.78
ELM	35.56	61.67	82.22	90.56	18.48	48.91	58.70	68.48

Table 6: A comparison of the performance outcomes for the uncertainty (U_{95}) analysis.

Combination	Models			
	LWLR	RF	MLR	ELM
*M*1	21.83	22.48	23.07	22.22
*M*2	19.73	22.33	23.04	22.27
*M*3	21.77	22.99	23.06	22.21
*M*4	20.62	20.79	21.89	20.69
*M*5	23.38	22.70	24.48	23.00
Without feature selection tool (all inputs)	21.87	22.23	22.76	22.27

the objective of this work. In the first scenario, all the models used are presented based on all the available input variables. Furthermore, in this scenario, four standard prediction models have been developed to predict the shear strength capacity of reinforced concrete deep beams with and without web reinforcement. The models are extreme learning machine (ELM), random forest (RF), multiple linear regression (MLR), and locally weighted linear regression (LWLR). The second scenario is created using assumed feature selection (FS) to select the most impressive input variables. Then, these variables are introduced into the prediction models to estimate the ultimate shear capacity of the deep bars. In this case, five input combinations are created based on the assumed FS (see Table 3). The main purpose of using GAITH as a feature selection tool is to remove the repetitive information from the dataset and thus improve the prediction accuracy. Finally, to evaluate the performance of the adopted models, we used various statistical parameters, including error measures and accuracy indices, as well as a graphical representation. According to the error measures, the proposed model (LWLR) of this study yielded lower prediction errors than comparable models (MAE = 13.249, RMSE = 22.563, NSE = 0.974, WI = 0.993). From this table, it can be inferred that the LWLR model provided more accurate estimates on all statistical measures, followed by the RF, ELM, and MLR models.

3.1. First Scenario: Standard Models. This part of the study looks at the performance results obtained with the standard models using all input parameters. The performances of the models used, such as extreme learning machine (ELM), random forest (RF), multiple linear regression (MLR), and locally weighted linear regression (LWLR) during the training and testing phases, are presented in Table 4. In general, all the models used performed well in the training set, yielding high values for NSE and WI. In this phase, WI ranged between 0.967 and 0.993, while NSE varied between 0.879 and 0.974. From these parameters, it can be seen that the LWLR model performed better than the other models, while the MLR model had lower prediction accuracy.

To select the best model, the higher performance of this model in the training phase is not sufficient because, in this step, the model receives input variables and their corresponding target. However, the testing phase is crucial and more reliable to assess the performance of a model. According to the results shown in Table 4, the LWLR model provided higher and desired accuracy in predicting the shear strength capacity compared to other models. This model achieved a higher agreement with the actual values with WI of 0.984, NSE of 0.941, and less prediction error (MAE = 33.933, RMSE = 57.776). However, the MLR model performed very poorly and therefore provided undesirable estimation accuracy (MAE = 61.165, RMSE = 89.651,

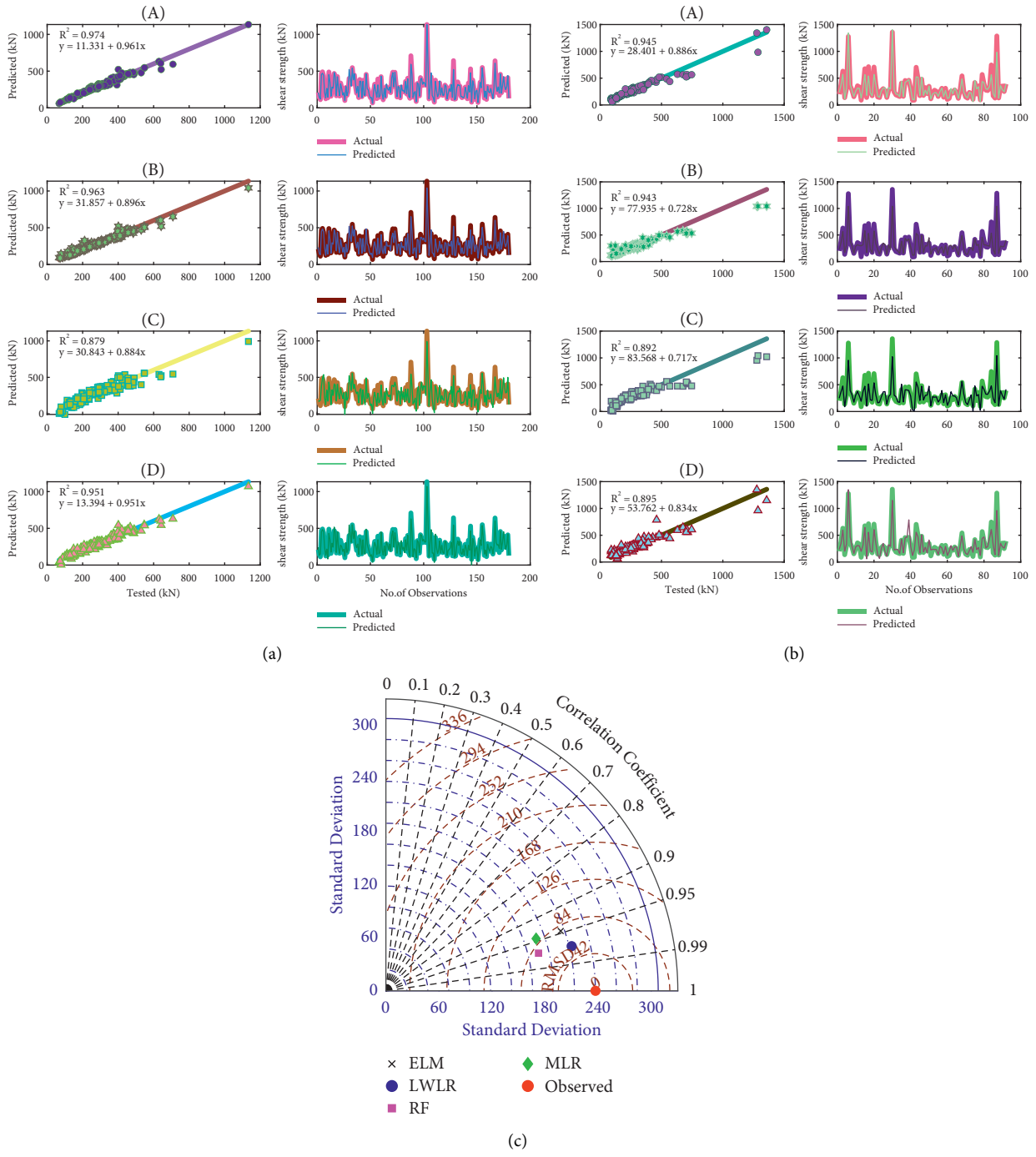

FIGURE 6: A comparison between the objectives of the models: (A)–(D) represent the LWLR, RF, MLR, and ELM models, respectively. Figures (a) and (b) show scatter plots and line plots for the training and test data, respectively, while figure (c) is a Taylor plot based on the test data. (a) Training data. (b) Testing data. (c) Taylor diagram.

NSE = 0.857, WI = 0.953). The other important observation can be drawn from the same table (Table 4): RF and ELM performed well compared to the MLR model and provided lower prediction accuracy than the LWLR model. However, the RF model provided a slightly better prediction than ELM with an RMSE of 77.712, MAE of 49.068, WI of 0.964, and an NSE of 0.892. Furthermore, ELM is considered the third best model and provides much better estimates of shear strength capacity than the MLR model (MAE = 51.999, RMSE = 78.22, NSE = 0.891, WI = 0.968). After quantitative evaluation, the superiority of the LWLR model is determined by its ability to reduce the RMSE criteria during the test phase. Specifically, the results showed a 34.51%, 55.17%, and 35.35% improvement in estimation by the LWLR model compared to the RF, MLR, and ELM models, respectively.

Table 5 evaluates the performance of the adopted models in terms of their efficiency in reducing the absolute relative error. According to the reported results, the LWLR model

Table 7: The statistical description of the proposed models using GAITH.

Model	Training phase				Testing phase			
	MAE (kN)	RMSE (kN)	NSE	WI	MAE (kN)	RMSE (kN)	NSE	WI
GAITH – $LWLR_{M1}$	7.934	17.599	0.984	0.996	37.052	58.095	0.940	0.985
GAITH – RF_{M1}	16.656	30.707	0.952	0.987	48.841	90.397	0.854	0.949
GAITH – MLR_{M1}	37.119	51.348	0.865	0.963	63.395	102.509	0.813	0.934
GAITH – ELM_{M1}	25.233	33.696	0.942	0.985	48.096	73.227	0.904	0.972
GAITH – $LWLR_{M2}$	7.277	17.217	0.985	0.996	33.617	49.519	0.956	0.988
GAITH – RF_{M2}	16.683	28.597	0.958	0.988	47.823	83.513	0.876	0.957
GAITH – MLR_{M2}	37.201	51.366	0.865	0.963	62.842	101.058	0.818	0.937
GAITH – ELM_{M2}	20.898	28.153	0.959	0.990	54.135	80.528	0.884	0.966
GAITH – $LWLR_{M3}$	8.985	18.180	0.983	0.996	34.583	52.704	0.951	0.986
GAITH – RF_{M3}	17.898	35.099	0.937	0.981	55.390	111.414	0.779	0.914
GAITH – MLR_{M3}	37.641	51.961	0.862	0.962	62.530	101.179	0.818	0.936
GAITH – ELM_{M3}	22.415	30.417	0.953	0.988	50.890	75.503	0.898	0.969
GAITH – $LWLR_{M4}$	11.650	20.318	0.979	0.995	35.284	59.671	0.937	0.981
GAITH – RF_{M4}	17.444	27.220	0.962	0.990	43.132	69.895	0.913	0.972
GAITH – MLR_{M4}	38.457	54.231	0.849	0.958	66.434	115.355	0.763	0.911
GAITH – ELM_{M4}	15.754	23.483	0.972	0.993	47.852	70.912	0.910	0.975
GAITH – $LWLR_{M5}$	37.165	49.937	0.872	0.963	62.673	117.293	0.755	0.907
GAITH – RF_{M5}	20.321	35.994	0.934	0.981	59.634	97.587	0.830	0.938
GAITH – MLR_{M5}	50.638	71.069	0.741	0.919	76.135	140.787	0.647	0.851
GAITH – ELM_{M5}	22.061	30.406	0.953	0.988	59.217	114.584	0.766	0.923

Table 8: A comparison between the suggested models' efficiency in the presence of GAITH.

Model	Distribution of data in terms of relative error for each model							
	Training phase				Testing phase			
	5%	10%	15%	20%	5%	10%	15%	20%
GAITH – $LWLR_{M1}$	81.67	95.00	96.67	99.44	32.61	57.61	72.83	83.70
GAITH – RF_{M1}	63.33	77.78	89.44	93.89	31.52	46.74	63.04	71.74
GAITH – MLR_{M1}	26.67	45.56	61.11	70.56	19.57	38.04	50.00	61.96
GAITH – ELM_{M1}	33.89	60.56	77.22	86.67	20.65	44.57	60.87	70.65
GAITH – $LWLR_{M2}$	82.22	95.56	97.22	99.44	33.70	62.78	77.91	86.78
GAITH – RF_{M2}	60.56	82.78	91.67	93.89	27.17	53.26	65.22	75.00
GAITH – MLR_{M2}	25.56	45.00	61.67	70.56	19.57	38.04	52.17	61.96
GAITH – ELM_{M2}	37.22	65.00	82.22	92.22	21.74	43.48	60.87	71.74
GAITH – $LWLR_{M3}$	80.56	93.89	97.78	99.44	30.43	60.87	77.17	85.87
GAITH – RF_{M3}	61.11	83.89	90.00	92.22	28.26	50.00	61.96	73.91
GAITH – MLR_{M3}	27.22	45.56	60.00	71.67	21.74	39.13	48.91	63.04
GAITH – ELM_{M3}	35.56	65.56	84.44	91.67	21.74	36.96	57.61	71.74
GAITH – $LWLR_{M4}$	66.67	91.11	97.22	98.89	33.70	60.87	78.26	85.87
GAITH – RF_{M4}	55.56	78.89	89.44	92.78	29.35	51.09	67.39	75.00
GAITH – MLR_{M4}	25.00	41.11	61.11	72.78	18.48	40.22	51.09	63.04
GAITH – ELM_{M4}	51.67	81.67	92.78	97.22	22.83	48.91	66.30	72.83
GAITH – $LWLR_{M5}$	23.33	42.22	61.67	75.00	16.30	39.13	52.17	68.48
GAITH – RF_{M5}	57.22	74.44	85.00	90.56	18.48	35.87	54.35	64.13
GAITH – MLR_{M5}	16.11	33.33	43.33	56.11	14.13	29.35	42.39	57.61
GAITH – ELM_{M5}	36.67	65.56	83.33	92.22	22.83	42.39	59.78	71.74

performed excellently in the test series. 85.87% of the data had an absolute relative error of less than 20%. The percentage of data that had an absolute relative error of less than 20% was 75%, 59.78%, and 68.48% for RF, MLR, and ELM, respectively.

A more comprehensive statistical analysis can be seen in Table 6. The primary purpose of uncertainty analysis is to restrict the predicted range in which the actual value of an experiment's outcome lies. The uncertainty interval describes the estimated range as an interval in this context. The results provided in that table showed that the LWLR-M2 model had the lowest value for uncertainty with a 95% confidence level (U95 = 19.73).

Visualisation assessment is critical to see how each model handles a single sample. Scatter plots and line plots provide essential information about the behaviour of a model and show the deviation between the actual and predicted values of shear strength (see Figures 6(a) and 6(b)).

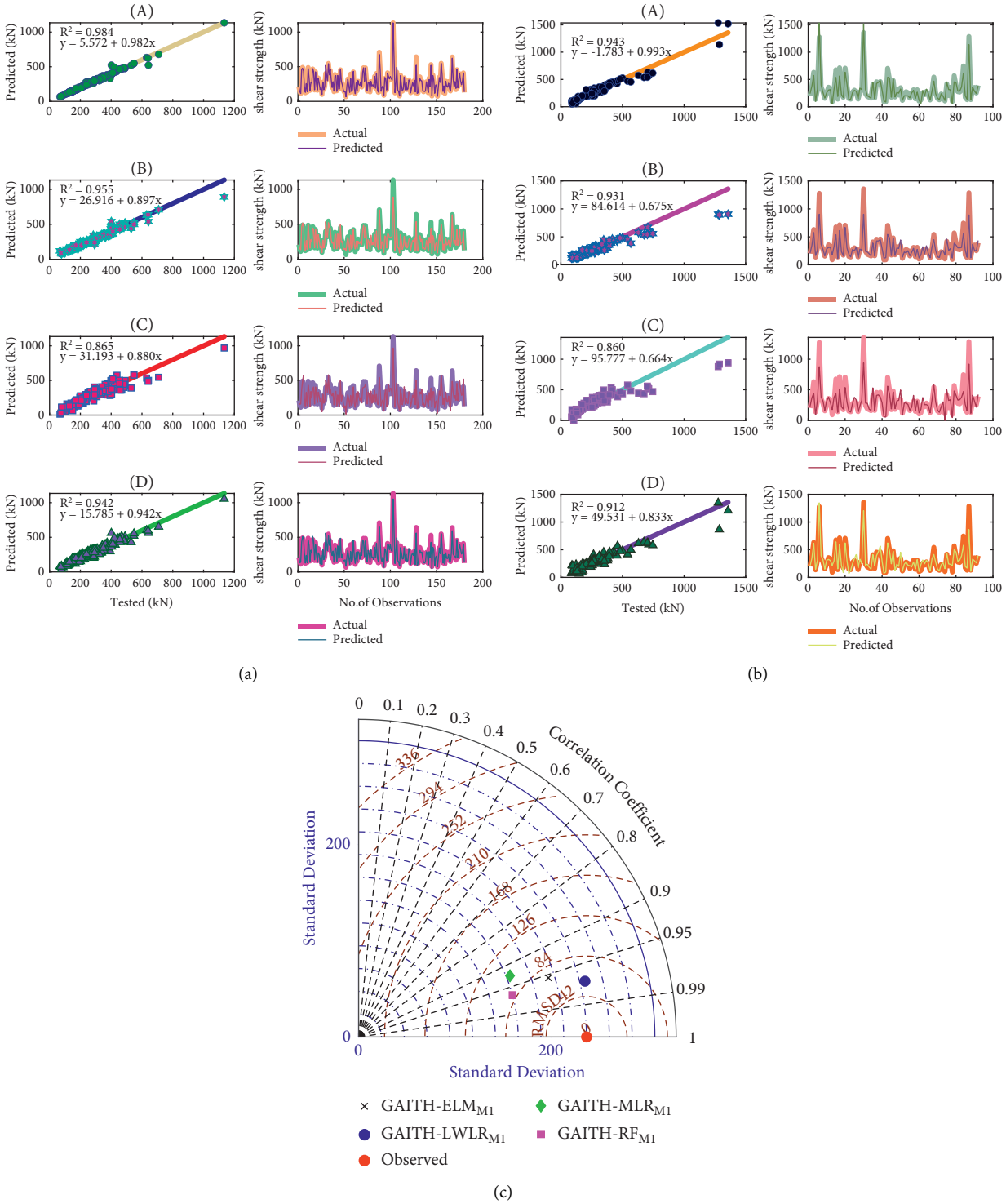

FIGURE 7: A comparison between the objectives of the models: (A)–(D) represent the GAITH – LWLR$_{M1}$, GAITH – RF$_{M1}$, GAITH – MLR$_{M1}$, and GAITH – ELM$_{M1}$ models, respectively. Figures (a) and (b) show scatter plots and line plots for the training and test data, respectively, while figure (c) is a Taylor plot based on the test data. (a) Training data. (b) Testing data. (c) Taylor diagram.

Figure 6 shows that the performance of all models generally gives a satisfactory prediction. However, the testing phase was crucial, and some models gave poor predictions. It is important to note that the model proposed in this study (LWLR) was superior to the others in estimating the shear strength capacity with the highest accuracy (R^2 = 0.945). The RF models showed good prediction accuracy with R^2 = 0.943, followed by the ELM model with R^2 = 0.895 and the MLR model (R^2 = 0.892). Another important observation is that the LWLR model showed an excellent ability to predict extreme values compared to the other models. Moreover, all the proposed models except the LWLR model showed that

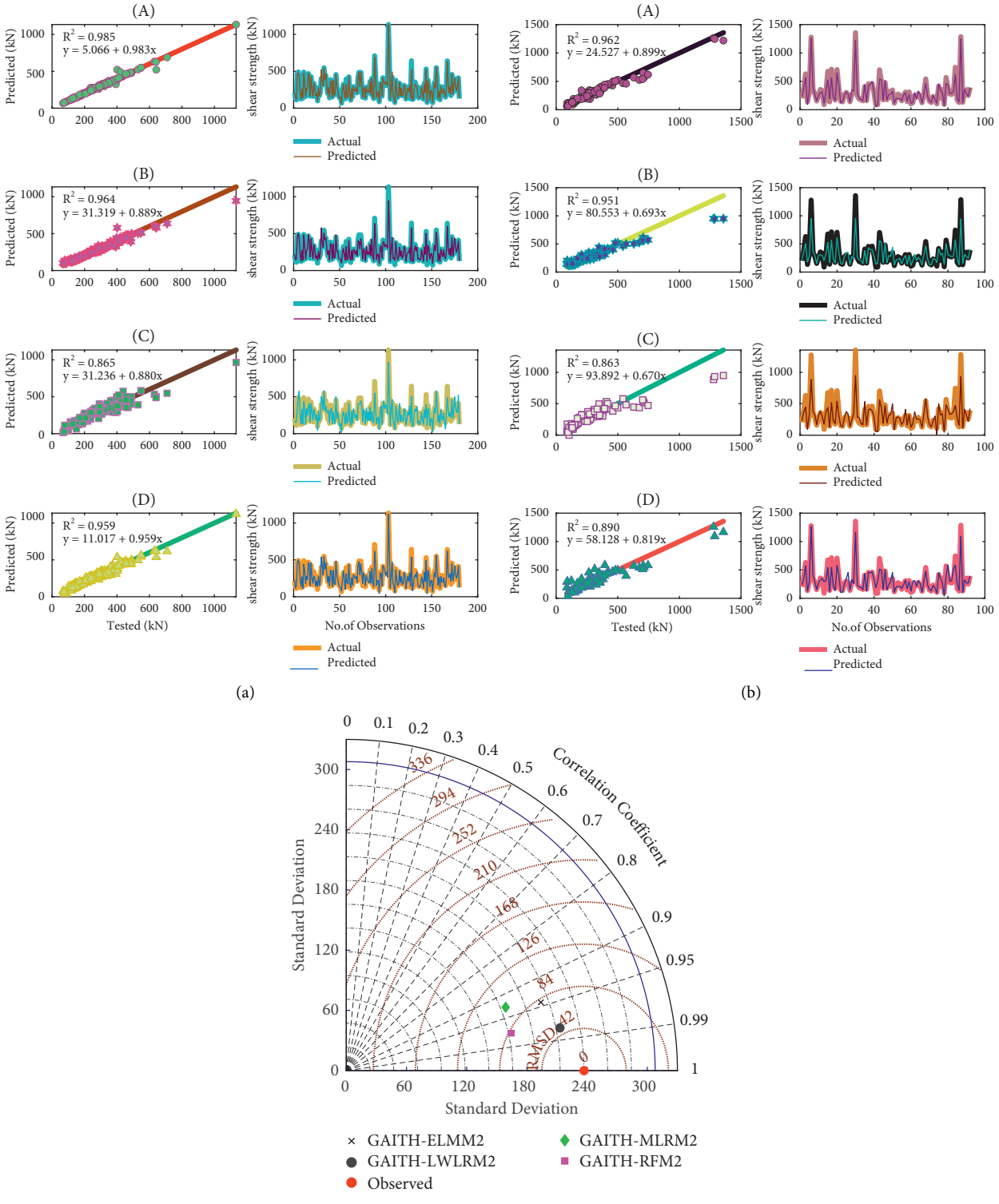

FIGURE 8: A comparison between the objectives of the models: (A)–(D) represent the GAITH – LWLR$_{M2}$, GAITH – RF$_{M2}$, GAITH – MLR$_{M2}$, and GAITH – ELM$_{M2}$ models, respectively. Figures (a) and (b) show scatter plots and line plots for the training and test data, respectively, while figure (c) is a Taylor plot based on the test data. (a) Training data. (b) Testing data. (c) Taylor diagram.

several predicted samples are far from the ideal line. The Tayler diagram is one of the most important figures for visually assessing the performance of a particular prediction model. This figure summarises three important statistical criteria: root mean square error (RMSE), standard deviation, and correlation coefficient. Figure 6(c) shows that the LWLR model is close to the actual data set compared to the other models. It has the highest correlation coefficient, the lowest

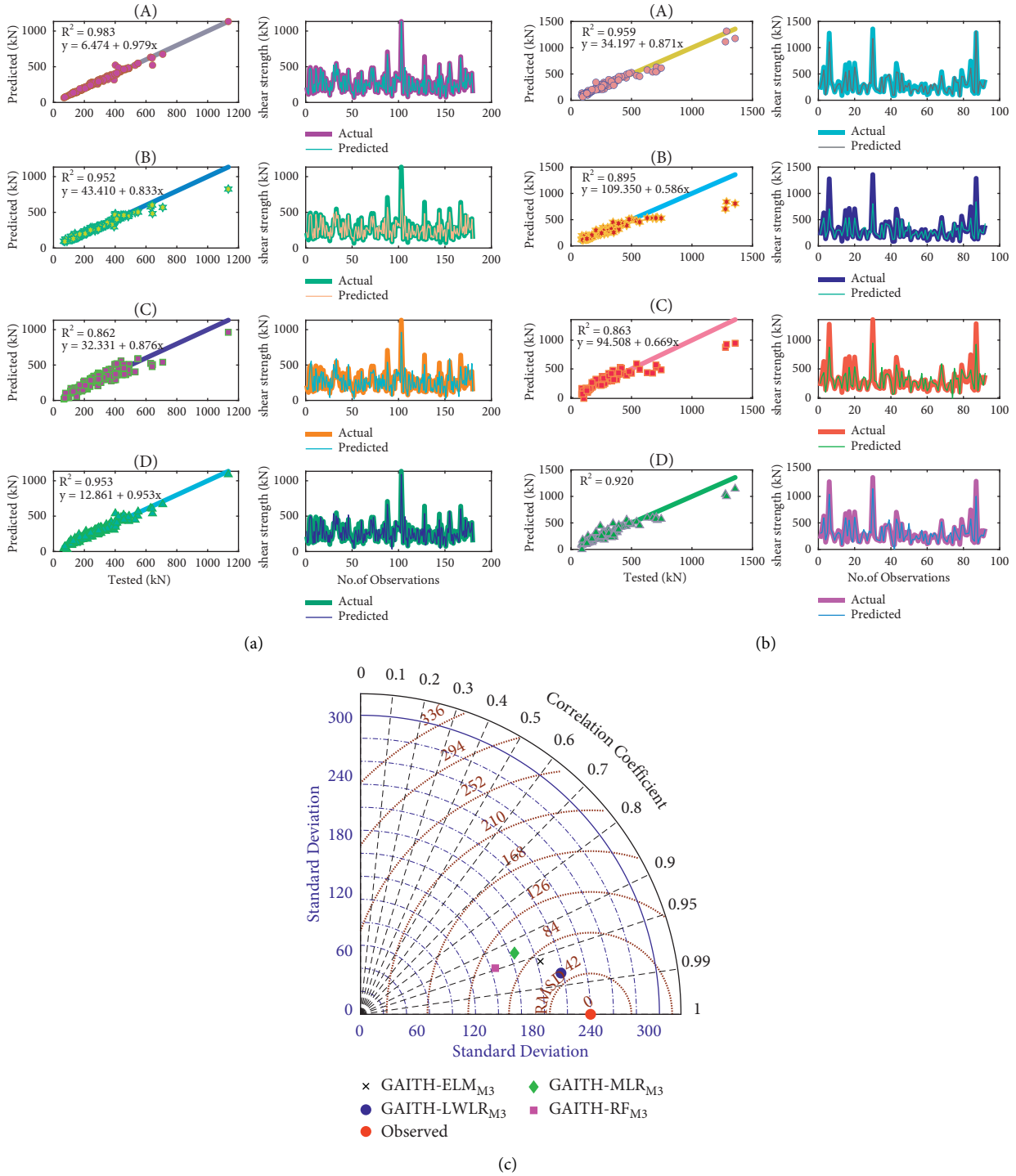

FIGURE 9: A comparison between the objectives of the models: (A)–(D) represent the GAITH – LWLR$_{M3}$, GAITH – RF$_{M3}$, GAITH – MLR$_{M3}$, and GAITH – ELM$_{M3}$ models, respectively. Figures (a) and (b) show scatter plots and line plots for the training and test data, respectively, while figure (c) is a Taylor plot based on the test data. (a) Training data. (b) Testing data. (c) Taylor diagram.

RMSE, and a lower standard deviation than the observed data set.

3.2. Second Scenario: Selection of Features Based on Prediction Models. This section focuses on using GAITH, a feature selection tool based on a mixture of information theory and genetic algorithms. The main advantage of using GAITH is to select the most efficient input variables that have the most significant impact on shear strength capacity and to minimise redundant information between variables. As mentioned earlier, five input combinations were selected using the GAITH algorithm. Table 7 summarises the performance of the models used based on GAITH. From Table 7, it can be

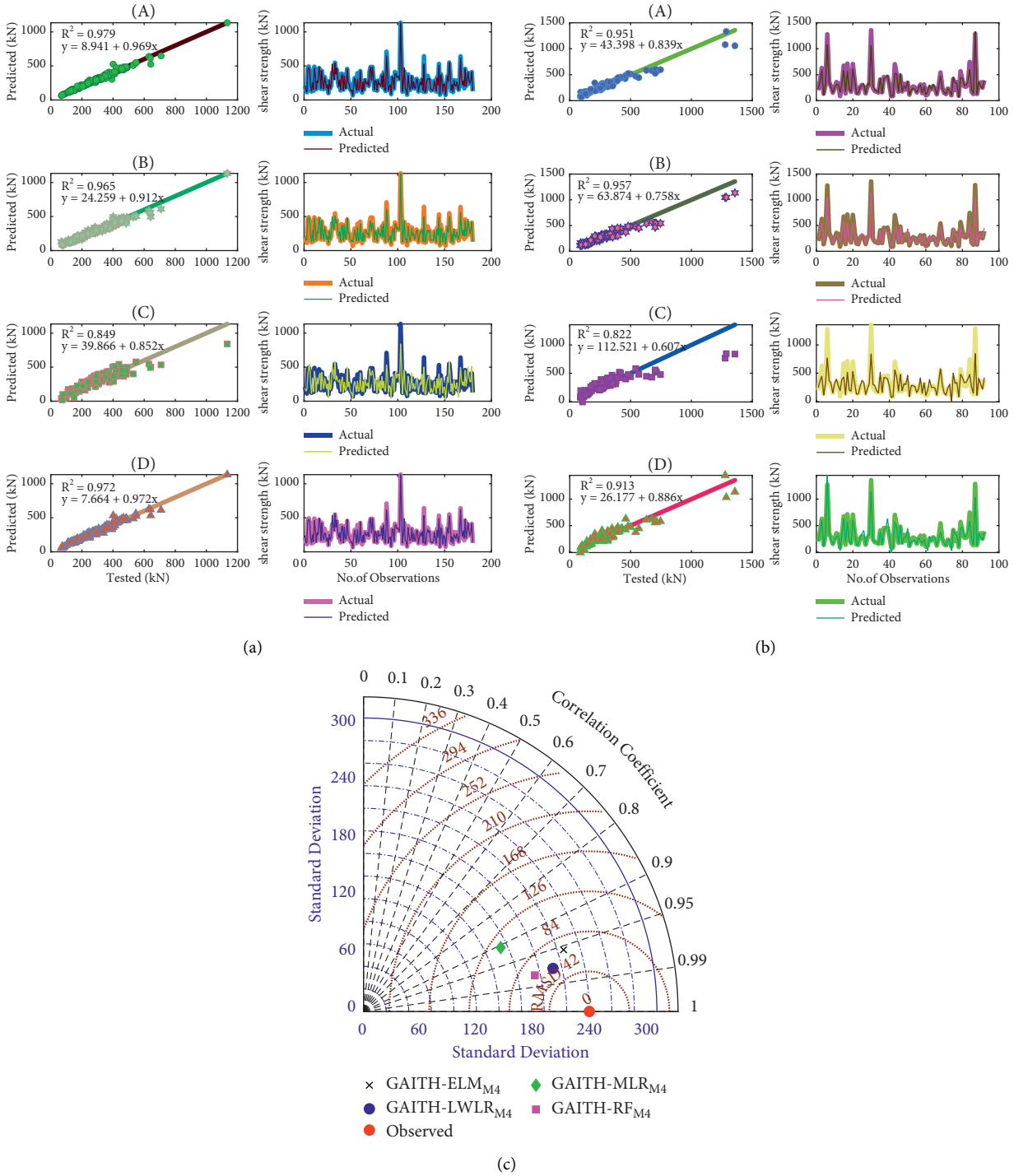

Figure 10: A comparison between the objectives of the models: (A)–(D) represent the GLWLR$_{M4}$, GAITH – RF$_{M4}$, GAITH – MLR$_{M4}$, and GAITH – ELM$_{M4}$ models, respectively. Figures (a) and (b) show scatter plots and line plots for the training and test data, respectively, while figure (c) is a Taylor plot based on the test data. (a) Training data. (b) Testing data. (c) Taylor diagram.

seen that the GAITH-based LWLR model (GAITH – LWLR$_{M2}$) showed excellent performance in predicting shear strength capacity over comparable models in the training and testing phases. For example, GAITH – LWLR$_{M2}$ gave the lowest measured error (RMSE = 49.519, MAE = 33.617) and higher prediction accuracy (NSE = 0.954 and WI = 0.988). Based on the evaluations shown in this table, the RF model with the m4 combination gave a good estimate (RMSE = 69.895, MAE = 43.132, NSE = 0.913, and WI = 0.972) but relatively lower than that of the LWLR model. However, the MLR model is found to provide the worst estimates as it could not account for the nonlinear relationship between the shear strength capacity and the geometric and concrete and steel properties. On the other

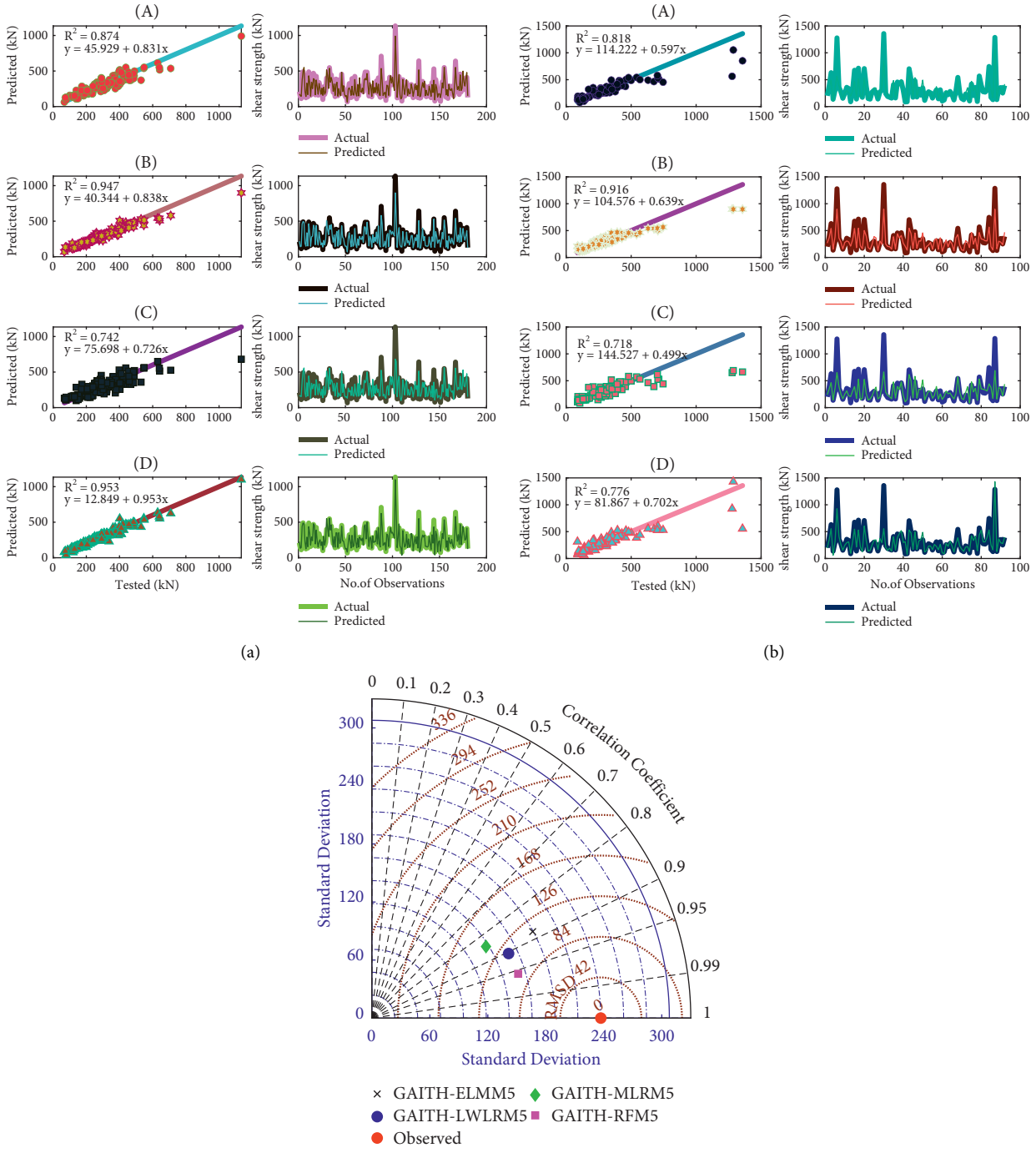

FIGURE 11: A comparison between the objectives of the models: (A)–(D) represent the GLWLR$_{M4}$, GAITH − RF$_{M4}$, GAITH − MLR$_{M4}$, and GAITH − ELM$_{M4}$ models, respectively. Figures (a) and (b) show scatter plots and line plots for the training and test data, respectively, while figure (c) is a Taylor plot based on the test data. (a) Training data. (b) Testing data. (c) Taylor diagram.

hand, ELM proved to be much better than MLR for the first combination (m1) and provided good prediction accuracy (RMSE = 58.095, MAE = 37.052, NSE = 0.940, WI = 0.98), which was, however, slightly lower than that of the RF model. For further evaluation, the cumulative percentage of absolute relative error was calculated and summarised in Table 8. The main result is that the proposed model (LWLR) produced a large percentage of data with less than the absolute relative benchmark error in each input combination (i.e., 5%, 10%, 15%, and 20%). For the M2 combination, the proposed model (GAITH − LWLR$_{M2}$) showed efficient performance, and 86.78% of the data set had an absolute relative error of less than 20%. Moreover, for the combination *m*4, the table shows that more than 78% of the shear

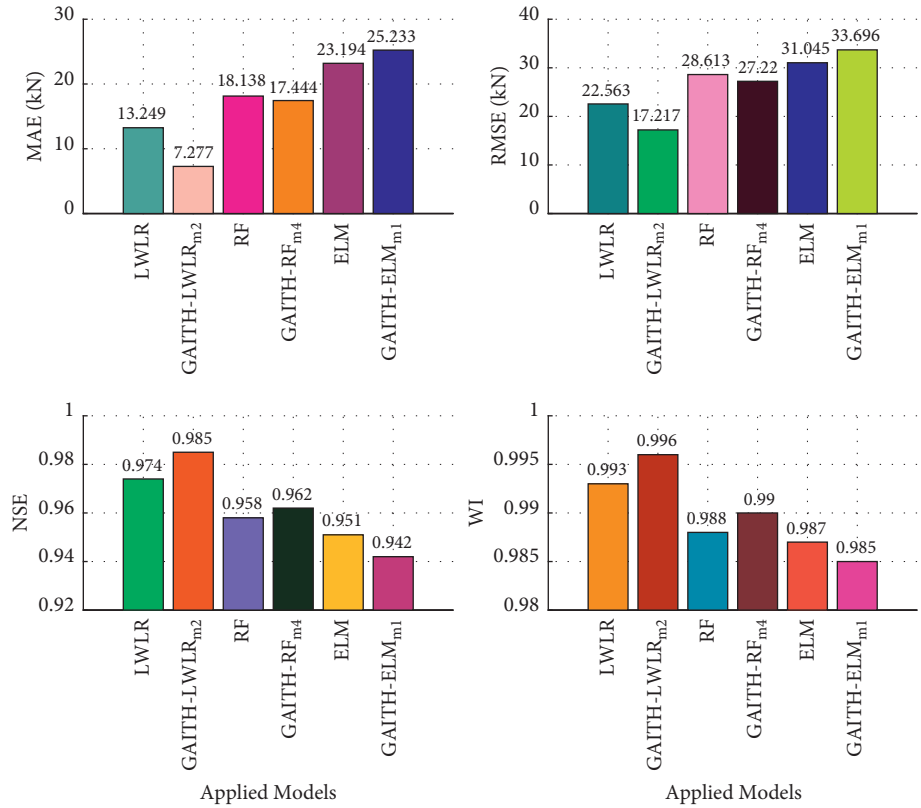

Figure 12: Comparison between the proposed models before and after using feature selection algorithm: training phase.

strength capacity estimated with the LWLR had an absolute relative error of less than 15%, while the corresponding values for the RF, MLR, and ELM models were 67.26%, 51.09%, and 66.30%, respectively. In this respect, MLR showed undesirable accuracy in all cases compared to the other prediction models.

Several graphs were generated during the training and testing datasets to further evaluate the impact of the GAITH approach on the predicted models (Figures 7–11). These figures provide essential information about the performance of each proposed model based on different input parameters. In general, the LWLR, in combination with GAITH, provided much more accurate estimates than other comparable models. It can also be visually seen that the $M2$ combination performed best in terms of the highest prediction accuracy. Among all the proposed models built with five input combinations, the GAITH – LWLR$_{M2}$ model stood out as the best model. The accuracy of this model was the highest with $R^2 = 0.962$ during the testing phase in terms of shear strength prediction. The Taylor diagram in Figure 8(c) shows a satisfactory agreement between the actual and estimated data to illustrate the comparison between the adopted models better. It also shows that the estimates for GAITH – LWLR$_{M2}$ are closest to the point corresponding to the actual data. Thus, these results prove that the GAITH – LWLR$_{M2}$ model was the best in terms of generalisation abilities and performed satisfactorily in both the training and testing phases.

The improvement of each model during the training and testing phase through GAITH is summarised in Figures 12–14. It is important to note that the MLR showed very poor estimates and therefore should not be used as a comparative model at this stage. In general, LWLR improved more significantly than other models due to the presence of the GAITH algorithm. More specifically, the performance of the hybrid model (GAITH – LWLR$_{M2}$) outperformed the standard model (LWLR) during the training phase in terms of reducing the predicted errors by 45.08% and 23.69% for MAE and RMSE, respectively. Looking at the performance of the RF model before and after using the feature selection tool, a slight improvement is observed after using the GAITH algorithm, with the reduction in RMSE and MAE being 4.87% and 3.83%, respectively. However, the ELM model was not run efficiently with fewer input parameters. This model required an extensive data set and complete input vectors to learn well, while other models performed efficiently with fewer input parameters. Nevertheless, all models used in the test phase improved their capacity prediction with the presence of the GAITH algorithm. The LWLR and GAITH algorithm combination provided the most accurate predictions compared to the other models. The superiority of GAITH – LWLR$_{M2}$ was clearly shown in the reduction of RMS parameters by 29.15% and 47.88% compared to the GAITH – RF$_{M4}$ and GAITH – ELM$_{M1}$ models, respectively. Finally, Taylor plots (see Figures 15 and 16) are produced throughout the training and testing phase, showing that there is perfect agreement between the shear strength data predicted by the GAITH – LWLR$_{M2}$ model and the actual values.

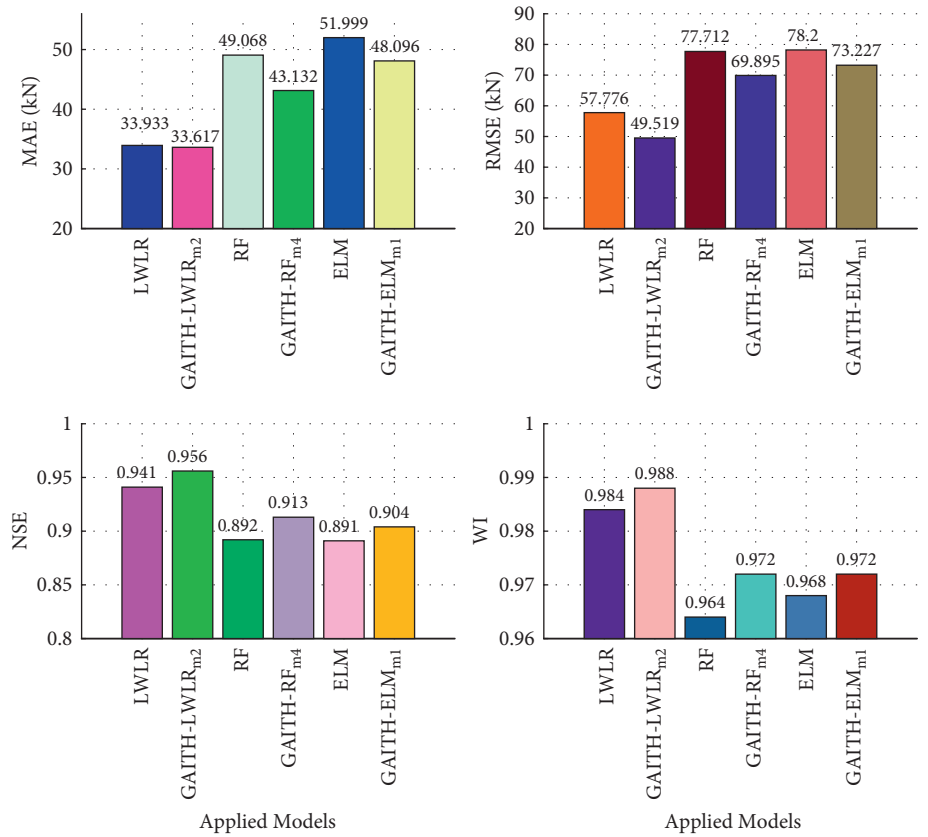

Figure 13: Comparison between the proposed models before and after using feature selection algorithm: testing phase.

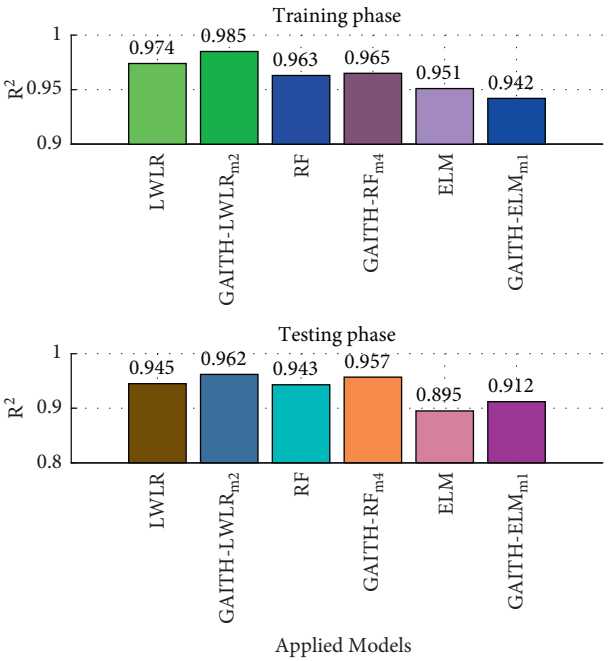

Figure 14: Improvement of the correlation of determination in the proposed models using the feature selection algorithm.

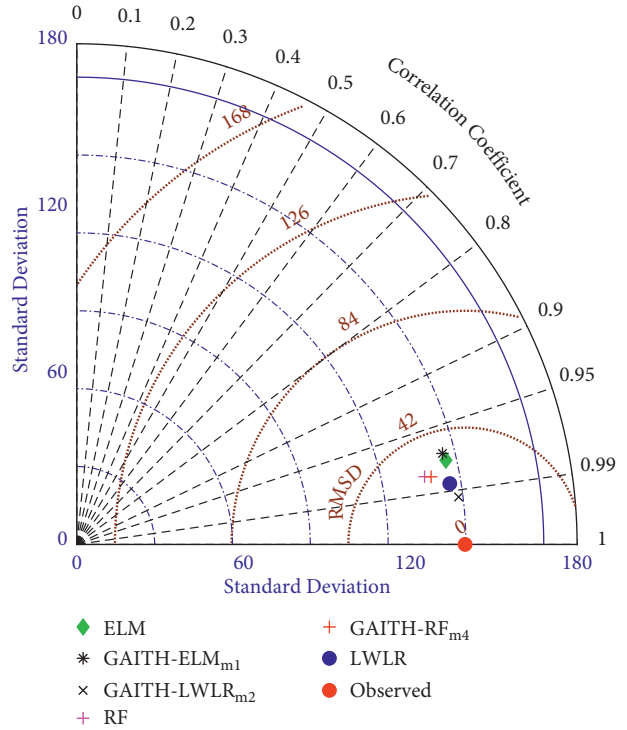

Figure 15: The Taylor diagram shows the improvement in prediction due to the presence of a feature selection algorithm: training phase.

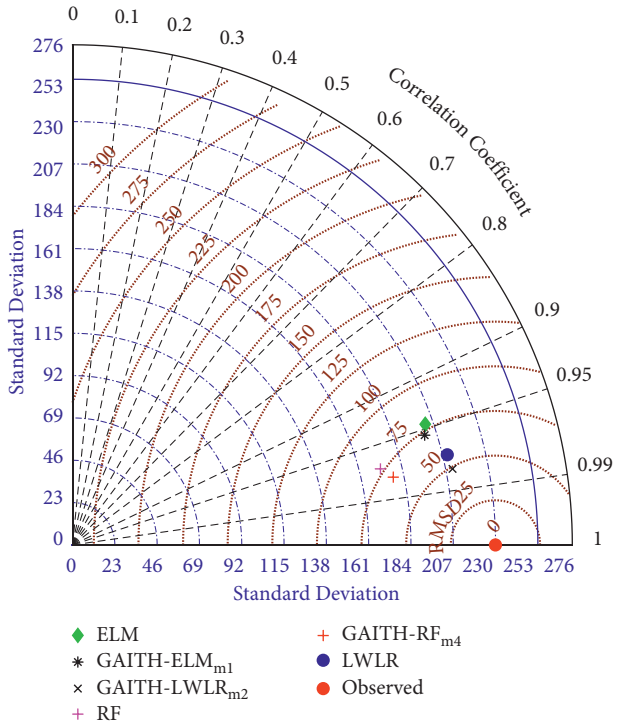

Figure 16: The Taylor diagram shows the improvement in prediction by the feature selection algorithm: testing phase.

4. Conclusion

As the reinforced concrete deep beams are essential components for load distribution, the design is still challenging due to the problem of shear stress. Several nonlinear factors influence the behaviour of the shear strength capacity, making the accurate estimation of this parameter challenging. Accurate estimation of shear stress for deep beams would help designers to design a better and safer structure to prevent structural failure, thus saving lives and property. One of the most critical factors for an efficient and accurate prediction model is the selection of input combinations. In this study, GAITH is introduced based on the integration of genetic algorithm and mutual information to determine the most influential input parameters. This method is developed to overcome some of the shortcomings of classical data-driven input selection. Instead of the trial-and-error technique or the linear correlation, this study presented a robust method for selecting input combinations for prediction models. The structure of the proposed models includes locally linear regression (LWLR) based on the radial basis kernel function, multiple linear regression (MLR), random forest (RF), and extreme learning machine (ELM). The integration between the GAITH algorithm and the aforementioned data-driven models yields promising results. Moreover, the performance of the models (except MLR) is significantly improved by the GAITH algorithm in terms of shear strength prediction. More specifically, the LWLR-GAITH model achieved the highest prediction accuracy in reducing root mean square error by 29.15% to 47.88% compared to the applied models (MLR – GAITH, ELM – GAITH, and RF – GAITH). The main reason for the improvement in prediction is the presence of the GAITH algorithm, which selects the most influential input combination that contains a minimum of redundant data and a maximum of useful information. Redundant data complicate the model's training process and have a negative impact on the generalisation of the model. Another important finding of this study is that the LWLR – GAITH model needs only two input variables to achieve the best prediction accuracy, while the other comparable models need four predictors. It is essential to mention that among the different parameters (i.e., geometry, concrete, and steel properties), the effective height (h_o) and f_y are the most critical parameters that greatly influence the shear strength capacity. In conclusion, this study recommends the application of the methodology used (LWLR – GAITH) to solve various problems related to the structure.

Abbreviations

b:	Beam width
h:	Beam height
A:	Shear span
h_o:	Effective height
l_o:	Beam span
a/h_o:	Shear span to-effective height ratio
l_o/h_o:	Beam span to-effective height ratio
S_v:	Vertical reinforcement spacing
fy_v:	Vertical reinforcement strength
ρ_v:	Vertical reinforcement ratio
S_h:	Horizontal reinforcement spacing
fy_h:	Horizontal reinforcement strength
ρ_h:	Horizontal reinforcement ratio
fy_l:	Longitudinal reinforcement strength
ρ_l:	Longitudinal reinforcement ratio
$f_c\prime$:	Concrete strength
V_u:	Beam shear strength
GA:	Genetic algorithm
ANN:	Artificial neural network
LM:	Levenberg–marquardt
QN:	Quasi-Newton method
GG:	Conjugate gradient
GD:	Gradient descent
NN:	Neural network
OSVM-AEW:	Optimized support vector machines with adaptive ensemble weighting
LS-SVM:	Least-squares support vector machine
SOS:	Symbiotic organisms search
R:	Coefficient of correlation
R^2:	Coefficient of determination
MAE:	Mean absolute error
MAPE:	Mean absolute percentage error
RMSE:	Root mean square error
SVR:	Support vector regression

GBDTs: Gradient boosted decision trees
NSE: Nash-efficiency coefficient
WI: Willmott-index
ACI: American concrete institute
CSA: Canadian standard association
SFA: Smart artificial firefly colony algorithm
LS: Least-squares
RBF: Radial basis function kernel
RF: Random forest
AdaBoost: Adoptive boosting
GBRT: Gradient boosting regression tree
DT: Decision tree
EMARS: Evolutionary multivariate adaptive regression splines
BPNN: Back-propagation neural network
RBFNN: Radial basis function neural network
STD: Standard deviation
COV: Coefficient of variation
AVG: Average
CSTM: Cracking strut-and-tie model.

Data Availability

All data are available upon request.

Conflicts of Interest

The authors declare that they have no conflicts of interest.

Acknowledgments

The authors would like to thank Al-Maarif University College for funding this research.

References

[1] J. Liu and B. I. Mihaylov, "A comparative study of models for shear strength of reinforced concrete deep beams," *Engineering Structures*, vol. 112, pp. 81–89, 2016.

[2] C. Xu, M. Nait Amar, M. A. Ghriga, H. Ouaer, X. Zhang, and M. Hasanipanah, "Evolving Support Vector Regression Using Grey Wolf Optimization; Forecasting the Geomechanical Properties of Rock," *Engineering with Computers*, vol. 38, pp. 1819–1833, 2020.

[3] D. Prayogo, M.-Y. Cheng, Y.-W. Wu, and D.-H. Tran, "Combining machine learning models via adaptive ensemble weighting for prediction of shear capacity of reinforced-concrete deep beams," *Engineering with Computers*, vol. 36, no. 3, pp. 1135–1153, 2020.

[4] J.-S. Chou, N.-T. Ngo, and A.-D. Pham, "Shear strength prediction in reinforced concrete deep beams using nature-inspired metaheuristic support vector regression," *Journal of Computing in Civil Engineering*, vol. 30, no. 1, Article ID 04015002, 2016.

[5] A. C. Institute, *318-14: Building Code Requirements for Structural Concrete and Commentary*, American Concrete Institute, Indianapolis, IN, United States, 2014.

[6] C. S. Association, *CSA Standard A23. 3–14 Design of Concrete Structures*, Canada, Ottawa, 2014.

[7] P. Code, *Eurocode 2: Design of concrete Structures-Part 1–1: General Rules and Rules for Buildings*, Br. Stand. Institution, London, 2005.

[8] R. A. Sanabria Díaz, S. J. Sarmiento Nova, M. C. A. Teixeira da Silva, L. Mouta Trautwein, and L. C. de Almeida, "Reliability analysis of shear strength of reinforced concrete deep beams using NLFEA," *Engineering Structures*, vol. 203, Article ID 109760, 2020.

[9] A. C. I. Aci, "318-11: building code requirements for structural concrete," *Farmingt. Hills, MI Am. Concr. Inst*, vol. 505, 2011.

[10] O. Arup, *The Design of Deep Beams in Reinforced concrete*, Construction Industry Research and Information Association, 1977.

[11] C. S. A. Csa, *Design of concrete Structures: Structures (Design)—a National Standard of Canada*, pp. 3–94, CAN-A23, Canada, 1994.

[12] M. S. Barkhordari, D.-C. Feng, and M. Tehranizadeh, "Efficiency of hybrid algorithms for estimating the shear strength of deep reinforced concrete beams," *Periodica Polytechnica: Civil Engineering*, 2022.

[13] K. H. Tan, L. W. Weng, and S. Teng, "A strut-and-tie model for deep beams subjected to combined top-and-bottom loading," *Structural Engineer*, vol. 75, no. 13, 1997.

[14] J. Amani and R. Moeini, "Prediction of shear strength of reinforced concrete beams using adaptive neuro-fuzzy inference system and artificial neural network," *Scientia Iranica*, vol. 19, no. 2, pp. 242–248, 2012.

[15] D.-C. Feng, W.-J. Wang, S. Mangalathu, G. Hu, and T. Wu, "Implementing ensemble learning methods to predict the shear strength of RC deep beams with/without web reinforcements," *Engineering Structures*, vol. 235, Article ID 111979, 2021.

[16] B. Salman and M. M. Kadhum, "Predicting of load carrying capacity of reactive powder concrete and normal strength concrete column specimens using artificial neural network," *Knowledge-Based Eng. Sci*, vol. 3, no. 1, pp. 45–53, 2022.

[17] J. Zhang, Y. Sun, G. Li, Y. Wang, J. Sun, and J. Li, "Machine-learning-assisted shear strength prediction of reinforced concrete beams with and without stirrups," *Engineering with Computers*, vol. 38, no. 2, pp. 1293–1307, 2020.

[18] M. M. Hameed, M. A. Abed, N. Al-Ansari, and M. K. Alomar, "Predicting compressive strength of concrete containing industrial waste materials: novel and hybrid machine learning model," *Advances in Civil Engineering*, vol. 2022, p. 19, 2022.

[19] L. Lixin, X. Lili, and C. Meng, "The shear strength capability of reinforced concrete deep flexural member," *Build. Struct*, vol. 30, no. 10, pp. 19–22, 2000.

[20] V. Ramakrishnan and Y. Ananthanarayana, "Ultimate strength of deep beams in shear," *ACI J. Proc*, vol. 65, no. 2, 1968.

[21] J. B. Butcher, C. R. Day, J. C. Austin, P. W. Haycock, D. Verstraeten, and B. Schrauwen, "Defect detection in reinforced concrete using random neural architectures," *Computer-Aided Civil and Infrastructure Engineering*, vol. 29, no. 3, pp. 191–207, Mar. 2014.

[22] G. Aguilar, A. B. Matamoros, G. J. Parra-Montesinos, J. A. Ramírez, and J. K. Wight, "Experimental evaluation of design procedures for shear strength of deep reinforced concrete beams," *ACI Structural Journal*, vol. 99, no. 4, pp. 539–548, 2002.

[23] M. M. Hameed and M. K. AlOmar, *Prediction of Compressive Strength of High-Performance Concrete: Hybrid Artificial Intelligence Technique BT-Applied Computing to Support Industry: Innovation and Technology*, M. I. Khalaf, D. Al-

Jumeily, and A. Lisitsa, Eds., Springer International Publishing, Cham, Switzerland, 2020.

[24] C. G. Atkeson, A. W. Moore, and S. Schaal, "Locally weighted learning for control," *Lazy Learning*, vol. 11, no. 11, pp. 75–113, 1997.

[25] G. Armano, M. Marchesi, and A. Murru, "A hybrid genetic-neural architecture for stock indexes forecasting," *Information Sciences*, vol. 170, no. 1, pp. 3–33, 2005.

[26] M. K. AlOmar, M. M. Hameed, N. Al-Ansari, and M. A. AlSaadi, "Data-driven model for the prediction of total dissolved gas: robust artificial intelligence approach," *Advances in Civil Engineering*, vol. 2020, pp. 1–20, 2020.

[27] G. B. Huang, Q.-Y. Zhu, and C.-K. Siew, "Extreme Learning Machine: Theory and Applications," *Neurocomputing*, vol. 70, no. 1-3, pp. 489–501, 2006.

[28] G.-B. Huang, X. Ding, and H. Zhou, "Optimization method based extreme learning machine for classification," *Neurocomputing*, vol. 74, no. 1-3, pp. 155–163, 2010.

[29] G.-B. Huang and L. Chen, "Enhanced random search based incremental extreme learning machine," *Neurocomputing*, vol. 71, no. 16-18, pp. 3460–3468, 2008.

[30] T. Hastie, J. Friedman, and R. Tibshirani, "The elements of statistical learning," no. 10, Springer series in statistics, New York, 2001.

[31] R. Díaz-Uriarte and S. Alvarez de Andrés, "Gene selection and classification of microarray data using random forest," *BMC Bioinformatics*, vol. 7, no. 1, p. 3, 2006.

[32] T. M. Cover, *Elements of Information Theory*, John Wiley & Sons, Hoboken, New Jersey, 1999.

[33] K. Krippendorff, "Mathematical theory of communication," *Dep. Pap*, vol. 169, 2009.

[34] A. Kertesz-Farkas, A. Kocsor, and S. Pongor, *The Application of Data Compression-Based Distances to Biological Sequences BT - Information Theory and Statistical Learning*, Eds., pp. 83–100, Springer US, Boston, MA, 2009.

[35] J. H. Holland, *Adaptation in Natural and Artificial Systems: An Introductory Analysis with Applications to Biology, Control, and Artificial Intelligence*, MIT press, Cambridge, MA, 1992.

[36] W.-Y. Lu, "Shear strength prediction for steel reinforced concrete deep beams," *Journal of Constructional Steel Research*, vol. 62, no. 10, pp. 933–942, 2006.

[37] O. Ludwig and U. Nunes, "Novel maximum-margin training algorithms for supervised neural networks," *IEEE Transactions on Neural Networks*, vol. 21, no. 6, pp. 972–984, 2010.

[38] M. M. Hameed, M. K. AlOmar, F. Khaleel, and N. Al-Ansari, "An extra tree regression model for discharge coefficient prediction: novel, practical applications in the hydraulic sector and future research directions," *Mathematical Problems in Engineering*, vol. 2021, p. 19, 2021.

[39] M. M. Hameed, M. K. AlOmar, W. J. Baniya, and M. A. AlSaadi, "Prediction of high-strength concrete: high-order response surface methodology modeling approach," *Engineering with Computers*, vol. 38, pp. 1655–1668, 2022.

[40] M. Z. Naser and A. H. Alavi, "Error metrics and performance fitness indicators for artificial intelligence and machine learning in engineering and sciences," *Architecture, Structures and Construction*, 2021.

[41] O. Ludwig, U. Nunes, R. Araújo, L. Schnitman, and H. A. Lepikson, "Applications of information theory, genetic algorithms, and neural models to predict oil flow," *Communications in Nonlinear Science and Numerical Simulation*, vol. 14, no. 7, pp. 2870–2885, 2009.

[42] T.-A. Nguyen, H.-B. Ly, H.-V. T. Mai, and V. Q. Tran, "On the training algorithms for artificial neural network in predicting the shear strength of deep beams," *Complexity*, vol. 2021, pp. 1–18, 2021.

[43] S. A. Yaseen, O. Q. Aziz, and B. H. A. Bakar, "Prediction of Shear Strength of Ultra High Performance Reinforced Concrete Deep Beams without Stirrups by Neural Network," *Eurasian Journal of Science and Engineering*, vol. 3.

[44] G. Zhang, Z. H. Ali, M. S. Aldlemy et al., "Reinforced concrete deep beam shear strength capacity modelling using an integrative bio-inspired algorithm with an artificial intelligence model," *Engineering with Computers*, vol. 38, no. S1, pp. 15–28, 2020.

[45] A. H. Gandomi, G. J. Yun, and A. H. Alavi, "An evolutionary approach for modeling of shear strength of RC deep beams," *Materials and Structures*, vol. 46, no. 12, pp. 2109–2119, 2013.

[46] M. Tasleema, M. A. Kumar, and J. L. Raj, "Evaluation of shear strength of deep beams using artificial neural networks," *International Conference on Advances in Civil EngineeringICACE-2019)*, vol. 7, pp. 341–345, 2019.

[47] H. Chen, W.-J. Yi, and H.-J. Hwang, "Cracking strut-and-tie model for shear strength evaluation of reinforced concrete deep beams," *Engineering Structures*, vol. 163, pp. 396–408, 2018.

[48] P. P. S. Kumar, G. S. Harsha, and P. P. Raju, "Development of shear strength expression for RC deep beams using strut-and-tie model," *International Conference on Advances in Civil EngineeringICACE-2019)*, vol. 21, p. 23, 2019.

[49] T. Wakjira, M. Ibrahim, B. Sajjad, and U. Ebead, "Shear capacity of reinforced concrete deep beams using genetic algorithm," *IOP Conference Series: Materials Science and Engineering*, vol. 910, no. 1, Article ID 012002, 2020.

[50] K.-H. Yang, A. F. Ashour, J.-K. Song, and E.-T. Lee, "Neural network modelling of RC deep beam shear strength," *Proceedings of the Institution of Civil Engineers - Structures and Buildings*, vol. 161, no. 1, pp. 29–39, 2008.

[51] M.-Y. Cheng and M.-T. Cao, "Evolutionary multivariate adaptive regression splines for estimating shear strength in reinforced-concrete deep beams," *Engineering Applications of Artificial Intelligence*, vol. 28, pp. 86–96, 2014.

[52] M. Pal and S. Deswal, "Support vector regression based shear strength modelling of deep beams," *Computers & Structures*, vol. 89, no. 13-14, pp. 1430–1439, 2011.

[53] T. T. C. Hsu, "Softened truss model theory for shear and torsion," *ACI Structural Journal*, vol. 85, no. 6, pp. 624–635, 1988.

[54] P. G. Bakir and H. M. Boduroğlu, "Mechanical behaviour and non-linear analysis of short beams using softened truss and direct strut & tie models," *Engineering Structures*, vol. 27, no. 4, pp. 639–651, 2005.

[55] F. J. Vecchio, "Analysis of shear-critical reinforced concrete beams," *ACI Structural Journal*, vol. 97, no. 1, pp. 102–110, 2000.

[56] F. J. Vecchio and M. P. Collins, "The modified compression-field theory for reinforced concrete elements subjected to shear," *ACI Journal Proceedings*, vol. 83, no. 2, pp. 219–231, 1986.

[57] J. Zaborac, J. Choi, and O. Bayrak, "Assessment of deep beams with inadequate web reinforcement using strut-and-tie

models," *Engineering Structures*, vol. 218, Article ID 110832, 2020.
[58] K. N. Smith and A. S. Vantsiotis, "Shear strength of deep beams," *Journal Proceedings*, vol. 79, no. 3, pp. 201–213, 1982.
[59] A. P. Clark, "Diagonal tension in reinforced concrete beams," *ACI Journal Proceedings*, vol. 48, no. 10, 1951.
[60] N. K. Subedi, A. E. Vardy, and N. Kubotat, "Reinforced concrete deep beams some test results," *Magazine of Concrete Research*, vol. 38, no. 137, pp. 206–219, 1986.
[61] F. K. Kong, P. J. Robins, and D. F. Cole, "Web reinforcement effects on deep beams," *ACI Journal Proceedings*, vol. 67, no. 12, pp. 1010–1017, 1970.
[62] A. Windisch, "Shear strength of reinforced concrete deep beams," *ACI Structural Journal*, vol. 111, no. 3, pp. 718–720, 2014.
[63] P. R. Muñoz, "Strength of struts in deep concrete members designed using strut-and-tie method," *ACI Structural Journal*, vol. 104, no. 3, pp. 375-376, 2007.

Hindawi
Complexity
Volume 2022, Article ID 1172805, 19 pages
https://doi.org/10.1155/2022/1172805

Research Article

Characterization of Meteorological Drought Using Monte Carlo Feature Selection and Steady-State Probabilities

Rizwan Niaz,[1] **Fahad Tanveer**,[1] **Mohammed M. A. Almazah**,[2,3] **Ijaz Hussain**,[1] **Soliman Alkhatib**,[4] **and A.Y. Al-Razami**[5,6]

[1]*Department of Statistics, Quaid-i-Azam University, Islamabad, Pakistan*
[2]*Department of Mathematics, College of Sciences and Arts (Muhyil), King Khalid University, Muhyil 61421, Saudi Arabia*
[3]*Department of Mathematics and Computer, College of Sciences, Ibb University, Ibb 70270, Yemen*
[4]*Engineering Mathematics and Physics Department, Faculty of Engineering and Technology, Future University Egypt, New Cairo 11835, Egypt*
[5]*Mathematics Department, Prince Sattam Bin Abdulaziz University, Al-Kharj 16278, Saudi Arabia*
[6]*Department of Statistics and Information, Sana'a University, Sana'a, Yemen*

Correspondence should be addressed to Rizwan Niaz; razwanniaz11@gmail.com and Mohammed M. A. Almazah; mmalmazah@kku.edu.sa

Received 2 March 2022; Revised 28 April 2022; Accepted 7 May 2022; Published 31 May 2022

Academic Editor: Haitham Abdulmohsin Afan

Drought is a creeping phenomenon that slowly holds an area over time and can be continued for many years. The impacts of drought occurrences can affect communities and environments worldwide in several ways. Thus, assessment and monitoring of drought occurrences in a region are crucial for reducing its vulnerability to the negative impacts of drought. Therefore, comprehensive drought assessment techniques and methods are required to develop adaptive strategies that a region can undertake to reduce its vulnerability to drought substantially. For this purpose, this study proposes a new method known as a regional comprehensive assessment of meteorological drought (RCAMD). The Standardized Precipitation Index (SPI), Standardized Precipitation Evapotranspiration Index (SPEI), and Standardized Precipitation and Temperature Index (SPTI) are jointly used for the development of the RCAMD. Further, the RCAMD employs Monte Carlo feature selection (MCFS) and steady-state probabilities (SSPs) to comprehensively collect information from various stations and drought indices. Moreover, the RCAMD is validated on the six selected stations in the northern areas of Pakistan. The outcomes associated with the RCAMD provide a comprehensive regional assessment of meteorological drought and become the initial source for bringing more considerations to drought monitoring and early warning systems.

1. Introduction

Drought is a multifaceted phenomenon triggered by a deficiency of precipitation, and its related impacts have severe effects on weather-related events, natural ecosystems, forestry, economy, agriculture, and environment [1–5]. It progressively holds an area over time, can be persisted for a long time, and distressed agricultural [6–8], environmental [9–11], and socioeconomic conditions [12–14]. Furthermore, it exhibits substantial spatial and temporal variability in various climates and regions. Several authors have proposed various procedures and frameworks to address the spatial and temporal variability of drought events [15–20]. However, it is considered a highly variable complicated phenomenon, and it is challenging to discover its onset and termination periods [21–24]. The complication in drought assessment and monitoring underpins the need for new drought assessment and monitoring methods and procedures [25–28].

Wilhite and Glantz [1] categorized the drought into several categories, i.e., "meteorological, agricultural, hydrological, and socioeconomic." Yihdego et al. [29] have defined meteorological drought as a prolonged precipitation deficit over time. The precipitation data have been used as a single input variable to mark meteorological drought occurrences and onsets [25, 26, 28, 30–33]. The continuous shortfall in precipitation interlinks the meteorological drought to the

agricultural drought. The agricultural drought manifests itself as a deficiency in precipitation, a deficit in soil moisture condition, crop failure, etc. [34, 35]. Further, the prolonged period without rainfall becomes the root of the hydrological drought [36, 37]. Hydrological drought manifests itself as decreased streamflow eviction and falling water level in lakes, groundwater, or reservoirs [38]. The hydrological drought can be damaging and cause severe societal impacts if not alleviated timely. The drought of socioeconomic concerns the supply and demands of the economic goods and is associated with the other three types of drought [39]. An extended period with a deficit in precipitation leads to crop failure issues, a shortage of water supply, and industrial and economic productivity [40]. Increasing demand for goods can lead to exploitation, resulting in vast socioeconomic influences and conflicts. In the recent past, drought has become one of the most dangerous natural hazards and disturbed economic and environmental sectors worldwide [41–44].

Distinctively, drought has been assessed under meteorological, agricultural, hydrological, and socioeconomic aspects by developing various indices that have been discussed and employed in various publications [45–58]. The indices are essential components for assessing and monitoring drought since they simply quantify the complicated interrelationships between varying climate and climate-related parameters [59–63]. Wilhite et al. (2000) have defined that indices are developed to communicate information related to climate anomalies to diverse users and allow researchers to evaluate climate anomalies quantitatively in terms of spatial extent. Several drought indices are established and employed to quantitatively assess the impacts of several kinds of droughts to provide helpful information for planning, organizing, and various management applications of water resources associated with several users and the environment [45–51, 64–67].

Along with the numerous indices proposed for assessing the meteorological drought, some specific indices are extensively used. In particular, Palmer's Drought Severity Index (PDSI) was presented and used [68, 69]. The index was created to " measure the cumulative departure of moisture supply." The PDSI is commonly used by the United States (USA). Further, instead of precipitation variability, the PSDI expands its assurance of drought on water supply and demand. The PDSI comprises important determinants, including data on soil temperature and precipitation. By incorporating these determinants as inputs, the PDSI analyzes four terms in the water balance equation ("evapotranspiration, moisture, soil recharge, and runoff"). Another extensively used index for the characterization of the meteorological drought is the Standardized Precipitation Index (SPI) [46, 70–73]. The SPI comprises only a single determinant, which is precipitation, and thus, SPI uses precipitation as an input to describe the water deficit. SPI is a renowned index, extensively used to assess and monitor meteorological drought. The SPI is less complicated than the PDSI. Therefore, it can be applied in any place by transforming the precipitation data from a skewed distribution to a normal distribution. Moreover, SPI with longer time scales can indicate the agricultural and hydrological drought [71, 74, 75]. For instance, the SPI for a nine-month time scale with a value less than −1.5 is an alert for the agricultural drought [59]. The streamflow, reservoir level, etc., can be reflected by positioning SPI at a twelve-month time scale. Therefore, SPI is famous and operational in numerous papers and publications [51, 76]. Further, the Standardized Precipitation Evapotranspiration Index (SPEI) is also a well-known index proposed by [50] that triggers the effect of temperature variability on drought estimation. Numerous analyses have employed SPEI for the drought evaluation [77–83], and Standardized Precipitation and Temperature Index (SPTI) by [84] is also considered in multiple studies for the assessment of meteorological drought [76, 84–86].

Considerable research has been done to quantify and understand the complex and meteoric nature of the drought [77, 78, 80, 81, 83, 87–90]. However, the manifestation of the drought nature is very complex [91]. The complexity of determining its pattern reinforces the development of new techniques and methods [92, 93]. The appropriate methods and procedures can help to minimize its meteoric influence in various parts of the world [87] [94] [90, 95]. However, the applications of the new methods may be better described by investigating drought at the regional level. Recently, numerous studies have been done to timely examine the drought occurrences in various regions. Therefore, the study of the particular region has significant importance; thus, current research is applied to the specific region. The selected region has a homogeneous pattern of drought occurrences concerning specific drought indices and a time scale (one-month time scale) [76, 96–99]. Ali et al. [96] examined meteorological drought based on three indices (SPI, SPEI, and SPTI). The study found that the three indices provide similar information about the selected region for the particular time scale. Hence, investigating meteorological drought from the selected homogeneous locations using several meteorological indices (SPI, SPEI, and SPTI) becomes counterproductive. This issue underpins the use of some new drought assessment methods that provide comprehensive information based on these indices. Therefore, this study proposes a new method, known as regional comprehensive assessment for meteorological drought (RCAMD). The RCAMD comprehensively collects information from several stations and drought indices using Monte Carlo feature selection (MCFS) and steady-state probabilities (SSPs). Further, the RCAMD mainly helps to overcome two issues. For instance, the first phase of the RCAMD chooses important stations more comprehensively for three indices from six homogeneous stations. In the presence of influential climatic factors in estimating the drought indices, the second phase of RCAMD characterizes several drought classes more comprehensively and accurately among the three indices (SPI, SPEI, and SPTI). Moreover, the six stations in the northern areas of Pakistan are selected to validate RCAMD. The findings associated with the RCAMD propose a comprehensive regional assessment of meteorological drought and create the initial basis for taking more considerations for assessing and monitoring drought at the regional level.

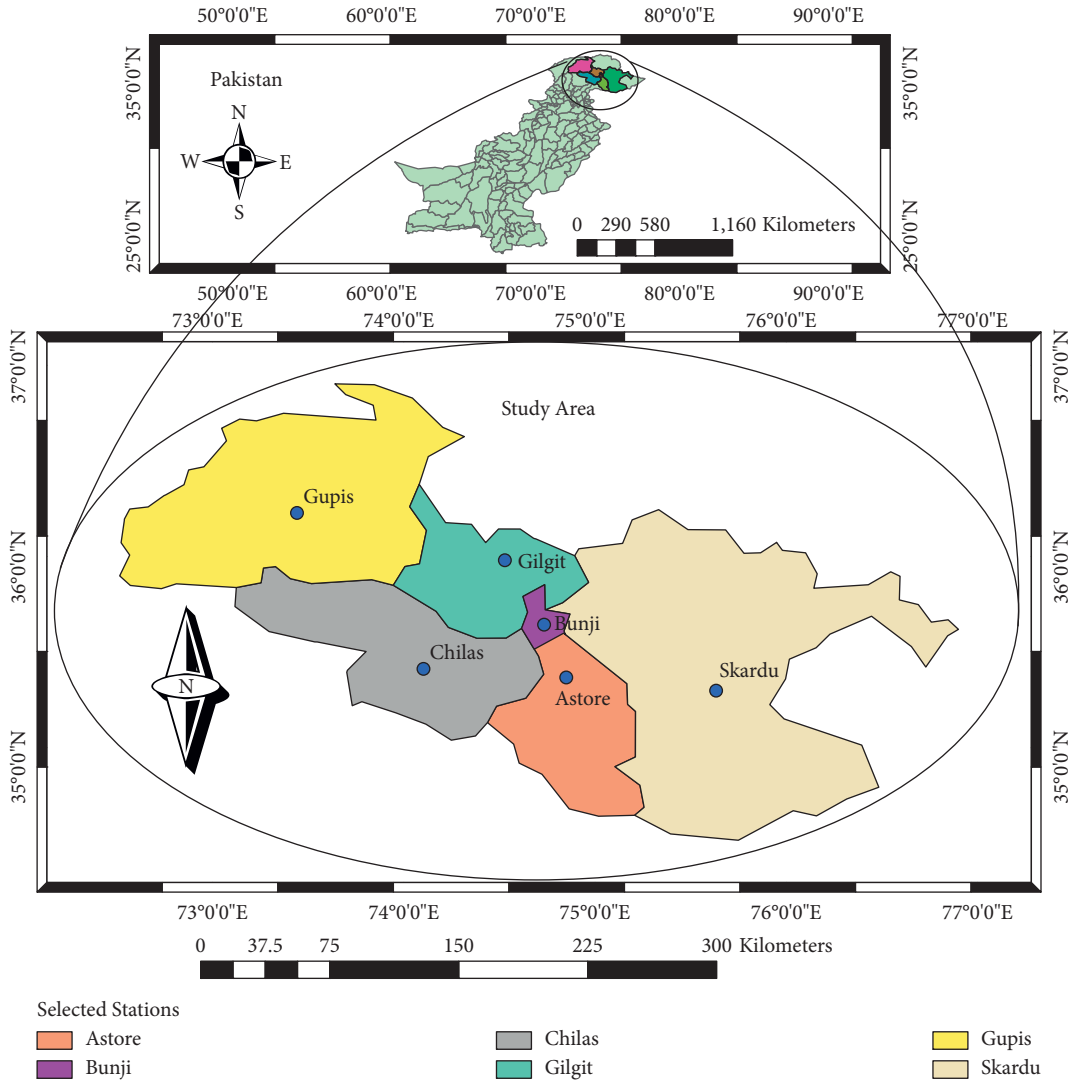

Figure 1: Geographical locations of the six selected stations in northern areas of Pakistan. The selected stations are important for the reservoir systems of the country. Most of the agricultural lands of the country depend on the reservoir systems that are linked to the selected stations. Several publications related to drought analysis [86, 97–99] have been based on these stations. Based on these publications and importance of the stations for the reservoir systems, therefore, these stations are selected for the current analysis.

2. Material and Methods

2.1. Description of the Study Area. The substantial climate changes have increasingly become a primary global task that endangers ecological, human, and natural systems [100–102]. Pakistan is extremely in danger of the undesirable influences of climate change, specifically extreme hydrometeorological activities [103–108]. The selected region is located in the northeastern part of Pakistan, spread over 72,971 square km, almost half of which covers peaks of mountains, glaciers, highlands, and lakes. The selected region has structural significance for other parts of the country. It has a key role in the agricultural sectors and the reservoir system of the country [109, 110]. However, it is highly at risk of climate change due to its geological composition, fragile mountain, topography, ecosystem, geographic locations, socioeconomic conditions, and scattered population [111]. Thus, the selected region requires more consideration for assessing the drought manifestations by developing comprehensive and proficient methods and procedures. Hence, the RCAMD method is designed for the selected region, enhancing the ability to assess drought events and facilitating drought monitoring and water resource management in the selected area (Figure 1).

2.2. Data and Methods. The data ranging from January 1971 to December 2017 are processed in the current analysis. The six stations in the northern areas are selected to calculate the indices (SPI, SPEI, and SPTI). These indices use information from the indicators (precipitation and temperature) to classify drought classes in the selected stations. The data of these indicators have been used in several publications [86, 97, 98, 112–114]. The various drought classes of the selected stations and indices are used to propose RCAMD. The new proposed RCAMD uses MCFS and SSP to assess the information more intensively for the drought classes from

the selected stations and indices. Moreover, the outcomes associated with RCAMD comprehensively assess drought classes for the homogeneous region. The RCAMD develops a new way of taking more consideration for evaluating and monitoring drought at the regional level.

2.2.1. Monte Carlo Feature Selection (MCFS). Niaz et al. [85] used MCFS for selecting informative stations for their analysis. They applied MCFS in the Punjab region of Pakistan and selected important stations based on SPTI. However, in this study, MCFS uses three drought indices (SPI, SPEI, and SPTI) to select important stations. Thus, the MCFS selects an important meteorological station for each drought index. For example, for SPI the MCFS selects Astore as an important station; for SPEI, the MCFS selects Gilgit as an important station. Further, for SPTI, the MCFS selects Astore as an important station for the preliminary analysis. The MCFS input enables the RCAMD to collect information from various stations comprehensively. The suitable stations are chosen based on relative importance (RI) values. The mathematical detail about the RI is given in [85]. For the current analysis, the Astore Station with RI value of 0.1385 is higher than other selected stations for SPI. For SPTI and SPEI, the Astore and Gilgit are selected, respectively. In Astore, the RI value for SPTI is 0.1920, while SPEI for Gilgit has RI value of 0.7617.

2.2.2. Steady-State Probabilities (SSPs). A Markov process can be expressed as the probabilities come up to the SSP when certain periods have been passed. The comprehensive mathematical details associated with the SSP of the Markov chain were described in Stewart (2009). The application of SSP is provided in several publications [76, 97]. Niaz et al. [85] used SSP as a weighting scheme from the long-run time-series data for different drought classes in the northern region of Pakistan. The proposed weighting scheme was used to accumulate information from the selected homogeneous stations. Further, Niaz et al. [97] used SSP to substantiate the prevalence of drought intensities in the northern region of Pakistan. Moreover, Niaz et al. [98] proposed a new technique based on SSP to accumulate information from various indices. Recently, Niaz et al. [99] incorporated SSP in their study to assess the probability of drought severity in the selected region. The SSP is used broadly in several publications to develop new methods and procedures [97–99, 113]. Therefore, in RCAMD, SSP is used to propagate weights for various drought categories over several stations and indices to achieve a particular aspect. In the current analysis, SSP mainly helps to characterize the new vector of drought classes. The inclusion of MCFS and SSP in RCAMD makes the study innovative. This innovation provides a comprehensive procedure to collect information from several stations and indices.

2.2.3. Regional Comprehensive Assessment of Meteorological Drought (RCAMD). The RCAMD employs MCFS and SSP to mainly determine drought events that are likely to occur in the region from numerous stations and drought indices. The MCFS technique is used to accumulate comprehensive information on several time-series data of meteorological stations. The mathematical detail of MCFS is given in Niaz et al. [85]. In the first phase of the RCAMD, the MCFS allows the selection of more important stations based on several selected indices. Three drought indices (SPI, SPEI, and SPTI) are used in RCAMD to determine important stations. Hence, the MCFS selects an important meteorological station for each drought index separately. The criteria for selecting an important station are based on relative importance (RI). The higher values corresponding to any stations show that the stations are important for the preliminary investigation. For example, based on the higher value of RI using SPEI, the MCFS chooses Gilgit as an important station, and for SPI, the MCFS takes Astore as an important station. Moreover, for SPTI the MCFS picks Astore as an important station for the computation of RCAMD. In the second phase of the RCAMD, the SSP is applied to characterize several drought classes among the three indices (SPI, SPEI, and SPI). The complete mathematical detail related to the SSP of the Markov chain is given in Stewart (2009). The SSP is used in several publications to develop new procedures and methodologies [76, 97]. The SSP characterizes various drought categories among selected stations and indices in this study. The SSP for each drought category (k) (("Extremely Dry (ED)," Extremely Wet (EW)," "Severely Dry (SD)," "Severely Wet (SW)," Median Dry (MD)," "Median Wet (MW)," and "Normal Dry (ND)") for each index (l) (SPI, SPEI, and SPTI) in the particular station (m) can be expressed in a vector as $(\mathrm{SSP})_{\mathrm{klm}}$. The obtained SSP for the varying drought categories can be described as the visit of the drought category in the long run. These long-run SSP of several drought categories is counted as weights. These weights are further utilized for the computation of RCAMD. The calculation of RCAMD is based on the vector of the stationary drought categories propagating on different drought indices, which can be identified as follows:

$$\begin{aligned}
\prod_i (\mathrm{SPI}) &= \left[\prod_1 (\mathrm{ED}_{\mathrm{SPI}}) \prod_2 (\mathrm{EW}_{\mathrm{SPI}}) \prod_3 (\mathrm{SD}_{\mathrm{SPI}}) \prod_4 (\mathrm{SW}_{\mathrm{SPI}}) \prod_5 (\mathrm{MD}_{\mathrm{SPI}}) \prod_6 (\mathrm{MW}_{\mathrm{SPI}}) \prod_7 (\mathrm{ND}_{\mathrm{SPI}})\right], \\
\prod_i (\mathrm{SPTI}) &= \left[\prod_1 (\mathrm{ED}_{\mathrm{SPTI}}) \prod_2 (\mathrm{EW}_{\mathrm{SPTI}}) \prod_3 (\mathrm{SD}_{\mathrm{SPTI}}) \prod_4 (\mathrm{SW}_{\mathrm{SPTI}}) \prod_5 (\mathrm{MD}_{\mathrm{SPTI}}) \prod_6 (\mathrm{MW}_{\mathrm{SPTI}}) \prod_7 (\mathrm{ND}_{\mathrm{SPTI}})\right], \\
\prod_i (\mathrm{SPEI}) &= \left[\prod_1 (\mathrm{ED}_{\mathrm{SPEI}}) \prod_2 (\mathrm{EW}_{\mathrm{SPEI}}) \prod_3 (\mathrm{SD}_{\mathrm{SPEI}}) \prod_4 (\mathrm{SW}_{\mathrm{SPEI}}) \prod_5 (\mathrm{MD}_{\mathrm{SPEI}}) \prod_6 (\mathrm{MW}_{\mathrm{SPEI}}) \prod_7 (\mathrm{ND}_{\mathrm{SPEI}})\right].
\end{aligned} \tag{1}$$

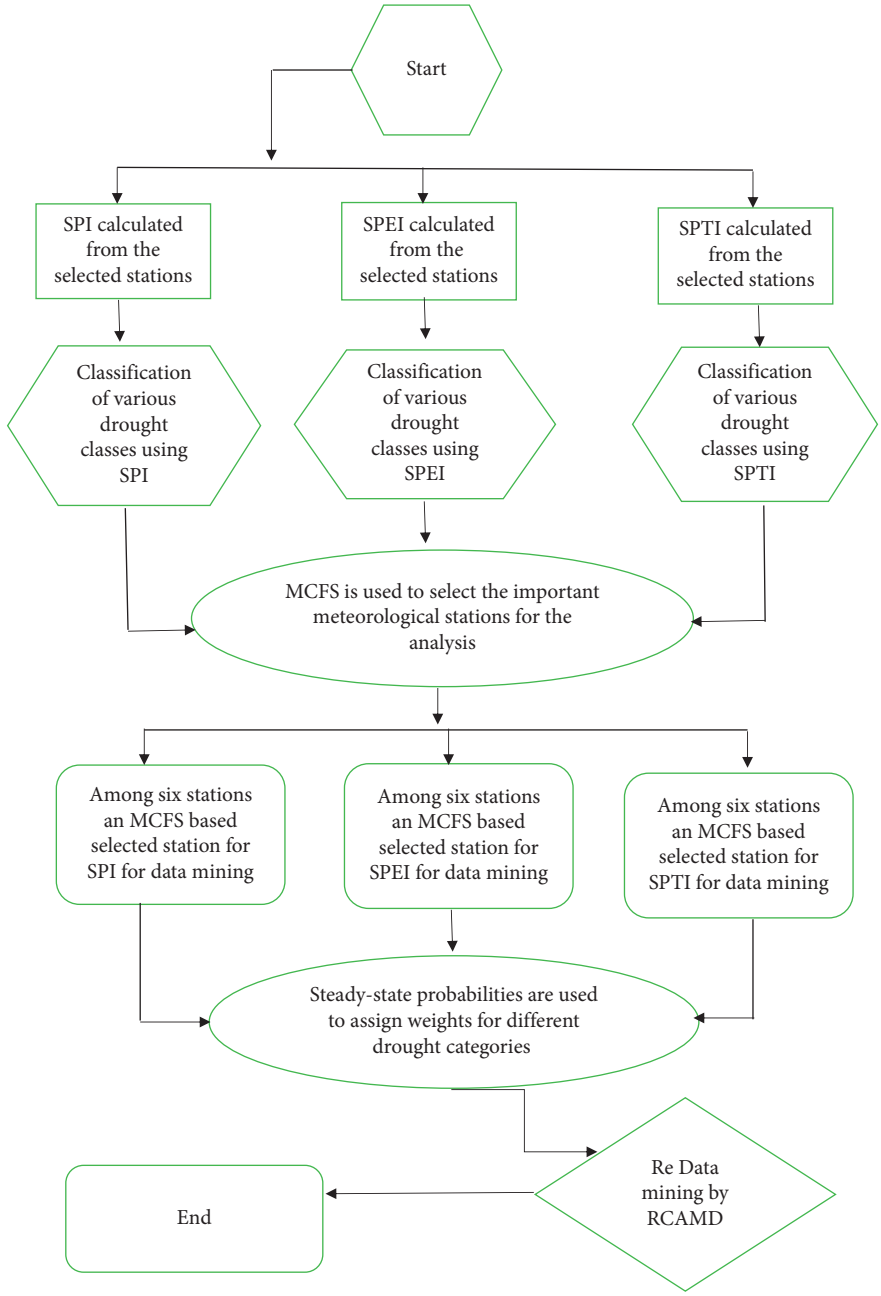

Figure 2: Flowchart of the RCAMD. In starting the RCAMD, three varying indices are calculated for the drought analysis. These calculated indices are further used for the drought classification. The drought classification criteria implemented in several publications [115] and Niaz et al. [76, 96, 97, 99] are used in the current research. In the next step, the MCFS is applied using three drought indices (SPI, SPEI, and SPTI) for selecting important stations. Consequently, the MCFS chooses an important meteorological station for each drought index. The use of MCFS input enables the RCAMD to accumulate information from various stations comprehensively. Moreover, in RCAMD, SSP is employed to disseminate weights for numerous drought categories over various stations and indices. The SSP mainly employs to characterize the new vector of drought categories. Conclusively, the resultant data mining vector based on MCFS and SSP in RCAMD provides a comprehensive information from several stations and indices.

The obtained limiting probabilities ($\prod_i$(SPI), , $\prod_i$(SPTI), $\prod_i$(SPEI)) can be referred to as the proportion or average of long-run probabilities of the drought states or categories for the varying indices (SPI, SPTI, and SPEI) on selected stations. These probabilities are used as weights for the computation of the RCAMD, which assigns the comprehensive weights to the varying drought categories from the selected stations. The flowchart of the RCAMD is given in Figure 2. Moreover, the drought states among selected drought indices (SPI, SPTI, and SPEI) that take maximum weights are chosen for the RCAMD. Hence, in the current research, the RCAMD selects the appropriate vector of drought classes from the time-series dataset for January 1971 to December 2017. The RCAMD enables a clearer, though

Table 1: Climatological features of the monthly precipitation data observed in numerous locations (stations) in the northern areas. The mean (40.91) of precipitation in Astore is observed higher among other stations. The standard deviation (St.Dev) of the Astore is also larger than any other selected stations. Moreover, other characteristics of the Astore and other stations can be followed accordingly.

Variable		Astore	Bunji	Gupis	Chilas	Gilgit	Skardu
Precipitation	Mean	40.91	14.34	16.86	16.76	12.42	20.63
	1st quartile	10.80	1.30	0.00	0.95	1.10	2.30
	Median	25.70	7.10	5.70	7.00	6.05	9.10
	3rd quartile	52.63	17.10	19.38	19.33	14.73	26.75
	Kurtosis	3.01	7.67	14.05	9.02	10.08	5.70
	St.Dev	41.93	18.90	30.21	23.53	16.57	25.90

Table 2: Climatological features of the monthly minimum temperature (MinT) data are given. The minimum temperature was observed in several stations. The mean MinT in Chilas is 15.14, which is higher than other selected stations. The minimum mean of the MinT is observed in Astore. The mean value of MinT in Astore is 4.34. The St.Dev in Chilas is 9.08, and in Astore, the St.Dev is 7.48. The larger St.Dev is observed in Chilas Station. Moreover, other climatological features of the selected stations can be observed accordingly.

Variable		Astore	Bunji	Gupis	Chilas	Gilgit	Skardu
Minimum temperature	Mean	4.34	11.86	6.74	15.14	8.07	5.06
	1st quartile	−2.43	3.78	−1.10	5.68	0.60	−2.73
	Median	4.30	11.50	6.90	14.30	7.75	5.55
	3rd quartile	10.70	17.70	13.33	23.20	13.53	11.80
	Kurtosis	−1.22	−1.24	−1.26	−1.41	−1.24	−1.17
	St.Dev	7.48	7.80	8.06	9.08	7.30	8.36

Table 3: Climatological features of the monthly maximum temperature (MaxT) are given. The MaxT was observed in varying stations for the selected time period. The mean of MaxT in Gilgit is observed high. The mean value of the MaxT in Gilgit is 25.46. In Skardu, the mean of the MaxT is 19.92. In Skardu, the St.Dev of the MaxT is 9.82. The highest St.Dev is observed in Chilas Station, which is 9.66. The smallest St.Dev of the MaxT was observed in Bunji Station. Further, other features of the MaxT can be found accordingly.

Variable		Astore	Bunji	Gupis	Chilas	Gilgit	Skardu
Maximum temperature	Mean	16.66	25.19	19.95	27.92	25.46	19.92
	1st quartile	7.38	15.78	10.33	17.68	15.60	9.95
	Median	16.70	24.95	19.70	27.35	25.15	20.05
	3rd quartile	23.86	32.02	27.40	35.63	32.80	27.90
	Kurtosis	−1.36	−1.32	−1.30	−1.38	−1.33	−1.24
	St.Dev	8.65	8.98	9.46	9.66	9.21	9.82

complicated, representation of how interconnected indices are further associated and linkable to a distinctive set of comprehensive outcomes. Further, RCAMD can be utilized to locate the proper vector of drought classes for any long time-series data in a homogeneous environment. The outcomes associated with the RCAMD provide a comprehensive regional assessment of meteorological drought and become the initial source for bringing more considerations to drought monitoring and early warning systems.

3. Results

The time-series data are collected for six meteorological stations from the northern areas of Pakistan. The varying features, including mean, 1st quartile, median, 3rd quartile, kurtosis, and standard deviation (St.Dev) of the precipitation, are given in Table 1. Table 2 contains the varying characteristics of the minimum temperature. The various features of the maximum temperature are given in Table 3. Further, these climatological features are presented in various figures. For example, the climatological features of the monthly precipitation observed in varying stations are presented on various maps in Figure 3. The climatological characteristics of the observed minimum temperature in various stations are presented in Figure 4. The climatological features of the observed maximum temperature in various stations are presented in Figure 5. Further, the drought categories are classified according to Li et al. [115]. The varying behavior of the classes can be observed in the selected time-series data. However, for simplicity, the results for the specific year (2017) based on SPI, SPEI, and SPTI are provided. In Table 4, the results for the year 2017 based on SPI are given. The varying drought classes can be observed in varying months of the selected year. Further, the index values corresponding to each drought category are provided. Table 5 contains the classified values based on SPEI, and the classified values observed in varying months and their corresponding index values based on SPTI are given in Table 6. The temporal behavior in the selected period, January 1971 to December 2017, in varying stations for the

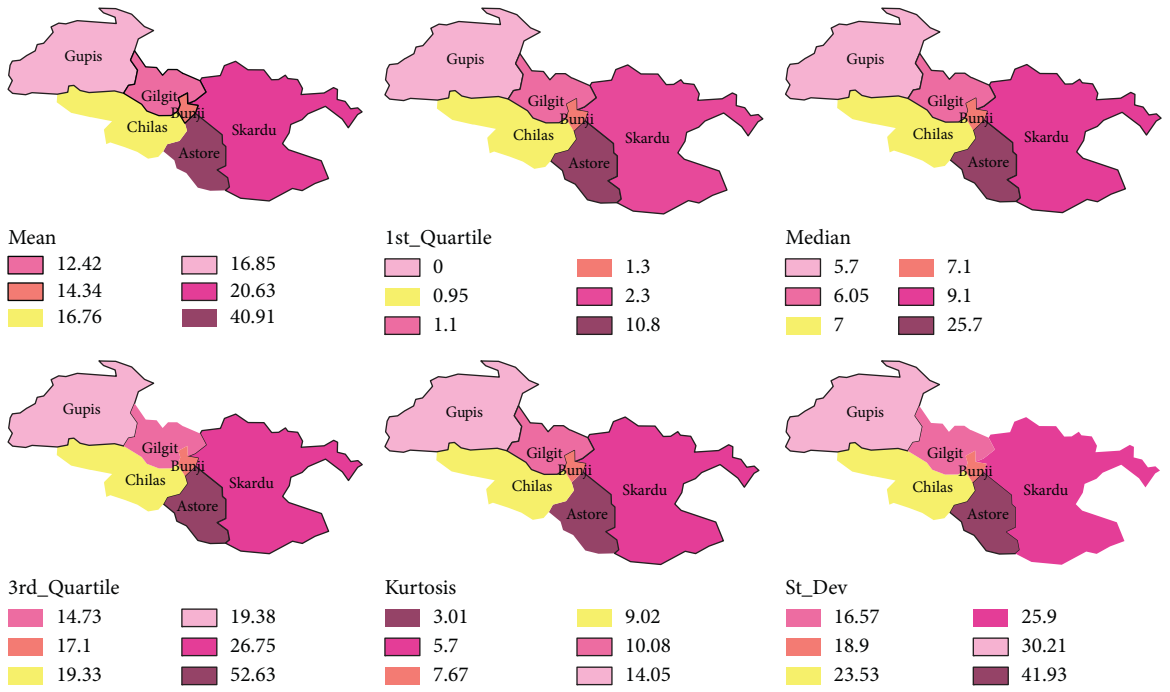

Figure 3: Climatological characteristics of the observed precipitation in various stations.

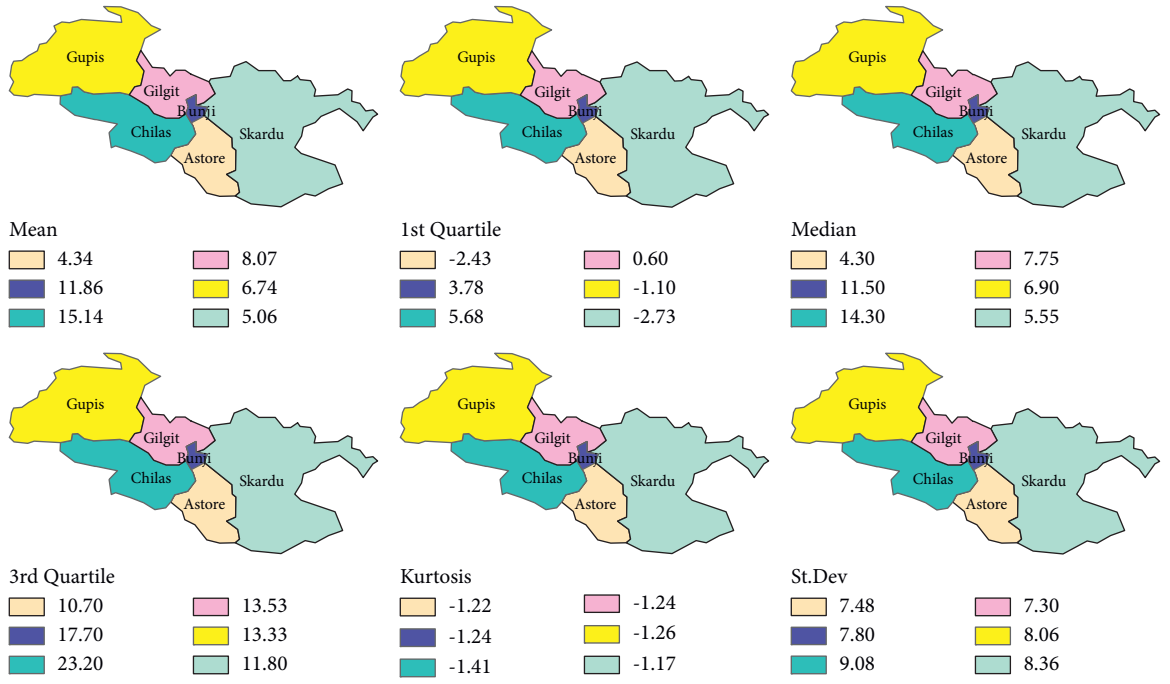

Figure 4: Climatological characteristics of the observed minimum temperature in various stations.

SPI at a one-month time scale (SPI-1) is presented in Figure 6. Figure 7 presents the temporal behavior of the SPEI on a one-month time scale (SPEI-1) at selected stations. Figure 8 shows the temporal behavior of the SPTI at a one-month time scale (SPTI-1) at various stations. Moreover, the varying drought categories observed in various stations for SPI at a one-month time scale are presented in Figure 9. Figure 10 contains various maps for the varying drought categories observed in various stations for SPEI at a one-month time scale. The drought categories classified based on SPTI at a one-month time scale and observed in varying stations are presented in Figure 11. The northern zones of Pakistan (i.e., Astore, Bunji, Chilas, Gupis, Skardu, and Gilgit) have a homogeneous pattern of the drought classes for the specific drought indices and time scale [76, 96, 97, 99] and therefore selected for the current analysis. Three indices,

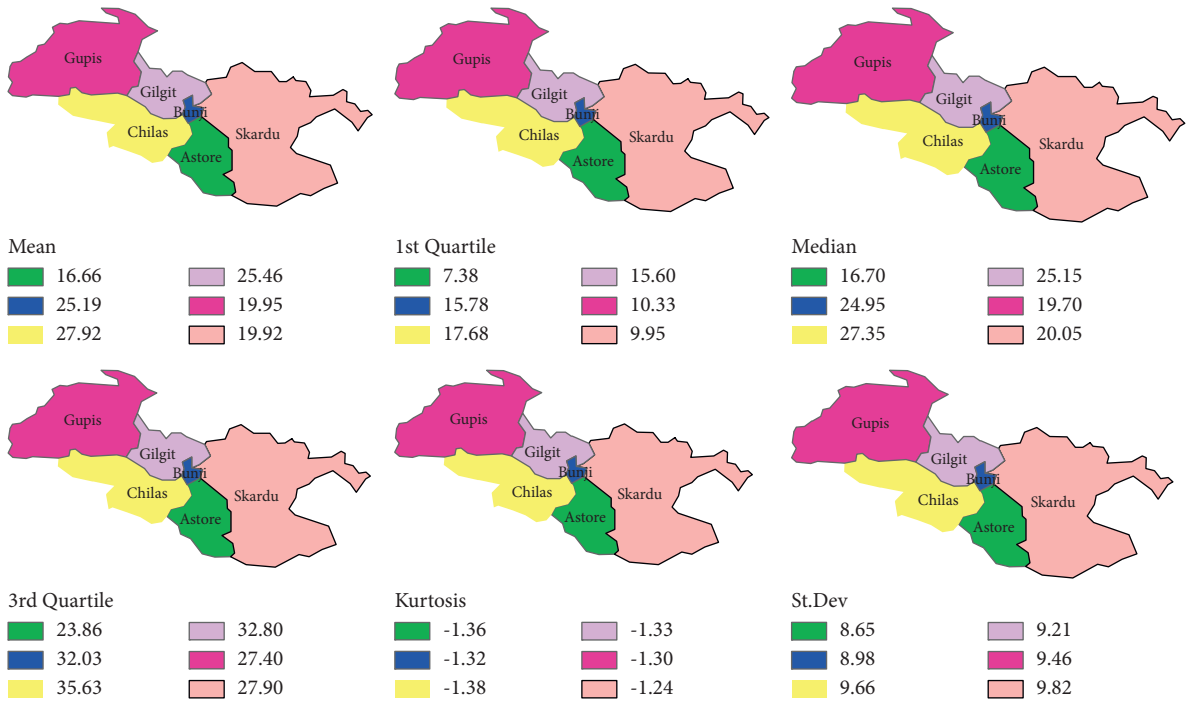

Figure 5: Climatological characteristics of the observed maximum temperature in various stations.

Table 4: Classified (Classif.) drought categories in varying stations based on SPI-1 for the year 2017 are given. The various months of 2017 are categorized by numerical numbers. For example, January is denoted by 1, 2 for February, and 3 for March. April, May, June, July, August, September, October, November, and December are presented by 4, 5, 6, 7, 8, 9, 10, 11, and 12, respectively. The classification criterion used by Li et al. (2015) is adopted for the current analysis. In January in Astore Station, the index value is -1.8044, and according to the classification criteria, the SD category of the drought occurred. Similarly, based on the classification criteria the drought classes are classified in varying months and stations for a specific year.

Month	Astore		Bunji		Gupis		Chilas		Gilgit		Skardu	
	Index	Classif.	Index	Classif.	Index	Classif.	Index	Classif.	Index	Classif.	Index	Classif.
1	−1.8044	SD	−1.2152	MD	−1.0805	MD	−0.3254	ND	−0.2296	ND	−0.4827	ND
2	−1.8044	SD	0.2629	ND	−1.0805	MD	0.8075	ND	0.2014	ND	−1.2581	ND
3	−0.4745	ND	−1.1059	MD	−0.6655	ND	−0.1535	ND	−1.0523	MD	−0.3096	ND
4	1.8879	SW	0.9377	ND	1.2811	MW	2.2094	EW	1.8283	SW	1.0615	EW
5	0.3314	ND	0.6975	ND	0.9813	ND	0.8297	ND	0.9724	ND	0.0796	ND
6	−0.3302	ND	−0.6380	ND	−0.2883	ND	−0.0637	ND	0.9309	ND	−0.8574	ND
7	−0.1857	ND	0.8192	ND	0.7872	ND	0.1366	ND	1.0574	MW	−0.2401	ND
8	−0.1967	ND	0.7181	ND	1.1317	MW	0.2058	ND	0.3864	ND	0.0086	ND
9	−0.5938	ND	0.2824	ND	0.4029	ND	0.1937	ND	0.4759	ND	0.0739	ND
10	−1.7685	SD	−1.1576	MD	−0.2883	ND	−1.0539	MD	−0.9569	ND	−1.2581	MD
11	−1.8044	SD	−1.2806	MD	−1.0805	MD	−1.0995	MD	−1.3227	MD	−1.2581	MD
12	−1.2499	MD	−1.2806	MD	−0.0621	ND	−1.0539	MD	−1.2398	MD	−1.2168	MD

SPI, SPEI, and SPTI, have shown a significant correlation and provided similar information in varying stations at a one-month time scale [76, 96, 116]. However, this study found a gap in the above research and proposed a new method that provides more comprehensive results. The mentioned research considered all stations for their analysis. Thus, considering all stations for drought analysis in a region with a similar pattern of drought occurrences seems counterproductive. It underpins a new gap that should be tackled by comprehensively accumulating information. Based on this gap, this study proposed to provide a more comprehensive drought assessment procedure for the region. For this purpose, the current research comprehensively offers an RCAMD method to accumulate information from numerous stations and drought indices. The RCAMD is based on two phases. In the first phase of the RCAMD, the MCFS technique is applied. The MCFS was utilized by Niaz et al. [85] for selecting more illustrative stations in the region of Punjab in Pakistan. The mathematical detail of the MCFS is available in [85].

Further, the selected stations for the current analysis have shown a similar pattern for all stations. Therefore, it underpins a rationale to apply MCFS for selecting only important stations for the analysis. Thus, the MCFS is

Table 5: Classif. drought categories in varying stations based on SPEI-1 are provided for the year 2017. In January in Bunji Station, ND occurred with a 0.9796 is the quantitative value of the index. The index value of 1.0670 is computed in Gilgit, which is classified as MW. Further, it can be observed that in most of the months of 2017 the ND appears based on SPEI. In Skardu, none of the other classified drought categories appear except ND for a whole year. In Skardu, the ND is a prevalent drought category.

Month	Astore		Bunji		Gupis		Chilas		Gilgit		Skardu	
	Index	Classif.	Index	Classif.	Index	Classif.	Index	Classif.	Index	Classif.	Index	Classif.
1	0.2741	ND	0.9796	ND	0.7679	ND	0.9039	ND	1.0670	MW	0.8220	ND
2	0.0829	ND	0.8384	ND	0.4871	ND	0.9296	ND	0.7976	ND	0.4919	ND
3	−0.1682	ND	0.1045	ND	0.0219	ND	0.1193	ND	0.1447	ND	0.1232	ND
4	1.4903	MW	0.0887	ND	0.3163	ND	1.3240	MW	0.6436	ND	0.1957	ND
5	−0.8214	ND	−1.0027	MD	−0.7708	ND	−0.8617	ND	−0.7646	ND	−0.9650	ND
6	−1.3547	MD	−1.3982	MD	−1.4032	MD	−1.3619	MD	−1.0659	MD	−1.4873	MD
7	−1.2755	MD	−1.0733	MD	−1.2931	MD	−1.3665	MD	−1.0312	MD	−1.3089	MD
8	−0.9560	ND	−0.7027	ND	−0.4335	ND	−0.8499	ND	−0.6704	ND	−0.8895	ND
9	−0.7888	ND	−0.4535	ND	−0.5996	ND	−0.4873	ND	−0.3957	ND	−0.4748	ND
10	−0.4409	ND	0.0387	ND	−0.0183	ND	0.0061	ND	0.0157	ND	−0.0880	ND
11	0.0596	ND	0.7154	ND	0.5016	ND	0.6265	ND	0.6878	ND	0.4532	ND
12	0.2411	ND	0.9475	ND	0.8261	ND	0.8367	ND	0.9538	ND	0.6461	ND

Table 6: Classif. drought categories in selected stations based on SPTI-1 are presented for the year 2017. The index value of -1.5398 is given in January, which indicates that the SD occurred in the Astore Station. Further, in January the MD occurred in Bunji and Gupis with index values of -1.2001 and -1.1305, respectively. The varying drought categories can be seen in various months accordingly.

Month	Astore		Bunji		Gupis		Chilas		Gilgit		Skardu	
	Index	Classif.	Index	Classif.	Index	Classif.	Index	Classif.	Index	Classif.	Index	Classif.
1	−1.5398	SD	−1.2001	MD	−1.1305	MD	−0.0928	ND	0.1063	ND	−0.0381	ND
2	−1.5398	SD	0.4943	ND	−1.1305	MD	0.9832	ND	0.4553	ND	−0.5366	ND
3	−0.3434	ND	−1.1119	MD	−0.6169	ND	−0.0695	ND	−1.0747	MD	−0.2155	ND
4	1.4038	MW	0.9448	ND	1.2422	MW	2.0709	EW	1.8490	SW	0.7164	ND
5	0.0369	ND	0.5504	ND	0.7799	ND	0.6277	ND	0.8382	ND	−0.1299	ND
6	−0.5360	ND	−0.7646	ND	−0.4345	ND	−0.2150	ND	0.6983	ND	−0.4870	ND
7	−0.4439	ND	0.5654	ND	0.5086	ND	−0.0537	ND	0.7859	ND	−0.3234	ND
8	−0.4273	ND	0.5021	ND	0.8873	ND	0.0310	ND	0.2006	ND	−0.2084	ND
9	−0.6874	ND	0.1387	ND	0.2467	ND	0.0446	ND	0.3438	ND	−0.1356	ND
10	−1.5153	SD	−1.1878	MD	−0.3152	ND	−0.9993	ND	−1.0048	MD	−0.5366	ND
11	−1.5398	SD	−1.3078	MD	−1.1305	MD	−1.0394	MD	−1.4267	MD	−0.5366	ND
12	−0.9624	ND	−1.3078	MD	0.2099	ND	−0.9757	ND	−1.2671	MD	−0.5264	ND

applied in the current analysis to select more important stations among the selected stations for various drought indices. This selection of the important stations is based on the relative importance (RI) values (Figure 12). The corresponding higher values of RIs in any station show that the station is to consider for the drought assessment. For example, the Astore Station with RI value of 0.1385 for SPI is higher than other selected stations. For SPTI and SPEI, the Astore and Gilgit are selected, respectively. In Astore, the RI value for SPTI is 0.1920, while SPEI for Bunji has RI value of 0.7617 (Table 7).

Moreover, in the presence of influential climatic factors in estimating the drought indices, the second phase of RCAMD comprehensively characterizes numerous drought categories among the selected indices (SPI, SPEI, and SPI) (Figure 13). Niaz et al. [76] proposed a method based on a steady-state weighting scheme. They selected the classes from various stations based on the maximum weights; hence, the classes that received maximum weights among different stations were selected for the analysis. The weights from three indices (SPI, SPEI, and SPTI) for the varying drought categories for a specific year, 2017, are provided in Tables 8–10, respectively. Recently, Niaz et al. [97] proposed a weighting scheme based on steady-state probabilities for selecting classes among the three indices (SPI, SPEI, and SPI). These indices are correlated for a one-month time scale and present similar information for the six stations in the northern areas [85, 96, 117]. The mathematical detail of the weighting scheme is available in [76].

Similarly, based on the mentioned studies, this study uses the SSP as a weighting scheme in the second phase of the RCAMD for selecting varying drought classes. Conclusively, to accomplish a specific task (i.e., characterize drought classes more comprehensively), therefore, in RCAMD, SSP is utilized to disseminate weights for several drought categories over various stations and indices. The use of SSP mainly characterizes the new vector of drought classes. The RCAMD suggests a comprehensive regional method for assessing meteorological drought and developing the base for taking more considerations for evaluating and monitoring drought at the regional level.

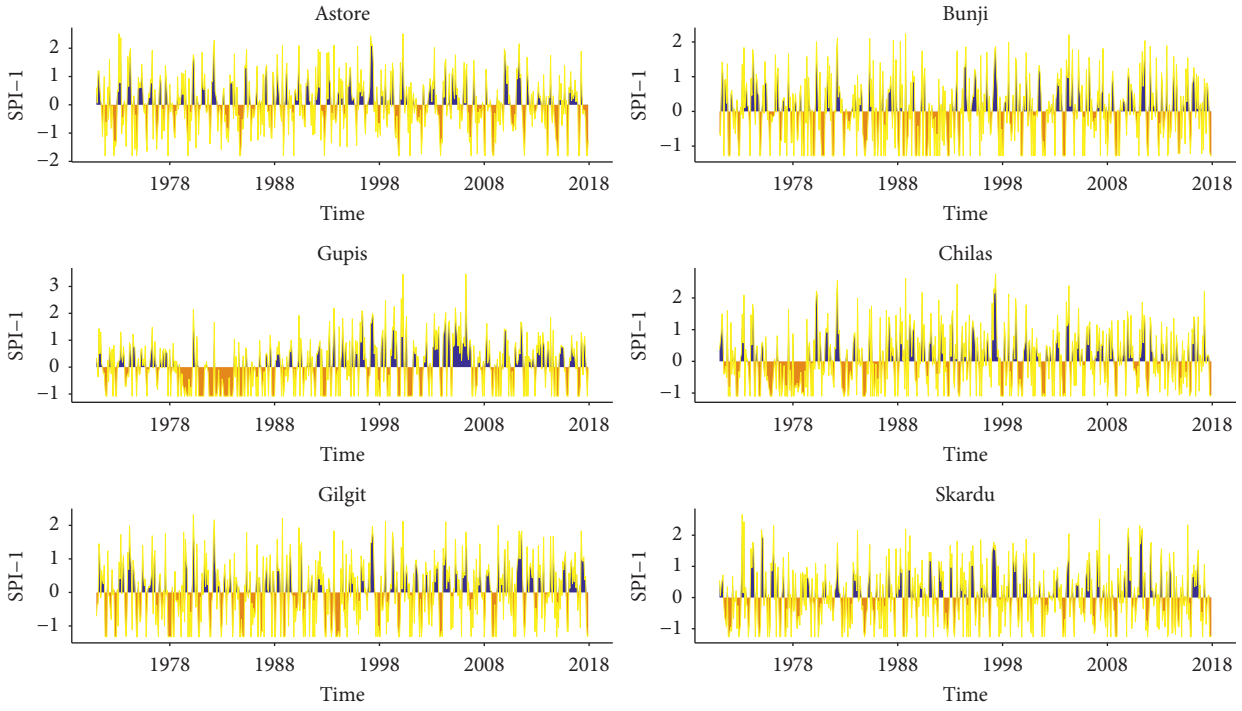

Figure 6: Temporal plots for selected stations based on SPI-1.

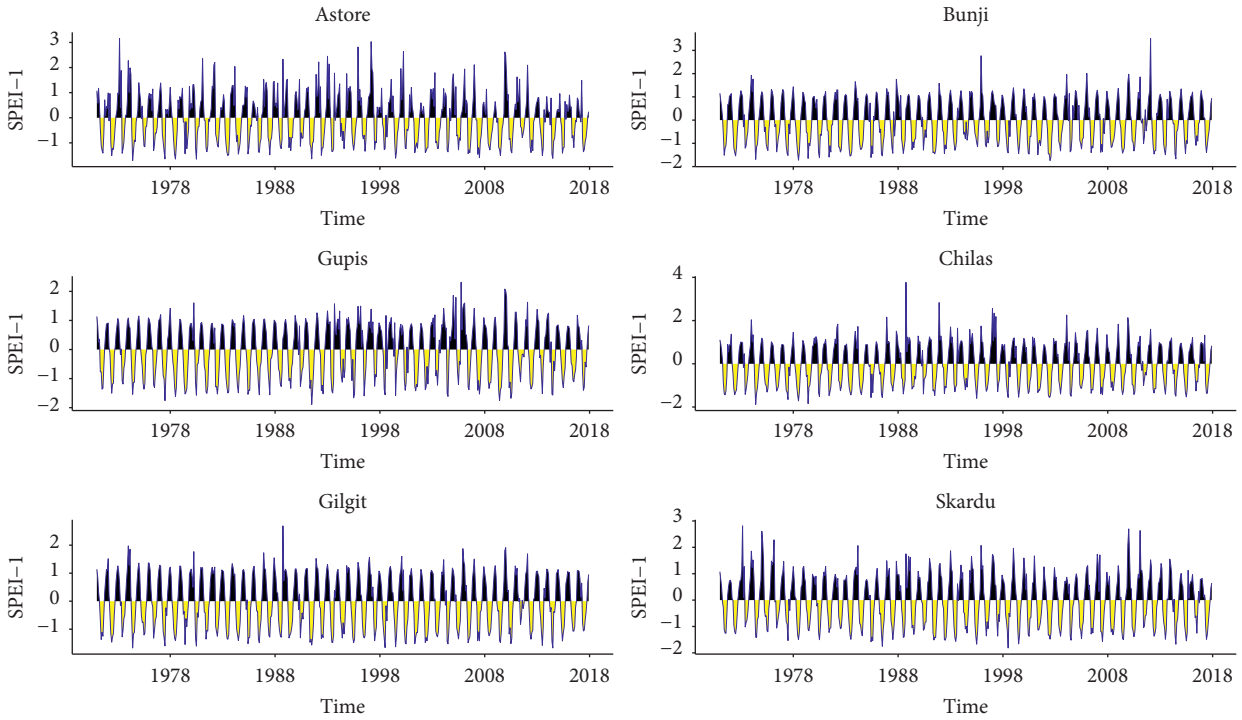

Figure 7: Temporal plots for selected stations based on SPEI-1.

4. Discussion

The data with varying features (precipitation, maximum and minimum temperature) are processed for the current analysis. The six stations in the northern areas are designated for data processing. The observed data are sufficient to calculate the varying SDI (SPI, SPEI, and SPTI). These SDIs are used to assess the drought severity in the selected region. The classification criteria are adopted from Li et al. [115] to characterize drought severity for the selected stations. The characterization and monitoring of the drought occurrences are vital components for the management and planning of

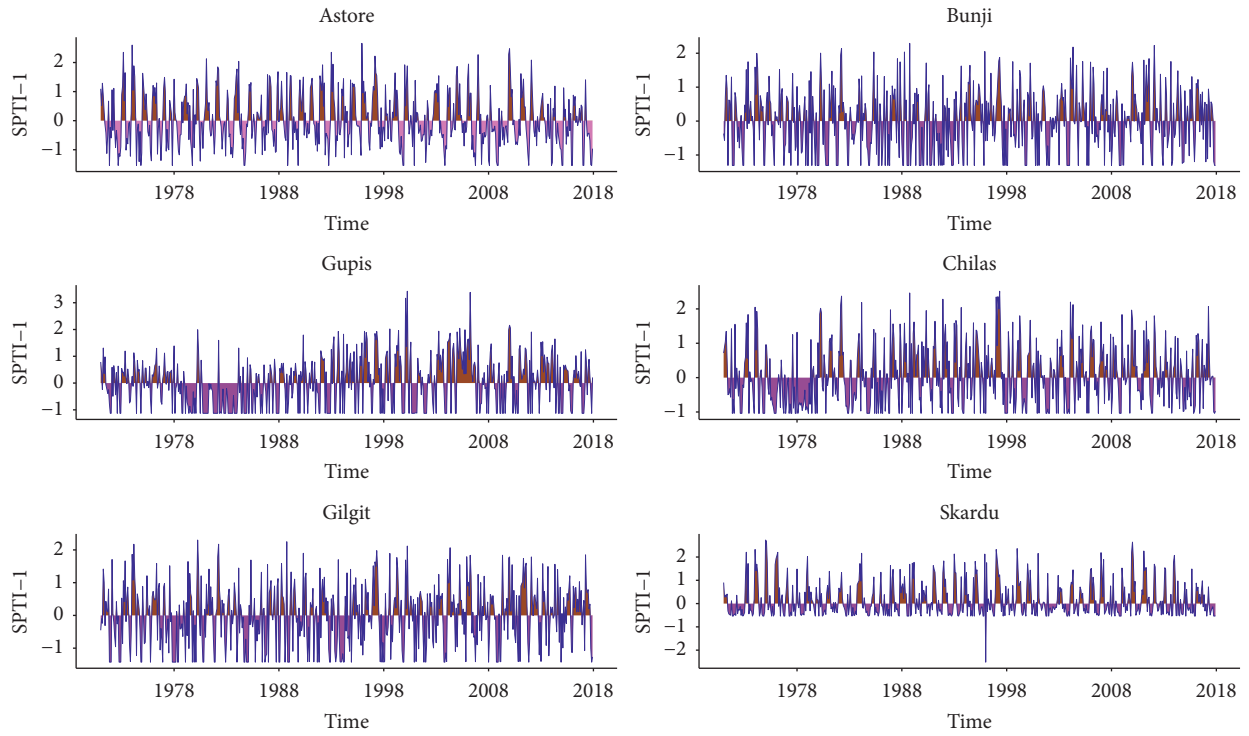

Figure 8: Temporal plots for selected stations based on SPTI-1.

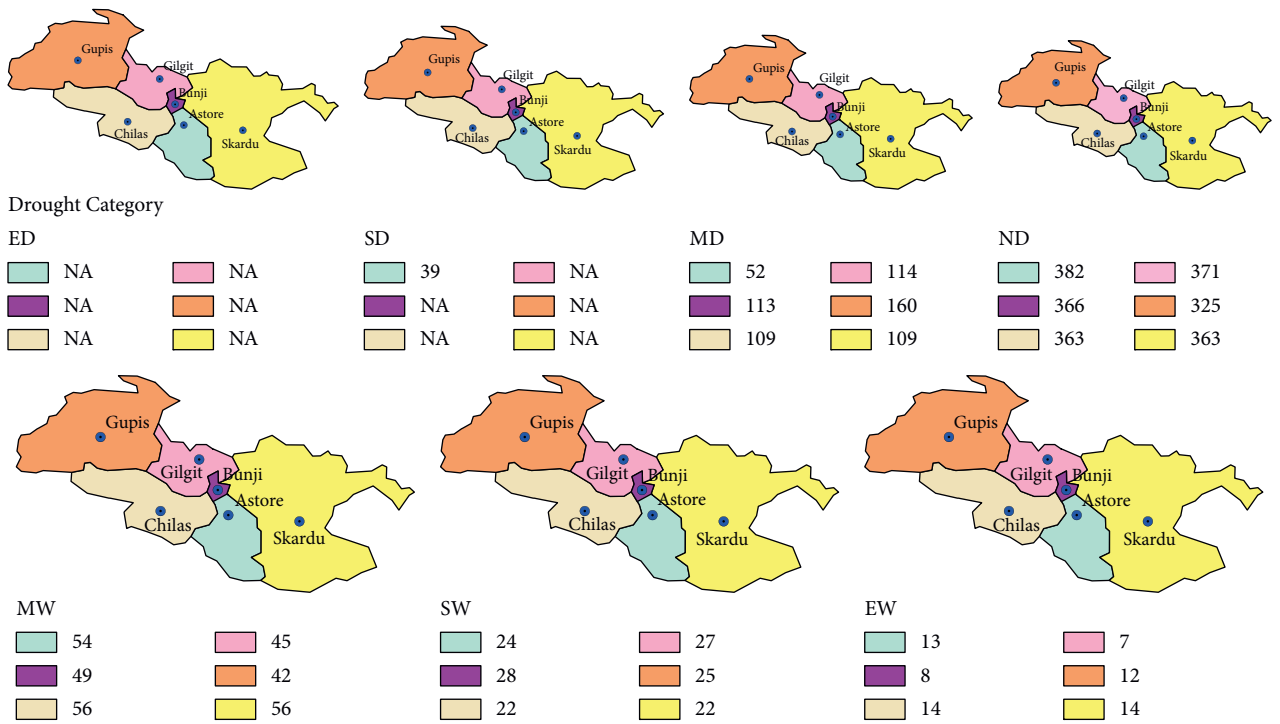

Figure 9: Varying drought categories observed in various stations for SPI-1. NA corresponding to any color shows that the specific drought category is not observed in the particular station. For instance, in Astore the ED is not observed; therefore, the NA is assigned corresponding to its color. The MD occurs 109 times in the selected time period ("January 1971 to December 2017") in Skardu Station. The ND appears 363 times in Skardu Station. The MW occurs 56 times in Skardu Station and so on. The remaining numerical values corresponding to each station and color can be observed accordingly for varying drought categories.

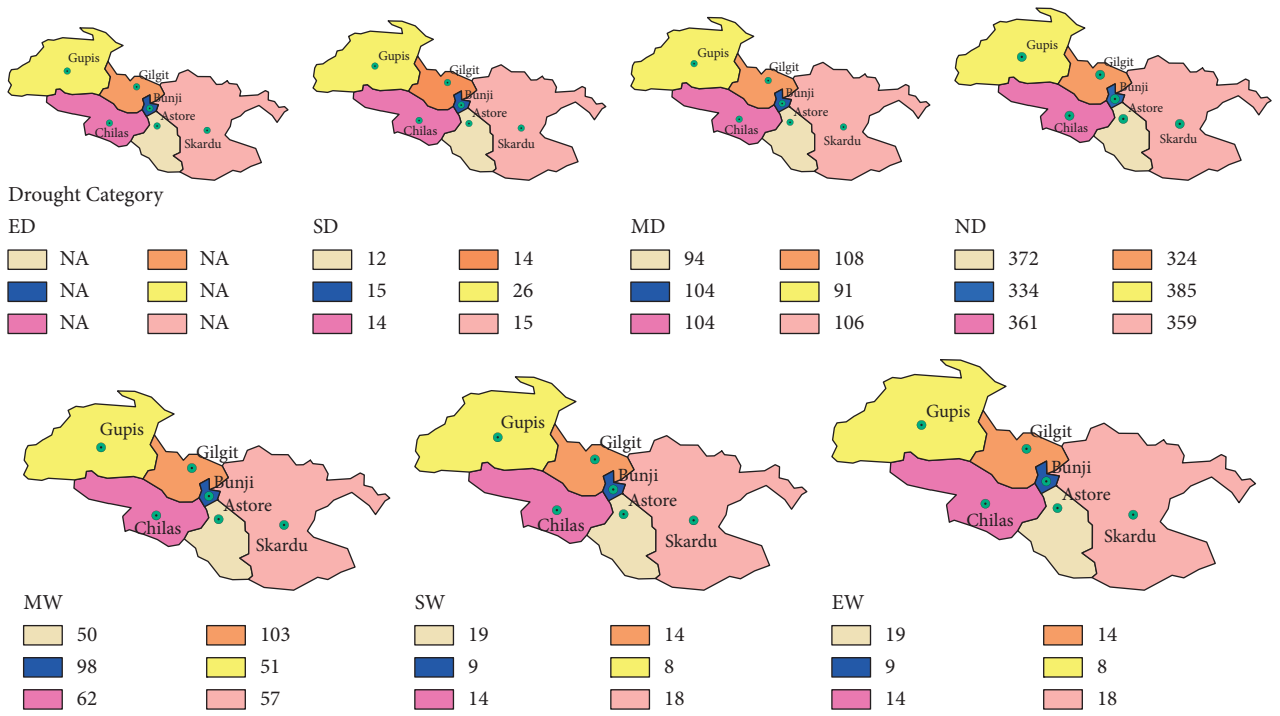

Figure 10: Varying drought categories observed in various stations for SPEI-1. Based on SPEI, MD occurs 91 times in Gupis during the selected time period ("January 1971 to December 2017"). In Gupis, the ND appears 385 times. MW drought category occurs 51 times in Gupis. 8 times it is observed that EW occurs in Gupis. The remaining drought categories observed in various stations can be perceived from the colors corresponding to each station.

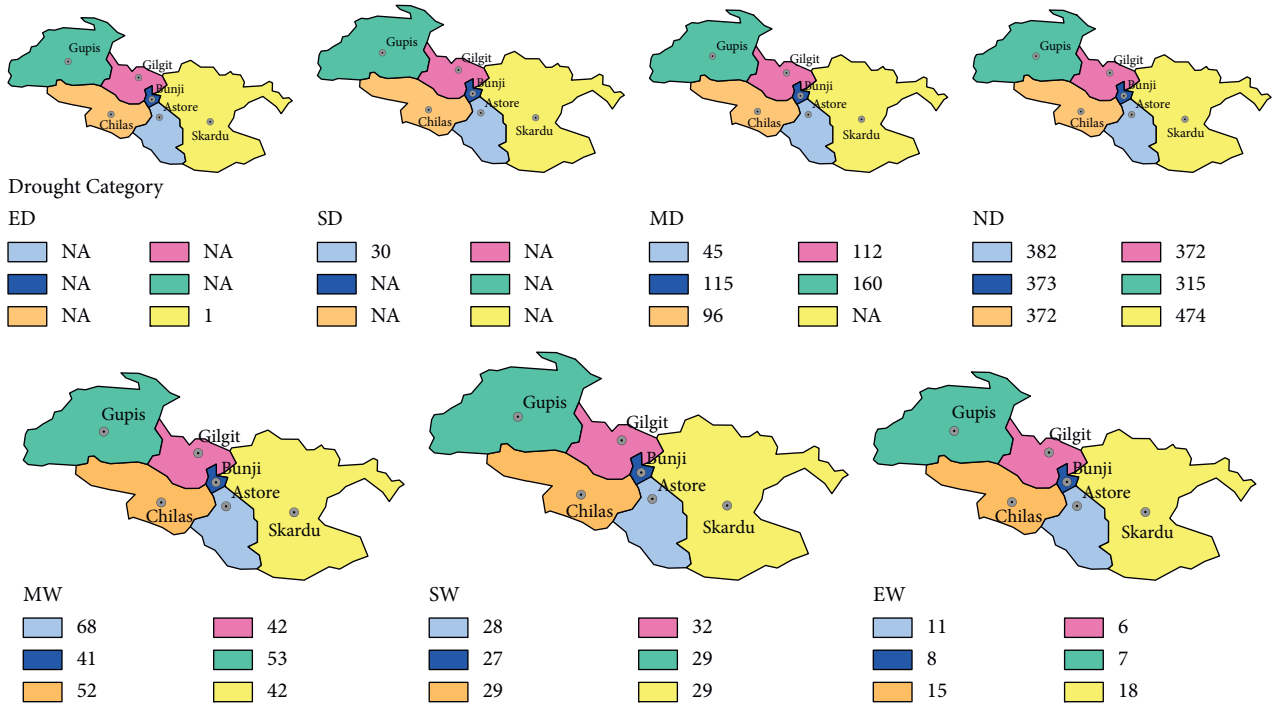

Figure 11: Varying drought categories observed in various stations for SPTI-1. Based on SPTI, the several drought categories appeared in selected stations. The higher the category values means the drought category is prevalent among other drought categories, which means possible measures should be prepared according to the drought category that is most prevalent in any station. The ND category has most likely to occur in several stations. For example, in Skardu the ND has occurred 474 times and in Astore ND has occurred 382 times. In Gupis, ND occurred 315 times, and in Bunji and Gilgit, it has occurred 373 and 372 times, respectively.

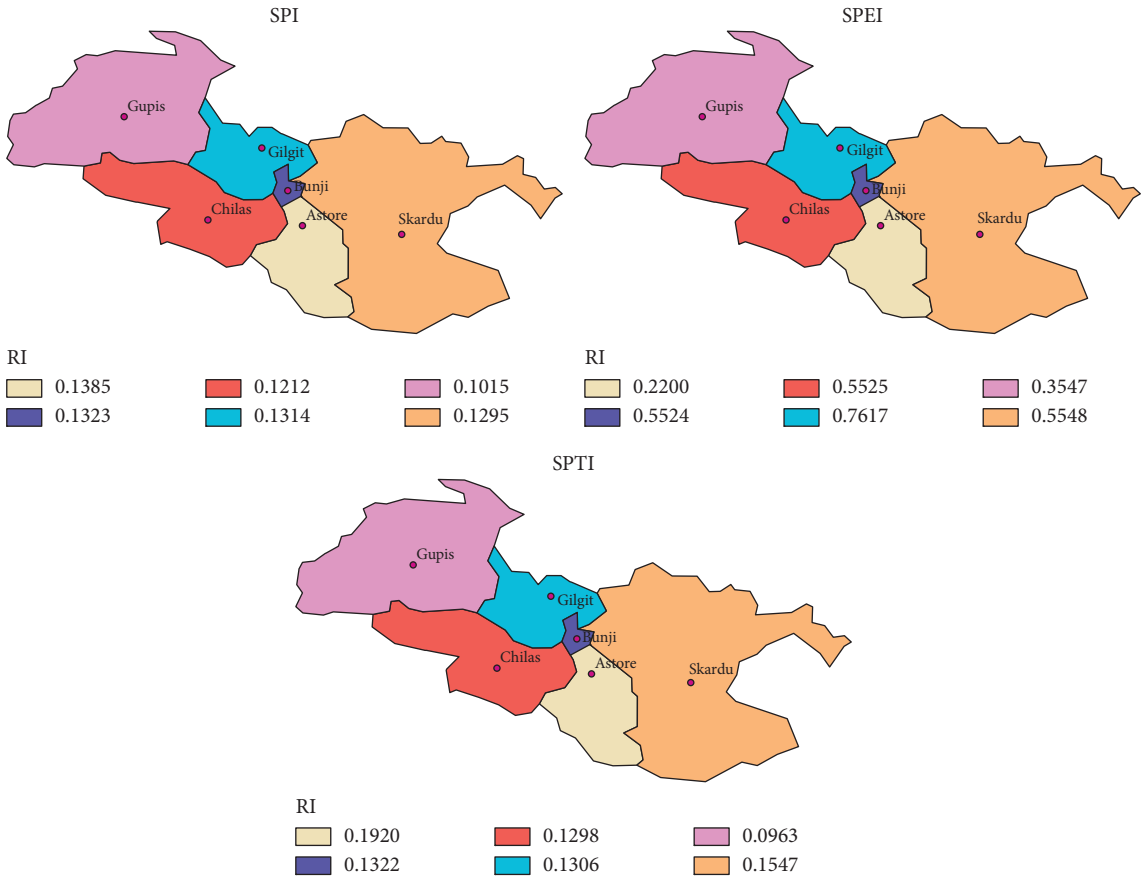

Figure 12: RI values calculated for various stations using three indices (SPI, SPEI, and SPTI).

Table 7: Relative importance (RI) values computed for three selected drought indices. The varying RI values can be observed for various indices. For example, for SPI, in the Astore Station, the RI value is 0.1385, and in Bunji, the RI value is 0.1323. The RI values of 0.1015, 0.1212, 0.1314, and 0.1295 are computed for Gupis, Chilas, Gilgit, and Skardu, respectively. The RI value in Astore is higher than other stations for SPI. In SPEI, RI value is 0.2200 for Astore Station. The RI value of 0.5524 is calculated for Bunji Station. For Gupis, Chilas, Gilgit, and Skardu, the RI values are 0.3547, 0.5525, 0.7617, and 0.5548, respectively. Based on SPEI, the Gilgit receives higher weights. In SPTI, the Astore has a higher RI value of 0.1922.

	Relative importance (RI)		
	SPI	SPEI	SPTI
Astore	0.1385	0.2200	0.1922
Bunji	0.1323	0.5524	0.1322
Gupis	0.1015	0.3547	0.0963
Chilas	0.1212	0.5525	0.1298
Gilgit	0.1314	0.7617	0.1306
Skardu	0.1295	0.5548	0.1547

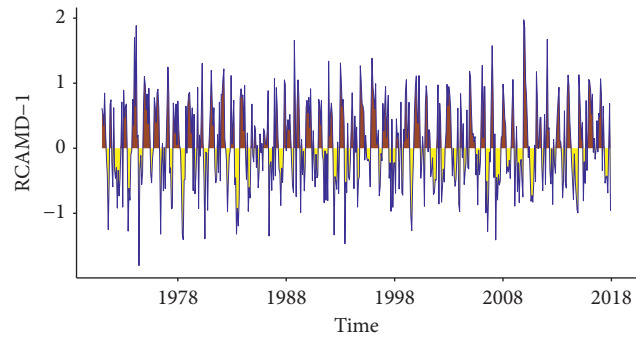

Figure 13: Temporal plots for selected stations based on SPTI at a one-month time scale.

water resources, mitigation strategies, and the creation of a climate-resilient society [25–27, 118–120]. Therefore, this study proposes an RCAMD to comprehensively and accurately characterize drought occurrences. The RCAMD employs MCFS and SSP to collect information from several stations and drought indices. The selected stations have a homogeneous pattern of drought occurrences among each other for specific indices. Ali et al. [96] cited these stations as homogeneous regions in their study. They used three SDIs (SPI, SPEI, and SPTI) and found that these stations are more and less similar in a specific time scale for three indices. Recently, Niaz et al. [76] considered these stations as homogeneous and developed a comprehensive index procedure to assimilate information. Further, Niaz et al. [98] considered these stations as homogeneous and proposed a regional-level propagation framework that is used to collect information from various indices. However, this study found a gap in their research; the mentioned research had considered all stations for the analysis, given that those

Table 8: Classif. drought categories received weights (steady-state weights (SSWs)) in various months using SPI-1 for the year 2017 in particular stations. For example, for the Astore Station in January the SD receives SSW with a value of 0.0695. In Astore, during March the ND receives the SSW with a value of 0.6765. The ND weight is a higher weight among the selected drought categories. This indicates that ND is the prevalent drought category in the Astore Station. Moreover, the weights can be observed for selected drought classes in other stations.

Month	Astore		Bunji		Gupis		Chilas		Gilgit		Skardu	
	Classif.	Weights	Classif.	Weights	Classif.	Weights	Classif.	Weights	Classif.	Weights	Classif.	Weights
1	SD	0.0695	MD	0.2012	MD	0.2842	ND	0.6426	ND	0.6569	ND	0.6836
2	SD	0.0695	ND	0.6480	MD	0.2842	ND	0.6426	ND	0.6569	ND	0.6836
3	ND	0.6765	MD	0.2012	ND	0.5755	ND	0.6426	MD	0.2030	ND	0.6836
4	SW	0.0425	ND	0.6480	MW	0.0746	EW	0.0248	SW	0.0479	EW	0.0231
5	ND	0.6765	ND	0.6480	ND	0.5755	ND	0.6426	ND	0.6569	ND	0.6836
6	ND	0.6765	ND	0.6480	ND	0.5755	ND	0.6426	ND	0.6569	ND	0.6836
7	ND	0.6765	ND	0.6480	ND	0.5755	ND	0.6426	MW	0.0798	ND	0.6836
8	ND	0.6765	ND	0.6480	MW	0.0746	ND	0.6426	ND	0.6569	ND	0.6836
9	ND	0.6765	ND	0.6480	ND	0.5755	ND	0.6426	ND	0.6569	ND	0.6836
10	SD	0.0695	MD	0.2012	ND	0.5755	MD	0.1940	ND	0.6569	MD	0.1566
11	SD	0.0695	MD	0.2012	MD	0.2842	MD	0.1940	MD	0.2030	MD	0.1566
12	MD	0.0925	MD	0.2012	ND	0.5755	MD	0.1940	MD	0.2030	MD	0.1566

Table 9: Classif. drought categories received SSW in various months. The SSW is computed based on the SPEI-1 for the year, 2017, in chosen stations. For instance, in the Skardu Station ND receives SSW with a value of 0.6378. In June of Skardu, the MD receives SSW with a value of 0.1887. It can be observed that ND category received greater weights than other selected drought categories. It can be observed in most of the selected stations and drought indices that the ND is prevalent. Further, the weights of other drought categories in varying stations can be noted accordingly.

Month	Astore		Bunji		Gupis		Chilas		Gilgit		Skardu	
	Classif.	Weights	Classif.	Weights	Classif.	Weights	Classif.	Weights	Classif.	Weights	Classif.	Weights
1	ND	0.6611	ND	0.5937	ND	0.6836	ND	0.6413	MW	0.1800	ND	0.6378
2	ND	0.6611	ND	0.5937	ND	0.6836	ND	0.6413	ND	0.5760	ND	0.6378
3	ND	0.6611	ND	0.5937	ND	0.6836	ND	0.6413	ND	0.5760	ND	0.6378
4	MW	0.0866	ND	0.5937	ND	0.6836	MW	0.1079	ND	0.5760	ND	0.6378
5	ND	0.6611	MD	0.1853	ND	0.6836	ND	0.6413	ND	0.5760	ND	0.6378
6	MD	0.1672	MD	0.1853	MD	0.1620	MD	0.1852	MD	0.1926	MD	0.1887
7	MD	0.1672	MD	0.1853	MD	0.1620	MD	0.1852	MD	0.1926	MD	0.1887
8	ND	0.6611	ND	0.5937	ND	0.6836	ND	0.6413	ND	0.5760	ND	0.6378
9	ND	0.6611	ND	0.5937	ND	0.6836	ND	0.6413	ND	0.5760	ND	0.6378
10	ND	0.6611	ND	0.5937	ND	0.6836	ND	0.6413	ND	0.5760	ND	0.6378
11	ND	0.6611	ND	0.5937	ND	0.6836	ND	0.6413	ND	0.5760	ND	0.6378
12	ND	0.6611	ND	0.5937	ND	0.6836	ND	0.6413	ND	0.5760	ND	0.6378

Table 10: Classif. drought categories received SSW in several months. The SSW is calculated based on SPTI-1 for the year, 2017, in certain stations. Using SPTI-1 in January of Gupis, MD occurred. The MD received SSW by a value of 0.2842. Further, in December (Dec) of Gupis ND received SSW by a value of 0.5577. In December of Skardu, ND received SSW by a value of 0.8401. The varying behavior of SSW for several stations and months can be examined accordingly.

Month	Astore		Bunji		Gupis		Chilas		Gilgit		Skardu	
	Classif.	Weights	Classif.	Weights	Classif.	Weights	Classif.	Weights	Classif.	Weights	Classif.	Weights
1	SD	0.0534	MD	0.2047	MD	0.2842	ND	0.6590	ND	0.6587	ND	0.8401
2	SD	0.0534	ND	0.6604	MD	0.2842	ND	0.6590	ND	0.6587	ND	0.8401
3	ND	0.6789	MD	0.2047	ND	0.5577	ND	0.6590	MD	0.1994	ND	0.8401
4	MW	0.1187	ND	0.6604	MW	0.0941	EW	0.0266	SW	0.0568	ND	0.8401
5	ND	0.6789	ND	0.6604	ND	0.5577	ND	0.6590	ND	0.6587	ND	0.8401
6	ND	0.6789	ND	0.6604	ND	0.5577	ND	0.6590	ND	0.6587	ND	0.8401
7	ND	0.6789	ND	0.6604	ND	0.5577	ND	0.6590	ND	0.6587	ND	0.8401
8	ND	0.6789	ND	0.6604	ND	0.5577	ND	0.6590	ND	0.6587	ND	0.8401
9	ND	0.6789	ND	0.6604	ND	0.5577	ND	0.6590	ND	0.6587	ND	0.8401
10	SD	0.0534	MD	0.2047	ND	0.5577	ND	0.6590	MD	0.1994	ND	0.8401
11	SD	0.0534	MD	0.2047	MD	0.2842	MD	0.1705	MD	0.1994	ND	0.8401
12	ND	0.6789	MD	0.2047	ND	0.5577	ND	0.6590	MD	0.1994	ND	0.8401

stations were homogeneous. Hence, it was counterproductive to study all stations in a homogeneous environment. It underpins a gap addressed in this current research by accumulating more comprehensive information. The present research proposes a new method, RCAMD, which provides more comprehensive results. In the first phase, the RCAMD employed MCFS to separately provide important stations for each index. For example, there are three indices (SPI, SPEI, and SPTI) and six stations in the current analysis. The MCFS uses SPI for selecting important stations among six selected stations. Then, MCFS uses SPEI to select the important station from six selected stations, and similarly, it employs SPTI for selecting an important station from the selected stations. Hence, three vectors of the observations are computed by MCFS for each index separately in the first phase. In the second phase, using SSP the RCAMD provides comprehensive information about various drought classes among selected indices and stations. Hence, the results related to the RCAMD provide a comprehensive assessment of meteorological drought at the regional level and bring a new method to consider more on drought assessment and monitoring. The RCAMD can efficiently work for early warning and mitigation policies. It can be used to make better management and planning to enhance the capabilities of forecasting procedures to decrease the vulnerability of society to drought and its forgoing impacts.

5. Conclusion

Drought is one of the multifaceted natural hazards that has adverse impacts on the economy, water resources, and other environmental structures worldwide. However, the assessment and analysis of drought are crucial, specifically to sound water resource planning and management at the regional level. Therefore, the assessment and monitoring of drought in a region are thus vital to decrease its vulnerability to negative impacts. Therefore, this study proposes an RCAMD. The RCAMD employs MCFS and SSP to accumulate information from several stations and drought indices comprehensively. The three commonly used SDIs are jointly analyzed for the computation of RCAMD. The RCAMD is performed at the six designated stations in the northern areas of Pakistan. The results related to the RCAMD provide a comprehensive assessment of meteorological drought at the regional level and bring a new method to take more consideration on drought assessment and monitoring. Moreover, the RCAMD considers the initial state, and the transition probabilities are constant by assuming time homogeneous progression; however, it can be considered temporal characteristics to improve drought monitoring efficiency for the selected stations. Further, the results of RCAMD would be entertained for the current scenario and application site; however, it cannot be generalized for other climatic conditions. The climatology conditions of the selected stations will change the outcomes and influence the extrapolations. Moreover, the categorization of the given data from other indices in the selected stations can implicitly be useful to increase the capabilities for drought monitoring.

Data Availability

The data and codes used to prepare the manuscript are available from the corresponding author and can be provided upon request.

Ethical Approval

All procedures followed were in accordance with the ethical standards of the Helsinki Declaration of 1975, as revised in 2000.

Consent

All authors voluntarily agreed to participate in this research study and agreed to publication; there is no legal constraint in publishing the data used in the manuscript.

Conflicts of Interest

The authors declare that there are no conflicts of interest.

Authors' Contributions

All authors contributed equally.

Acknowledgments

The author extends his appreciation to the Deanship of Scientific Research at King Khalid University for funding this work under grant number (RGP.2/34/43), received by Mohammed M. Almazah (http://www.kku.edu.sa/).

References

[1] D. A. Wilhite and M. H. Glantz, "Understanding: the drought phenomenon: the role of definitions," *Water International*, vol. 10, no. 3, pp. 111–120, 1985.

[2] Z. Kalantari, C. S. S. Ferreira, S. Keesstra, and G. Destouni, "Nature-based solutions for flood-drought risk mitigation in vulnerable urbanizing parts of East-Africa," *Current Opinion in Environmental Science & Health*, vol. 5, pp. 73–78, 2018.

[3] G. van der Schrier, R. P. Allan, A. Ossó et al., "The 1921 European drought: impacts, reconstruction and drivers," *Climate of the Past*, vol. 17, no. 5, pp. 2201–2221, 2021.

[4] S. Ruwanza, G. Thondhlana, and M. Falayi, "Research progress and conceptual insights on drought impacts and responses among smallholder farmers in South Africa: a review," *Land*, vol. 11, no. 2, p. 159, 2022.

[5] Y. Qu, X. Yang, W. Chang, J. Lv, and Z. Su, "Recurrence analysis of extreme historical drought under the current defense conditions in China," *The Science of the Total Environment*, vol. 822, Article ID 153400, 2022.

[6] R. J. Araneda-Cabrera, M. Bermúdez, and J. Puertas, "Benchmarking of drought and climate indices for agricultural drought monitoring in Argentina," *The Science of the Total Environment*, vol. 790, Article ID 148090, 2021.

[7] K. A. Kumar, G. O. Reddy, P. Masilamani, S. Y. Turkar, and P. Sandeep, "Integrated drought monitoring index: a tool to monitor agricultural drought by using time-series datasets of space-based earth observation satellites," *Advances in Space Research*, vol. 67, no. 1, pp. 298–315, 2021.

[8] M. Sugg, J. Runkle, R. Leeper et al., "A scoping review of drought impacts on health and society in North America," *Climatic Change*, vol. 162, no. 3, pp. 1177–1195, 2020.

[9] C. P. Kala, "Environmental and socio-economic impacts of drought in India: lessons for drought management," *Applied Ecology and Environmental Sciences*, vol. 5, no. 2, pp. 43–48, 2017.

[10] K. R. Kumawat and N. K. Sharma, "Effect of drought stress on plants growth," *Popular Kheti*, vol. 6, pp. 239–241, 2018.

[11] T. Zhang, X. Su, G. Zhang, H. Wu, G. Wang, and J. Chu, "Evaluation of the impacts of human activities on propagation from meteorological drought to hydrological drought in the Weihe River Basin, China," *The Science of the Total Environment*, vol. 819, Article ID 153030, 2022.

[12] S. Mansoor, N. Kour, S. Manhas et al., "Biochar as a tool for effective management of drought and heavy metal toxicity," *Chemosphere*, vol. 271, Article ID 129458, 2021.

[13] C. Greene, "Drought isn't just water, it is living": narratives of drought vulnerability in California's San Joaquin Valley," *Geoforum*, vol. 121, pp. 33–43, 2021.

[14] K. Bogati and M. Walczak, "The impact of drought stress on soil microbial community, enzyme activities and plants," *Agronomy*, vol. 12, no. 1, p. 189, 2022.

[15] K. S. Dayal, R. C. Deo, and A. A. Apan, "Spatio-temporal drought risk mapping approach and its application in the drought-prone region of south-east Queensland, Australia," *Natural Hazards*, vol. 93, no. 2, pp. 823–847, 2018.

[16] H. Aladaileh, M. Al Qinna, B. Karoly, E. Al-Karablieh, and J. Rakonczai, "An investigation into the spatial and temporal variability of the meteorological drought in Jordan," *Climate*, vol. 7, no. 6, p. 82, 2019.

[17] Z. Noorisameleh, W. A. Gough, and M. Mirza, "Persistence and spatial–temporal variability of drought severity in Iran," *Environmental Science and Pollution Research*, vol. 28, no. 35, pp. 48808–48822, 2021.

[18] J. E. Lee, M. Azam, S. U. Rehman et al., "Spatio-temporal variability of drought characteristics across Pakistan," *Paddy and Water Environment*, vol. 20, pp. 1–19, 2022.

[19] M. Esit and M. I. Yuce, *Copula-Based Bivariate Drought Severity and Duration Frequency Analysis Considering Spatial-Temporal Variability in the Ceyhan Basin*, Research Square, Turkey, 2022.

[20] H. Li, S. Liu, M. Yin et al., "Spatial and temporal variability and risk assessment of regional climate change in northern China: a case study in Shandong Province," *Natural Hazards*, vol. 111, pp. 1–38, 2022.

[21] R. Below, E. Grover-Kopec, and M. Dilley, "Documenting drought-related disasters: a global reassessment," *The Journal of Environment & Development*, vol. 16, no. 3, pp. 328–344, 2007.

[22] B. Sivakumar, "Global climate change and its impacts on water resources planning and management: assessment and challenges," *Stochastic Environmental Research and Risk Assessment*, vol. 25, no. 4, pp. 583–600, 2011.

[23] G. G. Haile, Q. Tang, S. M. Hosseini-Moghari et al., "Projected impacts of climate change on drought patterns over East Africa," *Earth's Future*, vol. 8, no. 7, Article ID e2020EF001502, 2020.

[24] A. R. Salvacion, "Multiscale drought hazard assessment in the Philippines," in *Computers in Earth and Environmental Sciences*, pp. 169–179, Elsevier, Amsterdam, Netherlands, 2022.

[25] J. Keyantash and J. A. Dracup, "The quantification of drought: an evaluation of drought indices," *Bulletin of the American Meteorological Society*, vol. 83, no. 8, pp. 1167–1180, 2002.

[26] M. Wens, J. M. Johnson, C. Zagaria, and T. I. Veldkamp, "Integrating human behavior dynamics into drought risk assessment—a sociohydrologic, agent-based approach," *Wiley Interdisciplinary Reviews: Water*, vol. 6, no. 4, p. e1345, 2019.

[27] A. Danandeh Mehr, A. Rikhtehgar Ghiasi, Z. M. Yaseen, A. U. Sorman, and L. Abualigah, "A novel intelligent deep learning predictive model for meteorological drought forecasting," *Journal of Ambient Intelligence and Humanized Computing*, pp. 1–15, 2022.

[28] S. Deng, S. Liu, and X. Mo, "Assessment and attribution of China's droughts using an integrated drought index derived from GRACE and GRACE-FO data," *Journal of Hydrology*, vol. 603, Article ID 127170, 2021.

[29] Y. Yihdego, B. Vaheddoost, and R. A. Al-Weshah, "Drought indices and indicators revisited," *Arabian Journal of Geosciences*, vol. 12, no. 3, pp. 1–12, 2019.

[30] A. R. Zarei, "Analysis of changes trend in spatial and temporal pattern of drought over south of Iran using standardized precipitation index (SPI)," *SN Applied Sciences*, vol. 1, no. 5, pp. 1–14, 2019.

[31] D. D. Zuo, W. Hou, Q. Zhang, and P. C. Yan, "Sensitivity analysis of standardized precipitation index to climate state selection in China," *Advances in Climate Change Research*, vol. 13, 2021.

[32] L. J. Cerpa Reyes, H. Ávila Rangel, and L. C. S. Herazo, "Adjustment of the standardized precipitation index (SPI) for the evaluation of drought in the arroyo pechelín basin, Colombia, under zero monthly precipitation conditions," *Atmosphere*, vol. 13, no. 2, p. 236, 2022.

[33] P. Dukat, E. Bednorz, K. Ziemblińska, and M. Urbaniak, "Trends in drought occurrence and severity at mid-latitude European stations (1951–2015) estimated using standardized precipitation (SPI) and precipitation and evapotranspiration (SPEI) indices," *Meteorology and Atmospheric Physics*, vol. 134, no. 1, pp. 1–21, 2022.

[34] J. Berger, J. Palta, and V. Vadez, "An integrated framework for crop adaptation to dry environments: responses to transient and terminal drought," *Plant Science*, vol. 253, pp. 58–67, 2016.

[35] J. Dar and A. Q. Dar, "Spatio-temporal variability of meteorological drought over India with footprints on agricultural production," *Environmental Science and Pollution Research*, vol. 28, pp. 55796–55809, 2021.

[36] L. Ma, Q. Huang, S. Huang et al., "Propagation dynamics and causes of hydrological drought in response to meteorological drought at seasonal timescales," *Hydrology Research*, vol. 53, no. 1, pp. 193–205, 2022.

[37] J. Wu, X. Chen, X. Yuan, H. Yao, Y. Zhao, and A. AghaKouchak, "The interactions between hydrological drought evolution and precipitation-streamflow relationship," *Journal of Hydrology*, vol. 597, Article ID 126210, 2021.

[38] M. Abdelkader and C. Yerdelen, "Hydrological drought variability and its teleconnections with climate indices," *Journal of Hydrology*, vol. 605, Article ID 127290, 2021.

[39] A. Kundu, D. Dutta, N. R. Patel, D. M. Denis, and K. K. Chattoraj, "Evaluation of socio-economic drought risk over bundelkhand region of India using analytic hierarchy process (AHP) and geo-spatial techniques," *Journal of the Indian Society of Remote Sensing*, vol. 49, no. 6, pp. 1365–1377, 2021.

[40] J. Han and Y. Yang, "The socio-economic effects of extreme drought events in northern China on the Ming dynasty in the late fifteenth century," *Climatic Change*, vol. 164, no. 3, pp. 1–17, 2021.

[41] M. Svoboda, D. LeComte, M. Hayes et al., "The drought monitor," *Bulletin of the American Meteorological Society*, vol. 83, no. 8, pp. 1181–1190, 2002.

[42] D. J. Williams, J. M. Gutiérrez, J. J. Calvete et al., "Ending the drought: new strategies for improving the flow of affordable, effective antivenoms in Asia and Africa," *Journal of Proteomics*, vol. 74, no. 9, pp. 1735–1767, 2011.

[43] T. Raziei, B. Saghafian, A. A. Paulo, L. S. Pereira, and I. Bordi, "Spatial patterns and temporal variability of drought in western Iran," *Water Resources Management*, vol. 23, no. 3, pp. 439–455, 2009.

[44] H. Wang, Y. Chen, Y. Pan, and W. Li, "Spatial and temporal variability of drought in the arid region of China and its relationships to teleconnection indices," *Journal of hydrology*, vol. 523, pp. 283–296, 2015.

[45] H. N. Bhalme and D. A. Mooley, "Large-scale droughts/floods and monsoon circulation," 1980, https://journals.ametsoc.org/view/journals/mwre/108/8/1520-0493_1980_108_1197_lsdamc_2_0_co_2.xml.

[46] T. B. McKee, N. J. Doesken, and J. Kleist, "The relationship of drought frequency and duration to time scales," in *Proceedings of the 8th Conference on Applied Climatology*, vol. 17, no. 22, pp. 179–183, American Meteorological Society, Anaheim, California, 17 January 1993.

[47] G. Tsakiris and H. J. E. W. Vangelis, "Establishing a drought index incorporating evapotranspiration," *European water*, vol. 9, no. 10, pp. 3–11, 2005.

[48] K. C. Mo, "Model-based drought indices over the United States," *Journal of Hydrometeorology*, vol. 9, no. 6, pp. 1212–1230, 2008.

[49] S. Shukla and A. W. Wood, "Use of a standardized runoff index for characterizing hydrologic drought," *Geophysical Research Letters*, vol. 35, no. 2, 2008.

[50] S. M. Vicente-Serrano, S. Beguería, and J. I. López-Moreno, "A multiscalar drought index sensitive to global warming: the standardized precipitation evapotranspiration index," *Journal of Climate*, vol. 23, no. 7, pp. 1696–1718, 2010.

[51] A. K. Mishra and V. P. Singh, "A review of drought concepts," *Journal of hydrology*, vol. 391, no. 1-2, pp. 202–216, 2010.

[52] M. D. Svoboda and B. A. Fuchs, *Handbook of Drought Indicators and Indices*, pp. 1–44, World Meteorological Organization, Geneva, Switzerland, 2016.

[53] Y. Bayissa, S. Maskey, T. Tadesse et al., "Comparison of the performance of six drought indices in characterizing historical drought for the upper Blue Nile basin, Ethiopia," *Geosciences*, vol. 8, no. 3, p. 81, 2018.

[54] S. Mukherjee, A. Mishra, and K. E. Trenberth, "Climate change and drought: a perspective on drought indices," *Current Climate Change Reports*, vol. 4, no. 2, pp. 145–163, 2018.

[55] A. S. Tefera, J. O. Ayoade, and N. J. Bello, "Comparative analyses of SPI and SPEI as drought assessment tools in Tigray Region, Northern Ethiopia," *SN Applied Sciences*, vol. 1, no. 10, pp. 1–14, 2019.

[56] D. M. Kimwatu, C. N. Mundia, and G. O. Makokha, "Developing a new socio-economic drought index for monitoring drought proliferation: a case study of Upper Ewaso Ngiro River Basin in Kenya," *Environmental Monitoring and Assessment*, vol. 193, no. 4, pp. 1–22, 2021.

[57] S. Bahmani, S. R. Naganna, M. A. Ghorbani, M. Shahabi, E. Asadi, and S. Shahid, "Geographically weighted regression hybridized with kriging model for delineation of drought-prone areas," *Environmental Modeling & Assessment*, vol. 26, no. 5, pp. 803–821, 2021.

[58] M. A. Faiz, Y. Zhang, N. Ma, F. Baig, F. Naz, and Y. Niaz, "Drought indices: aggregation is necessary or is it only the researcher's choice?" *Water Supply*, vol. 21, no. 8, pp. 3987–4002, 2021.

[59] A. Zargar, R. Sadiq, B. Naser, and F. I. Khan, "A review of drought indices," *Environmental Reviews*, vol. 19, no. NA, pp. 333–349, 2011.

[60] V. Blauhut, L. Gudmundsson, and K. Stahl, "Towards pan-European drought risk maps: quantifying the link between drought indices and reported drought impacts," *Environmental Research Letters*, vol. 10, no. 1, Article ID 014008, 2015.

[61] D. Tigkas, H. Vangelis, and G. Tsakiris, "Drought characterisation based on an agriculture-oriented standardised precipitation index," *Theoretical and Applied Climatology*, vol. 135, no. 3, pp. 1435–1447, 2019.

[62] T. Javed, Y. Li, S. Rashid et al., "Performance and relationship of four different agricultural drought indices for drought monitoring in China's mainland using remote sensing data," *The Science of the Total Environment*, vol. 759, Article ID 143530, 2021.

[63] E. Savelli, M. Rusca, H. Cloke, and G. Di Baldassarre, *Drought and Society: Scientific Progress, Blind Spots, and Future Prospects*, , p. e761, Wiley Interdisciplinary Reviews: Climate Change, 2022.

[64] F. Baret, G. Guyot, and D. J. Major, "July). TSAVI: a vegetation index which minimizes soil brightness effects on LAI and APAR estimation," in *12th Canadian Symposium on Remote Sensing Geoscience and Remote Sensing Symposium*vol. 3, , pp. 1355–1358, IEEE, 1989.

[65] A. Anyamba, C. J. Tucker, and J. R. Eastman, "NDVI anomaly patterns over Africa during the 1997/98 ENSO warm event," *International Journal of Remote Sensing*, vol. 22, no. 10, pp. 1847–1860, 2001.

[66] G. Tsakiris, D. Pangalou, and H. Vangelis, "Regional drought assessment based on the reconnaissance drought index (RDI)," *Water Resources Management*, vol. 21, no. 5, pp. 821–833, 2007.

[67] J. F. Brown, B. D. Wardlow, T. Tadesse, M. J. Hayes, and B. C. Reed, "The Vegetation Drought Response Index (VegDRI): a new integrated approach for monitoring drought stress in vegetation," *GIScience and Remote Sensing*, vol. 45, no. 1, pp. 16–46, 2008.

[68] W. C. Palmer, *Meteorological Drought*, vol. 58, US Weather Bureau, Washington, DC, 1965, Research paper no. 45.

[69] N. B. Guttman, J. R. Wallis, and J. R. M. Hosking, "Spatial comparability OF the palmer drought severity index 1," *JAWRA Journal of the American Water Resources Association*, vol. 28, no. 6, pp. 1111–1119, 1992.

[70] H. Ezzine, A. Bouziane, and D. Ouazar, "Seasonal comparisons of meteorological and agricultural drought indices in Morocco using open short time-series data," *International Journal of Applied Earth Observation and Geoinformation*, vol. 26, pp. 36–48, 2014.

[71] V. Poonia, S. Jha, and M. K. Goyal, "Copula based analysis of meteorological, hydrological and agricultural drought characteristics across Indian river basins," *International Journal of Climatology*, vol. 41, no. 9, pp. 4637–4652, 2021.

[72] F. Wang, H. Lai, Y. Li et al., "Dynamic variation of meteorological drought and its relationships with agricultural drought across China," *Agricultural Water Management*, vol. 261, Article ID 107301, 2022.

[73] S. Cao, L. Zhang, Y. He et al., "Effects and contributions of meteorological drought on agricultural drought under different climatic zones and vegetation types in Northwest China," *The Science of the Total Environment*, vol. 821, Article ID 153270, 2022.

[74] K. Duan and Y. Mei, "Comparison of meteorological, hydrological and agricultural drought responses to climate change and uncertainty assessment," *Water Resources Management*, vol. 28, no. 14, pp. 5039–5054, 2014.

[75] Y. Ding, X. Gong, Z. Xing et al., "Attribution of meteorological, hydrological and agricultural drought propagation in different climatic regions of China," *Agricultural Water Management*, vol. 255, Article ID 106996, 2021.

[76] R. Niaz, I. Hussain, Z. Ali et al., "A novel spatially weighted accumulative procedure for regional drought monitoring," *Tellus: DynamicMeteorologyandOceanography*, vol. 72, no. 1, pp. 1–13, 2020a.

[77] S. A. Banimahd and D. Khalili, "Factors influencing Markov chains predictability characteristics, utilizing SPI, RDI, EDI and SPEI drought indices in different climatic zones," *Water Resources Management*, vol. 27, no. 11, pp. 3911–3928, 2013.

[78] S. Beguería, S. M. Vicente-Serrano, F. Reig, and B. Latorre, "Standardized precipitation evapotranspiration index (SPEI) revisited: parameter fitting, evapotranspiration models, tools, datasets and drought monitoring," *International Journal of Climatology*, vol. 34, no. 10, pp. 3001–3023, 2014.

[79] J. H. Stagge, L. M. Tallaksen, L. Gudmundsson, A. F. Van Loon, and K. Stahl, "Candidate distributions for climatological drought indices (SPI and SPEI)," *International Journal of Climatology*, vol. 35, no. 13, pp. 4027–4040, 2015.

[80] M. J. Um, Y. Kim, D. Park, and J. Kim, "Effects of different reference periods on drought index (SPEI) estimations from 1901 to 2014," *Hydrology and Earth System Sciences*, vol. 21, no. 10, pp. 4989–5007, 2017.

[81] A. Manzano, M. A. Clemente, A. Morata et al., "Analysis of the atmospheric circulation pattern effects over SPEI drought index in Spain," *Atmospheric Research*, vol. 230, Article ID 104630, 2019.

[82] D. Hoffmann, A. J. Gallant, and J. M. Arblaster, "Uncertainties in drought from index and data selection," *Journal of Geophysical Research: Atmospheres*, vol. 125, no. 18, Article ID e2019JD031946, 2020.

[83] A. Dikshit, B. Pradhan, and A. Huete, "An improved SPEI drought forecasting approach using the long short-term memory neural network," *Journal of Environmental Management*, vol. 283, Article ID 111979, 2021.

[84] Z. Ali, I. Hussain, M. Faisal et al., "A novel multi-scalar drought index for monitoring drought: the standardized precipitation temperature index," *Water Resources Management*, vol. 31, no. 15, pp. 4957–4969, 2017.

[85] R. Niaz, I. M. Almanjahie, Z. Ali, M. Faisal, and I. Hussain, "A novel framework for selecting informative meteorological stations using Monte Carlo feature selection (MCFS) algorithm," *Advances in Meteorology*, vol. 2020, Article ID 5014280, 13 pages, 2020b.

[86] R. Niaz, M. Almazah, X. Zhang, I. Hussain, and M. Faisal, "Prediction for various drought classes using spatiotemporal categorical sequences," *Complexity*, vol. 2021, Article ID 7145168, 11 pages, 2021c.

[87] M. A. Asadi Zarch, H. Malekinezhad, M. H. Mobin, M. T. Dastorani, and M. R. Kousari, "Drought monitoring by reconnaissance drought index (RDI) in Iran," *Water Resources Management*, vol. 25, no. 13, pp. 3485–3504, 2011.

[88] Z. Hao and A. AghaKouchak, "Multivariate standardized drought index: a parametric multi-index model," *Advances in Water Resources*, vol. 57, pp. 12–18, 2013.

[89] M. A. A. Zarch, B. Sivakumar, and A. Sharma, "Droughts in a warming climate: a global assessment of Standardized precipitation index (SPI) and Reconnaissance drought index (RDI)," *Journal of hydrology*, vol. 526, pp. 183–195, 2015.

[90] S. Kim, P. Parhi, H. Jun, and J. Lee, "Evaluation of drought severity with a Bayesian network analysis of multiple drought indices," *Journal of Water Resources Planning and Management*, vol. 144, no. 1, Article ID 05017016, 2018.

[91] D. Rajsekhar, V. P. Singh, and A. K. Mishra, "Multivariate drought index: an information theory based approach for integrated drought assessment," *Journal of Hydrology*, vol. 526, pp. 164–182, 2015.

[92] M. Peña-Gallardo, S. M. Vicente-Serrano, F. Domínguez-Castro et al., "Effectiveness of drought indices in identifying impacts on major crops across the USA," *Climate Research*, vol. 75, no. 3, pp. 221–240, 2018.

[93] M. Peña-Gallardo, S. M. Vicente-Serrano, J. Hannaford et al., "Complex influences of meteorological drought time-scales on hydrological droughts in natural basins of the contiguous Unites States," *Journal of Hydrology*, vol. 568, pp. 611–625, 2019.

[94] M. A. Asadi Zarch, H. Malekinezhad, M. H. Mobin, M. T. Dastorani, and M. R. Kousari, "Drought monitoring by reconnaissance drought index (RDI) in Iran," *Water Resources Management*, vol. 25, no. 13, pp. 3485–3504, 2011.

[95] P. Das, S. R. Naganna, P. C. Deka, and J. Pushparaj, "Hybrid wavelet packet machine learning approaches for drought modeling," *Environmental Earth Sciences*, vol. 79, no. 10, pp. 1–18, 2020.

[96] Z. Ali, I. Hussain, M. Faisal et al., "A probabilistic weighted joint aggregative drought index (PWJADI) criterion for drought monitoring systems," *Tellus A: Dynamic Meteorology and Oceanography*, vol. 71, no. 1, Article ID 1588584, 2019.

[97] R. Niaz, M. Almazah, and I. Hussain, "A new framework to substantiate the prevalence of drought intensities," *Theoretical and Applied Climatology*, vol. 147, pp. 1–12, 2021a.

[98] R. Niaz, X. Zhang, Z. Ali et al., "A new propagation-based framework to enhance competency in regional drought monitoring," *Tellus A: Dynamic Meteorology and Oceanography*, vol. 73, no. 1, pp. 1–12, 2021b.

[99] R. Niaz, X. Almazah, and I. Hussain, "Assessing the probability of drought severity in a homogenous region," *Complexity*, vol. 2022, Article ID 3139870, 8 pages, 2022.

[100] P. A. Van Lange and D. G. Rand, "Human cooperation and the crises of climate change, COVID-19, and misinformation," *Annual Review of Psychology*, vol. 73, pp. 379–402, 2022.

[101] M. Puchlik, J. Piekutin, and K. Dyczewska, "Analysis of the impact of climate change on surface water quality in north-eastern Poland," *Energies*, vol. 15, no. 1, p. 164, 2022.

[102] S. Das and A. J. Mishra, "Dynamics of indigenous community's food and culture in the time of climate change in the Himalayan region," *Journal of Ethnic Foods*, vol. 9, no. 1, pp. 1–15, 2022.

[103] M. A. Khan, A. Tahir, N. Khurshid, M. Ahmed, and H. Boughanmi, "Economic effects of climate change-induced

loss of agricultural production by 2050: a case study of Pakistan," *Sustainability*, vol. 12, no. 3, p. 1216, 2020.
[104] S. Fahad and J. Wang, "Climate change, vulnerability, and its impacts in rural Pakistan: a review," *Environmental Science and Pollution Research*, vol. 27, no. 2, pp. 1334–1338, 2020.
[105] A. A. Chandio, H. Magsi, and I. Ozturk, "Examining the effects of climate change on rice production: case study of Pakistan," *Environmental Science and Pollution Research*, vol. 27, no. 8, pp. 7812–7822, 2020.
[106] Z. Munir, S. Shrestha, M. Zaman, M. I. Khan, M. M. Akram, and M. N. Tahir, "Climate change impacts on wheat yield: a multi-modeling case study of central Punjab, Pakistan," *Climate Research*, vol. 87, pp. 13–37, 2022.
[107] S. Abbas, "Climate change and major crop production: evidence from Pakistan," *Environmental Science and Pollution Research*, vol. 29, no. 4, pp. 5406–5414, 2022.
[108] S. Rasool, I. A. Rana, and S. Ahmad, "Linking flood risk perceptions and psychological distancing to climate change: a case study of rural communities along Indus and Chenab rivers, Pakistan," *International Journal of Disaster Risk Reduction*, vol. 70, Article ID 102787, 2022.
[109] M. Raza, "Analysis OF precipitation trends IN gilgit-baltistan (gb), Pakistan," *Journal of Mountain Area Research*, vol. 4, pp. 16–23, 2019.
[110] M. Ali, B. Jan, F. A. K. Afridi, and M. Yonus, "The best fitted probabilistic modelling for seasonal extreme rainfall of Gilgit-Baltistan, Pakistan," *International Journal of Global Warming*, vol. 23, no. 4, pp. 355–369, 2021.
[111] Z. Iqbal, S. Shahid, K. Ahmed, T. Ismail, and N. Nawaz, "Spatial distribution of the trends in precipitation and precipitation extremes in the sub-Himalayan region of Pakistan," *Theoretical and Applied Climatology*, vol. 137, no. 3, pp. 2755–2769, 2019.
[112] R. Niaz, X. Zhang, N. Iqbal, M. Almazah, T. Hussain, and I. Hussain, "Logistic regression analysis for spatial patterns of drought persistence," *Complexity*, vol. 2021, Article ID 3724919, 13 pages, 2021d.
[113] R. Niaz, I. Hussain, Z. Ali, and M. Faisal, "A novel framework for regional pattern recognition of drought intensities," *Arabian Journal of Geosciences*, vol. 14, no. 16, pp. 1–16, 2021e.
[114] R. Niaz, I. Hussain, X. Zhang et al., "Prediction of drought severity using model-based clustering," *Mathematical Problems in Engineering*, vol. 2021, Article ID 9954293, 10 pages, 2021f.
[115] X. Li, B. He, X. Quan, Z. Liao, and X. Bai, "Use of the standardized precipitation evapotranspiration index (SPEI) to characterize the drying trend in southwest China from 1982–2012," *Remote Sensing*, vol. 7, no. 8, pp. 10917–10937, 2015.
[116] Z. Ali, I. Hussain, M. Faisal et al., "Propagation of the multi-scalar aggregative standardized precipitation temperature index and its application," *Water Resources Management*, vol. 34, no. 2, pp. 699–714, 2020.
[117] Z. Ali, I. M. Almanjahie, I. Hussain, M. Ismail, and M. Faisal, "A novel generalized combinative procedure for Multi-Scalar standardized drought Indices-The long average weighted joint aggregative criterion," *Tellus A: Dynamic Meteorology and Oceanography*, vol. 72, no. 1, pp. 1–23, 2020.
[118] M. Waseem, M. Ajmal, and T. W. Kim, "Development of a new composite drought index for multivariate drought assessment," *Journal of Hydrology*, vol. 527, pp. 30–37, 2015.
[119] J. Kwak, H. Joo, J. Jung, J. Lee, S. Kim, and H. S. Kim, "A case study: bivariate drought identification on the Andong dam, South Korea," *Stochastic Environmental Research and Risk Assessment*, vol. 35, no. 3, pp. 549–560, 2021.
[120] H. S. Esfandabadi, M. G. Asl, Z. S. Esfandabadi, S. Gautam, and M. Ranjbari, "Drought assessment in paddy rice fields using remote sensing technology towards achieving food security and SDG2," *British Food Journal*, 2022.

Hindawi
Complexity
Volume 2022, Article ID 5433474, 22 pages
https://doi.org/10.1155/2022/5433474

Research Article

Compressive Strength Prediction Using Coupled Deep Learning Model with Extreme Gradient Boosting Algorithm: Environmentally Friendly Concrete Incorporating Recycled Aggregate

Mayadah W. Falah,[1] **Sadaam Hadee Hussein**,[2] **Mohammed Ayad Saad**,[3] **Zainab Hasan Ali**,[4] **Tan Huy Tran**,[5] **Rania M. Ghoniem**,[6] **and Ahmed A. Ewees**[7,8]

[1]*Building and Construction Engineering Technology Department, AL-Mustaqbal University College, Hillah 51001, Iraq*
[2]*Department of Civil Engineering, Al-Maarif University College, Ramadi 31001, Iraq*
[3]*Department of Medical Instrumentations Technique Engineering, Alkitab University, Kirkuk, Iraq*
[4]*Civil Engineering Department, College of Engineering, University of Diyala, Baquba 32001, Iraq*
[5]*Faculty of Civil Engineering, Ton Duc Thang University, Ho Chi Minh City, Vietnam*
[6]*Department of Information Technology, College of Computer and Information Sciences, Princess Nourah bint Abdulrahman University, P.O. Box 84428, Riyadh 11671, Saudi Arabia*
[7]*Department of e-Systems, University of Bisha, Bisha 61922, Saudi Arabia*
[8]*Department of Computer, Damietta University, Damietta 34511, Egypt*

Correspondence should be addressed to Tan Huy Tran; trantanhuy@tdtu.edu.vn

Received 7 January 2022; Revised 26 February 2022; Accepted 9 April 2022; Published 14 May 2022

Academic Editor: M. De Aguiar

The application of recycled aggregate as a sustainable material in construction projects is considered a promising approach to decrease the carbon footprint of concrete structures. Prediction of compressive strength (CS) of environmentally friendly (EF) concrete containing recycled aggregate is important for understanding sustainable structures' concrete behaviour. In this research, the capability of the deep learning neural network (DLNN) approach is examined on the simulation of CS of EF concrete. The developed approach is compared to the well-known artificial intelligence (AI) approaches named multivariate adaptive regression spline (MARS), extreme learning machines (ELMs), and random forests (RFs). The dataset was divided into three scenarios 70%-30%, 80%-20%, and 90%-10% for training/testing to explore the impact of data division percentage on the capacity of the developed AI model. Extreme gradient boosting (XGBoost) was integrated with the developed AI models to select the influencing variables on the CS prediction. Several statistical measures and graphical methods were generated to evaluate the efficiency of the presented models. In this regard, the results confirmed that the DLNN model attained the highest value of prediction performance with minimal root mean squared error (RMSE = 2.23). The study revealed that the highest prediction performance could be attained by increasing the number of variables in the prediction problem and using 90%-10% data division. The results demonstrated the robustness of the DLNN model over the other AI models in handling the complex behaviour of concrete. Due to the high accuracy of the DLNN model, the developed method can be used as a practical approach for future use of CS prediction of EF concrete.

1. Introduction

Consideration of sustainable development is an important requirement in the new era of the construction industry [1, 2]. Sustainable development is applied by reducing environmental impact and protecting natural resources. Increasing population growth led to the high demand for construction and, as a result, depletion of natural resources needed in concrete construction [3, 4]. Recently, many researchers have studied the production of environmental

friendly (EF) concrete, which has less harmful effects on nature [5–8]. One of the methods studied by the researchers is using recycled aggregate [9]. Production of construction debris and waste has been increasing using recycled materials in concrete production in the last years. The use of recycled aggregate in a construction project is considered a promising method to decrease the carbon footprint of a concrete project [10–13]. In recent years, EF concrete has been studied experimentally and mathematically [14, 15].

Early investigation on the mechanical behaviour of EF concrete was conducted using stone dust in concrete production [16]. The modelling results showed that the compressive strength of EF concrete is higher. The durability of concrete was studied and confirmed to produce high performance using recycled material [14]. Two researches have adopted an investigation of experimental analysis for the effect of using additive material such as fly ash and silica fume beside recycled aggregate on the mechanical properties of concrete [17, 18]. The studies indicated that using additive materials and recycled aggregate can enhance the strength and durability of concrete. Recycled aggregate usage in concrete enhances pore distribution and frost resistance [19]. The addition of agriculture waste to the concrete mix was considered and was investigated to enhance the properties of concrete using silica fume [20]. Calcium carbide residue was examined over the literature as industrial material [21]. Compressive strength and failure modes of concrete containing recycled nylon fiber fabric were studied [22]. Other researchers confirmed the potential of the produced EF concrete, and some researchers studied the utilization of agriculture and local waste in Africa for concrete production [23]. Others discussed the properties of lightweight interlocking concrete by adding sawdust and laterite in the concrete production [24]. All the reported literature on the experimental developed EF concrete elaborated the significance of producing such product material that can help essentially on the construction field and material sustainability. In addition, studies showed the importance of using recycled waste as environmental material in concrete production.

Owing to the complexity and nonlinearity of concrete behaviour and various parameters that affect CS, the necessity of developing an effective technique that can examine the properties of concrete can be noted. In recent years, artificial intelligence (AI) models have been effectively applied in concrete structure research [25–29]. AI models have the ability to solve nonlinear, stochastic problems and deal with complex systems [30–32]. Literature studies on AI models reported massively in this domain; artificial neural network (ANN) model with response surface methodology (RSM) was developed for predicting CS of recycled aggregate concrete [33]. The study concluded that the ANN-based model exhibits better performance than the RSM model. The development of adaptive neuro-fuzzy inference system, ANFIS, together with ANN model was adopted to estimate self-compacting concrete's CS [34]. The results demonstrated that the developed model accurately predicted concrete compressive strength. In another study, adaptive boosting (AdaBoost), ANN and support vector machine (SVM) were developed for the prediction process of compressive strength [35]. The study demonstrated that AdaBoost model exhibited better prediction achievement than other models. Examination of the feasibility of ANN model in the prediction process of concrete CS involving furnace slag of ground granulated blast was conducted by [36]. The study was integrated ANN with a multiobjective salp optimization algorithm and compared it with M5P model for CS prediction. The research was concluded that the proposed AI models successfully predicted CS. The incorporation of socio-political algorithm (ICA) with extreme gradient boosting (XGBoost), ANN, SVM, and ANFIS was tested for predicting of CS of recycled aggregate concrete, and was reported by [26]. The study revealed that the developed model (ICA-XGBoost) achieved better capacity than the other proposed models in the prediction process. The ability of ANN model was evaluated in the prediction of CS of Geopolymer Concrete (GPC) [37]. The results indicated that the proposed model attained high prediction capability of compressive strength. Boosted decision tree regression (BDTR) and SVM models were developed to predict EF concrete's compressive strength [38]. The researcher concluded that the BDTR model performed better than the SVM model with good accuracy prediction. The modelling accuracy of ANN, RSM, and gene expression programming (GEP) was tested for predicting the CS of engineering Geopolymer composites concrete [39]. The study showed that ANN and RSM models performed better than GEP model in the prediction process. Hybridization of three optimization algorithms called genetic algorithm (GA), salp swarm optimization (SSA), and grasshopper optimization algorithm (GOA) with ANN model were conducted for predicting CS of the concrete utilizing recycled aggregate [40]. The researchers indicated that ANN-SSA achieved better prediction performance than other models. Several other researches were adopted on testing the feasibility of the AI models for modelling the CS of concrete and confirmed the potential of those new computer-aided models in solving such a kind of complex material engineering problem [41–45].

Previous studies show that the use of recycled aggregate as a sustainable material in concrete production is highly emphasized by several researchers [46, 47]. Most of these studies examined the impact of recycled aggregate experimentally and there is a limited number of researchers who have explored the properties of EF concrete by a mathematical model. Due to the rapid advancement of AI models and computer vision, exploring a new approach that can handle the complex relationship between different parameters and the compressive strength of concrete is very important. Deep learning neural network (DLNN) is a new version of AI models that have achieved a reliable performance in solving complex and nonlinear systems [48–50]. DLNN outperformed other traditional AI models in various applications owing to their capacity on analyzing through the deep layers learning process. DLNN has been successfully applied and performed better prediction precision in several engineering problems [51–54]. The other concern that highly matters to the machine learning modelling is the feature selection for the appropriate

predictors. Hence, the current research focused on integrating a new feature selection approach.

This paper aims to provide an effective computer-aided model for predicting CS of recycled aggregate concrete. This approach can help determine the performance of EF concrete on the improvement of concrete strength and identify the appropriate mix designs of concrete. To achieve the research aim, the DLNN model is developed and compared with extreme learning machine (ELM), multivariate adaptive regression spline (MARS), and random forest (RF). Due to the important role of input parameters in CS prediction, XGBoost as an advanced algorithm is used that abstracts the most correlated variables in the modelling process. The proposed approach is helpful in many applications of a concrete structure and can be applied to examine the compressive strength of EF concrete.

2. Methodology Overview

2.1. Deep Learning Neural Network (DLNN). In recent years, the concept of the deep learning method has been introduced as an advanced algorithm of neural networks. Deep neural network is a traditional neural network with extra numbers of hidden layers that are added to the structure [55]. The deep learning algorithm was developed by Hinton et al. as he introduced a layer-wise-greedy-learning method [56]. According to this method, an unsupervised learning method is used to pertain the neural network before the training phase with layer by layer. Herein, deep learning is a popular AI model for some reasons: its ability to deal with big training data, avoid overfitting problems, and non-random value can be assigned to the network before learning process [55]. From these features, the algorithm can make a good performance through the training process among deep learning types. The backpropagation neural network is used in this study due to its popularity and robustness in many applications [51]. This type used multiple hidden layers and backpropagation with gradient descent algorithm. The main concept of this algorithm is yielding new variables based on the connection between hidden layers and the input layers. The new variables are reached to the output layer, and then the target value is predicted through the training process. The nonlinear relationship between multiple hidden layers gave the algorithm the capability to handle nonlinear relationships in different complex systems [57]. The structure of a deep neural network is shown in Figure 1 with the input layer, hidden layers, and output layer. The mathematical expression of the algorithm is discussed as follows:

$$M^I = f\left(w^I \varphi^{I-1} + b^I\right), \quad \text{for } 0 < I < L, \tag{1}$$

where f is the activation function, b is the bias, and w is the weight matrix of the hidden neurons. Input layer is described by 0 and L represents the output layer. The activation matrix used in this study is tanh function because of its capability to get good prediction performance in the explored problem.

2.2. Multivariate Adaptive Regression Spline Model (MARS). Multivariate adaptive regression spline model, a robustn machine learning model, was developed by [58]. MARS is a nonlinear flexible model recently used in many applications in engineering subjects [59]. The MARS model has three principle components: the basic functions (BFs), spline functions, and the knots [60]. The relationship between target value and predicted variables is addressed by BFs and it is expressed by max $(0, c - x)$ or max $(0, x - c)$, where x represents threshold value and c indicates the value of input variable. In this context, the knots indicate the function for the base as well as base endpoints. Spline functions contain one or more BFs and its role is developing a regression model for each node [61]. The predicted value in MARS model is based on linear combination of BFs components. The main processes of MARS model are as follows: Assuming Y represents the target variable whereas X is the matrix of input variable, then the mathematical expression of MARS model is described as follows:

$$Y = f(X) = \beta_0 + \sum_{m=1}^{M} \beta_0 BF_m(X), \tag{2}$$

where β_0 represents the initial value; and BF_m is the basis function that is used to fit MARS model; whereas M denotes the whole number of BFs [62]. There are two main phases in MARS model named forward phase and backward phase as shown in Figure 2. In forward phase, the model selects the optimum combination of input parameters. The overfitting problem can appear in the forward phase due to a series of splits, and the model cannot achieve good performance during the prediction process. The model uses the backward phase to remove undesirable parameters that have been selected and then enhance the prediction accuracy of a regression model. The basis deletion criteria in the backward phase are a generalized cross validation, which is indicated as GCV and can be computed as follows:

$$GCV(M) = \frac{(1/N)\sum_{i=1}^{N}\left(O_i - f(x_i)\right)^2}{\left(1 - (C(M)/N)\right)^2},$$
$$C(M) = (d+1) \times M, \tag{3}$$

where O_i denotes the observed value; N is the total number of data; $f(x_i)$ is the predicted value of x, M represents the whole number of BFs; and $(C(M))$ indicates the penalty factor. d represents the optimization cost of BFs and its range $2 \le d \le 4$. The systematic structure of MARS model is described in Figure 2.

2.3. Extreme Learning Machine (ELM). ELM is one of the advanced models that have been used in recent years to train the developed single layer feedforward neural network [63]. Each layer in ELM model has a number of neurons and the model contains input, hidden, and output layer. The sigmoid function is commonly utilized as activation function for the hidden layer, while the activation function in input and output layer is linear

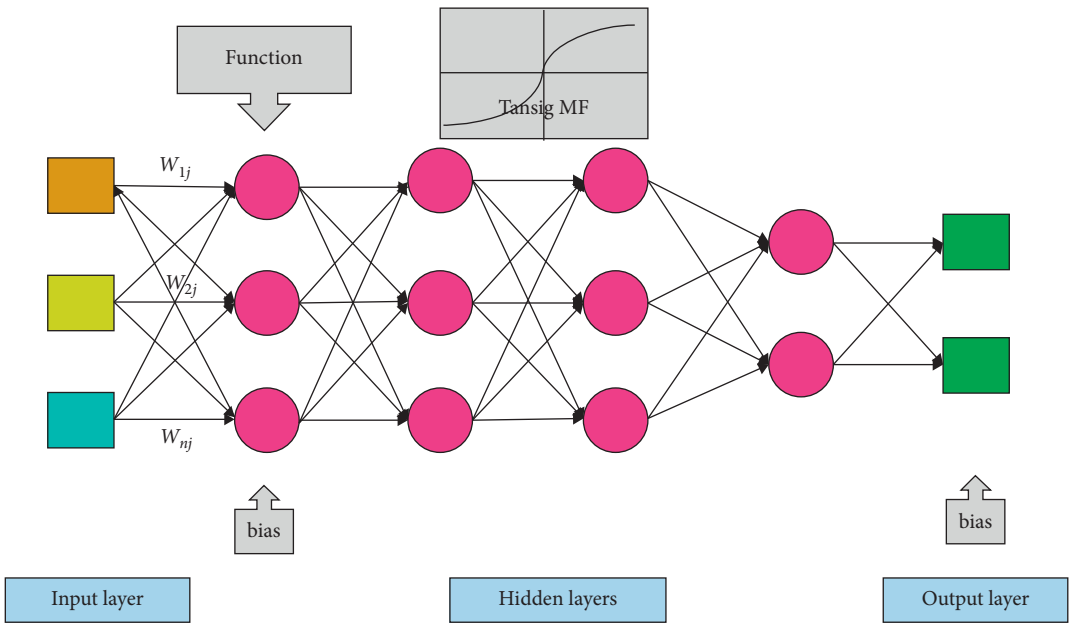

Figure 1: The architecture of the constructed DLNN model.

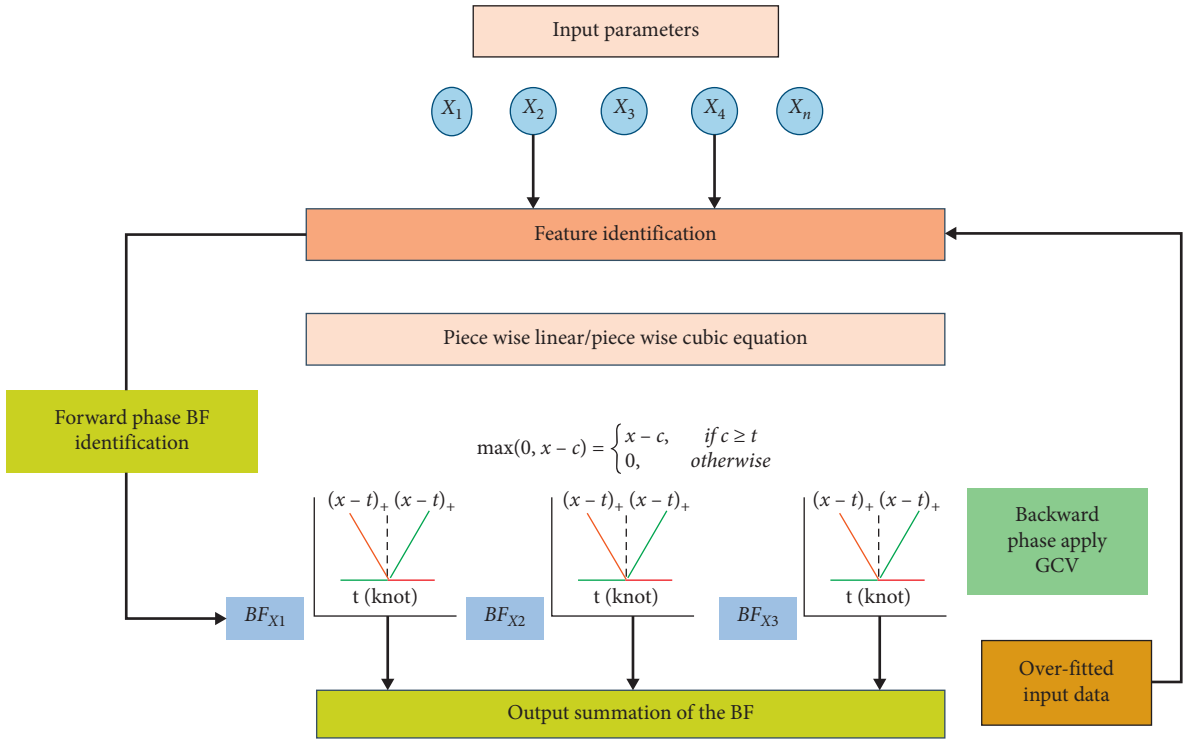

Figure 2: MARS model architecture.

function [64]. To achieve the optimum linear system solution, developing the ELM model required the determination of random input weight and hidden biases, then using the Moore Penrose generalized inverse method [65, 66]. ELM model has been used in many engineering tasks owing to fast learning, no parameter tuning, and its strong ability to achieve generalized model [67–69]. In ELM model, the first step is linear mapping the input vectors into an L-dimensional feature map as shown below:

$$\widetilde{t}_i = \sum_{i=1}^{L} \beta_i . g\left(w_l . x_i + b_l\right),\ i = 1, 2, \ldots, N, \tag{4}$$

where N denotes the size of training data, $\widetilde{t}_i$ represents the output vector, and x_i the input vector. β_i refers to the weight vector which represents the connection between hidden neuron and output layer; w_l is the weight vector that links the hidden neuron to the first layer; b_l represents the bias; while g symbolizes the activation function. In this regard, the structure of ELM model is illustrated in Figure 3.

According to the ELM model, a traditional single layer ANN can handle all sample data zero variation as shown in the below mathematical expression:

$$\sum_{i=1}^{N} t_i - \widetilde{t}_i = \sum_{i=1}^{N} t_i - \sum_{l=1}^{L} \beta_i . g\left(w_l . x_i + b_l\right) = 0, \tag{5}$$

where t_i represents the output vector. x_i denotes the input vector. Herein, the previous equation can be reconstructed as shown below:

$$H\beta = T, \tag{6}$$

where

$$H = \begin{bmatrix} g\left(w_1 \cdot x_1 + b_1\right) & \cdots & g\left(w_L \cdot x_1 + b_L\right) \\ \vdots & \ddots & \vdots \\ g\left(w_1 \cdot x_N + b_1\right) & \cdots & g\left(w_L \cdot x_N + b_L\right) \end{bmatrix}_{N \times I},$$

$$\beta = \begin{bmatrix} \beta_{1,1} & \cdots & \beta_{1,m} \\ \vdots & \ddots & \vdots \\ \beta_{L,1} & \cdots & \beta_{L,m} \end{bmatrix}_{L \times m}, \tag{7}$$

$$T = \begin{bmatrix} t_{1,1} & \cdots & t_{1,m} \\ \vdots & \ddots & \vdots \\ t_{N,1} & \cdots & t_{N,m} \end{bmatrix}_{N \times m},$$

where β indicates the weight for the matrix which links hidden and output layer; H is output matrix of hidden layer; and T is the output matrix of target value based on N training data.

By assuming that hidden biases along with input weight are both constant; it suggests that the model can be described as linear system where H and T indicate an output matrix from hidden layer and output target. While β is the weight of the matrix optimized during the training phase. The least-squares solution of the linear system can be expressed as follows:

$$\widetilde{\beta} = H^{\dagger} T, \tag{8}$$

where $H^{\dagger}$ represents Moore Penrose generalized inverse matrix.

2.4. Random Forest (RF). Random forest (RF) is a robust AI method based on classification and regression tree and developed by [70]. RF model was applied in classification and regression problems and gave an excellent performance in many fields of engineering applications [71, 72]. The work of RF model is based on the abstraction of multiple samples from the original sample by using the bootstrap resampling method, and then a decision tree model is developed for each bootstrap sample, and various outputs of decision tree models are combined to get the final result of prediction. Modifying the model parameters led to the use of many types of decision trees and then developed different trees models.

The modelling process of RF algorithm includes the following phases: using bootstrap resampling method to extract N predictors training data from the original problem data [73]. During training phase, the training data of RF model should be equal to 2/3 of the original data size. The utilized data is called in-bag data and the remaining 1/3 dataset is called out-of-bag data. The regression tree (RT) is developed for each training bootstrap data and a random forest algorithm is built based on the developing N predictors of RT models [74]. The variation of regression trees can be determined during the training data process by randomly selecting the optimal attribute from the maximum depth attributes; this process increases the capability of the RF model. The sequence of regression model can be attained by training the algorithm several times and this sequence is helpful for the developing of random forest system. The prediction results of N predictors are collected and final regression model for the new sample is calculated by using the average method [75]. The mathematical equation of regressions model in RF algorithm is as follows:

$$\widehat{f}_{rf}^{K}(x) = \frac{1}{K} \sum_{k=1}^{K} t_i(x), \tag{9}$$

where $\widehat{f}_{rf}^{K}(x)$ represents the regression model of random forest, t_i is the regression model of each regression tree, and K represents the number of regression tree model. The structure of RF model is shown in Figure 4:

2.5. Extreme Gradient Boosting (XGBoost). XGBoost is an advanced algorithm that was used recently in the feature selection process. It was developed as an extension and improvement of gradient boosting tree [76, 77]. The main structure of the algorithm depends on the efficient construction of boosted trees [78]. In feature selection problem, the main objective of XGBoost is to construct boosted trees to achieve the feature importance of input variables that are used for training process [79]. Boost trees are classified into classification and regression trees. The features' importance is extracted using three methods: gain, frequency, and cover [80]. The gain method calculates the importance of the features, frequency computes the number of trees in the boosted trees, and cover calculates the relative value for the observation [79]. The feature importance is calculated by weight using XGBoost as follows [81]:

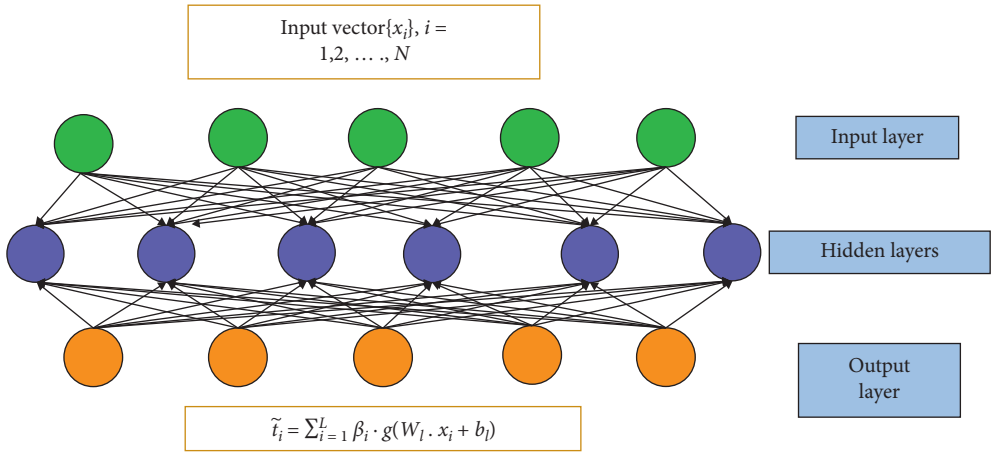

Figure 3: Paradigm of extreme learning machine model.

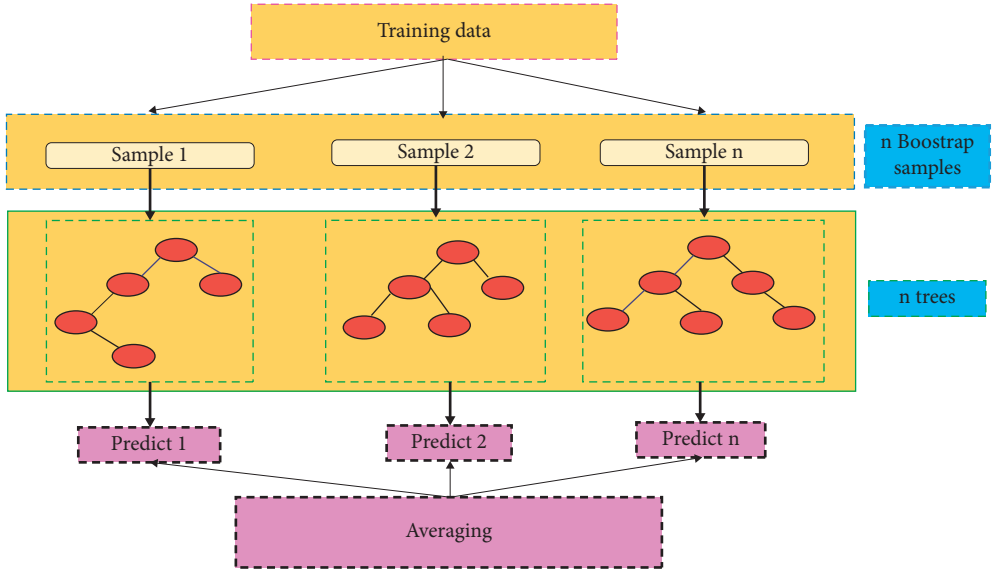

Figure 4: Random Forest model structure.

$$N_v = \sum_{L=1}^{L} \sum_{l=1}^{X=1} I\left(V_L^l, v\right),$$
$$\left(V_L^l, v\right) = f(x) = \begin{cases} 1 \text{if} V_L^l = v \\ 0, \text{otherwise} \end{cases}, \tag{10}$$

where L represents the number of trees, N indicates the number of leaf nodes, (V_L^l) is the feature of node l, and I is the indicator function.

3. Data Collection and Model Development

For the development of the proposed AI model, datasets were taken from open-source datasets [82]. The datasets contain 353 parameters of environmentally friendly concrete samples and their compressive strength. The datasets include water, (C: cement), (FA: fine aggregate), (CA: coarse aggregate), (RA: recycled aggregate), (AS: age strength), and (CS: compressive strength). The statistical characteristics of the datasets are reported in Table 1. These statistical characteristics include maximum value, minimum value, mean, standard deviation, skewness, and kurtosis. Figure 5 demonstrates the histogram for all input and output variables. The CS of the EF concrete ranges from 13 to 88.3, with mean value equal to 42.11, indicating high variance and giving the noticeable complexity of prediction problem. Table 1 and Figure 5 show that the data are well distributed and nearly to normal distribution.

The correlation matrix between input and output variables is depicted in Figure 6. Correlation statistics showed a good correlation between cement quantity and compressive strength. Increased cement quantity led to increasing the compressive strength of concrete. Figure 6 also demonstrates that there is a small correlation between value of coarse aggregate and compressive strength. There is also a small negative correlation between water, fine aggregate, recycled aggregate, and compressive strength. Increases of water, fine

Table 1: Statistical measures of the studied dataset.

Parameters	Minimum	Maximum	Mean	Std. deviation	Skewness	Kurtosis
Water (kg/m^3)	120	244	184.1	27.136	0.285	0.3497
C (kg/m^3)	220	750	394.9	83.942	1.101	2.889
FA (kg/m^3)	365	1020	710.3	108.452	0.313	1.435
CA (kg/m^3)	0	1366	564.8	438.708	-0.099	-1.458
RA (kg/m^3)	0	1259	504.3	414.588	0.218	-1.418
AS (days)	7	180	45.25	43.956	1.768	2.174
CS (MPa)	13	88.3	42.11	13.126	0.639	0.728

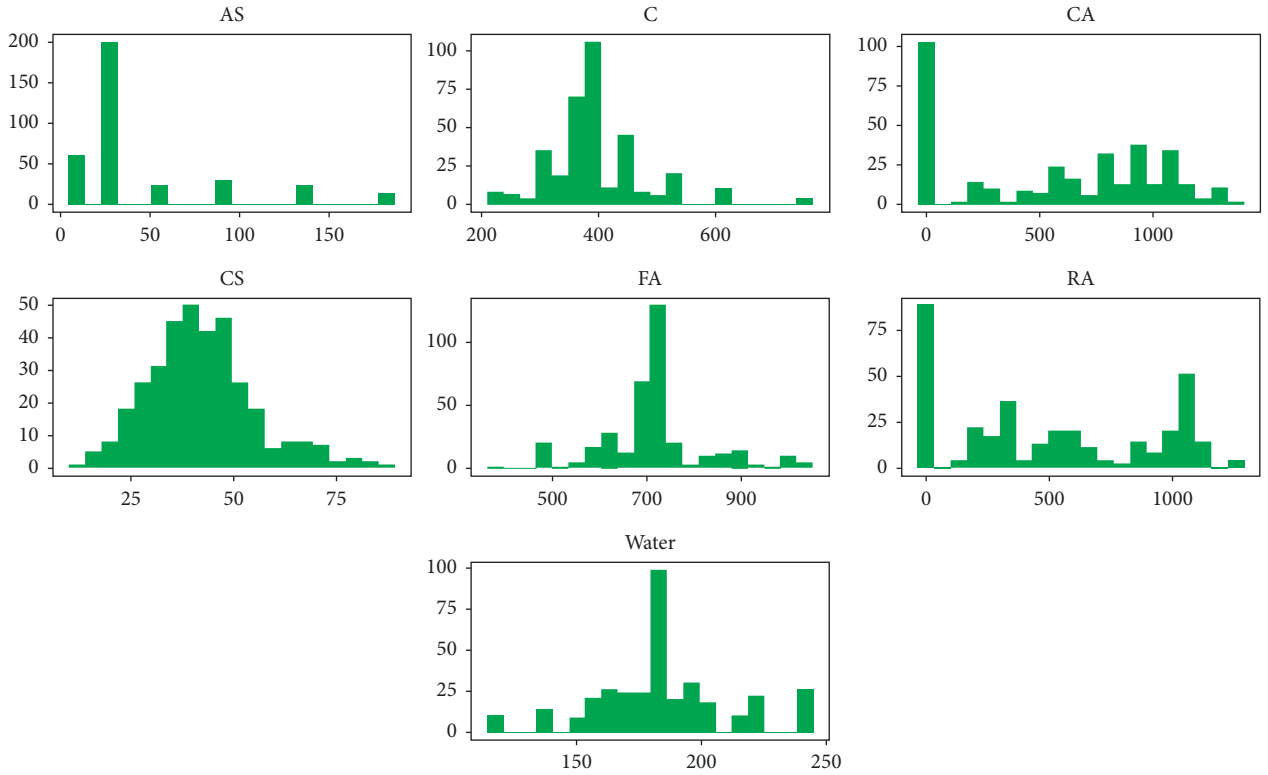

Figure 5: Histograms of the dataset used in the study.

aggregate, and recycled aggregate decreases the compressive strength of concrete.

Four AI models were adopted for the modelling process, i.e., DLNN, ELM, MARS, and RF. Dataset was split into three scenarios including 70-30%, 80-20%, and 90-10% to examine the best size of training and testing dataset suitable for modelling problems. XGBoost was used as a robust model to abstract the highly correlated variables of the best size of training and testing dataset for CS prediction. The input combinations of CS prediction are reported as in Table 2. It can be noted that the most relevant variable of CS prediction is the quantity of cement. The second input combinations of CS prediction are quantity of cement and water. Input combinations of XGBoost model showed that negatively correlated parameters and cement quantity are important variables in CS prediction. The procedure of the developed AI model is illustrated in Figure 7.

The accuracy of modelling is evaluated by using different statistical indicators including determination coefficient (R^2), mean absolute percentage error (MAPE), root mean square error (RMSE), mean absolute error (MAE), Nash–Sutcliffe efficiency (NSE), and Willmott' index (WI) [83, 84].

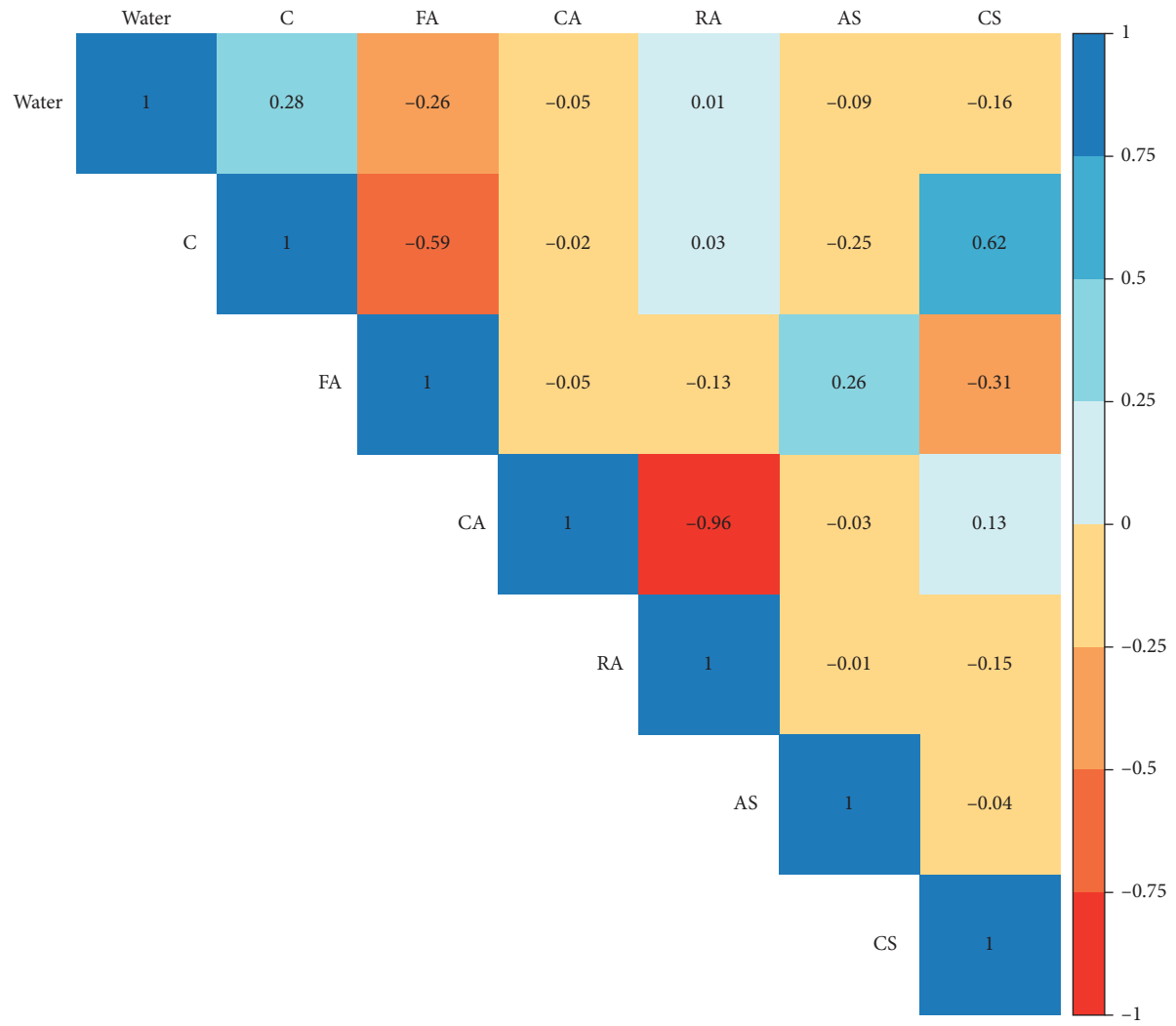

Figure 6: Correlation statistics between concrete parameters in the dataset.

Table 2: The abstracted input combination using XGBoost model.

Models	Input combinations
Model I	$CS = C$
Model II	$CS = C$, Water
Model III	$CS = C$, Water, FA
Model IV	$CS = C$, Water, FA, CA
Model V	$CS = C$, Water, FA, CA, AS
Model VI	$CS = C$, Water, FA, CA, AS, RA

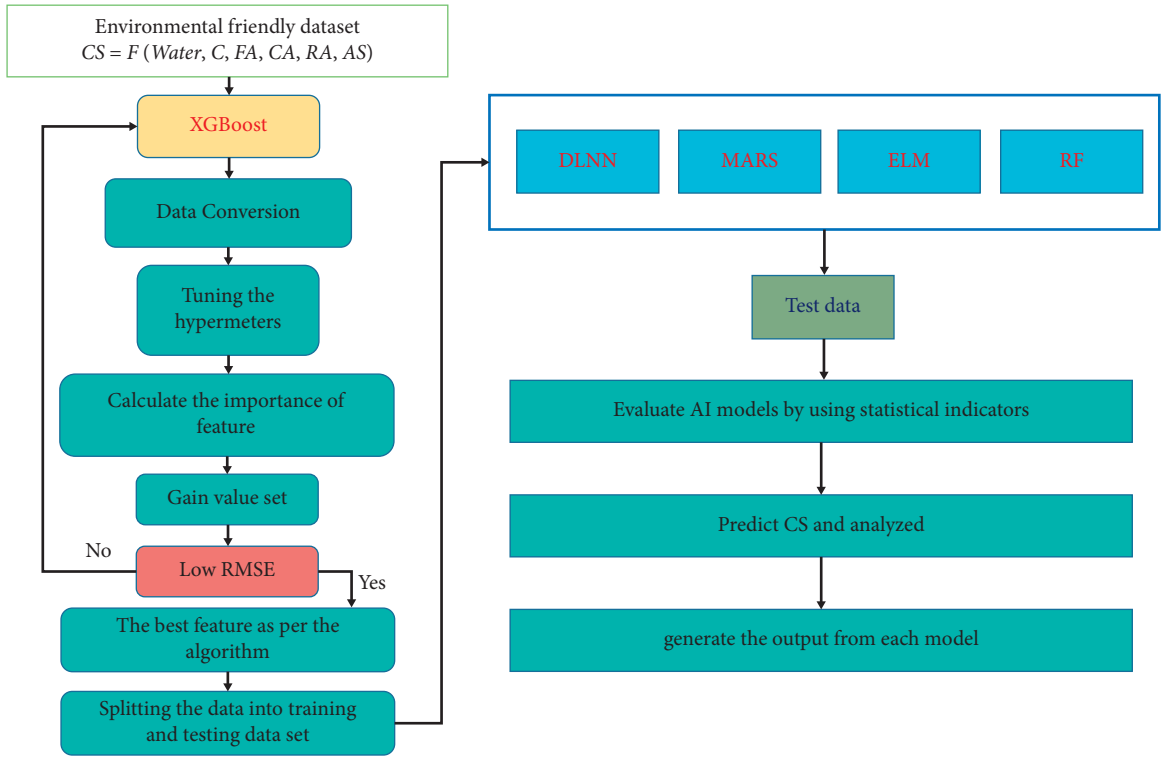

Figure 7: The developed AI models for CS prediction EF concrete.

$$
\begin{aligned}
R^2 &= \left(\frac{\sum_{i=1}^{N} \left(y_p - \overline{y_p}\right) \cdot \left(y_o - \overline{y_o}\right)}{\sqrt{\sum_{i=1}^{N} \left(y_p - \overline{y_p}\right)^2 \sum_{i=1}^{N} \left(y_o - \overline{y_o}\right)^2}} \right)^2, \\
\text{MAPE} &= \frac{1}{n} \sum_{i=1}^{n} \left| \frac{y_p - y_o}{y_o} \right|, \\
\text{RMSE} &= \sqrt{\frac{\sum_{i=1}^{N} \left(y_p - y_o\right)^2}{n}}, \\
\text{MAE} &= \frac{\sum_{i=1}^{N} \left| y_p - y_o \right|}{N}, \\
\text{NSE} &= 1 - \frac{\sum_{i=1}^{N} \left(y_p - y_o\right)^2}{\sum_{i=1}^{N} \left(y_o - \overline{y_o}\right)^2}, \\
WI &= 1 - \left[\frac{\sum_{i=1}^{N} \left(y_p - y_o\right)^2}{\sum_{i=1}^{N} \left(\left| y_p - \overline{y_o} \right| + \left| y_o - \overline{y_o} \right| \right)^2} \right],
\end{aligned}
\tag{11}
$$

where y_p and y_o represent the predicted and observed value of compressive strength; $\overline{y_o}$ is the mean value of the observed value of compressive strength; and N represents the number of experiment samples.

4. Results and Discussion

In this research, four AI models were established to predict the compressive strength of EF concrete containing recycled aggregate. The main idea from developing AI models is to examine the ability of the developed model to predict the compressive strength of EF concrete, and therefore three data division scenarios were used to test the size of dataset suitable for CS prediction.

Tables 2–4 describe the statistical indicators of the developed models (DLNN, MARS, ELM, and RF) over the training phase for the three data division scenarios. In general, the results indicated that all the developed models performed good prediction performance. This indicated that the developed models are reliable and they are capable to build a robust approach of CS prediction. However, the reported results showed the superiority of DLNN model over the other developed models through all data division scenarios. The prediction performance is gained by using DLNN model for 80-20% data division scenario with $R^2 = 0.99$, MAPE = 0.02, RMSE = 1.29, MAE = 0.74, NSE = 0.98, and WI = 0.99 (Tables 3 and 4).

The results of test phase are shown in Tables 5–7 with respect to the developed AI models in all scenarios. The results reported that the DLNN model performed the best predictive accuracy over the three adopted scenarios. The results indicated that using different data division scenarios

Table 3: The statistical measurements for the developed AI model over the training phase for 70-30% data division scenario.

Models	R^2	MAPE	RMSE	MAE	NSE	WI
DLNN	0.98	0.03	1.74	1.07	0.98	1.00
MARS	0.88	0.09	4.60	3.57	0.88	0.97
ELM	0.93	0.07	3.62	2.61	0.93	0.98
RF	0.87	0.10	4.98	3.79	0.86	0.96

Table 4: The statistical measurements for the developed model AI model over the training phase for 80-20% data division scenario.

Models	R^2	MAPE	RMSE	MAE	NSE	WI
DLNN	0.99	0.02	1.30	0.74	0.99	1.00
MARS	0.86	0.10	4.85	3.81	0.86	0.96
ELM	0.91	0.07	3.98	2.87	0.91	0.98
RF	0.88	0.09	4.70	3.59	0.87	0.96

Table 5: Statistical measures for the developed AI model across the training phase for 90-10% data division scenario.

Models	R^2	MAPE	RMSE	MAE	NSE	WI
DLNN	0.98	0.04	2.01	1.37	0.98	0.99
MARS	0.88	0.09	4.59	3.45	0.88	0.97
ELM	0.91	0.08	4.01	2.89	0.91	0.98
RF	0.89	0.09	4.54	3.41	0.88	0.96

Table 6: Statistical measurements for the developed AI model in the test phase by using 70-30% data division scenario.

Models	R^2	MAPE	RMSE	MAE	NSE	WI
DLNN	0.90	0.08	4.00	2.99	0.90	0.97
MARS	0.80	0.13	6.04	4.75	0.76	0.94
ELM	0.65	0.16	8.21	5.63	0.56	0.89
RF	0.89	0.08	4.33	3.19	0.88	0.96

Table 7: Statistical measurements for the developed AI model in the test phase by using 80-20% data division scenario.

Models	R^2	MAPE	RMSE	MAE	NSE	WI
DLNN	0.94	0.06	3.37	2.35	0.94	0.98
MARS	0.83	0.10	5.58	4.14	0.83	0.95
ELM	0.82	0.12	5.81	4.35	0.81	0.95
RF	0.89	0.08	4.67	3.32	0.88	0.96

Table 8: Statistical measurements for the developed AI model across the testing phase for 90-10% data division scenario.

Models	R^2	MAPE	RMSE	MAE	NSE	WI
DLNN	0.97	0.05	2.24	1.63	0.97	0.99
MARS	0.84	0.09	5.20	3.90	0.84	0.96
ELM	0.82	0.12	5.78	4.37	0.80	0.95
RF	0.94	0.07	3.60	2.75	0.92	0.98

has an essential role in training the developed AI model. Using 90% of dataset for the training process contributes to improving the predictive performance of AI model. The best prediction accuracy is attained by DLNN model and 90-10% scenario with $R^2 = 0.97$, MAPE = 0.04, RMSE = 2.23, MAE = 1.63, NSE = 0.93, and WI = 0.99 (Tables 6–8).

Scatter plots were created to examine the linear relationship among the actual and predicted values for EF concrete compressive strength. The scatter plots for the three scenarios (70-30%, 80-20%, and 90-10%), and the developed AI models (DLNN, MARS, ELM, and RF) are depicted in Figures 8–10. The 90-10% scenario achieved the best linear relationship between actual and predicted compressive strength values for the testing period using the DLNN model. Figure 10 indicates that the best prediction improvement is attained by the DLNN model with a maximum coefficient of determination $R^2 = 0.97$.

A two-dimensional graphical presentation named Taylor diagram is generated for investigating the performance for the developed AI model [85]. Taylor diagram is developed based on three statistical metrics correlation, RMSE, and standard deviation of the developed AI models as depicted in Figure 11. According to the location of the developed AI models on Taylor diagram, it can be noted that DLNN model achieved the best prediction performance for compressive strength of EF concrete by using a data division scenario of 90-10%.

Another graphical presentation is created to give a good explanation for the performance of the developed AI models. The developed AI models were investigated by using relative error percentages for the three tested data division scenarios. Figure 12 illustrates the relative error results of the developed model for scenarios 1, 2, and 3. According to the relative error results, the DLNN model attained the best predictive performance with a small relative error for scenario 3 with 90-10% data division.

Tables 9–12 present the statistical measurement for integrating XGBoost combinations with the developed AI models over training and testing phase for scenario 3. The results indicated that DLNN and RF models performed better prediction than ELM and MARS models. The results also reported that the best results were achieved by including al input parameters in the modelling problem. The best prediction accuracy during training phase was attained by DLNN model with $R^2 = 0.97724$, MAPE = 0.03867, RMSE = 2.0072, MAE = 1.37395, NSE = 0.97667, and WI = 0.99398. The testing phase results showed that DLNN model achieved highest prediction performance with $R^2 = 0.97106$, MAPE = 0.04552, RMSE = 2.23648, MAE = 1.63199, NSE = 0.96952, and WI = 0.99160. From the reported results, it can be observed that compressive strength of concrete is affected by all input variables including cement, water, fine aggregate, recycled aggregate, age strength, and coarse aggregate.

Figure 13 demonstrates the scatter plot diagram for all the developed model combinations. The DLNN model achieves the best results with highest value of the coefficient of determination $R^2 = 0.97$. The diagram shows that the best prediction performance is achieved by using all influencing input variables. Applying all input variables increases prediction performance for all developed models (DLNN, MARS, ELM, RF).

The Taylor diagram demonstrates the relationship between correlation, RMSE, and standard deviation for all

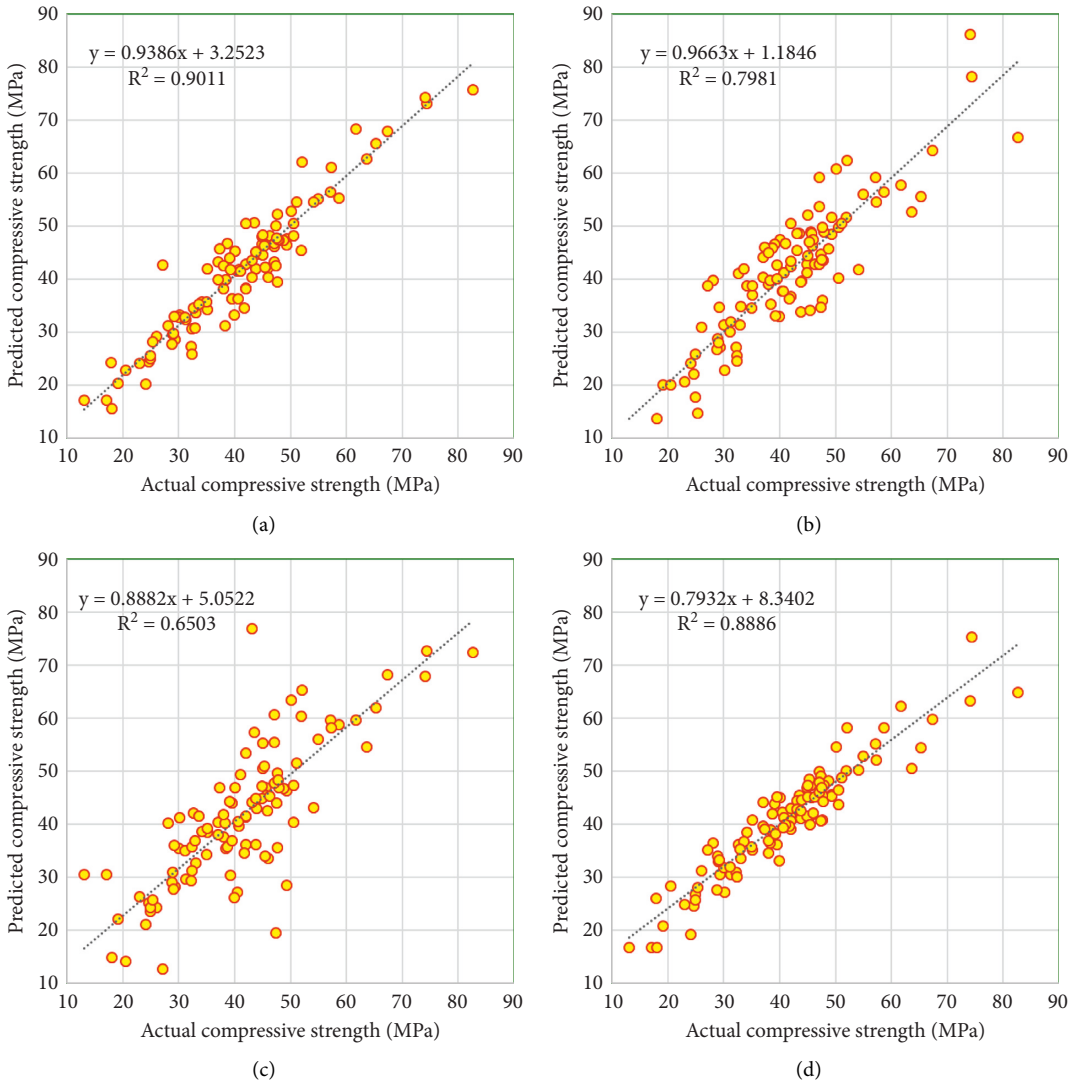

Figure 8: Scatter plot presentation using the developed AI model and for (70%-30%) data division scenario. (a) DLNN model. (b) MARS model. (c) ELM model. (d) RF model.

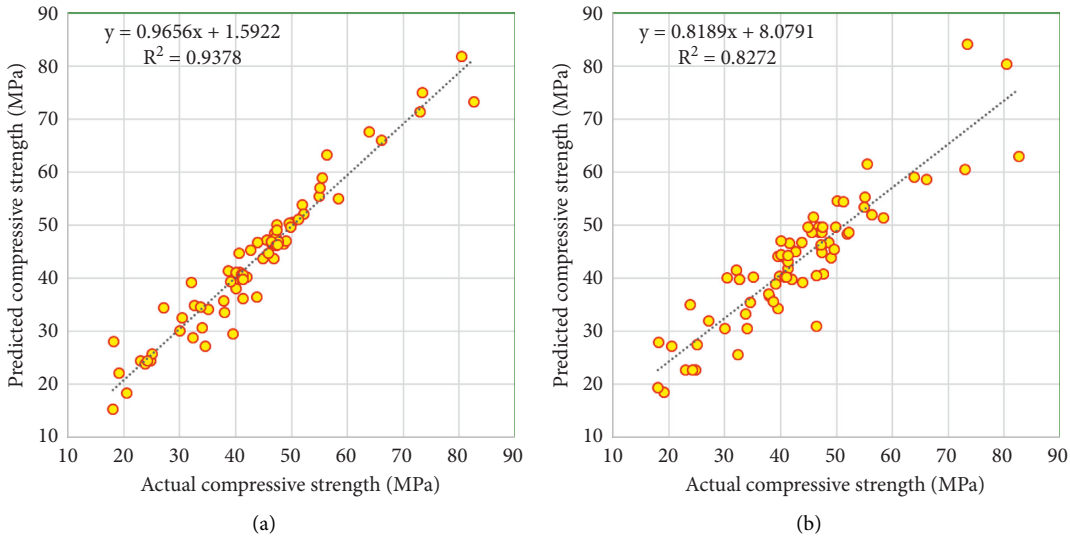

Figure 9: Continued.

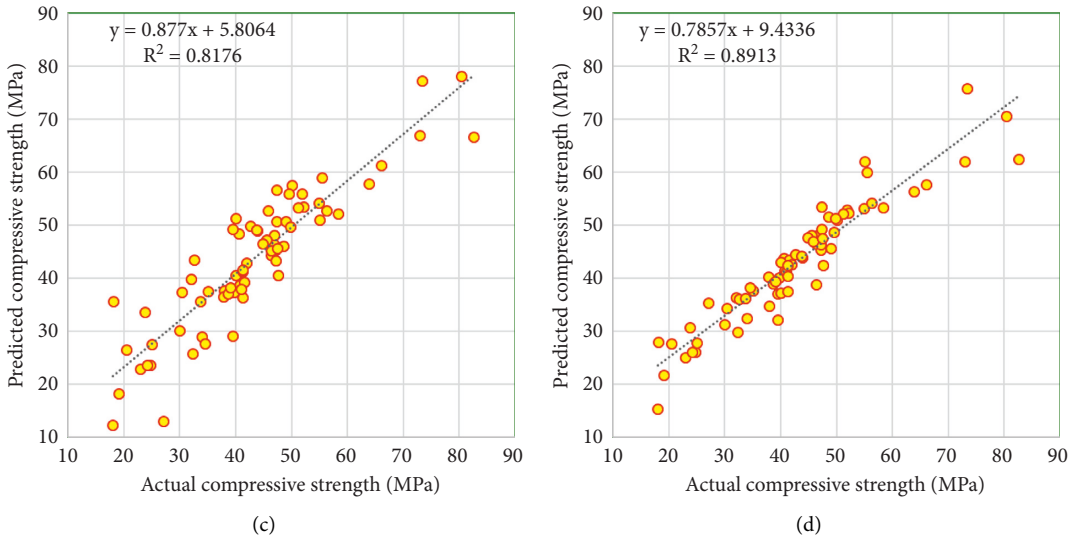

FIGURE 9: Scatter plot presentation using the developed AI model and for (80%-20%) data division scenario. (a) DLNN model. (b) MARS model. (c) ELM model. (d) RF model.

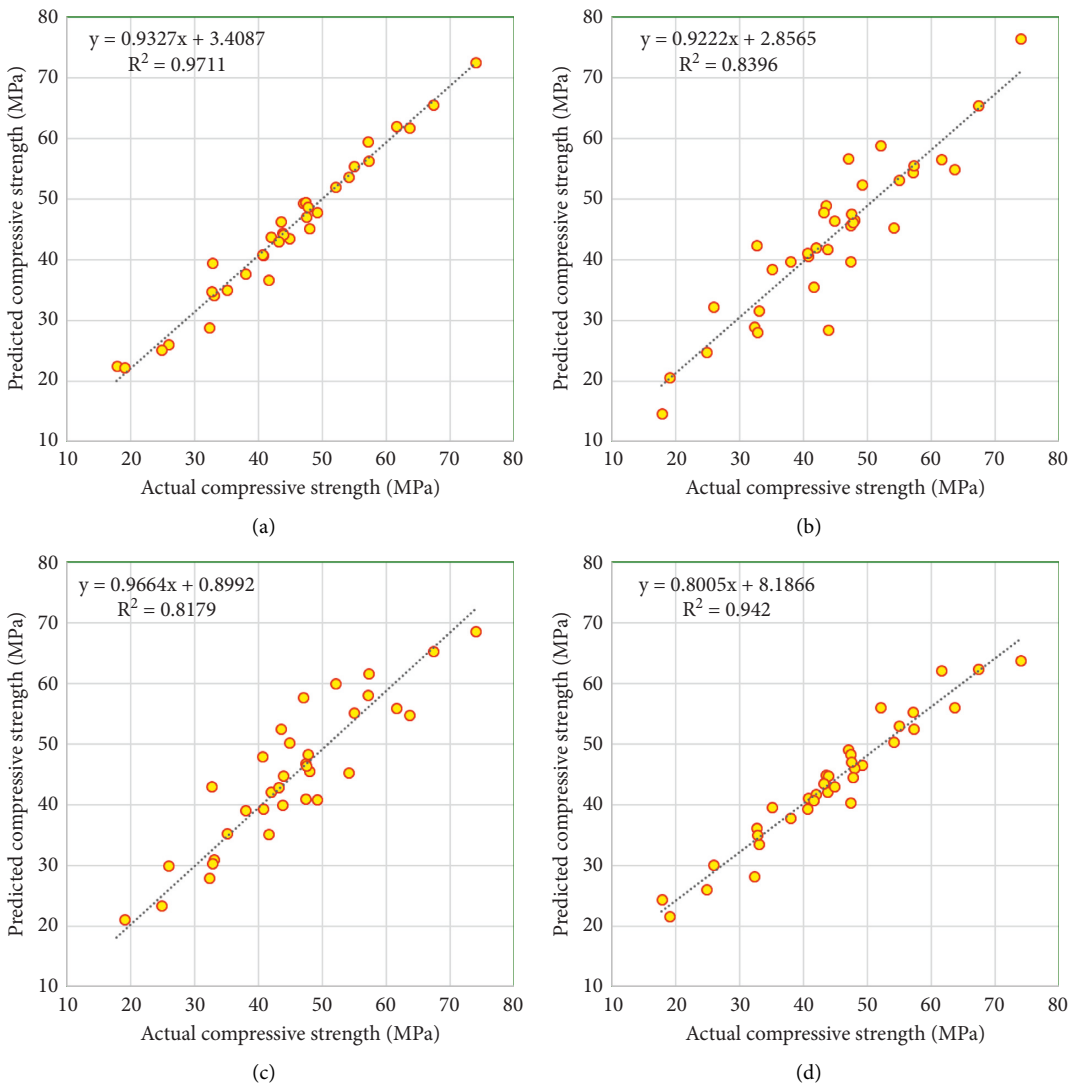

FIGURE 10: Scatter plot presentation using the developed AI model and for (90%-10%) data division scenario. (a) DLNN model. (b) MARS model. (c) ELM model. (d) RF model.

Table 9: Statistical measurements for DLNN model over training and testing phase for all input combinations.

Models	R^2	MAPE	RMSE	MAE	NSE	WI
Training phase						
DLNN-model I	0.67	0.14	7.52	5.59	0.67	0.89
DLNN-model II	0.82	0.11	5.64	4.29	0.82	0.95
DLNN-model III	0.82	0.11	5.57	4.19	0.82	0.95
DLNN-model IV	0.91	0.08	3.90	2.99	0.91	0.98
DLNN-model V	0.98	0.03	1.99	1.20	0.98	0.99
DLNN-model VI	0.98	0.04	2.01	1.37	0.98	0.99
Testing phase						
DLNN-model I	0.68	0.14	7.33	5.45	0.67	0.87
DLNN-model II	0.88	0.09	4.43	3.52	0.88	0.97
DLNN-model III	0.90	0.08	4.07	3.16	0.90	0.97
DLNN-model IV	0.89	0.09	4.17	3.39	0.89	0.97
DLNN-model V	0.93	0.06	3.28	2.41	0.93	0.98
DLNN-model VI	0.97	0.05	2.24	1.63	0.97	0.99

Table 10: Statistical measurements for MARS model over training and testing phase for all input combinations.

Models	R^2	MAPE	RMSE	MAE	NSE	WI
Training phase						
MARS-model I	0.43	0.19	7.52	5.59	0.67	0.89
MARS-model II	0.72	0.14	6.99	5.44	0.72	0.91
MARS-model III	0.77	0.13	6.36	4.98	0.77	0.93
MARS-model IV	0.80	0.12	5.88	4.66	0.80	0.94
MARS-model V	0.86	0.10	4.91	3.79	0.86	0.96
MARS-model VI	0.88	0.09	4.59	3.45	0.88	0.97
Testing phase						
MARS-model I	0.35	0.21	10.18	7.79	0.37	0.72
MARS-model II	0.75	0.12	6.33	4.91	0.76	0.92
MARS-model III	0.81	0.11	5.53	4.51	0.81	0.94
MARS-model IV	0.81	0.10	5.50	4.33	0.82	0.95
MARS-model V	0.84	0.10	5.23	4.20	0.83	0.96
MARS-model VI	0.84	0.09	5.20	3.90	0.84	0.96

Table 11: Statistical measurements for ELM model over training and testing phase for all input combinations.

Models	R^2	MAPE	RMSE	MAE	NSE	WI
Training phase						
ELM-model I	0.41	0.19	10.13	7.60	0.41	0.74
ELM-model II	0.69	0.14	7.28	5.61	0.69	0.90
ELM-model III	0.76	0.12	6.41	4.96	0.76	0.93
ELM-model IV	0.83	0.11	5.43	4.18	0.83	0.95
ELM-model V	0.91	0.08	4.01	2.98	0.91	0.98
ELM-model VI	0.91	0.08	4.01	2.89	0.91	0.98
Testing phase						
ELM-model I	0.39	0.20	9.84	7.49	0.41	0.74
ELM-model II	0.70	0.13	6.94	5.52	0.71	0.91
ELM-model III	0.73	0.13	6.54	5.34	0.74	0.92
ELM-model IV	0.74	0.13	6.38	5.13	0.75	0.92
ELM-model V	0.78	0.12	6.13	4.68	0.77	0.94
ELM-model VI	0.82	0.12	5.78	4.37	0.80	0.95

input combinations, as shown in Figure 14. Taylor's presentation revealed that the developed AI models achieved good prediction using sixth combinations with all input parameters. DLNN model attained the best prediction performance using all input variables with the nearest position to the actual value.

Table 12: Statistical measurements for RF model over training and testing phase for all input combinations.

Models	R^2	MAPE	RMSE	MAE	NSE	WI
Training phase						
RF-model I	0.64	0.15	7.89	5.83	0.64	0.89
RF-model II	0.74	0.13	6.74	5.13	0.74	0.92
RF-model III	0.74	0.13	6.72	5.14	0.74	0.92
RF-model IV	0.79	0.13	36.78	4.86	0.79	0.94
RF-model V	0.89	0.08	4.48	3.28	0.88	0.97
RF-model VI	0.89	0.09	4.54	3.41	0.88	0.96
Testing phase						
RF-model I	0.61	0.16	7.92	5.56	0.62	0.85
RF-model II	0.85	0.10	4.90	3.89	0.85	0.96
RF-model III	0.87	0.13	4.54	3.56	0.87	0.96
RF-model IV	0.87	0.10	4.64	3.89	0.87	0.96
RF-model V	0.90	0.07	4.04	2.91	0.90	0.97
RF-model VI	0.94	0.07	3.60	2.75	0.92	0.98

Relative error presentation for the proposed AI models with all abstracted combinations is illustrated in Figure 15. Graphical presentation of relative error percentages showed that modelling with six parameters attained low percentage error compared with the other combinations for all AI models. DLNN model with the sixth combination achieved the lowest relative error among the other three AI models (MARS, ELM, and RF).

In the current study, a robust AI model was suggested for predicting the compressive strength for EF concrete. An advanced XGBoost algorithm was integrated with the developed AI model and the comparable once to investigate the best combinations of input parameters suitable for predicting EF concrete compressive strength. The results reported that the presented models realized an efficient prediction model that has the capability to handle the complex behaviour of concrete. This approach can improve concrete performance and the strength of EF concrete. Based on the reported results, it was observed that the size of data used for training AI model remarkably affects the accuracy of prediction performance. An accurate selection of training data size helps the modeller reduce an underfitting problem associated with the modelling process. The current study presented that 90% of training data is suitable to provide an accurate prediction of EF concrete compressive strength. The integration of XGBoost algorithm with AI models showed that an accurate prediction could be achieved by including all input parameters in the prediction problems. All six variables including cement, water, fine aggregate, recycled aggregate, age strength, and coarse aggregate are necessary to achieve good prediction accuracy of compressive strength. The results also reported that DLNN model provided an excellent ability to understand the nonlinearity between the contributed variables as well as the compressive strength of concrete. The statistical metrics and the graphical presentations established the robustness

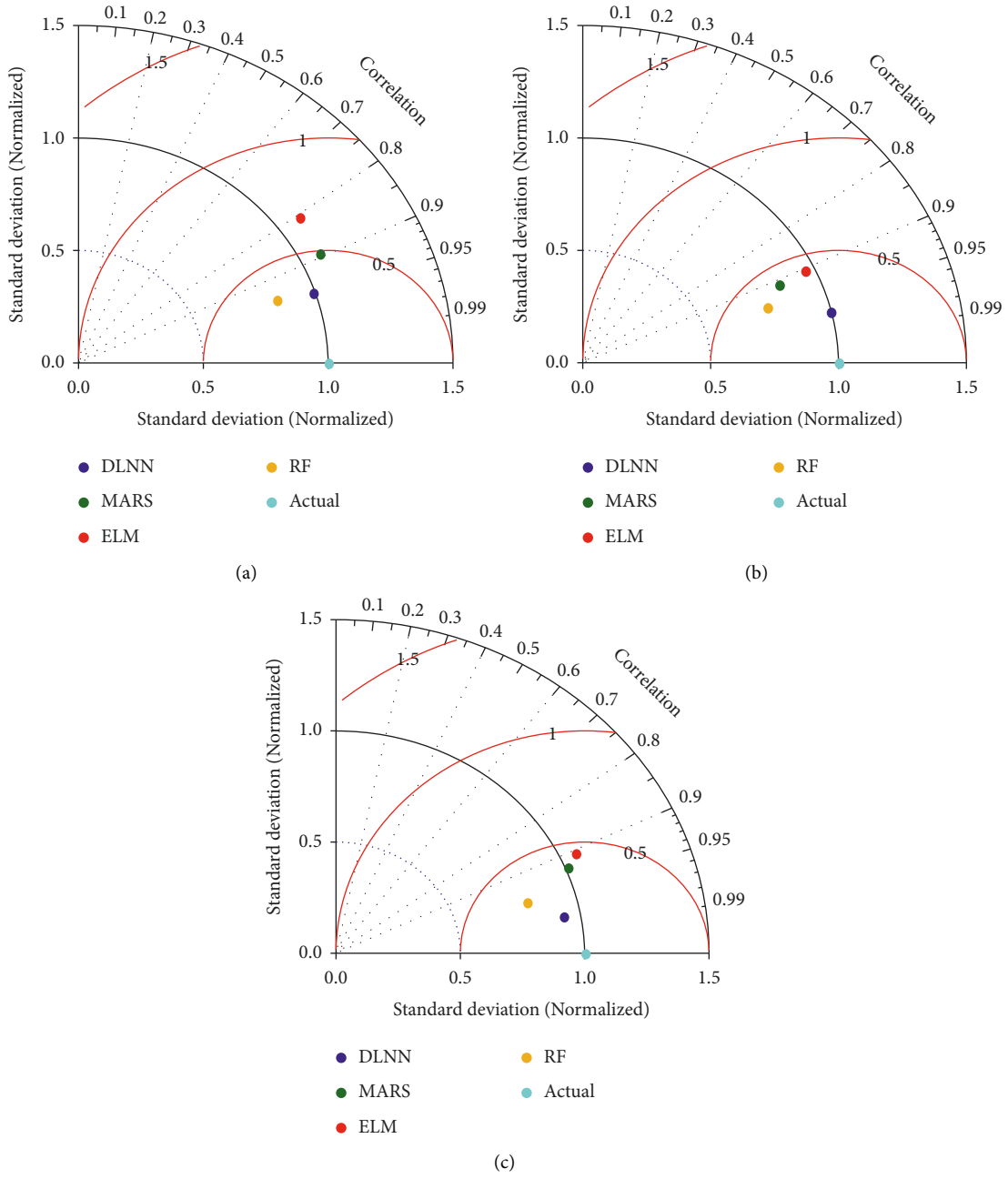

Figure 11: Taylor diagram for the developed AI model over all data division scenarios. (a) Scenario I. (b) Scenario II. (c) Scenario III.

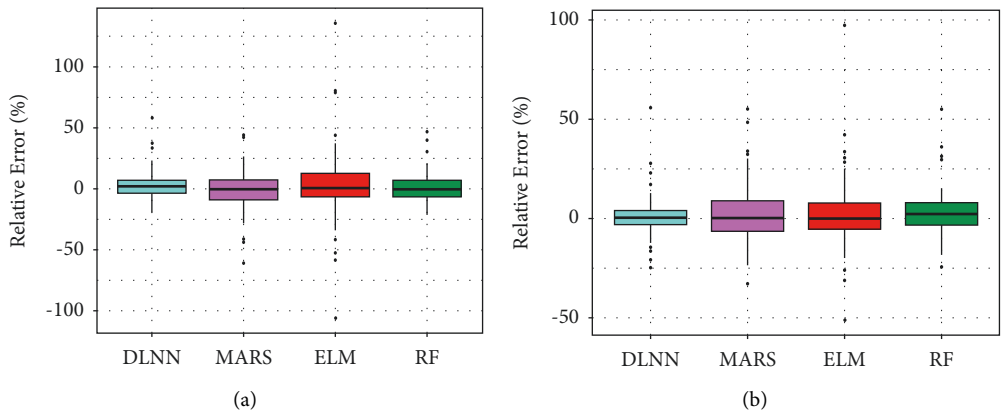

Figure 12: Continued.

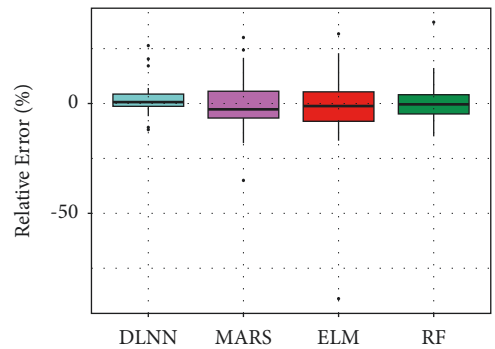

Figure 12: Relative error percentages of the developed AI models for the three tested scenarios. (a) Scenario I. (b) Scenario II. (c) Scenario III.

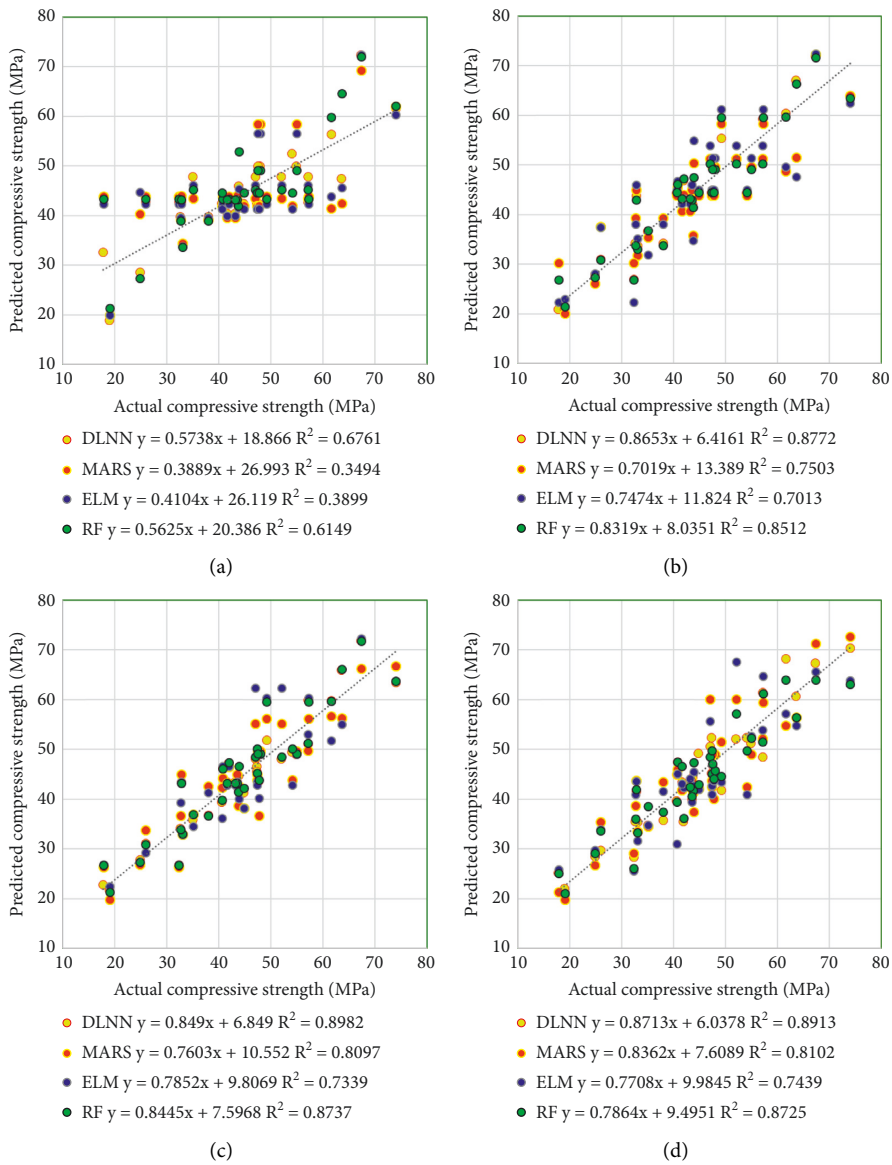

Figure 13: Continued.

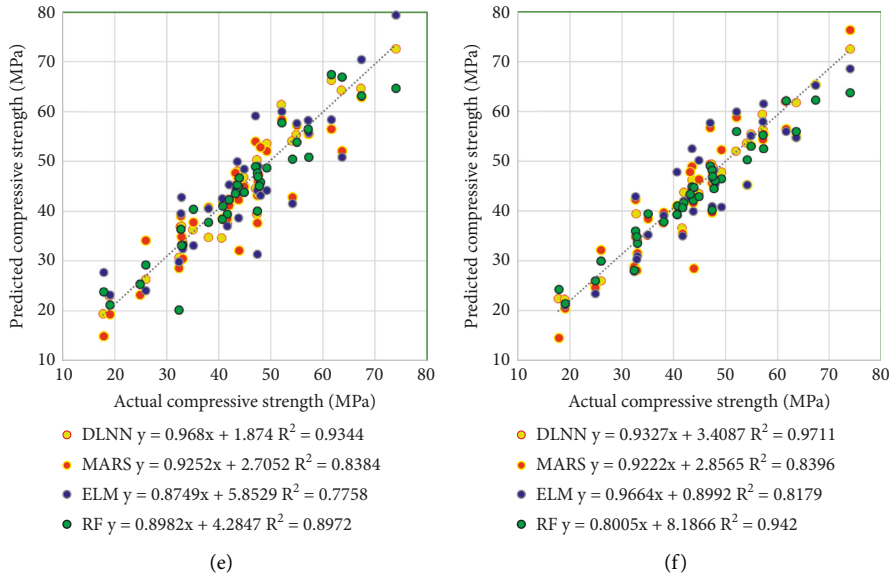

FIGURE 13: Scatter plot diagram for the developed AI models using all input combinations. (a) Model I. (b) Model II. (c) Model III. (d) Model IV. (e) Model V. (f) Model VI.

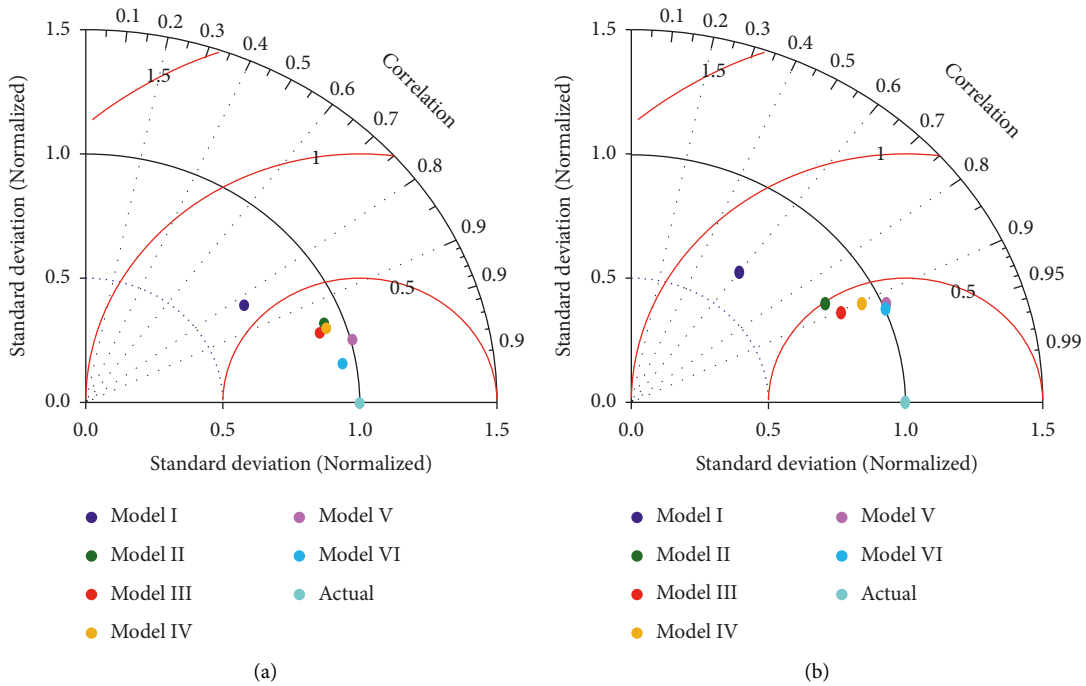

FIGURE 14: Continued.

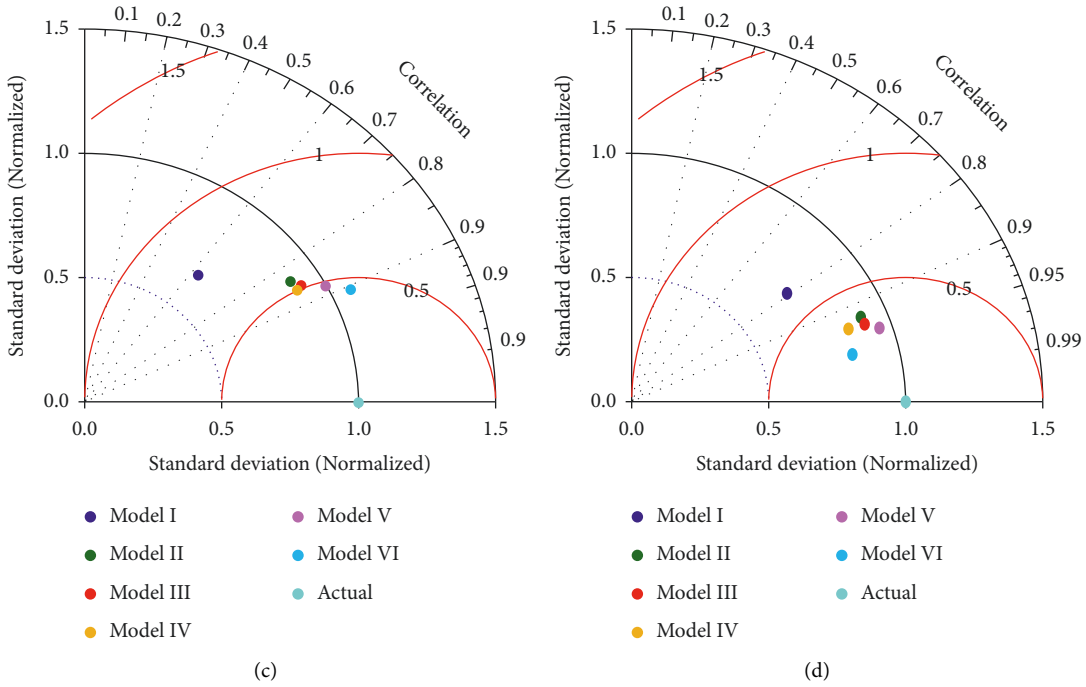

Figure 14: Taylor diagram for the developed AI models using all input combinations. (a) DLNN model. (b) MARS-model. (c) ELM-model. (d) RF-model.

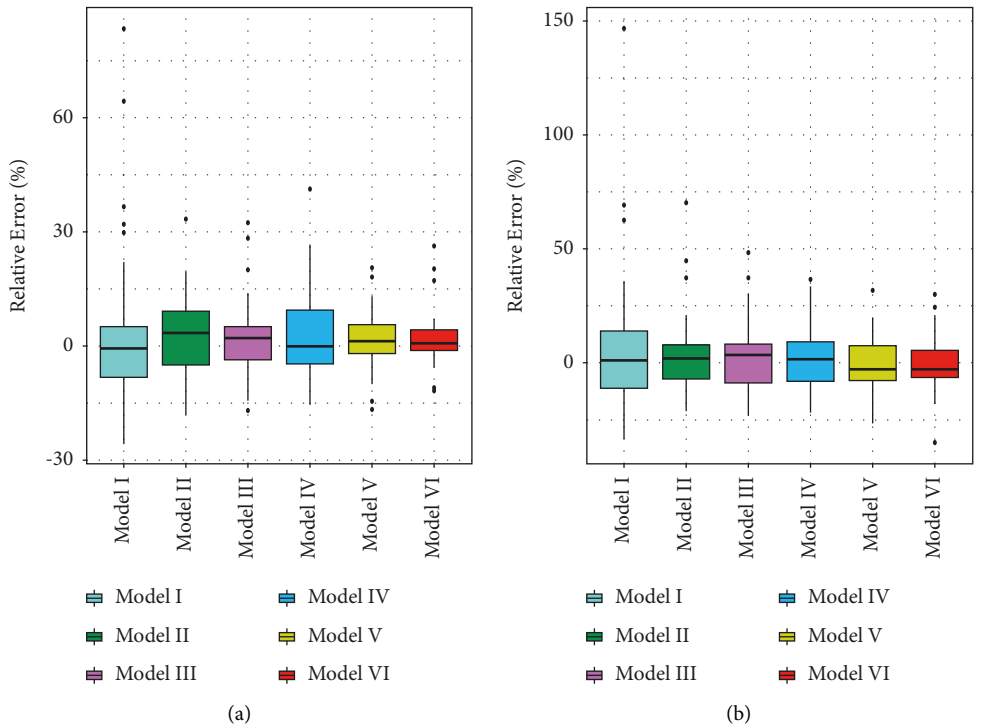

Figure 15: Continued.

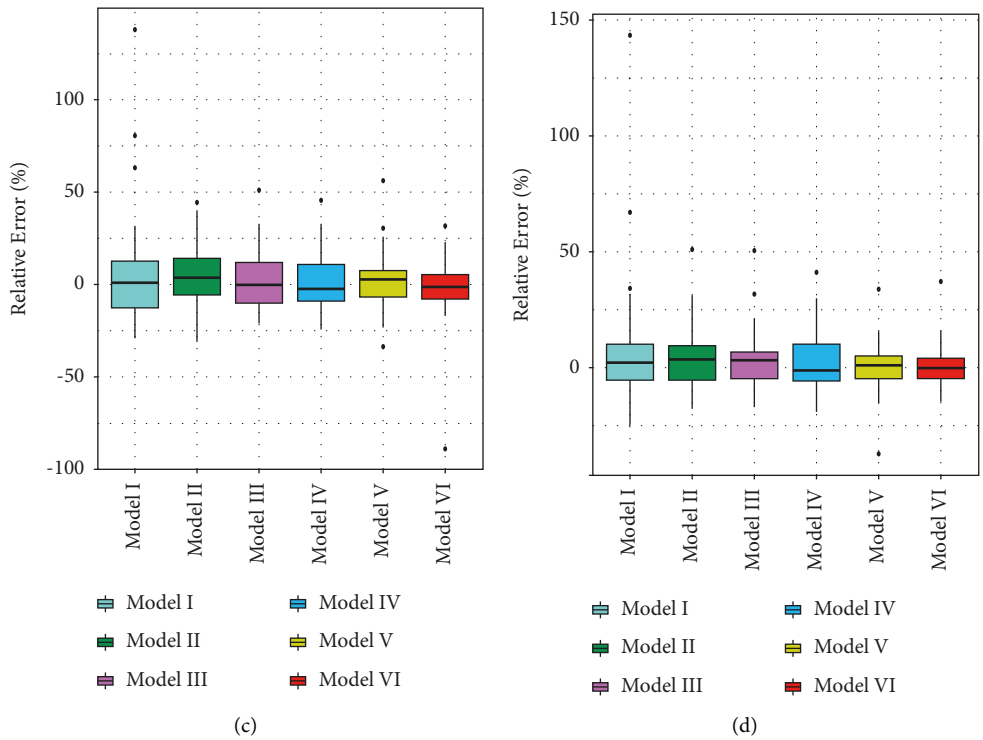

Figure 15: Relative error percentages of the developed AI models for the three tested scenarios. (a) DLNN model. (b) MARS-model. (c) ELM-model. (d) RF-model.

of the developed DLNN model for predicting the compressive strength of EF concrete. The proposed model indicated a robust machine learning model that can be implemented in actual practice to calculate the compressive strength of concrete as a prior stage for material design. This is giving credit to the application of computer-aided models to take place of an essential alternative technology. For future studies, the advanced models of AI can be introduced to improve the predictability of standalone AI models for compressive strength prediction of EF concrete such as [86, 87]. The application of uncertainty analysis can be examined to investigate the efficiency of input variables and the sensitivity of the developed model [88].

5. Conclusion

Accurate prediction of the compressive strength of EF concrete is very important in the sustainable development of concrete structures. Four AI approaches called DLNN, MARS, ELM, and RF were developed using 353 experiment samples collected from open-source literature. Three data division scenarios (70%-30%, 80%-20%, and 90%-10%) were applied to investigate the effect of changing training data size on the modelling process of compressive strength. XGBoost algorithm abstracted the most correlated input parameters needed to achieve the best prediction performance. The capacity of the developed model was examined by using statistical metrics and graphical presentations. The results reflected that the DLNN model attained the highest accuracy of prediction performance and, therefore, is suitable for the CS prediction of EF concrete. The results also demonstrated that using of 90%-10% data division scenario revealed a better prediction ability. It is found that the data size used for training the developed model has a considerable impact on the predicted model accuracy. The application of XGBoost as a feature selection approach plays an essential role in abstracting the most correlated variables in CS prediction. The study revealed that the highest prediction performance could be attained by incorporating all input variables in the prediction problem. The results reflected that the DLNN model attains the best prediction accuracy with the sixth input combination. In addition, the study demonstrated that the DLNN model provided an outstanding ability to capture the nonlinear relationship among the input variables as well as the compressive strength of concrete.

Data Availability

Data will be available upon request from the authors.

Conflicts of Interest

The authors declare that they have no conflicts of interest.

Acknowledgments

This study was supported by Princess Nourah bint Abdulrahman University Researchers Supporting Project number (PNURSP2022R138), Princess Nourah bint Abdulrahman University, Riyadh, Saudi Arabia. The first author would like

to thank Al-Mustaqbal University College for providing technical support for this research.

References

[1] R. Mi, G. Pan, K. M. Liew, and T. Kuang, "Utilizing recycled aggregate concrete in sustainable construction for a required compressive strength ratio," *Journal of Cleaner Production*, vol. 276, Article ID 124249, 2020.

[2] M. A. B. Omer and T. Noguchi, "A conceptual framework for understanding the contribution of building materials in the achievement of Sustainable Development Goals (SDGs)," *Sustainable Cities and Society*, vol. 52, Article ID 101869, 2020.

[3] D. Oh, T. Noguchi, R. Kitagaki, and H. Choi, "Proposal of demolished concrete recycling system based on performance evaluation of inorganic building materials manufactured from waste concrete powder," *Renewable and Sustainable Energy Reviews*, vol. 135, Article ID 110147, 2021.

[4] M. S. Nasr, I. M. Ali, A. M. Hussein, A. A. Shubbar, Q. T. Kareem, and A. T. AbdulAmeer, "Utilization of locally produced waste in the production of sustainable mortar," *Case Studies in Construction Materials*, vol. 13, Article ID e00464, 2020.

[5] M. Soltaninejad, M. Soltaninejad, F. S. K, M. K. Moshizi, V. Sadeghi, and P. Jahanbakhsh, "Environmental-friendly mortar produced with treated and untreated coal wastes as cement replacement materials," *Clean Technologies and Environmental Policy*, vol. 23, no. 10, pp. 2843–2860, 2021.

[6] M. Sandanayake, C. Gunasekara, D. Law, G. Zhang, S. Setunge, and D. Wanijuru, "Sustainable criterion selection framework for green building materials - an optimisation based study of fly-ash Geopolymer concrete," *Sustainable Materials and Technologies*, vol. 25, Article ID e00178, 2020.

[7] R. Yang, R. Yu, Z. Shui et al., "Environmental and economical friendly ultra-high performance-concrete incorporating appropriate quarry-stone powders," *Journal of Cleaner Production*, vol. 260, Article ID 121112, 2020.

[8] N. N. Hilal, A. S. Mohammed, and T. K. M. Ali, "Properties of eco-friendly concrete contained limestone and ceramic tiles waste exposed to high temperature," *Arabian Journal for Science and Engineering*, vol. 45, no. 5, pp. 4387–4404, 2020.

[9] B. Wang, L. Yan, Q. Fu, and B. Kasal, "A comprehensive review on recycled aggregate and recycled aggregate concrete," *Resources, Conservation and Recycling*, vol. 171, Article ID 105565, 2021.

[10] H. Naderpour, A. H. Rafiean, and P. Fakharian, "Compressive strength prediction of environmentally friendly concrete using artificial neural networks," *Journal of Building Engineering*, vol. 16, pp. 213–219, 2018.

[11] H. Naderpour and M. Mirrashid, "Estimating the compressive strength of eco-friendly concrete incorporating recycled coarse aggregate using neuro-fuzzy approach," *Journal of Cleaner Production*, vol. 265, Article ID 121886, 2020.

[12] J. Xie, W. Chen, J. Wang, C. Fang, B. Zhang, and F. Liu, "Coupling effects of recycled aggregate and GGBS/metakaolin on physicochemical properties of geopolymer concrete," *Construction and Building Materials*, vol. 226, pp. 345–359, 2019.

[13] J. Xie, J. Zhao, J. Wang, C. Wang, P. Huang, and C. Fang, "Sulfate resistance of recycled aggregate concrete with GGBS and fly ash-based geopolymer," *Materials*, vol. 12, no. 8, p. 1247, 2019.

[14] T. R. Naik and G. Moriconi, "Environmental-friendly durable concrete made with recycled materials for sustainable concrete construction," in *Proceedings of the International Symposium on Sustainable Development of Cement, Concrete and Concrete Structures*, pp. 5–7, Toronto, Ontario, October, 2005.

[15] R. Ahmmad, U. J. Alengaram, M. Z. Jumaat, N. H. R. Sulong, M. O. Yusuf, and M. A. Rehman, "Feasibility study on the use of high volume palm oil clinker waste in environmental friendly lightweight concrete," *Construction and Building Materials*, vol. 135, 2017.

[16] T. Kibriya and S. Khan, "Performance of ecologically friendly waste in high strength concrete," in *Proceedings of the IV Regional Conference on Civil Engineering Technology, Joint ASCE/ESIE Conference*, pp. 7–9, Cairo, June, 2005.

[17] R. Corral Higuera, S. P. Arredondo Rea, J. M. V. Gómez Soberón, D. C. Gámez García, J. M. Mendevil, and J. L. Almaral Sánchez, "Strength and durability parameters of an environmentally friendly concrete," in *Proceedings of the Twelfth International Conference on Recent Advances in concrete Technology and Sustainability Issues*, pp. 229–243, Prague, Czech Republic, October, 2012.

[18] M. Reiner, S. A. Durham, and K. L. Rens, "Development and analysis of high-performance green concrete in the urban infrastructure," *International Journal of Sustainable Engineering*, vol. 3, no. 3, pp. 198–210, 2010.

[19] Y. Wei, J. Chai, Y. Qin, Z. Xu, and X. Zhang, "Performance evaluation of green-concrete pavement material containing selected C&D waste and FA in cold regions," *Journal of Material Cycles and Waste Management*, vol. 21, no. 6, pp. 1550–1562, 2019.

[20] C. M. Grădinaru, A. A. Şerbănoiu, D. T. Babor, G. C. Sârbu, I. V. Petrescu-Mag, and A. C. Grădinaru, "When agricultural waste transforms into an environmentally friendly material: the case of green concrete as alternative to natural resources depletion," *Journal of Agricultural and Environmental Ethics*, vol. 32, no. 1, pp. 77–93, 2019.

[21] A. Abdulmatin, W. Tangchirapat, and C. Jaturapitakkul, "Environmentally friendly interlocking concrete paving block containing new cementing material and recycled concrete aggregate," *European Journal of Environmental and Civil Engineering*, vol. 23, no. 12, pp. 1467–1484, 2019.

[22] Y. Qin, X. Zhang, and J. Chai, "Damage performance and compressive behavior of early-age green concrete with recycled nylon fiber fabric under an axial load," *Construction and Building Materials*, vol. 209, pp. 105–114, 2019.

[23] E. Agbenyeku and F. Okonta, "Green economy and innovation: compressive strength potential of blended cement cassava peels ash and laterised concrete," *African Journal of Science, Technology, Innovation and Development*, vol. 6, no. 2, pp. 105–110, 2014.

[24] A. O. Sojobi, "Evaluation of the performance of eco-friendly lightweight interlocking concrete paving units incorporating sawdust wastes and laterite," *Cogent Engineering*, vol. 3, no. 1, Article ID 1255168, 2016.

[25] G. Zhang, "Reinforced concrete deep beam shear strength capacity modelling using an integrative bio-inspired algorithm with an artificial intelligence model," *Eng. Comput*, vol. 38, 2020.

[26] J. Duan, P. G. Asteris, H. Nguyen, X.-N. Bui, and H. Moayedi, "A novel artificial intelligence technique to predict compressive strength of recycled aggregate concrete using ICA-XGBoost model," *Engineering with Computers*, vol. 37, no. 4, pp. 3329–3346, 2021.

[27] H. Q. Nguyen, H.-B. Ly, V. Q. Tran, T.-A. Nguyen, T.-T. Le, and B. T. Pham, "Optimization of artificial intelligence system

by evolutionary algorithm for prediction of axial capacity of rectangular concrete filled steel tubes under compression," *Materials*, vol. 13, no. 5, p. 1205, 2020.

[28] A. A. Al-Musawi, "Determination of shear strength of steel fiber RC beams: application of data-intelligence models," *Frontiers of Structural and Civil Engineering*, vol. 13, 2019.

[29] A. A. Al-Musawi, A. A. H. Alwanas, S. Q. Salih, Z. H. Ali, M. T. Tran, and Z. M. Yaseen, "Shear strength of SFRCB without stirrups simulation: implementation of hybrid artificial intelligence model," *Engineering with Computers*, vol. 36, no. 1, pp. 1–11, 2020.

[30] Z. M. Yaseen, R. C. Deo, A. Hilal et al., "Predicting compressive strength of lightweight foamed concrete using extreme learning machine model," *Advances in Engineering Software*, vol. 115, pp. 112–125, 2018.

[31] Z. M. Yaseen, M. T. Tran, S. Kim, T. Bakhshpoori, and R. C. Deo, "Shear strength prediction of steel fiber reinforced concrete beam using hybrid intelligence models: a new approach," *Engineering Structures*, vol. 177, no. April, pp. 244–255, 2018.

[32] A. Shubbar, Z. Al-khafaji, M. Nasr, and M. Falah, "Using NON-destructive tests for evaluating flyover footbridge: case study," *Knowledge-Based Engineering and Sciences*, vol. 1, no. 01, pp. 23–39, 2020.

[33] A. Hammoudi, K. Moussaceb, C. Belebchouche, and F. Dahmoune, "Comparison of artificial neural network (ANN) and response surface methodology (RSM) prediction in compressive strength of recycled concrete aggregates," *Construction and Building Materials*, vol. 209, pp. 425–436, 2019.

[34] T. Al-Mughanam, T. H. H. Aldhyani, B. AlSubari, and M. Al-Yaari, "Modeling of compressive strength of sustainable self-compacting concrete incorporating treated palm oil fuel ash using artificial neural network," *Sustainability*, vol. 12, no. 22, p. 9322, 2020.

[35] D.-C. Feng, Z.-T. Liu, X.-D. Wang et al., "Machine learning-based compressive strength prediction for concrete: an adaptive boosting approach," *Construction and Building Materials*, vol. 230, Article ID 117000, 2020.

[36] A. Kandiri, E. Mohammadi Golafshani, and A. Behnood, "Estimation of the compressive strength of concretes containing ground granulated blast furnace slag using hybridized multi-objective ANN and salp swarm algorithm," *Construction and Building Materials*, vol. 248, Article ID 118676, 2020.

[37] A. A. Shahmansouri, M. Yazdani, S. Ghanbari, H. Akbarzadeh Bengar, A. Jafari, and H. Farrokh Ghatte, "Artificial neural network model to predict the compressive strength of eco-friendly geopolymer concrete incorporating silica fume and natural zeolite," *Journal of Cleaner Production*, vol. 279, Article ID 123697, 2021.

[38] S. D. Latif, "Developing a boosted decision tree regression prediction model as a sustainable tool for compressive strength of environmentally friendly concrete," *Environmental Science and Pollution Research*, vol. 28, no. 46, Article ID 65935, 2021.

[39] K. K. Yaswanth, J. Revathy, and P. Gajalakshmi, "Soft computing techniques for the prediction and analysis of compressive strength of alkali-activated Alumino-silicate based strain-hardening Geopolymer composites," *Silicon*, vol. 14, no. 5, pp. 1985–2008, 2021.

[40] A. Kandiri, F. Sartipi, and M. Kioumarsi, "Predicting compressive strength of concrete containing recycled aggregate using modified ann with different optimization algorithms," *Applied Sciences*, vol. 11, no. 2, p. 485, 2021.

[41] H. Naseri, H. Jahanbakhsh, P. Hosseini, and F. Moghadas Nejad, "Designing sustainable concrete mixture by developing a new machine learning technique," *J. Clean. Prod*, vol. 258, 2020.

[42] X. Huang, J. Zhang, J. Sresakoolchai, and S. Kaewunruen, "Machine learning aided design and prediction of environmentally friendly rubberised concrete," *Sustain*, vol. 13, 2021.

[43] I. Nunez, A. Marani, and M. L. Nehdi, "Mixture optimization of recycled aggregate concrete using hybrid machine learning model," *Materials (Basel)*, vol. 13, 2020.

[44] M. A. Khan, "Simulation of depth of wear of eco-friendly concrete using machine learning based computational approaches," *Materials*, vol. 15, no. 1, 2022.

[45] V. Quan Tran, V. Quoc Dang, and L. Si Ho, "Evaluating compressive strength of concrete made with recycled concrete aggregates using machine learning approach," *Construction and Building Materials*, vol. 323, Article ID 126578, 2022.

[46] A. W. Al Zand, E. Hosseinpour, W. H. W. Badaruzzaman, M. M. Ali, Z. M. Yaseen, and A. N. Hanoon, "Performance of the novel C-purlin tubular beams filled with recycled-lightweight concrete strengthened with CFRP sheet," *Journal of Building Engineering*, vol. 43, Article ID 102532, 2021.

[47] S. Arafa, A. Milad, N. I. M. Yusoff, N. Al-Ansari, and Z. M. Yaseen, "Investigation into the permeability and strength of pervious geopolymer concrete containing coated biomass aggregate material," *Journal of Materials Research and Technology*, vol. 15, pp. 2075–2087, 2021.

[48] Z. Yang, Y. Wang, J. Li, L. Liu, J. Ma, and Y. Zhong, "Airport arrival flow prediction considering meteorological factors based on deep-learning methods," *Complexity*, vol. 2020, Article ID 6309272, 11 pages, 2020.

[49] X. B. Jin, H. X. Wang, X. Y. Wang, Y. T. Bai, T. L. Su, and J. L. Kong, "Deep-learning prediction model with serial two-level decomposition based on bayesian optimization," *Complexity*, vol. 2020, Article ID 4346803, 14 pages, 2020.

[50] Y. Hou, Z. Deng, and H. Cui, "Short-term traffic flow prediction with weather conditions: based on deep learning algorithms and data fusion," *Complexity*, vol. 2021, Article ID 6662959, 14 pages, 2021.

[51] J. A. Khalaf, A. A. Majeed, M. S. Aldlemy et al., "Hybridized deep learning model for perfobond rib shear strength connector prediction," *Complexity*, vol. 2021, Article ID 6611885, 21 pages, 2021.

[52] C. Wang, D. Shi, and S. Li, "A study on establishing a microstructure-related hardness model with precipitate segmentation using deep learning method," *Materials (Basel)*, vol. 13, 2020.

[53] Z. M. Yaseen, H. A. Afan, and M.-T. Tran, "Beam-column joint shear prediction using hybridized deep learning neural network with genetic algorithm," *IOP Conference Series: Earth and Environmental Science*, vol. 143, Article ID 012025, 2018.

[54] C. A. Jeyasehar and K. Sumangala, "Nondestructive evaluation of prestressed concrete beams using an artificial neural network (ANN) approach," *Structural Health Monitoring*, vol. 5, no. 4, pp. 313–323, 2006.

[55] A. M. Araba, Z. A. Memon, M. Alhawat, M. Ali, and A. Milad, "Estimation at completion in civil engineering projects:

review of regression and soft computing models," *Knowledge-Based Engineering and Sciences*, vol. 2, no. 2, pp. 1–12, 2021.

[56] G. E. Hinton, S. Osindero, and Y.-W. Teh, "A fast learning algorithm for deep belief nets," *Neural Computation*, vol. 18, no. 7, pp. 1527–1554, 2006.

[57] S. V. Moghadam, A. Sharafati, H. Feizi, S. M. S. Marjaie, S. B. H. S. Asadollah, and D. Motta, "An efficient strategy for predicting river dissolved oxygen concentration: application of deep recurrent neural network model," *Environmental Monitoring and Assessment*, vol. 193, no. 12, p. 798, 2021.

[58] J. H. Friedman, "Multivariate adaptive regression splines," *Annals of Statistics*, vol. 19, no. 1, pp. 1–67, 1991.

[59] F. Yerlikaya-Özkurt, İ. Batmaz, and G.-W. Weber, "A review and new contribution on conic multivariate adaptive regression splines (CMARS): a powerful tool for predictive data mining," in *Modeling, Dynamics, Optimization and Bioeconomics I*, pp. 695–722, Springer, New york, NY, USA, 2014.

[60] M. A. Sahraei, H. Duman, M. Y. Çodur, and E. Eyduran, "Prediction of transportation energy demand: multivariate adaptive regression splines," *Energy*, vol. 224, Article ID 120090, 2021.

[61] G. Zheng, W. Zhang, H. Zhou, and P. Yang, "Multivariate adaptive regression splines model for prediction of the liquefaction-induced settlement of shallow foundations," *Soil Dynamics and Earthquake Engineering*, vol. 132, Article ID 106097, 2020.

[62] Q. S. Xu, "Multivariate Adaptive Regression Splines - Studies of HIV Reverse Transcriptase Inhibitors," *Chemom. Intell. Lab. Syst*, vol. 72, 2004.

[63] N.-Y. Nan-Ying Liang, G.-B. Guang-Bin Huang, P. Saratchandran, and N. Sundararajan, "A fast and accurate online sequential learning algorithm for feedforward networks," *IEEE Transactions on Neural Networks*, vol. 17, no. 6, pp. 1411–1423, 2006.

[64] M. Hou, T. Zhang, F. Weng, M. Ali, N. Al-Ansari, and Z. Yaseen, "Global solar radiation prediction using hybrid online sequential extreme learning machine model," *Energies*, vol. 11, no. 12, p. 3415, 2018.

[65] L. Zhang and D. Zhang, "Evolutionary cost-sensitive extreme learning machine," *IEEE Transactions on Neural Networks and Learning Systems*, vol. 28, no. 12, pp. 3045–3060, 2017.

[66] H. Yang, L. Gao, and G. Li, "Underwater acoustic signal prediction based on MVMD and optimized kernel extreme learning machine," *Complexity*, vol. 2020, Article ID 6947059, 14 pages, 2020.

[67] G. Huang, G. B. Huang, S. Song, and K. You, "Trends in extreme learning machines: a review," *Neural Networks*, vol. 61, pp. 32–48, 2015.

[68] M. Ali and R. Prasad, "Significant wave height forecasting via an extreme learning machine model integrated with improved complete ensemble empirical mode decomposition," *Renewable and Sustainable Energy Reviews*, vol. 104, pp. 281–295, 2019.

[69] S. Sekhar Roy, R. Roy, and V. E. Balas, "Estimating heating load in buildings using multivariate adaptive regression splines, extreme learning machine, a hybrid model of MARS and ELM," *Renewable and Sustainable Energy Reviews*, vol. 82, pp. 4256–4268, Feb. 2018.

[70] T. K. Ho, "Random decision forests," *Proceedings of 3rd international conference on document analysis and recognition*, vol. 1, pp. 278–282, 1995.

[71] F. Farooq, M. Nasir Amin, K. Khan et al., "A comparative study of random forest and genetic engineering programming for the prediction of compressive strength of high strength concrete (HSC)," *Applied Sciences*, vol. 10, no. 20, p. 7330, 2020.

[72] M. Ali, R. Prasad, Y. Xiang et al., "Variational mode decomposition based random forest model for solar radiation forecasting: new emerging machine learning technology," *Energy Reports*, vol. 7, pp. 6700–6717, 2021.

[73] A. Sharafati, S. B. H. S. Asadollah, and M. Hosseinzadeh, "The potential of new ensemble machine learning models for effluent quality parameters prediction and related uncertainty," *Process Safety and Environmental Protection*, vol. 140, pp. 68–78, 2020.

[74] M. M. Hameed, M. K. AlOmar, S. F. Mohd Razali et al., "Application of artificial intelligence models for evapotranspiration prediction along the southern coast of Turkey," *Complexity*, vol. 2021, Article ID 8850243, 20 pages, 2021.

[75] M. A. Khan, S. A. Memon, F. Farooq, M. F. Javed, F. Aslam, and R. Alyousef, "Compressive strength of fly-ash-based geopolymer concrete by gene expression programming and random forest," *Advances in Civil Engineering*, vol. 2021, Article ID 6618407, 17 pages, 2021.

[76] X. Shi, Y. D. Wong, M. Z.-F. Li, C. Palanisamy, and C. Chai, "A feature learning approach based on XGBoost for driving assessment and risk prediction," *Accident Analysis & Prevention*, vol. 129, pp. 170–179, 2019.

[77] Z. Wan, Y. Xu, and B. Šavija, "On the use of machine learning models for prediction of compressive strength of concrete: influence of dimensionality reduction on the model performance," *Materials*, vol. 14, no. 4, p. 713, 2021.

[78] A. Torres-Barrán, Á. Alonso, and J. R. Dorronsoro, "Regression Tree Ensembles for Wind Energy and Solar Radiation Prediction," *Neurocomputing*, vol. 326-327, 2017.

[79] S. R. Naganna, B. H. Beyaztas, N. Bokde, and A. M. Armanuos, "ON the evaluation OF the gradient tree boosting model for groundwater level forecasting," *Knowledge-Based Engineering and Sciences*, vol. 1, no. 01, pp. 48–57, 2020.

[80] T. Hastie, R. Tibshirani, and J. Friedman, *The Elements of Statistical Learning: Data Mining, Inference, and Prediction*, Springer Science & Business Media, Berlin/Heidelberg, Germany, 2009.

[81] A. Sharafati, S. B. H. S. Asadollah, and A. Neshat, "A new artificial intelligence strategy for predicting the groundwater level over the Rafsanjan aquifer in Iran," *Journal of Hydrology*, vol. 591, Article ID 125468, 2020.

[82] A. Ashrafian, "Toward an Innovative Fuzzy Computational Intelligence on the Compressive Strength Prediction of Environmental-Friendly concrete Containing Construction Waste Products," *Mendeley Data*, vol. 38, 2021.

[83] R. E. Walpole, R. H. Myers, S. L. Myers, and K. Ye, "Probability and statistics for engineers and scientists," *Macmillan*, vol. 5, 1993.

[84] H. V. Gupta, H. Kling, K. K. Yilmaz, and G. F. Martinez, "Decomposition of the mean squared error and NSE performance criteria: implications for improving hydrological modelling," *Journal of Hydrology*, vol. 377, no. 1-2, pp. 80–91, 2009.

[85] K. E. Taylor, "Summarizing multiple aspects of model performance in a single diagram," *Journal of Geophysical Research: Atmospheres*, vol. 106, no. D7, pp. 7183–7192, 2001.
[86] M. Ehteram, A. Sharafati, S. B. H. S. Asadollah, and A. Neshat, "Estimating the transient storage parameters for pollution modeling in small streams: a comparison of newly developed hybrid optimization algorithms," *Environmental Monitoring and Assessment*, vol. 193, no. 8, p. 475, 2021.
[87] M. Haghbin, A. Sharafati, and D. Motta, "Prediction of channel sinuosity in perennial rivers using Bayesian Mutual Information theory and support vector regression coupled with meta-heuristic algorithms," *Earth Science India*, vol. 14, no. 4, pp. 2279–2292, 2021.
[88] M. S. T. Nguyen and S.-E. Kim, "A hybrid machine learning approach in prediction and uncertainty quantification of ultimate compressive strength of RCFST columns," *Construction and Building Materials*, vol. 302, Article ID 124208, 2021.